INSIGHTS IN CROP AND PRODUCT PHYSIOLOGY: 2021

EDITED BY: Leo Marcelis
PUBLISHED IN: Frontiers in Plant Science

frontiers Research Topics

ISSN 1664-8714
ISBN 978-2-83250-128-3
DOI 10.3389/978-2-83250-128-3

About Frontiers

Frontiers is more than just an open-access publisher of scholarly articles: it is a pioneering approach to the world of academia, radically improving the way scholarly research is managed. The grand vision of Frontiers is a world where all people have an equal opportunity to seek, share and generate knowledge. Frontiers provides immediate and permanent online open access to all its publications, but this alone is not enough to realize our grand goals.

Frontiers Journal Series

The Frontiers Journal Series is a multi-tier and interdisciplinary set of open-access, online journals, promising a paradigm shift from the current review, selection and dissemination processes in academic publishing. All Frontiers journals are driven by researchers for researchers; therefore, they constitute a service to the scholarly community. At the same time, the Frontiers Journal Series operates on a revolutionary invention, the tiered publishing system, initially addressing specific communities of scholars, and gradually climbing up to broader public understanding, thus serving the interests of the lay society, too.

Dedication to Quality

Each Frontiers article is a landmark of the highest quality, thanks to genuinely collaborative interactions between authors and review editors, who include some of the world's best academicians. Research must be certified by peers before entering a stream of knowledge that may eventually reach the public - and shape society; therefore, Frontiers only applies the most rigorous and unbiased reviews.
Frontiers revolutionizes research publishing by freely delivering the most outstanding research, evaluated with no bias from both the academic and social point of view. By applying the most advanced information technologies, Frontiers is catapulting scholarly publishing into a new generation.

What are Frontiers Research Topics?

Frontiers Research Topics are very popular trademarks of the Frontiers Journals Series: they are collections of at least ten articles, all centered on a particular subject. With their unique mix of varied contributions from Original Research to Review Articles, Frontiers Research Topics unify the most influential researchers, the latest key findings and historical advances in a hot research area! Find out more on how to host your own Frontiers Research Topic or contribute to one as an author by contacting the Frontiers Editorial Office: frontiersin.org/about/contact

INSIGHTS IN CROP AND PRODUCT PHYSIOLOGY: 2021

Topic Editor:
Leo Marcelis, Wageningen University and Research, Netherlands

Citation: Marcelis, L., ed. (2022). Insights in Crop and Product Physiology: 2021
Lausanne: Frontiers Media SA. doi: 10.3389/978-2-83250-128-3

Table of Contents

frontiers in Plant Science

ORIGINAL RESEARCH
published: 29 November 2021
doi: 10.3389/fpls.2021.782465

Acclimating Cucumber Plants to Blue Supplemental Light Promotes Growth in Full Sunlight

Chenqian Kang[1†], Yuqi Zhang[1,2†], Ruifeng Cheng[1], Elias Kaiser[2], Qichang Yang[1,3] and Tao Li[1]*

[1] Institute of Environment and Sustainable Development in Agriculture, Chinese Academy of Agricultural Sciences, Beijing, China, [2] Horticulture and Product Physiology, Wageningen University and Research, Wageningen, Netherlands, [3] Institute of Urban Agriculture, Chinese Academy of Agricultural Sciences, Chengdu, China

OPEN ACCESS

Edited by:
Oliver Körner, Leibniz Institute of Vegetable and Ornamental Crops, Germany

Reviewed by:
Alfred Holzwarth, Max Planck Institute for Chemical Energy Conversion, Germany
Vladimir Spunda, University of Ostrava, Czechia

***Correspondence:**
Tao Li
litao06@caas.cn

[†] These authors have contributed equally to this work and share first authorship

Specialty section:
This article was submitted to Crop and Product Physiology, a section of the journal Frontiers in Plant Science

Received: *24 September 2021*
Accepted: *01 November 2021*
Published: *29 November 2021*

Citation:
Kang C, Zhang Y, Cheng R, Kaiser E, Yang Q and Li T (2021) Acclimating Cucumber Plants to Blue Supplemental Light Promotes Growth in Full Sunlight. Front. Plant Sci. 12:782465. doi: 10.3389/fpls.2021.782465

Raising young plants is important for modern greenhouse production. Upon transfer from the raising to the production environment, young plants should maximize light use efficiency while minimizing deleterious effects associated with exposure to high light (HL) intensity. The light spectrum may be used to establish desired traits, but how plants acclimated to a given spectrum respond to HL intensity exposure is less well explored. Cucumber (*Cucumis sativus*) seedlings were grown in a greenhouse in low-intensity sunlight (control; ∼2.7 mol photons m^{-2} day^{-1}) and were treated with white, red, blue, or green supplemental light (4.3 mol photons m^{-2} day^{-1}) for 10 days. Photosynthetic capacity was highest in leaves treated with blue light, followed by white, red, and green, and was positively correlated with leaf thickness, nitrogen, and chlorophyll concentration. Acclimation to different spectra did not affect the rate of photosynthetic induction, but leaves grown under blue light showed faster induction and relaxation of non-photochemical quenching (NPQ) under alternating HL and LL intensity. Blue-light-acclimated leaves showed reduced photoinhibition after HL intensity exposure, as indicated by a high maximum quantum yield of photosystem II photochemistry (F_v/F_m). Although plants grown under different supplemental light spectra for 10 days had similar shoot biomass, blue-light-grown plants (B-grown plants) showed a more compact morphology with smaller leaf areas and shorter stems. However, after subsequent, week-long exposure to full sunlight (10.7 mol photons m^{-2} day^{-1}), B-grown plants showed similar leaf area and 15% higher shoot biomass, compared to plants that had been acclimated to other spectra. The faster growth rate in blue-light-acclimated plants compared to other plants was mainly due to a higher photosynthetic capacity and highly regulated NPQ performance under intermittent high solar light. Acclimation to blue supplemental light can improve light use efficiency and diminish photoinhibition under high solar light exposure, which can benefit plant growth.

Keywords: supplemental light, photosynthesis, photoprotection, dynamic light, cucumber, greenhouse

INTRODUCTION

Light quality strongly affects the operation and formation of the leaf photosynthetic apparatus and plant growth (Hogewoning et al., 2010; Bugbee, 2016). Wavebands, such as blue, red, or green light, have distinct effects on plant physiological and morphological processes (Claypool and Lieth, 2020; Gao et al., 2020). In modern crop production, plants are often raised by specialized companies before their transfer to the production environment. Specific light spectra may be applied during plant raising to form traits that are desirable for later production, which may occur in greenhouses or the open field. Under full sunlight, plants will experience a longer duration of high light (HL) intensity or a high frequency of HL intensity and low light (LL) intensity transitions, due to variations of the solar angle, cloud cover, overlapping leaves, and greenhouse structures (Li et al., 2014, 2016; Marcelis et al., 2018). Plants need to maximize the efficiency of light energy used for photosynthesis while minimizing deleterious effects associated with exposure to HL intensity. However, how plants acclimated to a given spectrum respond to the dynamic HL intensity exposure is less well explored.

Growing plants under different light spectra involve acclimatory adjustments in the photosynthetic apparatus and plant morphology (Dueck et al., 2016; Landi et al., 2020), but so far most conclusions have been drawn based on experiments in climate chambers (Claypool and Lieth, 2020; Gao et al., 2020). Monochromatic red light often induces the "red light syndrome," which is characterized by a dysfunctional leaf photosynthetic apparatus and reduced photosynthetic capacity (Hogewoning et al., 2010). Acclimation to blue light, on the other hand, is known to produce "sun-type" plants whose leaves possess high photosynthetic capacity (Savvides et al., 2012). As for plant morphology, increasing the proportion of blue light tends to reduce plant height, whereas monochromatic blue light again increases it, as seen in cucumber (Hernández and Kubota, 2016; Liang et al., 2021), petunia, geranium, calibrachoa, and marigold (Kong et al., 2018). In addition, a green light may penetrate to lower layers of the canopy to benefit photosynthesis in shaded leaves, and increases in the green: blue ratio may serve as a shade signal to promote stem extension and leaf expansion, which may facilitate canopy light interception (Folta and Maruhnich, 2007; Smith et al., 2017). A range of light spectra is currently used in supplemental greenhouse lighting to increase crop growth and to form desired traits. Of course, background sunlight, which exists on top of supplemental light, changes the overall light spectrum to a variable extent and is likely to induce different results compared to results in climate chamber studies (Kaiser et al., 2019; Claypool and Lieth, 2020). Therefore, it is highly relevant to explore acclimation to light spectrum with solar light as a background and to explore how such acclimation affects plant growth and function during exposure to HL intensity.

Plant growth, to a large extent, depends on photosynthetic performance. When exposed to full sunlight, plants often experience dynamic light intensities, such that net photosynthesis rate (A; $\mu mol\ m^{-2}\ s^{-1}$) is rarely at a steady state (Kaiser et al., 2015; Li et al., 2016; Marcelis et al., 2018). When light intensity impinging on a shade-adapted leaf increases suddenly, A may take 10–30 min to reach a steady state, such that it might not reach a steady state before light intensity decreases again (McAusland and Murchie, 2020). This process, photosynthetic induction, can potentially limit daily CO_2 fixation by 10–50% (Taylor and Long, 2017; Morales et al., 2018), compared to a hypothetical, instantaneous response of A to increases in light intensity. Thus, a promising strategy for increasing light use efficiency in the field is to improve the rate of photosynthetic induction (Taylor and Long, 2017). The stomatal limitation is one of the major determinants of the rate of photosynthetic induction (Sakoda et al., 2021) and is often affected by the growth light spectrum (O' Carrigan et al., 2014). Therefore, the light spectrum might also affect the rate of photosynthetic induction. A previous study from our lab showed growth-chamber tomato (*Solanum lycopersicum*) plants that were acclimated to different red/blue ratios showed identical photosynthetic induction rates after dark–light transitions (Zhang et al., 2019). However, it is unknown whether acclimation to green and white light affects the photosynthetic induction rate.

When plants are exposed to sunlight, HL intensity can also cause damage to the photosynthetic machinery. The likelihood and severity of deleterious effects of HL intensity exposure are minimized by a set of photoprotective mechanisms. One key process is the controlled dissipation of energy from chlorophyll within PSII, known as non-photochemical quenching (NPQ; Bilger and Björkman, 1990). NPQ may play at least two opposing roles in plant productivity; on the one hand, it reduces photoinhibition and maintains maximal photosynthesis under HL intensity; on the other hand, it momentarily reduces the quantum efficiency of photosynthesis immediately following HL to LL transitions, due to transient overprotection (Murchie and Ruban, 2020). Therefore, a fast speed of formation of NPQ under HL intensity along with a fast relaxation in NPQ under LL is an important target to improve plant productivity under dynamic light (Zhu et al., 2004; Kromdijk et al., 2016; Morales et al., 2018; Foo et al., 2020; Wang et al., 2020). Acclimating plants to different light spectra may modulate NPQ under dynamic light intensity; in tomato and rice (*Oryza sativa*), blue-light-grown

Abbreviations: A, net CO_2 assimilation rate; A_i, steady-state net photosynthesis rate at 50 $\mu mol\ m^{-2}\ s^{-1}$ photosynthetic photon flux density; A_f, steady-state net photosynthesis rate at 1,000 $\mu mol\ m^{-2}\ s^{-1}$ photosynthetic photon flux density; A_{max}, maximum net photosynthesis rate; α, apparent quantum yield; A_{300}, integrated A during the first 300 s of high light; Ab, Rf, Tr, leaf absorptance, reflectance, transmittance; C, total leaf carbon content; Chl $a+b$, total chlorophyll a and b contents; Chl a:b, chlorophyll a and b ratio; C_i, substomatal cavity CO_2 partial pressure; DMC, dry mass content; DMP, dry mass partitioning; HL, high light; LL, low light; FL, fluctuating light; F_s, chlorophyll fluorescence yield under light; F_m', maximum chlorophyll fluorescence under light; F_0, minimal chlorophyll fluorescence under dark; F_m, maximal chlorophyll fluorescence under dark; F_m'', maximum fluorescence after 10 min of dark relaxation; F_v/F_m, maximum photosystem II (PSII) efficiency; g_s, stomatal conductance; gs_i, steady-state stomatal conductance at 50 $\mu mol\ m^{-2}\ s^{-1}$ photosynthetic photon flux density; gs_f, stomatal conductance after 42 min of fluctuating light; IS_{60}, photosynthetic induction state at 60 s; IS_{300}, photosynthetic induction state at 300 s; LED, light-emitting diode; LMA, leaf mass area; N, total leaf nitrogen; NPQ, non-photochemical quenching; PPFD, photosynthetic photon flux density; PSII, photosystem II; Φ_{PSII}, photosystem II operating efficiency; qE, energy-dependent quenching; qI, photoinhibitory quenching; R_{dark}, dark respiration rate; SSL, shade solar light; $VPD_{leaf-air}$, leaf-to-air vapor pressure deficit.

leaves (B-grown leaves) displayed faster induction and higher steady-state NPQ, compared to red-light grown leaves (R-grown leaves) (Hamdani et al., 2019; Zhang et al., 2019). Thus, we hypothesize that in greenhouse-grown plants, acclimation to blue supplemental light could enhance NPQ formation and relaxation and biomass production after HL intensity exposure, relative to acclimation to extra red light.

The aim of this study is to investigate how acclimation to a given spectrum in LL "prepares" plants for HL intensity exposure. Photosynthetic and photoprotective responses to stable and dynamically changing HL intensity, and the consequences of this acclimation for plant growth under full sunlight were investigated.

MATERIALS AND METHODS

Plant Materials and Growth Conditions

Cucumber (*Cucumis sativus* cv. Xiamei No. 2) seeds (130–150 seeds per batch of experiment) were sown in Rockwool plugs (Grodan, Roermond, Netherlands) and germinated in a growth chamber at a photoperiod of 16 h, photosynthetic photon flux density (PPFD) of 100 μmol m^{-2} s^{-1} provided by white light-emitting diode (LEDs), and at an ambient CO_2 partial pressure, the temperature of 23 ± 1°C, and relative humidity of 70 ± 10%. When plants unfolded the 1st true leaf (2 weeks after sowing), seedlings were transplanted to Rockwool cubes (10 cm × 10 cm × 6.5 cm, Grodan, Roermond, Netherlands); ∼100 seedlings per batch of experiment, and transferred to a Venlo-type glasshouse (Beijing, China, 40°N, 116°E) for experimental treatment (refer to **Table 1** for environmental conditions).

A white sunscreen (Harmony 6145, transmission of 39%, Ludvig Svensson, Kinna, Sweden) was placed at the top of the greenhouse (below the gutter) to reduce the incoming sunlight intensity during the experiment unless specified. Five cultivation tables with aluminum alloy frames (200 cm L × 120 cm W × 180 cm H) were arranged from east to west with 80 cm between tables. The top and sides of each frame were covered by white sunscreen for further shading. Five light treatments were arranged randomly, one per cultivation table: control (C, without supplemental light on), white (W), red (R), blue (B), and green (G). All treatments received identical amounts of background solar light (**Table 1**). LED lamps (ZWS01D-LED120-180, Panan Greenlight, Jinhua, China) were installed 70 cm above the cultivation table and were turned on from 08:00 to 18:00, at an intensity of 120 μmol m^{-2} s^{-1} measured 20 cm above the cultivation table. Peak wavelengths of R, B, and G LEDs were 656, 451, and 519 nm, respectively (**Supplementary Figure 1**). The LED lamp intensity was monitored with a spectroradiometer (Avaspec-2048CL, Avates, Apeldoorn, Netherlands). PPFD of solar light inside the greenhouse (**Table 1**) was recorded continuously with a line sensor (Licor191R, Li-COR, Lincoln, NE, United States).

The greenhouse experiment was performed from June 28, 2020 to September 27, 2020, during which four batches of plants were grown in succession (**Table 1**). Daily light integral (DLI) from sunlight was ∼2–3.5 mol photons m^{-2} d^{-1}, depending on the batch (**Table 1**). Per batch, treatments were re-arranged randomly, and 12–20 plants per treatment and batch were grown for 10 days. Additionally, in the fourth batch, after 10 days of treatment, sunscreens were removed and plants from all treatments were exposed to full solar light, without supplemental light, for 1 week (refer to **Table 1** for environmental conditions during the complete experiment and **Supplementary Figure 2** for daily environmental conditions during full solar light exposure).

Plants were irrigated with modified Hoagland nutrient solution (pH = 5.8, EC = 2.0 dS m^{-1}) regularly, and plants within treatments were rotated randomly every day. Greenhouse temperature, relative humidity, and CO_2 partial pressure were continuously recorded with a climate sensor (TR-76Ui, T&D Co. Ltd., Nagano, Tokyo, Japan; **Table 1**).

Measurements

The number of traits pertaining to plant growth and photosynthetic acclimation was quantified after 10 days of treatment and after 7 days of subsequent exposure to full sunlight. Unless specified, all leaf-level measurements were conducted on the youngest fully expanded leaf (∼15-cm width). Measurements conducted in each experimental batch are detailed in **Table 2**. Three to six biological replicates (plants) were performed per treatment per experimental batch.

Leaf Biochemical Components

Leaf discs (4 × 1.0 cm^2) were stored for 36 h in darkness in 8 ml 95% ethanol at 4°C. The absorbance of the extract was measured at 470, 649, and 665 nm, using a spectrophotometer (UV-1800, Shimadzu, Kyoto, Japan). Chlorophyll and carotenoid contents were calculated according to Wellburn (1994). Dry leaf samples (0.2 g) were ground to powder and used to measure total nitrogen (N) and carbon (C) content with a C/N analyzer (vario PYRO cube, Isoprime, Cheadle Hulme, United Kingdom).

Leaf Optical Properties

Leaf reflectance (Rf) and transmittance (Tr) were measured with a spectrophotometer (USB2000 +, Ocean Optics, Dunedin, FL, United States) with two integrating spheres (FOIS-1, ISP-REF, Ocean Optics, Dunedin, FL, United States). Leaf absorptance (Ab) was calculated as Ab = 1 − (Rf + Tr).

Stomatal Morphology

The silicon rubber impression technique (Savvides et al., 2012) was used to determine stomatal traits of both leaf surfaces. As a stomatal impression needed to be made on flat leaves, we used the leaves under the cultivation irradiance that had been detached immediately before (within 5 s from detachment to the application of silicon rubber on the table). Epidermal impressions were observed with an optical microscope (XSP-13 CC, Shanghai Caikon Optical Instruments, Shanghai, China) that was equipped with a digital camera (CK-300, Shanghai Caikon Optical Instruments, Shanghai, China). Under a magnification of × 400, five visual fields (19678.08 μm^2) were randomly selected per sample, and numbers of stomatal and epidermal cells were counted. About 20 stomata per visual field were picked

TABLE 1 | Growth conditions during four batches of the experiment.

Batch number	Duration	Photoperiod (h)	DLI of solar light (mol m^{-2} day^{-1})	DLI of solar light and LED (mol m^{-2} day^{-1})	Average T (day/night) (°C)	Average RH (day/night) (%)	$[CO_2]$ range (μmol mol^{-1})
1	June 28 to July 7	14.9	3.5	7.8	26/23	73/83	400–430
2	July 22 to July 31	14.5	2.8	7.1	27/24	76/86	
3	August 12 to August 21	13.6	2.1	6.4	28/25	72/86	
4	September 11 to September 20	12.4	2.4	6.7	25/21	56/62	
4 (FSL)	September 21 to September 27	12.4	10.7	-	24/20	67/79	

DLI, daily light integral; T, temperature; RH, relative humidity; $[CO_2]$, CO_2 partial pressure; FSL, full solar light treatment.

randomly to measure stomatal length and width, and pore length and aperture; from these, pore and stomatal area were calculated under the assumption that these were elliptical. Stomatal density, stomatal index, and pore area per leaf area were calculated according to Savvides et al. (2012).

Leaf Cross-Section Microscopy

Leaf segments (2 × 1 cm) of the youngest fully expanded leaves were cut and fixed in a formaldehyde-based fixative formalin-aceto-alcohol (FAA) for at least 24 h. After that, leaf segments were dehydrated and embedded in paraffin, and sectioned with a microtome (RM2016, Leica Microsystems, Shanghai, China). The sections were stained with safranin along with Fast Green and were examined using a microscope (BX53, Olympus Optical Co. Ltd., Tokyo, Japan).

Gas Exchange and Chlorophyll Fluorescence

Steady-state and dynamic leaf photosynthetic gas exchange was measured using the LI-6400 XT photosynthesis system (LI-COR Biosciences, Lincoln, NE, United States) equipped with the leaf chamber fluorometer (LI-COR Part No. 6400-40, enclosed leaf area: 2 cm^2). During measurements, CO_2 partial pressure was 400 μbar, leaf temperature was approximately 25°C, leaf vapor pressure deficit was 0.7–1.0 kPa, and air flow rate through the system was 500 μmol s^{-1}. PPFD was provided by a mixture of red (90%; 635 nm) and blue (10%; 465 nm) LEDs in the leaf chamber.

TABLE 2 | Measurements conducted in each batch of the experiment.

Measurement	Batch number			
	1	2	3	4
Leaf biochemical components	√		√	√
Leaf optical properties			√	
Leaf cross-section microscopy			√	
Stomatal morphological traits			√	
Plant growth analysis	√	√	√	√
Gas exchange and chlorophyll fluorescence measurement using LI-6400XT		√	√	√
Chlorophyll fluorescence imaging			√	
Photosynthesis and growth analysis after full solar light exposure				√

Light Response Curves of Leaf Photosynthesis

Leaves were firstly adapted to 1500 μmol m^{-2} s^{-1} PPFD, until *A* was stable, after which they were exposed to 1,000, 800, 600, 400, 200, 150, 100, 50, and 0 μmol m^{-2} s^{-1} PPFDs. When *A* reached steady-state at each PPFD (3–5 min), *A*, g_s, and C_i were logged continuously (every 5 s) for 1 min, and averaged values were used. Light response curves were fitted to a non-rectangular hyperbolic function (Cannell and Thornley, 1998), and the parameters maximum net photosynthesis rate (A_{max}), dark respiration rate (R_{dark}), and apparent quantum yield (α) were derived.

Dynamic Photosynthetic Responses to Step Changes in Irradiance

To evaluate gas exchange and chlorophyll fluorescence responses to a step change in PPFD, plants were adapted in a dark room for ∼30 min. After that, selected leaflets were placed in the LI-6400 XT cuvette, and minimal (F_0) and maximal (F_m) chlorophyll fluorescence were recorded to determine the maximum quantum efficiency of PSII photochemistry (F_v/F_m). PPFD was then increased to 50 μmol m^{-2} s^{-1}, and leaves were adapted at this PPFD until *A* and stomatal conductance (g_s) were at a steady state (approximately 30 min). After that, leaves were subjected to six cycles of 2 min LL (50 μmol m^{-2} s^{-1}) followed by 5 min of HL intensity (1,000 μmol m^{-2} s^{-1}) each, for a total of 42 min. In the end, leaves were subjected to 10 min of darkness. Gas exchange was logged once per second and transient *A*, g_s, and C_i responses were averaged over five data points to reduce measurement noise, using a moving average filter. Photosynthetic induction state was calculated, and the following parameters: (1) photosynthetic induction state 60 and 300 s after illumination (IS_{60} and IS_{300}); and (2) A_{300}, integrated *A* during the first 300 s of photosynthetic induction.

Chlorophyll fluorescence was measured once per minute, using the multiphase flash (MPF) routine. "Steady-state" fluorescence yield (F_s) and maximum fluorescence (F_m') in the light were determined. MPF settings were as follows: measuring intensity was 1 μmol m^{-2} s^{-1}, the maximum flash intensity was 8,000 μmol m^{-2} s^{-1}, flash intensity reduced by 60% during the 2nd phase of the MPF, and the duration of the three flash phases were 0.3, 0.6, and 0.3 s, respectively. Photosystem II operating efficiency (Φ_{PSII}) was calculated as $\Phi_{PSII} = (F_m'-F_s)/F_m'$, and NPQ was calculated as $NPQ = F_m/F_m'-1$ (Baker, 2008). Two components of NPQ, photoinhibitory quenching (qI) and energy-dependent quenching (qE), were calculated: qE and

qI before the dark relaxation period were calculated according to Liu and Last (2015) as qI = (F_m-F_m'')/F_m'', and qE = F_m/F_m'-F_m/F_m'', where F_m' is maximum fluorescence immediately before dark relaxation, and F_m'' is maximum fluorescence after 10 min of dark relaxation.

Chlorophyll Fluorescence Imaging After High Light Stress

To evaluate leaf photoprotective capacity, F_v/F_m before and after HL treatment was measured using the Imaging-PAM Chlorophyll Fluorescence System (MAXI-PAM, Heinz Walz GmbH, Effeltrich, Germany). Plants were first dark-adapted for 30 min, and F_0 and F_m of the youngest fully developed leaves (target leaves) were recorded to determine F_v/F_m. Then, plants were moved to the greenhouse (low-intensity sunlight) for ∼60 min to reach a low-light adapted state. Plants were then moved to a customized facility with white LEDs and exposed to HL of 1,100 μmol m^{-2} s^{-1} for 30 min. Later, plants were dark-adapted for 30 min, and F_v/F_m was determined once more.

Leaf Photosynthetic Capacity After Full Solar Light Exposure

To follow photosynthetic capacity in single leaves after full solar light exposure, the 2nd true leaf, counted from the bottom of the plant, was used for measurements. At 0, 2, 4, and 6 days after exposing plants to full sunlight, leaves were exposed to 1,000 μmol m^{-2} s^{-1} PPFD (close to the light saturation point), using the LI-6400 XT. When *A* was stable, gas exchange parameters were logged continuously (every 5 s) for 1 min, and averages of 12 values were used.

Growth Analysis

Growth analysis was conducted after 10 days of treatment and after 1 week of full solar light exposure. Leaf area was measured using a leaf area meter (LI-3100C, LI_COR Biosciences, Lincoln, NE, United States). Leaves and stems were dried in a ventilated oven (DHG-9070A, Shanghai Jinghong, Shanghai, China) at 80°C for at least 72 h. Leaf mass area (LMA) was calculated as leaf dry weight/leaf area.

Data Analysis

Statistical analysis was performed using IBM SPSS version 23 (IBM Corp., Armonk, NY, United States). For measurements conducted in several batches of experiments (**Table 2**), the average value per batch was treated as one statistical replicate. For measurements conducted only in one batch of the experiment (**Table 2**), each plant was treated as one biological replicate. One-way ANOVA was performed followed by Duncan's test at 95% CI. Data were plotted using SigmaPlot 12.5 (Systat Software, Inc., San Jose, CA, United States).

RESULTS

Leaf Thickness, Pigmentation, and Stomatal Traits

Leaf mass area (LMA) in plants grown under supplemental light increased by 27–55% (**Table 3**), compared to control plants. Growth under blue light produced the thickest leaves, as these showed ∼12% greater LMA than W-, R-, and G-grown leaves (**Table 3**); these leaves were visibly thicker (**Supplementary Figure 3**). All supplemental light treatments increased chlorophyll (Chl $a + b$), carotenoid (cars), and nitrogen and carbon concentrations (**Table 3**) compared to control. Similar to LMA, the largest concentrations of these components were found under B, followed by W, R, and G treatments (**Table 3**). The Chl *a*:*b* ratio was unaffected by treatments (**Table 3**). Leaf light absorption was 5–7% higher in leaves grown under supplemental light compared to control, without differences among supplemental light treatments (**Table 3** and **Supplementary Figure 4**).

Stomatal traits were measured in one batch of the experiment. Growth under supplemental light increased stomatal density on both leaf surfaces, although this was not significant on the adaxial side (**Table 4** and **Supplementary Figure 5**). B significantly increased the single stomatal area, as B-grown leaves had the longest and widest stomata. Total pore area per leaf area on the abaxial side was largely increased by supplemental light, particularly for B-grown leaves, where the total pore area per leaf area was ∼80% greater than that in control leaves (**Table 4**).

Steady-State Photosynthesis Traits

Steady-state *A* increased remarkably by acclimation to supplemental light, as shown by *A* in response to PPFD (*A*/PPFD curve, **Figure 1A**). When PPFD was above 150 μmol m^{-2} s^{-1}, B-grown leaves displayed the highest *A*, followed by W-, R-, and G-grown leaves, resulting in an A_{max} that was more than twice as high in B leaves compared to control leaves (**Table 3**). Blue light accounted for 72%, 26%, 17%, and 10% of PAR in B, W, G, and R supplemental light treatments, respectively. We found a positive correlation between blue light proportion during growth and A_{max} (**Supplementary Figure 6**). In addition, stomatal conductance (g_s) across a range of PPFD tended to be the highest in B-grown leaves (**Figure 1B**). The ratio of leaf internal to ambient CO_2 partial pressure (C_i C_a^{-1}) was unaffected by treatments (**Figure 1C**). Across treatments, A_{max} correlated positively with Chl $a + b$, N content, and LMA (**Figures 1D–F**). Dark respiration (R_{dark}) was significantly higher under supplemental light treatments and was highest under B, followed by W, R, and G (**Table 3**). Photosynthetic quantum yield (α) was not affected (**Table 3**).

Dynamic Responses of Leaf Photosynthesis During Changes in Irradiance Intensity

When leaves initially adapted to LL (50 μmol m^{-2} s^{-1}) were exposed to a series of lightflecks [5 min HL (1,000 μmol m^{-2} s^{-1}), interspersed with 2 min LL], *A* increased gradually in all treatments during HL phases (**Figure 2A**). At any time during fluctuating light (FL), B-grown leaves displayed the highest *A*, followed by W, R, G, and control leaves (**Figure 2A**). Not surprisingly, integrated *A* during the first 300 s of HL (A_{300}) was 35–65% higher in B-grown leaves compared to values from other treatments, which did not differ from one another (**Supplementary Table 1**). Leaves that grew under B also

TABLE 3 | Leaf biochemical, photosynthetic, and morphological traits of cucumber plants grown under different supplemental light spectra.

Parameter	Light quality					*p*-value
	Control	White	Red	Blue	Green	
Chl $a + b$(mg m^{-2})	242 ± 29d	319 ± 30 ab	310 ± 19 bc	342 ± 27 a	286 ± 31 c	<0.001
Chl *a:b*	2.72 ± 0.08	2.79 ± 0.05	2.78 ± 0.01	2.72 ± 0.08	2.71 ± 0.03	0.609
Carotenoid (mg m^{-2})	33.8 ± 5.2 c	46.5 ± 3.3 a	45.0 ± 2.0 a	48.9 ± 4.0 a	39.4 ± 3.1 b	<0.001
N (g m^{-2})	0.82 ± 0.06 d	1.13 ± 0.09 b	1.03 ± 0.05 c	1.35 ± 0.13 a	1.02 ± 0.09 c	<0.001
C (g m^{-2})	5.26 ± 0.34 d	7.26 ± 0.26 b	7.06 ± 0.28 b	8.18 ± 0.46 a	6.74 ± 0.42 c	<0.001
A_{max} (μmol m^{-2} s^{-1})	12.6 ± 0.7 d	21.7 ± 1.3 b	17.9 ± 0.7 c	26.7 ± 0.9 a	16.9 ± 0.8 c	<0.001
α (μmol m^{-2} s^{-1})	0.065 ± 0.003	0.067 ± 0.001	0.065 ± 0.002	0.069 ± 0.003	0.063 ± 0.002	0.545
R_{dark} (μmol m^{-2} s^{-1})	1.40 ± 0.10 c	1.93 ± 0.15 ab	1.79 ± 0.08 b	2.15 ± 0.08 a	1.62 ± 0.14 bc	0.005
LMA (g cm^{-2})	12.8 ± 1.0 d	17.7 ± 0.8 b	17.0 ± 0.8 bc	19.9 ± 1.5 a	16.3 ± 1.2 c	<0.001
Light absorption (%)	81.8 ± 0.9 b	87.5 ± 0.4 a	87.8 ± 0.2 a	86.7 ± 0.1 a	86.3 ± 0.2 a	<0.001

Control, shade solar light; Chl a + b, total chlorophyll a and b contents; Chl a:b, chlorophyll a and b ratio; N, total leaf nitrogen content; C, total leaf carbon content; A_{max}, maximum net photosynthesis rate; α, apparent quantum yield; R_{dark}, dark respiration rate; LMA, leaf mass area. Mean value ± SEM of three experimental batches is shown (n = 3) except in light absorption, the mean value ± SEM of six biological replicates in one experiment is shown. The p-values of treatment effect are shown, and different letters indicate significant treatment effect.

TABLE 4 | Stomatal traits on the adaxial and abaxial surfaces of cucumber leaves.

	Light quality					*p*-value
	Control	White	Red	Blue	Green	
Stomatal density (no.mm^{-2})						
Adaxial	270 ± 12	510 ± 24	442 ± 75	473 ± 44	449 ± 70	0.059
Abaxial	358 ± 39 b	695 ± 22 a	570 ± 44 a	635 ± 69 a	560 ± 45 a	0.005
Stomatal index (–)						
Adaxial	0.12 ± 0	0.13 ± 0.01	0.11 ± 0.01	0.16 ± 0	0.14 ± 0.02	0.093
Abaxial	0.19 ± 0	0.19 ± 0.02	0.33 ± 0.18	0.22 ± 0.01	0.18 ± 0.02	0.712
Stomatal area (μm^2)						
Adaxial	164 ± 7 b	164 ± 12 b	153 ± 12 b	206 ± 2 a	174 ± 5 b	0.010
Abaxial	166 ± 4 b	174 ± 3 b	182 ± 3 b	209 ± 11 a	176 ± 1 b	0.004
Stomatal length (μm)						
Adaxial	19.3 ± 0.5	17.6 ± 1.1	17.1 ± 1.4	19.8 ± 0.2	18.6 ± 0.4	0.241
Abaxial	18.7 ± 0.2 ab	18.1 ± 0.4 b	18.8 ± 0.2 ab	19.5 ± 0.3 a	18.3 ± 0.1 b	0.032
Stomatal width (μm)						
Adaxial	10.9 ± 0.2 c	11.9 ± 0.2 b	11.4 ± 0.1 bc	13.3 ± 0.3 a	11.9 ± 0.4 b	0.001
Abaxial	11.3 ± 0.1 c	12.2 ± 0.3 bc	12.3 ± 0.2 b	13.5 ± 0.5 a	12.2 ± 0.1 bc	0.005
Pore aperture (μm)						
Adaxial	2.8 ± 0.2	3.5 ± 0.5	3.3 ± 0.3	4.4 ± 0.4	3.8 ± 0.6	0.184
Abaxial	3.8 ± 0.1	4.2 ± 0.4	4.1 ± 0.1	5.1 ± 0.3	4.3 ± 0.4	0.085
Pore length (μm)						
Adaxial	10.8 ± 0.6	9.0 ± 0.8	9.5 ± 1.1	9.6 ± 0.2	10.7 ± 0.5	0.360
Abaxial	11.1 ± 0.6	10.0 ± 0.3	12.2 ± 0.4	11.0 ± 0.2	10.6 ± 0.6	0.063
Pore area per leaf area (μm^2 mm^{-2})						
Adaxial	6360 ± 234	13193 ± 2951	10683 ± 1634	15916 ± 2167	15091 ± 4883	0.194
Abaxial	9087 ± 468 c	23251 ± 3406 ab	22325 ± 1216 ab	28112 ± 3477 a	15712 ± 1051 bc	0.001

Cucumber plants were grown for 10 days under different supplemental light spectra: Control, shade solar light; White, supplemental white light; Red, supplemental red light; Blue, supplemental blue light; and Green, supplemental green light. Mean value ± SEM of three biological replicates in one experimental batch is shown (n = 3). The p-values of treatment effect are shown, and different letters indicate significant treatment effect.

displayed significantly higher g_s during FL compared with all other leaves (**Figure 2B**). However, the rate of photosynthetic induction was similar in all treatments, as shown by similar photosynthetic induction states at 60 and 300 s (IS_{60} and IS_{300}) after a LL to HL transition (**Supplementary Table 1**). Control leaves displayed a higher C_i during HL compared to leaves in other treatments (**Figure 2C**). A high C_i along with low *A* (**Figure 2A**) indicates that photosynthetic limitation

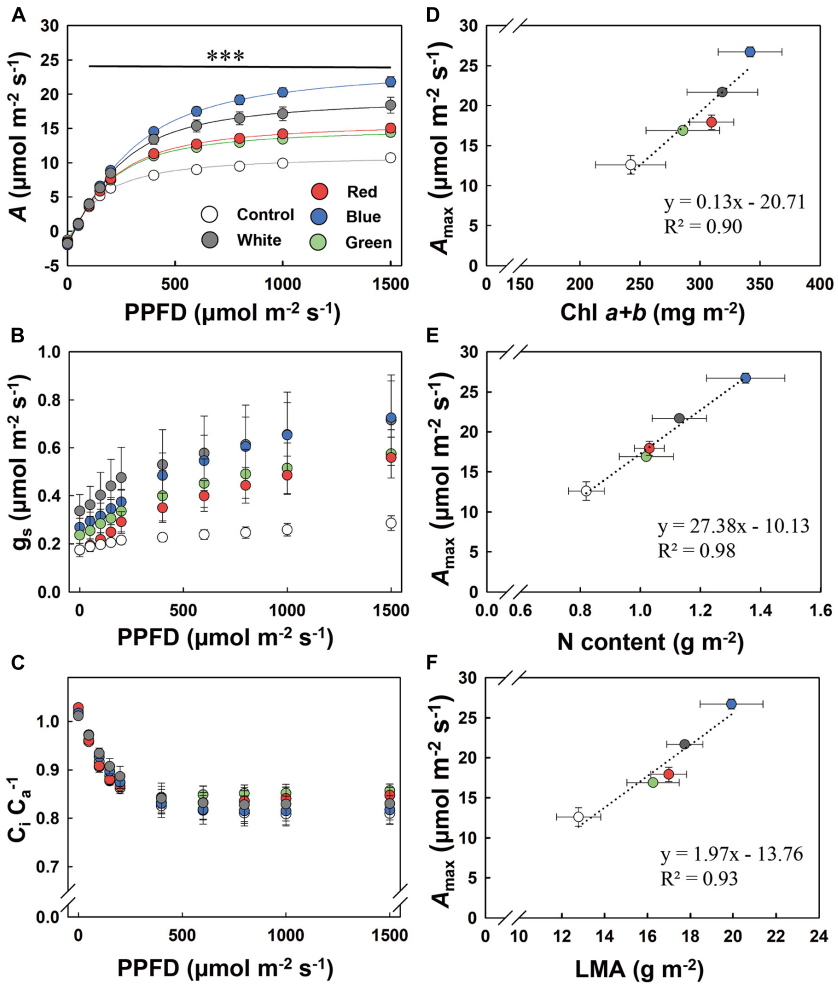

FIGURE 1 | Response of steady-state net leaf photosynthesis (*A*; **A**), stomatal conductance (g_s; **B**), and leaf internal CO_2 partial pressure relative to that of the air ($C_iC_a^{-1}$; **C**) to photosynthetic photon flux density (PPFD), and relationship of maximum photosynthesis rate (A_{max}) to chlorophyll *a* and *b* contents (Chl *a* + *b*; **D**), N content per leaf area (N; **E**), and leaf mass area (LMA; **F**). Control, shade solar light. Mean value ± SEM of 3–4 experimental batches is shown (n = 3–4), with four to six replicate plants per experimental batch. The asterisks in **(A)** indicate significant differences between treatments, ***$p < 0.001$. The dotted line in **(D–F)** represents a significant linear regression, with equations and R^2 coefficients shown.

in control leaves was mainly due to biochemical rather than stomatal limitation.

At any moment during FL, B leaves showed the highest values for Φ_{PSII}, followed by W, R, G, and control leaves (**Figure 2D**). During the initial LL to HL transition, NPQ increased gradually within 5 min in all treatments, with the highest value in B-grown leaves (**Figure 2E**). However, during the following LL–HL transitions, NPQ showed different patterns among treatments: in B- and W-grown leaves, NPQ increased toward a peak value and then relaxed toward a lower value (**Figure 2E**). In R- and G-grown leaves, NPQ quickly reached a plateau and did not decrease during HL. Finally, in control leaves, NPQ increased continuously during HL, resulting in a substantially higher value compared with the other treatments (**Figure 2E**). When light intensity decreased from HL to LL or darkness, NPQ relaxed to a lesser extent in control leaves than in the four supplemental light treatments, whereas B-grown leaves showed the fastest NPQ relaxation rate (**Figure 2E**). At the transition point from FL to darkness, B-grown leaves showed the highest qE and lowest qI, whereas control leaves showed the highest qI (**Figure 2F**).

Quantum Efficiency of Photosystem II in Response to High Light Intensity

F_v/F_m before and after HL was measured in one batch of the experiment. Before exposure to HL, F_v/F_m in leaves of all treatments was > 0.8, with a slightly lower value (0.80) in R (**Figure 3C**). After leaves were exposed to HL (1,100 μmol m^{-2} s^{-1}) for 30 min, differences in F_v/F_m started to show (**Figure 3B**): B leaves showed the highest F_v/F_m (∼0.76, 6% decrease from initial value), and control leaves showed the lowest F_v/F_m (∼0.68, 16% decrease from initial value), whereas W, G, and R leaves showed intermediate drops in F_v/F_m (**Figure 3C**). Besides, B leaves showed more homogeneity in

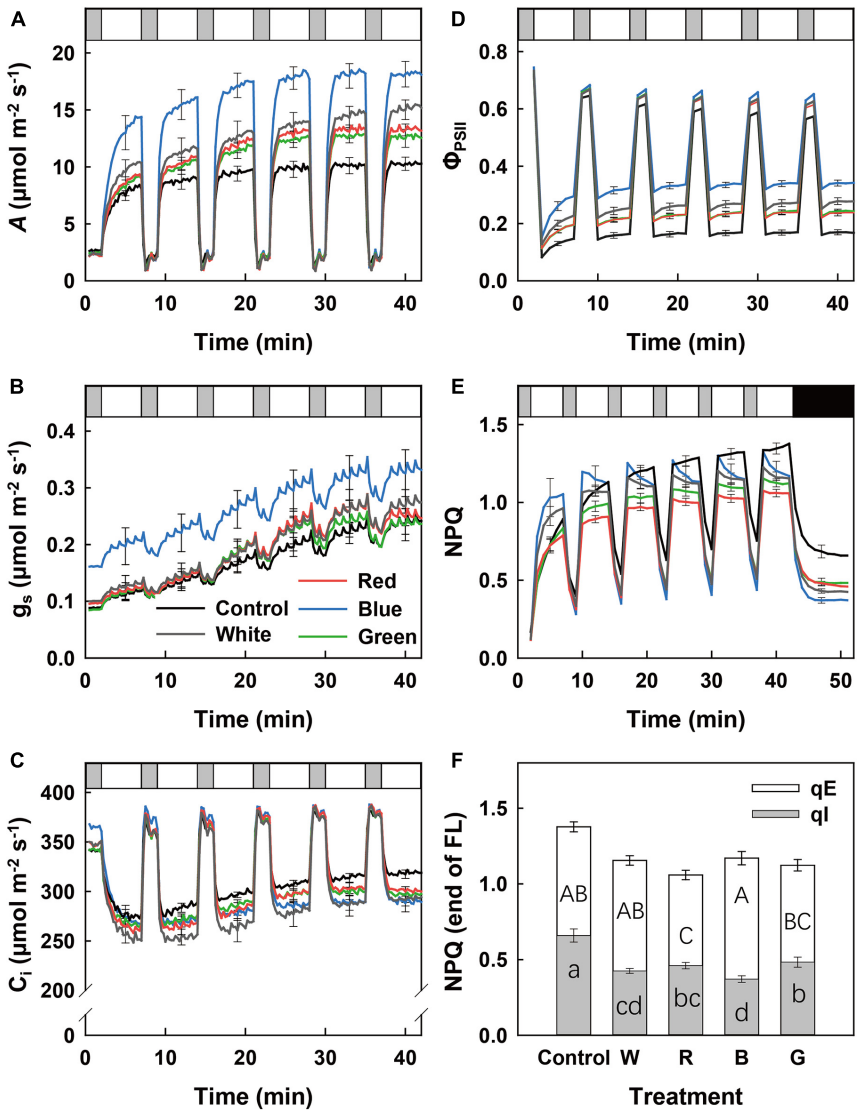

FIGURE 2 | Dynamic leaf photosynthetic traits of cucumber plants grown under different light treatments in response to fluctuating light (FL) intensity. Time courses of net photosynthesis rate (*A*; **A**), stomatal conductance (g_s; **B**), leaf internal CO_2 partial pressure (C_i; **C**), photosystem II electron transport efficiency (Φ_{PSII}; **D**), and non-photochemical fluorescence quenching (NPQ; **E**) when a leaf adapted to low irradiance (50 μmol m^{-2} s^{-1}) was exposed to FL between 2 min of low light (LL) (50 μmol m^{-2} s^{-1}) and 5 min of high light (HL) intensity (1,000 μmol m^{-2} s^{-1}) for 42 min (five repeated cycles). NPQ dark relaxation was recorded for another 10 min after FL in panel **(E)**. LL, HL, and darkness are visualized as gray, white, and black bars, respectively. Energy and zeaxanthin-depended quenching (qE) and photoinhibitory quenching (qI) at the transition from HL to darkness are shown in panel **(F)**. Control (C, shade solar light), white (W), red (R), blue (B), and green (G). Mean value ± SEM of three experimental batches are shown (n = 3), with three replicate plants per experimental batch. Different letters in panel **(F)** indicate significant treatment effects on qE (capital letter) and qI (lowercase letter), respectively.

F_v/F_m distribution after HL exposure compared to leaves in other treatments (**Figure 3B**).

Plant Growth and Morphology

Plant morphology was strongly affected by the growth light spectrum (**Figure 3A**). Stems of B-grown plants were the shortest (**Table 5**). Leaf number, fresh weight, and dry weight of leaves, stems, and whole shoots were similarly increased under all supplemental light treatments (**Table 5**). Leaf area was increased by 78–94% in W-, R-, and G-grown plants compared with control, whereas in B-grown plants it was only increased by 43% (**Table 5**). Compared to other treatments, B-grown plants had a tendency to partition more biomass to leaves at the cost of stem biomass (**Table 5**).

Photosynthesis and Plant Growth After Exposure to Full Sunlight

In the last batch of the experiment, plants from all treatments were transferred to full sunlight for 1 week. *A* at 1,000 μmol m^{-2} s^{-1} PPFD (A_{1000}; measured every 2 days) was the highest

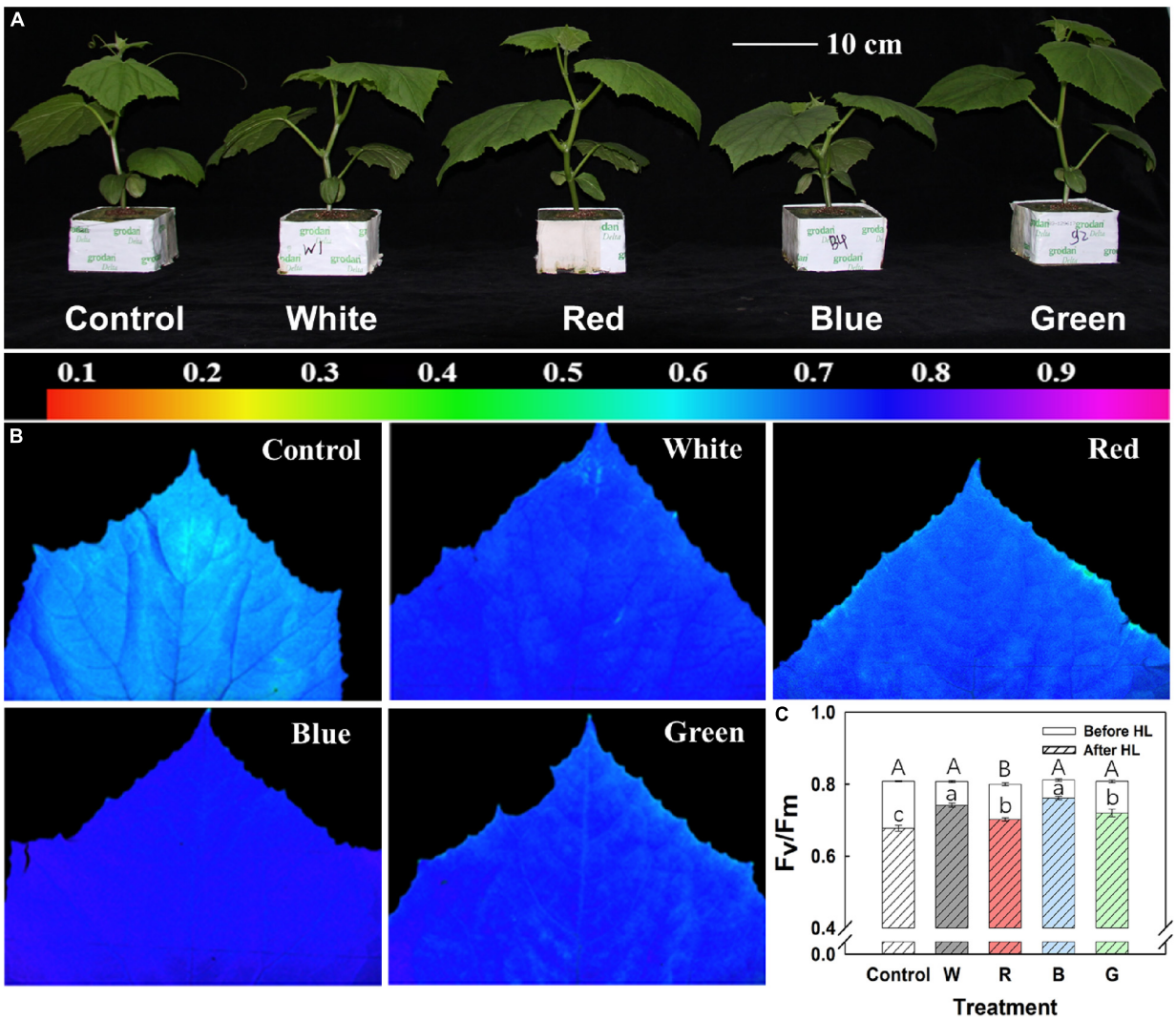

FIGURE 3 | Plant morphology and photoinhibition. **(A)** Representative images showing cucumber plants grown for 10 days under different supplemental light spectra: Control (C, shade solar light), white (W), red (R), blue (B), and green (G). **(B)** Representative false color images of maximum quantum efficiency of photosystem II photochemistry (F_v/F_m) distribution after high light (HL, 30 min, 1,100 μmol m^{-2} s^{-1}) treatment, including color scale. **(C)** Averaged F_v/F_m before and after HL treatment. Mean values ± SEM of four biological replicates in one experimental batch are shown (n = 4). Different letters in panel **(C)** indicate a significant treatment effect on F_v/F_m before (capital letter) and after (lowercase letter) HL, respectively ($p < 0.05$).

and most constant in B-grown leaves (**Figure 4A**). Leaves from all other treatments tended to show a larger temporal variability of A_{1000}, until, on day 6, A_{1000} in control leaves displayed a major drop to approximately half of its initial value (**Figure 4A**). After a week of growth under full sunlight, total leaf area was similar among supplemental light treatments (**Figure 4B**), though before full solar light exposure B-grown plants had smaller leaf area compared to plants grown under G, R, and W (**Table 5**). In addition, despite similar leaf and shoot biomass among G-, R-, W-, and B-grown plants before full sunlight exposure (**Table 5**), a week of full solar light exposure resulted in the highest leaf and shoot biomass in B-grown plants among the treatments (**Figure 4C** and **Supplementary Table 2**). This revealed a higher growth rate in B-grown plants during full solar light exposure.

DISCUSSION

We investigated how acclimation to different supplemental light spectra in the greenhouse with low-intensity sunlight as background affects the plant's capacity to cope with high and variable light intensity. Our focus was on both photosynthetic and photoprotective capacity, and their kinetics upon light intensity fluctuations. We found that while any supplemental light prepared plants for subsequent HL intensity exposure to some extent (compared to a control without any supplemental light), especially blue light prepared leaves for high solar light exposure best. Thus, leaves grown under supplemental blue light had a higher photosynthetic and photoprotective capacity (compared to other supplemental light spectra) and were able to

TABLE 5 | Growth and morphological traits of cucumber plants grown under different supplemental light spectra.

Parameter	Light quality					*p*-value
	Control	White	Red	Blue	Green	
Leaf						
Leaf number (>5 cm)	3.7 ± 0.2b	4.4 ± 0.5 a	4.5 ± 0.5 a	4.3 ± 0.5 a	4.4 ± 0.5 a	0.005
Leaf area (cm^2 $plant^{-1}$)	314 ± 34 c	589 ± 105 a	610 ± 125 a	450 ± 72 b	559 ± 87 ab	0.002
Fresh weight (g $plant^{-1}$)	4.4 ± 0.3 b	9.6 ± 1.5 a	9.6 ± 1.7a	8.1 ± 1.1 a	8.5 ± 1.0 a	<0.001
Dry weight (g $plant^{-1}$)	0.40 ± 0.04 b	1.03 ± 0.17 a	1.02 ± 0.17 a	0.88 ± 0.11 a	0.89 ± 0.12 a	<0.001
Stem						
Stem length (cm)	23.0 ± 2.6 ab	24.9 ± 5.9 a	28.0 ± 7.8 a	16.6 ± 2.7 b	30.2 ± 6.2 a	0.022
Fresh weight (g $plant^{-1}$)	3.5 ± 0.3 b	7.0 ± 2.0 a	7.3 ± 2.2 a	4.9 ± 1.2 ab	7.2 ± 1.5 a	0.023
Dry weight (g $plant^{-1}$)	0.12 ± 0.01 c	0.27 ± 0.07 ab	0.29 ± 0.08 a	0.19 ± 0.04 bc	0.27 ± 0.05 ab	0.014
Shoot						
Fresh weight (g $plant^{-1}$)	8.9 ± 0.7 b	19.6 ± 4.3 a	19.9 ± 4.6 a	15.2 ± 2.9 a	18.2 ± 2.9 a	0.005
Dry weight (g $plant^{-1}$)	0.56 ± 0.05 b	1.42 ± 0.26 a	1.42 ± 0.28 a	1.16 ± 0.16 a	1.26 ± 0.17 a	<0.001
DMC (%)	6.26 ± 0.30 c	7.40 ± 0.36 ab	7.32 ± 0.29 ab	7.81 ± 0.53 a	7.03 ± 0.34 b	<0.001
DMP_leaf (%)	71.1 ± 1.2 c	73.9 ± 1.9 ab	72.8 ± 2.4 bc	76.4 ± 1.5 a	71.0 ± 1.6 c	0.004
DMP_stem (%)	22.3 ± 0.9 a	18.5 ± 1.6 c	19.8 ± 2.0 bc	16.0 ± 1.0 d	21.6 ± 1.5 ab	<0.001

Control (C, shade solar light). DMC, dry mass content; DMP, dry mass partitioning. Mean value ± SEM of four experimental batches is shown (n = 4), with six replicate plants per experimental batch. The p-values of treatment effect are shown, and different letters indicate significant treatment effect.

confer superior plant growth upon transition to higher and more variable solar light.

Acclimation to Blue Light in Low Solar Light Confers Faster Growth Under High Solar Light

Whole-plant CO_2 fixation depends on both leaf photosynthetic rate and plant morphology (light interception; Zhu et al., 2010). A high fraction of blue light often led to a compact plant morphology (Hernández and Kubota, 2016; Izzo et al., 2021), and this was characterized by smaller leaf area and shorter stem length compared with other supplemental light treatments in this study (**Table 5** and **Figure 3A**). A similar phenotype was also observed in growth chamber-grown cucumbers (Liang et al., 2021). However, acclimation to blue light conferred a faster growth under high solar light (**Figure 4**) though with a morphology unfavorable for canopy light interception. Therefore, we ascribe a faster growth rate in blue-light-acclimated plants to efficient utilization of light energy and less deleterious effects associated with exposure to an HL intensity, rather than morphology, compared to plants acclimated to other spectra. The traits in blue-light-acclimated leaves were related to high photosynthetic and photoprotective capacity and the ability of NPQ to induce and decrease quickly upon light intensity changes, as discussed below.

High Photosynthetic Capacity in Blue-Light-Acclimated Plants

Manipulating the light spectrum often impacts photosynthesis. Importantly, the effects of monochromatic supplemental light in the greenhouse are likely different from those in the growth chamber, as the realized light spectrum is affected by a broad, solar background light of variable intensity (Kaiser et al., 2019). Specific photosynthetic acclimatory syndromes under a monochromatic spectrum are unlikely in greenhouses. Instead, treatment differences are likely caused by different proportions of wavebands in a broad spectrum.

Previous studies with fully artificial light showed that leaf photosynthetic capacity increases with increases in the fraction of blue light (0–50%) in tomato (Zhang et al., 2019), lettuce (Wang et al., 2016), and cucumber (Hogewoning et al., 2010); our study confirms and expands on these findings, as we found an increase in A_{max} between 10 and 76% (**Supplementary Figure 6**). The increase in A_{max} scaled very well with chlorophyll and nitrogen contents per unit leaf area, leaf thickness (**Figures 1D–F**), and Φ_{PSII} (**Figure 2D**). In addition, g_s roughly scaled with A_{max} (**Figures 1B**, **2B**), and a higher g_s under blue-light-acclimated leaves was not due to an increased stomatal density, but a significant increase in stomatal size (**Table 4**). Acclimation to a given waveband, therefore, resulted in a concerted change of all components related to photosynthesis, be it CO_2 diffusion (**Figure 1B**), electron transport (**Figure 2D**), or carboxylation. At a molecular level, blue light can activate cryptochrome and mediate transcription and expression of genes encoding PSII components, assuring a normal development of the photosynthetic apparatus (Walters, 2005; Kleine et al., 2007; Li et al., 2020). At the same time, blue light has been shown to regulate stomatal development (Kang et al., 2009), facilitating CO_2 availability to improve photosynthetic capacity. Furthermore, blue light might also trigger specific retrograde signals from the chloroplast to the nucleus in a photoreceptor-independent pathway, which can also play an important role in photosynthetic acclimation (Duan et al., 2020; Gommers, 2020).

Improved Photoprotective Performance in Blue-Light-Acclimated Leaves

In this study, leaves acclimated to blue light developed the greatest photoprotective capacity under dynamic light intensity,

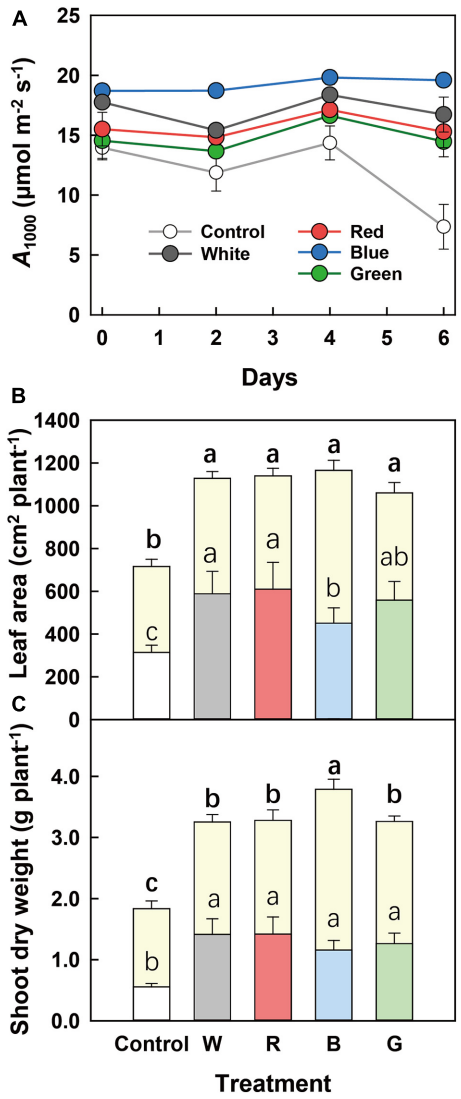

FIGURE 4 | Plant growth and photosynthesis after plant exposure to full sunlight for 1 week. **(A)** Time course of the steady-state net leaf photosynthesis rate at PPFD of 1,000 μmol m^{-2} s^{-1} (A_{1000}) during 6 days of full solar light exposure. **(B)** Leaf area and **(C)** shoot dry weight of cucumber plants before and after 7 days of full solar light exposure, indicated by the lower and upper part of columns, respectively. Before full solar light exposure, cucumber plants were grown for 10 days under different supplemental light spectra: Control (C, shade solar light), white (W), red (R), blue (B), and green (G). Mean values ± SEM of three to five biological replicates in one experimental batch are shown (n = 3–5). Different letters indicate a significant treatment effect ($p < 0.05$).

and under constant HL intensity. This was characterized by a highly induced and relaxed NPQ under dynamic light (**Figure 2E**) and the highest F_v/F_m after HL treatment (**Figures 3B,C**).

Non-photochemical quenching plays a key role in plant fitness and productivity, especially under FL. Consistent with previous studies conducted in growth chambers (Zhang et al., 2019; Duan et al., 2020), our study showed that acclimation to blue light can induce the faster formation of NPQ under HL intensity compared to red-light-acclimated leaves. In addition to this, our study showed a faster NPQ formation and relaxation rate in blue-light-acclimated leaves than R-, G-, and W-acclimated leaves (**Figure 2E**). Therefore, the fast NPQ relaxation in leaves grown under blue light (**Figure 2E**) may reduce foregone A under FL (Murchie and Ruban, 2020). NPQ comprises several components, which are determined by their induction and relaxation time scales. The fastest, and by far largest (under most circumstances), component is qE (Murchie and Ruban, 2020), which enables rapid adjustment of light-harvesting efficiency to incident light. qE can be induced within 10–200 s after a LL to HL intensity transition (**Figure 2E**). qE is regulated by ΔpH across the thylakoid membrane, which is sensed by PsbS that confers changes in the light-harvesting complex II, where qE takes place and is modulated by the concentration of zeaxanthin (Bassi and Dall'Osto, 2021). A recent study in rice showed that blue light-induced higher PsbS transcript levels, thereby increasing qE capacity in HL intensity, and rate of NPQ relaxation upon a transfer from HL to LL (Duan et al., 2020). We hypothesize that a faster induction of qE in B (during the 1st LL to HL transition, **Figure 2E**) in our study may be due to increased PsbS concentrations (Duan et al., 2020), and/or faster transthylakoid ΔpH changes due to more rapid electron and proton transport (suggested by larger initial Φ_{PSII}, **Figure 2D**).

An effective method for monitoring photoinhibition is the measurement of F_v/F_m after light stress (Külheim et al., 2002). Leaves acclimated to a high proportion of blue light (B and W light) had the highest values of F_v/F_m after HL treatment (**Figure 3C**), again indicating a larger photoprotective capacity compared to leaves in other treatments. The movement of chloroplasts away from HL intensity is an important photoprotective and adaptive mechanism to prevent or recover from the deleterious effects of photoinhibitory light (Liu et al., 2019). Although blue-light-acclimated leaves possessed the highest content of chlorophylls and the thickest leaves (**Table 3** and **Supplementary Figure 3**), surprisingly they did not possess the highest leaf light absorptance (**Table 3**). This could be related to blue-light-induced chloroplast movement mediated by activated phototropin, which can reduce leaf light absorptance, and may be another protecting mechanism against excess light in blue-light-acclimated plants (Shinkai et al., 2002).

Altogether, a higher proportion of blue light, higher A along with higher NPQ capacity, and faster induction and relaxation of qE can not only decrease excess light but also decrease reactive oxygen species production (Liu et al., 2019).

Acclimation to Supplemental Light Does Not Affect Photosynthesis Dynamics

Under direct light, plants in the greenhouse often experience large variations in light intensity, which are caused by the shade of construction parts and equipment (**Supplementary Figure 7**). Time-integrated A depends not only on the magnitude of steady-state A but also on the rapidity of the A response to changes in PPFD. The rate at which A responds to FL is usually quantified

as the rate of photosynthetic induction after low-to-high PPFD transitions (Kaiser et al., 2018; Tanaka et al., 2019).

Under a series of lightflecks aimed at probing *A* under dynamic light, we found differences between treatments during exposure to HL intensity (**Figure 2A**) that scaled well with those seen from steady-state light responses of *A* (**Figure 1A**). However, none of the treatments affected the rate of photosynthetic induction (**Supplementary Table 1**), agreeing with our previous study showing that in tomatoes, acclimation to different R/B ratios had only minor effects on the rapidity of the *A* under FL (Zhang et al., 2019). Photosynthetic induction rate is mainly determined by (1) Calvin cycle enzyme activities, e.g., Rubisco activation rate and (2) CO_2 diffusional limitation, e.g., transient stomatal limitation (Taylor et al., 2020; Sakoda et al., 2021). Our results again indicate that manipulating the PAR light spectrum does not change Rubisco activation properties or transient stomatal limitation.

Limitations of Our Study

In this study, we have provided some insights into how the light spectrum can "prepare" plants for HL intensity exposure. Mostly, we base our conclusions on leaf photosynthetic, photoprotective, and biochemical data that were gathered in several independent experiments (**Table 2**); these results can thus be viewed as very solid. However, for some other measurements, e.g., the growth analysis after full solar light exposure, they were only conducted once (**Table 2**); these results are only from pseudo-replications rather than statistical replications. Second, to investigate how acclimation to a given spectrum affects plants growth under HL intensity exposure, young cucumber seedlings were transferred to full solar light for 1 week in this study. Ideally, an extension of the HL treatment, e.g., to several weeks, even to a reproductive growth stage (e.g., the fruit yield), will provide a more complete picture as to how long-lasting the effects described here are. Third, strictly speaking, the phrase "full solar light" is not precise: in greenhouses, not only the intensity of solar light is decreased, but also UV radiation is considerably reduced, compared to full solar light in the open field. Therefore, the degree of HL stress after exposure to "full solar light" in the greenhouse is rather mild, compared to that impacting plants in the open field. However, still, it can be hypothesized that plants acclimated to blue light would show a growth advantage when transferred to the open field.

CONCLUSION

Our study shows that blue supplemental light in the background of LL can "prepare" plants to develop a high photosynthetic and photoprotective capacity, which subsequently can improve plant growth under full solar light. Although the rate of photosynthetic induction cannot be manipulated by acclimation to supplemental light, maximum leaf photosynthetic capacity and a highly flexible NPQ can be achieved; this may improve light use efficiency and diminish photoinhibition under full solar light exposure, which means both high and highly variable light intensities. Our results may help to bridge the gap between the establishment of young seedlings under different spectra and plant performance after transfer to the open field or greenhouse.

DATA AVAILABILITY STATEMENT

The original contributions presented in the study are included in the article/**Supplementary Material**, further inquiries can be directed to the corresponding author.

AUTHOR CONTRIBUTIONS

CK and YZ performed the experimental work and drafted the manuscript. RC and QY managed the project. EK revised the manuscript. TL conceived and supervised the study. All authors have read and agreed to the final version of the manuscript.

FUNDING

This study was financially supported by the National Natural Science Foundation of China (No. 31872955), and Central Public-Interest Scientific Institution Basal Research Fund (Nos. BSRF201911 and BSRF202107).

SUPPLEMENTARY MATERIAL

The Supplementary Material for this article can be found online at: https://www.frontiersin.org/articles/10.3389/fpls.2021.782465/full#supplementary-material

REFERENCES

Baker, N. R. (2008). Chlorophyll fluorescence: a probe of photosynthesis in vivo. *Annu. Rev. Plant Biol.* 59, 89–113.

Bassi, R., and Dall'Osto, L. (2021). Dissipation of light energy absorbed in excess: the molecular mechanisms. *Annu. Rev. Plant Biol.* 72, 47–76.

Bilger, W., and Björkman, O. (1990). Role of the xanthophyll cycle in photoprotection elucidated by measurements of light-induced absorbance changes, fluorescence and photosynthesis in leaves of *Hedera canariensis*. *Photosynth. Res.* 25, 173–185. doi: 10.1007/BF00033159

Bugbee, B. (2016). Toward an optimal spectral quality for plant growth and development: the importance of radiation capture. *Acta Hortic.* 1134, 1–12. doi: 10.17660/actahortic.2016.1134.1

Cannell, M. G. R., and Thornley, J. G. M. (1998). Temperature and CO_2 responses of leaf and canopy photosynthesis: a clarification using the non-rectangular hyperbola model of photosynthesis. *Ann. Bot.* 82, 883–892. doi: 10.1006/anbo.1998.0777

Claypool, N. B., and Lieth, J. H. (2020). Physiological responses of pepper seedlings to various ratios of blue, green, and red light using LED lamps. *Sci. Hortic.* 268:109371.

Duan, L., Ruiz-Sola, M. A., Couso, A., Veciana, N., and Monte, E. (2020). Red and blue light differentially impact retrograde signalling and photoprotection in rice. *Philos. Trans. R. Soc. Lond. B Biol. Sci.* 375:20190402. doi: 10.1098/rstb.2019.0402

Dueck, T., van Ieperen, W., and Taulavuori, K. (2016). Light perception, signalling and plant responses to spectral quality and photoperiod in natural and horticultural environments. *Environ. Exp. Bot.* 121, 1–3.

Folta, K. M., and Maruhnich, S. A. (2007). Green light: a signal to slow down or stop. *J. Exp. Bot.* 58, 3099–3111.

Foo, C. C., Burgess, A. J., Retkute, R., Tree-Intong, P., Ruban, A. V., and Murchie, E. H. (2020). Photoprotective energy dissipation is greater in the lower, not the upper regions of a rice canopy: a 3D analysis. *J Exp Bot.* 71, 7382–7392. doi: 10.1093/jxb/eraa411

Gao, S., Liu, X., Liu, Y., Cao, B., Chen, Z., and Xu, K. (2020). Photosynthetic characteristics and chloroplast ultrastructure of welsh onion (*Allium fistulosum* L.) grown under different LED wavelengths. *BMC Plant Biol.* 20:78. doi: 10.1186/s12870-020-2282-0

Gommers, C. (2020). The photobiology paradox resolved: photoreceptors drive photosynthesis and vice versa. *Plant Physiol.* 184, 6–7. doi: 10.1104/pp.20.00993

Hamdani, S., Khan, N., Perveen, S., Qu, M., Jiang, J., Govindjee, et al. (2019). Changes in the photosynthesis properties and photoprotection capacity in rice (*Oryza sativa*) grown under red, blue, or white light. *Photosynth. Res.* 139, 107–121. doi: 10.1007/s11120-018-0589-6

Hernández, R., and Kubota, C. (2016). Physiological responses of cucumber seedlings under different blue and red photon flux ratios using LEDs. *Environ. Exp. Bot.* 121, 66–74. doi: 10.1016/j.envexpbot.2015.04.001

Hogewoning, S. W., Trouwborst, G., Maljaars, H., Poorter, H., van Ieperen, W., and Harbinson, J. (2010). Blue light dose-responses of leaf photosynthesis, morphology, and chemical composition of *Cucumis sativus* grown under different combinations of red and blue light. *J. Exp. Bot.* 61, 3107–3117. doi: 10.1093/jxb/erq132

Izzo, L. G., Mickens, M. A., Aronne, G., and Gomez, C. (2021). Spectral effects of blue and red light on growth, anatomy, and physiology of lettuce. *Physiol. Plant.* 172, 2191–2202. doi: 10.1111/ppl.13395

Kaiser, E., Morales, A., and Harbinson, J. (2018). Fluctuating light takes crop photosynthesis on a rollercoaster ride. *Plant Physiol.* 176, 977–989. doi: 10.1104/pp.17.01250

Kaiser, E., Morales, A., Harbinson, J., Kromdijk, J., Heuvelink, E., and Marcelis, L. F. (2015). Dynamic photosynthesis in different environmental conditions. *J. Exp. Bot.* 66, 2415–2426. doi: 10.1093/jxb/eru406

Kaiser, E., Ouzounis, T., Giday, H., Schipper, R., Heuvelink, E., and Marcelis, L. F. M. (2019). Adding blue to red supplemental light increases biomass and yield of greenhouse-grown tomatoes, but only to an optimum. *Front. Plant Sci.* 9:2002. doi: 10.3389/fpls.2018.02002

Kang, C. Y., Lian, H. L., Wang, F. F., Huang, J. R., and Yang, H. Q. (2009). Cryptochromes, phytochromes, and COP1 regulate light-controlled stomatal development in Arabidopsis. *Plant Cell* 21, 2624–2641. doi: 10.1105/tpc.109.069765

Kleine, T., Kindgren, P., Benedict, C., Hendrickson, L., and Strand, A. (2007). Genome-wide gene expression analysis reveals a critical role for CRYPTOCHROME1 in the response of Arabidopsis to high irradiance. *Plant Physiol.* 144, 1391–1406. doi: 10.1104/pp.107.098293

Kong, Y., Stasiak, M., Dixon, M. A., and Zheng, Y. (2018). Blue light associated with low phytochrome activity can promote elongation growth as shade-avoidance response: a comparison with red light in four bedding plant species. *Environ. Exp. Bot.* 155, 345–359. doi: 10.1016/j.envexpbot.2018.07.021

Kromdijk, J., Glowacka, K., Leonelli, L., Gabilly, S. T., Iwai, M., Niyogi, K. K., et al. (2016). Improving photosynthesis and crop productivity by accelerating recovery from photoprotection. *Science* 354, 857–861. doi: 10.1126/science.aai8878

Külheim, C., Ågren, J., and Jansson, S. (2002). Rapid regulation of light harvesting and plant fitness in the field. *Science* 297, 91–93. doi: 10.1126/science.1072359

Landi, M., Zivcak, M., Sytar, O., Brestic, M., and Allakhverdiev, S. I. (2020). Plasticity of photosynthetic processes and the accumulation of secondary metabolites in plants in response to monochromatic light environments: a review. *Biochim. Biophys. Acta Bioenerg.* 1861:148131. doi: 10.1016/j.bbabio.2019.148131

Li, T., Heuvelink, E., Dueck, T. A., Janse, J., Gort, G., and Marcelis, L. F. M. (2014). Enhancement of crop photosynthesis by diffuse light: quantifying the contributing factors. *Ann. Bot.* 114, 145–156. doi: 10.1093/aob/mcu071

Li, T., Kromdijk, J., Heuvelink, E., van Noort, F. R., Kaiser, E., and Marcelis, L. F. (2016). Effects of diffuse light on radiation use efficiency of two anthurium cultivars depend on the response of stomatal conductance to dynamic light intensity. *Front. Plant Sci.* 7:56. doi: 10.3389/fpls.2016.00056

Li, X., Wang, H. B., and Jin, H. L. (2020). Light signaling-dependent regulation of PSII biogenesis and functional maintenance. *Plant Physiol.* 183, 1855–1868. doi: 10.1104/pp.20.00200

Liang, Y., Kang, C., Kaiser, E., Kuang, Y., Yang, Q., and Li, T. (2021). Red/blue light ratios induce morphology and physiology alterations differently in cucumber and tomato. *Sci. Hortic.* 281:109995.

Liu, J., and Last, R. L. (2015). A land plant-specific thylakoid membrane protein contributes to photosystem II maintenance in *Arabidopsis thaliana*. *Plant J.* 82, 731–743. doi: 10.1111/tpj.12845

Liu, J., Lu, Y., Hua, W., and Last, R. L. (2019). A new light on photosystem II maintenance in oxygenic photosynthesis. *Front. Plant Sci.* 10:975.

Marcelis, L. F. M., Kaiser, E., van Westreenen, A., and Heuvelink, E. (2018). Sustainable crop production in greenhouses based on understanding crop physiology. *Acta Hortic.* 1227, 1–12.

McAusland, L., and Murchie, E. (2020). Start me up; harnessing natural variation in photosynthetic induction to improve crop yields. *New Phytol.* 227, 989–991. doi: 10.1111/nph.16634

Morales, A., Kaiser, E., Yin, X., Harbinson, J., Molenaar, J., Driever, S. M., et al. (2018). Dynamic modelling of limitations on improving leaf CO2 assimilation under fluctuating irradiance. *Plant Cell Environ.* 41, 589–604. doi: 10.1111/pce.13119

Murchie, E. H., and Ruban, A. V. (2020). Dynamic non-photochemical quenching in plants: from molecular mechanism to productivity. *Plant J.* 101, 885–896. doi: 10.1111/tpj.14601

O' Carrigan, A., Babla, M., Wang, F., Liu, X., Mak, M., Thomas, R., et al. (2014). Analysis of gas exchange, stomatal behaviour and micronutrients uncovers dynamic response and adaptation of tomato plants to monochromatic light treatments. *Plant Physiol. Biochem.* 82, 105–115. doi: 10.1016/j.plaphy.2014.05.012

Sakoda, K., Yamori, W., Groszmann, M., and Evans, J. R. (2021). Stomatal, mesophyll conductance, and biochemical limitations to photosynthesis during induction. *Plant Physiol.* 185, 146–160. doi: 10.1093/plphys/kiaa011

Savvides, A., Fanourakis, D., and van Ieperen, W. (2012). Co-ordination of hydraulic and stomatal conductances across light qualities in cucumber leaves. *J. Exp. Bot.* 63, 1135–1143. doi: 10.1093/jxb/err348

Shinkai, K., Mohrs, M., and Locksley, R. M. (2002). Helper T cells regulate type-2 innate immunity in vivo. *Nature* 420, 829–832.

Smith, H. L., McAusland, L., and Murchie, E. H. (2017). Don't ignore the green light: exploring diverse roles in plant processes. *J. Exp. Bot.* 68, 2099–2110. doi: 10.1093/jxb/erx098

Tanaka, Y., Adachi, S., and Yamori, W. (2019). Natural genetic variation of the photosynthetic induction response to fluctuating light environment. *Curr. Opin. Plant Biol.* 49, 52–59. doi: 10.1016/j.pbi.2019.04.010

Taylor, S. H., and Long, S. P. (2017). Slow induction of photosynthesis on shade to sun transitions in wheat may cost at least 21% of productivity. *Philos. Trans. R. Soc. Lond. B Biol. Sci.* 372:20160543. doi: 10.1098/rstb.2016.0543

Taylor, S. H., Orr, D. J., Carmo-Silva, A. E., and Long, S. P. (2020). During photosynthetic induction, biochemical and stomatal limitations differ between Brassica crops. *Plant Cell Environ.* 43, 2623–2636. doi: 10.1111/pce.13862

Walters, R. G. (2005). Towards an understanding of photosynthetic acclimation. *J. Exp. Bot.* 56, 435–447. doi: 10.1093/jxb/eri060

Wang, J., Lu, W., Tong, Y., and Yang, Q. (2016). Leaf morphology, photosynthetic performance, chlorophyll fluorescence, stomatal development of lettuce (*Lactuca sativa* L.) exposed to different ratios of red light to blue light. *Front. Plant Sci.* 7:250. doi: 10.3389/fpls.2016.00250

Wang, Y., Burgess, S. J., de Becker, E. M., and Long, S. P. (2020). Photosynthesis in the fleeting shadows: an overlooked opportunity for increasing crop productivity? *Plant J.* 101, 874–884. doi: 10.1111/tpj.14663

Wellburn, A. R. (1994). The spectral determination of chlorophylls a and b, as well as total carotenoids, using various solvents with spectrophotometers of different resolution. *J. Plant Physiol.* 144, 307–313.

Zhang, Y., Kaiser, E., Zhang, Y., Yang, Q., and Li, T. (2019). Red/blue light ratio strongly affects steady-state photosynthesis, but hardly affects photosynthetic

induction in tomato (*Solanum lycopersicum*). *Physiol. Plant.* 167, 144–158. doi: 10.1111/ppl.12876

Zhu, X. G., Long, S. P., and Ort, D. R. (2010). Improving photosynthetic efficiency for greater yield. *Annu. Rev. Plant Physiol.* 61, 235–261.

Zhu, X. G., Ort, D. R., Whitmarsh, J., and Long, S. P. (2004). The slow reversibility of photosystem II thermal energy dissipation on transfer from high to low light may cause large losses in carbon gain by crop canopies: a theoretical analysis. *J. Exp. Bot.* 55, 1167–1175. doi: 10.1093/jxb/erh141

Conflict of Interest: The authors declare that the research was conducted in the absence of any commercial or financial relationships that could be construed as a potential conflict of interest.

Publisher's Note: All claims expressed in this article are solely those of the authors and do not necessarily represent those of their affiliated organizations, or those of the publisher, the editors and the reviewers. Any product that may be evaluated in this article, or claim that may be made by its manufacturer, is not guaranteed or endorsed by the publisher.

frontiers in Plant Science

ORIGINAL RESEARCH
published: 14 March 2022
doi: 10.3389/fpls.2022.853651

Patterns of Volatile Diversity Yield Insights Into the Genetics and Biochemistry of the Date Palm Fruit Volatilome

Jonathan M. Flowers[1‡], Khaled M. Hazzouri[1,2‡], Alain Lemansour[3†], Tiago Capote[1], Muriel Gros-Balthazard[1†], Sylvie Ferrand[1], Marc Lebrun[4,5], Khaled M. A. Amiri[2,6] and Michael D. Purugganan[1,7]**

[1] Center for Genomics and Systems Biology, New York University Abu Dhabi, Abu Dhabi, United Arab Emirates, [2] Khalifa Center for Genetic Engineering and Biotechnology, United Arab Emirates University, Al Ain, United Arab Emirates, [3] Date Palm Research and Development Unit, UAE University, Al Ain, United Arab Emirates, [4] CIRAD, UMR Qualisud, Montpellier, France, [5] Qualisud, Univ. Montpellier, Avignon Université, CIRAD, Institut Agro, IRD, Université de La Réunion, Montpellier, France, [6] Department of Biology, College of Science, UAE University, Al Ain, United Arab Emirates, [7] Center for Genomics and Systems Biology, New York University, New York, NY, United States

Volatile organic compounds are key components of the fruit metabolome that contribute to traits such as aroma and taste. Here we report on the diversity of 90 flavor-related fruit traits in date palms (*Phoenix dactylifera* L.) including 80 volatile organic compounds, which collectively represent the fruit volatilome, as well as 6 organic acids, and 4 sugars in tree-ripened fruits. We characterize these traits in 148 date palms representing 135 varieties using headspace solid-phase microextraction gas chromatography. We discovered new volatile compounds unknown in date palm including 2-methoxy-4-vinylphenol, an attractant of the red palm weevil (*Rhynchophorus ferrugineus* Olivier), a key pest that threatens the date palm crop. Associations between volatile composition and sugar and moisture content suggest that differences among fruits in these traits may be characterized by system-wide differences in fruit metabolism. Correlations between volatiles indicate medium chain and long chain fatty acid ester volatiles are regulated independently, possibly reflecting differences in the biochemistry of fatty acid precursors. Finally, we took advantage of date palm clones in our analysis to estimate broad-sense heritabilities of volatiles and demonstrate that at least some of volatile diversity has a genetic basis.

Keywords: volatile organic compound, aroma, flavor, fatty acid ester, metabolic network, volatilome

OPEN ACCESS

Edited by:
Brian Farneti,
Fondazione Edmund Mach, Italy

Reviewed by:
Natasha Spadafora,
University of Calabria, Italy
Cosimo Taiti,
University of Florence, Italy

***Correspondence:**
Khaled M. A. Amiri
k.amiri@uaeu.ac.ae
Michael D. Purugganan
mp132@nyu.edu

†Present addresses:
Alain Lemansour,
Plant Palm Lab Biotechnology, Chateauvieux, France

Muriel Gros-Balthazard, DIADE, Univ. Montpellier, CIRAD, IRD, Montpellier, France

‡*These authors have contributed equally to this work*

Specialty section:
This article was submitted to Crop and Product Physiology, a section of the journal Frontiers in Plant Science

Received: *12 January 2022*
Accepted: *03 February 2022*
Published: *14 March 2022*

Citation:
Flowers JM, Hazzouri KM, Lemansour A, Capote T, Gros-Balthazard M, Ferrand S, Lebrun M, Amiri KMA and Purugganan MD (2022) Patterns of Volatile Diversity Yield Insights Into the Genetics and Biochemistry of the Date Palm Fruit Volatilome. Front. Plant Sci. 13:853651. doi: 10.3389/fpls.2022.853651

INTRODUCTION

Fruit quality traits have been subject to selection by farmers and breeders since the origin of fruit crop agriculture. This process has contributed to the evolution of physical characteristics of fruits such as their size (Fuller, 2018) and to changes in chemosensory traits including fruit flavor compounds that distinguish domesticated species from their crop wild relatives (Aharoni et al., 2004). Flavor-related traits in fruit crops are an important component of fruit quality (Song and Forney, 2008) that include organic acids and sugars that influence taste and volatile organic

compounds (VOCs) that determine fruit aroma. In some cases, selection on flavor traits has improved the palatability of fruits (Tadmor et al., 2002; Aharoni et al., 2004), while in others, intense breeding has contributed to a loss of flavor (Klee and Tieman, 2018).

Date palms are a subtropical fruit crop that consists of approximately 3,000 vegetatively propagated cultivars (Zaid and Arias-Jiménez, 1999), or varieties, that include a small number of commercially important elite cultivars that are valued primarily for their sweet, nutritious fruit (Ghnimi et al., 2017). The domesticated crop is divided broadly into two gene pools consisting of a Western population in North Africa and an Eastern population in West Asia (Arabnezhad et al., 2012; Hazzouri et al., 2015), each defined by distinct genetic ancestries (Flowers et al., 2019). The fruits ("dates") are a drupe with a lignified stone surrounded by a sugar-rich fibrous pulp whose commercial grade depends on their appearance, texture, and sugar content. Fruits are produced by pollination of female palms in the spring followed by harvest in the summer or fall at either the *khalal* (or *besser*) stage when fruits are unripe and moisture content is at its peak or after the onset of ripening at the *rutab* (ripened) or *tamar* (mature) stage. The *khalal* stage is most familiar to consumers in date growing countries where small numbers of varieties (e.g., "Barhee," "Um Dhin," "Khenezi," and "Hayany") are consumed at this stage, while dried mature fruits are familiar to consumers worldwide. Fruit development in date palms is generally thought to be climacteric (i.e., ethylene dependent; Abbas and Ibrahim, 1996; Serrano et al., 2001), however, there is evidence that fruits of at least one variety ("Barhee") may develop in an ethylene-independent fashion (Marondedze et al., 2014).

In date palms, flavor is determined by a complex array of primary and secondary metabolites that vary by fruit developmental stage (Ahmed et al., 1995; Myhara et al., 1999; El Arem et al., 2011; Hatem et al., 2018) and frequently differ quantitatively among varieties (Al-Farsi and Lee, 2008; El Arem et al., 2011). Variation in flavor compounds contributes to diverse flavor profiles (Zaid and de Wet, 2002); for example, some fruits are characterized by nutty flavor notes (e.g., "Asharasi" and "Kenta" varieties; Popenoe, 1913) while others have sweet, honey-like characteristics (e.g., "Halawi"; Popenoe, 1913).

Variation in organic acids is an important determinant of differences in flavor among fruits of date palms. Many studies have reported differences in organic acids among varieties (Al-Farsi et al., 2005; Elshibli and Korpelainen, 2009; Farag et al., 2014; Hamad et al., 2015; Abdul-Hamid et al., 2018; Ghnimi et al., 2018; Kamal-Eldin and Ghnimi, 2018; Hazzouri et al., 2019), and malic acid has been identified as a key acid that differs among date palm fruits and may contribute to flavor differences (Farag et al., 2014; Kamal-Eldin and Ghnimi, 2018).

Sugar composition also varies prominently among varieties (Cook and Furr, 1953; Kanner et al., 1978; Samarawira, 1983; Fayadh and Al-Showiman, 1990; Ahmed et al., 1995; Al-Hooti et al., 1997; Chaira et al., 2009; Elshibli and Korpelainen, 2009; Haider et al., 2014; Hazzouri et al., 2019). Varieties can be classified as "reducing-type" (e.g., "Khalas"), which fully invert sucrose to glucose and fructose during ripening, or "sucrose-type" (e.g., "Sukary"), which deposit sucrose in the mesocarp (i.e., pulp) of the ripened fruit (Dowson and Aten, 1962). While sugar is a strong elicitor of the perception of sweet flavors in date palms, aroma compounds may contribute to the sweet taste of many fruits through the phenomenon of odor-induced changes in taste perception (Djordjevic et al., 2004). In apples, for example, volatiles explain 33% of perceived sweetness suggesting an important role for aroma compounds in either enhancing ("sweet congruent" compounds) or negating sweet perception (Aprea et al., 2017).

Date aroma is determined by a complex mixture of volatiles (Reynes et al., 1996), now referred to as the volatilome, that vary during the course of fruit development (El Arem et al., 2011). Classes of compounds including alcohols, aldehydes, ketones and esters are the most dominant classes of volatile in date palm fruits (El Arem et al., 2011, 2012; Hatem et al., 2018), while aliphatic hydrocarbons may be less important (Jaddou et al., 1984). Many of the most dominant volatiles are derived from fatty-acid and phenylpropanoid pathways and are likely important determinants of date aroma (Khalil et al., 2017). Varieties frequently differ in their volatile composition (Harrak et al., 2005; Khalil et al., 2017; Mezroua et al., 2017; Arif and Lombarkia, 2018; Hatem et al., 2018), but the causes are unknown.

Here we address questions about volatile diversity and biosynthesis that may contribute to differences in date palm flavor-related traits. We profile volatiles in tree-ripened fruit harvested from a panel of 148 palms representing 135 varieties. Our results on volatilome diversity provide new insight into the metabolism of volatiles and other flavor-related compounds in date fruits.

MATERIALS AND METHODS

Fruit Collection

The sampling population used in this study includes both elite and minor cultivars of date palm with most originating from the West Asian population and a smaller number representing the North African gene pool (Hazzouri et al., 2019). The original sampling of tree-ripened fruits from 148 date palms in this study was first reported in Hazzouri et al. (2019; **Supplementary Table 1**) and data for sugar, organic acid, and moisture content provided in that study. Date palms in this study consisted of adult female fruit-bearing palms located at two farms in the United Arab Emirates. The minimum age range is from roughly 10 years on the Al Falassi farm (Al Schweib, Abu Dhabi, UAE) and 17 years on the farm in Al Hamria (Ras-Al-Khaima, UAE). Both use drip irrigation with ∼750 liters of water per palm every two weeks. The Al Hamria farm uses organic fertilizer (75 kg cow/sheep/chicken dung mix) applied once a year per palm, while the Al Falassi farm is fertilized twice a year with the same mixture. Furthermore, the Al Falassi farm adds potassium sulfate fertilizer at 0.75 kg per palm per year. Finally, the Al Falassi farm is treated with several pesticides (including Dimethoate, Chloropyrifos, Triclorophon, Primiphos Methyl, Malathion) as needed, while there is no phytosanitary treatment in the Al Hamria farm. In both farms, females were pollinated with pollen mixtures from

various males that included Ghanami, Sekka, Alkhour, as well as those of unknown provenance.

Fruits of 148 palms used for volatile profiling in this study and for organic acid and sugar quantification in Hazzouri et al. (2019) were allowed to ripen completely to the mature "tamar" stage on the fruit stalk prior to harvest. Ripe fruit in the "tamar" stage was determined by visual inspection and as the stage where fruit abscission occurs. Fruits for different varieties were harvested asynchronously at the abscission stage to allow different varieties to reach the desired developmental stage. Note that for all trees fruit thinning was practiced and the developing fruit stalk bunch covered as standard agronomic practice. Approximately 20–25 fruit were harvested per date palm by removing each fruit from its spike and freezing immediately on dry ice. Fruits were maintained at –40°C up to 24 days prior to shipment on dry ice to Montpellier, France where samples were stored at –20°C prior to volatile quantification.

Volatile Profiling

Volatile profiling was conducted by repeating the following procedure three times per sample and the outputs treated as technical replicates in downstream analysis. Approximately 10–15 frozen fruits from each of the 148 date palms were crushed and stones removed prior to grinding the fruit flesh to powder on liquid nitrogen. Samples were then stored at –20°C until processing at which time they were divided in two. One part was retained for organic acid and sugar profiling reported previously (Hazzouri et al., 2019) and the remainder for volatile analysis. Volatile compounds were extracted using headspace solid-phase microextraction gas chromatography (SPME/GC). Each sample was analyzed in triplicate. Samples (1 g) were placed in headspace vials (10 mL) with butanol (Sigma-Aldrich) (5 μL/100 mL) as internal standard for semi-quantification.

Extraction was performed at 60°C with 15 min incubation and 60 min trapping on polydimethylsiloxane (PDMS)/DVB (divinylbenzene)/Carboxen fiber (Stableflex^{TM} 50/30μm, Supelco, Bellefonte, Pennsylvania, United States). Analysis was carried out with a gas chromatograph 6890/MSD 5973 system (Agilent Technologies, Palo Alto, United States) with a Gerstel Multipurpose Sampler MPS-2, equipped with a DB-WAX Ultra Inert (UI) polar column 30 m, 0.25 mm, 0.25 μm film thickness (Agilent J&W GC column). Hydrogen was used as carrier gas at 1.2 mL/min at constant flow. Fiber was desorbed at 250°C with the injector port in the gas chromatograph set to Splitless mode. The oven temperature increased from 40°C by 3°C/min to 170°C and then 10°C/min to 240°C. The oven was held at the final temperature for 10 min. The mass spectrometer operated in electron impact (EI+) ionization mode at 70 eV with a scan range of 40–350 Dalton.

Data were analyzed with MassHunter version B 08.00 (Agilent Technologies, Palo Alto, United States). Peaks were identified by comparing the obtained mass spectra with those of the National Institute of Standards and Technology (NIST, Gaithersburg, Maryland, United States) 14 database. Co-injection of series of alkanes, from C8 to C20 (Sigma-Aldrich), was used for the calculation of Kovats retention indices that were then compared with those found in the literature (Pubchem website[1] and NIST). After careful revision and removal of artifacts and pollution coming from fiber and column, the list of volatiles was reduced to 80 molecules. The raw data consisted of 3 technical replicates of each of the 148 date palm fruit samples and 80 volatiles (see section "Data Availability").

To allow for sample comparison, semi-quantitative determinations were carried out and expressed in butanol equivalents. The volatile quantification was performed as follows for each technical replicate: m_i (μg/100 g dried dates) = $K_i/K_{EI} \times A_i/A_{EI} \times m_{EI}/m_p \times 100$, where K_i is the coefficient of response of the unknown molecule, K_{EI} is the coefficient of response of the internal standard, A_i is the peak area of the volatile compound, A_{EI} is the peak area of butanol, m_{EI} is the quantity of butanol, m_p is the quantity of date fruit powder. Calculations were performed with setting $K_i/K_{EI} = 1$. Our results are therefore a semi-quantification where the concentration is used as a mean of relative comparison pertinent to our study. This semi-quantification allows direct comparison of measurements of each volatile, but precludes rigorous quantification of quantities such as total volatile emissions or volatile emissions per class (e.g., alcohols).

The raw data matrix with three technical replicates was then processed to remove low quality data points using the following procedure. First, any volatile from a single fruit sample with coefficient of variation (CV) > 50% across the three technical replicates was evaluated to determine if one of the technical replicates deviated substantially (as defined below) from the other two. Deviations were calculated for each of the minimum and maximum technical replicates as a percentage of the median replicate as | (replicate—median replicate)| /median replicate. In cases where the minimum or maximum replicates deviated from the median replicate by < 35% and the other by > 55%, the replicate with the larger deviation from the median was excluded. Second, in cases where the CV was > 50% for the three technical replicates, but one of the replicates could not be identified as low quality using the above criterion, information across volatiles to determine if one of the three technical replicate runs consistently yielded low quality data points across volatiles was used. In this case, the technical replicate corresponding to the low quality run was excluded for volatiles with CV > 50% for the date palm sample.

After cleaning of the raw SPME/GC mass spectroscopy (SPME/GCMS) data, the means of the technical replicate m_i values were calculated per volatile per sample. These values are estimates of the number of butanol equivalents of each volatile per fruit sample with units μg/100 g and were included as trait values in a volatile 148 × 80 phenotype matrix with 3.28% (412/12,580) missing data. This matrix was used in downstream analysis of volatiles. Finally, a second matrix was created for comparison of volatiles to other fruit traits collected for a subset of the same date palm samples. The volatile matrix was merged with fruit organic acid, sugar composition, and fruit color data from Hazzouri et al. (2019) and then subsetted to exclude

[1] https://pubchem.ncbi.nlm.nih.gov/

clonal replicates (see below) and remove samples with volatile phenotypes but without whole genome resequencing data.

Volatile Data Analysis

We ran principal component analysis (PCA) with the prcomp function in R (version 4.1.1). The input matrix to the PCA was modified by (i) imputing missing data with the median value calculated separately for each volatile, (ii) adding a constant (i.e., the minimum non-zero value) to all observations for any volatile with one or more zero values, (iii) taking the logarithm of the value, and (iv) both centering and scaling the values in the call to the prcomp function. PC1 (19.3%) and PC2 (18.7%) explained similar percentages of the overall variation. Thirty volatiles for hierarchical clustering in **Figure 1A** were chosen, by identifying the 15 volatiles with most extreme positive or negative loadings (i.e., absolute value) on each axis.

Heatmaps and associated hierarchical clustering was performed using the ComplexHeatmap (v. 2.8.0; Gu, 2016) package in R. Prior to clustering and heatmap generation, volatile trait values were adjusted by adding a constant to traits with zero values (using the same procedure as in the PCA) followed by Z-score transformation of log-transformed values. Z-score values less than –3 or greater than 3 were set to –3 and 3, respectively prior to calling the Heatmap function. Hierarchical clustering on both the sample and volatile axis of the heatmap was performed using Euclidean distances.

Clustering of volatiles was performed with the pvclust package (v. 2.2-0) in R using 1—Spearman's rank correlation as the distance measure. Node support was estimated as approximately unbiased ("AU"; see pvclust documentation) *P*-values obtained from 1,000 bootstrap replicates. The output was then plotted using the dendextend R package (v. 1.15.1) with pvclust_show_signif argument alpha = 0.05 to highlight nodes supported at this level. Manipulation of correlation matrices (e.g., **Supplementary Table 2**) was performed with the corrr R package (v. 0.4.3).

SNP Processing

Unprocessed SNPs from Hazzouri et al. (2019) were filtered to remove variants mapping to the chloroplast genome followed by use of VariantFiltration and SelectVariants (GATK, v. 4.1.9.0) tools to retain only biallelic SNPs, exclude SNPs within 10 bp of indels in the unfiltered original call set, remove SNPs with a genotype call rate of less than 85%, and to exclude variants meeting the following conditions: QUAL < 30.0, DP < 785 (i.e., SNPs with less than 5X coverage averaged across samples), DP > 2063 (i.e., SNPs with greater than 1.5X the coverage summed across samples; The 1000 Genomes Project Consortium), QD < 5.0, SOR > 3.0, FS > 60.0, MQ < 40.0, MQRankSum < -12.5, ReadPosRankSum < -8.0. Variant Call Format (VCF) tag definitions can be found in the archived VCF file. SNPs not in Hardy-Weinberg equilibrium ($P < 0.05$) were subsequently removed using vcftools (v. 0.1.14). Imputation was performed on this call set with Beagle (v4.1; Browning and Browning, 2016) using the -gl option. This approach uses the genotype likelihoods in the filtered VCF to call genotypes and uses LD information to improve genotype calls while imputing missing genotypes in the original GATK callset. Imputation was performed with the default uniform recombination rate of 1 cM/Mb and without a reference panel or pedigree information. This VCF was used to identify clonal samples (see below).

Kinship Analysis

Kinship coefficients were estimated on the VCF with ngsRelate (v. 2) using command line arguments "-T GT -c 1." Given an expected kinship for clones of 0.5, we identified 16 independent pairs ($n = 32$ samples) with kinship ∼0.5 and one set of three clones ($n = 3$ samples) consisting of two named varieties "Khenezi" ($n = 2$) and "Mablasi" ($n = 1$) (**Supplementary Table 3**). Therefore, 35 of the 148 samples were verified by genome sequencing as being members of a clone pair ($n = 2$) or group ($n = 3$) (**Supplementary Table 3**). We inspected the *khalal* stage fruits of inferred clones bearing different variety names and confirmed the fruits have the same color and shape. We conclude these samples are clones, but they may be either cases where the same clone was assigned different variety names or cases in which one of the samples had been mis-labeled on one of the two farms. Three other pairs of samples shared a variety name (i.e., "Deglet Al Emam," "Nebtet Seif," and "Nagal") but only one of the samples was sequenced preventing confirmation of clonal identity.

Clonal Analysis of Volatile Composition

We tested the hypothesis that vegetative clone pairs are more similar in their volatile profiles than expected by chance using a randomization procedure. Each replicate of the procedure consisted of randomly choosing n pairs of samples from the 148 samples in our volatile dataset and assigning them as pseudo-clone pairs, where n corresponds to the observed number of clones (**Supplementary Table 3**). We then calculated the Euclidean distance between volatile profiles separately for each pair of pseudo-clones and determined the mean for the n pseudo-clone pairs. This procedure was repeated 10,000 times. The *P*-value was calculated as the proportion of the 10,000 replicates where the mean Euclidean distance between pseudo-clone pairs was less than the observed mean. Samples considered clones in this analysis included only those that could be verified based on whole genome sequencing. Analysis of broad sense heritability was conducted using the approach of Einspahr et al. (1963) and Zsuffa (1975) on clones in our analysis represented by two palms. Analysis of Variance (ANOVA) summary statistics for the calculations were obtained using the aov function in the base R (v. 4.1.1) stats package and data tidying performed with the Broom package (v. 0.7.10) in R.

RESULTS AND DISCUSSION

Variation in Fruit Volatile Composition

We measured volatile composition of fruit from 148 date palms representing 135 varieties on two farms in the United Arab Emirates using headspace SPME/GC mass spectroscopy (**Supplementary Table 1**). The two farms (the Al Falassi farm in Abu Dhabi and the Al Hamria farm in Ras Al-Khaimah) are pre-existing farms that are unique in that they contain a large

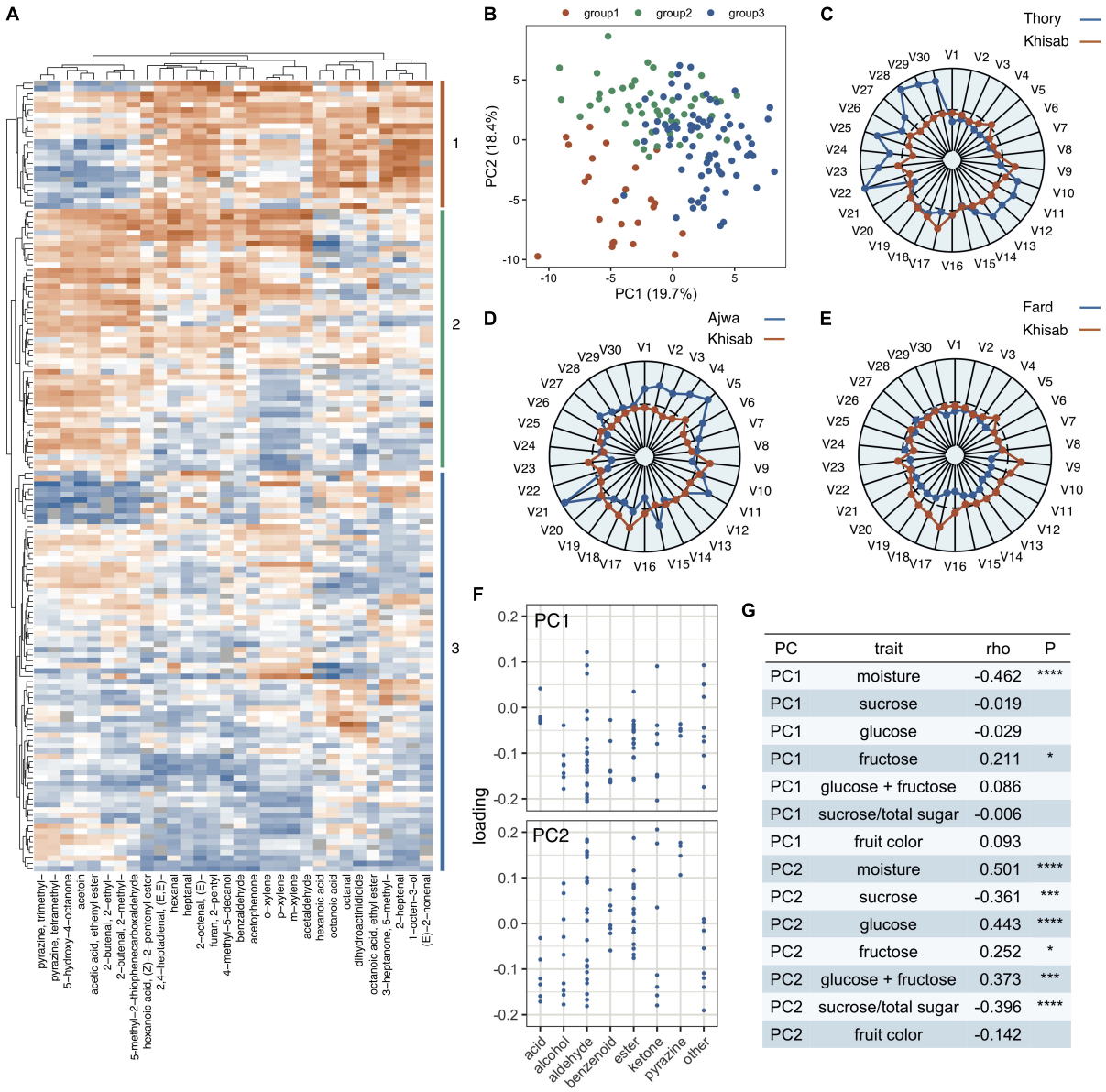

PC	trait	rho	P
PC1	moisture	-0.462	****
PC1	sucrose	-0.019	
PC1	glucose	-0.029	
PC1	fructose	0.211	*
PC1	glucose + fructose	0.086	
PC1	sucrose/total sugar	-0.006	
PC1	fruit color	0.093	
PC2	moisture	0.501	****
PC2	sucrose	-0.361	***
PC2	glucose	0.443	****
PC2	fructose	0.252	*
PC2	glucose + fructose	0.373	***
PC2	sucrose/total sugar	-0.396	****
PC2	fruit color	-0.142	

FIGURE 1 | Variation in volatile composition of fruits from 148 date palms (*Phoenix dactylifera*). **(A)** Hierarchical clustering of date palm samples (vertical axis) and volatiles (horizontal axis) based on 30 volatiles. The heatmap represents transformed volatile concentrations (orange = high, blue = low). **(B)** PCA of 148 date palms based on 80 volatiles. **(C–E)** Radar plots contrasting volatile composition in "Thory," "Ajwa," and "Fard" varieties representing groups 1,2 and 3, respectively, contrasted with the "Khisab" variety. Volatiles (V1-30) correspond to the 30 volatiles in **(A)** read from left to right. **(F)** Loadings for axes 1 and 2 of the PCA in **(B)** for volatiles categorized by their class as defined in **Table 1**. **(G)** Table of Spearman's Correlations of fruit traits and volatiles across date palm samples. Statistical significance is represented as $^{*}P < 0.05$, $^{***}P < 0.0005$, and $^{****}P < 0.00005$, All analyses in **(A–F)** were conducted on log-transformed values scaled by Z-score transformation separately for each volatile. Outlier Z-score values were collapsed to –3 and 3 prior to clustering, heatmap, and radar plot production.

number of varieties planted together; as far as is known, these are two of the largest living collections of date palm varieties that exists. The two farms differ in various aspects of farm management and are located ∼100 km apart; nevertheless the environments are sufficiently similar that fruit samples from these different farms have been successfully used together in genetic mapping studies (Hazzouri et al., 2019). Given the structure of the populations it was not possible to obtain biological replicates per genotype/variety for volatile levels, so our sampling is similar to wild sampling and at this level any difference between sample cannot be attributed solely to variety. In several genotypes, however, there were replicate trees in the two different farms and we could estimate genetic effects (see below).

Tree-ripened fruits were harvested at the fully ripened stage (i.e., *tamar* stage, indicated by fruit abscission) from an individual

tree; individual fruits were pooled and volatiles semi-quantified to allow relative comparison of varieties in subsequent analysis. A total of 80 volatiles were recorded across samples in our volatilome analysis, including acids (6), alcohols (9), aldehydes (23), esters (16), ketones (7), pyrazines (4), benzenoids (7), and other compounds (8) (**Table 1**). Thirty of the volatiles in **Table 1**, excluding potentially novel isoforms (i.e., *m*- and *o*-xylene), have not previously been reported in date palm fruit. These include dominant compounds in our analysis such as hexadecanoic acid, methyl ester, other fatty acid esters, branch chain aldehydes, furans, pyrazines, pyrrols, pyrrazoles, and 2-methoxy-4-vinylphenol, an attractant of the red palm weevil (*Rhynchophorus ferrugineus*), a major pest of the date palm crop (**Table 1**). Dominant compounds are indicated in **Table 1**. However, we note that the semi-quantification approach we adopted allows comparisons across samples for each volatile, but prevents a rigorous assessment of the relative abundance of different volatiles or volatile classes. Finally, one of the volatile compounds—acetic acid, ethenyl ester—was detected in our study but we could not rule out that it was a contaminant from storing the harvested date fruits in plastic bags.

The volatiles detected in our study include a number of compounds that either have not previously been reported or were rarely detected in date palm fruit. For example, pyrazines are produced by non-enzymatic processes during heating (Garcia et al., 2020) or as products of fermentation (Müller and Rappert, 2010). This class of compounds have been rarely observed in date palm fruit (El Arem et al., 2012); in contrast we find that trimethyl pyrazine is among the most dominant volatiles in our study. In other cases, we did not detect volatiles reported as dominant in prior studies (e.g., 2-propanol and isopentyl alcohol, El Arem et al., 2012; methyl propionoate, Hatem et al., 2018). Differences in assay sensitivity, experimental protocols, and the analytical procedure are possible contributing factors, but our approach of harvesting mature, tree-ripened fruits may also contribute to this observation. Our goal was to sample each variety at the same developmental stage and apply the same experimental protocol, while minimizing post-harvest handling, which contrasts with other study designs where volatiles have been profiled in dried fruits or after harvesting at an earlier stage.

Two volatiles in our analysis, 2-methoxy-4-vinylphenol and 1-octen-3-ol are of interest in the context of date palm pest management. The red palm weevil (RPW) is a severe threat to the crop in date-growing regions (El-Sabea et al., 2009) and volatile attractants are a primary means of limiting crop loss. RPW are attracted to fermenting plant material and traps are often baited both with RPW aggregation pheromones and date fruit baits, that act synergistically to lure the weevils (Soroker et al., 2015; Oehlschlager, 2016). 2-methoxy-4-vinylphenol is an aggregation pheromone produced by RPW (El-Sayed, 2021) that we also report in date fruits for the first time. This observation raises the possibility that 2-methoxy-4-vinylphenol is a natural coattractant of RPW that may contribute to the effectiveness of date fruit baits (Soroker et al., 2015). 2-methoxy-4-vinylphenol is also produced by coconut palm (*Cocus nucifera* L.) bark where it acts as a natural attractant for RPW (Gunawardena et al., 1998). Another interesting volatile compound in the context of

TABLE 1 | Date palm fruit volatiles identified by SPME/GC-MS and included in the present study.

Volatile	Formula	RI Exp	Ri Lit[a]	CAS registry no.	Volatile studies[b,c,d]
Acids					
*Acetic acid	$C_2H_4O_2$	1,453	1,449	64-19-7	
Decanoic acid	$C_{10}H_{20}O_2$	2,281	2,276	334-48-5	
Hexanoic acid	$C_6H_{12}O_2$	1,876	1,866[e]	142-62-1	E
Hexanoic acid, 2-ethyl-	$C_8H_{16}O_2$	1,973	1,960	149-57-5	C
Nonanoic acid	$C_9H_{18}O_2$	2,166	2,171	112-05-0	
Octanoic acid	$C_8H_{16}O_2$	2,063	2,060	124-07-2	C
Alcohols					
Benzyl alcohol	C_7H_8O	1,899	1,890[e]	100-51-6	G
Ethanol	C_2H_6O	985	932	64-17-5	G,J
Hexanol	$C_6H_{14}O$	1,366	1,355	111-27-3	A,B,C,D,I,J
4-methyl-5-decanol	$C_{11}H_{24}O$	1,656	–	213547-15-0	
(E,E)-3,5-octadien-2-ol	$C_8H_{14}O$	1,405	–	69668-82-2	
Octanol	$C_8H_{18}O$	1,577	1,557	111-87-5	A,B,C,D,E,H,I,J
1-octen-3-ol	$C_8H_{16}O$	1,455	1,450	3391-86-4	A,B,C,D,E,I
2-octen-1-ol, (E)-	$C_8H_{16}O$	1,644	1,626[e]	18409-17-1	D
Phenylethyl alcohol	$C_8H_{10}O$	1,930	1,906	60-12-8	A,C,D,E,I
Aldehydes					
Acetaldehyde	C_2H_4O	720	702	75-07-0	G
*Benzaldehyde	C_7H_6O	1,511	1,520	100-52-7	A,C
Butanal, 2-methyl-	$C_5H_{10}O$	916	914	96-17-3	E,J
Butanal, 3-methyl-	$C_5H_{10}O$	919	918	590-86-3	
2-Butenal, (E)-	C_4H_6O	1,030	1,039	123-73-9	J
2-Butenal, 2-ethenyl-	C_6H_8O	1,270	1,303	20521-42-0	
2-Butenal, 2-methyl-	C_5H_8O	1,077	1,095	1115-11-3	
2-Butenal, 2-ethyl-	$C_6H_{10}O$	1,143	1,145	19780-25-7	
β-cyclocitral	$C_{10}H_{16}O$	1,619	1,611	432-25-7	A,C,D,E,I
*2-Furancarboxaldehyde, 5-methyl-	$C_6H_6O_2$	1,569	1,570	620-02-0	G
*Furan-3-carboxaldehyde	$C_5H_4O_2$	1,463	1,454	498-60-2	
1H-pyrrole-2-carboxaldehyde, 1-ethyl-	C_7H_9NO	1,613	1,610	2167-14-8	
2,4-Heptadienal, (E,E)-	$C_7H_{10}O$	1,490	1,495	4313-03-5	B,C
*Heptanal	$C_7H_{14}O$	1,178	1,184	111-71-7	B,C,E,H,J
2-Heptenal	$C_7H_{12}O$	1,323	1,323	2463-63-0	B
Hexanal	$C_6H_{12}O$	1,084	1,083	66-25-1	A,B,C,D,H,I,J
(E)-2-Hexenal	$C_6H_{10}O$	1,216	1,216	6728-26-3	B,C
5-Methyl-2-thiophene carboxaldehyde	C_6H_6OS	1,717	1,735[e]	13679-70-4	
*Nonanal	$C_9H_{18}O$	1,393	1,391	124-19-6	A,B,D,H,I,J
(E)-2-Nonenal	$C_9H_{16}O$	1,506	1,537	18829-56-6	B,C,D,E,G
Octanal	$C_8H_{16}O$	1,295	1,289	124-13-0	A,B,C,D,G,H,J
2-Octenal, (E)-	$C_8H_{14}O$	1,426	1,429	2548-87-0	B,C,D,I
2-Phenyl-2-butenal	$C_{10}H_{10}O$	1,937	1,929	4411-89-6	
Esters					
Acetic acid, ethenyl ester	$C_4H_6O_2$	902	890	108-05-4	
Acetic acid, butyl ester	$C_6H_{12}O_2$	1,072	1,074	123-86-4	G
Butanoic acid, butyl ester	$C_8H_{16}O_2$	1,219	1,220	109-21-7	
Decanoic acid, methyl ester	$C_{11}H_{22}O_2$	1,613	1,593	110-42-9	C,D
Dodecanoic acid, methyl ester	$C_{13}H_{26}O_2$	1,836	1,834[e]	111-82-0	D
Ethyl acetate	$C_4H_8O_2$	902	888	141-78-6	A,D,E,G,I,J
*Hexadecanoic acid, methyl ester	$C_{17}H_{34}O_2$	2,212	2,208	112-39-0	
Hexadecanoic acid, ethyl ester	$C_{18}H_{36}O_2$	2,255	2,251	628-97-7	E,I
Hexanoic acid, (Z)-2-pentenyl ester	$C_{11}H_{20}O_2$	1,668	–	74298-89-8	

(Continued)

TABLE 1 | (Continued)

Volatile	Formula	RI Exp	Ri Lit[a]	CAS registry no.	Volatile studies[b,c,d]
Nonanoic acid, methyl ester	$C_{10}H_{20}O_2$	1,499	1,491	1731-84-6	C
Octadecanoic acid, ethyl ester	$C_{20}H_{40}O_2$	2,451	2,451	111-61-5	G
*Octadecanoic acid, methyl ester	$C_{19}H_{38}O_2$	2,419	2,418	112-61-8	G
8E,11E-Octadecadienoic acid, methyl ester	$C_{19}H_{34}O_2$	2,477	–	56599-58-7	F
Octanoic acid, ethyl ester	$C_{10}H_{20}O_2$	1,439	1,435	106-32-1	C,D,E,I
Pentadecanoic acid, methyl ester	$C_{16}H_{32}O_2$	2,110	2,108	7132-64-1	
Tetradecanoic acid, methyl ester	$C_{15}H_{30}O_2$	2,024	2,005	124-10-7	D
Ketones					
*Acetoin	$C_4H_8O_2$	1,290	1,284	513-86-0	
Acetophenone	C_8H_8O	1,650	1,647	98-86-2	C,G
Ethanone, 1-(1H-pyrrol-2-yl)	C_6H_7NO	1,985	1,973	1072-83-9	
3-Heptanone, 5-methyl-	$C_8H_{16}O$	1,256	1,265	541-85-5	
5-Hepten-2-one, 6-methyl-	$C_8H_{14}O$	1,340	1,338	110-93-0	A,B,C,D,I,J
5-Hydroxy-4-octanone	$C_8H_{16}O_2$	1,423	1,443	496-77-5	
β-ionone	$C_{13}H_{20}O$	1,947	1,971	79-77-6	A,B,C,D,E,I,J
Pyrazines					
Pyrazine, 3,5,-diethyl-2-methyl-	$C_9H_{14}N_2$	1,516	1,496	18138-05-1	
Pyrazine, 2-ethyl-6-methyl-	$C_7H_{10}N_2$	1,386	1,386	13925-03-6	
Pyrazine, tetramethyl-	$C_8H_{12}N_2$	1,477	1,469	1124-11-4	
*Pyrazine, trimethyl-	$C_7H_{10}N_2$	1,405	1,402	14667-55-1	
Benzenoids					
Ethylbenzene	C_8H_{10}	1,130	1,129	100-41-4	
p-cymene	C_10H_{14}	1,261	1,272	99-87-6	J
Styrene	C_8H_8	1,254	1,261	100-42-5	D,F
Toluene	C_7H_8	1,030	1,042	108-88-3	
m-xylene	C_8H_{10}	1,139	1,143	108-38-3	
o-xylene	C_8H_{10}	1,171	1,186	95-47-6	
p-xylene	C_8H_{10}	1,121	1,138	106-42-3	F
Other					
2(4H)-benzofuranone, 5,6,7,7a-tetrahydro-4,4,7a- trimethyl-, (R)-	$C_{11}H_{16}O_2$	2,290	2,325[e]	17092-92-1	C
γ-butyrolactone	$C_4H_6O_2$	1,622	1,632	96-48-0	A
Furan, 2-pentyl-	$C_9H_{14}O$	1,229	1,231	3777-69-3	C,D
1H-pyrazole, 4,5-dihydro-5,5-dimethyl-4-isopropylidene-	$C_8H_{14}N_2$	1,396	–	106251-09-6	
2-Methoxy-4-vinylphenol	$C_9H_{10}O_2$	2,167	2,188	7786-61-0	
Phenol, 4-ethyl-2-methoxy	$C_9H_{12}O_2$	2,167	2,188	2785-89-9	A,E,I
2-Pyrrolidinone	C_4H_7NO	2,029	2,017	616-45-5	
Vanillin	$C_8H_8O_3$	2,531	2,540[e]	121-33-5	F

Stereoisomers are indicated where they could be resolved. For compounds with multiple possible stereoisomers, reference to a compound in a prior study may or may not refer to the same stereoisomer detected in the present work.

**Major volatile in the present study.*

[a]*RI lit retention index coming from the NIST 14 database.*

[b]*Compound previously reported in date fruit by A = El Arem et al. (2011), B = Reynes et al. (1996), C = Khalil et al. (2017), D = Mezroua et al. (2017), E = Hatem et al. (2018), F = Arif and Lombarkia (2018), G = Narain (2007), H = Jaddou et al. (1984), I = El Arem et al. (2012), J = Harrak et al. (2005).*

[c]*No overlapping compounds were found with Siddeeg et al. (2019) and Aldulaimi et al. (2020).*

[d]*Acetic acid has previously been reported in non-volatile studies and is not considered novel to this study.*

[e]*RI lit retention index coming from Pubchem.*

RPW is a 1-octen-3-ol, which is weevil repellant that reduces feeding and oviposition activity (Guarino et al., 2015). Further inquiry into these compounds and the causes of variation among varieties is warranted.

Clustering of Volatile and Other Fruit Traits

PCA on the 80 volatiles collected from 148 date palm samples was conducted, and hierarchical clustering performed using 30 volatiles chosen based on their contribution to separating samples in the PCA. Membership of samples in the three basal-most groups in the hierarchical clustering (illustrated on the vertical axis of a heatmap, **Figure 1A** and **Supplementary Figure 1**) were used to color samples in the original PCA (**Figure 1B**). Interestingly, we do not find any individual samples, or groups of samples, as being distinct from others.

The profiles of 30 volatiles contributing most to diversity across samples in the PCA are shown for date palm samples labeled "Thory," "Ajwa," and "Fard" in contrast to the widely grown "Khisab" in **Figures 1C–E**. While differences among samples are primarily quantitative, some patterns are apparent. For example, "Thory" represents samples labeled as group 1 of the hierarchical clustering analysis (**Figure 1A**) and located primarily in the lower left quadrant of the PCA plot (**Figure 1B**). "Thory" and similar samples have consistently greater abundance of alcohols, aldehydes and carboxylic acids primarily with 6–8 carbon chains compared with other samples (**Figures 1A,C–E** and **Supplementary Figure 1**).

We determined if individual volatiles or volatile classes (e.g., alcohols; **Table 1**) disproportionately contribute to quantitative variation in volatile composition among samples by extracting the loadings on the first and second PC axes for each compound. **Figure 1F** shows that loadings are low for all volatiles on a scale from –0.3 to 0.3. Therefore, no individual volatile or class appears to contribute disproportionately to differences among samples in volatile composition in tree-ripened fruit. This is in contrast to results in Muscadine grapes, for example, where 29 volatile compounds are responsible for significant differences between 5 varieties (Deng et al., 2021).

To gain additional insight into factors that contribute to fruit volatile diversity, we tested for significant correlations between PC1 and PC2 from the volatile PCA and traits, including fruit moisture content, sugar composition and the color of the fruit epicarp (i.e., measured at the *khalal* stage Hazzouri et al., 2019). Fruit moisture content was negatively correlated with PC1 ($P < 0.00005$, **Figure 1G**) and positively with PC2 ($P < 0.00005$, **Figure 1G**). Glucose ($P < 0.00005$, **Figure 1G**) and glucose + fructose ($P < 0.0005$, **Figure 1G**) were positively correlated with PC2, while sucrose ($P < 0.0005$, **Figure 1G**) and sucrose/total sugar ($P < 0.00005$), **Figure 1G**) were negatively correlated with this PC. The opposing relationship of reducing and invert sugars with respect to PC2 are likely related to the inverse correlation between these sugars in date fruits (Hazzouri et al., 2019). Fruit color was not associated with either PC axis (**Figure 1G**).

The correlations between PC2 with both glucose and sucrose (**Figure 1G**) implies that sugar composition is associated with

the mixture of volatiles in ripened date palm fruits. Volatile composition as measured by PC1 and PC2 is also associated with moisture in our data (**Figure 1G**), although its unclear how this measure relates to the organoleptic properties of dry, semi-dry, and soft textures often used to characterize dried date fruits. Nevertheless, these correlations imply that differences among tree-ripened fruits in moisture and sugar content may be associated with system-wide metabolic differences in both volatile and non-volatile compounds that extend beyond sugar metabolism and the cellular processes controlling fruit moisture. This could be explained by differences in moisture content where the metabolism of fruits with low moisture content is arrested at an earlier stage than fruits with higher moisture content, which experience a greater degree of metabolic turnover during ripening (Diboun et al., 2015). In addition to correlations between volatiles and non-volatile traits, interesting correlations are found between specific volatiles that may reflect shared or distinct metabolic synthetic/catabolic pathways (see below).

Genetic Basis of Volatile Composition: Clonal Analysis

A key question is whether differences in volatile profiles among samples reflect genetic or non-genetic factors. We examined whether genetic factors contribute to volatile levels by capitalizing on clones in our analysis which originate from the practice of vegetatitve propagation in date palms (Chao and Krueger, 2007). We analyzed whole genome sequence data from Hazzouri et al. (2019) to confirm the clonal status of elite commercial cultivars "Fard," "Gharra," "Khalas," "Barhi," "Khisab," "Khenezi," "Sultana," "Chichi," and "Abou Kibal" each of which is represented by one palm on each of the two farms in our sampling populations. These samples had kinship coefficients estimated from whole genome sequences of ∼0.5 confirming their clonal identity (**Supplementary Table 3**). In addition to these clones, kinship analysis also revealed eight additional pairs of clones that bear different variety names (e.g., "Jeish Fatima" and "Jeish Mohammad Khalaf"), but had kinship coefficients of ∼0.5.

To test for a genetic effect on volatile composition, we asked if pairs of clones collectively have more similar volatile profiles then expected by chance. Using a randomization procedure, we found that the mean Euclidean distance between volatile profiles of pairs of clones bearing the same name ($n = 10$) were significantly less than expected by chance ($P < 0.01$). Application of this same procedure to all clones ($n = 16$ pairs), including those bearing different variety names, indicated these samples also have more similar volatile profiles between pairs of clones than expected by chance ($P < 0.05$). Thus, the shorter than expected mean pairwise volatile profile distance of clonal samples supports a genetic effect on volatile composition.

We took advantage of clonal pairs to estimate broad-sense heritabilities, H^2, of each volatile (Einspahr et al., 1963; Zsuffa, 1975). We estimated H^2 separately for the two overlapping sets of clones. One set consisted of clonal pairs in which clones had the same variety name ($n = 10$ pairs) and the other included four additional clones where members of each clone had different names ($n = 14$ pairs) (**Supplementary Table 4**). We find that the H^2 estimates using these two sets correlate well with each other (**Figure 2**), except for 3 volatiles (2-pyrrolidinone, benzyl alcohol, 2,4-heptadienal, (E,E)−) which we do not consider further. In the larger ($n = 14$) set, we find that 16 of the volatiles had negative heritability estimates (**Supplementary Table 4**), including m-,o- and p-xylene, and decanoic acid; these negative values may arise from the estimation procedure, but there is also some debate about the meaning of negative heritabilities (Steinsaltz et al., 2020), and we do not consider these estimates further. Of the remaining 61 volatiles with positive H^2 values, they range from 0.01 to 0.85. It should be noted that the H^2 values we estimate are probably less meaningful than the relative ranking of volatile heritabilities. In this regard, we note that volatiles with high estimated heritabilities ($H^2 > 0.6$), including 2-octen-1-ol, (E)-, hexanoic acid and butyrolactone, consist of volatiles representing different classes of compounds (e.g., alcohols, acids, etc.) and there is no class of volatiles with consistently high or low estimated heritability.

Correlations Among Volatiles

Correlations in metabolomic data can provide insight into metabolic networks (Camacho et al., 2005; Müller-Linow et al., 2007) and the biochemical pathways that produce poorly characterized volatile compounds (Tikunov et al., 2005; Mathieu et al., 2009). To gain insight into the date palm fruit volatiles, we follow the approach of Tikunov et al. (2005) and use our large sample of genotypes (i.e., 148 samples) to construct a matrix of Spearman's rank correlations for the 80 volatiles (3,160 pairwise comparisons) (**Figure 3** and **Supplementary Table 2**). This yielded 759 significant correlations (24%) after Bonferroni correction at $\alpha = 0.05$ of which 681 were positive and 78 were negative.

Positive correlations among metabolites suggest shared mechanisms of volatile production and clues to the pathway origins of compounds. In some cases, positive associations reflect shared pathways, while in others they reflect common regulation/genetic control. Many of the associations in our analysis reflect products of the same biochemical pathway. For instance, carotenoids accumulate at high concentrations in date palm fruits at early stages of fruit development and then are progressively broken down during maturation until they reach low concentrations in *tamar* stage fruits (Gross et al., 1983; Steingass et al., 2020). Degradation of these compounds produces apocarotenoids (Felemban et al., 2019). In tree-ripened date fruit, β-ionone, a breakdown product of β-carotene, is positively correlated with other apocarotenoids β-cyclocitral, 6-methyl-5-hepten-2-one, and dihydroactinidioide [i.e., 2(4H)-benzofuranone, 5,6,7,7a-tetrahydro-4,4,7a- trimethyl-, (R)-] consistent with their sharing precursors in the carotenoid pathway (**Figures 3**,**4A**, and **Supplementary Table 2**).

Negative correlations are less frequent in the volatile correlation matrix (**Figure 3** and **Supplementary Table 2**); for some of these examples it could be an indication of competition for precursor molecules during volatile biosynthesis or represent alternate metabolic states of different fruit samples. For example,

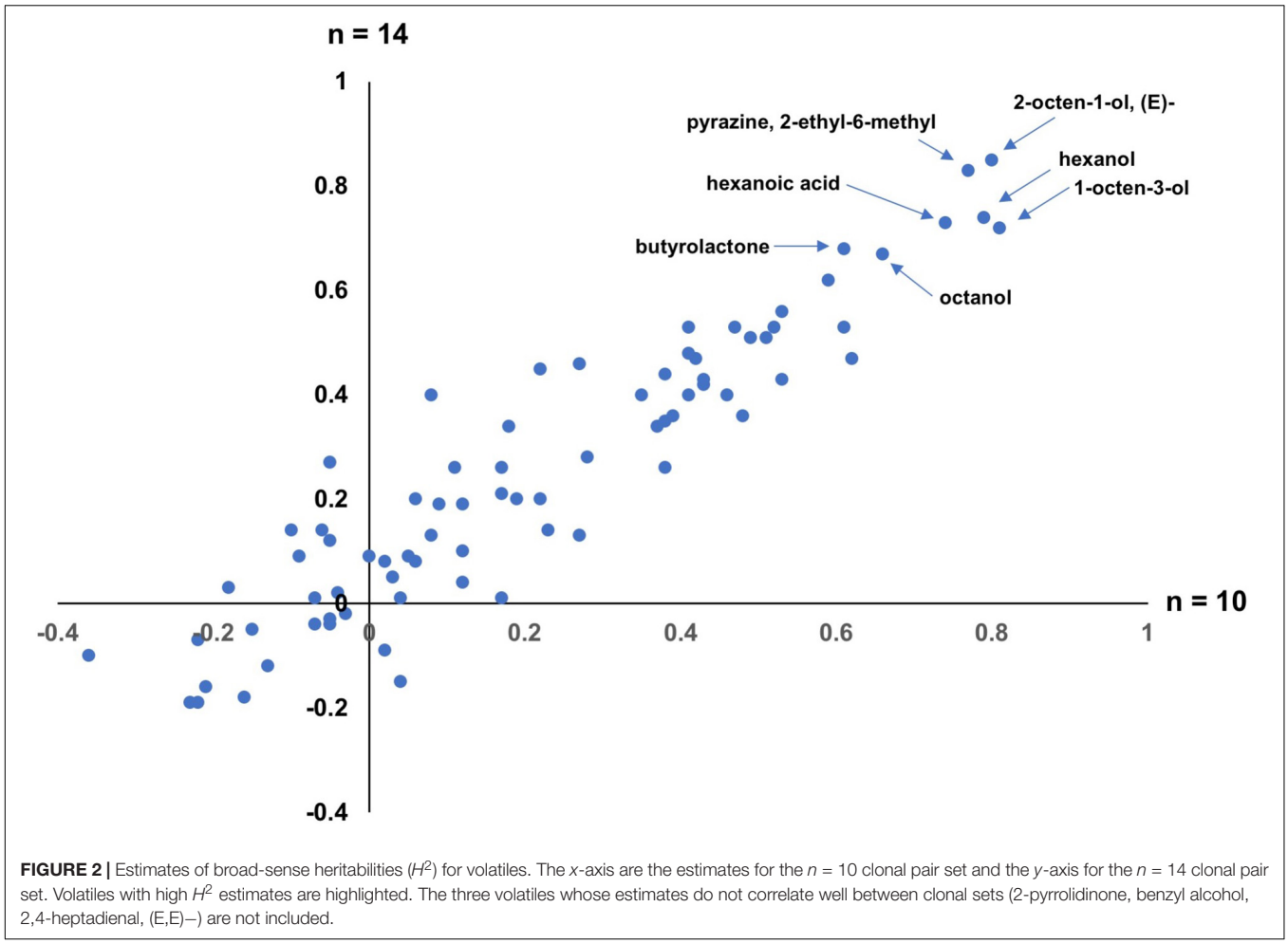

FIGURE 2 | Estimates of broad-sense heritabilities (H^2) for volatiles. The *x*-axis are the estimates for the $n = 10$ clonal pair set and the *y*-axis for the $n = 14$ clonal pair set. Volatiles with high H^2 estimates are highlighted. The three volatiles whose estimates do not correlate well between clonal sets (2-pyrrolidinone, benzyl alcohol, 2,4-heptadienal, (E,E)–) are not included.

γ-butyrolactone, an important flavor compound in coffee and almonds, is negatively correlated with 2-butenal, (E)- ($\rho = -0.67$; $P < 3.3 \times 10^{-20}$, **Figure 4B**) and three other branched aldehydes that are structurally similar to 2-butenal, (E)- (**Figure 4B**). Other relatively strong negative correlations are between 2-butenal, (E)- and furan-3-carboxaldehyde ($\rho = -0.68$, $P = 0.00$) and 2-butenal, (E)- and 2-furancarboxaldehyde, 5-methyl- ($\rho = -0.66$, $P < 1.97 \times 10^{-18}$) and between furan-3-carboxaldehyde and acetaldehyde ($\rho = -0.65$; $P = 0.00$), ethanol ($\rho = -0.57$; $P = 0.00$), and styrene ($\rho = -0.60$; 7.5×10^{-16}).

Clustering analysis based on Spearman's rank correlation distances (i.e., $1-\rho$) provides an alternate means of gaining insight into volatile correlations (Tikunov et al., 2005; Mathieu et al., 2009). Groups of compounds that cluster together in this analysis suggest common regulation. For example, there is a large, well-supported, cluster of long chain fatty acid methyl or ethyl esters (**Figure 5**) with fatty acid chains ranging in length from 14 to 18 carbons. This cluster includes two of the dominant volatiles in our analysis, namely octadecanoic acid, methyl ester and hexadecanoic acid, methyl ester (the methyl esters of palmitic and stearic acids) (**Table 1**). By contrast, medium chain fatty acid esters with fatty acid chains ranging from 8 carbons (octanoic acid, ethyl ester) to 12 carbons (dodecanoic acid, methyl ester) form a cluster independent of the long chain fatty acid esters (**Figure 5**).

This analysis suggests that medium chain and long chain fatty acid ester volatiles are regulated independently. Since date palm fruit retain only trace amounts of triacylglycerides (TAGs) (Bourgis et al., 2011), a potential source of fatty acid precursors is the breakdown of membrane phospholipids during ripening. Fatty acids produced during fruit ripening may initially be liberated by lipase or phospholipase activity and then further metabolized via the lipoxygenase (LOX) or β-oxidation pathways to produce straight chain fatty acids, alcohols, and aldehydes. Differences in regulation of medium and long chain fatty acid esters could be related to differences in regulatory control of fatty acid precursors, differences in properties of enzymes such as alcohol acyl transferase (AAT) responsible for ester formation in fruits (Ueda and Ogata, 1977), or due to completely independent synthetic pathways of medium and long chain esters possibly involving microbes in ripening fruit. For example, medium chain fatty acid esters responsible for the fruity notes in wines are yeast secondary metabolites produced during fermentation (Hu et al., 2018). Support for distinct clusters of long chain and medium chain fatty acid esters suggests common regulation within each class, but independent regulation between classes.

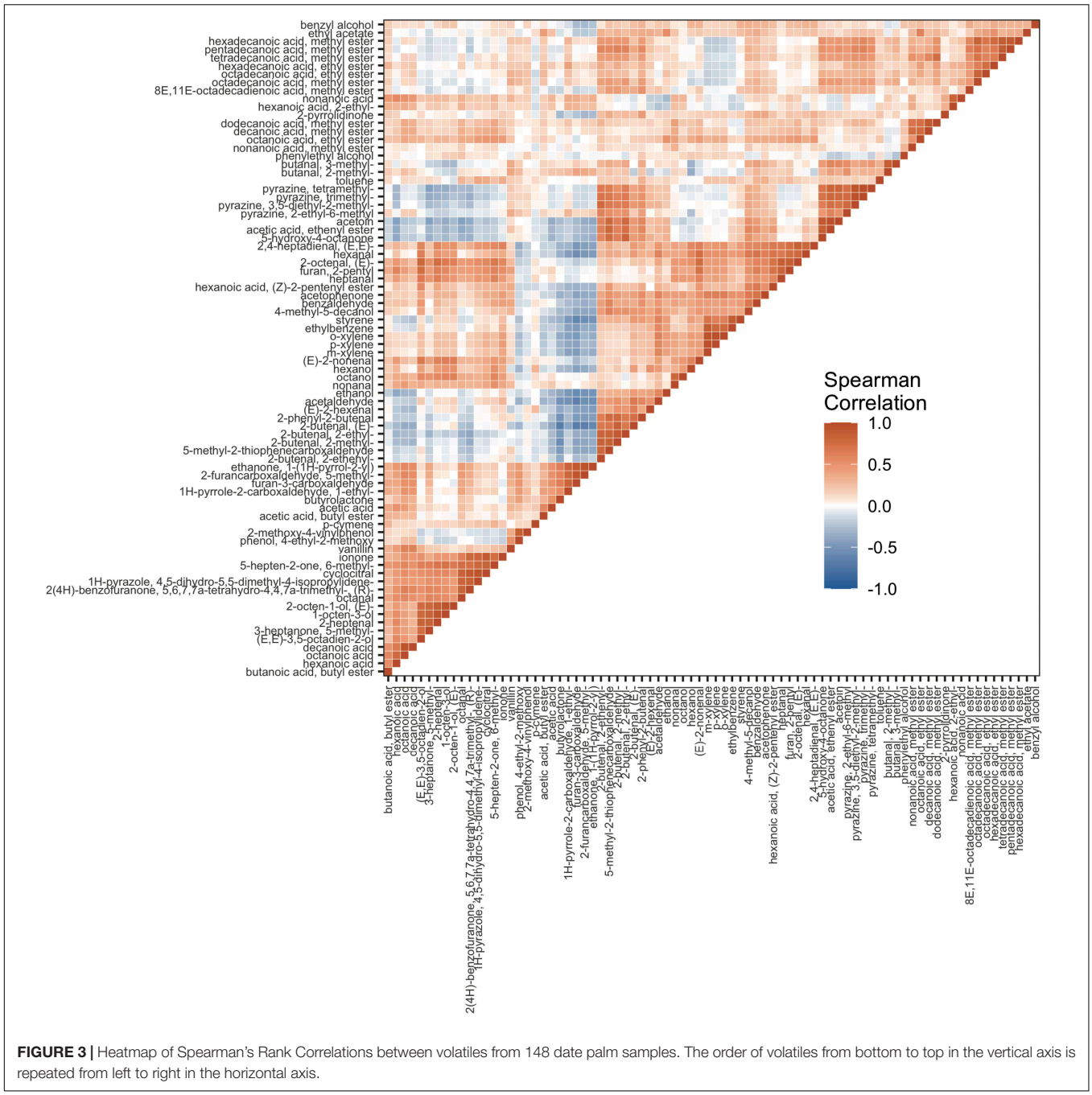

FIGURE 3 | Heatmap of Spearman's Rank Correlations between volatiles from 148 date palm samples. The order of volatiles from bottom to top in the vertical axis is repeated from left to right in the horizontal axis.

Other clusters include pyrazines, benzene derivatives, and apocarotenoids (**Figure 5**). Apocarotenoids β-ionone, β-cyclocitral, 5-hepten-2-one, 6-methyl, and dihydroactinidioide cluster with 1H-pyrazole, 4,5-dihydro-5,5-dimethyl-4-isopropylidene- and octanal (**Figure 5**). While the clustering of apocarotenoids is consistent with a shared carotenoid degradation pathway, the cause for clustering with unrelated compounds including octanal is less clear, although similar observations have been reported elsewhere (Mathieu et al., 2009; Rambla et al., 2017). Finally, 2-pentylfuran is found in a well-supported cluster with fatty acid derivates supporting a connection between this compound and fatty acid degradation (Tikunov et al., 2005; Rambla et al., 2017).

Correlations Among Volatiles, Organic Acids, Sugars, and Color Traits

Above, we reported correlations between sugar and moisture traits and PCs in the volatile PCA. Here, we test for correlations of these traits with individual volatiles, which have been reported previously for volatiles and organic acids and volatiles and fruit color (Ghnimi et al., 2018). We found no significant correlations

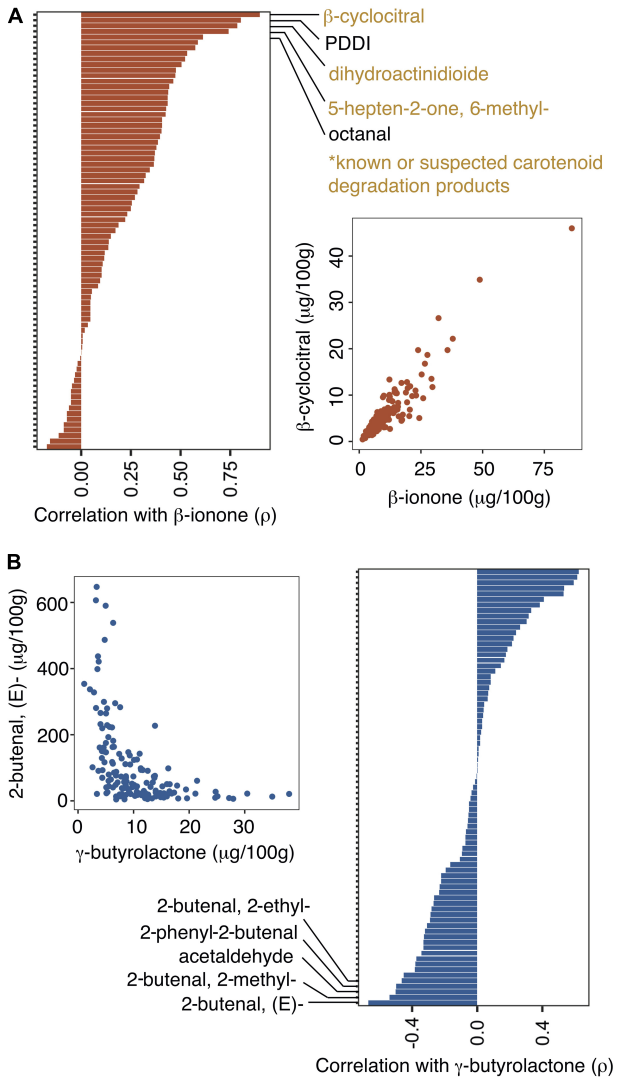

FIGURE 4 | Spearman's Rank Correlations among fruit volatile traits in 148 date palm fruit samples. **(A)** Correlations between β-ionone and other volatiles. Selected volatiles mentioned in the text are labeled. **(B)** Correlations between γ-butyrolactone and other volatiles. Selected volatiles mentioned in the text are labeled.

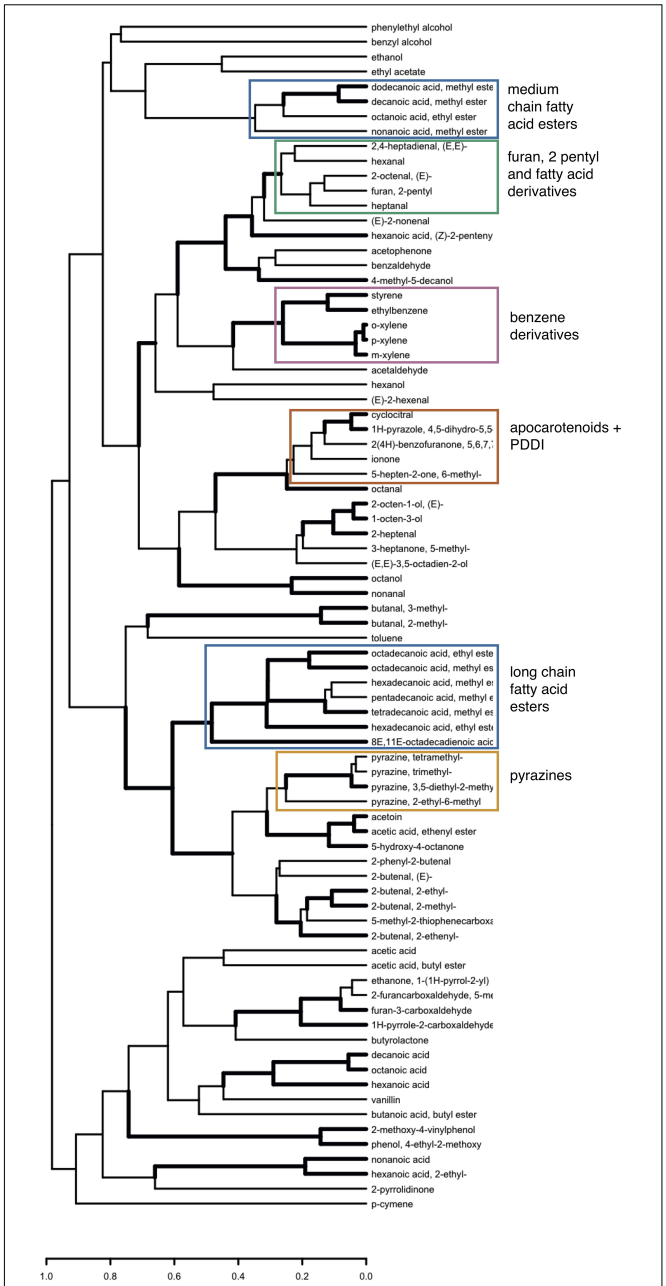

FIGURE 5 | Hierarchical clustering analysis of 80 volatiles across date palm samples based on Spearman's rank correlation. Distances used in clustering were calculated as $1-\rho$. Edges represented by heavy lines are supported by approximately unbiased *P*-values < 0.05 inferred from bootstrapping.

between fruit color or anthocyanin content and the 80 volatiles after Bonferroni correction at $\alpha = 0.05$ (**Supplementary Table 2**). We also tested for correlations between volatiles, sugars, and organic acids. We found a number of weak negative correlations between sucrose and some volatiles including 5-hydroxy-4-octanone ($\rho = -0.53$; $P < 3.5 \times 10^{-9}$). Correlations between all traits in our analysis are presented in **Supplementary Table 2**.

SUMMARY

Although volatile organic compounds are believed to underlie aroma and taste among varieties/cultivars of domesticated fruit tree species, there is remarkably few studies on fruit volatile diversity in these crops. Our study suggests substantial diversity in fruit volatile compounds between date palm varieties; such variation has also been observed in other fruit crop species such as Muscadine grapes (Deng et al., 2021), mangoes (Li et al., 2017), and strawberries (Zhao et al., 2020; Fan et al., 2021).

Date palm fruits differ in a number of commercially important traits, such as sugar content, which our analysis suggests is also correlated with volatile composition. Non-genetic factors,

including subtle or cryptic differences in developmental stage at time of harvest and environmental effects, likely contribute to volatile trait variation. Such effects may account for the observation that some samples (e.g., "Abou Kibal") have relatively large volatile profile distances between clonal pairs of samples (**Supplementary Figure 1**). Nevertheless, our clonal analysis indicates that fruit volatile diversity may indeed have a genetic basis, as date palm clones grown in different farms are more likely to share volatile profiles compared to non-related varieties. We have used this clonal structure to get estimates of broad-sense heritabilities for different volatile components, and we identified several volatiles with greater heritabilities compared to others within the sample sets. Identifying the genes underlying volatile composition is an obvious next step; unfortunately our sampling procedure as well as limited sample size precludes a genetic mapping analysis, and a full genetic study must await the availability of larger mapping populations.

The chemical basis of aroma has not been clearly defined in date palm, but appears to be explained by a complex mixture of volatiles. Presently, we know very little about which volatiles contribute to flavor perception. Hatem et al. (2018) suggested that alcohols and terpenes determine the herbaceous, fruity, citrus, floral and fungal aromas of date fruits and that 2-hexen-1-ol, 1-hexanol, and phenylethanol probably contribute to green, herbal, and floral aromas. El Arem et al. (2011) attributed the fresh and green notes of dates to nonanal and decanal straight chain aldehydes, of which the former was also detected in our study. In apples, approximately 350 volatiles have been reported (Song and Forney, 2008), but only around 20 are considered important for the distinctive flavors of apple varieties (Dixon and Hewett, 2000). We suspect this is similar in date palms and that only a small percentage of the volatiles we report impact flavor perception. Further advances in date fruit flavor research would benefit from sensory analysis that combines measurements of volatile, organic acid, and sugar composition in individual varieties with human sensory panels which is necessary to establish which compounds are most important in flavor perception (Ismail et al., 2001).

DATA AVAILABILITY STATEMENT

The original contributions presented in the study are publicly available. This data can be found here: https://doi.org/10.5061/dryad.mw6m905z8.

AUTHOR CONTRIBUTIONS

KH, ML, KA, and MP designed the research. KH and AL collected samples. ML performed headspace GC/MS and produced the raw volatile data. JF, ML, MP, SF, MG-B, and TC performed data collection and interpretation. JF performed the data analysis. JF and MP wrote the manuscript. All authors contributed to the article and approved the submitted version.

FUNDING

This project was funded by the Khalifa Center for Genetic Engineering and Biotechnology (KCGEB) and the New York University Abu Dhabi Research Institute (1205H).

ACKNOWLEDGMENTS

We thank Ahmad Al Falassi who graciously opened his farm to our research and kindly supported our efforts throughout the project. We also thank the UAE Ministry of Environment and Climate Change who granted access to the farm in Al Hamria, Ras-Al-Khaima and Sallah Abdulla Moussa for facilitating its use. We also thank the engineers at both farms for their assistance in accomplishing this work. We thank the Date Palm Research Unit at the UAEU for various roles in facilitating this work. We thank Robert R. Krueger, Khaled Masmoudi and the deceased Hussam S.M. Khierallah for helpful discussions on aspects of date palm agriculture and fruit development at the outset of this project. Gina M. Pham for helpful discussions on data curation and analysis, and Justin B. Renaud for helpful discussions on pyrazines. We thank Marc Arnoux and Nizar Drou for assistance with initial genomic data collection and processing. We thank members of the New York University and New York University Abu Dhabi High Performance Computing facilities for their assistance with technical issues concerning data processing.

SUPPLEMENTARY MATERIAL

The Supplementary Material for this article can be found online at: https://www.frontiersin.org/articles/10.3389/fpls.2022.853651/full#supplementary-material

REFERENCES

Abbas, M. F., and Ibrahim, M. A. (1996). The role of ethylene in the regulation of fruit ripening in the Hillawi date palm (*Phoenix dactylifera* L.). *J. Sci. Food Agric.* 72, 306–308.

Abdul-Hamid, N. A., Mediani, A., Maulidiani, M., Shadid, K., Ismail, I. S., Abas, F., et al. (2018). Metabolite characterization of different palm date varieties and the correlation with their NO inhibitory activity, texture and sweetness. *J. Food Sci. Technol.* 55, 1541–1551. doi: 10.1007/s13197-018-3073-6

Aharoni, A., Giri, A. P., Verstappen, F. W., Bertea, C. M., Sevenier, R., Sun, Z., et al. (2004). Gain and loss of fruit flavor compounds produced by wild and cultivated strawberry species. *Plant Cell* 16, 3110–3131. doi: 10.1105/tpc.104.023895

Ahmed, I. A., Ahmed, A. W. K., and Robinson, R. K. (1995). Chemical composition of date varieties influenced by the stage of ripening. *Food Chem.* 54, 305–309. doi: 10.1016/0308-8146(95)00051-j

Aldulaimi, A. K. O., Idan, A. H., Radhi, A. H., Aowda, S. A., Azziz, S., Salleh, W., et al. (2020). GCMS Analysis and biological activities of Iraq zahdi date palm *Phoenix dactylifera* L. volatile compositions. *Res. J. Pharm. Technol.* 13, 5207–5209.

Al-Farsi, M., Alasalvar, C., Morris, A., Baron, M., and Shahidi, F. (2005). Compositional and sensory characteristics of three native sun-dried date

(*Phoenix dactylifera* L.) varieties grown in Oman. *J. Agric. Food Chem.* 53, 7586–7591. doi: 10.1021/jf050578y

Al-Farsi, M., and Lee, C. (2008). Nutritional and functional properties of dates: a review. *Crit. Rev. Food Sci. Nutr.* 48, 877–887. doi: 10.1080/10408390701724264

Al-Hooti, S., Sidhu, J. S., and Qabazard, H. (1997). Physicochemical characteristics of five date fruit cultivars grown in the United Arab Emirates. *Plant Foods Hum. Nutr.* 50, 101–113. doi: 10.1007/BF02436030

Aprea, E., Charles, M., Endrizzi, I., Laura Corollaro, M., Betta, E., Biasioli, F., et al. (2017). Sweet taste in apple: the role of sorbitol, individual sugars, organic acids and volatile compounds. *Sci. Rep.* 7:44950. doi: 10.1038/srep44950

Arabnezhad, H., Bahar, M., Mohammadi, H. R., and Latifian, M. (2012). Development, characterization and use of microsatellite markers for germplasm analysis in date palm (*Phoenix dactylifera* L.). *Sci. Hortic.* 134, 150–156.

Arif, Y., and Lombarkia, N. (2018). Variability influence of the volatile compounds of three Algerian date cultivars (*Phoenix dactylifera* L.) on infestation rates of the date moth [(*Ectomyelois ceratoniae* Zell. (Lepidoptera: Pyralidae)]. *Cercet. Agron. Moldova* 51, 111–124.

Bourgis, F., Kilaru, A., Cao, X., Ngando-Ebongue, G.-F., Drira, N., Ohlrogge, J. B., et al. (2011). Comparative transcriptome and metabolite analysis of oil palm and date palm mesocarp that differ dramatically in carbon partitioning. *Proc. Natl. Acad. Sci. U.S.A.* 108, 12527–12532. doi: 10.1073/pnas.1106502108

Browning, S. R., and Browning, B. L. (2016). Genotype imputation with millions of reference samples. *Am. J. Hum. Genet.* 98, 116–126. doi: 10.1016/j.ajhg.2015.11.020

Camacho, D., de la Fuente, A., and Mendes, P. (2005). The origin of correlations in metabolomics data. *Metabolomics* 1, 53–63.

Chaira, N., Mrabet, A., and Ferchichi, A. (2009). Evaluation of antioxidant activity, phenolics, sugar and mineral contents in date palm fruits. *J. Food Biochem.* 33, 390–403. doi: 10.1186/s12944-019-1087-3

Chao, C. T., and Krueger, R. R. (2007). The date palm (*Phoenix dactylifera* l.): overview of biology, uses and cultivation. *Hortscience* 42, 1077–1082.

Cook, J., and Furr, J. (1953). Kinds and relative amount of sugar and their relation to texture in some American-grown date varieties. *Am. Soc. Hortic. Sci.* 61, 286–292.

Deng, H., He, R., Long, M., Li, Y., Zheng, Y., Lin, L., et al. (2021). Comparison of the fruit volatile profiles of five Muscadine grape cultivars (*Vitis rotundifolia* Michx.) using HS-SPME-GC/MS combined with multivariate statistical analysis. *Front. Plant Sci.* 12:728891. doi: 10.3389/fpls.2021.728891

Diboun, I., Mathew, S., Al-Rayyashi, M., Elrayess, M., Torres, M., Halama, A., et al. (2015). Metabolomics of dates (*Phoenix dactylifera*) reveals a highly dynamic ripening process accounting for major variation in fruit composition. *BMC Plant Biol.* 15:291. doi: 10.1186/s12870-015-0672-5

Dixon, J., and Hewett, E. W. (2000). Factors affecting apple aroma/flavor volatile concentration a review. *N. Z. J. Crop Hort. Sci.* 28, 155–173. doi: 10.1080/01140671.2000.9514136

Djordjevic, J., Zatorre, R. J., and Jones-Gotman, M. (2004). Odor-induced changes in taste perception. *Exp. Brain Res.* 159, 405–408. doi: 10.1007/s00221-004-2103-y

Dowson, V. H. W., and Aten, A. (1962). *Dates, Handling, Processing and Packing.* Rome: Food and Agriculture Organization.

Einspahr, D., Van Buijtenen, P., and Peckham, J. (1963). Natural variation and heritability in triploid Aspen. *Silvae Genet.* 12, 51–58.

El Arem, A., Flamini, G., Saffi, E. B., Issaoui, M., Zayene, N., Ferchichi, A., et al. (2011). Chemical and aroma volatile compositions of date palm (*Phoenix dactylifera* L.) fruits at three maturation stages. *Food Chem.* 127, 1744–1754. doi: 10.1016/j.foodchem.2011.02.051

El Arem, A., Saafi, E., Flamini, G., Issaoui, M., Ferchichi, A., Hammami, M., et al. (2012). Volatile and nonvolatile chemical composition of some date fruits (*Phoenix dactylifera* L.) harvested at different stages of maturity. *Int. J. Food Sci. Technol.* 47, 549–555.

El-Sabea, A. M. R., Faleiro, J. R., and Abo-El-Saad, M. M. (2009). The threat of red palm weevil *Rhynchophorus ferrugineus* to date plantations of the Gulf region in the Middle-East: an economic perspective. *Outlooks Pest Manage.* 20, 131–134.

El-Sayed, A. M. (2021). *The Pherobase: Database of Pheromones and Semiochemicals*. Available online at: https://www.pherobase.com (accessed April 6, 2021).

Elshibli, S., and Korpelainen, H. (2009). Biodiversity of date palms (*Phoenix dactylifera* L.) in Sudan: chemical, morphological and DNA polymorphisms of selected cultivars. *Plant Genet. Resour.* 7, 194–203.

Fan, Z., Hasing, T., Johnson, T. S., Johnson, T., Garner, D. M., Schwieterman, M. L., et al. (2021). Strawberry sweetness and consumer preference are enhanced by specific volatile compounds. *Hortic. Res.* 8:66.

Farag, M. A., Mohsen, M., Heinke, R., and Wessjohann, L. A. (2014). Metabolomic fingerprints of 21 date palm fruit varieties from Egypt using UPLC/PDA/ESI-qTOF-MS and GC-MS analyzed by chemometrics. *Food Res. Int.* 64, 218–226. doi: 10.1016/j.foodres.2014.06.021

Fayadh, J. M., and Al-Showiman, S. S. (1990). Chemical composition of date palm (*Phoenix dactylifera* L.). *J. Chem. Soc. Pak.* 12, 84–102.

Felemban, A., Braguy, J., Zurbriggen, M. D., and Al-Babili, S. (2019). Apocarotenoids involved in plant development and stress response. *Front. Plant Sci.* 10:1168. doi: 10.3389/fpls.2019.01168

Flowers, J. M., Hazzouri, K. M., Gros-Balthazard, M., Mo, Z., Koutroumpa, K., Perrakis, A., et al. (2019). Cross-species hybridization and the origin of North African date palms. *Proc. Nat. Acad. Sci. U.S.A.* 116, 1651–1658. doi: 10.1073/pnas.1817453116

Fuller, D. Q. (2018). Long and attenuated: comparative trends in the domestication of tree fruits. *Veg. Hist. Archaeobot.* 27, 165–176. doi: 10.1007/s00334-017-0659-2

Garcia, E. J., McDowell, T., Ketola, C., Jennings, M., Miller, J. D., and Renaud, J. B. (2020). Metabolomics reveals chemical changes in *Acer saccharum* sap over a maple syrup production season. *PLoS One* 15:e0235787. doi: 10.1371/journal.pone.0235787

Ghnimi, S., Al-Shibli, M., Al-Yammahi, H. R., Al-Dhaheri, A., Al-Jaberi, F., Jobe, B., et al. (2018). Reducing sugars, organic acids, size, color, and texture of 21 Emirati date fruit varieties (*Phoenix dactylifera*, L.). *NFS J.* 12, 1–10.

Ghnimi, S., Umer, S., Karim, A., and Kamal-Eldin, A. (2017). Date fruit (*Phoenix dactylifera* L.): an underutilized food seeking industrial valorization. *NFS J.* 6, 1–10.

Gross, J., Haber, O., and Ikan, R. (1983). The carotenoid pigments of the date. *Sci. Hortic.* 20, 251–257. doi: 10.1016/0304-4238(83)90005-5

Gu, Z. (2016). Complex heatmaps reveal patterns and correlations in multidimensional genomic data. *Bioinformatics* 32, 2847–2849. doi: 10.1093/bioinformatics/btw313

Guarino, S., Colazza, S., Peri, E., Bue, P. L., Germanà, M. P., Kuznetsova, T., et al. (2015). Behaviour-modifying compounds for management of the red palm weevil (*Rhynchophorus ferrugineus* Oliver). *Pest Manage. Sci.* 71, 1605–1610. doi: 10.1002/ps.3966

Gunawardena, N. E., Kern, F., Janssen, E., Meegoda, C., Schäfer, D., Vostrowsky, O., et al. (1998). Host attractants for red weevil *Rhynchophorus ferrugineus*: identification, electrophysiological activity, and laboratory bioassay. *J. Chem. Ecol.* 24, 425–437.

Haider, M. S., Khan, I. A., Jaskani, M. J., Naqvi, S. A., and Khan, M. M. (2014). Biochemical attributes of dates at three maturation stages. *Emirates J. Food Agric.* 26, 953–962.

Hamad, I., AbdElgawad, H., Al Jaouni, S., Zinta, G., Asard, H., Hassan, S., et al. (2015). Metabolic analysis of various date palm fruit (*Phoenix dactylifera* L.) cultivars from Saudi Arabia to assess their nutritional quality. *Molecules* 20, 13620–13641. doi: 10.3390/molecules200813620

Harrak, H., Reynes, M., Lebrun, M., Hamouda, A., and Brat, P. (2005). Identification and comparison of volatile components of fruits of eight Moroccan date varieties. *Fruits* 60, 267–278.

Hatem, A., Al-Khalifa, A. R., Farouk, A., and Shaheen, M. (2018). Effect of maturation stages on flavor profile and antioxidant activity of date palm fruits (*Phoenix dactylifera*) grown in Saudi Arabia. *Int. J. Pharm.* 14, 407–414.

Hazzouri, K. M., Flowers, J. M., Visser, H. J., Khierallah, H. S. M., Rosas, U., Pham, G. M., et al. (2015). Whole genome re-sequencing of date palms yields insights into diversification of a fruit tree crop. *Nat. Commun.* 6:8824. doi: 10.1038/ncomms9824

Hazzouri, K. M., Gros-Balthazard, M., Flowers, J. M., Copetti, D., Lemansour, A., Lebrun, M., et al. (2019). Genome-wide association mapping of date palm fruit traits. *Nat. Commun.* 10:4680. doi: 10.1038/s41467-019-12604-9

Hu, K., Jin, G.-J., Mei, W.-C., Li, T., and Tao, Y.-S. (2018). Increase of medium-chain fatty acid ethyl ester content in mixed H. uvarum/S. cerevisiae

fermentation leads to wine fruit aroma enhancement. *Food Chem.* 239, 495–501. doi: 10.1016/j.foodchem.2017.06.151

Ismail, B., Haffar, I., Baalbaki, R., and Henry, J. (2001). Development of a total quality scoring system based on consumer preference weightings and sensory profiles: application to fruit dates (Tamr). *Food Qual. Prefer.* 12, 499–506. doi: 10.1016/s0950-3293(01)00043-x

Jaddou, H., Mhaisen, M. T., and Al-Hakim, M. (1984). Flavour volatile analysis of Zahdi dates by gas liquid chromatography. *Date Palm. J.* 3, 367–379.

Kamal-Eldin, A., and Ghnimi, S. (2018). Classification of date fruit (*Phoenix dactylifera*, L.) based on chemometric analysis with multivariate approach. *J. Food Meas. Charact.* 12, 1020–1027.

Kanner, J., Elmaleh, H., Reuveni, O., and Ben-gera, I. (1978). Invertase (β-fructofuranosidase) activity in three date cultivars. *J. Agric. Food Chem.* 26, 1238–1240.

Khalil, M. N. A., Fekry, M. I., and Farag, M. A. (2017). Metabolome based volatiles profiling in 13 date palm fruit varieties from Egypt via SPME GC-MS and chemometrics. *Food Chem.* 217, 171–181. doi: 10.1016/j.foodchem.2016.08.089

Klee, H. J., and Tieman, D. M. (2018). The genetics of fruit flavour preferences. *Nat. Rev. Genet.* 19, 347–356. doi: 10.1038/s41576-018-0002-5

Li, L., Ma, X.-W., Zhan, R.-L., Wu, H.-X., Yao, Q.-S., Xu, W.-T., et al. (2017). Profiling of volatile fragrant components in a mini-core collection of mango germplasms from seven countries. *PLoS One* 12:e0187487. doi: 10.1371/journal.pone.0187487

Marondedze, C., Gehring, C., and Thomas, L. (2014). Dynamic changes in the date palm fruit proteome during development and ripening. *Hortic. Res.* 1:14039. doi: 10.1038/hortres.2014.39

Mathieu, S., Cin, V. D., Fei, Z., Li, H., Bliss, P., Taylor, M. G., et al. (2009). Flavour compounds in tomato fruits: identification of loci and potential pathways affecting volatile composition. *J. Exp. Bot.* 60, 325–337. doi: 10.1093/jxb/ern294

Mezroua, E. Y., Agli, A., Flamini, G., Boudalia, S., and Oulamara, H. (2017). Aroma characterization of ripe date fruits (*Phoenix dactylifera* L.) from Algeria. *Afr. J. Biotechnol.* 16, 2054–2061.

Müller, R., and Rappert, S. (2010). Pyrazines: occurrence, formation and biodegradation. *Appl. Microbiol. Biotechnol.* 85, 1315–1320. doi: 10.1007/s00253-009-2362-4

Müller-Linow, M., Weckwerth, W., and Hutt, M.-T. (2007). Consistency analysis of metabolic correlation networks. *BMC Syst. Biol.* 1:44. doi: 10.1186/1752-0509-1-44

Myhara, R. M., Karkalas, J., and Taylor, M. S. (1999). The composition of maturing Omani dates. *J. Sci. Food Agric.* 79, 1345–1350.

Narain, N. (2007). Volatile compounds in date palm fruit. *Acta Hortic.* 736, 261–266.

Oehlschlager, A. C. (2016). Palm weevils pheromones: discovery and use. *J. Chem. Ecol.* 42, 617–630.

Popenoe, P. B. (1913). *Date Growing in the Old World and the New*. Los Angeles, CA: Press of George Rice and Sons.

Rambla, J. L., Medina, A., Fernández-del-Carmen, A., Barrantes, W., Grandillo, S., Cammareri, M., et al. (2017). Identification, introgression, and validation of fruit volatile QTLs from a red-fruited wild tomato species. *J. Exp. Bot.* 68, 429–442. doi: 10.1093/jxb/erw455

Reynes, M., LeBrun, M., and Shaw, P. E. (1996). Identification of volatile date components and use of multivariate analysis to distinguish date varieties. *J. Food Qual.* 19, 505–514.

Samarawira, I. (1983). Date palm, potential source for refined sugar. *Econ. Bot.* 37, 181–186.

Serrano, M., Pretel, M. T., Botella, M. A., and Amoros, A. (2001). Physicochemical changes during date ripening related to ethylene production. *Food Sci. Technol. Int.* 7, 31–36. doi: 10.1177/108201301772662662

Siddeeg, A., Zeng, X. A., Ammar, A. F., and Han, Z. (2019). Sugar profile, volatile compounds, composition and antioxidant activity of Sukkari date palm fruit. *J. Food Sci. Technol.* 56, 754–762. doi: 10.1007/s13197-018-3534-y

Song, J., and Forney, C. F. (2008). Flavour volatile production and regulation in fruit. *Can. J. Plant Sci.* 88, 537–550.

Soroker, V., Harari, A., and Faleiro, J. R. (2015). "The role of semiochemicals in date pest management," in *Sustainable Pest Management in Date Palm: Current Status and Emerging Challenges*, eds W. Wakil, J. R. Faleiro, and T. Miller (Cham: Springer), 315–346.

Steingass, C. B., Vollmer, K., Metwali, E. M. R., Kadasa, N. M. S., Almaghrabi, O. A., Schweiggert, R., et al. (2020). Chlorophyll and carotenoid patterns of middle eastern date (*Phoenix dactylifera*) fruit at different maturity stages. *Int. J. Agric. Biol.* 23, 845–850.

Steinsaltz, D., Dahl, A., and Wachter, K. (2020). On negative heritability and negative estimates of heritability. *Genetics* 215, 343–357. doi: 10.1534/genetics.120.303161

Tadmor, Y., Fridman, E., Gur, A., Larkov, O., Lastochkin, E., Ravid, U., et al. (2002). Identification of malodorous, a wild species allele affecting tomato aroma that was selected against during domestication. *J. Agric. Food Chem.* 50, 2005–2009. doi: 10.1021/jf011237x

Tikunov, Y., Lommen, A., Ric de Vos, C. H., Verhoeven, H. A., Bino, R. J., Hall, R. D., et al. (2005). A novel approach to nontargeted data analysis for metabolomics. Large-scale profiling of tomato fruit volatiles. *Plant Physiol.* 139, 1125–1137. doi: 10.1104/pp.105.068130

Ueda, Y., and Ogata, K. (1977). Coenzyme A-dependent esterification of alcohols and acids in separated cells of banana pulp and its homogenate. *Nippon Shokuhin Kogyo Gakkaishi* 24, 624–630. doi: 10.3136/nskkk1962.24.624

Zaid, A., and Arias-Jiménez, E. J. (1999). *Date Palm Cultivation*. Rome: Food and Agriculture Organization.

Zaid, A., and de Wet, P. F. (2002). "Botanical and systematic description of the date palm," in *Date Palm Cultivation. FAO Plant Production and Protection Paper no. 156*, ed. A. Zaid (Rome: Food and Agriculture Organization), 1–28.

Zhao, J., Liu, J., Wang, F., Wang, S., Feng, H., Xie, X., et al. (2020). Volatile constituents and ellagic acid formation in strawberry fruits of selected cultivars. *Food Res. Int.* 138:109767. doi: 10.1016/j.foodres.2020.109767

Zsuffa, L. (1975). Broad sense heritability values and possible genetic gains in clonal selection of *Pinus griffithii* McClelland x *P. strobus* L. *Silvae Genet.* 24, 85–88.

Conflict of Interest: The authors declare that the research was conducted in the absence of any commercial or financial relationships that could be construed as a potential conflict of interest.

Publisher's Note: All claims expressed in this article are solely those of the authors and do not necessarily represent those of their affiliated organizations, or those of the publisher, the editors and the reviewers. Any product that may be evaluated in this article, or claim that may be made by its manufacturer, is not guaranteed or endorsed by the publisher.

frontiers in Plant Science

ORIGINAL RESEARCH
published: 22 March 2022
doi: 10.3389/fpls.2022.868319

Chemical Composition of Lipophilic Compounds From Rice (*Oryza sativa*) Straw: An Attractive Feedstock for Obtaining Valuable Phytochemicals

*Mario J. Rosado†, Gisela Marques†, Jorge Rencoret, Ana Gutiérrez and José C. del Río**

Instituto de Recursos Naturales y Agrobiología de Sevilla, CSIC, Seville, Spain

OPEN ACCESS

Edited by:
María Serrano, Miguel Hernández University of Elche, Spain

Reviewed by:
Simon Hammann, University of Erlangen Nuremberg, Germany
Nereida Cordeiro, University of Madeira, Portugal

***Correspondence:**
José C. del Río
delrio@irnase.csic.es

†These authors have contributed equally to this work and share first authorship

Specialty section:
This article was submitted to Crop and Product Physiology, a section of the journal Frontiers in Plant Science

Received: *02 February 2022*
Accepted: *04 March 2022*
Published: *22 March 2022*

Citation:
Rosado MJ, Marques G, Rencoret J, Gutiérrez A and del Río JC (2022) Chemical Composition of Lipophilic Compounds From Rice (Oryza sativa) Straw: An Attractive Feedstock for Obtaining Valuable Phytochemicals. Front. Plant Sci. 13:868319. doi: 10.3389/fpls.2022.868319

Rice (*Oryza sativa* L.) straw is a highly abundant, widely available, and low cost agricultural waste that can be used as a source to extract valuable phytochemicals of industrial interest. Hence, in the present work, the chemical composition of the lipophilic compounds present in rice straw was thoroughly characterized by gas chromatography and mass spectrometry using medium-length high-temperature capillary columns, which allowed the identification of a wide range of lipophilic compounds, from low molecular weight fatty acids to high molecular weight sterols esters, sterol glucosides, or triglycerides in the same chromatogram. The most abundant lipophilic compounds in rice straw were fatty acids, which accounted for up to 6,400 mg/kg (41.0% of all identified compounds), followed by free sterols (1,600 mg/kg; 10.2%), sterol glucosides (1,380 mg/kg; 8.8%), fatty alcohols (1,150 mg/kg; 7.4%), and triglycerides (1,140 mg/kg; 7.3%), along with lower amounts of high molecular weight wax esters (900 mg/kg; 5.8%), steroid ketones (900 mg/kg; 5.8%), monoglycerides (600 mg/kg; 3.8%), alkanes (400 mg/kg; 2.6%), diglycerides (380 mg/kg; 2.4%), sterol esters (380 mg/kg; 2.4%), tocopherols (340 mg/kg; 2.2%), and steroid hydrocarbons (60 mg/kg; 0.4%). This information is of great use for the valorization of rice straw to obtain valuable lipophilic compounds of interest for the nutraceutical, pharmaceutical, cosmetic, and chemical industries. Moreover, this knowledge is also useful for other industrial uses of rice straw, as in pulp and papermaking, since some lipophilic compounds are at the origin of the so-called pitch deposits during pulping.

Keywords: rice straw, phytochemicals, fatty acids, sterols, sterol glucosides, tocopherols

INTRODUCTION

Rice (*Oryza sativa* L.) is one of the most important staple food crops used for human nutrition worldwide. In 2020, paddy fields accounted for up to 164 million cultivated hectares with a global rice production of 757 million Mt., with Asia contributing 90% of the world rice production followed by Africa (5%), the Americas (4%), and Europe (1%; FAOSTAT, 2022). Rice harvesting generates large amounts of wastes such as rice straw, which includes stems, leaves, and spikelets. With an estimated grain/straw ratio of around 1.5 (Lal, 2005), the annual

world production of rice straw is estimated to be around 1,130 million Mt. Nearly half of the rice straw is burnt for cogeneration of heat and power with the subsequent environmental problems while the rest is traditionally used as fodder or left for decomposition in landfills (Matsumura et al., 2005; Wang et al., 2016; Bhattacharyya et al., 2020; Kumar and Verma, 2021). Rice straw is also widely used as a raw material for papermaking in a variety of countries (Kaur et al., 2017; Elhelece, 2020). In recent years, however, there is great interest in developing approaches to exploit the potential of rice straw for biorefining, through conversion to biofuels and bioproducts (Abraham et al., 2016).

Rice straw is a lignocellulosic material essentially constituted of cellulose (24.0%), hemicelluloses (27.8%), and lignin (13.5%), with important amounts of ash (17%) that correspond mostly to silica (Rosado et al., 2021). Due to the significant amounts of carbohydrates and lignin, and to its low price and high availability, rice straw has been considered a suitable feedstock for the production of biofuels, biochemicals, and biobased materials in the context of lignocellulosic biorefineries (Lal, 2005; Lu and Hsieh, 2012; Kalita et al., 2015; Abraham et al., 2016; Kumar et al., 2016; Gou et al., 2018; Swain et al., 2019; Bhattacharyya et al., 2020; Sharma et al., 2020). In addition, rice straw also presents significant amounts of lipophilic compounds (3.4%) that can also be used to obtain valuable phytochemicals of industrial interest (Rosado et al., 2021). Most of the functionally important plant-based compounds derive from food processing as by-products. Nevertheless, lignocellulosic wastes (cereal by-products such as wheat straw, rice husks, or maize fibers, among others) that are easily available at a very low cost are considered alternative sources for obtaining valuable phytochemicals (del Río et al., 2013a,b, 2015; Marques et al., 2020).

Plant lipophilic compounds comprise a wide range of chemical products (e.g., hydrocarbons, fatty acids, fatty alcohols, aldehydes, acylglycerols, terpenoids, and steroids) that present many applications in the pharmaceutical, nutraceutical, cosmetic, food, or chemical industries (Hernandez, 2005; Metzger and Bornscheuer, 2006; Tao, 2007; Rombaut et al., 2014; Sin et al., 2014; Carciochi et al., 2017; Attard et al., 2018). For example, fatty acids and acylglycerols are widely used for the production of biodiesel (Zhang et al., 2013) as well as cosmetics (Kalustian, 1985). Among the fatty acids, linoleic acid is an omega-6 essential unsaturated fatty acid of interest for the food and nutraceutical industries. Moreover, linoleic acid is also used in pharmaceutical and cosmetic products and is considered to influence the metabolic processes in the skin and to promote the activity of vitamins A and E and the restoration of the barrier properties of stratum corneum (Huang et al., 1999). On the other hand, plant sterols are also of interest in the food and nutraceutical industry because, when used as functional ingredients in foods, contribute to lowering blood cholesterol levels (Wilson et al., 2000; Quílez et al., 2003; Jones and AbuMweis, 2009), play an important role in the regulation of cardiovascular disease, and exhibit anticancer properties (Iwatsuki et al., 2003; Jones and AbuMweis, 2009). In addition, sterol ferulates, which are widely present in cereal bran oils, present anti-inflammatory effects and are also effective antitumor-promoters (Akihisa et al., 2000). Tocopherols and tocotrienols also have antioxidant properties and play a role in the prevention of certain types of cancer, heart disease, and other chronic ailments (Shahidi and De Camargo, 2016).

On the other hand, however, the presence of lipophilic compounds in the raw material can be detrimental during some industrial processing operations, such as during pulp and paper manufacturing. The lipophilic compounds can form organic deposits (called pitch) during pulp and paper production that have negative effects in the product as well as in the machinery and resulting in significant economic losses (del Río et al., 1998, 2000; Back and Allen, 2000; Gutiérrez et al., 2001, 2004). During alkaline cooking, the different lipophilic compounds exhibit different behavior. Thus, acylglycerols are completely hydrolyzed, and fatty acids are extensively dissolved forming fatty acid soaps. However, neutral compounds, particularly free sterols, fatty alcohols, sterol glycosides, steroid hydrocarbons, and steroid ketones, survive cooking and are difficult to remove in the washing stages due to their low water solubility, and therefore can be at the origin of the sticky deposits (pitch) in the pulp and in the machinery. It is, therefore, essential to know the exact nature of the lipophilic compounds in rice straw in order to maximize the exploitation of this important agricultural waste.

However, despite the importance and the enormous quantities of rice straw produced annually, there is a lack of studies reporting the detailed chemical composition of the lipophilic compounds in this material. Only a few studies describing the chemical composition of the lipophilic compounds in rice straw have been published, but with limited success. A previous work (Xiao et al., 2001) examined the composition of the lipophilic compounds in rice straw and reported free fatty acids, sterols, waxes, sterol esters, and triglycerides; however, the occurrence of significant amounts of resin acids, a group of compounds that is exclusively restricted to conifers, as well as other compounds such as cholesterol, which is not a typical plant sterol, raised the question of whether the sample studied was contaminated or whether the lipophilic compounds were properly identified. Another study reported only the composition of free fatty acids in rice straw, which were dominated by palmitic, and oleic acids, with significant amounts of linoleic and stearic acids (Zemnukhova et al., 2015). Finally, Zhao et al. (2007) also reported some lipophilic compounds in rice straw, including some tocopherols and steroid compounds, although the identities of the reported steroids presented many inconsistencies and most of them may have been misidentified because they are rarely present in plants. Therefore, a comprehensive and detailed description of the chemical composition of the lipophilic compounds present in rice straw is still pending.

In this work, the lipophilic compounds in rice straw were analyzed by gas chromatography-mass spectrometry (GC-MS) using a medium-length, high-temperature capillary column, with thin films, according to the method developed by our group that allowed the elution and identification of a wide range of components, from low molecular weight fatty acids to high molecular weight sterol esters or triglycerides (Gutiérrez et al., 1998, 2004). The results

presented here will greatly improve our understanding of the lipophilic compounds in rice straw and will help to maximize the exploitation of this important agricultural waste.

MATERIALS AND METHODS

Samples

Rice (*Oryza sativa* L., var. Indica, Puntal) was harvested from a paddy field in Isla Mayor (Southern Spain). Samples of rice straw were brought to the laboratory, air-dried, and crushed using an IKA knife mill (Janke and Kunkel, Staufen, Germany) with 1-mm screen. The samples were then extracted with acetone in a Soxhlet for 8 h. The extracts were brought to dryness using a rotary evaporator and were further determined gravimetrically, accounting for 3.4% ± 0.1 (dry-basis). The determination was performed in triplicate. The moisture content of the rice straw was determined by drying the sample in an oven at 105°C for 24 h.

GC-MS Analysis of Lipophilic Compounds in Rice Straw

The acetone extracts were redissolved in chloroform and subsequently analyzed by GC-MS both underivatized, and after derivatization with bis(trimethylsilyl)trifluoroacetamide (BSTFA), using the equipment and experimental conditions previously described (del Río et al., 2016). The different compounds were identified by comparison of their mass spectra with those in the NIST library, by comparison with literature (Lauer et al., 1970; Curstedt, 1974; Evershed et al., 1989; Snyder et al., 1993; Gutiérrez and del Río, 2001; del Río et al., 2009, 2013a, 2015, 2016), and when possible by comparison with authentic standards (alkanes from *n*-octadecane to *n*-hentriacontane, alcohols from *n*-hexadecanol to *n*-octacosanol, saturated fatty acids from *n*-tetracosanoic acid to *n*-eicosanoic acid, the unsaturated fatty acids oleic, linoleic, and linolenic acids; the sterols campesterol, stigmasterol, sitosterol, and their respective 3β-D-glucopyranosides; the sterol esters cholesteryl palmitate, cholesteryl oleate, and cholesteryl linoleate; the wax ester tetradecyl tetradecanoate; and the acylglycerols 1-monopalmitin, 1,3-dipalmitin, tripalmitin, triolein, and trilinolein). Quantification was performed by using a mixture of authentic external standards (palmitic acid, linoleic acid, stigmasterol, sitosterol, cholesteryl linoleate, sitosteryl 3β-D-glucopyranoside, 1-monopalmitin, 1,3-dipalmitin, tripalmitin, and tetracosane) in a concentration range between 0.1 and 1 mg/mL, and the calibration curves and response factors were determined for each of them. The correlation coefficient was higher than 0.99 in all cases. All peaks were quantified by peak area. Quantification was given as the mean of three replicates.

RESULTS AND DISCUSSION

Lipophilic Constituents in Rice Straw

The lipophilic compounds in rice straw accounted for 3.4% on a dry-basis. The composition of the lipophilic extracts (both underivatized and as their TMS-ether derivatives) were analyzed by GC-MS using high-temperature medium-length capillary columns according to the method previously described, that allowed the identification of high molecular weight compounds, as sterol glycosides, sterol esters, high molecular weight wax esters, and triglycerides (Gutiérrez et al., 1998, 2004). The chromatograms of the underivatized and the TMS-ether derivatives of the lipophilic compounds from rice straw are shown in **Figure 1**. The identities and abundances (as mg/kg, dry-weight basis) of the main lipophilic compounds identified are detailed in **Table 1**. Several classes of compounds were identified by GC-MS, including *n*-fatty acids, *n*-alkanes, tocopherols, steroid hydrocarbons, steroid ketones, free sterols, sterol esters, sterol glucosides, mono-, di-, and triglycerides, and high molecular weight ester waxes. Structures representatives of the main aliphatic compounds identified in rice straw are depicted in **Figure 2**, whereas structures representatives of the main steroid compounds are shown in **Figure 3**.

The relative abundances of the different classes of lipophilic compounds in rice straw are depicted in the histogram of **Figure 4**. The most abundant class of lipophilic compounds were series of fatty acids, that accounted for up to 41.0% of all compounds identified, followed by free sterols (10.2%), sterol glucosides (8.8%), fatty alcohols (7.4%), and triglycerides (7.3%), together with lower amounts of high molecular weight wax esters (5.8%), steroid ketones (5.8%), monoglycerides (3.8%), alkanes (2.6%), diglycerides (2.4%), sterol esters (2.4%), tocopherols (2.2%), and steroid hydrocarbons (0.4%). A series of peaks appeared in the chromatogram of the TMS-ether derivatives around 11–13 min (marked with asterisks), but their identities could not be fully established. The mass spectra of these peaks exhibited characteristic fragments of carbohydrates (*m/z* 147, 217, 361), suggesting that they might belong to glycolipids, but it did not show any other diagnostic fragment that might provide additional clues to their identities. Some glycolipids have been reported to occur among the lipophilic compounds of rice extracts, as the mono- and digalactosyl monoacylglycerols and the mono- and digalatosyl diacylglycerols (Moazzami et al., 2011). Interestingly, these peaks from unknown glycolipids also appeared in rice husks (Marques et al., 2020), suggesting that they might be typical compounds of rice.

It is important to note that the acetone extracts in rice straw represent 3.4% (dry-basis) or 34 mg/kg, while the sum of the amounts of the different lipophilic compounds identified in **Table 1** is around 15.6 mg/kg. This discrepancy is most likely due to the occurrence in the acetone extracts of polar compounds that have not been quantified, as well as high molecular weight compounds that are out of the analytical window of our procedure.

Aliphatic Series

The main aliphatic compounds identified in rice straw were series of free *n*-fatty acids, acylglycerols (mono-, di-, and triglycerides), high molecular weight esters, *n*-fatty alcohols, *n*-alkanes, as well as small amounts of tocopherols. The distributions of the series of *n*-alkanes, *n*-fatty alcohols, *n*-fatty acids, and monoglycerides are represented in the histograms of **Figure 5**.

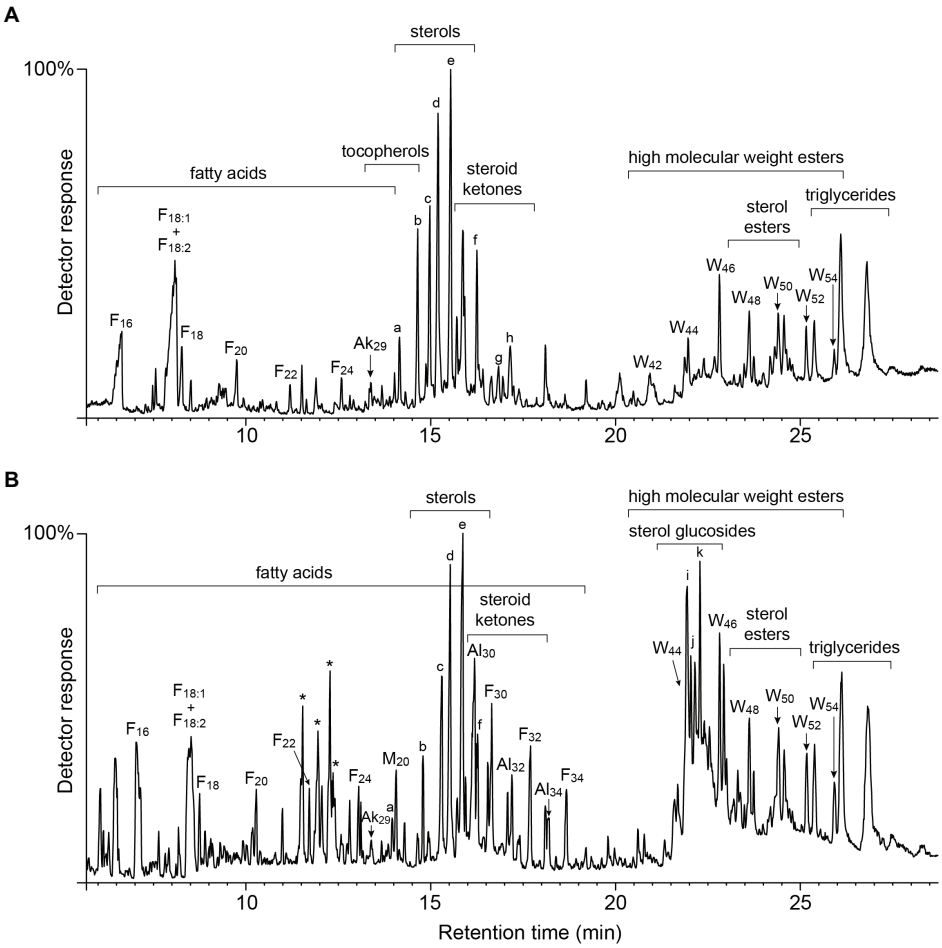

FIGURE 1 | GC-MS chromatograms of the acetone extracts from rice straw, **(A)** underivatized, and **(B)** as TMS-ether derivatives. F(n), *n*-fatty acid series; Al(n), *n*-fatty alcohol series; Ak(n), *n*-alkanes; M(n), monoglycerides; and W(n), high molecular weight esters. Labels for selected compounds are as: (**a**), γ-tocopherol; (**b**), α-tocopherol; (**c**), campesterol; (**d**), stigmasterol; (**e**), sitosterol; (**f**), stigmast-4-en-3-one; (**g**), ergostane-3,6-dione; (**h**), stigmastane-3,6-dione; (**i**), campesteryl 3β-D-glucopyranoside; (**j**), stigmasteryl 3β-D-glucopyranoside; and (**k**), sistosteryl 3β-D-glucopyranoside. *unknown compounds, possibly glycolipids, referred in the text.

The series of *n*-alkanes in rice straw accounted for 400 mg/kg, and ranged from *n*-pentacosane (C_{25}) to *n*-hentriacontane (C_{31}), with a strong predominance of the odd carbon atom number homologues and with maximum for *n*-nonacosane (C_{29}; **1**), that accounted for 152 mg/kg, as shown in **Figure 5A**. This is the first time that the series of *n*-alkanes have been reported in rice straw. A previous paper indicated the occurrence of tetratriacontane (C_{34}) and pentatriacontane (C_{35}) in rice straw (Zhao et al., 2007); however, the identities of these alkanes may have been erroneously assigned as their relative retention times did not correspond to these compounds; and in our opinion, this paper presented many inconsistencies and most of the identifications reported there should be taken with caution. Alkanes could not be identified in the respective rice husks waste (Marques et al., 2020) but were reported in similar amounts (371 m/kg) in the related wheat straw (del Río et al., 2013a).

The series of fatty alcohols was also identified in rice straw in important amounts, accounting for a total of 1,150 mg/kg. The series ranged from *n*-octacosanol (C_{28}) to *n*-hexatriacontanol (C_{36}), with the exclusive presence of the even carbon atom number homologues, and with maximum for *n*-triacontanol (C_{30}; **2**) that accounted for 440 mg/kg, as depicted in **Figure 5B**. This is the first time that the series of fatty alcohols were reported among the lipophilic compounds of rice straw as they were not identified in previous studies (Xiao et al., 2001; Zhao et al., 2007). Fatty alcohols were also reported, although to a lesser extent (340 mg/kg) in the respective rice husks waste (Marques et al., 2020), but higher amounts of alcohols (1,615 mg/kg) were reported in the related wheat straw (del Río et al., 2013a).

Free fatty acids were the most abundant class of lipophilic compounds in rice straw, accounting for a total of 6,400 mg/kg. The content of fatty acids was higher than in the respective rice husks, with 2,770 mg/kg (Marques et al., 2020), and in the related wheat straw, with only 2,080 mg/kg (del Río et al., 2013a). The series of saturated fatty acids ranged from *n*-hexadecanoic acid (C_{16}; palmitic acid, **3**) to *n*-tetratriacontanoic acid (C_{34}), with a strong predominance of the even carbon atom number homologues, and a bimodal distribution with

TABLE 1 | Composition and abundance (mg/kg, on a dry-basis) of the compounds identified in rice straw (in parenthesis are the percentages referred to the total compounds identified).

Compounds	mg/kg (%)		mg/kg (%)
***n*-Alkanes**	**400 ± 20 (2.6%)**	**Triglycerides**	**1,140 ± 120 (7.3%)**
n-pentacosane	32	C_{51} (tripalmitin)	180
n-hexacosane	12	C_{55} (palmitoyldiolein + palmitoyldilinolein)	492
n-heptacosane	70	C_{57} (trilinolein + triolein, **9**)	468
n-octacosane	30		
n-nonacosane (**1**)	152	**High molecular weight esters**	**900 ± 50 (5.8%)**
n-triacontane	40	esters C_{42}	36
n-hentriacontane	64	esters C_{44}	116
		esters C_{46} (**10**)	204
***n*-Fatty alcohols**	**1,150 ± 30 (7.4%)**	esters C_{48}	180
n-octacosanol	102	esters C_{50}	164
n-triacontanol (**2**)	440	esters C_{52}	124
n-dotriacontanol	370	esters C_{54}	76
n-tetratriacontanol	176		
n-hexatriacontanol	62	**Tocopherols**	**340 ± 40 (2.2%)**
		α-tocopherol (**11**)	220
***n*-Fatty acids**	**6,400 ± 200 (41.0%)**	α-tocopherol acetate (**12**)	30
n-hexadecanoic acid (**3**)	650	γ-tocopherol (**13**)	80
n-heptadecanoic acid	110	δ-tocopherol (**14**)	10
$C_{18:2}$ (*cis,cis*-octadeca-9,12-dienoic acid, **4**)	1,200		
$C_{18:1}$ (*cis*-octadec-9-enoic acid, **5**)	740	**Sterols**	**1,600 ± 50 (10.2%)**
n-octadecanoic acid	394	campesterol (**15**)	312
n-nonadecanoic acid	80	campestanol (**16**)	10
n-eicosanoic acid	375	stigmasterol (**17**)	528
n-heneicosanoic acid	100	sitosterol (**18**)	600
n-docosanoic acid	286	stigmastanol (**19**)	80
n-tricosanoic acid	114	7-oxo-sitosterol (**20**)	14
n-tetracosanoic acid	336	Δ^7-campesterol (**21**)	36
n-pentacosanoic acid	108	Δ^7-stigmastenol (**22**)	10
n-hexacosanoic acid	165	Δ^5-avenasterol (**23**)	10
n-heptacosanoic acid	40		
n-octacosanoic acid	296	**Steroid ketones**	**900 ± 20 (5.8%)**
n-nonacosanoic acid	54	ergost-4-en-3-one (**24**)	112
n-triacontanoic acid	520	stigmasta-4,22-dien-3-one (**25**)	360
n-hentriacontanoic acid	80	stigmasta-3,5-dien-7-one (**26**)	30
n-dotriacontanoic acid	464	stigmast-4-en-3-one (**27**)	248
n-tritriacontanoic acid	50	ergostane-3,6-dione (**28**)	50
n-tetratriacontanoic acid	238	stigmastane-3,6-dione (**29**)	100
Monoglycerides	**600 ± 80 (3.8%)**	**Steroid hydrocarbons**	**60 ± 10 (0.4)**
2,3-dihydroxypropyl hexadecanoate	68	stigmasta-3,5-diene	20
2,3-dihydroxypropyl octadeca-9,12-dienoate	86	stigmasta-3,5,22-triene (**30**)	40
2,3-dihydroxypropyl octadec-9-enoate	96		
2,3-dihydroxypropyl octadecanoate	40	**Sterol glucosides**	**1,380 ± 150 (8.8%)**
2,3-dihydroxypropyl eicosanoate (**6**)	220	campesteryl 3β-D-glucopyranoside	370
2,3-dihydroxypropyl docosanoate	56	stigmasteryl 3β-D-glucopyranoside	310
2,3-dihydroxypropyltetracosanoate	34	sitosteryl 3β-D-glucopyranoside (**31**)	700
Diglycerides	**380 ± 50 (2.4%)**	**Sterol sters**	**380 ± 30 (2.4%)**
1,2-dipalmitin	20	campesterol palmitate	26
1,3-dipalmitin	16	campesterol oleate/campesterol linoleate	58
1,2-palmitoylolein+1,2-palmitoyllinolein	60	stigmasterol palmitate	32
1,3-palmitoylolein+1,3-palmitoyllinolein	56	stigmasterol oleate/stigmasterol linoleate	76
1,2-diolein (**7**) +1,2-dilinolein+1,2-oleyllinolein	144	sitosterol palmitate	50
1,3-diolein (**8**) +1,3-dilinolein+1,3-oleyllinolein	84	sitosterol oleate/sitosterol linoleate (**32**)	138

Bold numbers in parenthesis refer to the structures depicted in **Figures 2**, **3**.

two maxima for *n*-hexadecanoic acid (650 mg/kg) and *n*-triacontanoic acid (C_{30}; 520 mg/kg), as depicted in **Figure 5C**. Large amounts of mono- ($C_{18:1}$; 740 mg/kg) and diunsaturated ($C_{18:2}$; 1,200 mg/kg) fatty acids were also identified. Although the experimental conditions used here, particularly the GC column, do not allow their unequivocal identification, they most likely correspond to oleic ($C_{18:1}$) and linoleic ($C_{18:2}$) acids, the most common unsaturated fatty acids in similar lignocellulosic residues. The distribution of free fatty acids is similar to that found in rice husks (Marques et al., 2020).

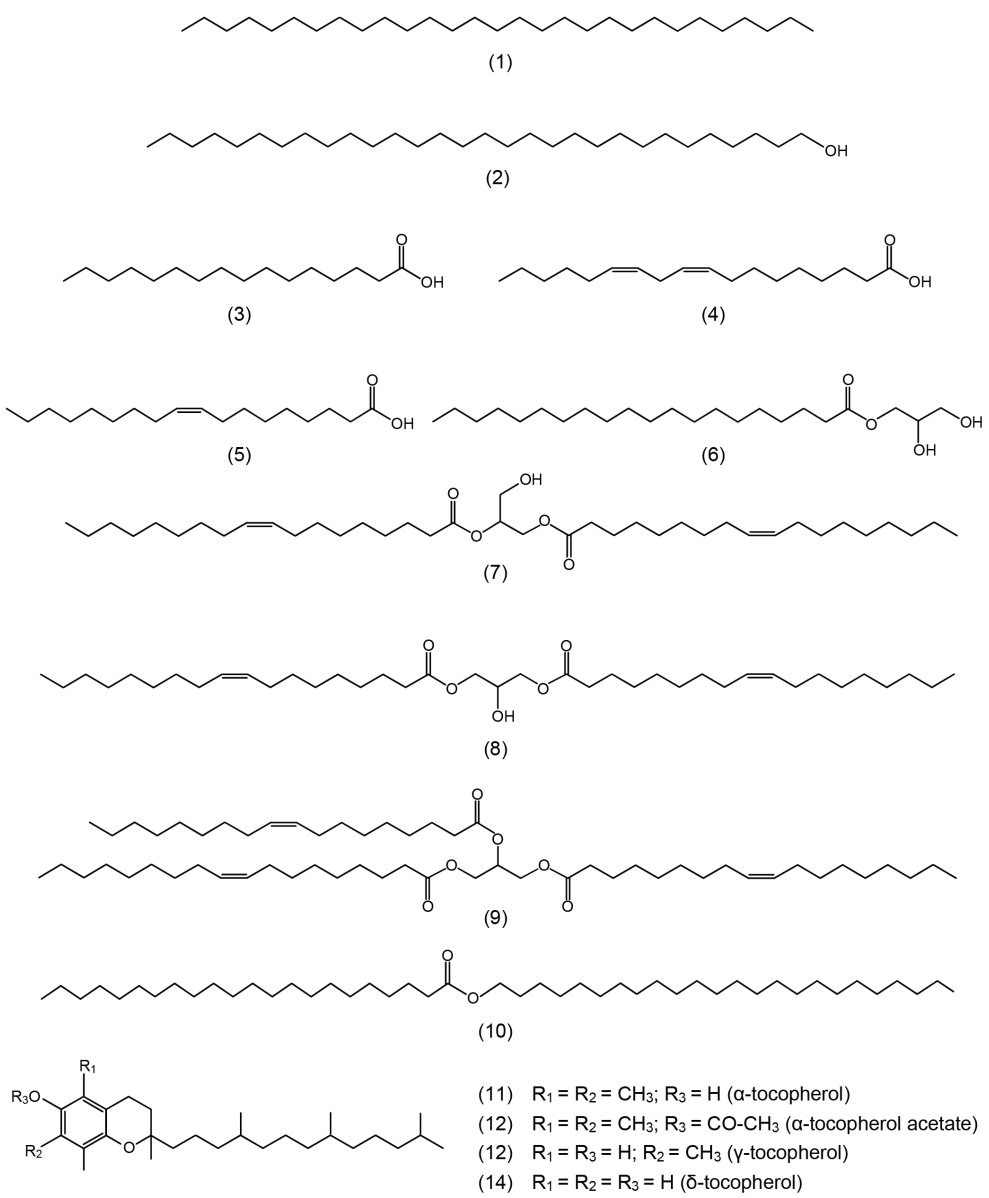

FIGURE 2 | Structures representative of the main aliphatic compounds identified in the acetone extracts of rice straw and referred in the text. **1**: *n*-nonacosane; **2**: *n*-triacontanol; **3**: *n*-hexadecanoic (palmitic) acid; **4**: *cis*,*cis*-octadeca-9,12-dienoic (linoleic) acid; **5**: *cis*-octadec-9-enoic (oleic) acid; **6**: 2,3-dihydroxypropyl eicosanoate; **7**: 1,2-diolein; **8**: 1,3-diolein; **9**: triolein; **10**: docosanoic acid, tetracosyl ester; **11**: α-tocopherol; **12**: α-tocopherol acetate; **13**: γ-tocopherol; and **14**: δ-tocopherol.

Previous works (Xiao et al., 2001; Zemnukhova et al., 2015) also reported a similar distribution of fatty acids in rice straw but failed to detect the high molecular weight fatty acids above tetracosanoic acid (C_{24}), which amounted up to a third of the total fatty acids identified. In the present work, the identification of the high molecular weight fatty acids was possible by the use of the methodology developed in our laboratories that used medium-length high-temperature capillary columns (Gutiérrez et al., 1998). Surprisingly, a previous work also reported the occurrence of abietic acid in rice straw (Xiao et al., 2001). However, abietic acid, like all other resin acids, is exclusively restricted to conifers and cannot occur in rice (a monocotyledonous plant), raising the question of whether this compound was misidentified or whether the sample studied was contaminated.

Acylglycerols (including mono-, di-, and triglycerides) were present in important amounts in rice straw, accounting for a total of 2,120 mg/kg. Triglycerides were the most abundant acylglycerols, accounting for 1,140 mg/kg, followed by monoglycerides (600 mg/kg) and diglycerides (380 mg/kg). In any case, the content of triglycerides in rice straw was much lower than those present in the respective rice husks where

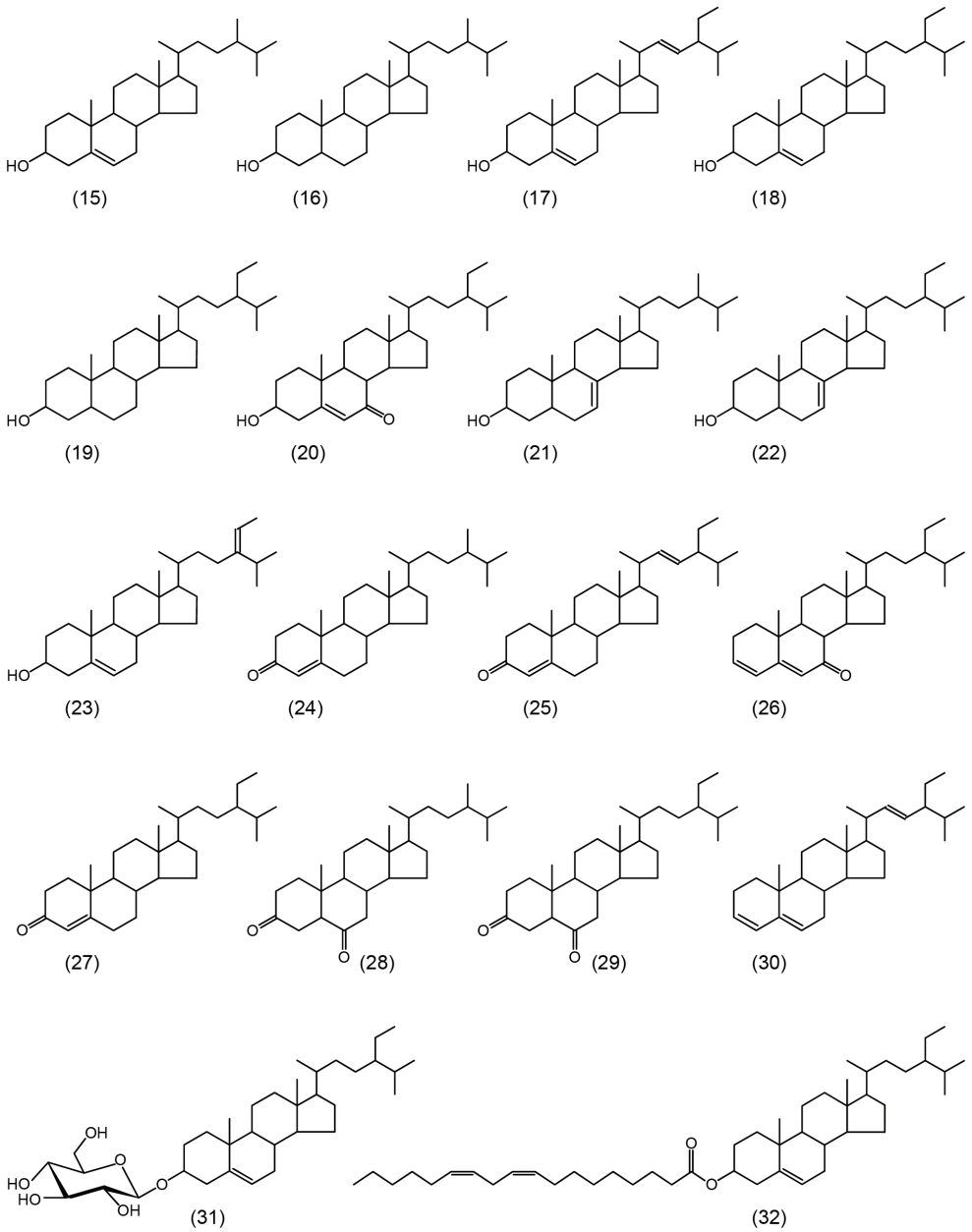

FIGURE 3 | Structures of the main steroid compounds identified in the acetone extracts of rice straw and referred in the text. **15**: campesterol; **16**: campestanol; **17**: stigmasterol; **18**: sitosterol; **19**: stigmastanol; **20**: 7-oxo-sitosterol; **21**: Δ^7-campesterol; **22**: Δ^7-stigmastenol; **23**: Δ^5-avenasterol; **24**: ergost-4-en-3-one; **25**: stigmasta-4,22-dien-3-one; **26**: stigmasta-3,5-dien-7-one; **27**: stigmast-4-en-3-one; **28**: ergostane-3,6-dione; **29**: stigmastane-3,6-dione; **30**: stigmasta-3,5,22-triene; **31**: sitosteryl 3β-D-glucopyranoside; and **32**: sitosteryl linoleate.

they accounted for up to 10,400 mg/kg (Marques et al., 2020). Previous papers only reported the occurrence of di- and triglycerides in rice straw but failed to detect monoglycerides (Xiao et al., 2001). In the present work, the series of monoglycerides were identified in the range from 2,3-dihydroxypropyl hexadecanoate (C_{16}, 1-monopalmitin) to 2,3-dihydroxypropyl tetracosanoate (C_{24}), with the occurrence of only the even carbon atom number homologues, and with 2,3-dihydroxypropyl eicosanoate (C_{20}, **6**) being the most abundant one (220 mg/kg), as depicted in **Figure 5D**. Significant amounts of the unsaturated 2,3-dihydroxypropyl octadec-9,12-dienoate ($C_{18:2}$, 1-monolinolein; 86 mg/kg) and 2,3-dihydroxypropyl octadec-9-enoate ($C_{18:1}$, 1-monoolein; 96 mg/kg) were also identified. On the other hand, the diglycerides identified in rice straw corresponded to different combinations of the saturated palmitic acid (C_{16}) and the unsaturated linoleic ($C_{18:2}$) and oleic ($C_{18:1}$) acids, with different substitution patterns (forming 1,2- and 1,3-isomers). The individual diglycerides could

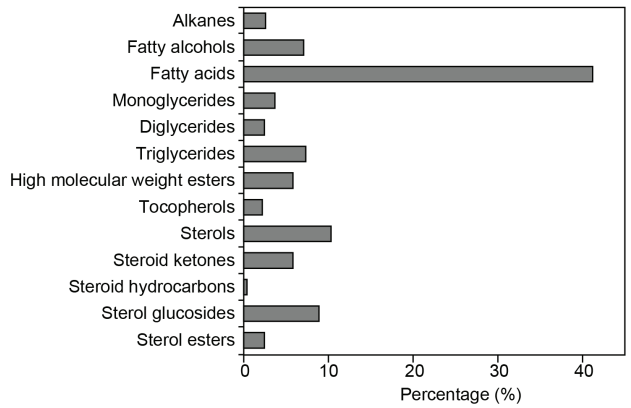

FIGURE 4 | Percentage of the main classes of lipophilic compounds identified in the acetone extracts of rice straw.

be identified by their mass spectra, as previously published (Curstedt, 1974). The diglycerides identified in rice straw were 1,2- and 1,3-dipalmitin, 1,2- and 1,3-palmitoylolein, 1,2- and 1,3-palmitoyllinolein, 1,2- and 1,3-diolein (**7**, and **8**), 1,2- and 1,3-dilinolein, and 1,2- and 1,3-oleyllinolein. Among the different diglycerides, a predominance of the 1,2- over the 1,3-isomers was observed, as also occurred with the diglycerides identified in the respective rice husks (Marques et al., 2020). A previous work reported only the occurrence of "dipalmitin" but did not indicate the substitution pattern (Xiao et al., 2001). Finally, triglycerides in rice straw appeared as a mixture of several compounds that eluted in three main chromatographic peaks that were separated by total carbon number (C_{51}, C_{55}, and C_{57}); however, identification of individual triglycerides in each peak could be achieved based on their mass spectra, as already reported (Lauer et al., 1970; del Río et al., 2016). The analyses indicated that the main triglycerides in rice straw were tripalmitin (180 mg/kg), palmitoyldiolein/palmitoyllinolein (492 mg/kg), and trilinolein/triolein (**9**, 468 mg/kg); a similar distribution pattern has been previously reported (Xiao et al., 2001).

A series of high molecular weight ester waxes were also found in rice straw in significant amounts (900 mg/kg). This series was formed by combinations of different long-chain fatty acids with different long-chain fatty alcohols that produced a wide variety of various long-chain ester waxes in the range from C_{42} to C_{54}. The identities of the different individual high molecular weight ester waxes were determined from their mass spectra, as already reported (del Río et al., 2009, 2013a). The mass spectra of long-chain esters were characterized by a base peak that corresponded to the protonated acid ion. Hence, the base peak provides information about the acid moiety while the molecular ion provided information of the total number of carbon atoms in the ester. It was then possible to determine the contribution of individual esters in every chromatographic peak by mass spectrometric determination of the molecular ion and the base peak. Quantitation of individual esters was accomplished by integrating the areas in the chromatographic profiles of the ions characteristic for the acidic moiety. The detailed composition of the different high molecular weight ester waxes identified in rice straw is shown in **Table 2**. The esterified fatty acids ranged from hexadecanoic (C_{16}) to tetracosanoic acid (C_{24}), whereas the esterified alcohols ranged from eicosanol (C_{20}) to tetratriacontanol (C_{34}). It is important to note the absence of unsaturated fatty acids forming long-chain ester waxes, despite the high abundance of unsaturated fatty acids (oleic and linoleic acids) present in free form in rice straw. The most prominent high molecular weight esters in rice straw were C_{46} (204 mg/kg), which was primarily constituted by docosanoic acid, tetracosyl ester (**10**), that accounted from 92 mg/kg. The high molecular weight ester waxes identified in the present work have not been reported previously in rice straw, although the occurrence of palmitic acid, palmityl ester, a C_{32} wax ester, along with smaller amounts of unsaturated esters, was reported in a previous paper (Xiao et al., 2001), but they could not be detected in the present work. High molecular weight esters were detected only in low amounts (60 mg/kg) in the respective rice husks (Marques et al., 2020), and in similar amounts (915 mg/kg) in the related wheat straw (del Río et al., 2013a).

Finally, different tocopherols were also found among the lipophilic compounds of rice straw, accounting for a total of 340 mg/kg. Tocopherols were identified by comparison with the mass spectra previously published (Snyder et al., 1993; del Río et al., 2015). The most predominant tocopherol was α-tocopherol (**11**) that accounted for 220 mg/kg, followed by γ-tocopherol (**13**, 80 mg/kg) and minor amounts of α-tocopherol acetate (**12**, 30 mg/kg) and δ-tocopherol (**14**, 10 mg/kg). The occurrence of α-tocopherol and α-tocopherol acetate in rice straw was already reported in a previous paper, although it failed to detect γ- and δ-tocopherols (Zhao et al., 2007). Among the tocopherols, α-tocopherol is the most abundant and active form of vitamin E in nature. Tocopherols have antioxidant properties and have a role in the prevention of certain types of cancer, as well as heart and other diseases (Shahidi and De Camargo, 2016). Tocopherols have been reported in rice husks (40 mg/kg), but in lower amounts than those found in the respective rice straw (Marques et al., 2020).

Steroid Compounds

Different families of steroid compounds were identified among the lipophilic compounds of rice straw, including steroid ketones, steroid hydrocarbons, free sterols, sterol glucosides, and sterol esters (**Table 1**; **Figure 3**), that in total amounted up to 4,320 mg/kg.

Free sterols were the most predominant class of steroids in rice straw, accounting for 1,600 mg/kg. The most important sterols identified were campesterol (**15**, 312 mg/kg), stigmasterol (**17**, 528 mg/kg), sitosterol (**18**, 600 mg/kg), and stigmastanol (**19**, 80 mg/kg). Other sterols were also identified in lower amounts, including campestanol (**16**, 10 mg/kg), 7-oxo-sitosterol (**20**, 14 mg/kg), Δ^7-campesterol (**21**, 36 mg/kg), Δ^7-stigmastenol (**22**, 10 mg/kg), and Δ^5-avenasterol (**23**, 10 mg/kg). Only stigmasterol and sitosterol, together with minor amounts of cholesterol, which is not a typical plant sterol, were previously

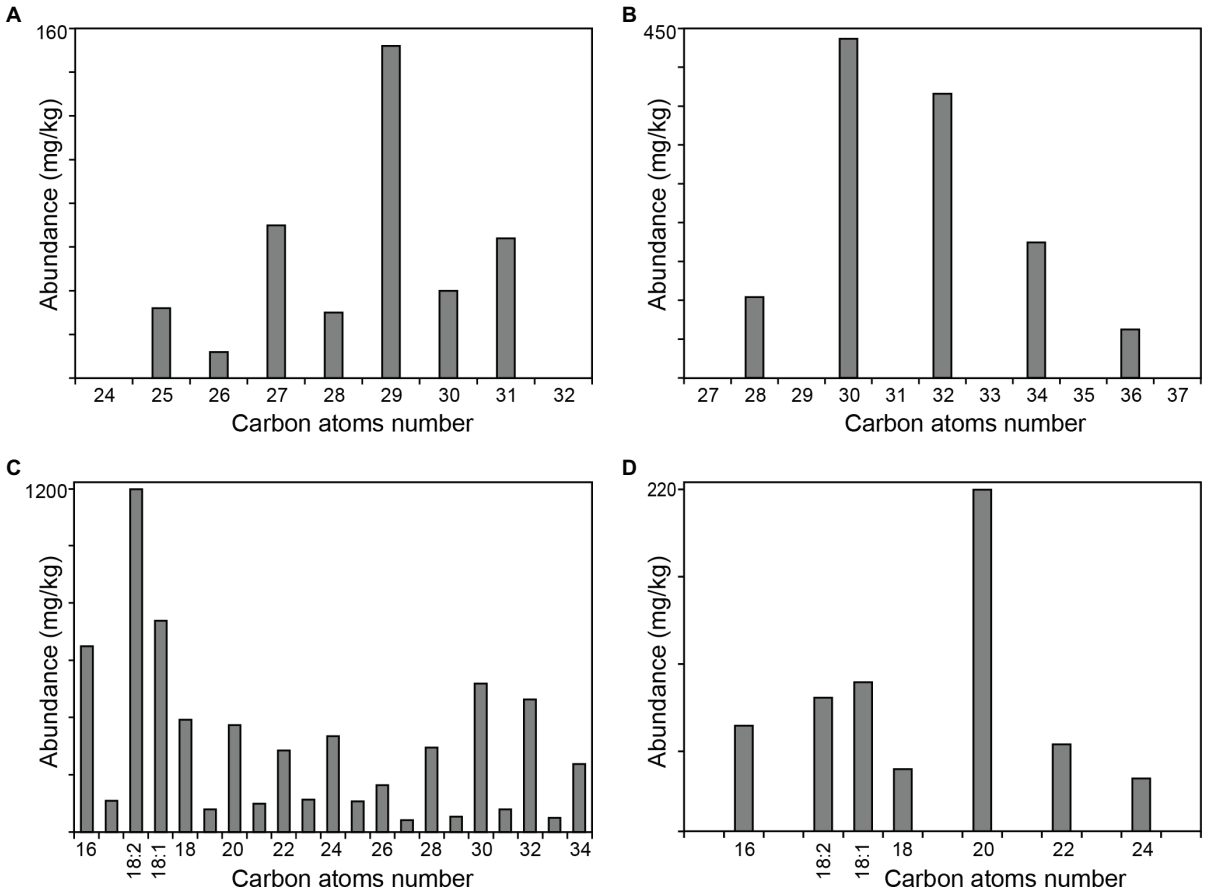

FIGURE 5 | Distribution of the main aliphatic series identified in the extracts of rice straw. **(A)** series of *n*-alkanes; **(B)** series of *n*-fatty alcohols; **(C)** series of *n*-fatty acids; and **(D)** series of monoglycerides. The histograms are scaled up to the abundance of the major compound in the series.

reported in rice straw (Xiao et al., 2001). However, a different paper (Zhao et al., 2007) reported a variety of rare and weird sterols (i.e., γ-sitosterol and stigmasta-3-en-6-ol, among others), but as said above, this paper presented many inconsistencies such as the identification of stigmasterol and 5,22-dien-3-stigmasterol (which are synonyms for the same compound) as two different sterols in the same sample, but could not detect sitosterol that is the most abundant sterol in rice straw (Zhao et al., 2007). Sterols were also found, although in lower amounts (250 mg/kg), in the respective rice husks (Marques et al., 2020). Likewise, lower amounts of sterols (1,121 mg/kg) were reported in the related wheat straw (del Río et al., 2013a).

Sterol glucosides were also found in rice straw in important amounts, accounting for 1,380 mg/kg. This is the first time that sterol glucosides have been reported in rice straw as they were not identified in previous studies (Xiao et al., 2001; Zhao et al., 2007). Their identification was made by comparison with the retention time and mass spectra of authentic standards (as their TMS-ether derivatives), as previously reported (Gutiérrez and del Río, 2001). The most abundant sterol glucoside in rice straw was sitosteryl 3β-D-glucopyranoside (**31**) that amounted up to 700 mg/kg, followed by campesteryl-3β-D-glucopyranoside (370 mg/kg) and stigmasteryl-3β-D-glucopyranoside (310 mg/kg). A similar distribution of sterol glucosides was found, although in much lower amounts (70 mg/kg) in the respective rice husks waste (Marques et al., 2020). Important amounts of sterol glucosides (680 mg/kg) were also reported in the related wheat straw (del Río et al., 2013a).

Significant amounts of sterol esters were also found in rice straw, accounting for 380 mg/g. Sterol esters were identified by comparison with the mass spectra of authentic standards that matched those previously published (Evershed et al., 1989), as well as by comparison with retention times and mass spectra of an enriched fraction of sterol esters isolated from abaca (del Río and Gutiérrez, 2006). The sterol esters identified corresponded to campesterol, stigmasterol, and sitosterol esterified with different fatty acids, particularly with palmitic, and with the mono- ($C_{18:1}$) and diunsaturated ($C_{18:2}$) fatty acids (that most likely correspond to oleic and linoleic acids). The most important sterol esters present in rice straw were a mixture of sitosterol esterified with the $C_{18:1}$ and $C_{18:2}$ unsaturated fatty acids, that most likely correspond to sitosterol oleate/sitosterol linoleate (**32**), accounting for 138 mg/kg. Small amounts of sterol esters (70 mg/kg) were found in the respective rice husks (Marques et al., 2020).

TABLE 2 | Composition and abundance (mg/kg, on a dry-basis) of the different individual esters found among the waxes identified in the extracts of rice straw.

Compound	Fatty acid:Fatty alcohol	Abundance
Esters C_{42}		**36**
hexadecanoic acid, hexacosyl ester	C_{16}:C_{26}	10
octadecanoic acid, tetracosyl ester	C_{18}:C_{24}	6
eicosanoic acid, docosyl ester	C_{20}:C_{22}	10
docosanoic acid, eicosyl ester	C_{22}:C_{20}	10
Esters C_{44}		**116**
hexadecanoic acid, octacosyl ester	C_{16}:C_{28}	16
octadecanoic acid, hexacosyl ester	C_{18}:C_{26}	10
eicosanoic acid, tetracosyl ester	C_{20}:C_{24}	40
docosanoic acid, docosyl ester	C_{22}:C_{22}	50
Esters C_{46}		**204**
hexadecanoic acid, triacontyl ester	C_{16}:C_{30}	50
octadecanoic acid, octacosyl ester	C_{18}:C_{28}	12
eicosanoic acid, hexacosyl ester	C_{20}:C_{26}	30
docosanoic acid, tetracosyl ester (**10**)	C_{22}:C_{24}	92
tetracosanoic acid, docosyl ester	C_{24}:C_{22}	20
Esters C_{48}		**180**
hexadecanoic acid, dotriacontyl ester	C_{16}:C_{32}	42
octadecanoic acid, triacontyl ester	C_{18}:C_{30}	30
eicosanoic acid, octacosyl ester	C_{20}:C_{28}	30
docosanoic acid, hexacosyl ester	C_{22}:C_{26}	32
tetracosanoic acid, tetracosyl ester	C_{24}:C_{24}	46
Esters C_{50}		**164**
hexadecanoic acid, tetratriacontyl ester	C_{16}:C_{34}	20
octadecanoic acid, dotriacontyl ester	C_{18}:C_{32}	16
eicosanoic acid, triacontyl ester	C_{20}:C_{30}	56
docosanoic acid, octacosyl ester	C_{22}:C_{28}	42
tetracosanoic acid, hexacosyl ester	C_{24}:C_{26}	30
Esters C_{52}		**124**
eicosanoic acid, dotriacontyl ester	C_{20}:C_{32}	36
docosanoic acid, triacontyl ester	C_{22}:C_{30}	62
tetracosanoic acid, octacosyl ester	C_{24}:C_{28}	26
Esters C_{54}		**76**
eicosanoic acid, tetratriacontyl ester	C_{20}:C_{34}	20
docosanoic acid, dotriacontyl ester	C_{22}:C_{32}	28
tetracosanoic acid, triacontyl ester	C_{24}:C_{30}	28

Bold number in parenthesis refers to the structure depicted in **Figure 2**.

Steroid ketones were found in significant amounts in rice straw, accounting for a total of 900 mg/kg. The most important steroid ketones identified were ergost-4-en-3-one (**24**, 112 mg/kg), stigmasta-4,22-dien-3-one (**25**, 360 mg/kg), stigmast-4-en-3-one (**27**, 248 mg/kg), and stigmastane-3,6-dione (**29**, 100 mg/kg), together with minor amounts of stigmasta-3,5-dien-7-one (**26**, 30 mg/kg) and ergostane-3,6-dione (**28**, 50 mg/kg). A previous paper (Zhao et al., 2007) reported the occurrence of stigmast-4-en-3-one, although they also reported other steroid ketones, such as spinasterone, 22,23-dihydrospinasterone, and cholest-4-en-3-one-26-oic acid, which are rare and uncommon steroid ketones, which could not be detected in the present work. Steroid ketones were only found in minor amounts (30 mg/kg) in the respective rice husks waste (Marques et al., 2020), as well as in the related wheat straw, where they amounted to only 88 mg/kg (del Río et al., 2013a).

Finally, small amounts of steroid hydrocarbons (60 mg/kg) were also identified, including stigmasta-3,5-diene (20 mg/kg) and stigmasta-3,5,22-triene (**30**, 40 mg/kg). These compounds are most likely degradation products arising from free and conjugated sterols, as previously indicated (Marques et al., 2020).

The occurrence of important amounts of steroid compounds in rice straw makes it an interesting and useful raw material for obtaining valuable compounds of interest to the nutraceutical, pharmaceutical, cosmetic, food, and other industries. In particular, phytosterols are well known for their nutraceutical and health-promoting benefits, thus helping to reduce blood cholesterol levels, regulating cardiovascular disease, as well as exhibiting anticancer properties (Wilson et al., 2000; Moreau et al., 2002; Iwatsuki et al., 2003; Quílez et al., 2003; Jones and AbuMweis, 2009; Awika, 2011). However, on the other hand, as in the case of using rice straw as raw material for pulp and papermaking, the important amounts of steroid compounds, particularly free and conjugated (esterified and glycosylated) sterols, present in this material can be problematic as these compounds contribute significantly to the pitch deposits (del Río et al., 1998, 2000; Gutiérrez et al., 2001, 2004; Gutiérrez and del Río, 2001).

CONCLUSION

The detailed composition of the lipophilic compounds in rice straw has been reported. The main compounds identified were *n*-fatty acids, *n*-alkanes, tocopherols, steroid hydrocarbons, steroid ketones, free sterols, sterol esters, sterol glucosides, mono-, di-, and triglycerides, and high molecular weight ester waxes. The data indicated that the amounts of most valuable phytochemicals are higher in rice straw than in the respective rice husks wastes or in other related cereal wastes such as in wheat straw. The composition of the lipophilic extractives reported here for rice straw, however, may vary depending on various factors (including cultivar., geographical location, age of crops, soil type, or climatic conditions, among others). Nevertheless, this information is of high interest for the valorization of rice straw as the lipophilic compounds can be obtained as a side-stream in a lignocellulosic biorefinery. These lipophilic compounds have a wide range of industrial applications and can be used for the nutraceutical, pharmaceutical, cosmetic, and chemical industries. In particularly, steroid compounds are of great interest in the pharmaceutical and nutraceutical as they have multiple health benefits, such as lowering plasma cholesterol levels, and they can be used as food supplements. However, for certain uses of rice straw, such as for pulp and papermaking, lipophilic compounds, and particularly the important amounts of free and conjugated sterols, represent a major problem because they are at the origin of the pitch deposits.

DATA AVAILABILITY STATEMENT

The raw data supporting the conclusions of this article will be made available by the authors, without undue reservation.

AUTHOR CONTRIBUTIONS

MJR and GM made the experimental work. AG and JR contributed to method development. JCR designed the work, processed the data, and wrote the article, with contributions from the rests of authors. All authors contributed to the article and approved the submitted version.

FUNDING

This work was supported by the projects AGL2017-83036-R and PID2020-118968RB-I00 (funded by MCIN/AEI/10.13039/501100011033 and, as appropriate, by "ERDF A way of making Europe") and the Regional Andalusian Government, Consejería de Transformación Económica, Industria, Conocimiento y Universidades/FEDER (project P20-00017). MJR acknowledges the Spanish Ministry of Science, Innovation and Universities for a FPI fellowship (PRE2018-083267).

ACKNOWLEDGMENTS

The authors thank Bernardo Hermosín (IRNAS-CSIC) for providing the samples of rice straw used for this work.

REFERENCES

Abraham, A., Mathew, A. K., Sindhu, R., Pandey, A., and Binod, P. (2016). Potential of rice straw for bio-refining: An overview. *Bioresour. Technol.* 215, 29–36. doi: 10.1016/j.biortech.2016.04.011

Akihisa, T., Yasukawa, K., Yamaura, M., Ukiya, M., Kimura, Y., Shimizu, N., et al. (2000). Triterpene alcohol and sterol ferulates from rice bran and their anti-inflammatory effects. *J. Agric. Food Chem.* 48, 2313–2319. doi: 10.1021/jf000135o

Attard, T. M., Bukhanko, N., Eriksson, D., Arshadi, M., Geladi, P., Bergsten, U., et al. (2018). Supercritical extraction of waxes and lipids from biomass: A valuable first step towards an integrated biorefinery. *J. Clean. Prod.* 177, 684–698. doi: 10.1016/j.jclepro.2017.12.155

Awika, J. M. (2011). "Health promoting effects of cereal and cereal products", in *Fruit and Cereal Bioactives – Sources Chemistry, and Applications*. eds. Ö. Tokusoglu and C. A. Hall (Boca Raton, FL: CRC Press), 9–17.

Back, E.L., and Allen, L.H. (2000). *Pitch Control, Wood Resin, and Deresination*. Atlanta: TAPPI Press.

Bhattacharyya, P., Bhaduri, D., Adak, T., Munda, S., Satapathy, B. S., Dash, P. K., et al. (2020). Characterization of rice straw from major cultivars for best alternative industrial uses to cutoff the menace of straw burning. *Ind. Crop. Prod.* 143:111919. doi: 10.1016/j.indcrop.2019.111919

Carciochi, R. A., D'Alessandro, L. G., Vauchel, P., Rodriguez, M. M., Nolasco, S. M., and Dimitrov, K. (2017). "Valorization of agrifood by-products by extracting valuable bioactive compounds using green processes," in *Ingredients Extraction by Physicochemical Methods in Food – Handbook of Food Bioengineering*. eds. A. M. Grumezescu and A. M. Holban (London, UK: Academic Press), 191–228.

Curstedt, T. (1974). Mass spectra of trimethylsilyl ethers of 2H-labelled mono- and diglycerides. *Biochim. Biophys. Acta* 360, 12–23. doi: 10.1016/0005-2760(74)90176-3

del Río, J. C., Evaristo, A. B., Marques, G., Martín-Ramos, P., Martín-Gil, J., and Gutiérrez, A. (2016). Chemical composition and thermal behavior of the pulp and kernel oils from macauba palm (*Acrocomia aculeata*) fruit. *Ind. Crop. Prod.* 84, 294–304. doi: 10.1016/j.indcrop.2016.02.018

del Río, J. C., and Gutiérrez, A. (2006). Chemical composition of abaca (*Musa textilis*) leaf fibers used for manufacturing of high quality paper pulps. *J. Agric. Food Chem.* 54, 4600–4610. doi: 10.1021/jf053016n

del Río, J. C., Gutiérrez, A., González-Vila, F. J., Martín, F., and Romero, J. (1998). Characterization of organic deposits produced in the Kraft pulping of *Eucalyptus globulus* wood. *J. Chromatogr. A* 823, 457–465. doi: 10.1016/S0021-9673(98)00179-4

del Río, J. C., Marques, G., Lino, A. G., Lima, C. F., Colodette, J. L., and Gutiérrez, A. (2015). Lipophilic phytochemicals from sugarcane bagasse and straw. *Ind. Crop. Prod.* 77, 992–1000. doi: 10.1016/j.indcrop.2015.09.064

del Río, J. C., Marques, G., Rodríguez, I. M., and Gutiérrez, A. (2009). Chemical composition of lipophilic extractives from jute (*Corchorus capsularis*) fibers used for manufacturing of high-quality paper pulps. *Ind. Crop. Prod.* 30, 241–249. doi: 10.1016/j.indcrop.2009.04.001

del Río, J. C., Prinsen, P., and Gutiérrez, A. (2013a). A comprehensive characterization of lipids in wheat straw. *J. Agric. Food Chem.* 61, 1904–1913. doi: 10.1021/jf304252m

del Río, J. C., Prinsen, P., and Gutiérrez, A. (2013b). Chemical composition of lipids in brewer's spent grain: A promising source of valuable phytochemicals. *J. Cereal Sci.* 58, 248–254. doi: 10.1016/j.jcs.2013.07.001

del Río, J. C., Romero, J., and Gutiérrez, A. (2000). Analysis of pitch deposits produced in Kraft pulp mills using totally chlorine free bleaching sequences. *J. Chromatogr. A* 874, 235–245. doi: 10.1016/S0021-9673(00)00111-4

Elhelece, W. A. (2020). "Rice straw as a raw material for pulp and paper production," in *Encyclopedia of Renewable and Sustainable Materials*. eds. I. A. Choudhury and S. Hashmi (Netherlands: Elsevier), 296–304.

Evershed, R. P., Prescott, M. C., Spooner, N., and Goad, L. J. (1989). Negative ion ammonia chemical ionization and electron impact ionization mass spectrometric analysis of steryl fatty acyl esters. *Steroids* 53, 285–309. doi: 10.1016/0039-128X(89)90016-0

FAOSTAT (2022). Food and Agriculture Organization of the United Nations. Available at: https://fao.org/faostat/ (Accessed January 17, 2022).

Gou, G., Wei, W., Jiang, M., Zhang, S., Lu, T., Xie, X., et al. (2018). "Environmentally friendly method for the separation of cellulose from steam-exploded rice straw and its high-value applications," in *Pulp and Paper Processing*. ed. S. N. Kazi (London, UK: IntechOpen), 133–154.

Gutiérrez, A., and del Río, J. C. (2001). Gas chromatography/mass spectrometry demonstration of steryl glycosides in eucalypt wood, Kraft pulp and process liquids. *Rapid Commun. Mass Spectrom.* 15, 2515–2520. doi: 10.1002/rcm.537

Gutiérrez, A., del Río, J. C., González-Vila, F. J., and Martín, F. (1998). Analysis of lipophilic extractives from wood and pitch deposits by solid-phase extraction and gas chromatography. *J. Chromatogr. A* 823, 449–455. doi: 10.1016/S0021-9673(98)00356-2

Gutiérrez, A., del Río, J. C., and Martínez, A. T. (2004). "Chemical analysis and biological removal of wood lipids forming pitch deposits in paper pulp manufacturing," in *Methods in Biotechnology: Environmental Biology: Methods and Protocols*. eds. J. M. Walker and J. F. T. Spencer (New Jersey: Humana Press), 189–202.

Gutiérrez, A., Romero, J., and del Río, J. C. (2001). Lipophilic extractives from *Eucalyptus globulus* pulp during Kraft cooking followed by TCF and ECF bleaching. *Holzforschung* 55, 260–264. doi: 10.1515/HF.2001.043

Hernandez, E. (2005). "Pharmaceutical and cosmetic use of lipids" in *Bailey's Industrial Oil and Fat Products. 6th Edn*. ed. F. Shahidi (New York: Wiley-Interscience), 391–411.

Huang, F. C., Ju, Y. H., and Chiang, J. C. (1999). γ-Linolenic acid-rich triacylglycerols derived from borage oil *via* lipase-catalyzed reactions. *J. Am. Oil Chem. Soc.* 76, 833–837. doi: 10.1007/s11746-999-0073-8

Iwatsuki, K., Akihisa, T., Tokuda, H., Ukiya, M., Higashihara, H., Mukainaka, T., et al. (2003). Sterol ferulates, sterols, and 5-alk(en)ylresorcinols from wheat, rye, and corn bran oils and their inhibitory effects on Epstein-Barr virus activation. *J. Agric. Food Chem.* 51, 6683–6688. doi: 10.1021/jf030371+

Jones, P. J., and AbuMweis, S. S. (2009). Phytosterols as functional food ingredients: linkages to cardiovascular disease and cancer. *Curr. Opin. Clin. Nutr. Metab. Care* 12, 147–151. doi: 10.1097/mco.0b013e328326770f

Kalita, E., Narth, B. K., Deb, P., Agan, F., Islam, M. R., and Saikia, K. (2015). High quality fluorescent cellulose nanofibers from endemic rice husk: isolation and characterization. *Carbohydr. Polym.* 122, 308–313. doi: 10.1016/j.carbpol.2014.12.075

Kalustian, P. (1985). Pharmaceutical and cosmetic uses of palm and lauric products. *J. Am. Oil Chem. Soc.* 62, 431–433. doi: 10.1007/BF02541417

Kaur, D., Bhardwaj, N. K., and Lohchab, R. K. (2017). Prospects of rice straw as a raw material for paper making. *Waste Manag.* 60, 127–139. doi: 10.1016/j.wasman.2016.08.001

Kumar, A. K., Parikh, B. S., and Pravakar, M. (2016). Natural deep eutectic solvent mediated pretreatment of rice straw: bioanalytical characterization of lignin extract and enzymatic hydrolysis of pretreated biomass residue. *Environ. Sci. Pollut. Res.* 23, 9265–9275. doi: 10.1007/s11356-015-4780-4

Kumar, B., and Verma, P. (2021). Biomass-based biorefineries: An important architype towards a circular economy. *Fuel* 288:119622. doi: 10.1016/j.fuel.2020.119622

Lal, R. (2005). World crop residues production and implications of its use as a biofuel. *Environ. Int.* 31, 575–584. doi: 10.1016/j.envint.2004.09.005

Lauer, W. M., Aasen, A. J., Graff, G., and Holman, R. T. (1970). Mass spectrometry of triglycerides: I. *Struc. Eff. Lipids* 5, 861–868. doi: 10.1007/BF02531117

Lu, P., and Hsieh, Y. L. (2012). Preparation and characterization of cellulose nanocrystals from rice straw. *Carbohydr. Polym.* 87, 564–573. doi: 10.1016/j.carbpol.2011.08.022

Marques, G., Rencoret, J., Gutiérrez, A., and del Río, J. C. (2020). Lipophilic compounds from maize fiber and rice husk residues - An abundant and inexpensive source of valuable phytochemicals. *Ind. Crop. Prod.* 146:112203. doi: 10.1016/j.indcrop.2020.112203

Matsumura, Y., Minowa, T., and Yamamoto, H. (2005). Amount, availability and potential use of rice straw (agricultural residue) biomass as an energy resource in Japan. *Biomass Bioenergy* 29, 347–354. doi: 10.1016/j.biombioe.2004.06.015

Metzger, J. O., and Bornscheuer, U. (2006). Lipids as renewable resources: current state of chemical and biotechnological conversion and diversification. *Appl. Microbiol. Biotechnol.* 71, 13–22. doi: 10.1007/s00253-006-0335-4

Moazzami, A. A., Lampi, A.-M., and Kamal-Eldin, A. (2011). "Bioactive lipids in cereals and cereal products," in *Fruit and Cereal Bioactives – Sources, Chemistry, and Applications*. eds. Ö. Tokusoglu and C. A. Hall (Boca Raton, FL: CRC Press), 229–249.

Moreau, R. A., Whitaker, B. D., and Hicks, K. B. (2002). Phytosterols, phytostanols, and their conjugates in foods: structural diversity, quantitative analysis, and health-promoting uses. *Prog. Lipid Res.* 41, 457–500. doi: 10.1016/S0163-7827(02)00006-1

Quílez, J., García-Lorda, P., and Salas-Salvadó, J. (2003). Potential uses and benefits of phytosterols in diet: present situation and future directions. *Clin. Nutr.* 22, 343–351. doi: 10.1016/s0261-5614(03)00060-8

Rombaut, N., Tixier, A.-S., Bily, A., and Chemat, F. (2014). Green extraction processes of natural products as tools for biorefinery. *Biofuels Bioprod. Biorefin.* 8, 530–544. doi: 10.1002/bbb.1486

Rosado, M. J., Rencoret, J., Marques, G., Gutiérrez, A., and del Río, J. C. (2021). Structural characteristics of the guaiacyl-rich lignins from rice (*Oryza sativa* L.) husks and straw. *Front. Plant Sci.* 12:640475. doi: 10.3389/fpls.2021.640475

Shahidi, F., and De Camargo, A. C. (2016). Tocopherols and tocotrienols in common and emerging dietary sources: occurrence, applications, and health benefits. *Int. J. Mol. Sci.* 17:1745. doi: 10.3390/ijms17101745

Sharma, A., Singh, G., and Arya, S. K. (2020). Biofuel from rice straw. *J. Clean. Prod.* 277:124101. doi: 10.1016/j.jclepro.2020.124101

Sin, E. H. K., Marriott, R., Hunt, A. J., and Clark, J. H. (2014). Identification, quantification and Chrastil modelling of wheat straw wax extraction using supercritical carbon dioxide. *C. R. Chim.* 17, 293–300. doi: 10.1016/j.crci.2013.12.001

Snyder, J.-M., Taylor, S. C., and King, J. W. (1993). Analysis of tocopherols by capillary supercritical fluid chromatography and mass spectrometry. *J. Am. Oil Chem. Soc.* 70, 349–354. doi: 10.1007/BF02552705

Swain, M. R., Singh, A., Sharma, A. K., and Tuli, D. K. (2019). "Bioethanol production from rice- and wheat straw: an overview," in *Bioethanol Production from Food Crops: Sustainable Sources, Interventions and Challenges*. eds. R. C. Ray and S. Ramachandra (London, UK: Academic Press), 213–231.

Tao, B. Y. (2007). "Industrial applications for plant oils and lipids" in *Bioprocessing for Value-Added Products From Renewable Resources – New Technologies and Applications*. ed. S.-T. Yang (Amsterdam: Elsevier), 611–627.

Wang, W., Wu, X., Chen, A., Xie, X., Wang, Y., and Yin, C. (2016). Mitigating effects of ex situ application of rice straw on CH_4 and N_2O emissions from paddy-upland coexisting system. *Sci. Rep.* 6:37402. doi: 10.1038/srep37402

Wilson, T. A., DeSimone, A. P., Romano, C. A., and Nicolosi, R. J. (2000). Corn fiber oil lower plasma cholesterol levels and increases cholesterol excretion greater than corn oil and similar to diets containing soy sterols and soy stanols in hamsters. *J. Nutr. Biochem.* 11, 443–449. doi: 10.1016/S0955-2863(00)00103-0

Xiao, B., Sun, X. F., and Sun, R. C. (2001). Extraction and characterization of lipophilic extractives from rice straw. Chemical composition. *J. Wood Chem. Technol.* 21, 397–411. doi: 10.1081/WCT-100108334

Zemnukhova, L. A., Isai, S. V., Busarova, N. G., and Arefieva, O. D. (2015). Study of lipids composition in the rice straw. *Appl. Mech. Mater.* 737, 646–648. doi: 10.4028/www.scientific.net/AMM.737.646

Zhang, Y., Wong, W.-T., and Yung, K.-F. (2013). One-step production of biodiesel from rice bran oil catalyzed by chlorosulfonic acid modified zirconia via simultaneous esterification and transesterification. *Bioresour. Technol.* 147, 59–64. doi: 10.1016/j.biortech.2013.07.152

Zhao, W., Zong, Z. M., Lin, J., Song, Y. M., Guo, X. F., Yao, Z. S., et al. (2007). Dewaxing from stalks with petroleum ether by different methods. *Energy Fuel* 21, 1165–1168. doi: 10.1021/ef060229l

Conflict of Interest: The authors declare that the research was conducted in the absence of any commercial or financial relationships that could be construed as a potential conflict of interest.

Publisher's Note: All claims expressed in this article are solely those of the authors and do not necessarily represent those of their affiliated organizations, or those of the publisher, the editors and the reviewers. Any product that may be evaluated in this article, or claim that may be made by its manufacturer, is not guaranteed or endorsed by the publisher.

frontiers | Frontiers in Plant Science

ORIGINAL RESEARCH
published: 07 April 2022
doi: 10.3389/fpls.2022.847743

Foliar Spray of Micronutrients Alleviates Heat and Moisture Stress in Lentil (*Lens culinaris* Medik) Grown Under Rainfed Field Conditions

Visha Kumari Venugopalan[1,2], Rajib Nath[1], Kajal Sengupta[1], Anjan K. Pal[3], Saon Banerjee[4], Purabi Banerjee[1], Malamal A. Sarath Chandran[2,4], Suman Roy[5], Laxmi Sharma[5], Akbar Hossain[6] and Kadambot H. M. Siddique[7]**

[1] Department of Agronomy, Bidhan Chandra Krishi Viswavidyalaya, Mohanpur, India, [2] Indian Council of Agricultural Research (ICAR)-Central Research Institute for Dryland Agriculture, Hyderabad, India, [3] Department of Crop Physiology, Bidhan Chandra Krishi Viswavidyalaya, Mohanpur, India, [4] Department of Agricultural Meteorology and Physics, Bidhan Chandra Krishi Viswavidyalaya, Mohanpur, India, [5] Indian Council of Agricultural Research (ICAR)-Central Research Institute for Jute and Allied Fibers, Kolkata, India, [6] Department of Agronomy, Bangladesh Wheat and Maize Research Institute, Dinajpur, Bangladesh, [7] The University of Western Australia (UWA) Institute of Agriculture and School of Agriculture and Environment, The University of Western Australia, Perth, WA, Australia

The simultaneous occurrence of high temperature and moisture stress during the reproductive stage of lentil (*Lens culinaris* Medik) constrains yield potential by disrupting the plant defense system. We studied the detrimental outcomes of heat and moisture stress on rainfed lentils under residual moisture in a field experiment conducted on clay loam soil (Aeric Haplaquept) in eastern India from 2018 to 2019 and from 2019 to 2020 in winter seasons. Lentil was sown on two dates (November and December) to expose the later sowing to higher temperatures and moisture stress. Foliar sprays of boron (0.2% B), zinc (0.5% Zn), and iron (0.5% Fe) were applied individually or in combination at the pre-flowering and pod development stages. High temperatures increased malondialdehyde (MDA) content due to membrane degradation and reduced leaf chlorophyll content, net photosynthetic rate, stomatal conductance, water potential, and yield (kg ha^{-1}). The nutrient treatments affected the growth and physiology of stressed lentil plants. The B+Fe treatment outperformed the other nutrient treatments for both sowing dates, increasing peroxidase (POX) and ascorbate peroxidase (APX) activities, chlorophyll content, net photosynthetic rate, stomatal conductance, relative leaf water content (RLWC), seed filling duration, seed growth rate, and yield per hectare. The B+Fe treatment increased seed yield by 35–38% in late-sown lentils (December). In addition, the micronutrient treatments positively impacted physiological responses under heat and moisture stress with B+Fe and B+Fe+Zn alleviating heat and moisture stress-induced perturbations. Moreover, the exogenous nutrients helped in improving physiochemical attributes, such as chlorophyll content, net photosynthetic rate, stomatal conductance, water potential, seed filling duration, and seed growth rate.

Keywords: Heat stress, chlorophyll, relative water content, antioxidant machinery, pollen

OPEN ACCESS

Edited by:
Maria Cecilia Rousseaux, Centro Regional de Investigaciones Científicas y Transferencia Tecnológica de La Rioja (CRILAR CONICET), Argentina

Reviewed by:
Arun K. Shanker, Central Research Institute for Dryland Agriculture (ICAR), India
Basharat Ali, University of Agriculture, Faisalabad, Pakistan

****Correspondence:***
Visha Kumari Venugopalan
visha.venugopal@gmail.com
Kadambot H. M. Siddique
kadambot.siddique@uwa.edu.au

Specialty section:
This article was submitted to Crop and Product Physiology, a section of the journal Frontiers in Plant Science

Received: *03 January 2022*
Accepted: *23 February 2022*
Published: *07 April 2022*

Citation:
Venugopalan VK, Nath R, Sengupta K, Pal AK, Banerjee S, Banerjee P, Chandran MAS, Roy S, Sharma L, Hossain A and Siddique KHM (2022) Foliar Spray of Micronutrients Alleviates Heat and Moisture Stress in Lentil (Lens culinaris Medik) Grown Under Rainfed Field Conditions. Front. Plant Sci. 13:847743. doi: 10.3389/fpls.2022.847743

INTRODUCTION

Abiotic stresses, such as elevated temperature and moisture stress, are key limiting factors for crop development and output. Climate change has intensified adverse crop environments, which result in significant economic losses in agricultural and horticultural crops (Beck et al., 2007). High temperatures are frequently associated with less water availability. The increased likelihood of combined drought and heat stress events in the future (IPCC, 2014) highlights the need to explore crop responses to these combined stresses and cost-effective management options.

Lentil is a versatile and profitable pulse crop. It is an excellent source of complex carbohydrates, protein, minerals, vitamins, and dietary fiber for humans, and valuable feed and fodder for livestock (Ninou et al., 2019). In India, lentil is a cool-season food legume crop often planted as a rainfed crop during winter. It is grown on 1.51 million ha, producing 1.56 million tons (1,032 kg ha^{-1}) (Directorate of Economics and Statistics, 2020). In India's vast fallow land, lentils can be cultivated on residual soil moisture after the previous rice harvest without additional irrigation. However, the short winter season and temperature fluctuations inhibit lentil growth and productivity. As with chickpea (Kaushal et al., 2013) and lentils (Sita et al., 2017a; Venugopalan et al., 2021a), cool-season food legumes are adapted to low and mild temperature environments and thus susceptible to heat stress (Sita et al., 2017b; Venugopalan et al., 2021b), particularly, during reproductive growth, significantly reducing seed yields (Sita et al., 2017b; Venugopalan et al., 2021b).

Temperatures exceeding 32/20°C (max/min) during lentil flowering and pod filling can significantly impact seed output and quality (Delahunty et al., 2015; Bourgault et al., 2018; Venugopalan et al., 2021b). Furthermore, in eastern India, long-duration rice production prevents the sowing of lentils as a sole crop. Long-term trend analysis data show that late-sown lentils face heat and moisture stress. The crop can experience initial or late moisture stress due to the hard layer of puddled rice soil that depletes soil moisture. The occurrence of moisture and heat stress during the reproductive stage (terminal stage) is a major concern for lentil yield.

Foliar sprays of micronutrients aid their rapid translocation, reducing plant stress, especially under late-sown conditions. Exogenous nutrition administration could be a useful strategy for reducing the adverse effects of heat (Waraich et al., 2012). Zinc (Zn) is essential during the reproductive phase of crops. Zinc-mediated regulation of water relations confers heat tolerance by maintaining cell water and osmotic potential under stress. Iron (Fe) is required for various plant metabolic reactions and helps during stress (Briat et al., 1995; Rout and Sahoo, 2015). Boron (B) is essential for plant reproduction and growth (Dear and Lipsett, 1987; Dell and Huang, 1997). Under stressful conditions, B enhances stomatal opening and gaseous exchange regulation (Chen et al., 2008).

We hypothesize that these micronutrients (Zn, B, and Fe) ameliorate heat and moisture stress in late-sown lentil crops, given their relevance in protecting crops from a wide range of abiotic stresses. We investigated the impact of micronutrient foliar sprays on photosynthesis, stomatal conductance, and reproduction. We conducted a field experiment to (1) determine the effect of sowing time and foliar sprays on the physiochemical properties and yield of lentils and (2) reveal the role of Zn, B, and Fe in alleviating the impact of high temperature and moisture stress.

TABLE 1 | Treatment description and abbreviation.

Treatment	Abbreviation
No spray (Control)	Control
Foliar spray: tap water	Tap water
Foliar spray: 0.5% Zn ($ZnSO_4.7H_2O$)	Zn@0.5%
Foliar spray: 0.5% Fe ($FeSO_4.7H_2O$)	Fe@0.5%
Foliar spray: 0.2% ($Na_2B_4O_7.10H_2O$)	B@0.2%
Foliar spray: 0.5% Zn + 0.2% B	Zn+B
Foliar spray: 0.5% Zn + 0.5% Fe	Zn+Fe
Foliar spray: 0.2% B + 0.5% Fe	B+Fe
Foliar spray: 0.5% Zn + 0.5% Fe + 0.2% B	Zn+B+Fe

MATERIALS AND METHODS

Site Characteristics

The field experiments were conducted during the period from 2018 to 19 and from 2019 to 20 in winter seasons at the Seed Farm of Bidhan Chandra Krishi Viswavidyalaya (22°58′ N and 88°32′ E; 9.75 m asl) in Kalyani, West Bengal, India. The study site is flat with a well-drained Gangetic alluvial soil (order: Inceptisol), belonging to the clayey loams, with medium fertility and almost neutral reaction. The soil is low in organic carbon (wet-digestion method), available nitrogen (alkaline permanganate-oxidizable), zinc [diethylenetriaminepentaacetic acid (DTPA)-extractable], boron (azomethine-H), and iron (DTPA-extractable) (0.52%, 138 kg ha^{-1}, 0.40 mg kg^{-1}, 0.49 mg kg^{-1}, and 0.45 mg kg^{-1}, respectively), and fairly rich in available P (Brays' P) and K (NH_4OAC-extractable) (13 and 132 kg ha^{-1}, respectively).

Treatment Description and Experimental Design

The experiments had a split-plot design with three replications. The main plots were two planting dates: November (normal) and December (late), and the subplots comprised foliar sprays of various micronutrients (see **Table 1** for treatment abbreviations and details). A popular red lentil type, *Moitree* (WBL 77), was used due to its medium duration and high production. The foliar sprays were applied during the flowering and pod development stages.

Crop Management

Seeds were sown in a 5 × 4 m experimental plot at 30 cm row spacing. Standard crop management procedures were used that include a uniform N: P: K fertilizer dose of 20: 17.5: 334 kg ha^{-1} and one hand weeding 25–30 days after sowing. No irrigation was

TABLE 2 | Mean rainfall and maximum and minimum temperatures during crop phenological stages.

Parameter	Year	Sowing time	Germination	Flowering	Pod initiation	Maturity
Rainfall (mm)	2018–19	Normal	0	21.4	0	0
		Late	5.2	13.6	0.6	51
	2019–20	Normal	0	15.4	0	0
		Late	0	0	0	0.3
Tmax (°C)	2018–19	Normal	29.6	26.4	24.7	25.9
		Late	25.7	24.3	26.5	29.4
	2019–20	Normal	30.1	25.5	23.1	26.4
		Late	27	22.4	24	29.8
Tmin (°C)	2018–19	Normal	17.7	13.6	9.2	10.7
		Late	10.5	9.6	11.9	11.5
	2019–20	Normal	18.1	13.6	11.5	12.8
		Late	15.4	11	11.1	16.7

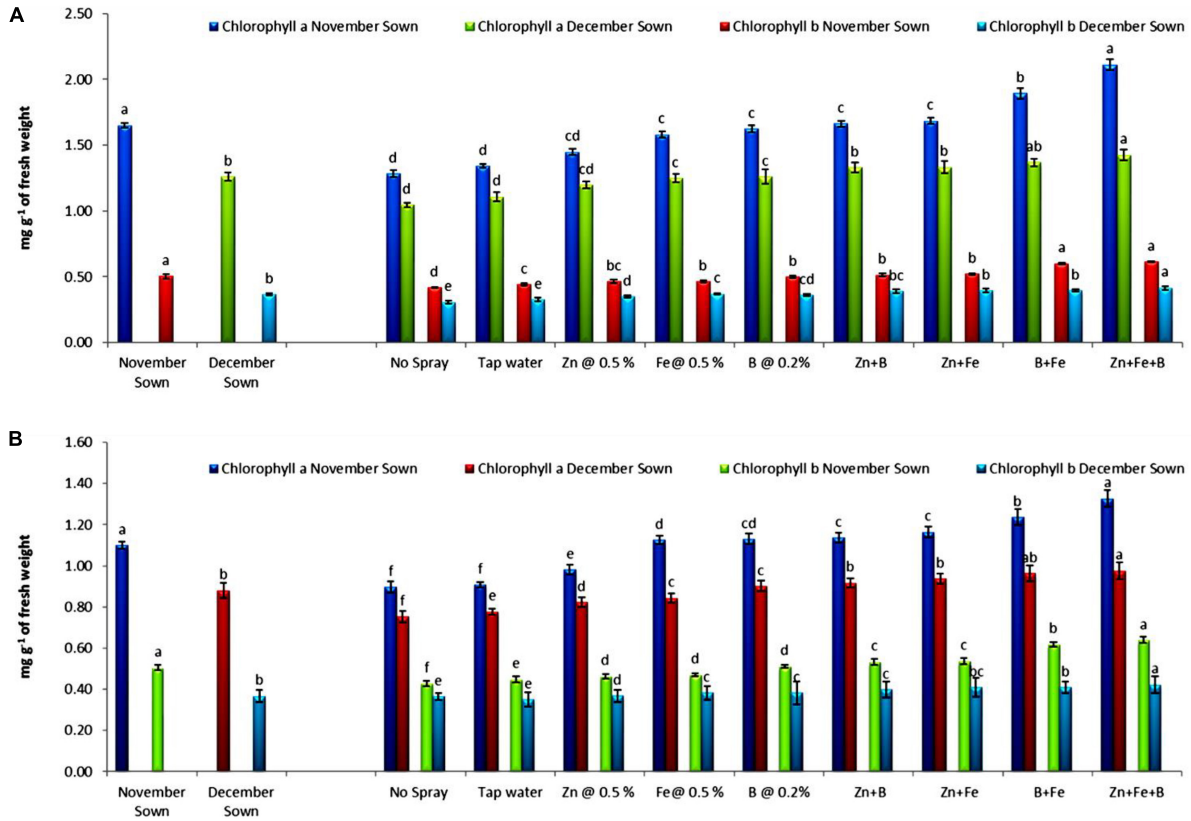

FIGURE 1 | Leaf chlorophyll a and b for different sowing dates and foliar spray treatments in the **(A)** 2018–19 and **(B)** 2019–20 lentil cropping seasons. Values are means, and bars represent ± SEM (n = 3). Different letters indicate significant differences between means.

provided because lentil is grown on residual soil moisture from rainfall during the winter season.

Meteorological data were collected from the All India Coordinated Research Project on Agrometeorology unit, Directorate of Research, Kalyani, West Bengal, from November 2018 to March 2019 and from November 2019 to March 2020. Phenological stage mean rainfall and maximum and minimum temperatures are shown in **Table 2**. The temperature and moisture status of the soil at various stages of crop growth in both years are given in **Supplementary Tables 1**, **2**.

Measurement of Physiological Parameters

Chlorophyll Content

The chlorophyll content in leaf samples was estimated as per Arnon (1949). Absorbance was read at 480, 510, 645, and 663 nm using a Systronics-105 spectrophotometer against a

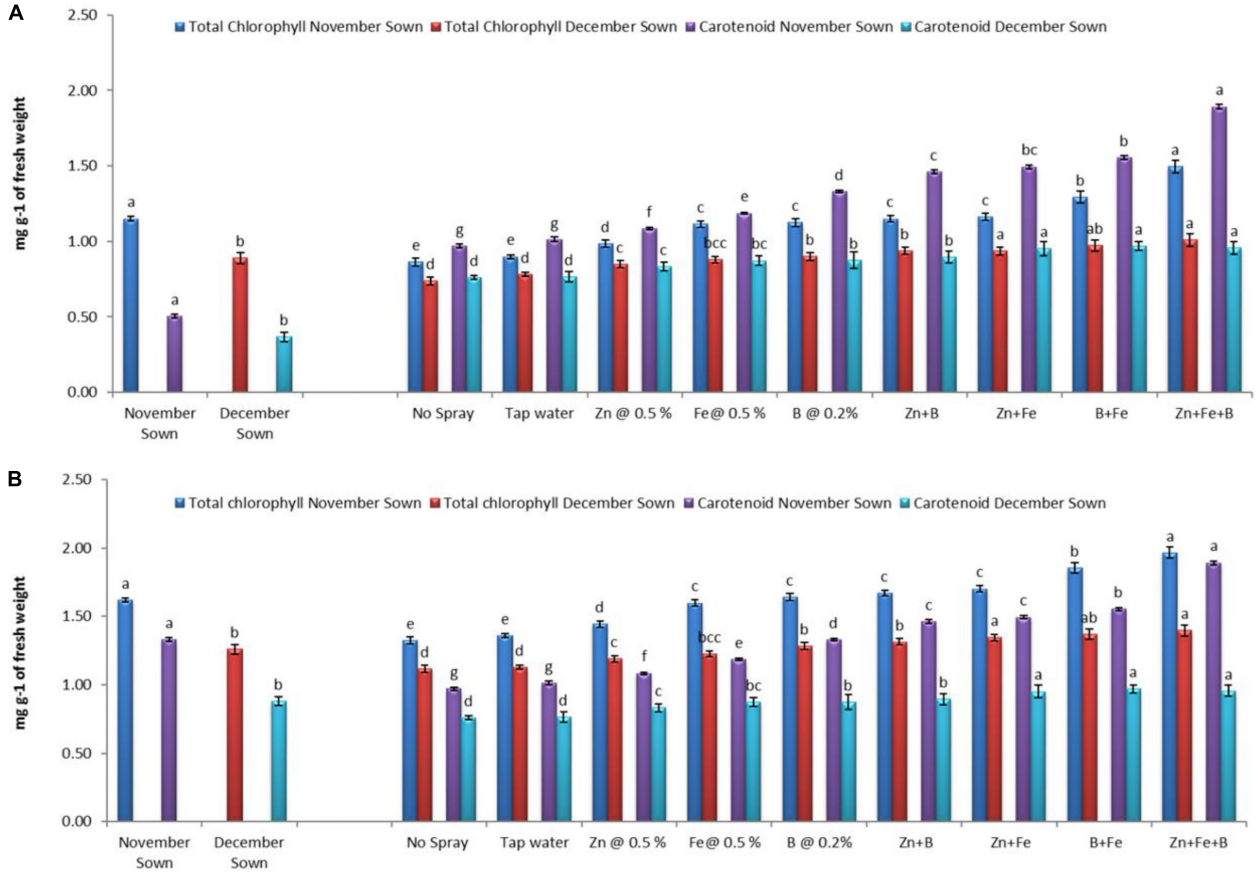

FIGURE 2 | Total chlorophyll content and carotenoid for different sowing dates and foliar spray treatments in the **(A)** 2018–19 and **(B)** 2019–20 lentil cropping seasons. Values are means, and bars represent ± SEM (n = 3). Different letters indicate significant differences between means.

blank containing 80% acetone. The amount of chlorophyll *a*, chlorophyll *b*, total chlorophyll, and carotenoids was estimated as follows:

mg of chlorophyll *a* g^{-1} of fresh weight

$$= [(12.7 \times A_{663}) - (2.69 \times A_{645})] \times \left(\frac{V}{W} \times 1,000\right)$$

mg of chlorophyll b g^{-1} of fresh weight

$$= [(22.9 \times A_{665}) - (4.68 \times A_{663})] \times \left(\frac{V}{W} \times 1,000\right)$$

mg of total chlorophyll g^{-1} of fresh weigh

$$= [(12.7 \times A_{663}) - (2.69 \times A_{645})] \times \left(\frac{V}{W} \times 1,000\right)$$

mg of carotenoid g^{-1} of fresh weight

$$= [(7.6 \times A_{480}) - (1.49 \times A_{510})] \times \left(\frac{V}{W} \times 1,000\right)$$

where V = volume of extract (ml), W = fresh weight (FW) of tissue (g), and A = absorbance.

Pollen Studies

Pollen viability was estimated by acetocarmine stain (Srinivasan and Gaur, 2011) and expressed in percentage. Pollen fertility was determined by their staining ability. Pollen germination was estimated as per Niles and Quesenberry (1992). Pollen germination was recorded at 30-min intervals for up to 90 min, by which time the pollen had reached maximum germination percentage. The slides were viewed under a microscope (10×).

Seed Growth Rate and Seed Filling Duration

Five pods per plant (three plants from each replicate; nine plants total) were tagged at the beginning of pod filling (pod size ≈1 cm) and followed to physiological maturity to investigate seed growth rate and seed-filling duration, as reported by Sehgal et al. (2019). Seed dry weight was recorded 7 days after pod filling started and at physiological maturity after oven-drying at 45°C for 5 days. The time (days) taken for tagged pods to complete seed filling was noted.

Relative Leaf Water Content

Relative leaf water content (RLWC) was estimated as per Perez et al. (2002). Leaves (250 mg) were collected from five plants in each replication, cut into small pieces, and pooled to record FW.

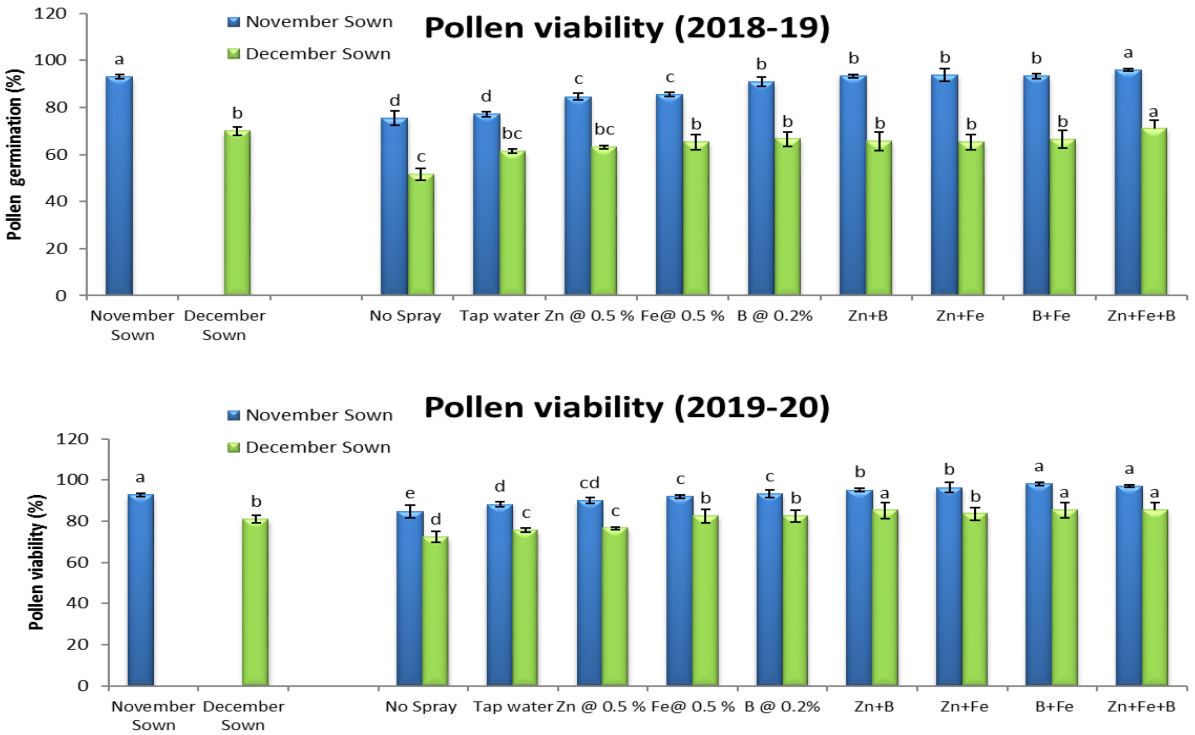

FIGURE 3 | Pollen viability (%) for different sowing dates and foliar spray treatments in the 2018–19 and 2019–20 lentil cropping seasons. Values are means, and bars represent ± SEM (n = 3). Different letters indicate significant differences between means.

The leaves were immersed in double-distilled water for 4 h, before recording turgid weight (TW), and then dried at 80 ± 1°C in a hot air oven to constant weight to record dry weight (DW). The RLWC was expressed as follows:

$$RLWC = \frac{FW - DW}{TW - DW} \times 100$$

Net Photosynthetic Rate, Transpiration Rate, and Stomatal Conductance

Leaf net photosynthetic rate (Pn), transpiration rate (E), and stomatal conductance (C) were measured using a portable handheld photosynthesis system (CI-340 Handheld Photosynthesis system, CID Bio-Science, Inc. Camas, WA 98607, United States). The measurements were taken from fully developed upper leaves of three selected plants on clear sunny days between 10.30 a.m. and 12.30 p.m. at the 100% pod development stage.

Enzyme Assays

Ascorbate peroxidase (APX) and peroxidase (POX) activities were measured according to the protocols by Nakano and Asada (1981) and Castillo et al. (1984), respectively. To extract the APX enzyme, a 1 g leaf sample was frozen in liquid nitrogen to suppress proteolytic activity, then ground in 10 ml of extraction buffer [0.1 M phosphate buffer, pH 7.5, with 0.5 mM ethylenediaminetetraacetic acid (EDTA)], passed through four layers of cheesecloth, and centrifuged at 15,000 g for 20 min. The absorbance of the supernatant was read at 290 nm at 1-min intervals for 5–10 min. The absorbance coefficient of ascorbic acid was 2.8 mM^{-1} cm^{-1}. The POX extract was prepared by freezing a 1 g leaf sample in liquid nitrogen to prevent proteolytic activity, then grinding with 10 ml of extraction buffer (0.1 M phosphate buffer pH 7.5, containing 0.5 mM EDTA). The absorbance due to the formation of tetra-guaiacol was recorded at 470 nm, and the enzyme activity was calculated as the extinction coefficient of its oxidation product, tetra-guaiacol ε = 26.2 mM^{-1} cm^{-1}.

Lipid Peroxidation

Lipid peroxidation is the oxidative degradation of lipid-fatty acid by reactive oxygen species (ROS). The level of lipid peroxidation is measured in terms of thiobarbituric acid (TBA) reactive substances content (Heath and Packer, 1968) and expressed as malondialdehyde (MDA). A total of 4 ml of 0.5% TBA in 20% trichloroacetic acid (TCA) was added to a 1.0 ml aliquot of the supernatant, heated at 95°C for 30 min in a laboratory water bath, and cooled in an ice bath. After cooling, the aliquot was centrifuged at 10,000 g for 10 min. The absorbance of the clear supernatant was recorded at 532 nm. Values of non-specific absorption recorded at 600 nm were subtracted from the values recorded at 532 nm. The MDA content is calculated according to its extinction coefficient ε = 155 mM cm^{-1}.

Proline

Free proline content in the leaves was determined using the method of Bates et al. (1973).

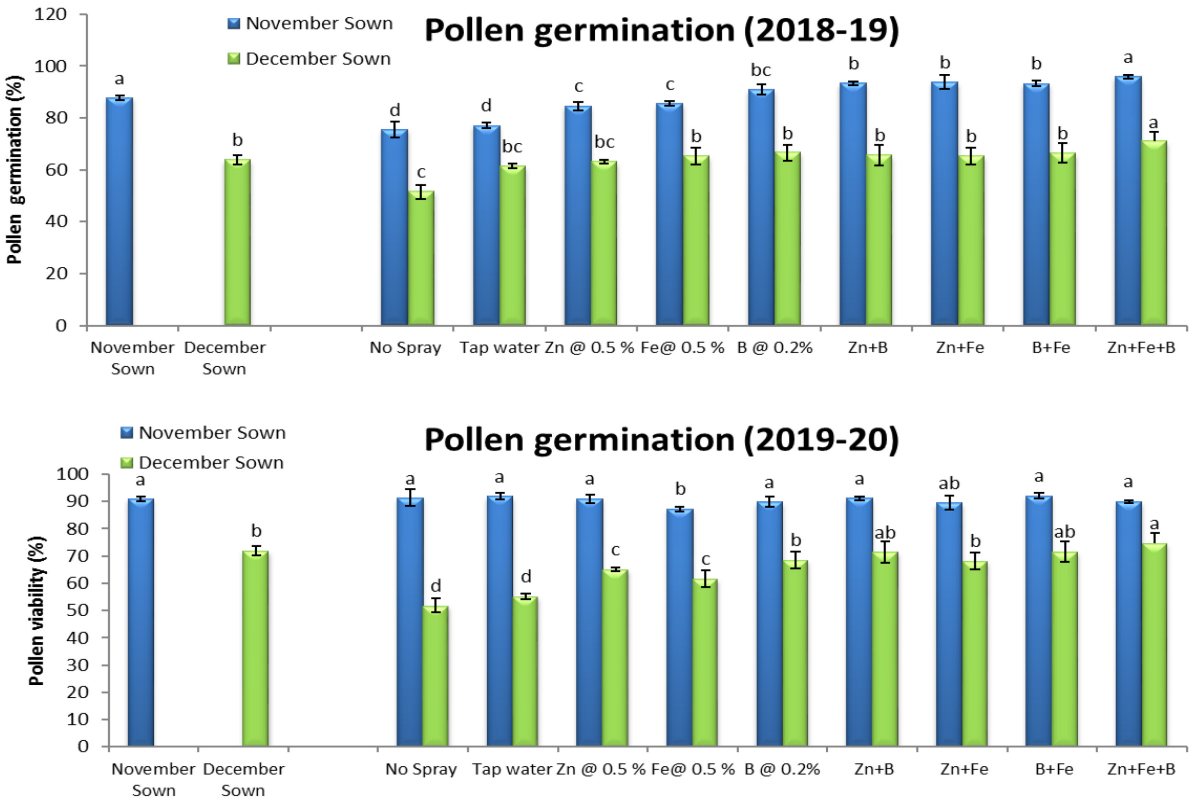

FIGURE 4 | Pollen germination (%) for different sowing dates and foliar spray treatments in the 2018–19 and 2019–20 lentil cropping seasons. Values are means, and bars represent ± SEM (n = 3). Different letters indicate significant differences between means.

TABLE 3 | Effect of sowing time and zinc, iron, and boron foliar sprays on seed growth rate and seed filling duration of lentil.

Treatments	Seed growth rate (g dry weight) (2018–19)		Seed growth rate (g dry weight) (2019–20)		Seed filling duration (days) (2018–19)		Seed filling duration (days) (2019–20)	
	Normal-sown	Late-sown	Normal-sown	Late-sown	Normal-sown	Late-sown	Normal-sown	Late-sown
Control	6.53 ± 0.05*c*	4.10 ± 0.30*e*	7.23 ± 0.15*c*	4.10 ± 0.12*c*	18.00 ± 0.24*c*	12.33 ± 0.01*c*	18.67 ± 0.21*c*	13.00 ± 0.02*d*
Tap water	6.80 ± 0.20*c*	4.17 ± 0.3*e*	7.33 ± 0.24*c*	4.20 ± 0.14*c*	18.00 ± 0.15*c*	12.00 ± 0.01*c*	18.67 ± 0.21*c*	13.33 ± 0.01*c*
Zn@0.5%	7.57 ± 0.40*b*	4.30 ± 0.50*d*	7.90 ± 0.31*b*	4.30 ± 0.12*c*	19.00 ± 0.12*b*	12.33 ± 0.01*c*	19.33 ± 0.34*b*	13.33 ± 0.31*c*
Fe@0.5%	8.07 ± 0.40*ab*	4.37 ± 0.40*d*	8.00 ± 0.30*b*	4.43 ± 0.14*b*	19.00 ± 0.31*b*	12.67 ± 0.02*b*	19.33 ± 0.11*b*	13.33 ± 0.21*c*
B@0.2%	8.20 ± 0.45*a*	4.2*d*3 ± 0.3*d*	8.20 ± 0.21*ab*	4.52 ± 0.22*b*	19.67 ± 0.02*a*	12.67 ± 0.57*b*	20.00 ± 0.25*a*	13.67 ± 0.24*b*
Zn+B	7.93 ± 0.05*b*	4.53 ± 0.05*c*	7.80 ± 0.24*b*	4.53 ± 0.20*b*	19.67 ± 0.14*a*	12.67 ± 0.57*b*	20.33 ± 0.32*a*	13.67 ± 0.21*b*
Zn+Fe	7.53 ± 0.20*b*	4.70 ± 0.36*b*	7.53 ± 0.24*c*	4.60 ± 0.31*b*	19.67 ± 0.12*a*	12.67 ± 0.54*b*	19.67 ± 0.32*b*	13.67 ± 0.12*b*
B+Fe	8.37 ± 0.66*a*	4.93 ± 0.15*a*	8.40 ± 0.25*a*	4.93 ± 0.25*a*	19.67 ± 0.12*a*	14.00 ± 0.45*a*	20.67 ± 0.14*a*	15.00 ± 0.14*a*
Zn+B+Fe	8.20 ± 0.62*a*	4.83 ± 0.30*a*	8.33 ± 0.24*a*	4.63 ± 0.47*b*	19.33 ± 0.14*b*	14.00 ± 0.48*a*	20.33 ± 0.24*a*	15.00 ± 0.14*a*

Values are means, and numbers with parentheses are ± SEM (n = 3). Different letters indicate significant differences between means.

Grain Micronutrient Concentration

Zinc and Fe were analyzed using an atomic absorption spectrometer (210/211 VGP, United States). Boron was estimated according to the azomethine-H method (Lohse, 1982).

Protein Analysis

The finely ground seed sample (0.5 g) was digested with concentrated H_2SO_4. Total nitrogen in seeds was determined by the micro-Kjeldahl method as per the procedure suggested by Baethgen and Alley (1989). Seed protein contents were calculated by multiplying the nitrogen values by 6.25. Triplicate analyses were carried out on each sample.

Soil Moisture Estimation

Soil moisture measurement was carried out gravimetrically. Moisture was recorded at three depths: 0–15 cm, 15–30 cm, and 30–45 cm. All samples were dried in an oven at

TABLE 4 | Effect of sowing time and zinc, iron, and boron foliar sprays on the relative leaf water content of lentil (%).

Treatments	2018–19		2019–20	
	Normal-sown	Late-sown	Normal-sown	Late-sown
Control	79.60 ± 1.62*c*	60.83 ± 0.72*c*	79.07 ± 0.99*c*	60.03 ± 0.73*c*
Tap water	80.53 ± 1.46*bc*	60.93 ± 0.68*c*	80.58 ± 0.55*bc*	60.68 ± 1.05*c*
Zn@0.5%	80.60 ± 1.03*b*	61.67 ± 1.03*b*	80.80 ± 0.48*b*	60.72 ± 0.74*bc*
Fe@0.5%	80.73 ± 0.40*b*	61.33 ± 1.25*b*	80.67 ± 0.58*b*	60.53 ± 1.08*c*
B@0.2%	80.67 ± 0.99*b*	61.08 ± 1.47*b*	81.62 ± 0.60*b*	61.43 ± 0.92*b*
Zn+B	81.83 ± 0.29*a*	61.77 ± 0.28	81.78 ± 0.52*b*	61.72 ± 1.29*b*
Zn+Fe	81.83 ± 1.53*a*	62.60 ± 1.49*a*	81.52 ± 0.38*b*	61.70 ± 0.96*b*
B+Fe	81.60 ± 0.55*a*	62.60 ± 1.57*a*	82.22 ± 0.54*a*	62.05 ± 1.08*a*
Zn+B+Fe	81.82 ± 0.78*a*	62.23 ± 1.32*a*	82.20 ± 0.79*a*	62.32 ± 0.25*a*

Values are means, and numbers with parentheses are ± SEM (n = 3). Different letters indicate significant differences between means.

105°C for 24–48 h to constant moisture. The dried soil samples were weighed on an electrical balance. Actual moisture content in each soil sample was calculated as follows:

$$\text{Soil moisture (\%)} = \frac{\textit{Fresh weight of soil } (g) - \textit{Dry weight of soil } (g)}{\textit{Dry weight of soil } (g)} \times 100$$

From percent soil moisture, soil moisture on depth basis was estimated using:

$$\text{Soil moisture (cm)} = \text{Soil moisture content (\%)} \times A_i \times D$$

Flower and Pod Numbers and Yield

The number of open flowers per plant was recorded daily, excluding the previous day's open flowers in the following day's count. Five plants were tagged in the central rows from each plot to calculate the total flower number. Five plants were randomly uprooted from the sampling rows of each plot at harvest to calculate the average pod number. The grain from each plot was dried to 12–13% moisture to calculate seed yield per hectare.

Statistical Analysis

The data were analyzed using analysis of variance (ANOVA) for split-plot design (Gomez and Gomez, 1984). IRRI's STAR software was used to perform the statistical analysis. Tukey's *post-hoc* test was applied to compare differences between the mean values.

RESULTS

Chlorophyll Content

Normal-sown (November) lentils had higher values of chlorophyll a, chlorophyll b, total chlorophyll, and carotenoid (1.15, 0.50, 1.65, and 1.36 mg g^{-1} FW) than late-sown (December) lentils (0.89, 0.37, 1.26, and 0.88 mg g^{-1} FW) in 2018–19 (**Figures 1**, **2**), with a similar trend in 2019–20. For normal-sown lentils in 2018–19, the micronutrient foliar sprays increased chlorophyll contents. The Zn+Fe+B treatment recorded the highest values for chlorophyll a, chlorophyll b,

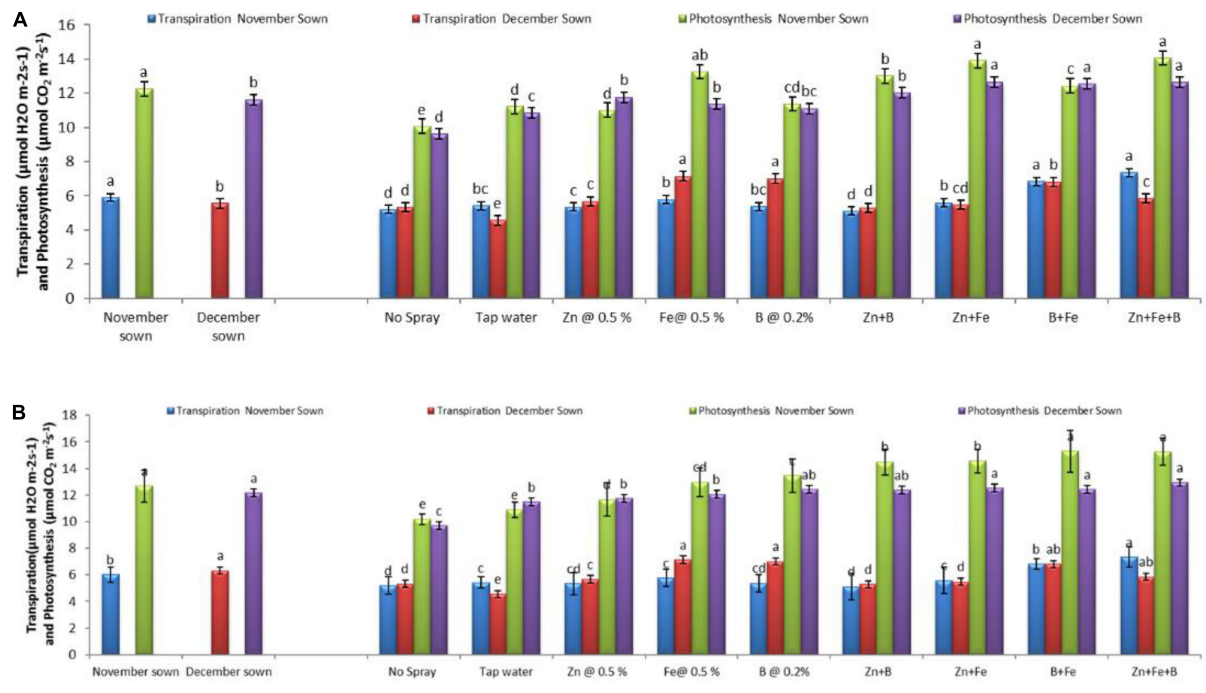

FIGURE 5 | Transpiration and photosynthesis (µmol CO_2 m^{-2} s^{-1}) for different sowing dates and foliar spray treatments in the **(A)** 2018–19 and **(B)** 2019–20 lentil cropping seasons. Values are means, and bars represent ± SEM (*n* = 3). Different letters indicate significant differences between means.

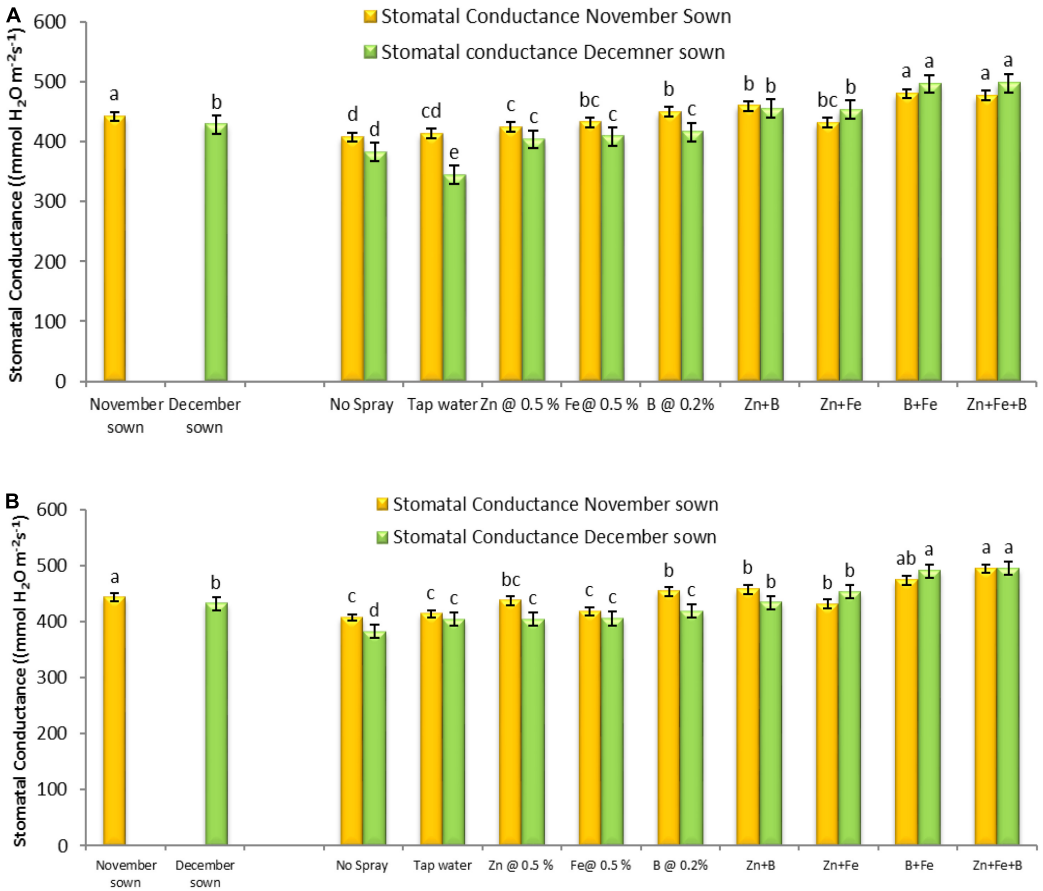

FIGURE 6 | Stomatal conductance (μmol CO_2 m^{-2} s^{-1}) for different sowing dates and foliar spray treatments in the **(A)** 2018–19 and **(B)** 2019–20 lentil cropping seasons. Values are means, and bars represent ± SEM (n = 3). Different letters indicate significant differences between means.

total chlorophyll, and carotenoid (1.48, 0.62, 2.11, and 1.89 mg g^{-1}) relative to the control (0.86, 0.42, 1.28, and 0.97 mg g^{-1}). Late-sown lentils had lower values than normal-sown lentils due to moisture and temperature stress, but the foliar sprays somewhat ameliorated the stress effects with higher values than the control. A similar trend occurred in 2019–20 (**Figures 1**, **2**).

Pollen Studies

Normal-sown lentils had 92% pollen viability and 88% pollen germination in 2018–19 as compared to 70 and 64%, respectively, for late-sown lentils (**Figures 3**, **4**). A similar trend occurred in 2019–20. The Zn+Fe+B and Fe+B foliar sprays produced the highest pollen viability and germination relative to the control (no spray) (**Supplementary Figure 1**).

Seed Growth Rate and Seed Filling Duration

Normal-sown lentils had a higher seed growth rate (7.69 and 7.75 g DW) than late-sown lentils (4.52 and 4.53 g DW) in 2018–19 and 2019–20, respectively. Stress reduced the days to maturity, resulting in a lower seed growth rate in the late-sown crop (**Table 3**). The B+Fe treatment had 25 and 14% higher seed growth rates in 2018–19 and 2019–20 than the control.

Relative Leaf Water Content

Relative leaf water content significantly differed between sowing dates and foliar sprays (**Table 4**). The late-sown crop had 23–24% lower RLWC than the normal sown crop in both years. Foliar spray of Zn+Fe, B+Fe, and Zn+B+Fe increased RLWC in both the years relative to the control.

Net Photosynthetic Rate, Transpiration Rate, and Stomatal Conductance

Normal-sown lentils had higher maximum net photosynthesis (12.26 and 12.68 μmol CO_2 m^{-2} s^{-1}), transpiration rate (5.90 and 6.01 μmol H_2O m^{-2} s^{-1}), and stomatal conductance (441.59 and 442.70 mmol H_2O m^{-2} s^{-1}) than late-sown lentils (11.62 and 12.15 μmol CO_2 m^{-2} s^{-1}, 5.55 and 6.32 μmol H_2O m^{-2} s^{-1}, and 428.65 and 431.63 mmol H_2O m^{-2} s^{-1}) in the period of 2018–19 and 2019–20,

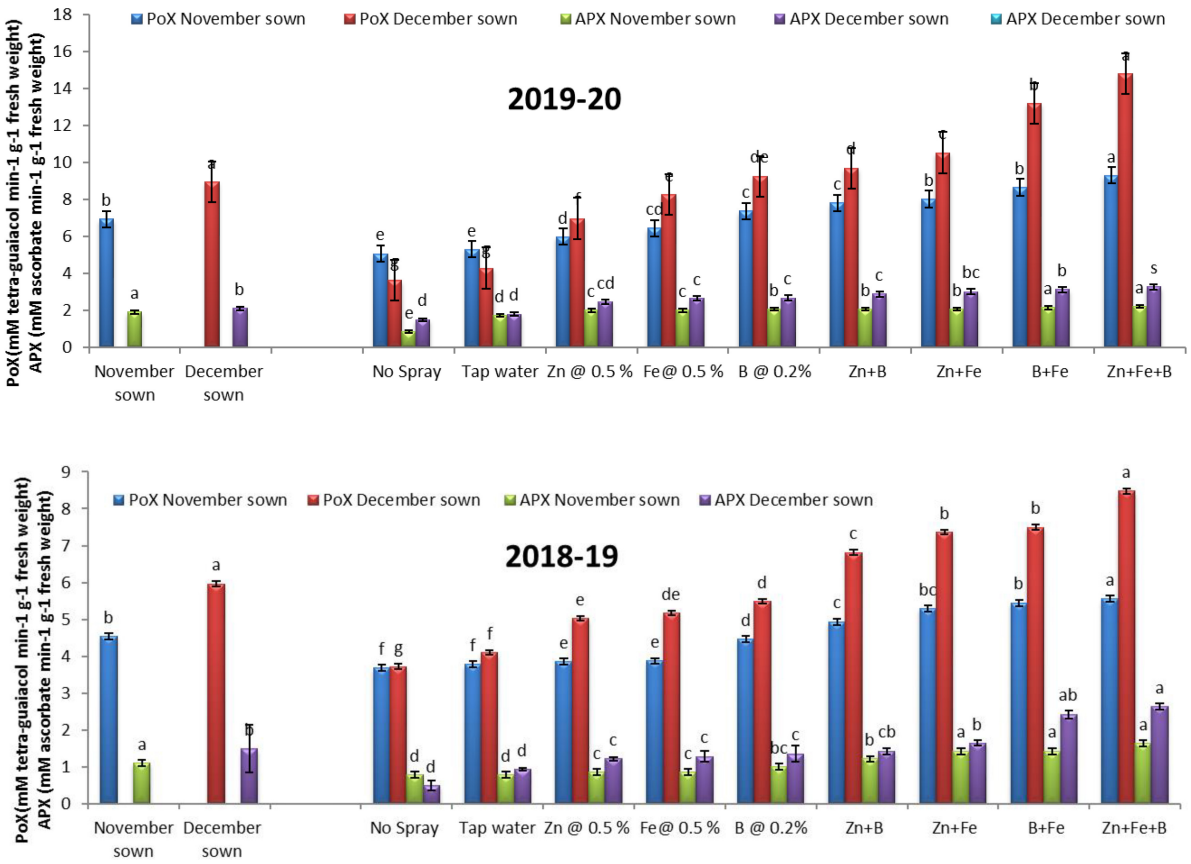

FIGURE 7 | Peroxidase (POX; mM tetra-guaiacol min^{-1} g^{-1} FW) and ascorbate peroxidase (APX; mM ascorbate min^{-1} g^{-1} FW) activities for different sowing dates and foliar spray treatments in 2018–19 and 2019–20 lentil cropping seasons. Values are means, and bars represent ± SEM (n = 3). Different letters indicate significant differences between means.

respectively. The foliar micronutrient sprays also affected net photosynthetic rate, transpiration rate, and stomatal conductance (**Figures 5**, **6**).

Enzymes

Late-sown lentils had higher POX (6.92 and 8.94 mM tetra-guaiacol min^{-1} g^{-1} FW) and APX (1.90 and 2.12 mM ascorbate min^{-1} g^{-1} FW) activities than normal-sown lentils (4.54 and 7.09 mM tetra-guaiacol min^{-1} g^{-1} FW and 1.34 and 1.48 mM ascorbate min^{-1} g^{-1} FW) in 2018–19 and 2019–20, respectively (**Figure 7**).

Lipid Peroxidation

Late-sown lentils had significantly higher lipid peroxidation than normal-sown lentils. The foliar spray treatments did not significantly affect MDA contents in normal-sown lentils but significantly increased them in late-sown lentils (**Figure 8**).

Proline

Late-sown lentils accumulated more proline (0.40 and 0.52 μmol g^{-1}) than normal-sown lentils (0.29 and 0.39 μmol g^{-1}) in 2018–19 and 2019–20, respectively (**Figure 9**).

Moisture Storage

Late-sown lentils had lower soil moisture content than normal-sown lentils throughout both growing seasons, except initially in the second year due to a fair amount of rain (15.4 mm) just before sowing. Changes in moisture storage over time are shown in **Figure 10**.

Seed Nutrient and Protein Contents

The Fe, Zn, and B contents did not significantly differ between growing seasons, so the data were pooled (**Table 5**). Late sowing significantly affected micronutrient accumulation and seed protein content. Late-sown lentils had 21.85–23.13% seed protein when compared with 24.32–25.05% in normal-sown lentils. Foliar sprays at the pre-flowering and pod development stages also significantly affected micronutrient accumulation.

Flowers Pods and Yield

Sowing date significantly affected pod number per plant in both growing seasons. Foliar spray of micronutrients at

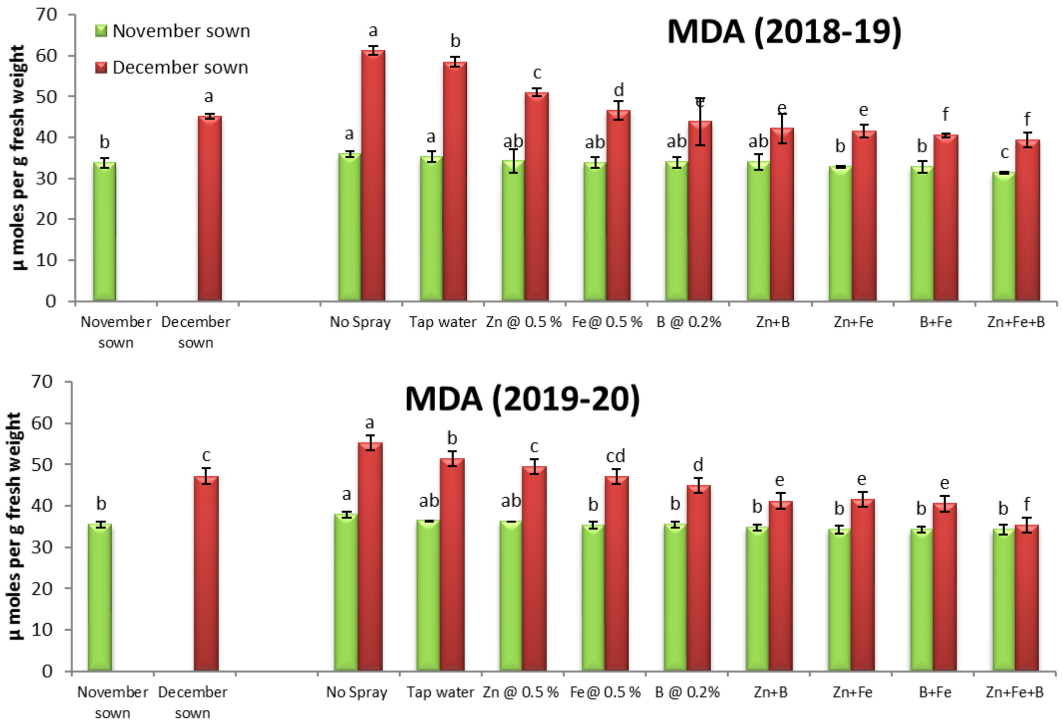

FIGURE 8 | Malondialdehyde (MDA; µmol g^{-1} FW) content for different sowing dates and foliar spray treatments in the 2018–19 and 2019–20 lentil cropping seasons. Values are means, and bars represent ± SEM (n = 3). Different letters indicate significant differences between means.

pre-flowering and pod development stages increased pod number per plant by 75–104.67 and 87.33–138.83 in 2018–19 and 2019–20, respectively, relative to the control (**Table 6**). Lentil seed yield significantly differed between treatments in both years (**Table 7**).

Correlation Studies

Pooled data for both years were used for the correlation analysis. The correlation coefficients for different crop parameters and grain yield indicated that most of the agro-physiological crop parameters were—flower number, pod number, seed growth rate, seed filling duration, total chlorophyll, and enzyme activities—positively correlated with yield, while lipid peroxidation and proline content were negatively correlated with growth and yield parameters (**Figure 11**).

The correlation matrix heatmap shows the Pearson's correlation coefficient values for all studied parameters, with positive values in red and negative values in blue. The values range from −1 to 1, where −1 indicates a perfect negative linear relationship, 1 indicates a perfect positive linear relationship, and 0 indicates no relationship between variables. The studied parameters were seed growth rate, seed filling duration, RLWC, pollen viability, pollen germination, total chlorophyll, pod number, seed yield, transpiration rate, net photosynthetic rate, stomatal conductance, lipid peroxidation, proline, and APX (color figure online).

DISCUSSION

Relative Water Content to Water Relations and Gas Exchange

In terms of the physiological consequences of cellular water shortage, the relative amount of water present in plant tissues is the most accurate indicator of plant water status (Barrs and Weatherly, 1962; Nilsen and Orcutt, 1996). Late-sown lentils had lower leaf relative water content (RWC) than normal-sown lentils due to low soil moisture and heat stress delaying seedling emergence (**Supplementary Tables 1**, **2**; Talukdar, 2013), leading to loss of turgor, reduced cell expansion, and suppressed plant growth and development. A decrease in leaf RWC in response to soil moisture stress has been reported in various species (Nayyar and Gupta, 2006). Late-sown lentils had considerably lower chlorophyll a, chlorophyll b, chlorophyll a/b ratio, carotenoids, stomatal conductance, and net photosynthetic rate than normal-sown lentils. The reduced pigment composition and stomatal conductance in late-sown lentils might have reduced the net photosynthetic rate. Higher stomatal conductance in plants increases CO_2 diffusion into leaves, favoring photosynthesis. Higher net CO_2 assimilation rates also increase biomass and crop yield (Saraswathi and Paliwal, 2011).

We observed improved pigment composition and photosynthetic rate in treatments sprayed with Fe+Zn+B and Fe+B. Iron is important for chlorophyll biosynthesis, energy transmission, and chloroplast development (Kim and Guerinot, 2007; Brumbarova et al., 2008; Gill and Tuteja, 2011), so the

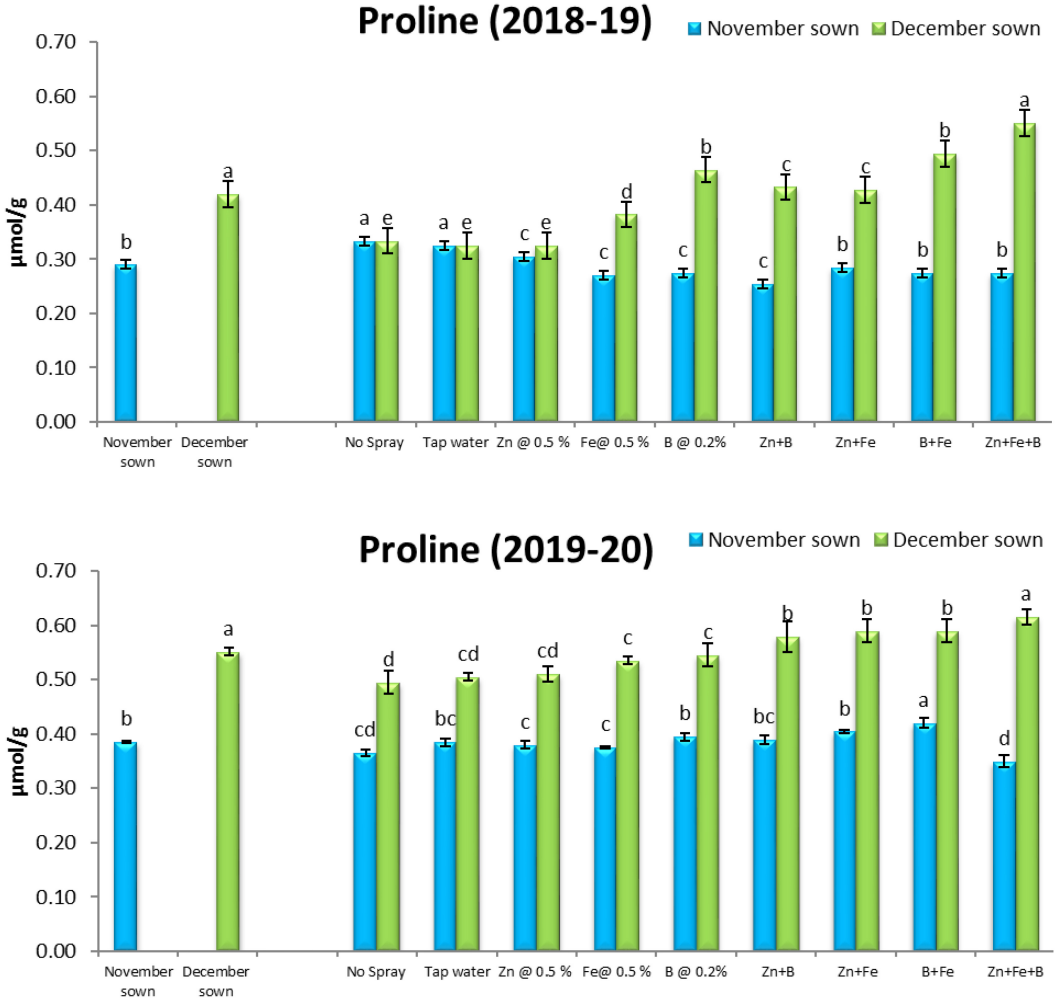

FIGURE 9 | Proline (µmol g^{-1}) content for different sowing dates and foliar spray treatments in the 2018–19 and 2019–20 lentil cropping seasons. Values are means, and bars represent ± SEM (n = 3). Different letters indicate significant differences between means.

Fe+Zn+B and Fe+B treatments might have improved chlorophyll content in our study. Kumawat et al. (2006) reported that Fe application to pulse crops increased leaf chlorophyll content attributing to Fe being a structural component of chlorophyll. Boron is an important nutrient for carbohydrate and hormone metabolism and translocation. In addition, B is involved in potassium transport into guard cells and thus stomatal opening (Romheld and Marschner, 1991) and photosynthesis. Zinc deficiency inhibits plant development and limits photosynthesis in many plant species (Wang and Jin, 2005). Chandan and Vijay (2018) reported that soil and foliar sprays of Fe and Zn improved chlorophyll content in lentils. Nandan et al. (2018) reported that combining foliar Zn and Fe sprays at the pre-flowering and pod development stages with the recommended fertilizer dose increased chlorophyll content in chickpea. We observed all of the above advantages of these micronutrients in improving various physiological traits in lentils. Zn, Fe, and B also help alleviate abiotic stress (Waraich et al., 2012), as evidenced by the improved leaf RWC, chlorophyll accumulation, and photosynthesis in late-sown lentils with Zn+Fe+B foliar spray.

High temperature decreases soil nutrient uptake, and moisture stress combined with high temperature further enhances the importance of an exogenous nutrient supply. Endogenous Zn, B, and Fe applications might modulate biochemical changes through antioxidant enzymes, as reported by Corrales et al. (2008); Upadhyaya et al. (2013), and Zahoor et al. (2017). Exogenous nutrient application upregulates chlorophyll biosynthesis, delays senescence, and enhances nutrient biofortification, consequently improving the photosynthetic rate and photosynthetic enzymes (Sarwar et al., 2019). Similarly, Zn-mediated regulation of water relations confers heat tolerance by sustaining cell water and osmotic potential under stress conditions. Boron availability enhances stomatal opening, regulating gaseous exchange in stressed environments (Jain et al., 2001; Stavrianakou et al., 2006). The combined application of Zn, Fe, and B spray treatments improved chlorophyll biosynthesis, photosynthetic rate, gaseous exchange regulation,

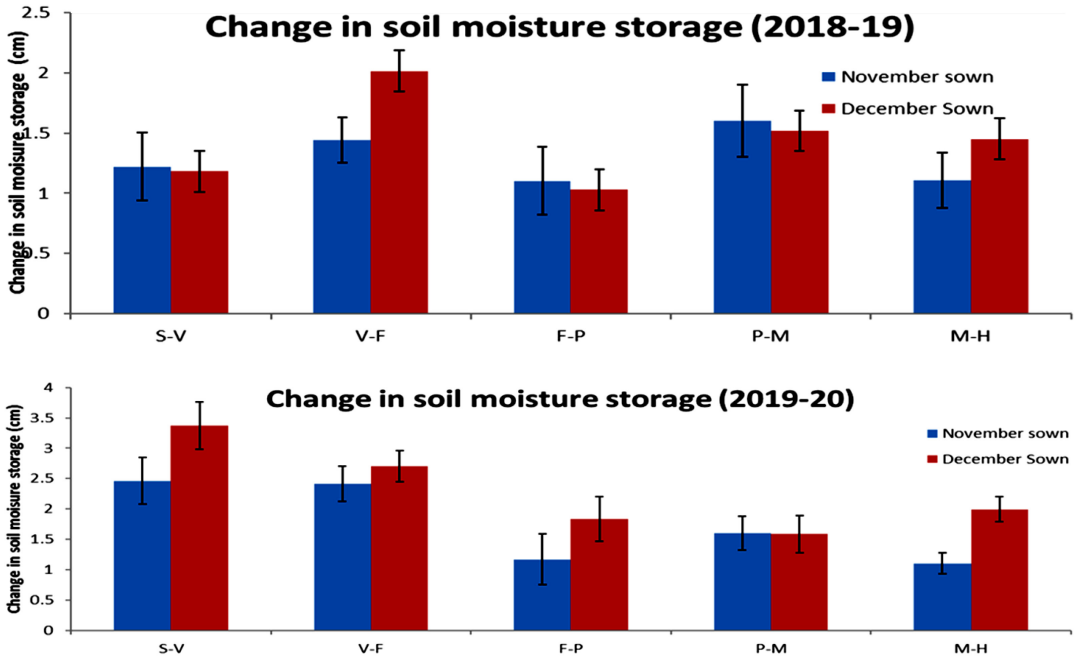

FIGURE 10 | Change in soil moisture storage (0–45 cm soil profile) for different sowing dates in the 2018–19 and 2019–20 lentil cropping seasons. Error bars represent the standard error of the mean. Values are means, and bars represent ± SEM (n = 3). Different letters indicate significant differences between means. S–V (sowing to the vegetative stage), V–F (vegetative to the flowering stage), F–P (flowering to pod development stage), P–M (pod development to maturity stage), and M–H (maturity to harvest stage).

TABLE 5 | Effect of sowing time and zinc, iron, and boron foliar sprays seed nutrients and seed protein.

Treatments	Fe (mg/100 g)		Zn (mg/100 g)		B (mg/100 g)		Seed protein (%)	
	Normal-sown	Late-sown	Normal-sown	Late-sown	Normal-sown	Late-sown	Normal-sown	Late-sown
Control	7.28 ± 0.2*b*	3.52 ± 0.2*b*	3.13 ± 0.3*b*	3.13 ± 0.2*b*	3.52 ± 0.2*b*	1.40 ± 0.2*d*	24.32 ± 0.3*b*	21.85 ± 0.4*c*
Tap water	7.32 ± 0.1*b*	3.50 ± 0.2*b*	3.25 ± 0.3*b*	3.25 ± 0.2*b*	3.50 ± 0.2*b*	1.47 ± 0.2*d*	24.58 ± 0.1*ab*	21.98 ± 0.2*c*
Zn@0.5%	7.33 ± 0.3*b*	4.13 ± 0.1*a*	3.35 ± 0.1*b*	3.35 ± 0.5*b*	4.13 ± 0.2*a*	1.90 ± 0.1*a*	24.90 ± 0.1*a*	22.17 ± 0.5*b*
Fe@0.5%	7.80 ± 0.2*a*	3.72 ± 0.2*b*	3.37 ± 0.2*b*	3.37 ± 0.2*b*	3.72 ± 0.6*b*	1.72 ± *c*0.2	24.80 ± 0.2*a*	22.35 ± 0.6*b*
B@0.2%	7.52 ± 0.3*b*	3.67 ± 0.3*b*	4.05 ± 0.2*a*	4.05 ± 0.1*a*	3.67 ± 0.2*b*	1.73 ± 0.3*c*	24.80 ± 0.2*a*	22.43 ± 0.1*b*
Zn+B	7.58 ± 0.2*b*	4.22 ± 0.4*a*	3.92 ± *a*0.1*b*	3.92 ± 0.1*ab*	4.22 ± 0.1*a*	1.83 ± 0.1*b*	24.90 ± 0.3*a*	22.87 ± 0.3*b*
Zn+Fe	7.88 ± 0.3*a*	4.33 ± 0.2*a*	3.48 ± 0.2*b*	3.48 ± 0.4*b*	4.33 ± 0.2*a*	1.95 ± 0.2*a*	24.98 ± 0.1*a*	22.82 ± 0.2*b*
B+Fe	7.78 ± 0.1*a*	3.78 ± 0.1*b*	4.02 ± 0.2*a*	4.02 ± 0.2*a*	3.78 ± 0.2*b*	1.90 ± 0.2*a*	25.03 ± 0.2*a*	22.90 ± 0.3*a*
Zn+B+Fe	7.77 ± 0.2*a*	4.18 ± 0.2*a*	4.00 ± 0.2*a*	4.00 ± 0.1*a*	4.18 ± 0.2*a*	1.92 ± 0.1*a*	25.05 ± 0.1*a*	23.12 ± 0.1*a*

Values are means, and numbers with parentheses are ± SEM (n = 3). Different letters indicate significant differences between means.

and osmoregulation, helping the late-sown lentil plants to alleviate stress and improve yield.

Enzyme Activities

Lipid membrane peroxidation by ROS indicates stress-induced damage at the cellular level. An increase in the lipid peroxidation product, MDA, is often used as a plant stress indicator (Jain et al., 2001), generally increasing with temperature extremities. We observed increased MDA content in the control and the treatment sprayed with tap water. High-temperature stress increased MDA content in French beans (Babu and Devraj, 2008) and rice (Pantoja-Benavides et al., 2021). Under normal sowing conditions (November sown), a well-coordinated and responsive antioxidant system balanced oxidative damage to cellular components. Improved RLWC in the treatments sprayed with micronutrients could help maintain membrane stability during stress. Similar to MDA, proline is important for maintaining osmoregulation and accumulating low molecular weight metabolites, such as sugars, organic acids, and amino acids (Gill et al., 2011; Chakhchar et al., 2015). Proline is a major osmoprotectant (Gill et al., 2011) involved in ROS scavenging, protecting cell membranes from oxidative damage. We observed an increased level of proline accumulation in the late-sown lentils and the Zn, Fe, and B treatment. In general, proline concentration increases in response to water stress, resulting in water transfer to plants (Sofo et al., 2004). Different enzymes and metabolites

TABLE 6 | Effect of sowing time and zinc, iron, and boron foliar sprays on flower and pod numbers.

Treatments	2018–19				2019–20			
	Flower number		Pod number		Flower number		Pod number	
	Normal-sown	Late-sown	Normal-sown	Late-sown	Normal-sown	Late-sown	Normal-sown	Late-sown
Control	275 ± 8.4*c*	204 ± 12.1*c*	83 ± 6.5*c*	68 ± 6.5*c*	288 ± 7.3*d*	218 ± 13.2*c*	92 ± 8.7*e*	83 ± 7.7*b*
Tap water	282 ± 8.7*c*	224 ± 11.2*c*	90 ± 6.4*c*	68 ± 3.5*c*	285 ± 4.5*d*	234 ± 9.2*bc*	104 ± 5.1*d*	85 ± 4.5*b*
Zn@0.5%	306 ± 5.6*b*	256 ± 10.3*b*	109 ± 3.5*ab*	71 ± 6.7*b*	313 ± 5.7*b*	256 ± 8.4*b*	134 ± 6.2*c*	87 ± 1.5*b*
Fe@0.5%	299 ± 2.3*c*	264 ± 9.5*a*	106 ± 2.7*ab*	81 ± 7.6*a*	307 ± 7.7*c*	268 ± 10.2*a*	144 ± 3.5*c*	90 ± 2.5*a*
B@0.2%	318 ± 6.4*b*	271 ± 6.8*a*	104 ± 7.8*ab*	79 ± 8.4*ab*	318 ± 15.1*b*	275 ± 5.4*a*	150 ± 4.1*b*	88 ± 4.8*b*
Zn+B	307 ± 11.2*b*	275 ± 8.9*a*	116 ± 8.4*a*	84 ± 6.5*a*	319 ± 5.7*b*	275 ± 6.5*a*	159 ± 9.5*b*	94 ± 9.5*a*
Zn+Fe	304 ± 12.5*bc*	249 ± 9.7*b*	129 ± 9.4*a*	73 ± 8.4*ab*	305 ± 6.1*c*	275 ± 11.2*a*	157 ± 7.4*b*	97 ± 6.5*a*
B+Fe	332 ± 9.8*a*	262 ± 9.7*a*	119 ± 8.4*a*	75 ± 7.8*ab*	341 ± 9.5*a*	269 ± 6.4*a*	179 ± 8.4*a*	99 ± 6.7*a*
Zn+B+Fe	357 ± 8.6*a*	289 ± 5.6*a*	101 ± 5.5*ab*	84 ± 9.7*a*	357 ± 6.2*a*	291 ± 7.2*a*	172 ± 8.7*a*	95 ± 5.8*a*

Values are means, and numbers with parentheses are ± SEM (n = 3). Different letters indicate significant differences between means.

TABLE 7 | Effect of sowing time and zinc, iron, and boron foliar sprays on seed yield (kg ha^{-1}).

Treatments	2018–19		2019–20	
	Normal-sown	Late-sown	Normal-sown	Late-sown
Control	1, 024 ± 24.9*e*	861 ± 35.2*e*	1, 011 ± 29.5*f*	865 ± 35.2*d*
Tap water	1, 033 ± 31.2*e*	887 ± 44.6*e*	1, 033 ± 60.1*f*	876 ± 63.2*d*
Zn@0.5%	1, 264 ± 22.0*d*	905 ± 28.5*d*	1, 288 ± 38.5*d*	919 ± 54.4*c*
Fe@0.5%	1, 194 ± 35.2*d*	924 ± 54.2*d*	1, 179 ± 53.2*e*	954 ± 29.5*c*
B@0.2%	1, 325 ± 46.2*c*	957 ± 24.5*cd*	1, 363 ± 46.2*c*	961 ± 36.5*bc*
Zn+B	1, 483 ± 32.8*b*	973 ± 36.4*c*	1, 496 ± 57.5*c*	965 ± 54.2*b*
Zn+Fe	1, 481 ± 19.7*b*	992 ± 29.5*c*	1, 492 ± 46.5*c*	996 ± 44.6*b*
B+Fe	1, 744 ± 38.1*a*	1, 183 ± 32.7*a*	1, 723 ± 54.9*a*	1, 073 ± 52.1*a*
Zn+B+Fe	1, 525 ± 55.8*b*	1, 064 ± 58.4*b*	1, 534 ± 81.4*b*	1, 004 ± 36.4*a*

Values are means, and numbers with parentheses are ± SEM (n = 3). Different letters indicate significant differences between means.

contribute to the antioxidant defense system. We studied the effect of APX and POX antioxidant enzymes that help protect cells by purifying and detoxifying ROS in cells and increasing stress tolerance (Farooq et al., 2009). This enzyme catalyzes the partitioning of O_2 into either ordinary molecular O_2 or H_2O_2 and is involved in the fine modulation of ROS for signaling (Lin et al., 2010). Late-sown lentils faced stress in both years due to low soil moisture and increased air temperatures, increasing proline, APX, and POX activities, as reported for canola (Rezayian et al., 2018) and chickpea (Khan et al., 2019). The Zn, Fe, and B foliar sprays induced physiological and biochemical responses, such as ROS scavenging, to cope with the stress. The higher proline concentration in water-stressed plants indicates an efficient mechanism for osmotic regulation, stabilization of sub-cellular structures, and cellular adaptation to water stress (Gunes et al., 2008). The decreased MDA buildup in the foliar spray treatments suggests that micronutrients have the potential to alleviate stress by activating the enzymatic response, as seen in cotton (Sarwar et al., 2019) and citrus (Sarwar et al., 2019). Studies have found that heat-tolerant cultivars exhibit higher antioxidant enzyme activity than sensitive wheat (Huseynova, 2012) and chickpea (Khan et al., 2019) cultivars. However, there may be a temperature threshold at which defensive enzyme activity declines, giving ROS the upper hand (Farooq et al., 2009). In our study, the decreased MDA level and increased proline accumulation with micronutrient foliar spray could be attributed to reduced oxidative stress caused by the ROS scavenging response.

Lentil requires low temperatures during vegetative growth and warm temperatures during reproductive growth. The optimal temperature during flowering and pod filling is 30/18°C (max/min); temperatures > 32/20°C (max/min) can drastically reduce lentil seed yield and quality (Saxena, 2009; Malik et al., 2015; Sita et al., 2018). Late-sown lentils had shorter cool and longer hot periods than normal-sown lentils, exposing the crop to heat and moisture stress, particularly, during the reproductive stage. Temperatures varied by 2–3°C between normal- and late-sown lentils during the reproductive stage (pod initiation to maturity) in both years. Furthermore, daily temperatures exceeded 32°C (T_{max}) for 3–5 consecutive days for late-sown lentils. The lentil crops were exposed to above-optimal temperatures in both years, especially when sown late. Due to the lack of irrigation, the crops also suffered moisture stress during the terminal stage, particularly, when sown late.

Seed Nutrients and Protein

Late-sown lentils had significantly lower vital minerals (Fe, Zn, and B) than normal-sown lentils due to heat and/or drought stress. The lower soil moisture might have inhibited mineral translocation into developing seeds, similar to Sehgal et al. (2019) who reported that moisture and heat stress reduced K, Ca, Fe, P, Mn, and Zn contents in lentils. The reduced seed protein content in late-sown lentils indicated impaired protein synthesis due to stress, consistent with drought-stressed beans (Ghanbari et al., 2013a), chickpea (Behboudian et al., 2001), and wheat (Begcy and Walia, 2015). Stress affects seed output by impairing symbiotic nitrogen fixation, increasing oxygen diffusion resistance to root bacteroides, reducing nitrogenase activity, and thus limiting nitrogen availability for protein biosynthesis (Purcell and King, 1996). While seed protein quality largely depends on genotype,

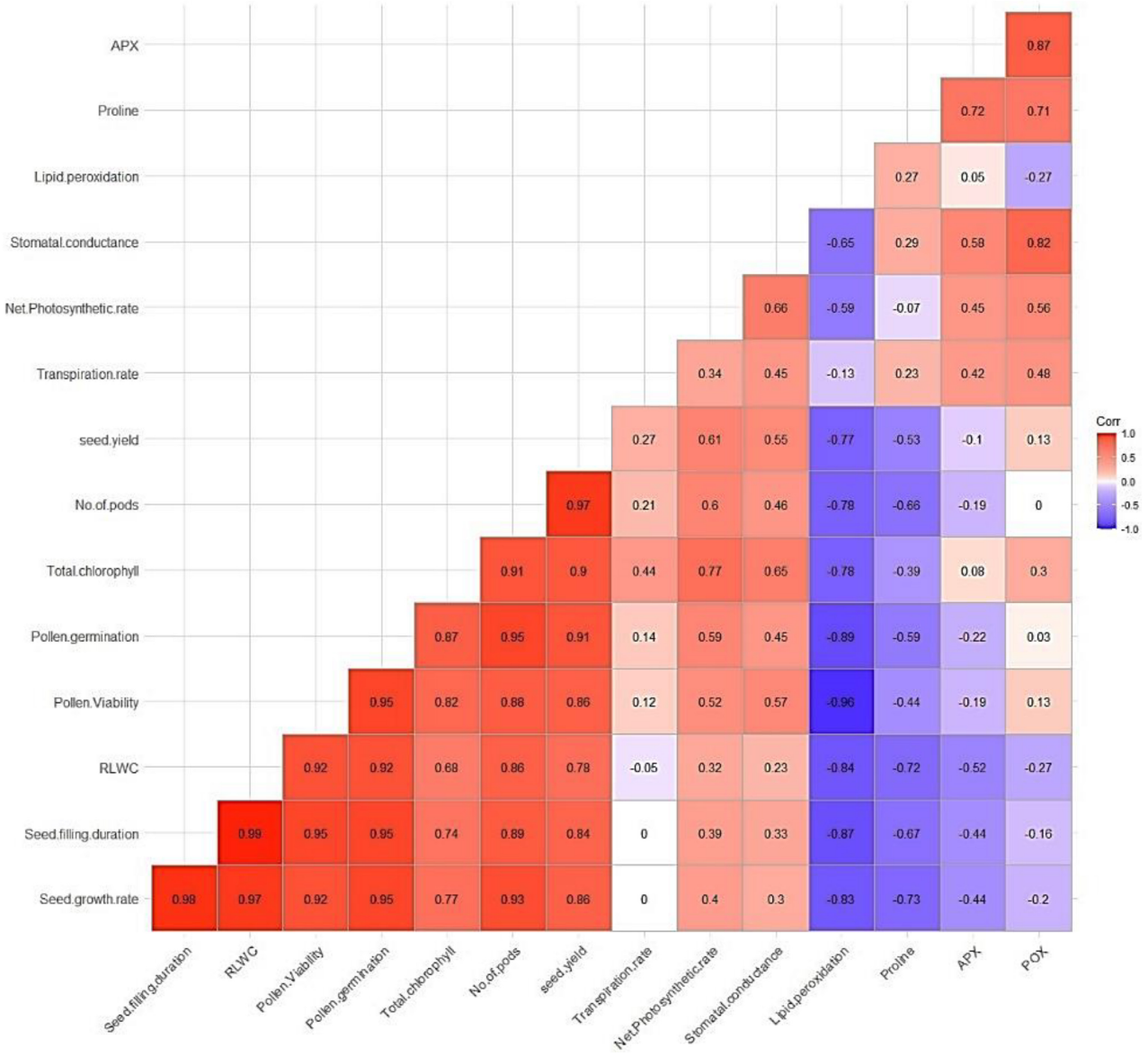

FIGURE 11 | Correlation analysis of physiological traits and yield.

environmental stresses can influence it (Triboï et al., 2003). Drought and heat stresses alter protein fractions primarily due to changes in total nitrogen accumulated during seed filling (Triboï et al., 2003). Some legume studies have reported that drought stress reduces mineral accumulation in developing seeds. For example, Fe, Zn, P, and N concentrations decreased in common bean under drought stress and correlated with reduced total protein content (Ghanbari et al., 2013b). In another study, drought stress during pod filling decreased seed nitrogen and protein contents in white, red, and "chitti" bean cultivars (Ghanbari et al., 2013a).

Foliar micronutrient sprays in the field increased N_2 fixation and nodule mass and thus grain N contents in chickpea, lentils, and lupin (Yanni, 1992). We found that foliar micronutrient sprays also improved grain Zn, Fe, and B contents, even in late-sown lentils. Other studies have reported that foliar micronutrient sprays affected the uptake of N, P, K, S, Zn, and B in rice (Hossain et al., 2001), soybean (Sarker et al., 2002), lentil (Okaz et al., 1994), and mung (Singh and Prasad, 2014) bean.

Flower and Pod Numbers and Yield

Terminal drought and high temperatures are becoming more common, impacting seed development in cool-season pulses, such as lentils. High temperature has been associated with reduced water availability (Barnabás et al., 2008). In cereals, such as wheat and maize, combined drought and heat stress decreased photosynthesis, stomatal conductance, leaf area, and water use efficiency (Shah and Paulsen, 2003), with similar results reported

for chickpea (Awasthi et al., 2014) and lentil (Sehgal et al., 2017, 2019). Cool-season food legumes, such as chickpea (Kaushal et al., 2013) and lentils (Sita et al., 2017a), are adapted to low and mild temperature environments and are thus highly sensitive to heat stress. Sowing date and micronutrient foliar sprays significantly affected lentil yield attributes. The micronutrient foliar sprays helped in reducing the adverse effects of heat and moisture stress to improve seed yield, even under late-sown conditions, particularly, the B+Fe foliar spray, which increased yield by 35–37% yield when compared to the control.

Flower and pod numbers per plant are the most influential yield components, which are closely correlated with seed yield. Zinc, B, and Mo enhanced pod numbers per plant in mung bean (Quddus et al., 2011), chickpea (Valenciano et al., 2011), Zn and B in green gram (Begum, 2014), Zn in French bean (Nasir et al., 2011), and B and Mo in cowpea (Chatterjee and Bandyopadhyay, 2017). Our study contributes to the growing body of literature on the effect of Zn, Fe, and B on lentils. The correlation analysis provides a clear picture of the relationship between improved yield and exogenous application of these micronutrients. The correlation coefficient between a causal factor and the effect (i.e., grain yield) is almost equal to its direct effect.

High temperatures and moisture stress during the reproductive stage reduced lentil yield by decreasing chlorophyll content and impeding photosynthesis. Exogenous application of Zn, Fe, and B improved chlorophyll content, net photosynthetic rate, water relations, and yield in lentil, especially, B+Fe and B+Zn+Fe, which upregulated antioxidant enzyme activities (POX, APX, proline, and MDA) and improved chlorophyll content, net photosynthetic rate, and yield.

CONCLUSION

High temperature and moisture stress at the reproductive stage in lentils reduced grain yield by reducing chlorophyll contents and impairing photosynthesis. Exogenous application of micronutrients (Zn, Fe, and B) ameliorated the stress effects. In particular, B+Fe and B+Zn+Fe upregulated antioxidant enzyme activities (POX, APX, proline, and MDA) and improved chlorophyll content, net photosynthetic rate, water relations, and yield. Our study revealed that foliar spray of Zn, Fe, and B ameliorated terminal heat and moisture stress in late-sown lentils. Furthermore, ameliorating high-temperature-induced oxidative stress using foliar micronutrient sprays opens up the possibility of improving plant growth at higher temperatures.

DATA AVAILABILITY STATEMENT

The original contributions presented in the study are included in the article/**Supplementary Material**, further inquiries can be directed to the corresponding authors.

AUTHOR CONTRIBUTIONS

VV, KS, RN, AP, and SB designed the study. VV and PB conducted the field experiment and data acquisition. VV, SR, LS, and AP conducted the lab analysis. VV, SR, and MC conducted the statistical analyses and wrote the manuscript. VV, AH, and KHS edited the final version of the manuscript. All authors contributed to the article and approved the submitted version.

FUNDING

This study was funded by the ICARDA project. The authors thank The UWA Institute of Agriculture and School of Agriculture and Environment, The University of Western Australia, Perth, Australia, for funding the publication.

ACKNOWLEDGMENTS

We extend our appreciation to International Center for Agricultural Research in the Dry Areas (ICARDA), and the first author thanks the Director, ICAR-CRIDA, for granting Ph.D. study leave.

SUPPLEMENTARY MATERIAL

The Supplementary Material for this article can be found online at: https://www.frontiersin.org/articles/10.3389/fpls.2022.847743/full#supplementary-material

REFERENCES

Arnon, D. I. (1949). Copper enzymes in isolated chloroplasts. Polyphenoloxidase in *Beta vulgaris*. *Plant Physiol.* 24:1. doi: 10.1104/pp.24.1.1

Awasthi, R., Kaushal, N., Vadez, V., Turner, N. C., Berger, J., Siddique, K. H. M., et al. (2014). Individual and combined effects of transient drought and heat stress on carbon assimilation and seed filling in chickpea. *Funct. Plant Biol.* 41, 1148–1167. doi: 10.1071/FP13340

Babu, N. R., and Devraj, V. R. (2008). High temperature and salt stress response in French bean (*Phaseolus vulgaris*). *Aust. J. Crop Sci.* 2, 40–48.

Baethgen, W. E., and Alley, M. M. (1989). A manual colorimetric procedure for measuring ammonium nitrogen in soil and plant Kjeldahl digests. *Commun. Soil Sci. Plant Anal.* 20, 961–969. doi: 10.1080/00103628909368129

Barnabás, B., Jäger, K., and Fehér, A. (2008). The effect of drought and heat stress on reproductive processes in cereals. *Plant Cell Environ.* 31, 11–38. doi: 10.1111/j.1365-3040.2007.01727.x

Barrs, H. D., and Weatherly, P. E. (1962). A re examination of relative turgidity for estimating water deficit in leaves. *Aust. J. Biol. Sci.* 15, 413–428. doi: 10.1071/bi9620413

Bates, L. S., Waldren, R. P., and Teare, I. D. (1973). Rapid determination of free proline for water stress studies. *Plant Soil* 39, 205–207. doi: 10.1007/bf00018060

Beck, E. H., Fettig, S., Knake, C., Hartig, K., and Bhattarai, T. (2007). Specific and unspecific responses of plants to cold and drought stress. *J. Biosci.* 32, 501–510. doi: 10.1007/s12038-007-0049-5

Begcy, K., and Walia, H. (2015). Drought stress delays endosperm development and misregulates genes associated with cytoskeleton organization and grain quality proteins in developing wheat seeds. *Plant Sci.* 240, 109–111. doi: 10.1016/j.plantsci.2015.08.024

Begum, R. (2014). *Effect of Some Micronutrients Application on Seed Yield and Quality in Green Gram*. Master's thesis. Odisha: Orissa University of Agriculture and Technology, Bhubaneswar.

Behboudian, M., Ma, Q. H., Turner, N. C., and Palta, J. A. (2001). Reactions of chickpea to water stress: yield and seed composition. *J. Sci. Food Agric.* 81, 1288–1291. doi: 10.1002/jsfa.939

Bourgault, M., Löw, M., Tausz-Posch, S., Nuttall, J. G., Delahunty, A. J., and Brand, J. (2018). Effect of heat wave on lentil grown under free-air CO_2 enrichment (FACE) in a semi-arid environment. *Crop Sci.* 58, 803–812. doi: 10.2135/cropsci2017.09.0565

Briat, J. F., Fobis-Loisy, N., Grignon, S., Lobréaux, N., Pascal, G., Savino, S., et al. (1995). Cellular and molecular aspects of iron metabolism in plants. *Biol. Cell*. 84, 69–81. doi: 10.1016/0248-4900(96)81320-7

Brumbarova, T., Matros, A., Mock, H. P., and Bauer, P. (2008). A Proteomic study showing differential regulation of stress, redox regulation and peroxidase proteins by iron supply and the transcription factor FER. *Plant J.* 54, 321–334. doi: 10.1111/j.1365-313X.2008.03421.x

Castillo, F. J., Penel, C., and Greppin, H. (1984). Peroxidase release induced by ozone in *Sedum album* leaves: involvement of Ca^{2+}. *Plant Physiol.* 74, 846–851. doi: 10.1104/pp.74.4.846

Chakhchar, A., Lamaoui, M., Wahbi, S., Ferradous, A., El Mousadik, A., Ibnsouda-Koraichi, S., et al. (2015). Leaf water status, osmoregulation and secondary metabolism as a model for depicting drought tolerance in *Arganias pinosa*. *Acta Physiol. Plant.* 37, 80–96.

Chandan, S., and Vijay, P. (2018). Biochemical responses of lentil (*Lens culinaris* Medik) to zinc and iron nutrition in zinc deficient soil. *J. Pharmacogn.* 7, 2344–2348.

Chatterjee, R., and Bandyopadhyay, S. (2017). Effect of boron, molybdenum and biofertilizers on growth and yield of cowpea (*Vigna unguiculata* L.Walp.) in acid soil of eastern Himalayan region. *J. Saudi Soc. Agric. Sci.* 16, 332–336. doi: 10.1016/j.jssas.2015.11.001

Chen, W., Yang, X., He, Z., Feng, Y., and Hu, F. (2008). Differential changes in photosynthetic capacity, 77 K chlorophyll fluorescence and chloroplast ultrastructure between Zn-efficient and Zn-inefficient rice genotypes (*Oryza sativa*) under low zinc stress. *Physiol. Plant.* 132, 89–101. doi: 10.1111/j.1399-3054.2007.00992.x

Corrales, I., Poschenrieder, C., and Barceló, J. (2008). Boron-induced amelioration of aluminium toxicity in a monocot and a dicot species. *J. Plant Physiol.* 165, 504–513. doi: 10.1016/j.jplph.2007.03.014

Dear, B. S., and Lipsett, J. (1987). The effect of boron supply on the growth and seed production of sub-terranean clover (*Trifolium subterraneum* L.). *Aust. J. Agric. Res.* 38, 537–546. doi: 10.1071/ar9870537

Delahunty, A., Nuttall, J., Nicolas, M., and Brand, J. (2015). "Genotypic heat tolerance in lentil," in *Proceedings of the 17th ASA Conference*, Hobart, TS, 20–24.

Dell, B., and Huang, L. (1997). Physiological response of plants to low boron. *Plant Soil* 193, 103–120. doi: 10.1007/978-94-011-5580-9_8

Directorate of Economics and Statistics (2020). *Agricultural Statistics at a Glance 2019 Government of India Ministry of Agriculture and Farmers Welfare Department of Agriculture, Cooperation and Farmers Welfare Directorate of Economics and Statistics*. New Delhi: Directorate of Economics and Statistics.

Farooq, M., Wahid, A., Kobayashi, N., Fujita, D., and Basra, S. M. A. (2009). Plant drought stress: effects, mechanisms and management. *Agron. Sustain. Dev.* 29, 185–212. doi: 10.1016/b978-0-323-85193-0.00011-5

Ghanbari, A. A., Mousavi, S. H., Mousapour Gorgi, A., and Rao, I. M. (2013a). Effects of water stress on leaves and seeds of bean (*Phaseolus vulgaris* L.). *Turk. J. Field Crops* 181, 73–77.

Ghanbari, A. A., Shakiba, M. R., Toorchi, M., and Choukan, R. (2013b). Nitrogen changes in the leaves and accumulation of some minerals in the seeds of red, white and chitti beans (*Phaseolus vulgaris*) under water deficit conditions. *Aust. J. Crop Sci.* 7, 706–712.

Gill, R., Lull, C., Boscaiu, M., Bautista, I., Lidon, A., and Vicente, O. (2011). Soluble carbohydrates as osmolytes in several halophytes from a Mediterranean salt marsh. *Bot. Hortic. Agrobot. Cluj Napoca* 39, 9–17.

Gill, S. S., and Tuteja, N. (2011). Cadmium stress tolerance in crop plants probing the role of sulfur. *Plant Signal. Behav.* 6, 215–222. doi: 10.4161/psb.6.2.14880

Gomez, K. A., and Gomez, A. A. (1984). *Statistical Procedures for Agricultural Research*, Edition 2 Edn. New York, NY: John Wiley & Sons.

Gunes, A., Inal, A., Adak, M. S., Bagci, E. G., Cicek, N., and Eraslan, F. (2008). Effect of drought stress implemented at pre- or post-anthesis stage some physiological as screening criteria in chickpea cultivars. *Russ. J. Plant Physiol.* 55, 59–67. doi: 10.1134/s102144370801007x

Heath, R. L., and Packer, L. (1968). Photoperoxidation in isolated chloroplasts. I. Kinetics and stoichiometry of fatty acid peroxidation. *Arch. Biochem. Biophys.* 125, 189–198. doi: 10.1016/0003-9861(68)90654-1

Hossain, M. B., Kumar, T. N., and Ahmed, S. (2001). Effect of zinc, boron and molybdenum application on the yield and nutrient uptake by BRRI Dhan 30. *J. Biol. Sci.* 1, 698–700. doi: 10.3923/jbs.2001.698.700

Huseynova, I. M. (2012). Photosynthetic characteristics and enzymatic antioxidant capacity of leaves from wheat cultivars exposed to drought. *Biochim. Biophys. Acta* 1817, 1516–1523. doi: 10.1016/j.bbabio.2012.02.037

IPCC (2014). *Climate Change 2014. Synthesis Report, Contribution of Working Group I, II and III to the Fifth Assessment Report of the Inter-Governmental Panel on Climate Change*. IPCC: Geneva, 151.

Jain, M., Mathur, G., Koul, S., and Sarin, N. B. (2001). Ameliorative effects of proline on salt stress induced lipid peroxidation in cell lines of groundnut *(Arachis hypogaea* L.). *Plant Cell Rep*. 20, 463–468. doi: 10.1007/s002990100353

Kaushal, N., Awasthi, R., Gupta, K., Gaur, P., Siddique, K. H. M., and Nayyar, H. (2013). Heat-stress-induced reproductive failures in chickpea (*Cicer arietinum*) are associated with impaired sucrose metabolism in leaves and anthers. *Funct. Plant Biol.* 40, 1334–1349. doi: 10.1071/FP13082

Khan, N., Bano, A., Rahman, M. A., Rathinasabapathi, B., and Babar, M. A. (2019). UPLC-HRMS-based untargeted metabolic profiling reveals changes in chickpea (*Cicer arietinum*) metabolome following long-term drought stress. *Plant Cell Environ.* 42, 115–132. doi: 10.1111/pce.13195

Kim, S. A., and Guerinot, M. L. (2007). Mining iron: iron uptake and transport in plants. *FEBS Lett.* 581, 2273–2280. doi: 10.1016/j.febslet.2007.04.043

Kumawat, R. N., Rathore, P. S., and Pareek, N. (2006). Response of mungbean to sulphur and iron nutrition grown on calcareous soil of Western Rajasthan. *Indian J. Pulse Res.* 19, 228–230.

Lin, K. H., Huang, H. C., and Lin, C. Y. (2010). Cloning, expression and physiological analysis of broccoli catalase gene and Chinese cabbage ascorbate peroxidase gene under heat stress. *Plant Cell Rep.* 29, 575–593. doi: 10.1007/s00299-010-0846-4

Lohse, G. (1982). Microanalytical azomethine-H method for boron determination in plant tissue. *Commun. Soil Sci. Plant Anal.* 13, 127–134. doi: 10.1080/00103628209367251

Malik, A. I., Ali, M. O., Zaman, M. S., Flower, K., Rahaman, M. M., and Erskine, W. (2015). Relay sowing of lentil to intensify rice-based cropping. *J. Agric. Sci.* 154, 850–857. doi: 10.1017/s0021859614001324

Nakano, Y., and Asada, K. (1981). Hydrogen peroxide is scavenged by ascorbate specific peroxidase in spinach chloroplasts. *Plant Cell Physiol.* 22, 867–880. doi: 10.1016/s0005-2728(00)00256-5

Nandan, B., Sharma, B. C., Chand, G., Bazgalia, K., Kumar, R., and Banotra, M. (2018). Agronomic fortification of Zn and Fe in chickpea an emerging tool for nutritional security – A Global Perspective. *Acta Sci. Nutr. Health*. 2, 12–19.

Nasir, M., Khalatbari, M., and Farahani, H. M. (2011). Zn-foliar application influence on quality and quality features in *Phaseolus vulgaris* under different levels of N and K fertilizers. *Adv. Environ. Biol.* 5, 839–846.

Nayyar, H., and Gupta, D. (2006). Differential sensitivity of C_3 and C_4 plants to water deficit stress: association with oxidative stress and antioxidants. *Environ. Exp. Bot.* 58, 106–113. doi: 10.1016/j.envexpbot.2005.06.021

Niles, W. L., and Quesenberry, K. H. (1992). Pollen germination of rhizoma peanut cv. Florigraze. *Peanut Sci.* 19, 105–107. doi: 10.3146/i0095-3679-19-2-11

Nilsen, E. T., and Orcutt, D. M. (1996). *Physiology of Plants Under Stress, Abiotic Factors*, 2 Edn. New York, NY: Wiley, 689.

Ninou, E., Papathanasiou, F., Vlachostergios, D. N., Mylonas, I., Kargiotidou, A., Pankou, C., et al. (2019). Intense breeding within lentil landraces for high-yielding pure lines sustained the seed quality characteristics. *Agriculture* 9:175. doi: 10.3390/agriculture9080175

Okaz, A. M. A., El-Gareib, E. A., Kadry, W., Negm, A. Y., and Zahran, F. A. F. (1994). "Micronutrient application to lentil plants grown on newly reclaimed sandy soils," in *Proceedings of the 6th Conference of Agronomy*, Vol. II, (Cairo: Al-Azhar University), 737–752.

Pantoja-Benavides, A. D., Garces-Varon, G., and Restrepo-Díaz, H. (2021). Foliar growth regulator sprays induced tolerance to combined heat stress by

enhancing physiological and biochemical responses in rice. *Front. Plant Sci.* 12:702892. doi: 10.3389/fpls.2021.702892

Perez, N., GarcÍfa-Espinosa, R., LóÓpez-Castañeda, C., Acosta-Gallegos, J. A., and Simpson, J. (2002). Water relations, histopathology and growth of common bean (*Phaseolus vulgaris* L.) during pathogenesis of *Macrophomina phaseolina* under drought stress. *Physiol. Mol. Plant Pathol.* 60, 185–195. doi: 10.1006/pmpp.2001.0388

Purcell, L. C., and King, C. A. (1996). Drought and nitrogen source effects on nitrogen nutrition, seed growth, and yield in soybean. *J. Plant Nutr.* 19, 969–993. doi: 10.1080/01904169609365173

Quddus, M. A., Rashhid, M. H., Hossain, M. A., and Naser, H. M. (2011). Effect of zinc and boron on yield and yield contributing characters of mungbean in low Ganges river flood plain soil at Madaripur, Bangladesh. *Bangladesh J. Agric. Res.* 36, 75–85. doi: 10.3329/bjar.v36i1.9231

Rezayian, M., Niknam, V., and Ebrahimzadeh, H. (2018). Effects of drought stress on the seedling growth, development, and metabolic activity in different cultivars of canola. *J. Soil Sci. Plant Nutr.* 64, 360–369. doi: 10.1080/00380768.2018.1436407

Romheld, V., and Marschner, H. (1991). "Function of micronutrients in plants," in *Micronutrients in Agriculture*, 2nd Edn, eds J. J. Mortvedt, F. R. Cox, L. M. Shuman, and R. M. Welch (Madison, WI: SSSA), 297–328. doi: 10.2136/sssabookser4.2ed.c9

Rout, G. R., and Sahoo, S. (2015). Role of iron in plant growth and metabolism. *Rev. Agric. Sci.* 3, 1–24. doi: 10.7831/ras.3.1

Saraswathi, S. G., and Paliwal, K. (2011). Drought induced changes in growth, leaf gas exchange and biomass production in *Albizia lebbeck* and *Cassia siamea* seedlings. *J. Environ. Biol.* 32, 173–178.

Sarker, S. K., Chowdhury, M. A. H., and Zakir, H. M. (2002). Sulphur and boron fertilization on yield quality and nutrient uptake by Bangladesh Soybean-4. *J. Biol. Sci.* 2, 729–733. doi: 10.3923/jbs.2002.729.733

Sarwar, M., Saleem, M. F. A., Ullah, N., Ali, S., Rizwan, M., Rizwan, M., et al. (2019). Role of mineral nutrition in alleviation of heat stress in cotton plants grown in glasshouse and field conditions. *Sci. Rep.* 9:13022. doi: 10.1038/s41598-019-49404-6

Saxena, M. C. (2009). "Plant morphology, anatomy and growth habit," in *The Lentil: Botany, Production and Uses*, 1st Edn, eds W. Erskine, F. Maeuhlbauer, A. Sarker, and B. Sharma (Wallingford: CABI Publishing), 34–46. doi: 10.1079/9781845934873.0034

Sehgal, A., Sita, K., Bhandari, K., Kumar, S., Kumar, J., Vara Prasad, P. V., et al. (2019). Influence of drought and heat stress, applied independently or in combination during seed development, on qualitative and quantitative aspects of seeds of lentil (*Lens culinaris* Medikus) genotypes, differing in drought sensitivity. *Plant Cell Environ.* 42, 198–211. doi: 10.1111/pce.13328

Sehgal, A., Sita, K., Kumar, J., Kumar, S., Singh, S., Siddique, K. H. M., et al. (2017). Effects of drought, heat and their interaction of the growth, yield and photosynthetic function of lentil (*Lens culinaris* Medikus) genotypes varying in heat and drought sensitivity. *Front. Plant Sci.* 8:1776. doi: 10.3389/fpls.2017.01776

Shah, N. H., and Paulsen, G. M. (2003). Interaction of drought and high temperature on photosynthesis and grain filling of wheat. *Plant Soil* 257, 219–226. doi: 10.1023/a:1026237816578

Singh, M. K., and Prasad, S. K. (2014). Agronomic aspects of zinc biofortification in rice (*Oryza sativa* L.). *Proc. Natl. Acad. Sci. India Section B Biol. Sci.* 84, 613–623. doi: 10.1007/s40011-014-0329-4

Sita, K., Sehgal, A., Bhandari, K., Kumar, J., Kumar, S., Singh, S., et al. (2018). Impact of heat stress during seed filling on seed quality and seed yield in lentil (*Lens culinaris* Medikus) genotypes. *J. Sci. Food Agric.* 98, 5134–5141. doi: 10.1002/jsfa.9054

Sita, K., Sehgal, A., Kumar, J., Kumar, S., Singh, S., Siddique, K. H. M., et al. (2017a). Identification of high-temperature tolerant lentil (*Lens culinaris* Medik.) genotypes through leaf and pollen traits. *Front. Plant Sci.* 8:744. doi: 10.3389/fpls.2017.00744

Sita, K., Sehgal, A., Hanumantha Rao, B., Nair, R. M., Prasad, P. V., Kumar, S., et al. (2017b). Food legumes and rising temperatures: effects, adaptive functional mechanisms specific to reproductive growth stage and strategies to improve heat tolerance. *Front. Plant Sci.* 8:1658. doi: 10.3389/fpls.2017.01658

Sofo, A., Dichio, B., Xiloyannis, C., and Masia, A. (2004). Effects of different irradiance levels on some antioxidant enzymes and on malondialdehyde content during re-watering in olive tree. *Plant Sci.* 166, 293–302. doi: 10.1016/j.plantsci.2003.09.018

Srinivasan, S., and Gaur, M. G. (2011). Genetics and characterization of an open flower mutant in chickpea. *J. Hered.* 103, 297–302. doi: 10.1093/jhered/esr125

Stavrianakou, S., Liakopoulos, G., and Karabourniotis, G. (2006). Boron deficiency effects on growth, photosynthesis and relative concentrations of phenolics of *Dittrichia viscose* (Asteraceae). *Environ. Exp.* 56, 293–300. doi: 10.1016/j.envexpbot.2005.03.007

Talukdar, D. (2013). Comparative morpho-physiological and bio-chemical responses of lentil and grass pea genotypes under water stress. *J. Nat. Sci. Biol. Med.* 4, 396–402. doi: 10.4103/0976-9668.116983

Triboï, E., Martre, P., and Triboï-Blondel, A. M. (2003). Environmentally-induced changes of protein composition for developing grains of wheat are related to changes in total protein content. *J. Exp. Bot.* 54, 1731–1742. doi: 10.1093/jxb/erg183

Upadhyaya, H., Dutta, B. K., and Panda, S. K. (2013). Zinc modulates drought-induced biochemical damages in tea (*Camellia sinensis* (L.) O Kuntze). *J. Agric. Food Chem.* 61, 6660–6670. doi: 10.1021/jf304254z

Valenciano, J. B., Boto, J. A., and Marcelo, V. (2011). Chickpea (*Cicer arietinum* L.) response to zinc, boron and molybdenum application under field conditions. *J. Crop Hortic. Sci.* 39, 217–229. doi: 10.1080/01140671.2011.577079

Venugopalan, V. K., Roy, A., Vijayan, R., Banerjee, P., Verma, V. C., Nalia, A., et al. (2021a). Drought and heat stress in cool-season food legumes in sub-tropical regions: consequences, adaptation, and mitigation strategies. *Plants* 10:1038. doi: 10.3390/plants10061038

Venugopalan, V. K., Nath, R., Sengupta, K., Nalia, A., Banerjee, S., Chandran, M. A. S., et al. (2021b). The response of lentil (*Lens culinaris* Medik.) to soil moisture and heat stress under different dates of sowing and foliar application of micronutrients. *Front. Plant Sci.* 12:679469. doi: 10.3389/fpls.2021.679469

Wang, H., and Jin, J. Y. (2005). Photosynthetic rate, chlorophyll fluorescence parameters, and lipid peroxidation of maize leaves as affected by zinc deficiency. *Photosynthetica* 43, 591–596.

Waraich, E., Ahmad, R., Halim, A., and Aziz, T. (2012). Alleviation of temperature stress by nutrient management in crop plants: a review. *J. Soil Sci. Plant Nutr.* 12, 221–244. doi: 10.4014/jmb.2105.05009

Yanni, Y. G. (1992). Performance of chickpea, lentil and lupin nodulated with indigenous or inoculated rhizobia micropartners under nitrogen, boron, cobalt and molybdenum fertilization schedules. *World J. Microbiol. Biotech.* 8, 607–613. doi: 10.1007/BF01238798

Zahoor, R., Zhao, W., Abid, M., Dong, H., and Zhou, Z. (2017). Potassium improves photosynthetic tolerance to and recovery from episodic drought stress in functional leaves of cotton (*Gossypium hirsutum* L.). *J. Plant Physiol.* 119, 21–32. doi: 10.1016/j.plaphy.2017.08.011

Conflict of Interest: The authors declare that the research was conducted in the absence of any commercial or financial relationships that could be construed as a potential conflict of interest.

Publisher's Note: All claims expressed in this article are solely those of the authors and do not necessarily represent those of their affiliated organizations, or those of the publisher, the editors and the reviewers. Any product that may be evaluated in this article, or claim that may be made by its manufacturer, is not guaranteed or endorsed by the publisher.

frontiers | Frontiers in Plant Science

ORIGINAL RESEARCH
published: 07 April 2022
doi: 10.3389/fpls.2022.852654

Lack of Blue Light Regulation of Antioxidants and Chilling Tolerance in Basil

*Dorthe H. Larsen[1], Hua Li[1], Samikshya Shrestha[1], Julian C. Verdonk[1], Celine C. S. Nicole[2], Leo F. M. Marcelis[1] and Ernst J. Woltering[1,3]**

[1] Horticulture and Product Physiology Group, Wageningen University and Research, Wageningen, Netherlands, [2] Signify Research Laboratories, Eindhoven, Netherlands, [3] Food and Biobased Research, Wageningen University and Research, Wageningen, Netherlands

Blue light, measuring from 400 to 500 nm, is generally assumed to increase the content of antioxidants in plants independent of the species. Blue light stimulates the biosynthesis of phenolic compounds such as flavonoids and their subclass anthocyanins from the phenylpropanoid pathway. Flavonoids, anthocyanins, and phenolic acids are strong reactive oxygen species (ROS) scavengers and may lessen the symptoms of abiotic stresses such as chilling. We tested the hypothesis that a high percentage of blue light induces the accumulation of antioxidants and that this effect depends on the photosynthetic photon flux density (PPFD, 400–700 nm). The effect may be more pronounced at a lower PPFD. We investigated the changes in primary and secondary metabolites of basil in response to the percentage of blue light (9, 33, 65, and 100%) applied either as a 5-day End-Of-Production (EOP) treatment or continuous throughout the growth cycle in the green cv. Dolly. We also studied if the response to the percentage of blue light (9 or 90%) was dependent on the total PPFD (100 or 300 μmol m^{-2} s^{-1} PPFD) when applied as a 5-day EOP treatment in the green cv. Dolly and the purple cv. Rosie. For both green and purple basil, it was found that the percentage of blue light had little effect on the levels of antioxidants (rosmarinic acid, total ascorbic acid, total flavonoids, and total anthocyanins) at harvest and no interactive effect with PPFD was found. Antioxidants generally decreased during postharvest storage, wherein the decrease was more pronounced at 4 than at 12°C. Chilling injury, as judged from a decrease in F_v/F_m values and from the occurrence of black necrotic areas, was not affected by the percentage of blue light. Particularly, chilling tolerance in the purple cultivar was increased in plants grown under higher PPFD. This may be related to the increased levels of soluble sugar and starch in leaves from high PPFD treated plants.

Keywords: blue light, basil, vertical farming, anthocyanins, antioxidants, chilling injury, quality

OPEN ACCESS

Edited by:
Youssef Rouphael, University of Naples Federico II, Italy

Reviewed by:
Aušra Brazaitytė, Lithuanian Research Centre for Agriculture and Forestry, Lithuania
Roberta Bulgari, University of Turin, Italy

***Correspondence:**
Ernst J. Woltering
ernst.woltering@wur.nl

Specialty section:
This article was submitted to Crop and Product Physiology, a section of the journal Frontiers in Plant Science

Received: *11 January 2022*
Accepted: *22 February 2022*
Published: *07 April 2022*

Citation:
Larsen DH, Li H, Shrestha S, Verdonk JC, Nicole CCS, Marcelis LFM and Woltering EJ (2022) Lack of Blue Light Regulation of Antioxidants and Chilling Tolerance in Basil. Front. Plant Sci. 13:852654. doi: 10.3389/fpls.2022.852654

INTRODUCTION

Basil (*Ocimum basilicum* L.) is rich in antioxidants, in particular, polyphenolic compounds from the phenylpropanoid pathway such as rosmarinic and chicoric acid (Kwee and Niemeyer, 2011). Basil also contains compounds from the flavonoid (sub) family such as quercetin, rutin, and kaempferol. Mostly basil exists as green varieties but some varieties are purple due to anthocyanins which are

a subgroup of flavonoids (McCance et al., 2016). Compounds such as anthocyanins, flavonoids, and phenolic acids have strong antioxidant capacity. Antioxidants can scavenge reactive oxygen species (ROS) and protect the plants from oxidative damage thus contributing to tolerance against abiotic stress such as chilling and drought (Ahmed et al., 2014). Chilling injury occurs in basil when it is exposed to temperatures below 10–12°C during growth, storage, or transport resulting in the development of dark necrotic spots (Lange and Cameron, 1994). During chilling, a cascade of events occurs: the lipid bilayer in the cell membranes can go from a flexible to a solid gel state which may result in membrane malfunction, ion leakage, and excessive formation of ROS. ROS will further lead to the damage of the DNA, membrane lipids, and proteins, thereby being severely damaging to the plant (Sevillano et al., 2009). Antioxidants, such as phenolic compounds, can counteract ROS and ameliorate chilling tolerance (Das and Roychoudhury, 2014). Increasing the content of antioxidants such as flavonoids and anthocyanins may improve the tolerance to chilling temperatures. In addition, an increase in sugars, starch, and antioxidants is beneficial for consumers as it improves the products' nutritional value. In the production phase, antioxidants can be increased through the modulation of the growth environment (Larsen et al., 2022). Such modulation can be facilitated by light-emitting diodes (LEDs) through which we can easily increase both the light intensity and change the light spectrum. LEDs are particularly used in greenhouses and in vertical farming (SharathKumar et al., 2020). Light intensity and spectrum can affect the content of phenolic acids, flavonoids, and anthocyanins. In particular, blue light (400–500 nm) has been found to stimulate the biosynthesis of compounds from the phenylpropanoid pathway such as flavonoid and anthocyanin content in several crops: in fruit and leaves of strawberry (Piovene et al., 2015; Zhang et al., 2018), lettuce (Samuoliene et al., 2013), and Arabidopsis (Chen et al., 2006). Blue light has also been found to stimulate the biosynthesis of rosmarinic acid, chicoric acid, chlorogenic acid, *p*-OH-cinnamic acid derivative, 2-*O*-feruloyl tartaric acid, and quercetin rhamnoside in green basil (Taulavuori et al., 2013, 2016), and phenolic acids in red lettuce (Ouzounis et al., 2015). In addition, blue light increased the content of vitamin C in pak choi with a photosynthetic photon flux density (PPFD, 400–700 nm) up until 100 μmol m^{-2} s^{-1} after which it decreased at a higher PPFD (Zheng et al., 2018). Although blue light has been widely accepted to stimulate the biosynthesis of compounds from the flavonoid branch of the phenylpropanoid pathway it is not fully understood why compounds such as vitamin C should increase. The energy content of a blue light photon is higher than its red counterparts due to blue light having a lower wavelength than red. Thus, blue photons might result in a stress reaction.

Application of increased light intensity during the last phase of the growth as an End-Of-Production (EOP) treatment showed to be sufficient to increase the content of secondary metabolites without having adverse effects on plant morphology (Gomez and Jimenez, 2020; Larsen et al., 2020, 2022; Min et al., 2021). In red lettuce, an EOP treatment with 69% blue light has increased anthocyanins but not flavonoids (Gomez and Jimenez, 2020). However, a change in the spectrum as EOP treatment is yet to be studied in basil. We hypothesized that an increased percentage of blue light would increase the content of antioxidants, such as phenolic acids, flavonoids, and anthocyanins, thereby improving chilling tolerance. Furthermore, we hypothesized that the effect of a high percentage of blue light might have an interactive effect on the PPFD (400–700 nm). Spectral effects may be less on the accumulation of antioxidants under higher PPFD as the PPFD might dominate the overall plant response.

First, we investigated the changes in primary and secondary metabolites of basil in response to the percentage of blue light (400–500 nm) in the spectrum applied either as an EOP treatment or continuous throughout the growth cycle. Second, we studied if the light intensity interacts with the percentage of blue light applied as EOP treatment in a green and purple cultivar and further if this improves the postharvest chilling tolerance.

MATERIALS AND METHODS

Experimental Set-Up

For this study, two cultivars of basil (*Ocimum basilicum* L.), cv. Dolly (green leaves) and cv. Rosie (purple leaves that are rich in anthocyanin) (Enza Zaden, Enkhuizen, the Netherlands) were grown in a climate chamber. Plants were grown according to Larsen et al. (2020, 2022). The seeds were sown as single seeds in stone wool plugs in trays of 240 plugs (Grodan Rockwool B.V., Roermond, the Netherlands). The most morphologically similar plants were transplanted to 7.5 cm × 7.5 cm × 6.5 cm stone wool blocks (Grodan Rockwool B.V., Roermond, the Netherlands) after 15 days. For the growth of the plants, a vertical farming set-up was used. Each compartment had a dimension of 0.8 m × 1.3 m × 1 m, (w × l × h) and a planting density of 123 plants m^{-2}. The two cvs were grown in different compartments to maintain a similar PPFD at the top of the plants. Throughout the experiments, the heights of the light frames were adjusted to maintain the desired PPFD. The light frames were kept 25 cm above the plants. In the climate chamber. the day/night temperature was set at 25°C, the relative humidity at 75%, and carbon dioxide (CO_2) was kept at ambient concentrations. The temperature and relative humidity deviated within ± 10% (RH) and 1°C (T) from the setpoints and were logged with KeyTag dataloggers (KTL-508, KeyTag, Leiderdorp, the Netherlands).

Plants were watered through an ebb and flow system. At all growth stages, plants were kept well-watered. Plants were watered with a nutrient solution of pH 5.7, EC 1.7 dS m^{-1}, 8.5 mM NO_3^-, 3.9 mM SO_4^{2-}, 1.5 mM HPO_4^{2-}, 1.5 mM NH_4^+, 5.5 mM K^+, Ca^{2+} 4 mM, 1.5 mM Mg^{2+}, 0.2 mM Cl^-, 30 μM Fe^{3+}/Fe^{2+}, 5 μM Mn^{2+}, 5 μM Zn^{2+}, 35 μM $H_2BO_3^-$, 1 μM Cu^+/Cu^{2+}, and 1 μM MoO_4^{2-} before transplanting. After transplanting, the EC measured 2.3 dS m^{-1} and the concentration of the nutrients was raised correspondingly.

The response to the light treatments on plant growth and morphology (i.e., plant height, leaf area, and fresh and dry mass at harvest) from these experiments were described by Larsen et al. (2020).

Blue Light Duration (Experiment 1)

In Experiment 1, we investigated the response of cv. Dolly to different percentages of blue light applied either as a continuous

treatment throughout the growth (i.e., for 25 days) or as EOP treatment during the last 5 days before harvest. Seedlings grew under red-white light from LEDs (Green Power LED production module, 120 cm, Philips Eindhoven, the Netherlands) with a PPFD of 150 μmol m^{-2} s^{-1}. The red-white light contained 9% blue (B) (400–500 nm), 19% green (G) (500–600 nm), and 70% red (R) (600–700 nm), as well as 1% far-red (FR) (700–800 nm) lights. For the blue light treatments, the different percentages of blue light were made by using pure blue (Green Power LED production module, 120 cm, Blue, Philips Eindhoven, the Netherlands), (Green Power LED research module, Blue, Philips Eindhoven, the Netherlands) and red-white LEDs. When the plants were transplanted, they were treated with four different blue light treatments for 25 days with a total PPFD of 300 μmol m^{-2} s^{-1} (**Table 1**.). In addition, plants were grown under red-white light (PPFD, 300 μmol m^{-2} s^{-1}) in three other treatments for 20 days after which they were treated with different blue light treatments for 5 days (**Table 1**). For all light treatments, the spectral intensity was measured with a spectroradiometer (USB2000 spectrometer, Ocean Optics, Duiven, 110 Netherlands). Throughout the experiment, the day length was 16 h. This whole experiment with a similar set-up was conducted 2 times.

Blue Light and the Interactive Effect With PPFD (Experiment 2)

In Experiment 2, we investigated the response of cultivars Rosie (purple) and Dolly (green) to EOP treatments with an increased percentage of blue light. We also investigated the interaction with PPFD during the last 5 days before harvest. Seedlings grew under 200 μmol m^{-2} s^{-1} red-white LED light. Plants were transplanted and continued to grow for another 15 days under 200 μmol m^{-2} s^{-1} red-white light. The last 5 days before harvest plants were treated with EOP treatments with either a low (100 μmol m^{-2} $s^{-}1$) or high (300 μmol m^{-2} s^{-1}) PPFD, in combination with a low (9%) and high (90%) percentage of blue light (**Table 1**). For the blue light treatments, the different percentages of blue light were made by using two types of pure blue LEDs (Green Power LED production module, 120 cm, Blue, Philips Eindhoven, the Netherlands) (Green Power LED research module, Blue, Philips Eindhoven, the Netherlands) and red-white LEDs. For all light treatments, the spectral intensity was measured with a spectroradiometer (USB2000 spectrometer, Ocean Optics, Duiven, 110 Netherlands). Throughout the growth, the day length was 18 h. This whole experiment with a similar set-up was conducted 3 times for cv. Dolly and 4 times for cv. Rosie.

Postharvest Storage and Sampling

The plants were harvested 40 (Experiment 1) or 35 (Experiment 2) days after sowing. The border plants were excluded from the sampling. The postharvest storage was done according to Larsen et al. (2022). For postharvest storage and sampling, three-leaf pairs were taken per plant. The oldest and youngest underdeveloped leaves were excluded. The leaves were stored in plastic boxes (16 cm × 11 cm × 6 cm), which combined leaves from two plants per box. The wetted filter paper was added to the bottom of the boxes to keep the humidity high. For the leaves to avoid direct contact with the wet filter paper, a small piece of plastic was added on top of it. The leaves from the two plants were separated by a piece of plastic. To avoid the build-up of CO_2 or ethylene, nine holes were made in the lids with a 1 mm syringe needle. During storage, the boxes were randomized in a cold cabinet in darkness at 4 or 12°C. In the boxes, the temperature and relative humidity deviated within ± 2% (RH) and 0.3°C (T) from the setpoints and were recorded with KeyTag dataloggers (KTL-508, KeyTag, Leiderdorp, the Netherlands).

In Experiment 1, measurement and sampling were done on day 0 (at harvest) and 5, 10, and 15 days after harvest for EOP treated plants. In Experiment 2, measurements and sampling were done on day 0 (day of harvest), while days 3 and 6 for cv. Dolly and for cv. Rosie the sampling continued on days 9 and 12. Two postharvest storage boxes (i.e., each containing leaves from two individual plants per block per light treatment) were sampled on each sampling day.

During sampling, an overall visual quality score was given to the leaves of each sampled plant to determine the chilling injury level. In Experiment 2, the maximum quantum yield of PSII (F_v/F_m) was measured in addition to the scoring. Following the scoring and measuring of F_v/F_m, the leaves were frozen in liquid nitrogen and ground with an IKA-A 11 basic analytical mill (im-lab, Boutersem, Belgium). Samples were stored at −80°C for further analysis of metabolite content. Each sample consisted of leaves derived from 4 plants.

Carbohydrates

Carbohydrates were measured according to Larsen et al. (2022). Briefly, 300 mg of frozen ground leaves were extracted with 5 ml of 85% ethanol in a shaking water bath at 80°C for 20 min. Samples were centrifuged for 5 min at 8,500 RCF (Universal 320R, Hettich, Sigma-Aldrich, Darmstadt, Germany) and 1 ml of the supernatant was dried with a vacuum centrifuge (Savant SpeedVac SPD2010, Thermo Fisher Scientific, Waltham, MA, United States) for 120 min at 50°C and 5.1 mbar. The remaining pellet with supernatant was later used for starch determination.

The dried samples were re-suspended in 2 ml of 0.01 N hydrochloric acid and sonicated for 10 min (Branson 2800, Richmond, VA, United States). The samples were vortexed and centrifuged at 21,100 RCF for 5 min (Sorvall Legend Micro 21R, Thermo Fisher Scientific, Waltham, MA, United States).

Amino acids and other amino compounds were removed from the sample solution by trapping with a SPE column (UCT CLEAN-UP BCX columns, BGB analytik Benelux B.V. Harderwijk, The Nethelands, 100 mg/1 ml), eluted with 0.01 N hydrochloric acid.

The samples were diluted ten times and glucose, fructose, and sucrose were quantified using High-Performance Anion Exchange Chromatography with Pulsed Amperometric Detection (HPAEC-PAD; Dionex ICS5000, Thermo Fisher Scientific, Waltham, MA, United States), with a CarboPac1 column (250 mm × 2 mm, Thermo Fisher Scientific, Waltham, MA, United States) and eluted with 100 mM NaOH at a flow rate of 0.25 ml/min at 25°C.

For starch determination, the stored pellet was used. The pellet was washed three times with 80% ethanol, dried for

TABLE 1 | Photosynthetic photon flux density (PPFD) (400–700 nm) and spectra of the treatments for Experiments 1 and 2.

Treatments	Treatment duration (days)	PPFD (μmol m^{-2} s^{-1})	Blue light (%)	Green light (%)	Red light (%)	Far-red light (%)
Exp. 1						
9%	25 and 5	300	9	19	70	1
33%	25 and 5	300	33	14	51	1
65%	25 and 5	300	65	7	26	0
100%	25 and 5	300	100	0	0	0
Exp. 2						
Low PPFD, low blue	5	100	9	19	70	1
Low PPFD, high blue	5	100	90	2	8	0
High PPFD, low blue	5	300	9	19	70	1
High PPFD, high blue	5	300	90	2	8	0

Percentages of the spectra; blue light (400–500 nm), green light (500–600 nm), red light (600–700 nm), far-red light (700–800 nm) are expressed as percentages of the total photon flux density (400–800 nm).

20 min in a vacuum centrifuge at 50°C and 5.1 mbar. For the resuspension of the dried pellet, 2 ml of 1 g/L thermostable alpha-amylase (SERVA Electrophoresis GmbH, Heidelberg, Germany) was used. The samples were incubated at 90°C for 30 min. Before further incubation at 60°C for 15 min, 1 ml of 0.5 g/L amyloglucosidases (10115 Sigma-Aldrich, Darmstadt, Germany) in 50 mM citrate buffer (pH 4.6) was added to the samples. The samples were centrifuged at 21,100 RCF for 5 min and diluted 50–100 times. Glucose was quantified using HPEAC-PAD (see description above).

A conversion factor was made for each sample to convert them from fresh weight to dry weight. In brief, 400 ± 40 mg of fresh frozen was weighed into a reaction tube and oven-dried for 8 h at 70°C. Data was expressed on the base of dry weight as mg/g DW.

Rosmarinic and Chicoric Acid

Phenolic acids were extracted according to Larsen et al. (2022). Briefly, 250 ± 20 mg of frozen ground leaves were extracted with 1.5 ml of 80% methanol with 2.5% formic acid for 15 min in an ultrasonic bath (Branson 2800, Richmond, VA, United States). The supernatant was filtered through a cellulose syringe filter 0.45 μm, and analyzed according to the method of Kwee and Niemeyer (2011), with modifications. In Experiment 1, samples were measured on an HPLC system (Waters, Knowloon, Hongkong) with a UV dual-wavelength detector and autosampler and a Vydac 201TP54 (C18, 5 μm, 300 Å, 4.6 mm × 250 mm) reverse-phase (RP) column. In Experiment 2, samples were measured on an HPLC system with a GS50 pump (Dionex, Thermo Fisher Scientific, Waltham, MA, United States), a 340S UV-VIS detector (Dionex, Thermo Fisher Scientific, Waltham, MA, United States), and a MIDAS autosampler (Spark, Emmen, the Netherlands) using a LiChrospher 100 RP-18 (5 μm), 150 × 4 mm column (Merck, Amsterdam, the Netherlands). Samples were eluted with 2.5% formic acid in H_2O (A) and acetonitril (B) with a linear gradient of: 85% A, 0 min; 75% A, 6 min; 0% A, 8.5 min [0% A, 9 min; 85% A, 11.5 min; 85% A, 14 min]. Analytes were detected at 330 nm.

For quantification, calibration curves were prepared with standards (Extrasynthese, Genay, France) from 0 to 500 mg/L. Data were expressed on the base of dry weight as mg/g DW.

Total Ascorbic Acid

Ascorbic acid (AsA) was measured according to Min et al. (2021). Total AsA (TAsA) is a large antioxidant group in leafy vegetables, also defined as vitamin C (Min et al., 2021). TAsA is the sum of AsA and dehydroascorbic acid (DHA). Extraction of AsA was done from 200 mg frozen ground leaves with 1 ml 3.3% meta-phosphoric acid (MPA) and sonicated (Branson 2800, Richmond, VA, United States) for 10 min in darkness at 0°C. The samples were centrifuged at 21,100 RCF (Sorvall Legend Micro 21R, Thermo Fisher Scientific, Waltham, MA, United States) for 10 min at 4°C. For analysis of AsA, the supernatant was filtered through a cellulose syringe filter of 0.45 μm of cellulose into an amber HPLC vial. Furthermore, for TAsA analysis, 100 μl of the filtered extract was transferred to another HPLC vial and 50 μl of 5 mM dithiothreitol in 400 mM Tris base was added. To convert DHA to AsA, the vials were kept in darkness at room temperature. The reaction was stopped after 15 min by adding 50 μl 8.5% o-phosphoric acid. AsA was measured on an HPLC consisting of a GS50 pump (Dionex, Thermo Fisher Scientific, Waltham, MA, United States), a 340S UV-VIS detector (Dionex, Thermo Fisher Scientific, Waltham, MA, United States) with a MIDAS autosampler (Spark, Emmen, the Netherlands), and a ProntoSIL 120-3 C18 AQ (250 × 3 mm column) (Knauer, Berlin, Germany). For the elution of column, 400 μL/L H3PO4 + 2.5 ml/L MeOH + 0.1 mM EDTA in H_2O was used with a wash step consisting of 30% acetonitrile in H_2O at a flow rate of 0.35 ml/min at 35°C. The detection of AsA was done at 243 nm. A standard with AsA in 3.3% MPA was used for calibration. The amount of TAsA was calculated as the sum of the AsA and the AsA converted from DHA. Data was expressed on the base of dry weight as mg/g DW.

Total Anthocyanin Content

Total anthocyanin content was extracted from 300 mg frozen ground basil tissue with 1.5 ml 50% MeOH along with 1% formic acid in an ultrasonic bath (Branson 2800, Richmond, VA, United States) for 15 min. Samples were centrifuged at 15,000 RCF (Sorvall Legend Micro 21R, Thermo Fisher Scientific, Waltham, MA, United States) at 4°C for 15 min. The supernatant was filtered through a 0.45 μm cellulose filter.

Samples were diluted 5 times and measured in a cuvette at wavelength of λ = 530 nm in a spectrophotometer (Genesys 50, Thermo Fisher Scientific, Waltham, MA, United States) against a blank. The total content of anthocyanins was expressed as mg/g with cyanidin chloride as standard in the range 1–25 mg/L.

Total Flavonoid Content

Total flavonoid content was determined by aluminum chloride colorimetric assay (Zhishen et al., 1999). Total flavonoid content was extracted from 300 mg of frozen ground basil and 1.5 ml of methanol/H_2O/acetone (60:30:10 v/v/v) in an ultrasonic bath (Branson 2800, Richmond, VA, United States) for 15 min. Samples were centrifuged at 15,000 RCF (Sorvall Legend Micro 21R, Thermo Fisher Scientific, Waltham, MA, United States) at 4°C for 10 min, and the supernatant was collected. Catechin was used as a quantifying standard. In a 3-ml cuvette, 50 μL of the extracted sample was mixed with 1.95 ml water and 75 μL of 5% $NaNO_2$. After 6 min 150 μL of 10% $AlCl_3$ was added and after another 5 min, 500 μL of 1 M NaOH was added. The absorbance was measured at a wavelength of λ = 250 nm in a spectrophotometer (Genesys 50, Thermo Fisher Scientific, Waltham, MA, United States) against a blank. Data was expressed on the base of dry weight as mg/g DW.

Hydrogen Peroxide

Hydrogen peroxide (H_2O_2) was determined according to Junglee et al. (2014) with some modifications. H_2O_2 was extracted from 0.1 g of frozen ground basil leaves with 0.4 ml of 0.1% TCA, 0.4 ml of potassium phosphate buffer (pH 7.6), and 0.8 ml of potassium iodide. After incubation for 10 min at 4°C, the samples were centrifuged at 15,000 RCF (Sorvall Legend Micro 21R, Thermo Fisher Scientific, Waltham, MA, United States) at 4°C for 10 min, and the supernatant was collected. Samples were measured in UV-cuvettes at a wavelength of λ = 350 nm in a spectrophotometer (Genesys 50, Thermo Fisher Scientific, Waltham, MA, United States) against the blank. For quantification, a calibration curve was prepared with H_2O_2 solutions with concentrations from 10 to 400 μmol/L. For each sample, three technical replicates were prepared. Data were expressed on the base of dry weight as mg/g DW.

Maximum Chlorophyll Fluorescence

Chilling injury was measured as an F_v/F_m ratio previously described by Larsen et al. (2022). F_v/F_m is the maximum quantum yield of the primary photochemical reactions or PSII in dark-adapted leaves. Per stored box, containing leaves from two plants, one leaf from the upper leaf-pair and one leaf from the middle leaf pair per plant were measured. First leaves were dark-adapted at 20°C for 20 min after which the measurement of chlorophyll fluorescence was done using a PSI closed Fluorcam 800-C chlorophyll fluorescence imaging system (PSI, Drasov, Czech Republic). To operate the fluorcam and analyze the images, the Fluorcam software version 7 was used, according to the method of Hogewoning and Harbinson (2007).

Overall Visual Quality

Overall visual quality (OVQ) was evaluated using a scoring system according to Larsen et al. (2022). The scores were given based on visual symptoms associated with chilling injury and general symptoms appearing at non-chilling temperatures. A score between 1 and 8 was given based on the visual symptoms (i.e., 1 being the worst and 8 being the best). The consumer acceptance limit was set at the score of 5, which represented the end of shelf life. The scores would be reduced due to symptoms such as dark spots/discoloration, fungal appearance, degree of crispness, degree of wilting, leaf shininess, and presence of characteristic curved leaf shape (**Supplementary Table 1**).

Statistical Setup and Analysis

The experiments were carried out in a complete randomized block design. The light treatments for the different cultivars in either the green cv. Dolly or the purple cv. Rosie were located in separate compartments. Experiment 1 was carried out two times (2 blocks) and Experiment 2 was carried out three times (3 blocks) for cv. Dolly and four times for cv. Rosie (4 blocks). The border plants were excluded from the analysis. For the chemical analysis at harvest, four replicate plants were sampled per light treatment in each block. The rest of the plants were stored for postharvest sampling. For postharvest storage at 4 and 12°C, the leaves from two plants were packed in one plastic box (see description above). Two boxes (i.e., leaves from four plants) per cv. and light treatment were sampled for overall visual quality and chemical analysis per postharvest timepoint. As one replicate an average value of each block was used for further statistical analysis. For each block, the chemical analysis was done on leaves from four plants as a pooled sample. The means are based on the number of blocks x four replicate plants.

The data were analyzed with Genstat (VSN International, 19th Edition). The assumptions of homogeneity and normality of the residuals were tested with Bartlett's test and the Shapiro-Wilk test. In the case that the data did not follow the assumption, the data were transformed with the natural logarithm, after which it followed the assumption. Thereafter, the data were analyzed using a two-way ANOVA per time point and storage temperature with the *post hoc* test Fisher's protected LSD. For Experiment 1, the test was conducted with a probability level of $\alpha = 0.1$ because the experiment only had two blocks, while for Experiment 2, the probability level was $\alpha = 0.05$

RESULTS

Metabolite Content in Response to Percentage and Duration of Blue Light

Soluble sugars (glucose, fructose, and sucrose) at harvest were not affected by the percentage of blue light during cultivation (25 days) or 5 days of EOP. Starch content was reduced by 30–50% with an increasing percentage of blue light for both EOP and continuously treated plants (**Figures 1A,B**). Rosmarinic acid at harvest was little affected by the percentage of blue. However, continuous blue (33, 65, and 100% blue) treatments

resulted in a 15–25% decrease compared to the shorter duration of EOP blue treatments (**Figure 1C**). Chicoric acid levels increased with an increasing percentage of blue whether it was provided continuously throughout cultivation or EOP, but the increase was stronger when applied throughout cultivation (+85%) compared to EOP (+45%) (**Figure 1D**). TAsA did not respond to either percentage of blue or duration of blue light (**Figure 1E**).

The changes in metabolites from the EOP treated plants were measured during postharvest storage. During storage at both 4 and 12°C, sugars increased whereas starch decreased over time (**Supplementary Figure 1**). However, the patterns of the time courses were not affected by the EOP blue light treatments. During postharvest storage at 4°C, rosmarinic acid, chicoric acid, and AAsA showed a steep decrease over time (**Supplementary Figure 2**). At 12°C, an initial increase was observed in chicoric and rosmarinic acids for all treatments, later followed by a decrease. TAsA at 12°C showed a similar pattern as at 4°C (**Supplementary Figure 2**).

Metabolite Content in Response to the Percentage of Blue Light at Different PPFD

We investigated the interactive effect between the percentage of blue light (low; 9% or high; 90%) and PPFD (low; 100 μmol m^{-2} s^{-1}, or high; 300 μmol m^{-2} s^{-1}) applied as EOP treatment the last 5 days before harvest on metabolites in green cv. Dolly and purple cv. Rosie (Experiment 2). The high PPFD and the low blue were the same as in Experiment 1.

High PPFD as EOP treatment increased soluble sugars and starch content at harvest in both the green cv. Dolly (**Figures 2A,B**) and the purple cv. Rosie (**Figures 3A,B**). Furthermore, for both cultivars, starch content was significantly higher in the high PPFD treatment combined with low blue compared to the high PPFD with high blue. A higher percentage of blue light increased the content of chicoric acid in both cultivars (**Figures 2D**, **3D**), while high PPFD also increased the content of chicoric acid in purple cv. Rosie. Rosmarinic acid was neither affected by PPFD nor by the percentage of blue light (**Figures 2C**, **3C**). Similarly, the total anthocyanin content in the purple cv. Rosie was not significantly affected by either PPFD or the percentage of blue light (**Figure 3G**). The green cv. Dolly did not contain anthocyanins. In contrast, total flavonoid content and the level of H_2O_2 were lower at high PPFD than at low PPFD in purple cv. Rosie (**Figures 3E,F**). However, for neither the green nor the purple cultivar did percentage of blue light and PPFD have an interactive effect on the content of metabolites.

Sugar levels were slightly higher and starch levels were considerably lower in purple cv. Rosie compared to green cv. Dolly (**Figures 2A**, **3A**). Rosmarinic acid, chicoric acid, and flavonoids were higher in purple cv. Rosie compared to green cv. Dolly. The purple cv. Rosie contained anthocyanin, which was absent (below the detection level) in the green cv. Dolly. Together it implies the purple cv. Rosie had a higher level of antioxidants (secondary metabolites) but a considerably lower level of carbohydrate reserves at harvest.

From Experiment 1 with the green cv. Dolly, it was clear that the pre-harvest blue light had little or no effects on the metabolite changes during the postharvest phase. Therefore, in Experiment 2 the green cv. Dolly was sampled only on days 3 and 6 during storage at 4 and 12°C. The purple cultivar Rosie was sampled in addition also at days 9 and 12. During storage soluble sugars increased at both 4 and 12°C for the green cv. Dolly (**Supplementary Figures 3A,B**) whereas for the purple cv. Rosie a slight decrease was observed at 12°C (**Supplementary Figure 4B**). The levels of sugars in the postharvest phase were generally higher in the samples derived from plants from high PPFD EOP treatments while the percentage of blue light did not have an effect on the postharvest content. During postharvest storage at both 4 and 12°C, the starch content remained the highest from high PPFD and low blue EOP treatments in both cvs Dolly and Rosie (**Supplementary Figures 3C,D, 4C,D**). The starch reserves, especially in the samples from low PPFD and high PPFD/high percentage of blue light treatments were depleted by days 3–6 in the purple cv. Rosie. At that time, depletion was not complete in the green cv. Dolly had higher starch levels at harvest. The starch breakdown was generally faster at 12 than at 4°C.

Overall, metabolites were unchanged at 12°C storage for both cultivars (**Figures 4**, **5**) but in the purple cv. Rosie a pronounced decrease in the metabolite levels was observed at 4°C. During the 6 days of storage, there was no clear effect of the EOP light treatments on the changes in metabolite levels in the green cv. Dolly. For the purple cv. Rosie, high PPFD during cultivation resulted in a slower decrease of metabolites (rosmarinic acid, chicoric acid, total flavonoid content, and total anthocyanin content) during dark storage at 4°C (**Figures 5A,C,E,G**). In addition, a low percentage of blue light resulted in a slower decrease of rosmarinic acid and total anthocyanin content compared to a high percentage of blue light in the purple cv. Rosie at 4°C (**Figures 5A,G**). The reverse effect was seen for chicoric acid, where a high percentage of blue light resulted in the slowest decrease for both cvs (**Figures 4C**, **5C**).

Chilling Tolerance in Response to the Percentage of Blue Light and PPFD

During the storage, F_v/F_m was measured as a marker for chilling injury. During dark storage at 12°C, there was little change over time and no effect of PPFD or the percentage of blue light during cultivation (**Figures 6B**, **7B**). For both cultivars, high PPFD during cultivation resulted in less chilling injury during 4°C storage (i.e., a slower decrease of F_v/F_m and a longer shelf life) (**Figures 6A**, **7A**). The high percentage of blue light showed a minor effect on the chilling injury for both cultivars. OVQ values were in line with F_v/F_m values. At 1°C, OVQ values slowly decreased and there were no clear effects of EOP PPFD or percentage of blue light (**Figures 6D**, **7D**). At 4°C a high PPFD had a positive effect on OVQ values for both cultivars (**Figures 6C**, **7C**) whereas the effect of percentage of blue light was limited.

During chilling injury, the content of H_2O_2 (i.e., a ROS) may increase due to chilling stress. At 12°C, the H_2O_2 content remained unchanged in the green cv. Dolly but decreased in

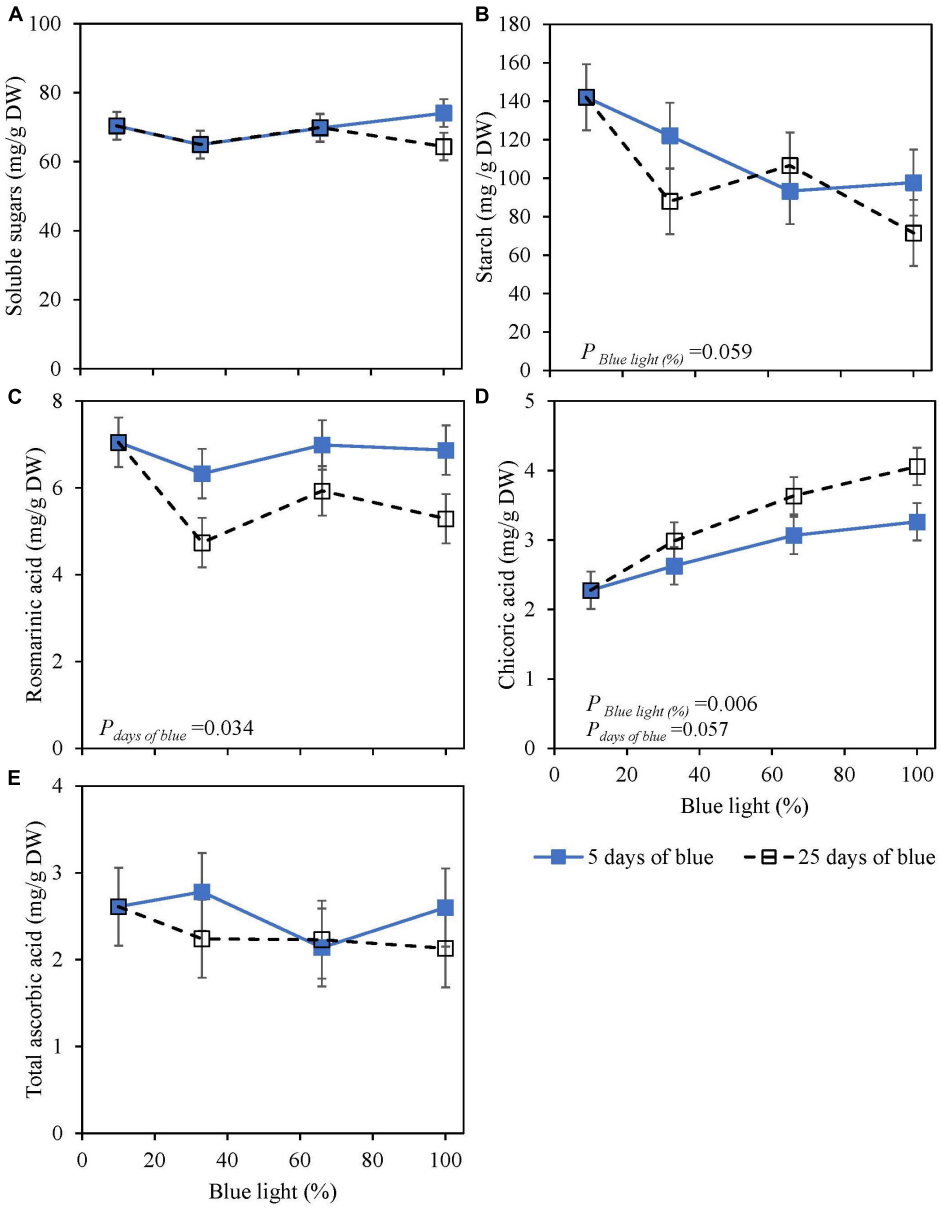

FIGURE 1 | Metabolite levels at harvest in basil cv. Dolly exposed either continuously (25 days) (open symbols) or for 5 days of End-Of-Production (EOP) (closed symbols) to different percentages of blue light. Plants were harvested after 40 days of cultivation. After 15 days, plants were transplanted. After the transplant, the continuously treated plants grew under different percentages of blue light until harvest [photon flux density (PPFD) of 300 μmol m^{-2} s^{-1}]. The EOP plants were grown under red-white (PPFD of 300 μmol m^{-2} s^{-1}, 9% blue) light and later exposed to different percentages of blue light (PPFD of 300 μmol m^{-2} s^{-1}) for the last 5 days before harvest as EOP treatments. **(A)** Soluble sugars (sum of glucose, fructose, and sucrose), **(B)** starch, **(C)** rosmarinic acid, **(D)** chicoric acid, **(E)** total ascorbic acid. All values are expressed per gram dry weight in the leaves. The data are means of two blocks (n = 2) (i.e., per block four replicate plants). Standard errors of means are shown as error bars. Significance of the main effects percentage of blue and days of blue (α = 10%) are depicted (Experiment 1).

the purple cv. Rosie (**Figures 6F**, **7F**). H_2O_2 levels in samples from low PPFD EOP treatments were generally higher than in samples from high PPFD in both cvs. There was no effect on the percentage of blue light. At 4°C, H_2O_2 levels in both cvs rapidly decreased, the decrease seemed to be more pronounced in samples from low PPFD EOP treatments; there was no effect of percentage of blue light on the observed patterns (**Figures 6E**, **7E**).

DISCUSSION

Blue Light Did Not Stimulate the Biosynthesis of Secondary Metabolites From the Phenylpropanoid Pathway

Blue light has been reported in numerous studies to increase the content of antioxidants in several plant species such as

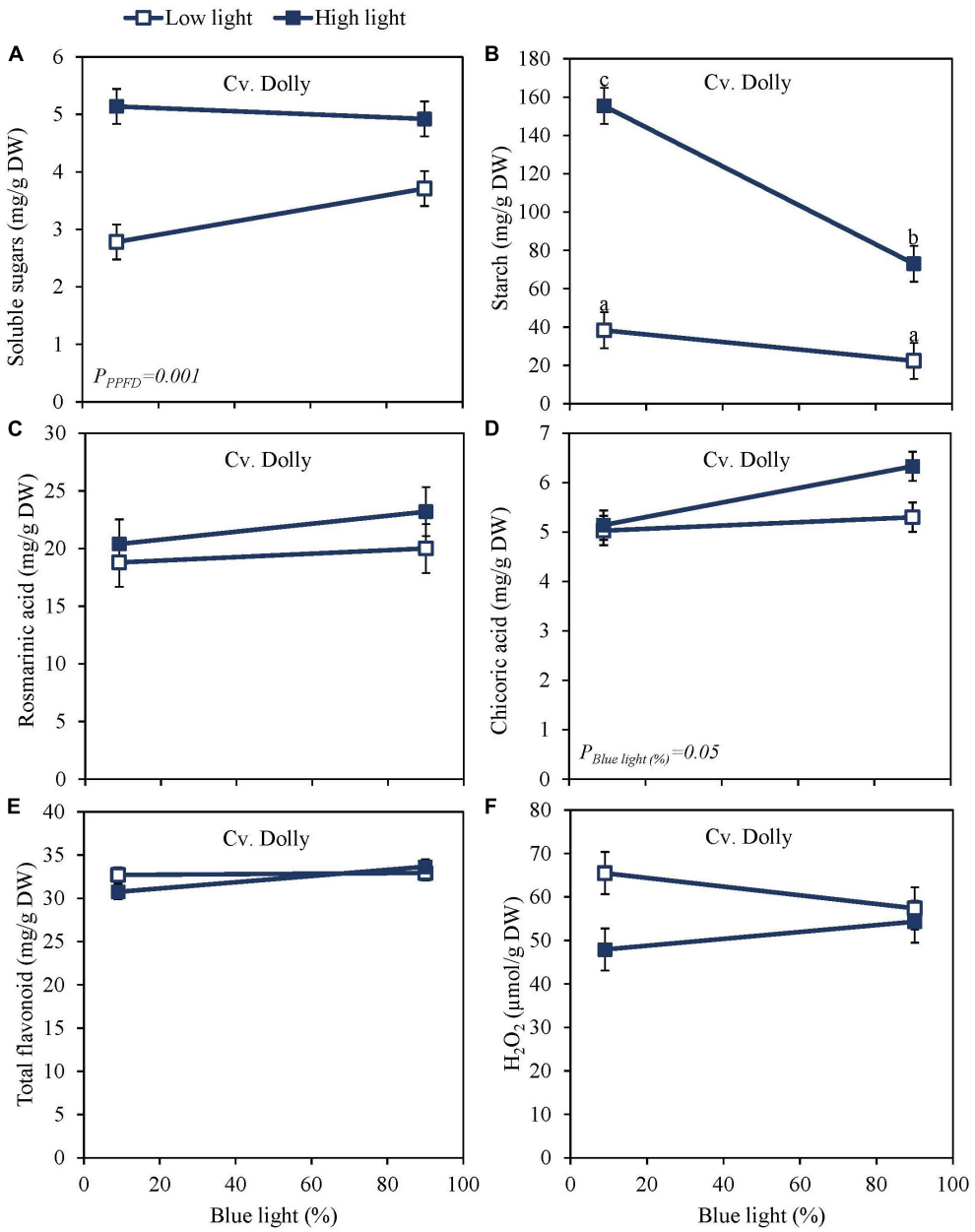

FIGURE 2 | Metabolite levels at harvest in basil, the green cv. Dolly were exposed to either 9% or 90% blue light at low PPFD (100 µmol m^{-2} s^{-1}) (open symbols) or high PPFD (300 µmol m^{-2} s^{-1}) (closed symbols) applied the last 5 days before harvest as EOP treatments. Before EOP treatments plants were grown under red-white light (PPFD of 200 µmol m^{-2} s^{-1}, 9% blue) for 30 days. **(A)** Soluble sugars (sum of glucose, fructose, and sucrose), **(B)** starch, **(C)** rosmarinic acid, **(D)** chicoric acid, **(E)** total flavonoids, **(F)** hydrogen peroxide (H_2O_2). All values are expressed per gram dry weight in the leaves. The data are means of three blocks (n = 3) (i.e., per block four replicate plants). Standard errors of means are shown as error bars. Significance of the main effects percentage of blue light and PPFD (α = 5%) are shown. Letters indicate and interactive effect between the two main effects (percentage of blue light and PPFD), (Experiment 2).

strawberry, green and red lettuce, green and red pak choi, and Arabidopsis (Chen et al., 2006; Samuoliene et al., 2013; Ouzounis et al., 2015; Zhang et al., 2018; Zheng et al., 2018). Thus, we hypothesized that blue light would increase the content of antioxidants at harvest in green and purple basil. Our findings indicate that a high percentage of blue light (up to 100%) during the whole cultivation period applied as a 5-day EOP treatment did not increase the content of rosmarinic acid in basil leaves (**Figures 1C**, **2C**, **3C**). Similar to Taulavuori et al. (2016), we found that a continuous application of a high percentage of blue light even negatively affected the content of rosmarinic acid (**Figure 1C**). Spectra that earlier have been reported to result in a high content of rosmarinic acid included red with supplementary far-red (Schwend et al., 2016), red light (Shiga et al., 2009), and

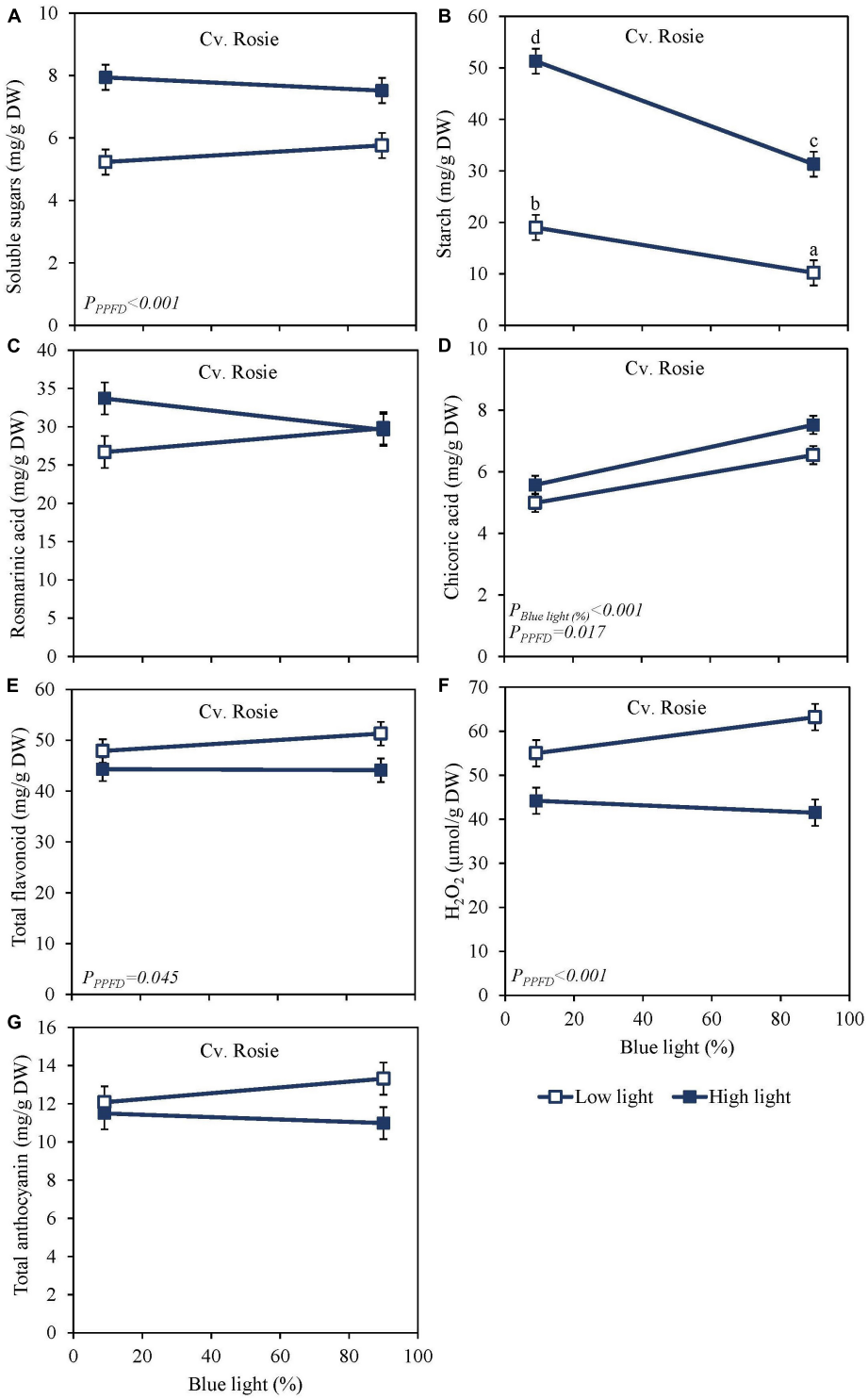

FIGURE 3 | Metabolite levels at harvest in basil the purple cv. Rosie were exposed to either 9% or 90% blue light at low PPFD (100 µmol m^{-2} s^{-1}) (open symbols) or high PPFD (300 µmol m^{-2} s^{-1}) (closed symbols) applied the last 5 days before harvest as EOP treatments. Before EOP treatments plants were grown under red-white light (PPFD of 200 µmol m^{-2} s^{-1}, 9% blue) for 30 days. **(A)** Soluble sugars (sum of glucose, fructose, and sucrose), **(B)** starch, **(C)** rosmarinic acid, **(D)** chicoric acid, **(E)** total flavonoids, **(F)** H_2O_2, **(G)** total anthocyanins. All values are expressed per gram dry weight in the leaves. The data are means of four blocks (n = 4) (i.e., per block four replicate plants). Standard errors of means are shown as error bars. Significance of the main effects percentage of blue light and PPFD (α = 5%) are shown. Letters indicate and interactive effect between the two main effects (percentage of blue light and PPFD), (Experiment 2).

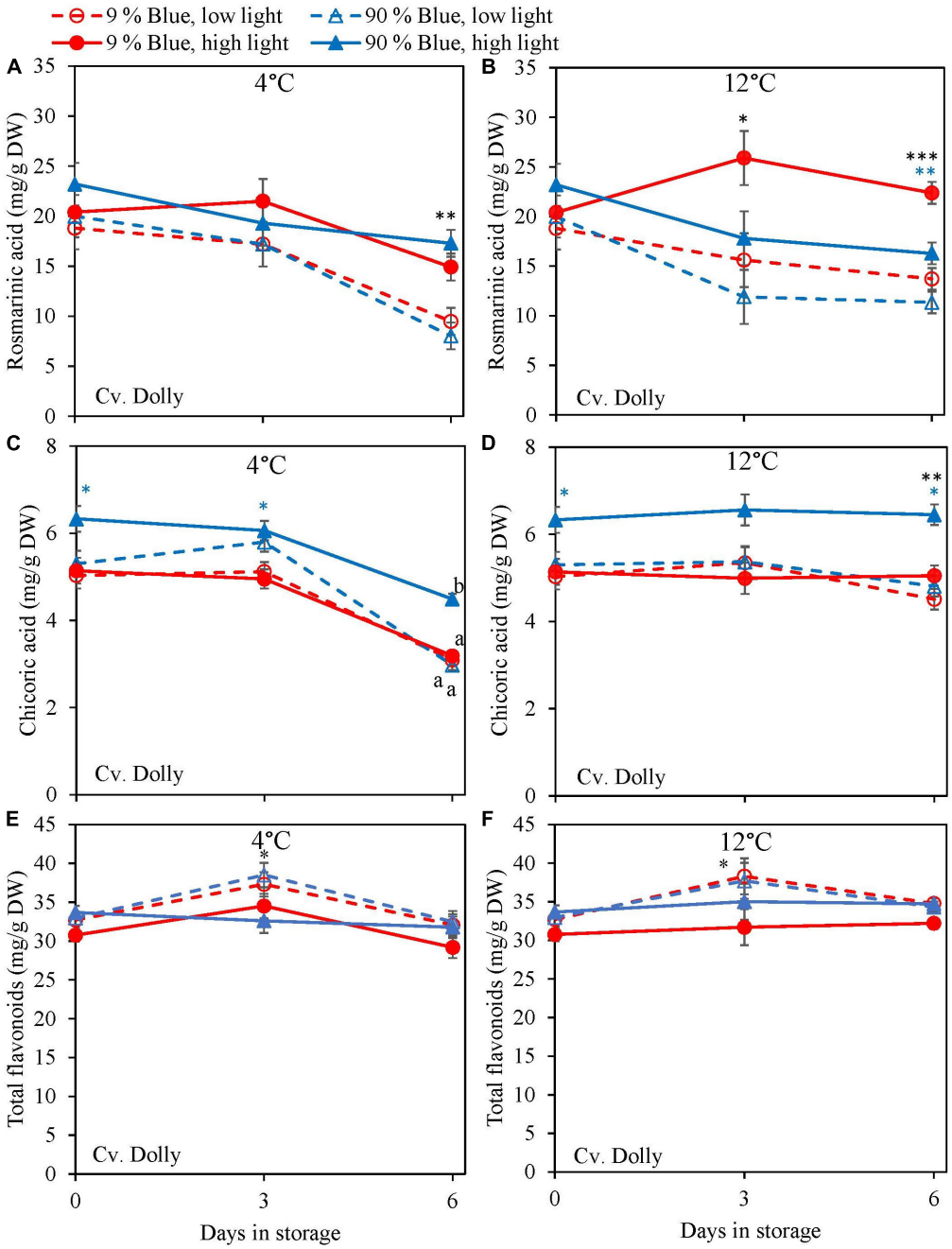

FIGURE 4 | Changes in metabolite levels during postharvest storage at 4 **(A,C,E)** and 12°C **(B,D,F)** in basil in the green cv. Dolly were exposed to EOP treatments. Plants were grown under red-white light (PPFD of 200 μmol m^{-2} s^{-1}, 9% blue) for 30 days. The last 5 days before harvest plants were exposed to different EOP blue light ratios 9 or 90% at low PPFD (100 μmol m^{-2} s^{-1}) (open symbols) or high PPFD (300 μmol m^{-2} s^{-1}) (closed symbols). **(A,B)** Change in rosmarinic acid, **(C,D)** change in chicoric acid, **(E,F)** change in total flavonoid content. All values are expressed per gram dry weight in the leaves. The data are means of three blocks (n = 3) (i.e., per block four replicate plants). Standard errors of means are shown as error bars. If no interaction was found but only the main effects were significant the indicated with p-values; *$p < 0.05$, **$p < 0.01$, ***$p < 0.001$ are depicted with either a blue (percentage of blue light) or black asterisk (PPFD). Letters indicate and interactive effect between the two main effects (percentage of blue light and PPFD), (Experiment 2).

blue light under greenhouse conditions. However, these studies did not consistently compare how the different percentages of the spectra affect the biosynthesis of rosmarinic acid (i.e., percentage of blue vs. green, red, and far-red). Chicoric acid generally constitutes a minor amount of the total level of phenolic compounds in the basil cultivars under study (**Figures 1D**, **2D**, **3D**). Although chicoric acid has been found to be a stronger antioxidant than rosmarinic acid (Dalby-Brown et al., 2005),

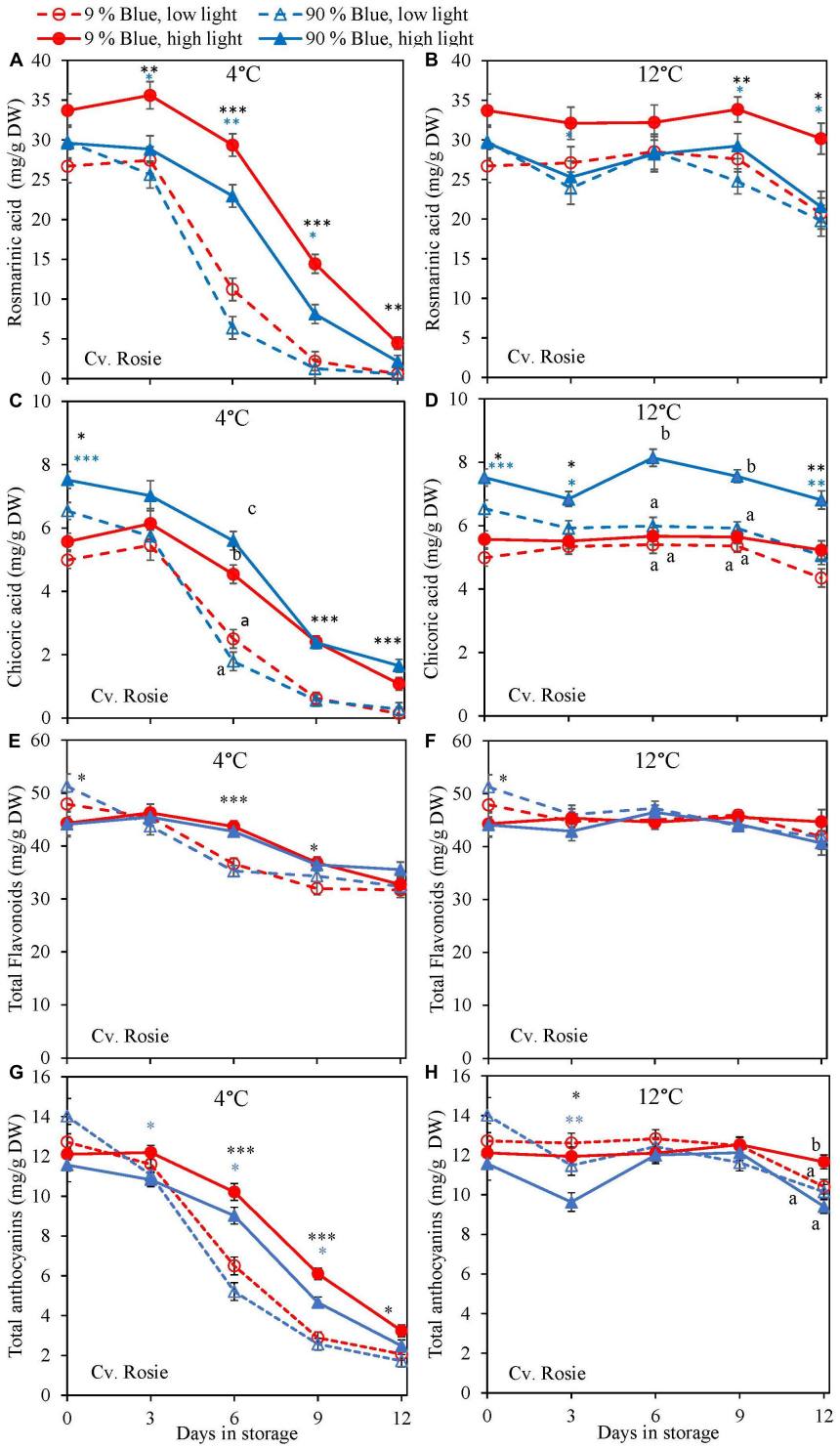

FIGURE 5 | Changes in metabolite levels during postharvest storage at 4 **(A,C,E,G)** and 12°C **(B,D,F,H)** in basil in the purple cv. Rosie were exposed to EOP treatments. Plants were grown under red-white light (PPFD of 200 μmol m^{-2} s^{-1}, 9% blue) for 30 days. The last 5 days before harvest plants were exposed to different EOP blue light ratios 9 or 90% at low PPFD (100 μmol m^{-2} s^{-1}) (open symbols) or high PPFD (300 μmol m^{-2} s^{-1}) (closed symbols). **(A,B)** Change in rosmarinic acid, **(C,D)** change in chicoric acid, **(E,F)** change in total flavonoid content, **(G,H)** change in total anthocyanin content. All values are expressed per gram dry weight in the leaves. The data are means of four blocks (n = 4) (i.e., per block four replicate plants). Standard errors of means are shown as error bars. If no interaction was found but only the main effects were significant the indicated with p-values; *$p < 0.05$, **$p < 0.01$, ***$p < 0.001$ are depicted with either a blue (percentage of blue light) or black asterisk (PPFD). Letters indicate and interactive effect between the two main effects (percentage of blue light and PPFD), (Experiment 2).

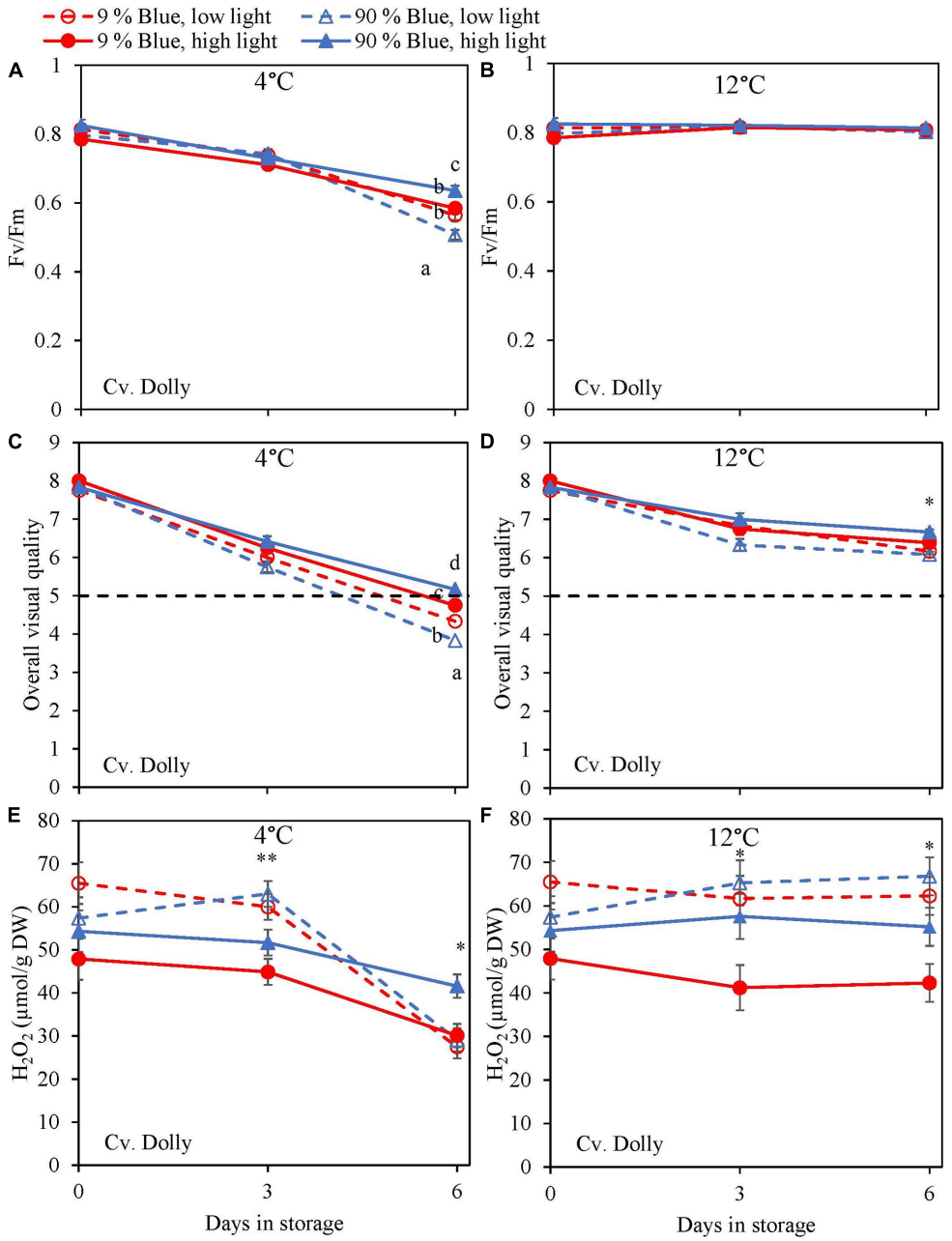

FIGURE 6 | Changes in chilling injury parameters during postharvest storage at 4 **(A,C,E)** and 12°C **(B,D,F)** in basil in the green cv. Dolly were exposed to EOP treatments. Plants were grown under red-white light (PPFD of 200 µmol m^{-2} s^{-1}, 9% blue) for 30 days. The last 5 days before harvest plants were exposed to different EOP blue light ratios 9 or 90% at low light (100 µmol m^{-2} s^{-1}) (open symbols) or high light (300 µmol m^{-2} s^{-1}) (closed symbols). **(A,B)** Change in maximum quantum yield of PSII of dark-adapted leaves (F_v/F_m), **(C,D)** change Overall Visual Quality (OVQ), **(E,F)** change in hydrogen peroxide (H_2O_2) content. All metabolite values are expressed per gram dry weight in leaves. The data are means of three blocks (n = 3) (i.e., per block four replicate plants). Standard errors of means are shown as error bars. If no interaction was found but only the main effects were significant the indicated with p-values; $^*p < 0.05$, $^{**}p < 0.01$, are depicted with either a blue (percentage of blue light) or black asterisk (PPFD). Letters indicate and interactive effect between the two main effects (percentage of blue light and PPFD), (Experiment 2).

it is unknown to what extent chicoric acid contributes to the overall scavenging activity of basil antioxidants. Similar to our results, Taulavuori et al. (2016) found blue light to have a positive effect on the content of chicoric acid. We found different absolute levels of especially rosmarinic acid content in the two experiments. However, the response to blue light remained the same between the two experiments (i.e., no effect of blue light). The main difference between the experiments was the initial

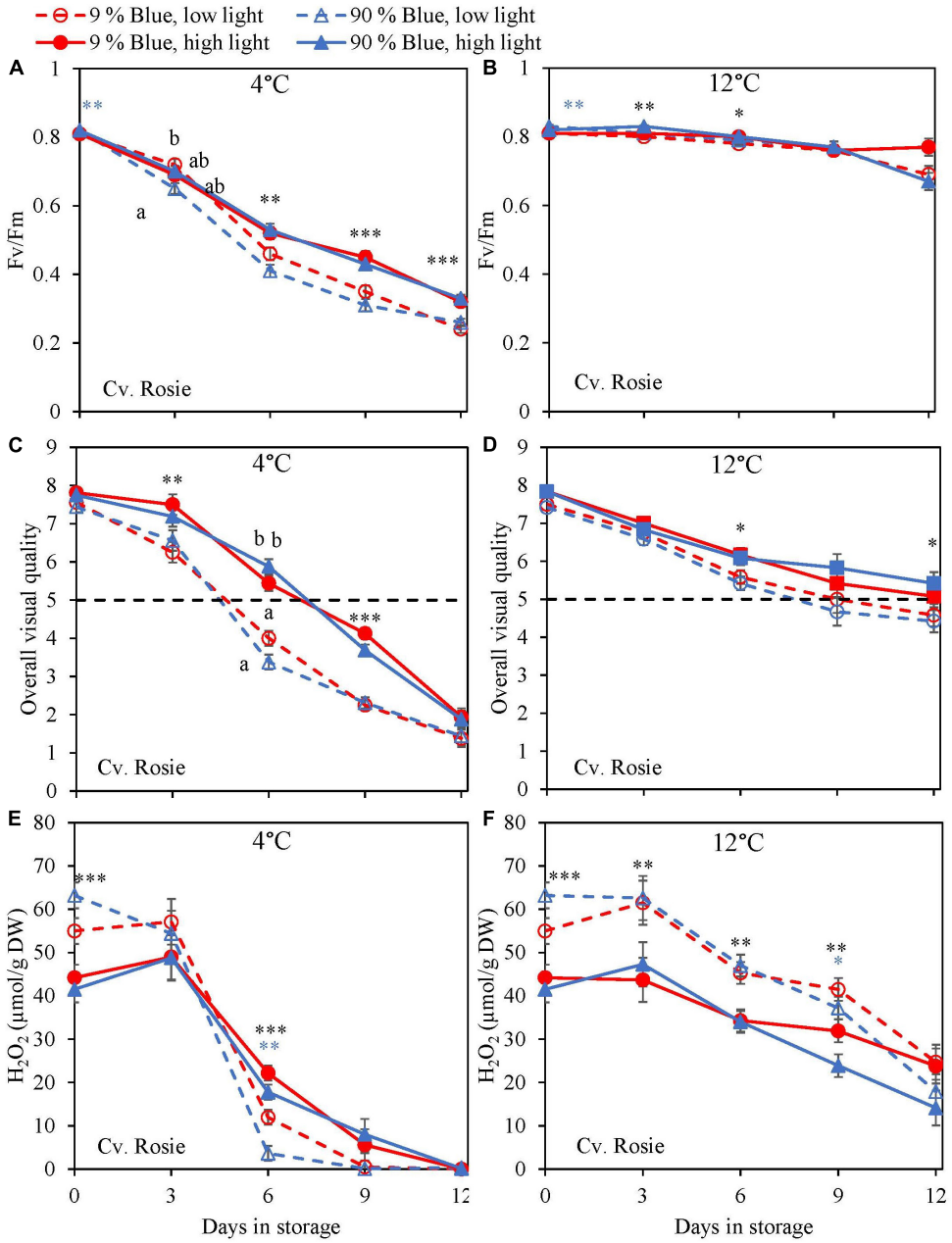

FIGURE 7 | Changes in chilling injury parameters during postharvest storage at 4 **(A,C,E)** and 12°C **(B,D,F)** in basil in the purple cv. Rosie was exposed to EOP treatments. Plants were grown under red-white light (PPFD of 200 µmol m^{-2} s^{-1}, 9% blue) for 30 days. The last 5 days before harvest plants were exposed to different EOP blue light ratios 9 or 90% at low light (100 µmol m^{-2} s^{-1}) (open symbols) or high light (300 µmol m^{-2} s^{-1}) (closed symbols). **(A,B)** Change in Maximum quantum yield of PSII of dark-adapted leaves (F_v/F_m), **(C,D)** change in OVQ, **(E,F)** change in H_2O_2 content. All metabolite values are expressed per gram dry weight in leaves. The data are means of four blocks (n = 4) (i.e., per block four replicate plants). Standard errors of means are shown as error bars. If no interaction was found but only the main effects were significant the indicated with p-values; *$p < 0.05$, **$p < 0.01$, ***$p < 0.001$ are depicted with either a blue (percentage of blue light) or black asterisk (PPFD). Letters indicate and interactive effect between the two main effects (percentage of blue light and PPFD), (Experiment 2).

PPFD; Experiment 1 had a PPFD of 300 µmol m^{-2} s^{-1} and Experiment 2 a PPFD of 200 µmol m^{-2} s^{-1}. Similar to the high content of rosmarinic acid in Experiment 2 our previous results in basil also showed increased PPFD as EOP treatment to increase rosmarinic acid (Larsen et al., 2022). Furthermore, the duration of Experiment 1 was 40 days while Experiment 2 was 35. The younger leaves in Experiment 2 may have additionally contributed to a higher content of rosmarinic acid at harvest.

Blue light is absorbed by photoreceptors such as cryptochromes (cry1 and cry2) which mediates plant responses. The genes involved in the biosynthesis of flavonoids and anthocyanins through the phenylpropanoid pathway are induced

through cry1 (Jenkins et al., 2001). The starting point for the flavonoid biosynthesis branch is chalcone synthase (CHS). The expression level of *CHS* has been found to increase by blue light in Arabidopsis cells (Christie and Jenkins, 1996) and increase anthocyanin and flavonoid content in several species. In pepper leaves, increasing blue light to 75% increased the content of anthocyanins but not flavonoids (Hoffmann et al., 2016). However, in our study total anthocyanin content did not increase with an increased percentage of blue light (**Figure 3G**), and neither did total flavonoid content in the green cultivar (**Figure 2E**) nor the purple cultivar (**Figure 3E**). Similarly, Dou et al. (2019) found that increasing the blue light from 16 to 24% did not increase the anthocyanin content in green or purple basil while they did find a positive effect on flavonoids in green basil. Findings by Pennisi et al. (2019) indicated an optimum at 23% blue light resulting in the highest total flavonoids content while 58% and 19% blue light resulted in the lowest total flavonoid content in green basil. In contrast, Piovene et al. (2015) found that a range of blue light from 10 to 40% did not increase the total flavonoid content in basil. In red lettuce, 47% blue light gave the highest content of flavonoids whereas 59% blue light yielded the highest content in green lettuce (Son and Oh, 2013). Although it is generally assumed that blue light will increase particularly the flavonoid and anthocyanin content there is no general consistency in the results; this makes it hard to predict which percentage of blue light may be required to increase the flavonoid and anthocyanin content if any. However, it should be noted that changes in the percentage of blue light also cause changes in the contribution of other wavelengths, that may contribute to the measured effects. Based on our results it seems that a low percentage of blue light (9%) in the spectrum is already sufficient for maximal biosynthesis of phenolic compounds (phenolic acids, flavonoids, and anthocyanins) in green and purple basil.

The Content of Secondary Metabolites in Response to the Percentage of Blue Light Did Not Depend on PPFD

We hypothesized that the response to blue light might be reduced by high PPFD (300 μmol $m^{-2}s^{-1}$). The accumulation of antioxidants in response to blue light may be more pronounced at a lower PPFD compared to a high PPFD as a high PPFD regardless of the spectrum leads to an increase in antioxidants (Larsen et al., 2022). In cannabis, the percentage of blue light at a PPFD of 750 and 900 μmol $m^{-2}s^{-1}$ did not affect secondary metabolites which were assumed to be attributed to saturated photoreceptors (i.e., less sensitivity to spectral effects) (Westmoreland et al., 2021). We tested if the effect of varying percentages of blue light was different when applied on a low or high PPFD background. We did not find such an effect on the metabolite content in either green or purple basil. This is in contrast to findings by Zheng et al. (2018) in green and red-leaved pak choi where the percentage of blue light and PPFD had an interactive effect on vitamin C, carotenoids, and total phenolic content.

At harvest, the dominant effect of light on metabolites came from the PPFD (**Figures 2**, **3**) which is in line with the results of Larsen et al. (2022) where increased PPFD increased both primary and secondary metabolites in basil. In red lettuce, anthocyanin and phenolic acids were not affected by PPFD whereas flavonoids increased (Becker et al., 2013). This is in accordance with our results where PPFD had no effect on anthocyanin content but a small increasing effect on flavonoid content at harvest (**Figure 3E**). In studies where anthocyanins have been reported to increase with an increase in PPFD, the much bigger difference between light intensities was applied; from 100 to 550–650 μmol m^{-2} s^{-1} (Page et al., 2012) from 50–350 to 750 μmol m^{-2} s^{-1} (Albert et al., 2009). To get an overview of the whole plant, we sampled all fully developed leaves at harvest except the oldest leaf pair. Young leaves contain higher amounts of anthocyanins than older leaves and by sampling young leaves along with more mature leaves, we could potentially have had a dilution effect (Chalker-Scott, 1999). In addition to antioxidants, we found that starch content was significantly decreased at a high PPFD and a high percentage of blue light in both green and purple basil (**Figures 1B**, **2B**, **3B**), this could negatively affect shelf life as starch is used for respiration (Enninghorst and Lippert, 2003). Although, we found that starch was decreased in both experiments the dry mass of the leaves only decreased with the percentage of blue light when continuously grown under a high PPFD (300 μmol m^{-2} s^{-1}) (Larsen et al., 2020).

High PPFD Resulted in a Slower Breakdown of Antioxidants and Improved Chilling Tolerance Postharvest

In lettuce (Min et al., 2021) and basil (Larsen et al., 2022), it was found that the stimulating effect of high PPFD on metabolites observed at harvest was maintained during postharvest storage. In the present experiments, levels at harvest were little affected by PPFD, but during postharvest storage at 4°C antioxidants (rosmarinic acid, chicoric acid, total anthocyanin content, and total flavonoid content) in the purple cv. Rosie from high PPFD EOP light treatments showed a slower breakdown than in samples from low PPFD treatments (**Figure 5**). The effect of PPFD on the rate of the postharvest breakdown of antioxidants was less pronounced in the green cv. Dolly (**Figure 4**). The slower breakdown of antioxidants during storage at 4°C coincided with a slower decrease in F_v/F_m and Overall visual quality (OVQ) (**Figures 6A,C**, **7A,C**). This indicates that the plants from high PPFD were more tolerant to the cold. Although antioxidants may scavenge ROS and in turn result in maintaining high F_v/F_m values we believe that another mechanism could also be in play here. In the purple cv. Rosie, high light did increase the soluble sugar and starch content (**Supplementary Figure 4**) which can protect against chilling stress (Santarius, 1973). Plants with an increased chilling tolerance may have had higher levels of hormones such as ABA and JA (Lado et al., 2016; Wang et al., 2016). However, this has yet to be studied in basil.

During excessive stress, H_2O_2 is not only formed in the mitochondria and chloroplasts but also in the peroxisomes resulting in lipid peroxidation (Corpas et al., 2001). Exposure of basil to chilling temperatures was expected to increase the content

of H_2O_2. However, during storage at 4°C, we observed a strong decrease of H_2O_2 in both cultivars (**Figures 6E**, **7E**). In contrast, the level of H_2O_2 at 12°C either remained constant in the green cv. Dolly (**Figure 6F**) or showed a slow decrease in the purple cv. Rosie (**Figure 7F**). The low H_2O_2 concentration at 4°C may be a result of scavenging by anthocyanins, flavonoids, rosmarinic acid, and chicoric acid, which all showed comparable decreasing trends at 4°C (**Figures 2**, **3**). Enzymatic antioxidants might also have been active in scavenging as the content is known to increase when plants are grown under high PPFD (Ali et al., 2005; Zhou et al., 2012).

CONCLUSION

Contrary to our hypothesis and general expectations, a high percentage of blue light applied either continuously throughout the growth or as EOP treatment did not increase antioxidants such as rosmarinic acid, total anthocyanin content, or total flavonoid content at harvest. The only antioxidant that was increased by a percentage of blue light was chicoric acid, which is only a minor part of the total antioxidant content. The absence of effects of blue light was observed both in green and purple basil cultivars, and the absence was also observed whether PPFD was high or low. Chilling tolerance is supposed to be related to the scavenging activity of antioxidants. The lack of effect of the percentage of blue light on antioxidant levels is in line with the absence of a percentage of blue light effects on chilling tolerance. Although a high percentage of blue light did not improve postharvest chilling tolerance in green or purple basil, high PPFD EOP treatments did. High PPFD as EOP treatment particularly improved chilling tolerance in the purple cultivar, reflected in a slower decrease in antioxidants than in samples from in low PPFD treatments. This may not be related to the levels of antioxidants but to the higher carbohydrate levels (soluble sugars and starch) in leaves from high PPFD grown plants.

DATA AVAILABILITY STATEMENT

The raw data supporting the conclusions of this article will be made available by the authors, without undue reservation.

AUTHOR CONTRIBUTIONS

DL, EW, CN, JV, and LM conceptualized the research plan. DL, EW, and LM designed the experiments. DL and HL established the methodology. DL and SS carried out the experiments. DL analyzed the data and wrote the manuscript. EW and LM provided critical feedback on the manuscript and supervised the research. CN, HL, JV, and SS provided critical comments on the overall structure of the manuscript. All authors reviewed and approved the final manuscript.

FUNDING

This work was funded by Signify, Eindhoven, Netherlands.

ACKNOWLEDGMENTS

We would like to thank Arjen van de Peppel and Kees van Kekem for their help during the analysis of metabolites. Furthermore, we thank Joke Oosterkamp for her help with fluorescence measurements. We thank the technical staff in Unifarm and Klima, in particular, Gerrit Stunnenberg, Taede Stoker, and David Brink.

SUPPLEMENTARY MATERIAL

The Supplementary Material for this article can be found online at: https://www.frontiersin.org/articles/10.3389/fpls.2022.852654/full#supplementary-material

REFERENCES

Ahmed, N. U., Park, J. I., Jung, H. J., Yang, T. J., Hur, Y., and Nou, I. S. (2014). Characterization of dihydroflavonol 4-reductase (DFR) genes and their association with cold and freezing stress in Brassica rapa. *Gene* 550, 46–55. doi: 10.1016/j.gene.2014.08.013

Albert, N. W., Lewis, D. H., Zhang, H., Irving, L. J., Jameson, P. E., and Davies, K. M. (2009). Light-induced vegetative anthocyanin pigmentation in Petunia. *J. Exp. Bot.* 60, 2191–2202. doi: 10.1093/jxb/erp097

Ali, M. B., Hahn, E.-J., and Paek, K.-Y. (2005). Effects of light intensities on antioxidant enzymes and malondialdehyde content during short-term acclimatization on micropropagated Phalaenopsis plantlet. *Environ. Exp. Bot.* 54, 109–120. doi: 10.1016/j.envexpbot.2004.06.005

Becker, C., Kläring, H. P., Kroh, L. W., and Krumbein, A. (2013). Temporary reduction of radiation does not permanently reduce flavonoid glycosides and phenolic acids in red lettuce. *Plant Physiol. Biochem.* 72, 154–160. doi: 10.1016/j.plaphy.2013.05.006

Chalker-Scott, L. (1999). Environmental significance of anthocyanins in plant stress responses. *Photobiol.* 70, 1–9. doi: 10.1111/j.1751-1097.1999.tb01944.x

Chen, D., Li, Z., Pan, R., and Wang, X. (2006). Anthocyanin Accumulation Mediated by Blue Light and Cytokinin in Arabidopsis Seedlings. *J. Integr. Plant Biol.* 48, 420–425. doi: 10.1016/j.plaphy.2021.01.047

Christie, J. M., and Jenkins, G. I. (1996). Distinct UV-B and UV-A / Blue Light Signal Transduction Pathways lnduce Chalcone Synthase Gene Exptession in Arabidopsis Cells. *Plant Cell* 8, 1555–1567.

Corpas, F. J., Barroso, J. B., and Luis, A. (2001). Peroxisomes as a source of reactive oxygen species and nitric oxide signal molecules in plant cells. *Trends Plant Sci.* 6, 145–150. doi: 10.1016/s1360-1385(01)01898-2

Dalby-Brown, L., Barsett, H., Landbo, A. K. R., Meyer, A. S., and Mølgaard, P. (2005). Synergistic antioxidative effects of alkamides, caffeic acid derivatives, and polysaccharide fractions from Echinacea purpurea on in vitro oxidation of human low-density lipoproteins. *J. Agric. Food Chem.* 53, 9413–9423. doi: 10.1021/jf0502395

Das, K., and Roychoudhury, A. (2014). Reactive oxygen species (ROS) and response of antioxidants as ROS-scavengers during environmental stress in plants. *Front. Environ. Sci.* 2:53. doi: 10.3389/fenvs.2014.00053

Dou, H., Niu, G., and Gu, M. (2019). Photosynthesis, morphology, yield, and phytochemical accumulation in basil plants influenced by substituting green light for partial red and/or blue light. *HortScience* 54, 1769–1776. doi: 10.21273/HORTSCI14282-19

Enninghorst, A., and Lippert, F. (2003). Postharvest changes in carbohydrate contetnt of Lamb's lettuce (Valerianella Locusta). *Acta Hortic.* 604, 553–558. doi: 10.17660/ActaHortic.2003.604.65

Gomez, C., and Jimenez, J. (2020). Effect of End-of-production High-energy Radiation on Nutritional Quality of Indoor-grown Red-leaf Lettuce. *HortScience* 55, 1–6. doi: 10.21273/HORTSCI15030-20

Hoffmann, A. M., Noga, G., and Hunsche, M. (2016). Alternating high and low intensity of blue light affects PSII photochemistry and raises the contents of carotenoids and anthocyanins in pepper leaves. *Plant Growth Regul.* 79, 275–285. doi: 10.1007/s10725-015-0132-0

Hogewoning, S. W., and Harbinson, J. (2007). Insights on the development, kinetics, and variation of photoinhibition using chlorophyll fluorescence imaging of a chilled, variegated leaf. *J. Exp. Bot.* 58, 453–463. doi: 10.1093/jxb/erl219

Jenkins, G. I., Long, J. C., Wade, H. K., Shenton, M. R., and Bibikova, T. N. (2001). UV and blue light signalling: Pathways regulating chalcone synthase gene expression in Arabidopsis. *New Phytol.* 151, 121–131. doi: 10.1046/J.1469-8137.2001.00151.X

Junglee, S., Urban, L., Sallanon, H., and Lopez-Lauri, F. (2014). Optimized Assay for Hydrogen Peroxide Determination in Plant Tissue Using Potassium Iodide. *Am. J. Anal. Chem.* 05, 730–736. doi: 10.4236/AJAC.2014.511081

Kwee, E. M., and Niemeyer, E. D. (2011). Variations in phenolic composition and antioxidant properties among 15 basil (Ocimum basilicum L.) cultivars. *Food Chem.* 128, 1044–1050. doi: 10.1016/j.foodchem.2011.04.011

Lado, J., Manzi, M., Sainz, M. M., Sotelo, M., and Zacarías, L. (2016). "Involvement of Plant Hormones in Cold Stress Tolerance," in *Plant Hormones under Challenging Environmental Factors*, eds G. J. Ahammed and J.-Q. Yu (Dordrecht: Springer Netherlands), 23–49. doi: 10.1007/978-94-017-7758-2_2

Lange, D. D., and Cameron, A. C. (1994). Postharvest shelf life of sweet basil (Ocimum basilicum). *HortScience* 29, 102–103.

Larsen, D. H., Li, H., van de Peppel, A. C., Nicole, C. C. S., Marcelis, L. F. M., and Woltering, E. J. (2022). High light intensity at End-Of-Production improves the nutritional value of basil but does not affect postharvest chilling tolerance. *Food Chem.* 369:130913. doi: 10.1016/J.FOODCHEM.2021.130913

Larsen, D. H., Woltering, E. J., Nicole, C. C. S., and Marcelis, L. F. M. (2020). Response of Basil Growth and Morphology to Light Intensity and Spectrum in a Vertical Farm. *Front. Plant Sci.* 11:597906. doi: 10.3389/fpls.2020.597906

McCance, K. R., Flanigan, P. M., Quick, M. M., and Niemeyer, E. D. (2016). Influence of plant maturity on anthocyanin concentrations, phenolic composition, and antioxidant properties of 3 purple basil (Ocimum basilicum L.) cultivars. *J. Food Compos. Anal.* 53, 30–39. doi: 10.1016/j.jfca.2016.08.009

Min, Q., Marcelis, L. F. M., Nicole, C. C. S., and Woltering, E. J. (2021). High Light Intensity Applied Shortly Before Harvest Improves Lettuce Nutritional Quality and Extends the Shelf Life. *Front. Plant Sci.* 12:615355. doi: 10.3389/fpls.2021.615355

Ouzounis, T., Razi Parjikolaei, B., Fretté, X., Rosenqvist, E., and Ottosen, C.-O. (2015). Predawn and high intensity application of supplemental blue light decreases the quantum yield of PSII and enhances the amount of phenolic acids, flavonoids, and pigments in Lactuca sativa. *Front. Plant Sci.* 6:19. doi: 10.3389/fpls.2015.00019

Page, M., Sultana, N., Paszkiewicz, K., Florance, H., and Smirnoff, N. (2012). The influence of ascorbate on anthocyanin accumulation during high light acclimation in Arabidopsis thaliana: Further evidence for redox control of anthocyanin synthesis. *Plant Cell Environ.* 35, 388–404. doi: 10.1111/j.1365-3040.2011.02369.x

Pennisi, G., Blasioli, S., Cellini, A., Maia, L., Crepaldi, A., Braschi, I., et al. (2019). Unraveling the Role of Red:Blue LED Lights on Resource Use Efficiency and Nutritional Properties of Indoor Grown Sweet Basil. *Front. Plant Sci.* 10:305. doi: 10.3389/fpls.2019.00305

Piovene, C., Orsini, F., Bosi, S., Sanoubar, R., Bregola, V., Dinelli, G., et al. (2015). Optimal red: Blue ratio in led lighting for nutraceutical indoor horticulture. *Sci. Hortic.* 193, 202–208. doi: 10.1016/j.scienta.2015.07.015

Samuoliene, G., Brazaityte, A., Sirtautas, R., Viršile, A., Sakalauskaite, J., Sakalauskiene, S., et al. (2013). LED illumination affects bioactive compounds in romaine baby leaf lettuce. *J. Sci. Food Agric.* 93, 3286–3291. doi: 10.1002/jsfa.6173

Santarius, K. A. (1973). The Protective Effect of Sugars on Chloroplast Membranes during Temperature and Water Stress and Its Relationship to Frost, Desiccation and Heat Resistance. *Planta.*113, 105–14. doi: 10.1007/BF00388196

Schwend, T., Prucker, D., Peisl, S., Nitsopoulos, A., and Mempel, H. (2016). The rosmarinic acid content of basil and borage correlates with the ratio of red and far-red light. *Eur. J. Horticult. Sci.* 81, 243–247. doi: 10.17660/eJHS.2016/81.5.2

Sevillano, L., Sanchez-Ballest, M. T., Romojaro, F., and Flores, F. B. (2009). Physiological, hormonal and molecular mechanisms regulating chilling injury in horticultural species. Postharvest technologies applied to reduce its impact. *J. Sci. Food Agric.* 89, 555–573. doi: 10.1002/jsfa.3468

SharathKumar, M., Heuvelink, E., and Marcelis, L. F. M. (2020). Trends in Plant Science Forum Vertical Farming: Moving from Genetic to Environmental Modification Trends in Plant Science. *Trends Plant Sci.* 25, 1–4. doi: 10.1016/j.tplants.2020.05.012

Shiga, T., Shoji, K., Shimada, H., Hashida, S., Goto, F., and Yoshihara, T. (2009). Effect of light quality on the polyphenol content andantioxidant activity of Sweet Basil (Ocimum basilicum L.). *Acta Hortic.* 26, 255–259. doi: 10.17660/ActaHortic.2011.907.10

Son, K. H., and Oh, M. M. (2013). Leaf shape, growth, and antioxidant phenolic compounds of two lettuce cultivars grown under various combinations of blue and red light-emitting diodes. *HortScience* 48, 988–995.

Taulavuori, K., Hyöky, V., Oksanen, J., Taulavuori, E., and Julkunen-Tiitto, R. (2016). Species-specific differences in synthesis of flavonoids and phenolic acids under increasing periods of enhanced blue light. *Environ. Exp. Bot.* 121, 145–150. doi: 10.1016/j.envexpbot.2015.04.002

Taulavuori, K., Julkunen-Tiitto, R., Hyoky, V., and Taulavuori, E. (2013). Blue Mood for Superfood. *Nat. Prod. Commun.* 8, 791–794. doi: 10.1002/ptr.3648

Wang, F., Guo, Z., Li, H., Wang, M., Onac, E., Zhou, J., et al. (2016). Phytochrome A and B Function Antagonistically to Regulate Cold Tolerance *via* Abscisic Acid-Dependent Jasmonate Signaling. *Plant Physiol.* 170, 459–471. doi: 10.1104/pp.15.01171

Westmoreland, F. M., Kusuma, P., and Bugbee, B. (2021). Cannabis lighting: Decreasing blue photon fraction increases yield but efficacy is more important for cost effective production of cannabinoids. *PLoS One* 16:e0248988. doi: 10.1371/JOURNAL.PONE.0248988

Zhang, Y., Jiang, L., Li, Y., Chen, Q., Ye, Y., Zhang, Y., et al. (2018). Effect of red and blue light on anthocyanin accumulation and differential gene expression in strawberry (Fragaria × ananassa). *Molecules* 23:820. doi: 10.3390/molecules23040820

Zheng, Y. J, Zhang, Y. T, Liu, H. C, Liu, L. H., Min, L. Y., Liang, L. Y., et al. (2018). Supplemental blue light increases growth and quality of greenhouse pak choi depending on cultivar and supplemental light intensity. *J. Integr. Agric* 17, 2245–2256. doi: 10.1016/S2095-3119(18)62064-7

Zhishen, J., Mengcheng, T., and Jianming, W. (1999). The determination of flavonoid contents in mulberry and their scavenging effects on superoxide radicals. *Food Chem.* 64, 555–559. doi: 10.1016/S0308-8146(98)00102-2

Zhou, W. L., Liu, W. K., and Yang, Q. C. (2012). Quality changes in hydroponic lettuce grown under pre-harvest short-duration continuous light of different intensities. *J. Hortic. Sci. Biotechnol.* 87, 429–434. doi: 10.1080/14620316.2012.11512890

Conflict of Interest: CN was employed by Signify Research Laboratories Ltd.

The remaining authors declare that the research was conducted in the absence of any commercial or financial relationships that could be construed as a potential conflict of interest.

Publisher's Note: All claims expressed in this article are solely those of the authors and do not necessarily represent those of their affiliated organizations, or those of the publisher, the editors and the reviewers. Any product that may be evaluated in this article, or claim that may be made by its manufacturer, is not guaranteed or endorsed by the publisher.

frontiers | Frontiers in Plant Science

ORIGINAL RESEARCH
published: 11 April 2022
doi: 10.3389/fpls.2022.863467

Melatonin Pre-harvest Treatments Leads to Maintenance of Sweet Cherry Quality During Storage by Increasing Antioxidant Systems

Alberto Carrión-Antolí[1], Domingo Martínez-Romero[1], Fabián Guillén[1], Pedro J. Zapata[1], María Serrano[2] and Daniel Valero[1]*

[1] Department of Agro-Food Technology, University Miguel Hernández, Orihuela, Spain, [2] Department of Applied Biology, University Miguel Hernández, Orihuela, Spain

Melatonin has been reported to have an important role in fruit ripening, although the effect of pre-harvest melatonin treatment on sweet cherry quality properties during storage is still unknown. In the present experiments, the effects of melatonin (0.1, 0.3, and 0.5 Mm) by foliar spray treatments of 'Prime Giant' and 'Sweet Heart' sweet cherry trees on fruit quality traits and antioxidants systems during storage was evaluated. Results showed that these treatments reduced weight losses during storage, as well as losses in firmness and titratable acidity. In addition, changes in fruit colour and total soluble solid content were also delayed in fruit from melatonin treated trees with respect to controls. Moreover, in general, total phenolic and anthocyanin concentrations were higher in fruit from treated trees than in those from control ones, either at harvest or during the whole storage period. Finally, the activity of the antioxidant enzymes catalase, ascorbate peroxidase and peroxidase was also enhanced as a consequence of melatonin treatment. Overall results show that pre-harvest melatonin treatment delayed the post-harvest ripening process of sweet cherry fruit, leading to maintenance of their quality properties in optimum levels for consumption 2 weeks more with respect to fruit from control trees. Antioxidant systems, both enzymatic and non-enzymatic ones, were also enhanced by melatonin treatments, which would account for the delay on fruit post-harvest ripening process and fruit quality maintenance during storage.

Keywords: ***Prunus avium*, phenolics, anthocyanins, firmness, colour, soluble sugars, acidity, antioxidant enzymes**

OPEN ACCESS

Edited by:
Leo Marcelis, Wageningen University and Research, Netherlands

Reviewed by:
Kaituo Wang, Chongqing Three Gorges University, China
Qingguo Wang, Shandong Agricultural University, China

****Correspondence:***
María Serrano
m.serrano@umh.es

Specialty section:
This article was submitted to Crop and Product Physiology, a section of the journal Frontiers in Plant Science

Received: *27 January 2022*
Accepted: *17 March 2022*
Published: *11 April 2022*

Citation:
Carrión-Antolí A, Martínez-Romero D, Guillén F, Zapata PJ, Serrano M and Valero D (2022) Melatonin Pre-harvest Treatments Leads to Maintenance of Sweet Cherry Quality During Storage by Increasing Antioxidant Systems. Front. Plant Sci. 13:863467. doi: 10.3389/fpls.2022.863467

INTRODUCTION

Sweet cherry fruit (*Prunus avium* L.) have excellent organoleptic and nutritional properties, such as appearance, colour, texture, flavour, juiciness, and sugar and organic acid content (Usenik et al., 2008; Díaz-Mula et al., 2009; Martínez-Esplá et al., 2014). In addition, sweet cherries are rich in bioactive compounds with antioxidant properties, mainly phenolics, and ascorbic acid, which are responsible for their health beneficial properties, namely, anti-inflammatory, antidiabetic, antimicrobial, and anticancer effects as well as cardiovascular and neuroprotection activities (McCune et al., 2011; Blando and Oomah, 2019; Faienza et al., 2020). However, they are very perishable fruit suffering from quickly quality losses after harvest even under storage in cold

conditions. Thus, different post-harvest treatments combined with cold storage have been reported to be useful to maintain sweet cherry fruit quality for longer time, such as alginate coating (Díaz-Mula et al., 2012), *Aloe vera* gel containing rosehip oil (Paladines et al., 2014), nano-silica coating (Meng et al., 2022), 1-methylcyclopropene and chlorine dioxide treatments, alone or in combination (Serradilla et al., 2019; Zhao et al., 2021) or salicylic (SA), acetylsalicylic (ASA), and oxalic (OA) acids treatments (Valero et al., 2011), as well as storage under modified atmosphere conditions (Cozzolino et al., 2019), among others (Correia et al., 2017).

In addition, different pre-harvest treatments, such as gibberellic acid (Einhorn et al., 2013), oxalic acid (Martínez-Esplá et al., 2014), salicylic acid (SA), acetyl salicylic acid (ASA), and methyl salicylate (MeSa) (Giménez et al., 2014, 2017; Valverde et al., 2015) have been performed aimed to increase sweet cherry fruit quality attributes at harvest. These treatments led to enhanced fruit size, firmness and total anthocyanin and phenolic contents at harvest and these quality parameters were maintained during storage, leading to fruit with increased shelf life. In addition, the activity of antioxidant enzymes, such as peroxidase (POD), catalase (CAT), ascorbate peroxidase (APX), and superoxide dismutase (SOD), was also enhanced by these salicylate treatments (Valverde et al., 2015; Giménez et al., 2017). These antioxidant enzymes are involved on scavenging reactive oxygen species (ROS) species, such as hydrogen peroxide (H_2O_2), superoxide radical ($O2^{\bullet-}$), hydroxyl radical ($OH^{\bullet}$), or $^1O^2$, which are inevitably generated in normal metabolism of plant cells but accumulated during fruit ripening and senescence, contributing to peroxidation of membrane lipids, damage to DNA and proteins, and acceleration of senescence processes. Thus, treatments aimed to increase the ability of fruit tissues to decrease ROS levels, by enhancing antioxidant enzyme activities and/or antioxidant compounds, such as phenolics or anthocyanins, have been reported to delay ripening and senescence process and, in turn, to maintain fruit quality in a wide range of fruit species including sweet cherry. In this sense, post-harvest treatments of sweet cherry with hexanal or 1-methylcyclopropene led to higher levels of SOD and APX activities during storage as compared with control cherries (Sharma et al., 2010). Similarly, higher antioxidant enzyme activities during storage were found in sweet cherry fruit coated with chitosan (Dang et al., 2010) or after vacuum cooling treatment (He et al., 2013), as well as in sweet cherry fruit from SA, ASA, or MeSa treated trees (Giménez et al., 2015; Valverde et al., 2015).

Recently, melatonin, which was identified in plants in 1995 (Dubbels et al., 1995), is gaining a broad interest as a universal plant signalling molecule having pivotal roles on regulating a wide range of plant physiological processes, with great potential for its application in the horticultural industry (Aghdam et al., 2020; Arnao and Hernández-Ruiz, 2020a; Tiwari et al., 2020). In particular, post-harvest melatonin treatments have been shown to delay fruit ripening in a wide range of fruit species (Xu et al., 2019; Arnao and Hernández-Ruiz, 2020b). For instance, dipping treatment with 0.5 mM melatonin delayed ripening in mangoes, due to inhibition of ABA and ethylene biosynthesis (Liu et al., 2020), as well as in banana fruit (Hu et al., 2017), which were dose-dependent in the range of 0.05–0.5 mM. Accordingly, a delay of ripening has been reported in peaches and nectarines after post-harvest melatonin treatment (Gao et al., 2016; Bal, 2021). However, the effects of melatonin applied as pre-harvest treatment on on-tree fruit ripening and quality traits have been evaluated in a very few papers and different effects have been found depending on concentration, application time and fruit species. Thus, tomato plant treatment with melatonin, applied in the irrigation system led to increases in lycopene and sugar contents, showing acceleration of the fruit ripening process (Liu et al., 2016). However, melatonin treatment by foliar spray of apricot trees did not affect the on-tree ripening process although positive effects were observed on crop yield and fruit quality parameters at harvest, which were maintained during storage, either at chilling or non-chilling temperatures, as compared with apricots from control trees (Abd El-Naby et al., 2019; Medina-Santamarina et al., 2021). Similar effects of melatonin pre-harvest treatments have been reported recently for 'Mollar de Elche' pomegranate (Lorente-Mento et al., 2021).

In sweet cherry fruit, post-harvest dipping melatonin treatments have been recently reported to maintain fruit quality during storage throughout a delay of the senescence process in 'Sunburst' (Wang et al., 2019), 'Siah Mashhad' (Sharafi et al., 2021), 'Santina,' and 'Royal Rainier' (Miranda et al., 2020) cultivars. On the other hand, melatonin treatment, applied directly to fruit surface during on-tree fruit development delayed fruit ripening in 'Prime Giant' cultivar (Tijero et al., 2019). On the contrary, foliar spray treatment with 0.5 mM melatonin 2 and 1 weeks prior to harvest accelerated fruit ripening of sweet cherry 'Ferrovia' (Michailidis et al., 2021). In our previous paper, pre-harvest foliar spray with 0.1, 0.3, and 0.5 mM melatonin led to fruit with enhanced quality traits at harvest, such as fruit weight, colour, firmness, total soluble solid content and titratable acidity (Carrión-Antolí et al., 2022). However, as far as we know, there is not available literature regarding the effect of pre-harvest melatonin treatment on the maintenance of sweet cherry fruit quality properties during storage. Thus, the aim of the present experiment was to evaluate the effects of melatonin foliar spray of sweet cherry trees of 'Prime Giant' and 'Sweet Heart' cultivars on fruit quality parameters, with especial interest on bioactive compounds and the activity of antioxidant enzymes.

MATERIALS AND METHODS

Plant Material and Experimental Design

The experiments were carried out in a commercial field located at Jumilla (Murcia, Spain, UTMX: 463.700 UTMY: 4.268.900) with 'Prime Giant' and 'Sweet Heart' sweet cherry (*P. avium* L.) cultivars, in 2019 and 2020 years, respectively. 'Prime Giant' was planted in January 2012 and 'Sweet Heart' in January 2015 and both were grafted onto SL-64 rootstock. Climatic conditions in the crop field were similar for 2019 and 2020 years: mean annual temperatures 15.24 and 15.30°C for 2019 and 2020, respectively, and accumulated rainfall of 357 and 352 mm for 2019 and 2020, respectively. Agronomic practices were similar for both

cultivars with fertilisation of 60:30:100 kg ha^{-1} N:P:K and base type open centre pruning. For each cultivar, three blocks of three trees were selected at random for 0 (control), 0.1, 0.3, and 0.5 mM melatonin treatments. Treatments were applied with a manual sprayer machine (3 L per tree) by using freshly prepared melatonin solutions (containing 1 mL L^{-1} Tween as surfactant) at three key points of fruit development (pit hardening, starting of colour changes and 3 days before harvest), according to previous reports (Giménez et al., 2017; Carrión-Antolí et al., 2022). Sweet cherries were harvested according to commercial practices, when reached their commercial ripening stage, based on the soluble solid content and skin colour of each cultivar. About 3 kg of fruit from each treatment and replicate were taken and transported to laboratory in 3 h. Then, lots of 20 fruits, homogenous in colour and size and without visual defects, were performed at random and stored at 2°C and 90% RH. After 0, 7, 14, 21, and 28 days of storage one lot of each replicate and treatment was taken to perform the following analytical determinations.

Quality Parameter

Fresh weight of each fruit lot was measured at harvest and at each sampling date during storage by using a digital balance KERN 440-35N (Balingen, Germany) and weight losses were expressed as percentage with respect to weight at day 0. Colour was measured with a Minolta colorimeter (CRC200, Minolta Camera Co., Osaka, Japan), at three equidistant points along the equatorial perimeter of each fruit and was expressed as a*/b* ratio by using the CIELab coordinates. Results are the mean ± SE. Fruit firmness was measured independently in each fruit by using a TX-XT2i Texture Analyzer (Stable Mycrosys-tems, Godalming, United Kingdom) equipped with a flat probe. A force to achieve a 5% fruit diameter deformation was applied and fruit firmness was expressed as the relation between the applied force and the travelled distance (N mm^{-1}). Results are the mean ± SE. Then, flesh of the 20 fruit of each replicate was cut in small pieces to obtain a homogeneous sample. A ≈50 g sample was used for total soluble solids (TSS) and titratable acidity (TA) measures, in duplicate, after being squeezed through two layers of cotton cloth. TSS in fruit juice were measured by using a digital refractometer (Atago PR-101, Atago Co. Ltd., Tokyo, Japan) and TA by titration of 1 mL of juice, diluted in 25 mL of distilled H_2O, with 0.1 N NaOH up to pH 8.1 by using an automatic titration system (785 DMP Titrino, Metrohm, Herisau, Switzerland). TSS and TA results are expressed as g 100 g^{-1} and are the mean ± SE. Other 50 g fruit sample was ground under liquid N_2, and stored at −20°C until total phenolic and anthocyanin concentrations and antioxidant enzyme activities were measured.

Total Phenolic and Anthocyanin Quantification

Phenolics were extracted by homogenising 5 g of frozen tissue with 10 mL of water:methanol (2:8) containing 2 mM NaF (to inactivate polyphenol oxidase activity and prevent phenolic degradation) in a Ultraturrax homogeniser (T18 basic, IKA, Berlin, Germany). Then, the extracts were centrifuged at 10,000 × *g* for 10 min at 4°C and total phenolics were quantified in duplicate in the supernatant by using the Folin-Ciocalteu reagent as previously described (Díaz-Mula et al., 2009). Results were expressed as mg gallic acid equivalent 100 g^{-1} and are the mean ± SE. Anthocyanins were extracted by homogenising 2 g of fruit sample with 10 mL of methanol/HCl/water (80:1:19, v/v/v) as addressed above. After centrifugation, anthocyanins were quantified in duplicate in the supernatant by reading absorbance at 530 in a spectrophotometer (UNICAM Helios-α, Artisan Technology Group, Champaign, IL, United States). Total anthocyanins were calculated by using cyanidin-3-glucoside molar absorption coefficient of 23,900 L cm^{-1} mol^{-1} and molecular weight of 449.2 g mol^{-1}. Results were expressed as mg cyanidin 3-glucoside equivalent 100 g^{-1} and were the mean ± SE.

Measure of Antioxidant Enzyme Activities

To obtain crude extract of POD, CAT and APX, 5 g of sweet cherry samples were homogenised with 10 mL of phosphate buffer 50 mM, pH 7.0, containing 1 mM ethylen-diamine-tetraacetic acid (EDTA) and 1% (w/v) polyvinylpyrrolidone. Then, the homogenate was centrifuged at 15,000 × *g* for 30 min at 4°C and antioxidant enzyme activities were measured in the supernatant as previously described (Giménez et al., 2017). Briefly, for POD determination, the reaction mixture contained 50 mM phosphate buffer pH 7.0, 14 mM guaiacol, 12 mM H_2O_2 and 100 μL of enzymatic extract in a total volume of 3 mL. The increase of absorbance at 470 nm from time 0 to 1 min, due to guaiacol oxidation, was measured and POD activity was expressed as U min^{-1} g^{-1}, one enzymatic unit (U) being defined as 0.01 absorbance increase per min. The reaction mixture for CAT activity contained 100 μL of the above extract and 2.9 mL 50 mM phosphate buffer pH 7.0, containing 15 mM H_2O_2 and the decrease of absorbance at 240 nm for 1 min due to H_2O_2 degradation was measured and CAT activity expressed as U min^{-1} g^{-1}, one enzymatic unit (U) being defined as 0.01 absorbance decrease per minute. Finally, the assay mixture for APX quantification contained 50 mM potassium phosphate pH 7.0, 0.5 mM ascorbic acid, 1 mM H_2O_2 and 100 μL of crude extract in a final volume of 3 mL. The decrease of absorbance at 290 nm during 1 min was measured and one enzymatic unit of APX (U) was defined as the amount of enzyme that oxidises 1 mmol of ascorbate per minute, and APX was expressed as U min^{-1} g^{-1}.

Statistical Analysis

The field experiments were performed by using three replicates of three trees per treatment for each cultivar in a completely randomised design. Fruit samples from each replicate were taken and used for storage experiment. Experimental data from each cultivar were independently subjected to ANOVA analysis. For each cultivar, sources of variation were treatment and storage time. All analyses were performed with SPSS software package v. 22.0 for Windows (SPSS, 2011). Least significant differences (LSD) at $p < 0.05$ were calculated and values shown in each figure.

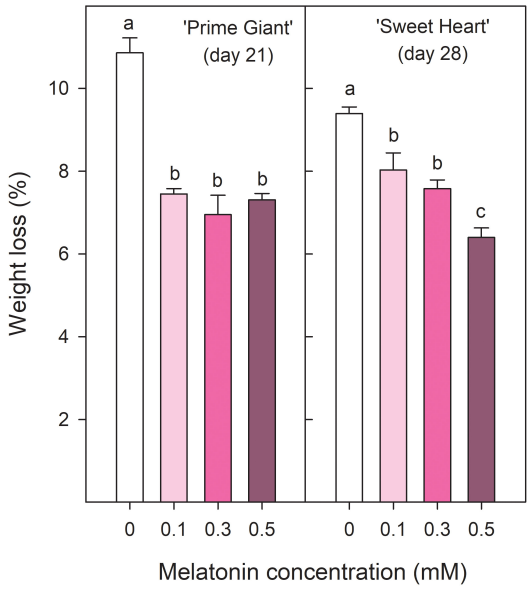

FIGURE 1 | Weight losses for 'Prime Giant' and 'Sweet Heart' cultivars after 21 and 28 days of storage at 2°C, respectively, as affected by melatonin pre-harvest treatments. Data are the mean ± SE of three replicates of 20 fruits. Different letters show significant differences ($p < 0.05$) among treatments for each cultivar.

RESULTS

Fruit Quality Parameters

'Prime Giant' and 'Sweet Heart' cultivars were stored for 21 and 28 days, respectively, until control fruit reached an over-ripening and senescence stage in which quality attributes were considered as not optimum for consumption. Weight loss increased during storage in both cherry cultivars, either in fruit from control trees as from treated trees, although they were delayed in the last ones. Thus, for 'Prime Giant' weight losses in control fruit reached values of 10.86 ± 0.36% after 21 days of storage while significantly ($p < 0.05$) lower values, ≈7% were reached in fruit from melatonin control trees independently of the applied dose. For 'Sweet Heart' cultivar, weight losses were also significantly lower ($p < 0.05$) and dose dependent in fruit from melatonin treated trees than in controls, the lowest weight losses being found for 0.5 mM dose, with values of 6.40 ± 0.23% after 28 days as compared to 9.39 ± 0.16% in controls (**Figure 1**). Colour index (a*/b*) at harvest was significantly increased ($p < 0.05$) as a consequence of melatonin treatments with respect to controls in both cultivars and a similar trend was observed during storage, with increases during the first 1–2 weeks and decreases thereafter, except for 'Prime Giant' from 0.5 mM melatonin treated fruit, in which no changes occurred from day 0 to day 14 of storage (**Figures 2A,C**). However, colour index showed higher values, 9.21, 7.77, and 11.63%, in fruit from 0.1, 0.3, and 0.5 mM treated trees, respectively, for 'Prime Giant' and 2.46, 7.86, and 8.48% for 'Sweet Heart' than in controls taking into account data from all sampling dates. Fruit firmness was also found at significantly higher levels ($p < 0.05$) in fruit from melatonin treated trees than in controls at harvest and these differences were maintained during the whole storage period, in spite of the firmness decreases observed in all fruit for both cultivars (**Figures 2B,D**). At harvest, the highest effect on fruit firmness was observed for 0.3 and 0.1 mM melatonin doses in 'Prime Giant' and 'Sweet Heart,' respectively. However, during storage, no significant differences were observed between melatonin doses, with 25–30 and 15–20% higher firmness levels in treated fruit than in controls for 'Prime Giant' and 'Sweet Heart' cultivars, respectively, taking into account data of all sampling dates.

Total soluble solids in control fruit at harvest were 20.43 ± 0.24 and 19.70 ± 0.21 g 100 g^{-1} for 'Prime Giant' and 'Sweet Heart,' respectively, and significant increases ($p < 0.05$) occurred during storage (**Figures 3A,C**). Melatonin pre-harvest treatments led to significant ($p < 0.05$) enhanced TSS concentrations at harvest, the highest effects being observed for 0.1 mM in 'Prime Giant' (24.45 ± 0.12 g 100 g^{-1}), while no significant differences among doses were observed for 'Sweet Heart' cultivar (≈21 g 100 g^{-1}). Nevertheless, it is worth noting that TSS was higher in fruit from melatonin treated trees than in controls during the whole storage period. TA at harvest was 1.05 ± 0.01 and 1.31 ± 0.02 g 100 g^{-1} in control fruit of 'Prime Giant' and 'Sweet Heart' cultivars, respectively, and significant decreases ($p < 0.05$) occurred during storage. However, in fruit from melatonin treated trees, TA losses were delayed with respect to controls in both cultivars, and significantly ($p < 0.05$) higher values, ca. 15 and 10%, were observed as a consequence of melatonin treatments, either at harvest or during storage, in 'Prime Giant' and 'Sweet Heart', respectively (**Figures 3B,D**).

Antioxidant Compounds and Antioxidant Enzymes

Total phenolic concentrations at harvest was significantly increased by melatonin treatments in a dose-dependent way, from 74.84 ± 4.23 mg 100 g^{-1} in fruit from control trees to 100.48 ± 3.67 mg 100 g^{-1} in those from 0.5 mM treated ones, in 'Prime Giant' and from 60.08 ± 2.14 to 72.36 ± 0.96 mg 100 g^{-1} in 'Sweet Heart.' During storage, total phenolics were maintained at higher levels in fruit from melatonin treated trees than in controls, although no significant differences among melatonin doses were observed (**Figures 4A,B**). With respect to anthocyanin concentration, significant enhanced ($p < 0.05$) values were also found, in general, as a consequence of melatonin treatments, either at harvest or during storage, for both cultivars (**Figures 4C,D**). Taking into account data of all sampling date, total phenolic and anthocyanin concentration was ca. 25% lower in 'Sweet Heart' than in 'Prime Giant,' while the increase in concentrations of these bioactive compounds by melatonin treatments was higher in 'Sweet Heart' than in 'Prime Giant.'

In general, the activity of antioxidant enzymes CAT, APX, and POD was significantly higher ($p < 0.05$) in fruit from 0.3 mM melatonin treated trees than in controls, either at harvest or during storage, except POD activity in 'Prime Giant' cultivar (**Figure 5**). The highest effects were found for CAT activity, which was 30 and 20% higher in treated fruits for 'Prime Giant' and 'Sweet Heart,' respectively, during the whole storage period, while ≈15% increases were observed for APX activity in both cultivars.

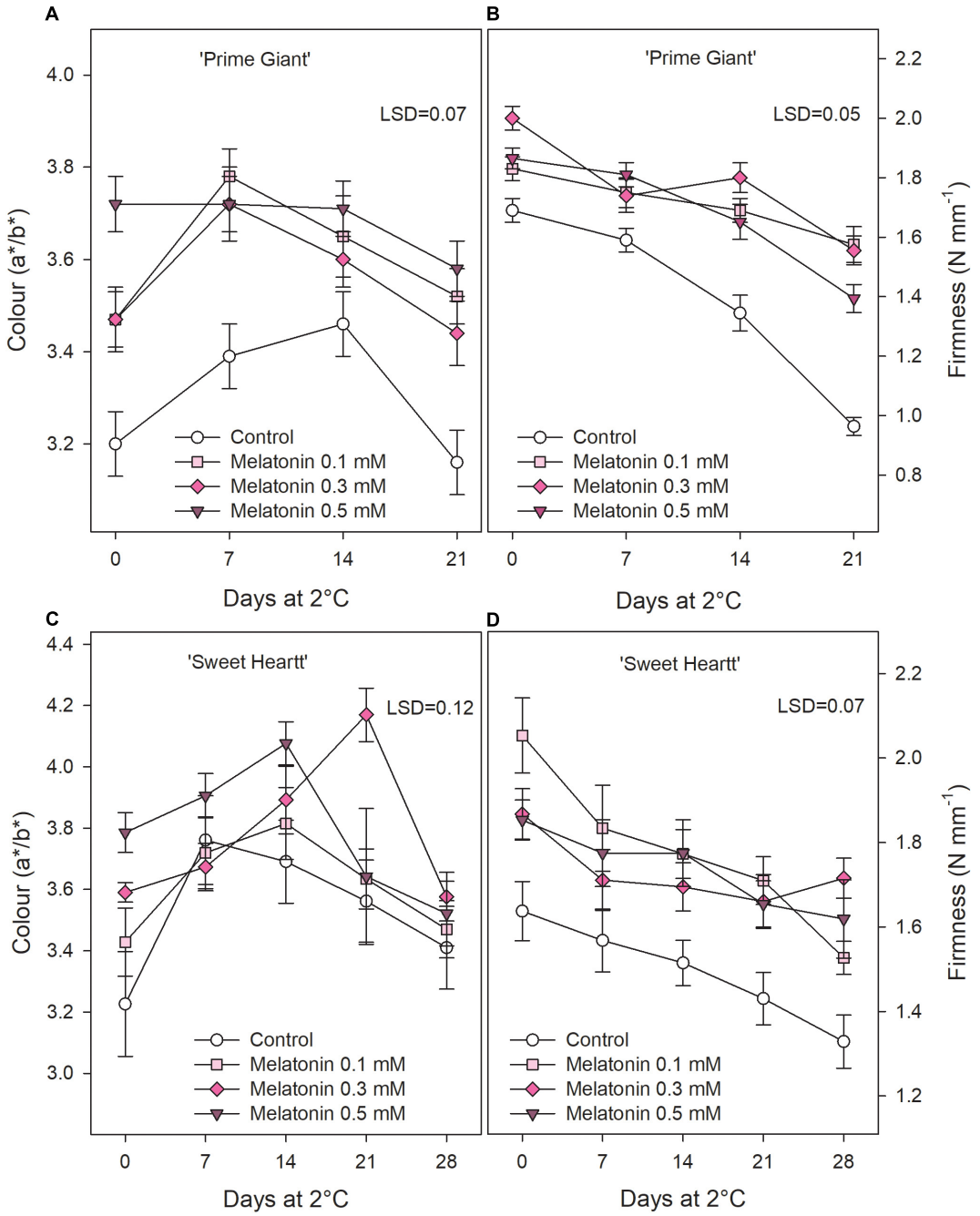

FIGURE 2 | Fruit colour **(A)** and firmness **(B)** for 'Prime Giant' and 'Sweet Heart' **(C,D)** cultivars during storage at 2°C as affected by melatonin pre-harvest treatments. Data are the mean ± SE of three replicates of 20 fruits. LSD values at ($p < 0.05$) are shown in each figure.

DISCUSSION

Sweet cherry fruit quality traits, such as absence of visual defects, fruit size, colour, stem freshness, and length, firmness, aroma, flavour, sweetness, and sourness are the major responsible for consumer purchase decisions, although important differences have been reported among cultivars (Díaz-Mula et al., 2009; Serradilla et al., 2012; Correia et al., 2017). However, these quality parameters evolved quickly during fruit storage, even if storage is performed at appropriate temperature, leading to fruit with no optimal quality for consumption (Serrano et al., 2009; Chockchaisawasdee et al., 2016; Giménez et al., 2017; Zhang et al., 2021). These changes are mainly related to softening, losses of fruit weight and TA, and increases in TSS and colour as well as to fruit decay and browning and desiccation of the pedicel. Accordingly, the present results show increases in weight loss,

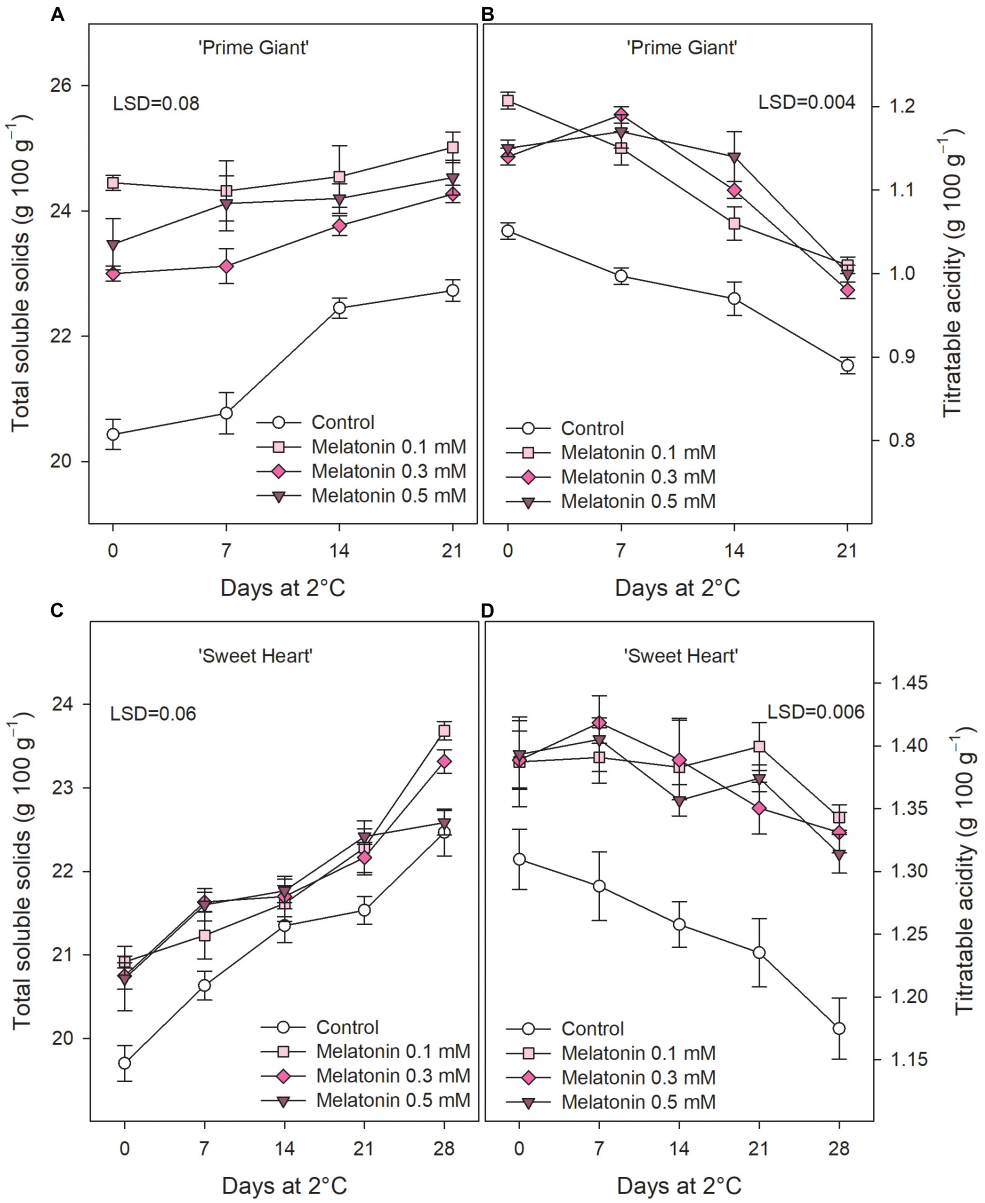

FIGURE 3 | Total soluble solids **(A)** and titratable acidity **(B)** for 'Prime Giant' and 'Sweet Heart' **(C,D)** cultivars during storage at 2°C as affected by melatonin pre-harvest treatments. Data are the mean ± SE of three replicates. LSD values at ($p < 0.05$) are shown in each figure.

TSS and colour and decreases in fruit firmness and TA, although these changes were significantly delayed in fruit from melatonin treated trees with respect to controls (**Figures 1–3**). Firmness and TA maintenance as a consequence of pre-harvest melatonin treatments are major factor contributing to preserve fruit during storage, since cherries with higher firmness are much appreciated by consumers and TA retention during storage led to cherries with the aroma and taste of recently harvested cherries (Valero et al., 2011; Díaz-Mula et al., 2012; Serradilla et al., 2012).

Thus, taking into account all these quality parameters, storage time with optimal fruit quality properties for consumption in control cherries for both cultivars was 14 days, while it could be extended up to 21 and 28 days in fruit from melatonin treated trees for 'Pime Giant' and 'Sweet Heart' cultivars, respectively. Accordingly, post-harvest ripening was delayed in 'Guifei' mangoes by 0.5 mM melatonin dipping treatment for 1 h (Liu et al., 2020) and in banana in a concentration dependent manner in the range of 0.05–0.5 mM (Hu et al., 2017), leading to extension of fruit shelf life. Similar results have been reported in peaches (Gao et al., 2016), and nectarines (Bal, 2021), and these effects were attributed to inhibition of ethylene production in those climacteric fruit species. Maintenance of fruit quality traits and extension of shelf-life seem to be general fruit responses to melatonin post-harvest dipping treatments since they have been

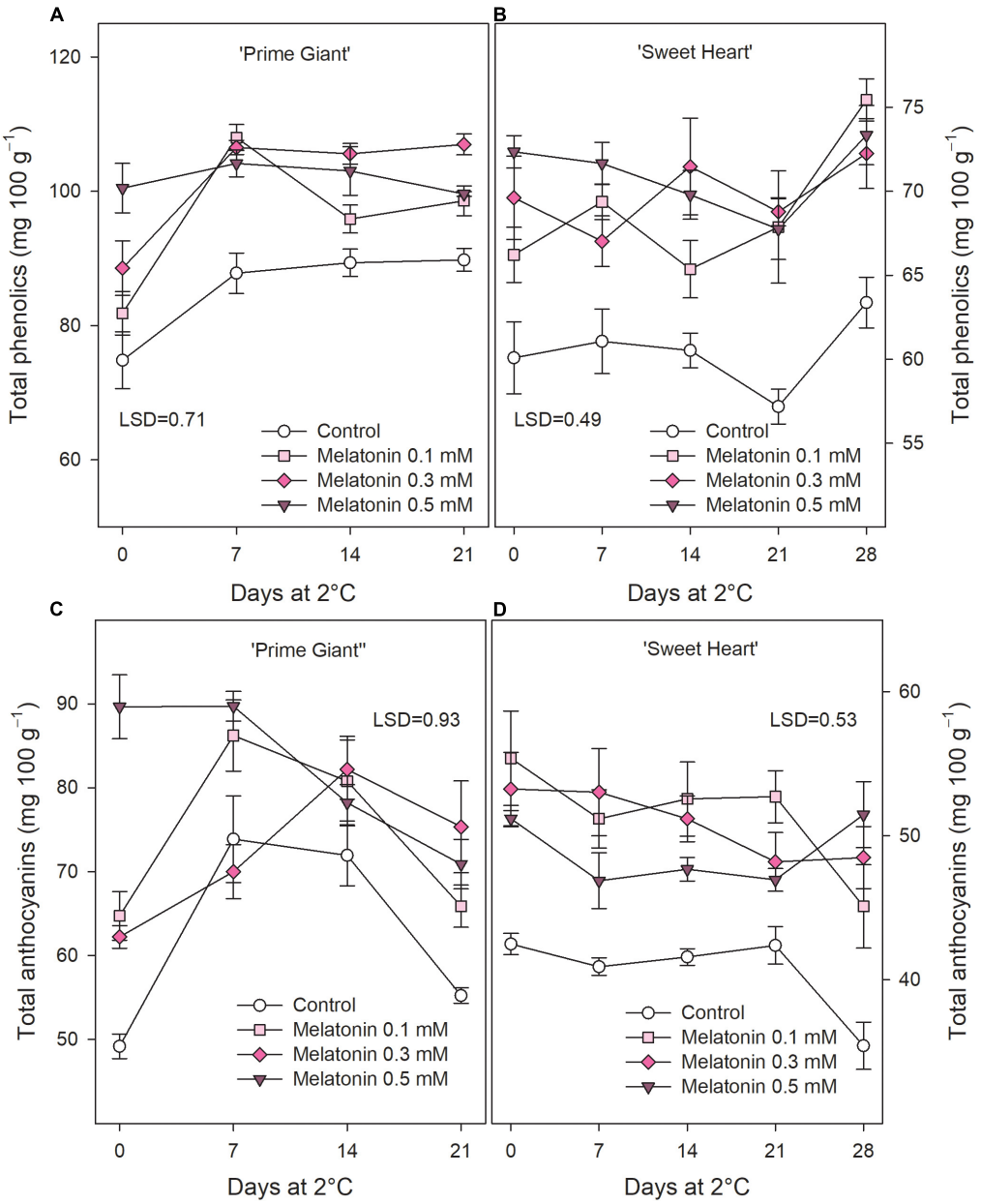

FIGURE 4 | Total phenolics **(A,B)** and total anthocyanins **(C,D)** for 'Prime Giant' and 'Sweet Heart' cultivars during storage at 2°C as affected by melatonin pre-harvest treatments. Data are the mean ± SE of three replicates. LSD values at ($p < 0.05$) are shown in each figure.

also reported in non-climacteric fruit, such as pomegranate and strawberry as recently revised by Ze et al. (2021). Specifically, in 'Sunburst' sweet cherries, post-harvest 0.05, 0.1, and 0.15 Mm melatonin treatments led to delay the post-harvest ripening process (Wang et al., 2019) and in 'Siah Mashhad' cultivar dipping with 0.001, 0.01, 0.1, and 1 mM melatonin reduced flesh browing and decay after 45 days of storage, the highest effect being found with 0.1 mM dose (Sharafi et al., 2021). However, post-harvest fruit treatments have consumers' concerns and legal restrictions and then, there is a need of research regarding pre-harvest treatments with effect on fruit quality properties at harvest and during storage. In this sense, pre-harvest treatments of apricot tree with melatonin increased fruit quality parameters at harvest and these quality traits were maintained during storage (Medina-Santamarina et al., 2021). Higher values of quality parameters, either at harvest or during storage, were observed on pomegranate fruit as a consequence of melatonin tree treatments during on-tree fruit development (Lorente-Mento et al., 2021). In sweet cherry, 0.05, 0.1, and 0.2 mM melatonin applied on tree canopy (3, 2, and 1 weeks before harvest) resulted in fruit with higher TSS and lower TA in the 'Hongdeng' cultivar (Xia et al., 2020), but no storage experiment was performed in this research.

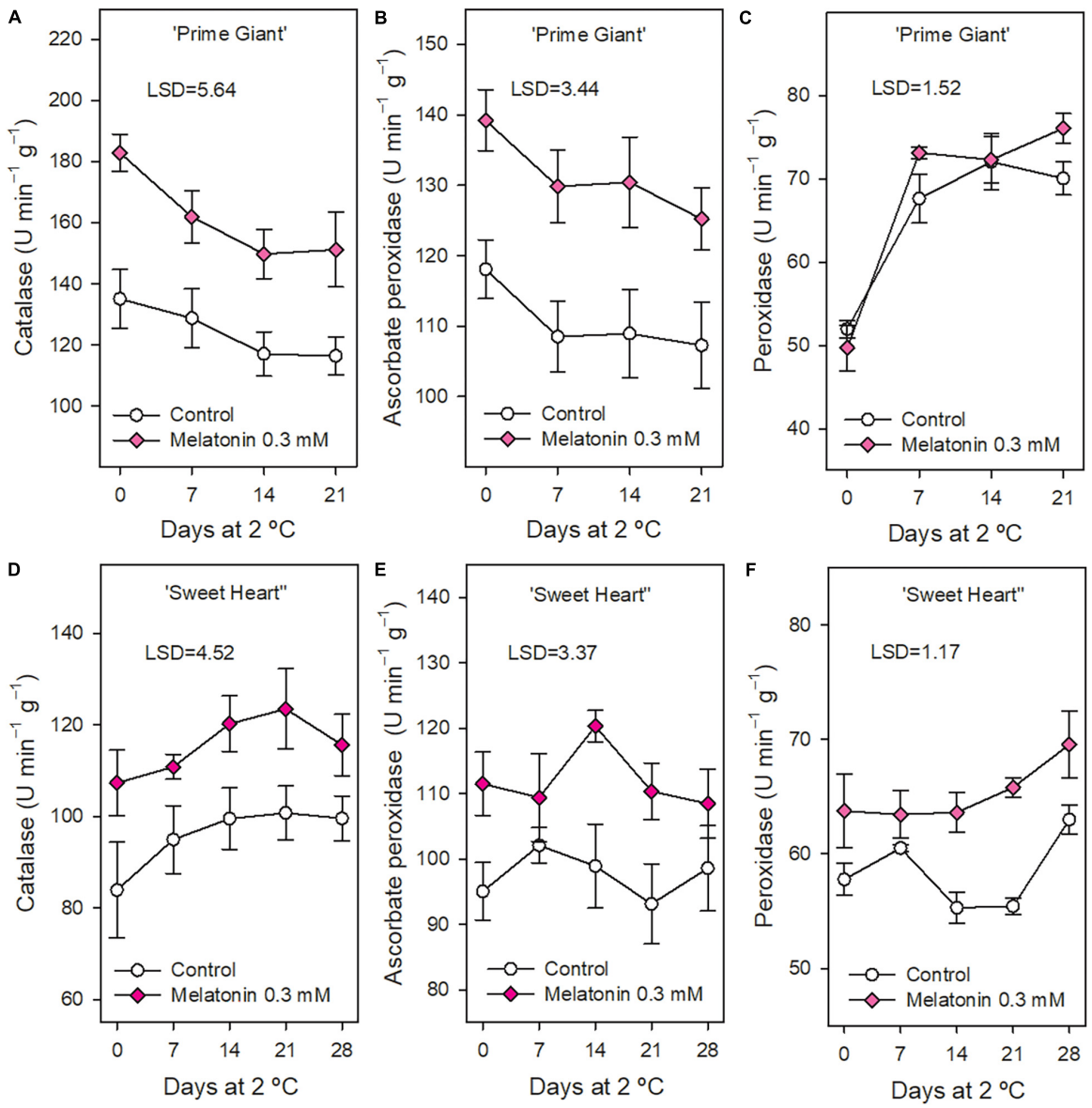

FIGURE 5 | Catalase, ascorbate peroxidase, and peroxidase activities in 'Prime Giant' (**A–C**, respectively) and 'Sweet Heart' (**D–F**, respectively) cultivars during storage at 2°C as affected by melatonin pre-harvest treatments. Data are the mean ± SE of three replicates. LSD values at ($p < 0.05$) are shown in each figure.

On the contrary, similar treatments with 0.5 mM melatonin did not show significant effect on 'Ferrovia' fruit quality parameters at harvest and softening was the only parameters related to fruit quality and senescence delayed after 14 days of cold storage (Michailidis et al., 2021). Thus, the effects of pre-harvest melatonin treatment on delaying fruit ripening and senescence will be different depending on cultivar, applied concentration or fruit developmental stage, among other factors.

In the last decade, special attention has been paid to the content on bioactive compounds with antioxidant activity, such as anthocyanins and other phenolic compounds, in sweet cherry due to their positive impact on human health, by reducing the risk of suffering from several degenerative diseases (Correia et al., 2017; Gonçalves et al., 2018, 2019; Antognoni et al., 2020; Faienza et al., 2020; Luo et al., 2021). In this fruit species, the red colour intensity is due to their content of anthocyanins and their profile, the major anthocyanin being cyanidin 3-*O*-rutinoside comprising around 90% of total anthocyanins, and 70% of total phenolic compounds, in most of the studied cultivars, including 'Prime Giant' and 'Sweet Heart' (Usenik et al., 2008; Serrano et al., 2009; Martínez-Esplá et al., 2014; Antognoni et al., 2020; Gonçalves et al., 2021; Carrión-Antolí et al., 2022). Total phenolic concentration showed an upward trend from day 0 until the end of storage in fruit from control and treated trees for both cultivars (**Figures 4A,B**), while total anthocyanins, generally, increased during the first

weeks of storage and decreased thereafter (**Figures 4C,D**). These results are in agreement with previous reports in other cherry cultivars, which have been related to the ongoing ripening process after harvesting (Serrano et al., 2009; Valero et al., 2011; Giménez et al., 2014; Sharafi et al., 2021). However, it is wort noting that phenolic and anthocyanin contents at harvest were enhanced as a result of melatonin treatments and maintained at higher levels in treated fruit than in controls during storage (**Figures 4A–D**). Accordingly, post-harvest melatonin dipping treatments have been reported to increase phenolic and anthocyanin concentrations during storage in some fruit species, such as strawberry (Liu et al., 2018), tomato (Sharafi et al., 2019), and pomegranate (Aghdam et al., 2020) and even in sweet cherry, as has been recently reported by Sharafi et al. (2021). These effects were attributed to melatonin stimulation of the phenylpropanoid pathway mainly by enhancing phenylalanine ammonialyase and chalcone synthase activities. However, literature regarding the impact of pre-harvest melatonin treatments on phenolic and anthocyanin evolution during storage is scarce.

In sweet cherry, the effects of pre-harvest melatonin treatments on anthocyanins and phenolic content have been reported only in three previous papers and contradictory results are observed. Thus, higher total phenolic and anthocyanin contents at harvest in 'Hongdeng' cultivar were found after tree treatment with 0.05 and 0.1 mM melatonin 3, 2, and 1 week before harvest (Xia et al., 2020). On the contrary, fruit treatment of 'Prime Giant' cultivar at stage II with 0.1 mM did not show impact on anthocyanin content at harvest while 0.01 mM dose led to twofold lower anthocyanin concentration as compared with control (Tijero et al., 2019). In 'Ferrovia' cultivar, 0.5 mM melatonin treatments, 2 and 1 week before harvest, had no effects on individual phenolic or anthocyanin compounds at harvest (Michailidis et al., 2021). However, as far as we know, only Michailidis et al. (2021) have reported the effects of cherry tree pre-harvest melatonin treatment on these bioactive compound evolution during storage and showed higher levels of neochlorogenic acid and cyaniding 3-*O*-rutinoside (the major phenolic and anthocyanin, respectively) after 12 days of cold storage in fruit from treated trees than in controls.

Fruit ripening and senescence are associated with ROS accumulation, such as H_2O_2, $O_2^{-\bullet}$ and $OH^{-\bullet}$, which are involved in DNA and proteins damage, peroxidation of membrane lipids and acceleration of senescence processes (Hodges et al., 2004). These ROS are generated in normal metabolism of plant cells and scavenged by antioxidant compounds (such as phenolics, tocopherols, carotenoids, and ascorbic acid) and by antioxidant enzymes, mainly superoxide dismutase (SOD), POD, CAT, and APX contributing to repair cell oxidative damage (Hodges et al., 2004; Kumar et al., 2014). Antioxidant enzymes were measured in fruit from control and 0.3 mM treated trees, since, in general, similar effects on maintaining cherry quality properties were observed for 0.3 and 0.5 mM concentrations, as well as on increasing crop yield (Carrión-Antolí et al., 2022). The results of the present study show higher activities of these antioxidant enzymes in melatonin treated trees than in controls during the whole storage period in both cultivars (**Figures 5A–F**). Thus, the occurrence of increased activity of antioxidant enzymes and enhanced content of the antioxidant compounds, phenolics and anthocyanins, could be responsible for the delay in the fruit post-harvest ripening process and maintenance of fruit quality attributes observed in sweet cherries from melatonin treated trees. Accordingly, different post-harvest treatments aimed to delay the sweet cherry post-harvest ripening and senescence processes also increased these antioxidant enzymes during storage. Thus, chitosan coating enhanced CAT and POD activities (Dang et al., 2010), as well as vacuum cooling treatment before storage (He et al., 2013) and 1-methylcyclopropene and hexanal increased SOD activity and reduced decreases in APX activity during storage compared to control cherries (Sharma et al., 2010). Nano-silica-chitosan solution and pressurised Argon treatment, and specially the combination of both treatments, led also to increased activities of CAT, APX, SOD, POD, and glutathione reductase (GR) and reduced accumulation of H_2O_2 and $O_2^{\bullet-}$ during sweet cherry storage as compared with controls, resulting in fruit with delayed senescence and extended shelf life (Meng et al., 2022). Pre-harvest sweet cherry treatments with SA, ASA, and SaMe led also to higher activities of CAT, POD, APX, and SOD and increased concentrations of phenolics and anthocyanins in treated fruit at harvest and during storage as compared with controls (Valverde et al., 2015; Giménez et al., 2017). Thus, treatments leading to increase sweet cherry ROS elimination systems, as observed in the present experiments for cherries from melatonin-treated trees, could contribute to delaying the post-harvest ripening and senescence processes and extending their shelf life. Accordingly, post-harvest melatonin treatment significantly induced enzymatic antioxidants and non-enzymatic antioxidants during storage in mango, kiwifruit, pomegranate, and peach fruit as reviewed by Xu et al. (2019) and Ze et al. (2021). The expression of genes encoding for antioxidant enzymes was upregulated by melatonin treatment, although the molecular mechanism underlying these effects needs further research. In sweet cherry, increased activity of antioxidant enzymes during storage due to post-harvest melatonin treatment has also been recently reported (Sharafi et al., 2021), although these effects due to melatonin applied as foliar spray treatment to sweet cherry trees have been reported for the first time in the present experiments.

CONCLUSION

Overall results showed that melatonin treatments during sweet cherry fruit on-tree development reduced weight and TA losses, softening and changes in fruit colour and TSS during cold storage. In addition, total phenolic and anthocyanin concentrations were higher in fruit from treated trees than in those from control ones, either at harvest or during the whole storage period. Finally, the activity of the antioxidant enzymes CAT, APX, and POD was also enhanced as a consequence of melatonin treatment. Thus, the storage period of fruit with quality properties in optimum levels for consumption was extended by one and 2 weeks for 'Prime Giant' and 'Sweet

Heart' cultivars, respectively, with respect to fruit from control trees. The increase of antioxidant systems, both enzymatic and non-enzymatic ones, as a consequence of melatonin treatments would lead to a more efficient ROS elimination accounting for delaying the post-harvest ripening process and maintaining fruit quality during storage.

DATA AVAILABILITY STATEMENT

The original contributions presented in the study are included in the article/supplementary material, further inquiries can be directed to the corresponding author.

AUTHOR CONTRIBUTIONS

DV and MS conceived and designed the work in association with other authors. AC-A performed field treatments and most of the analytical determination, in collaboration with DM-R, PJZ, FG, MS, and DV. MS and DV analysed the data and wrote the manuscript. DV and MS were responsible for funding acquisition. All authors contributed to review the article and approved the submitted version.

FUNDING

This work was funded by Spanish Ministry of Science, Innovation and Universities and European Commission with FEDER funds through Project RTI2018-099664-B-100 Ph.D scholarship FPU18/04112 funded by Ministry of Science, Innovation and Universities.

ACKNOWLEDGMENTS

We thank Spanish Ministry of Science, Innovation and Universities for Ph.D.-scholarship of AC-A and Finca Toli Frutas S.L. for providing field experiments.

REFERENCES

Abd El-Naby, S. K. M. A., Mohamed, A. A. A., and El-Naggar, Y. I. M. (2019). Effect of melatonin, GA3 and NAA on vegetative growth, yield and quality of 'Canino' apricot fruits. *Acta Sci. Pol. Hortorum Cultus* 18, 167–174. doi: 10.24326/asphc.2019.3.16

Aghdam, M. S., Luo, Z., Li, L., Jannatizadeh, A., Fard, J. R., and Pirzad, F. (2020). Melatonin treatment maintains nutraceutical properties of pomegranate fruits during cold storage. *Food Chem.* 303:125385. doi: 10.1016/j.foodchem.2019.125385

Antognoni, F., Potente, G., Mandrioli, R., Angeloni, C., Freschi, M., Malaguti, M., et al. (2020). Fruit quality characterization of new sweet cherry cultivars as a good source of bioactive phenolic compounds with antioxidant and neuroprotective potential. *Antioxidants* 2020:677. doi: 10.3390/antiox9080677

Arnao, M. B., and Hernández-Ruiz, J. (2020a). Is phytomelatonin a new plant hormone? *Agronomy* 10:95. doi: 10.3390/agronomy10010095

Arnao, M. B., and Hernández-Ruiz, J. (2020b). Melatonin in flowering, fruit set and fruit ripening. *Plant Reprod.* 33, 77–87. doi: 10.1007/s00497-020-00388-8

Bal, E. (2021). Effect of melatonin treatments on biochemical quality, and postharvest life of nectarines. *J. Food Meas. Charact.* 15, 288–295. doi: 10.1007/s11694-020-00636-5

Blando, F., and Oomah, B. D. (2019). Sweet and sour cherries: origin, distribution, nutritional composition and health benefits. *Trends Food Sci. Technol.* 86, 517–529. doi: 10.1016/j.tifs.2019.02.052

Carrión-Antolí, A., Lorente-Mento, J. M., Valverde, J. M., Castillo, S., Valero, D., and Serrano, M. (2022). Effects of melatonin treatment on sweet cherry tree yield and fruit quality. *Agronomy* 12:3. doi: 10.3390/agronomy12010003

Chockchaisawasdee, S., Golding, J. B., Vuong, Q. V., Papoutsis, K., and Stathopoulos, C. E. (2016). Sweet cherry: composition, postharvest preservation, processing and trends for its future use. *Trends Food Sci. Technol.* 55, 72–83. doi: 10.1016/j.tifs.2016.07.002

Correia, S., Schouten, R., Silva, A. P., and Gonçalves, B. (2017). Factors affecting quality and health promoting compounds during growth and postharvest life of sweet cherry (*Prunus avium* L.). *Front. Plant Sci.* 8:2166. doi: 10.3389/fpls.2017.02166

Cozzolino, R., Martignetti, A., Cefola, M., Pace, B., Capotorto, I., De Giulio, B., et al. (2019). Volatile metabolites, quality and sensory parameters of "Ferrovia" sweet cherry cold stored in air or packed in high CO2 modified atmospheres. *Food Chem.* 286, 659–668. doi: 10.1016/j.foodchem.2019.02.022

Dang, Q. F., Yan, J. Q., Li, Y., Cheng, X. J., Liu, C. S., and Chen, X. G. (2010). Chitosan acetate as an active coating material and its effects on the storing of *Prunus avium* L. *J. Food Sci.* 75, S125–S131.

Díaz-Mula, H. M., Castillo, S., Martínez-Romero, D., Valero, D., Zapata, P. J., Guillén, F., et al. (2009). Sensory, nutritive and functional properties of sweet cherry as affected by cultivar and ripening stage. *Food Sci. Technol. Int.* 15, 535–543. doi: 10.1177/1082013209351868

Díaz-Mula, H. M., Serrano, M., and Valero, D. (2012). Alginate coatings preserve fruit quality and bioactive compounds during storage of sweet cherry fruit. *Food Bioprocess Tech.* 5, 2990–2997.

Dubbels, R., Reiter, R. J., Klenke, E., Goebel, A., Schnakenberg, E., Ehleers, C., et al. (1995). Melatonin in edible plants identified by radioimmunoassay and by high performance liquid chromatography-mass spectrometry. *J. Pineal Res.* 18, 28–31. doi: 10.1111/j.1600-079X.1995.tb00136.x

Einhorn, T. C., Wang, Y., and Turner, J. (2013). Sweet cherry fruit firmness and postharvest quality of late-maturing cultivars are improved with low-rate, single applications of gibberellic acid. *HortScience* 48, 1010–1017. doi: 10.21273/HORTSCI.48.8.1010

Faienza, M. F., Corbo, F., Carocci, A., Catalano, A., Clodoveo, M. L., Grano, M., et al. (2020). Novel insights in health-promoting properties of sweet cherries. *J. Funct. Foods* 69:103945. doi: 10.1016/j.jff.2020.103945

Gao, H., Zhang, Z. K., Chai, H. K., Cheng, N., Yang, Y., and Wang, D. N. (2016). Melatonin treatment delays postharvest senescence and regulates reactive oxygen species metabolism in peach fruit. *Postharvest Biol. Technol.* 118, 103–110. doi: 10.1016/j.postharvbio.2016.03.006

Giménez, M. J., Serrano, M., Valverde, J. M., Martínez-Romero, D., Castillo, S., Valero, D., et al. (2017). Preharvest salicylic acid and acetylsalicylic acid treatments preserve quality and enhance antioxidant systems during postharvest storage of sweet cherry cultivars. *J. Sci. Food Agric.* 97, 1220–1228. doi: 10.1002/jsfa.7853

Giménez, M. J., Valverde, J. M., Valero, D., Guillén, F., Martínez-Romero, D., Serrano, M., et al. (2014). Quality and antioxidant properties on sweet cherries as affected by preharvest salicylic and acetylsalicylic acids treatments. *Food Chem.* 160, 226–232. doi: 10.1016/j.foodchem.2014.03.107

Giménez, M. J., Valverde, J. M., Valero, D., Díaz-Mula, H. M., Zapata, P. J., Serrano, M., et al. (2015). Methyl salicylate treatments of sweet cherry trees improve fruit quality at harvest and during storage. *Sci. Hortic.* 197, 665–673. doi: 10.1016/j.scienta.2015.10.033

Gonçalves, A. C., Bento, C., Jesus, F., Alves, G., and Silva, L. R. (2018). Sweet cherry phenolic compounds: identification, characterization, and health benefits. *Stud. Nat. Prod. Chem.* 59, 31–78. doi: 10.1016/B978-0-444-64179-3.00002-5

Gonçalves, A. C., Bento, C., Silva, B., Simões, M., and Silva, L. R. (2019). Nutrients, bioactive compounds and bioactivity: the health benefits of sweet cherries (*Prunus avium* L.). *Curr. Nutr. Food Sci.* 15, 208–227.

Gonçalves, A. C., Campos, G., Alves, G., García-Viguera, C., Moreno, D. A., and Silva, L. R. (2021). Physical and phytochemical composition of 23 Portuguese sweet cherries as conditioned by variety (or genotype). *Food Chem.* 335:127637. doi: 10.1016/j.foodchem.2020.127637

He, S. Y., Zhang, G. C., Yu, Y. Q., Li, R. G., and Yang, Q. R. (2013). Effects of vacuum cooling on the enzymatic antioxidant system of cherry and inhibition of surface-borne pathogens. *Int. J. Refrig.* 36, 2387–2394. doi: 10.1016/j.ijrefrig.2013.05.018

Hodges, D. M., Lester, G. E., Munro, K. D., and Toivonen, P. M. A. (2004). Oxidative stress: importance for postharvest quality. *HortScience* 39, 924–929. doi: 10.21273/HORTSCI.39.5.924

Hu, W., Yang, H., Tie, W. W., Yan, Y., Ding, Z., Liu, Y., et al. (2017). Natural variation in banana varieties highlights the role of melatonin in postharvest ripening and quality. *J Agric. Food Chem.* 65, 9987–9904. doi: 10.1021/acs.jafc.7b03354

Kumar, S., Yadav, P., Jain, V., and Malhotra, S. P. (2014). Isozymes of antioxidative enzymes during ripening and storage of ber (*Ziziphus mauritiana* Lamk.). *J. Food Sci. Technol.* 51, 329–334. doi: 10.1007/s13197-011-0489-7

Liu, C. H., Zheng, H. H., Sheng, K. L., Liu, W., and Zheng, L. (2018). Effects of melatonin treatment on the postharvest quality of strawberry fruit. *Postharvest Biol. Technol.* 139, 47–55. doi: 10.1016/j.postharvbio.2018.01.016

Liu, J., Zhang, R., Sun, Y., Liu, Z., Jin, W., and Sun, Y. (2016). The beneficial effects of exogenous melatonin on tomato fruit properties. *Sci. Hortic.* 207, 14–20. doi: 10.1016/j.scienta.2016.05.003

Liu, S., Huang, H., Huber, D. J., Pan, Y., Shi, X., and Zhang, Z. (2020). Delay of ripening and softening in 'Guifei' mango fruit by postharvest application of melatonin. *Postharvest Biol. Technol.* 163:111136. doi: 10.1016/j.postharvbio.2020.111136

Lorente-Mento, J. M., Guillén, F., Castillo, S., Martínez-Romero, D., Valverde, J. M., Valero, D., et al. (2021). Melatonin treatment to pomegranate trees enhances fruit bioactive compounds and quality traits at harvest and during postharvest storage. *Antioxidants* 10:820. doi: 10.3390/antiox10060820

Luo, J., Si, H., Jia, Z., and Liu, D. (2021). Dietary anti-aging polyphenols and potential mechanisms. *Antioxidants* 10:283. doi: 10.3390/antiox10020283

Martínez-Esplá, A., Zapata, P. J., Valero, D., García-Viguera, C., Castillo, S., and Serrano, M. (2014). Preharvest application of oxalic acid increased fruit size, bioactive compounds, and antioxidant capacity in sweet cherry cultivars (*Prunus avium* L.). *J. Agric. Food Chem.* 62, 3432–3437. doi: 10.1021/jf500224g

McCune, L. M., Kubota, C., Stendell-Hollins, N. R., and Thomson, C. A. (2011). Cherries and health: a review. *Crit. Rev. Food Sci. Nutr.* 51, 1–12.

Medina-Santamarina, J., Zapata, P. J., Valverde, J. M., Valero, D., Serrano, M., and Guillén, F. (2021). Melatonin treatment of apricot trees leads to maintenance of fruit quality attributes during storage at chilling and non-chilling temperatures. *Agronomy* 11:917. doi: 10.3390/agronomy11050917

Meng, X., Chen, C., Song, T., Xu, J., Zhang, X., Wang, J., et al. (2022). Effect of nano-silica coating combined with pressurized Ar treatment on postharvest quality and reactive oxygen species metabolism in sweet cherry fruit. *Food Chem.* 374:131715. doi: 10.1016/j.foodchem.2021.131715

Michailidis, M., Tanou, G., Sarrou, E., Karagiannis, E., Ganopoulos, I., Martens, S., et al. (2021). Pre- and Post-harvest melatonin application boosted phenolic compounds accumulation and altered respiratory characters in sweet cherry fruit. *Front. Nutr.* 8:695061. doi: 10.3389/fnut.2021.695061

Miranda, S., Vilches, P., Suazo, M., Pavez, L., García, K., Méndez, M., et al. (2020). Melatonin triggers metabolic and gene expression changes making possible improved quality traits of two sweet cherry cultivars during cold storage. *Food Chem.* 319:126360. doi: 10.1016/j.foodchem.2020.126360

Paladines, D., Valero, D., Valverde, J. M., Díaz-Mula, H., Serrano, M., and Martínez-Romero, D. (2014). The addition of rosehip oil improves the beneficial effect of Aloe vera gel on delaying ripening and maintaining postharvest quality of several stone fruit. *Postharvest Biol. Technol.* 92, 23–28. doi: 10.1016/j.postharvbio.2014.01.014

Serradilla, M. J., Falagán, N., Bohmer, B., Terry, L. A., and Alamar, M. C. (2019). The role of ethylene and 1-MCP in early-season sweet cherry 'Burlat' storage life. *Sci. Hortic.* 258:108787. doi: 10.1016/j.scienta.2019.108787

Serradilla, M. J., Martín, A., Ruiz-Moyano, S., Hernández, A., López-Corrales, M., and Córdoba, M. D. G. (2012). Physicochemical and sensorial characterisation of four sweet cherry cultivars grown in Jerte Valley (Spain). *Food Chem.* 133, 1551–1559. doi: 10.1016/j.foodchem.2012.02.048

Serrano, M., Díaz-Mula, H., Zapata, P. J., Castillo, S., Guilleìn, F., Martínez-Romero, D., et al. (2009). Maturity stage at harvest determines the fruit quality and antioxidant potential after storage of sweet cherry cultivars. *J. Agric. Food Chem.* 57, 3240–3246. doi: 10.1021/jf803949k

Sharafi, Y., Aghdam, M. S., Luo, Z., Jannatizadeh, A., Razavi, F., Fard, J. R., et al. (2019). Melatonin treatment promotes endoge-nous melatonin accumulation and triggers GABA shunt pathway activity in tomato fruits during cold storage. *Sci. Hortic.* 254, 222–227. doi: 10.1016/j.scienta.2019.04.056

Sharafi, Y., Jannatizadeh, A., Fard, J. R., and Aghdam, M. S. (2021). Melatonin treatment delays senescence and improves antioxidant potential of sweet cherry fruits during cold storage. *Sci. Hortic.* 288:110304. doi: 10.1016/j.scienta.2021.110304

Sharma, M., Jacob, J. K., Subramanian, J., and Paliyath, G. (2010). Hexanal and 1-MCP treatments for enhancing the shelf life and quality of sweet cherry (*Prunus avium* L.). *Sci. Hortic.* 125, 239–247.

SPSS (2011). *SPSS Software Version 22.0 for Windows*. Chicago, IL: SPSS Inc.

Tijero, V., Muñoz, P., and Munné-Bosch, S. (2019). Melatonin as an inhibitor of sweet cherries ripening in orchard trees. *Plant Physiol. Biochem.* 140, 88–95. doi: 10.1016/j.plaphy.2019.05.007

Tiwari, R. K., Lal, M. K., Naga, K. C., Kumar, R., Chourasia, K. N., Subhash, S., et al. (2020). Emerging roles of melatonin in mitigating abiotic and biotic stresses of horticultural crops. *Sci. Hortic.* 272:109592. doi: 10.1016/j.scienta.2020.109592

Usenik, V., Fabčič, J., and Štampar, F. (2008). Sugars, organic acids, phenolic composition and antioxidant activity of sweet cherry (*Prunus avium* L.). *Food Chem.* 107, 185–192. doi: 10.1016/j.foodchem.2007.08.004

Valero, D., Díaz-Mula, H. M., Zapata, P. J., Castillo, S., Guillén, F., Martínez-Romero, D., et al. (2011). Postharvest treatments with salicylic acid, acetylsalicylic acid or oxalic acid delayed ripening and enhanced bioactive compounds and antioxidant capacity in Sweet cherry. *J. Agric. Food Chem.* 59, 5483–5489. doi: 10.1021/jf200873j

Valverde, J. M., Giménez, M. J., Guillén, F., Valero, D., Martínez-Romero, D., and Serrano, M. (2015). Methyl salicylate treatments of sweet cherry trees increase antioxidant systems in fruit at harvest and during storage. *Postharvest Biol. Technol.* 109, 106–113. doi: 10.1016/j.postharvbio.2015.06.011

Wang, F., Zhang, X., Yang, Q., and Zhao, Q. (2019). Exogenous melatonin delays postharvest fruit senescence and maintains the quality of sweet cherries. *Food Chem.* 301:125311. doi: 10.1016/j.foodchem.2019.125311

Xia, H., Shen, Y., Shen, T., Wang, X., Zhang, X., Hu, P., et al. (2020). Melatonin accumulation in sweet cherry and its influence on fruit quality and antioxidant properties. *Molecules* 25:753. doi: 10.3390/molecules25030753

Xu, T., Chen, Y., and Kang, H. (2019). Melatonin is a potential target for improving post-harvest preservation of fruits and vegetables. *Front. Plant Sci.* 10:1388. doi: 10.3389/fpls.2019.01388

Ze, Y., Gao, H., Li, T., Yang, B., and Jiang, Y. (2021). Insights into the roles of melatonin in maintaining quality and extending shelf life of postharvest fruits. *Trends Food Sci. Technol.* 109, 569–578. doi: 10.1016/j.tifs.2021.01.051

Zhang, Y.-L., Cui, Q.-L., Wang, Y., Shi, F., Liu, J.-P., Liu, J.-L., et al. (2021). Effect of carboxymethyl chitosan-gelatin-based edible coatings on the quality and antioxidant properties of sweet cherry during postharvest storage. *Sci. Hortic.* 289:110462. doi: 10.1016/j.scienta.2021.110462

Zhao, H., Fu, M., Du, Y., Sun, F., Chen, Q., Jin, T., et al. (2021). Improvement of fruit quality and pedicel color of cold stored sweet cherry in response to pre-storage 1-methylciclopropene and chlorine dioxide treatments: combination treatment of 1-MCP plus ClO2 improves post-harvest quality of sweet cherry fruit. *Sci. Hortic.* 277:109806. doi: 10.1016/j.scienta.2020.109806

Conflict of Interest: The authors declare that the research was conducted in the absence of any commercial or financial relationships that could be construed as a potential conflict of interest.

Publisher's Note: All claims expressed in this article are solely those of the authors and do not necessarily represent those of their affiliated organizations, or those of the publisher, the editors and the reviewers. Any product that may be evaluated in this article, or claim that may be made by its manufacturer, is not guaranteed or endorsed by the publisher.

frontiers | Frontiers in Plant Science

REVIEW
published: 13 May 2022
doi: 10.3389/fpls.2022.881813

Overcoming Reproductive Compromise Under Heat Stress in Wheat: Physiological and Genetic Regulation, and Breeding Strategy

Min Li[1†], *Jiming Feng*[1†], *Han Zhou*[1], *Ullah Najeeb*[2], *Jincai Li*[1], *Youhong Song*[1*] *and Yulei Zhu*[1*]

[1] National Engineering Laboratory of Crop Stress Resistance Breeding, School of Agronomy, Anhui Agricultural University, Hefei, China, [2] Faculty of Science, Universiti Brunei Darussalam, Bandar Seri Begawan, Brunei

OPEN ACCESS

Edited by:
Leo Marcelis, Wageningen University and Research, Netherlands

Reviewed by:
Costas Delis, University of Peloponnese, Greece
Jauhar Ali, International Rice Research Institute (IRRI), Philippines

***Correspondence:**
Yulei Zhu
zhuyulei2011@126.com
Youhong Song
uqysong@163.com

[†] *These authors have contributed equally to this work*

Specialty section:
This article was submitted to Crop and Product Physiology, a section of the journal Frontiers in Plant Science

Received: *23 February 2022*
Accepted: *14 April 2022*
Published: *13 May 2022*

Citation:
Li M, Feng J, Zhou H, Najeeb U, Li J, Song Y and Zhu Y (2022) Overcoming Reproductive Compromise Under Heat Stress in Wheat: Physiological and Genetic Regulation, and Breeding Strategy. Front. Plant Sci. 13:881813. doi: 10.3389/fpls.2022.881813

The reproductive compromise under heat stress is a major obstacle to achieve high grain yield and quality in wheat worldwide. Securing reproductive success is the key solution to sustain wheat productivity by understanding the physiological mechanism and molecular basis in conferring heat tolerance and utilizing the candidate gene resources for breeding. In this study, we examined the performance on both carbon supply source (as leaf photosynthetic rate) and carbon sink intake (as grain yields and quality) in wheat under heat stress varying with timing, duration, and intensity, and we further surveyed physiological processes from source to sink and the associated genetic basis in regulating reproductive thermotolerance; in addition, we summarized the quantitative trait loci (QTLs) and genes identified for heat stress tolerance associated with reproductive stages. Discovery of novel genes for thermotolerance is made more efficient *via* the combination of transcriptomics, proteomics, metabolomics, and phenomics. Gene editing of specific genes for novel varieties governing heat tolerance is also discussed.

Keywords: ***Triticum aestivum*** **L, terminal heat stress, grain-filling stage, QTL, genetic regulation**

INTRODUCTION

Wheat (*Triticum aestivum* L.), one of most important cereal crops, is widely cultivated in diverse ecotypes across the world. However, wheat cultivation is often suffering from heat stress damage. According to the IPCC report in 2014, atmospheric temperatures have increased since the beginning of the twenty-first century and are predicted to continue to increase by ∼1.0–1.7°C by 2050. As such, wheat growth and development will be subjected to more frequent and severe heat stress as global climate changes (Liu et al., 2017).

Heat stress often occurred during reproduction from flowering to final maturation (Akter and Islam, 2017). It is reported that heat episode during the reproductive phase is fatal to yield and quality of grain by compromising grain setting and grain filling due to lower duration and activities of leaf photosynthesis (Sharkey, 2005), the compromised reproductive development (Farooq et al., 2011), and retarded grain sugar metabolism (Zhang et al., 2018). High temperature results in damages in anther/pollen structure and timing of development (Saini and Aspinall, 1982; Giorno et al., 2013).

Pollen development is most sensitive to heat. Pollen dysontogenesis, even abortion, has been reported while exposure to temperatures ≥30°C at this stage (Bheemanahalli et al., 2019; Ullah et al., 2021). Heat stress during rapid grain filling stage can cause photosynthetic capacity reduction, lower metabolic activities, increased oxidative reactive species, and reduced grain filling duration and grain filling rate (Farooq et al., 2011; Akter and Islam, 2017). In addition, high temperature combined with rainfall easily causes pre-harvest sprouting, which is a worldwide problem that reduces wheat yield and quality. The reason is that temperature is one of the most important environmental factors for maintaining dormancy during seed development and for inducing dormancy during seed imbibition (Ali et al., 2019).

Understanding of thermotolerance will help to find solutions to protect heat damage during wheat reproduction, including breeding tolerant cultivars. The physiological mechanisms in controlling the reproductive heat tolerance are focused on the analysis from the activities in both leaf source and grain sink. The enzymes in removing reactive oxygen species (ROS), and heat shock protein (HSP) aggravation, and stay-green traits were shown to be acting to protect heat damage. Meanwhile, efforts have been made to examine genetic markers or genes consistently observed across backgrounds and/or environments with a major or stable effect for heat stress tolerance in wheat. The increasing knowledge of molecular mechanisms of heat tolerance is likely to pave the way for engineering plants with favorable economic yields under heat stress.

EFFECTS OF HEAT STRESS ON LEAF PHOTOSYNTHETIC CAPACITY AND GRAIN YIELD FORMATION IN WHEAT

High temperature often occurs at the reproductive stage of wheat, and both carbon source supply and carbon sink intake in wheat are sensitive to heat stress varying with timing, duration, and intensity. Heat stress results in the destruction of photosynthetic systems, which ultimately results in a reduced rate of photosynthesis. Heat stress hindered the formation and development processes of grain, and affected grain filling, grain starch synthesis, eventually resulting into great yield loss.

Effects of Heat Stress on Leaf Photosynthetic Performance

Photosynthesis is one of most important physiological processes sensitive to elevated temperature (Wahid et al., 2007; Centritto et al., 2011). The major effect on leaf photosynthesis due to heat stress resulted from premature leaf senescence and impaired photosynthetic machinery (Kumar et al., 2010; Vijayalakshmi et al., 2010; Liu et al., 2017).

High-temperature stress may reduce Chlorophyll (Chl) biosynthesis, accelerated degradation, or a combination of both, and therefore, lesser accumulation of Chl from plants. The inhibition of Chl biosynthesis under high temperature is attributed to the destruction of many enzymes (Dutta et al., 2009). For instance, the activity of 5-aminolevulinate dehydratase, an important enzyme in the pyrrole biosynthesis pathway, decreased significantly in wheat under heat stress (Mohanty et al., 2006). High-temperature stress also accelerated degradation of chlorophyll a and chlorophyll b of leaves (Feng et al., 2014; Sattar et al., 2020). Photosynthetic pigments are present in the photosystems, and they are damaged by high-temperature stress, resulting in light absorbing efficiency of both photosystems (PSI and PSII) reduction (Geissler et al., 2009; Zhang et al., 2011). PSII has been considered as an important thermal-sensitive component in photosynthesis than PSI (Feng et al., 2014), which is due to disordering of thylakoid membrane fluidity and dissociation of the light-harvesting complex II from the PSII (Iwai et al., 2010). The inhibition of PSII under heat stress is indicated by a sharp increase of chlorophyll fluorescence (Ristic et al., 2007). The fluorescence induction parameter Fv, Fm, and its ratio are generally used as a response of metabolic disorders under stress. Fv/Fm ratio is an important parameter to determine the maximum quantum efficiency of PSII (Baker and Rosenqvist, 2004; Baker, 2008; Baczek-Kwinta et al., 2011).

Ribulose-1,5-bisphosphate carboxylase/oxygenase (Rubisco) acts as a key enzyme in regulating photosynthesis to heat stress. Rubisco activation (RCA) is a catalytic chaperone involved in modulating the Rubisco activity and heat stress tolerance in wheat (Kumar et al., 2019). In wheat, RCA was inhibited above 30°C; when the exposure of wheat leaf to high temperatures exceeded 40°C, dark or light treatment causes a great change in Rubisco and RCA, and such changes are irreversible under dark conditions (Mathur et al., 2011). RCA protected the nascent proteins from aggregation under heat stress, and removed the inhibitory sugar phosphates from the active site of Rubisco so as to activating it (Portis, 2003). Compared with other enzyme activities, Rubisco is more sensitive to temperature. This is an important reason that high temperature accelerates the rate of formation of dead-end product and decreases the rate of RCA reactivation, finally inhibiting the photosynthesis process (Qu et al., 2017). In addition, the inhibition of photosynthesis at high temperatures is partially attributed to an increase in photorespiration rate (Pinto et al., 2016, 2017). Respiration rate and mitochondrial activities, which are changed by heat stress, show an initial increase with a rise in temperature, reach a critical level, and then decline due to photorespiratory damage (Pinto et al., 2017). Photorespiration of wheat flag leaf significantly increases under heat stress because of changes in solubility of O_2 and CO_2 and the affinity of rubisco for these gases (Cossani and Reynolds, 2012).

Consequently, heat stress leads to the synthesis of blocked photosynthetic pigments, membrane disruption, particularly of thylakoid membranes, thereby inhibiting the activities of enzymes and destroying photosynthetic systems (PSII, PSI), which ultimately results in a reduced rate of photosynthesis (Ristic et al., 2008; Rexroth et al., 2011; Ashraf and Harris, 2013).

Effects of Heat Stress on Reproduction in Wheat

Short-term and prolonged exposure of high-temperature stress compromises grain yield and qualities (Feng et al., 2014). The

TABLE 1 | Effect of high-temperature treatment at different days after anthesis (DAA) on grain number (GN), 1,000-grain weight (TGW) and grain yield (GY) in wheat.

Variety	Method of high temperature	Duration	Time	Temperature	GN (%)	TGW (g) (%)	GY (%)	References
Fleisch 481, Soissons, Plainsman, Magma	Move pots in the phytotron heat stress chamber	10–24 DAA	8 h a day	35°C/20°C	37.3 (6.5↓)	30.6 (25.4↓)	1.2g/spike (30.1↓)	Bányai et al., 2014
		20–34 DAA	8 h a day	35°C/20°C	38.2 (4.3↓)	33.8 (17.6↓)	1.4g/spike (18.1)	
CK	Grown at controlled temperature in greenhouse				39.9	41.0	1.7g/spike	
Yang 16	Free–air temperature enhancement technique in the field	0–34 DAA	0:00–24:00	CK+1.5°C	40.9 (7.3↓)	40.4 (5.6↓)	7258.2 kg·hm^{-2} (13.0↓)	Bian et al., 2012
		0–34 DAA	7:00–19:00	CK+1.5°C	41.6 (5.7↓)	41.2 (3.9↓)	7600.9 kg·hm^{-2} (8.9↓)	
		0–34 DAA	19:00–7:00	CK+1.5°C	43.4 (1.7↓)	41.5 (3.0↓)	7547.1 kg·hm^{-2} (9.5↓)	
		0–34 DAA	0:00–24:00	CK+3°C	38.9 (11.8↓)	39.2 (8.5↓)	6718.2 kg·hm^{-2} (19.5↓)	
		0–34 DAA	7:00–19:00	CK+3°C	40.4 (8.5↓)	39.85 (6.9↓)	7087.2 kg·hm^{-2} (15.0↓)	
		0–34 DAA	19:00–7:00	CK+3°C	39.0 (11.6↓)	40.9 (4.4↓)	6899.8 kg·hm^{-2} (17.3↓)	
CK	Nature condition in the field				44.1	42.8	8342.2 kg·hm^{-2}	
Yang 5	Move the pots to a transparent automatic temperature and moisture controlled box	1–3 DAA	08:00–17:00	30°C		34.7 (15.1↓)		Feng et al., 2000
		5–7 DAA	08:00–17:00	30°C		34.1 (16.5↓)		
		12–14 DAA	08:00–17:00	30°C		32.8 (19.7↓)		
		20–22 DAA	08:00–17:00	30°C		31.4 (23.1↓)		
		28–30 DAA	08:00–17:00	30°C		38.2 (6.6↓)		
		20–22 DAA	08:00–17:00	40°C		31.4 (23.1↓)		
		20–22 DAA	08:00–17:00	40°C		31.4 (23.1↓)		
CK1	Nature condition in the field					40.9		
		20–22 DAA	08:00–17:00	30°C		38.5 (8.5↓)		
		20–22 DAA	08:00–17:00	40°C		37.4 (11.0↓)		
CK2	Nature condition in the field					42.0		
Lira–Sa−92, Sakha−8, Gemmeiza−7	Sown late in field					48.1 (15.6↓)	54.9g/plant (24.9↓)	Hassan et al., 2016
CK	Optimal sowing dates in field					57.0	73.1g/plant	
Bainongaikang 58, Luohan 2	Move pots to the walking–in chambers	10–11 DAA	11:00–16:00	38 °C		36.2 (17.7↓)	38.3g/pot (19.1↓)	Jing et al., 2010
		20–21 DAA	11:00–16:00	38 °C		33.2 (24.6↓)	35.9g/pot (24.2↓)	
CK	Nature condition in the field					44.0	47.4g/pot	
Yang 9, Yang 12	Move pots to the artificial intelligence greenhouse	1–3 DAA	8:00–18:00	25°C		37.6 (11.1↓)		Liu et al., 2007
		6–8 DAA	8:00–18:00	25°C		37.4 (11.5↓)		

(Continued)

TABLE 1 | Continued

Variety	Method of high temperature	Duration	Time	Temperature	GN (%)	TGW (g) (%)	GY (%)	References
		13–15 DAA	8:00–18:00	25°C		37.0 (12.4↓)		
		19–21 DAA	8:00–18:00	25°C		36.7 (13.1↓)		
		25–27 DAA	8:00–18:00	25°C		37.3 (11.7↓)		
		33–35 DAA	8:00–18:00	25°C		39.7 (6.0↓)		
		36–38 DAA	8:00–18:00	25°C		40.8 (3.5↓)		
		1–3 DAA	8:00–18:00	30°C		36.2 (14.3↓)		
		6–8 DAA	8:00–18:00	30°C		38.1 (9.9↓)		
		13–15 DAA	8:00–18:00	30°C		37.3 (11.6↓)		
		19–21 DAA	8:00–18:00	30°C		36.2 (14.4↓)		
		25–27 DAA	8:00–18:00	30°C		39.2 (7.3↓)		
		33–35 DAA	8:00–18:00	30°C		41.4 (1.9↓)		
		36–38 DAA	8:00–18:00	30°C		42.4 (0.4↑)		
		1–3 DAA	8:00–18:00	35°C		28.1 (33.5↓)		
		6–8 DAA	8:00–18:00	35°C		27.0 (36.1↓)		
		13–15 DAA	8:00–18:00	35°C		36.3 (14.2↓)		
		19–21 DAA	8:00–18:00	35°C		35.0 (17.2↓)		
		25–27 DAA	8:00–18:00	35°C		35.9 (15.1↓)		
		33–35 DAA	8:00–18:00	35°C		39.5 (6.5↓)		
		36–38 DAA	8:00–18:00	35°C		40.3 (4.5↓)		
		1–3 DAA	8:00–18:00	40°C		19.8 (53.2↓)		
		6–8 DAA	8:00–18:00	40°C		8.8 (79.2↓)		
		13–15 DAA	8:00–18:00	40°C		34.7 (18.0↓)		
		19–21 DAA	8:00–18:00	40°C		33.7 (20.2↓)		
		25–27 DAA	8:00–18:00	40°C		35.0 (17.7↓)		
		33–35 DAA	8:00–18:00	40°C		37.9 (10.3↓)		
		36–38 DAA	8:00–18:00	40°C		39.3 (6.9↓)		
CK	Nature condition in the field					42.3		
Berkut/Krichauff, DH	Late sown in field					25.6 (26.3↓)	1975.8 Kg/hm^2 (45.8↓)	Tiwari et al., 2012
CK	Normal sown in field					34.7	3647.6 Kg/hm^2	
Ji 20, Wennong 6	Plastic shed in the field	1–5 DAA	8:00–18:00	CK+3°C	31.2 (21.8↓)	35.2 (2.5↓)	531.8 (22.8↓)	Yang et al., 2014
CK	Nature condition in the field				39.9	36.1	688.5g/m^2	

reduction of grain yield under high temperature is mainly due to the loss of grain number and decreased grain weight (**Table 1**).

Grain Setting

Grain setting is sensitive to elevated temperature (**Table 1**). The temperature favorable for anthesis ranges from 12°C to 22°C in wheat (Farooq et al., 2011). Wheat plants exposed to the abovementioned temperatures can significantly increase floret abortion (Bányai et al., 2014) and reduce the number of spikelet and grains per spike (Semenov, 2009; Kaur and Behl, 2010). Temperature above 30°C during anthesis affects pollen cell and microspore resulting into complete male sterility (Kumar et al., 2014). Even 42°C for 2 h at the anthesis stage could reduce the pollen viability as well as growth of the pollen tip (Kumar et al., 2014). When the duration of heat stress during anthesis is less than 3 days, the anther of wheat florets is structurally abnormal and nonfunctional (Hedhly et al., 2009). In addition, a substantial lowering in grain yield plants was observed when plants are exposed to 30°C for 1–3 days between the beginning of meiosis and anthesis (Kumar et al., 2014). When wheat plants were exposed to high temperature for 20 h, pollen mother cells (PMCs) exposed to 35°C were less likely to progress than those exposed to 30°C, and grain number per spike was reduced at 30°C, and further at 35°C (Draeger and Moore, 2017).

Grain Filling, Grain Starch Synthesis, and Grain Quality

Grain-filling duration (GFD) and grain-filling rate (GFR) are important factors in determining the grain yield. High temperature inhibits wheat grain-filling (Jing et al., 2020) and reduces the GFD (Liu et al., 2007). Under high temperature, wheat crop completes its life cycle much quicker than under

TABLE 2 | Heat shock protein genes involved in sensing and response to heat stress.

Gene	Source	Trans-host/expression analysis	Function	References
TaHsfA6f	Cloned the TaHsfA6f gene from the heat and drought tolerant wheat cv. TAM107.	*Arabidopsis*	Through up-regulation of a number of genes involved in ABA metabolism and signaling, and other stress-associated genes.	Bi et al., 2020
sHSP26	Cloned the TaHsfA6f gene from bread wheat cv. CPAN1676	Transgenic rice and *Arabidopsis*	Transgenic *Arabidopsis* plants were substantially tolerant under con tinuous high temperature regimen than wild-type plants, as measured by photosystem II (PSII) activity, accumulation of more photosynthetic pigments, higher biomass and seed yield. Transgenic plants produced bold seeds under high temperature, having higher germination potential than the wild-type plants.	Chauhan et al., 2012
TaHsfA2d	Homology clone from rice gene rice OsHsfA2d	*Arabidopsis*	A heat shock factor (HSF) gene expressing preferentially in developing seed tissues of wheat grown under high temperatures, possess higher tolerance toward high temperature, also showed higher yield and biomass accumulation under constant heat stress conditions.	Chauhan et al., 2013
TaHsfC2a-B	Using the sequences of Hsf DNA-binding domains from rice and *Arabidopsis* Hsf proteins for searching T. aestivum Hsf expressed sequence tags (ESTs) from the NBCI EST database	Transgenic wheat Fielder	A transcriptional activator of heat protection genes and serves as a proactive mechanism for heat protection in developing wheat grains via the ABA-mediated regulatory pathway.	Hu et al., 2018
HSP90	Clone from C-306 cultivar of wheat	Expression analysis of HSP90 gene in wheat C-306	A high HSP90 transcript level along with high activities of antioxidant isoenzymes and low proline accumulation is a promising target for developing wheat genotypes with tolerance to heat stress.	Kumar et al., 2013
HSP70	Clone from a thermotolerant cultivar C306) of wheat	Expression analysis of HSP90 gene in wheat C-306	The expression of *HSP70* could decrease membrane stability and enhance total antioxidant capacity under heat stress.	Kumar et al., 2016

normal temperature conditions due to accelerated development. Heat stress decreases the grain-filling duration, reducing the time to apoptosis and maturity (Altenbach, 2012). For instance, an increase of 5.4°C above normal temperature reduces the GFD by 8 days in wheat (Tiwari et al., 2012). The time of GFD is shortened to capture resources between anthesis and filling, ultimately reducing the grain yield (Liu et al., 2007; Tiwari et al., 2012). The interesting thing is that high temperature accelerates the GFR, but shortens the GFD; however, under 30°C, the reduced GFD cannot be compensated by high GFR to enhance growth rate (Yang et al., 2014).

Starch makes up ∼70% of the dry grain weight; high temperature during grain filling has a great influence on contents and compositions of starch (Wang et al., 2015), and the decrease in yield is mainly attributed to a reduction in the starch content (Li et al., 2017). ADP-glucose pyrophosphorylase (AGPase), soluble starch synthase (SSS), granule-bound starch synthase (GBSS), starch branching enzyme (SBE), and sucrose synthase (SS) are the key enzymes for starch synthesis during grain filling in wheat, and this activity was positively correlated with the starch accumulation rate (Yan et al., 2007; Li et al., 2017). The activity of AGPase, SSS, GBSS, and the content of starch was decreased under high-temperature treatment during grain filling (Yan et al., 2007). Overexpression of the rice soluble starch synthase I (*SSI*) gene in transgenic wheat can improve wheat productivity under terminal heat stress, with the increase in photosynthetic duration and 1,000 grain weight by 21–34% in T2 and T3 transgenic plants compared with the non-transgenic control plants (Tian et al., 2018). Starch accumulation is correlated with the sucrose content of the kernels (Yan et al., 2008); on the one hand, high temperature decreases the inactivation of key enzymes in starch synthesis and inhibits the conversion of sucrose into starch (Asthir et al., 2009); on the other hand, high temperature decreased the time of the maximum grain dry weight and resulted in reduced starch accumulation (Dupont and Altenbach, 2003). High temperature altered the timing of the starch biosynthetic process and resulted in an earlier peak in the gene expression during starch biosynthesis due to an enhanced -amylase activity (Li et al., 2017). A low sucrose content and a decline in the enzymatic activity involved in starch synthesis are responsible for the reduction of starch accumulation (Balla et al., 2011).

Protein is an important characteristic to define grain quality. High-temperature stress affects protein content of the grain, which has a great relationship with leaf nitrogen content (Iqbal et al., 2017). Moderate nighttime warming is more conducive to accumulate protein and increase gluten content in grain, especially the increase of glutenin content (Bian et al., 2012). However, high-temperature stress reduces total protein content, thus shortening the sedimentation time of protein in grains (Labuschagne et al., 2009); meanwhile, high temperature reduces the amino acid level and sedimentation index of grains (Dias et al., 2008).

THE PHYSIOLOGICAL MECHANISMS OF HEAT TOLERANCE

Air temperature exceeding certain threshold levels cause excessive accumulation of ROS, oxidative stress, excess membrane damage (Bita and Gerats, 2013; Hasanuzzaman et al., 2013), irreversible degeneration of proteins, and even protein misfolding and raft disruption (Goraya et al., 2017; Lippmann et al., 2019). Plants use various methods to resist heat stress injury, such as mobilizing antioxidant protection system, HSP, phytohormone, prolonging stay-green time, and regulating sugar metabolism of heat tolerance.

Antioxidant Protection for Heat Tolerance

When the temperature is favorable for the plant, ROS in the form of hydrogen peroxide (H_2O_2), superoxide anions ($O_2^{\bullet-}$), hydroxyl radical (OH•), and singlet oxygen ($^1O_2$) is present in plant vacuoles at lower levels. However, when plants are exposed to temperatures beyond the optimum, ROS level can be significantly enhanced, which will cause negative effects on cell metabolism (Esfandiari et al., 2007). Hence, an efficient antioxidant defense system is important for protecting plants against heat stress (Farooq et al., 2011). Both antioxidant defense system and non-enzymatic antioxidant systems contributed to scavenging ROS. Antioxidant defense system includes superoxide dismutase (SOD), peroxidase (POD), catalase (CAT), ascorbate peroxidase (APX), monodehydroascorbate reductase (MDHAR), glutathione peroxidase (GPX), dehydroascorbate reductase (DHAR), peroxiredoxin (PRX), glutathione S-transferase (GST), and glutathione reductase (GR) (Farooq et al., 2011; You and Chan, 2015); non-enzymic antioxidants include glutathione (GSH), ascorbic acid (AsA), ascorbate, and tocopherols (Farooq et al., 2011; You and Chan, 2015).

Heat Shock Protein for Heat Tolerance

Heat stress can disturb cellular homeostasis and hindering reproduction in wheat (Sehgal et al., 2018; Hütsch et al., 2019). HSPs play a multifaceted role in plant heat tolerance (**Table 2**) (Hu et al., 2010; Jacob et al., 2017; Bi et al., 2020), such as protecting proteins from aggregation under heat stress and promoting protein refolding during recovery (Li and Howell, 2021), and involvement in heat stress independent signaling (Liu et al., 2011; Kumar et al., 2016; Jacob et al., 2017; Malik and Lone, 2021). HSPs fall into five categories, namely, HSP110, HSP90, HSP70, HSP60, and small heat shock proteins (sHSPs), respectively (Thomas et al., 2005). It was reported that HSPs regulate the transcription of *HSP* genes (Schoffl et al., 1998); some genes of protective proteins involved in sensing and responding to heat stress during grain filling stage were characterized by overexpression/expression in *Arabidopsis* or wheat (Kumar et al., 2017; Lu et al., 2018). The wheat chloroplastic sHSP (sHSP26) is involved in seed maturation and germination, and greater tolerance to heat stress (Chauhan et al., 2012). Transgenic *Arabidopsis* plants overexpressing *TaHsfA2d* produced greater biomass and grain yield under constant heat stress conditions (Chauhan et al., 2013). Overexpressed *TaHsfC2a*, a transcriptional activator of heat protection genes that serves as a proactive mechanism for heat protection in developing grains, in transgenic wheat, improved the thermotolerance, but did not contribute to dehydration tolerance (Hu et al., 2018). The expression of heat shock factor *Tahsfa6f* is increased in wheat leaves by overexpressing *TaHsfA6f,* which could increase abscisic acid (ABA) levels and enhance tolerance to heat stress in transgenic plants (Bi et al., 2020).

Phytohormone for Heat Tolerance

Plant hormones are the endogenous signal molecules that play a key role in the response to the extreme heat during grain filling in wheat (Kumar et al., 2015). ABA is an important signaling molecule under high-temperature stress (Suzuki et al., 2016). ABA reduces the damage of chloroplast structure by preventing photoinhibition and improving PSII efficiency (Li et al., 2020), activating various antioxidant mechanisms by producing various osmolytes, and improving ability of basic and acquired resistance high temperature (Rezaul et al., 2019; Li et al., 2020). For example, ABA induces the expression of NADPH oxidase (RBOHs) in the *Arabidopsis* genome, known as respiratory burst oxidase homologs (RBOHs), to induce ROS (Suzuki et al., 2011; Kaya et al., 2019) and antioxidant protection (Li et al., 2014; Rezaul et al., 2019). In addition, ABA can activate the expression of sucrose transporter gene and metabolism-related genes in heat stress, for instance, sucrose transporter, sucrose synthase gene, and sucrose invertase genes to maintain ATP formation to enhance heat tolerance of plants (Chen et al., 2019; Rezaul et al., 2019). Cytokinins (CTKs) play a key role in the response to temperature stress (O'Brien and Benkova, 2013), which is the most potent general coordinator between the stay-green trait and senescence (Yang et al., 2016), and promotion of grain filling under heat stress (Zavaleta-Mancera et al., 2007; Wang et al., 2012; Hoenig et al., 2018). CTKs protect plants from the deleterious effects of heat stress by activating antioxidant mechanisms, reducing lipid peroxidation protecting photosynthetic apparatus, and delaying senescence (Liu and Huang, 2002). Brassinosteroids (BRs) enhanced activities of enzymes involved in the ascorbate–glutathione (AsA-GSH) cycle and expression of genes encoding these enzymes to resist heat stress; in addition, BRs could increase the production of HSPs against irreversible heat-induced damage (Wu et al., 2014; Jin et al., 2015; Li et al., 2018). Jasmonates (JAs) could activate the defense system to resist heat stress in rice by improved antioxidant enzyme activity, increased proline content, and enhanced osmotic regulation ability (Clarke et al., 2009;

Farhangi-Abriz and Ghassemi-Golezani, 2019; Sharma et al., 2019; Yang et al., 2020). The airborne ethylene (ET) may reduce thermotolerance to heat stress by deterring antioxidant defenses (Munne-Bosch et al., 2004). Expression patterns of a heat-responsive gene, *TaGASR1*, revealed that it was strongly induced by stress factors, such as high temperature, drought, high salinity and oxidation, as well as the phytohormones, including methyl jasmonate and ABA, which suggested that the *TaGASR1* gene might participate in these stress and hormone signal transduction pathways.

Stay-Green Traits Regulating Heat Tolerance

Stay-green, antagonist to senescence, chlorophyll, and photosynthetic capacity of leaves were maintained or prolonged, which is considered an indicator of heat tolerance (Fokar et al., 1998). Since the loss of chlorophyll is associated with senescence, stay-green genotypes are better able to maintain green area of photosynthesis, resulting in a high percentage of carbohydrates. Compared with the stay-green varieties, the yield and inferior grains of no-stay-green cultivar were much more influenced by high-temperature stress (Yang et al., 2014). Moreover, a study showed that high temperatures during reproduction resulted in a significant decline in C and N assimilation and translocation in the heat-susceptible rice (Shi et al., 2013). The stay-green genotype has the characteristics of delayed C-N transfer, or when the transfer occurs, the process of N re-transfer is slower (Thomas and Ougham, 2014). A stay-green cultivar Wennong 6 had relatively higher grain yield under heat stress due to a lower gibberellin (GA_3) content and a higher zeatin riboside (ZR) content (Yang et al., 2016). The stay-green character showed its potential use in plant breeding, as wheat genotypes in maintaining stay-green of photosynthetic tissues had a greater capacity for grain filling, resulting in increased average weight of grains (Kumar et al., 2010).

Sugar Metabolism Regulates Heat Tolerance

Previous studies suggested that the high sensitivity of reproductive development to heat stress is attributed to the sugar starvation in non-wheat crops (Frank et al., 2009; Liu et al., 2013, 2019; Ruan, 2014), which could be due to reduced photosynthesis, increased respiration, or compromised sugar unloading into grains (Mittler and Blumwald, 2010; Zhang et al., 2018).

It is reported that soluble sugars have been directly linked to the production rates of ROS (Couee et al., 2006) in regulating ROS metabolic pathways, such as mitochondrial respiration or photosynthesis. Sugars may act as signaling molecules for plant development (Zhang and Zhou, 2013), for instance, higher concentrations of sugars may be ROS scavengers in plants, while lower concentrations of sugars may act as substrates or as a stress signal (Van den Ende and Valluru, 2009). Soluble carbohydrate plays an important role in stabilizing cell membrane and maintaining turgor pressure (Peshev and Ende, 2013). The protective characteristics of soluble sugars during oxidative stress are usually attributed to the production of ROS scavengers and/or repair enzymes triggered by direct or indirect signals (Van den Ende and Valluru, 2009). Fructan and hexose contents in grains were significantly reduced under high-temperature stress (Hütsch et al., 2019), for example, hexose is mainly used in starch synthesis, which directly affects starch accumulation (Hütsch et al., 2019). Further study reveals that sucrose and fructan have premium ROS scavenging properties (Keunen et al., 2013; Peshev and Ende, 2013). Heat stress reduces vacuolar invertase activity in maize grains, thereby preventing sucrose degradation to hexose and reducing starch biosynthesis in the endosperm (Cheikh and Jones, 1995). Due to heat stress leading to oxidative stress, they further proved that galactinol and raffinose at an appropriate concentration have good antioxidant capacity and can protect plant cells from oxidative damage (Nishizawa et al., 2008). However, further study is needed to illustrate how sugar participates in the metabolic process of wheat organisms.

BREEDING STRATEGIES COPING WITH HEAT STRESS

To cope with high-temperature stress at the reproductive stage, appropriate measures have been taken to improve crop yield. Strategies to improve heat stress tolerance in wheat include selecting heat tolerance varieties, identifying QTL/genes and exploitation of closely linked markers, and application of closely linked markers in selecting heat-tolerant varieties and marker-assisted breeding in wheat.

Selection of Heat-Tolerant Varieties

Some traits such as grain yield, 1,000-grain weight, canopy temperature (CT) depression, stay-green, and membrane thermostability that appear to be effective indicators could be used in selecting heat-tolerant varieties, though there is no direct screening method to select heat-tolerant varieties (Ni et al., 2018). Stable yield performance of genotypes under heat stress conditions is vital to identify heat-tolerant genotypes (Mason et al., 2010). Thus, the relative performance of yield traits under heat-stressed and non-stressed environments has been widely used as an indicator to identify heat-tolerant wheat genotypes (Sharma et al., 2016). The heat susceptibility index (HSI) was shown to be a reliable indicator of yield stability and a proxy for heat tolerance (Geng et al., 2016; Chen et al., 2017; Zhang et al., 2020). Twenty-six wheat varieties with stable heat resistance were screened using the HSI of 1,000-grain weight and yield all less than 1; even 11 varieties had relatively strong heat resistance with HSI less than 1 in consecutive years (Zhang et al., 2020). Using integrated HSI of yield-related traits and cell membrane thermostability as selection criteria, seven wheat varieties (lines) were selected with heat tolerance (Geng et al., 2016). Leaf senescence is an early response to heat stress, so delayed senescence/stay-green genotypes are important germplasm for resistance heat stress (Abdelrahman et al., 2017). Compared with non-stay-green varieties, stay-green varieties are of agronomic interest, as although the photosynthetic capacity is maintained, the onset of senescence is delayed or the

development of senescence is slowed under heat stress (Thomas and Ougham, 2014). CT can be successfully used as an important selection parameter in breeding program at field, which showed a significant and negative correlation with grain yield, biomass, and 1,000-grain weight, and a positive correlation with spike number per plant during wheat growing period, especially after flowering (Gautam et al., 2015). Lower CT during late grain-filling protected chlorophyll and photosynthesis, exhibiting a greater degree of tolerance to terminal heat (Gautam et al., 2015).

Based on these conventional methods, a series of heat-resistant varieties were selected from existing varieties (**Table 3**), and these germplasm resources were defined as carriers with actual or potential utilization value and biological genetic information. However, traditional phenotypic screening for heat stress tolerance in wheat is slow, laborious, and expensive, which has trailed the high-speed development of genomics and transcriptomics, thereby restricting crop breeding and functional genomics study. More attention needs to be paid to high-precision and high-throughput phenomics studies, in particular, phenomics and multiomics joint analysis in identifying heat-tolerant germplasm resources (Cobb et al., 2013; Zhou et al., 2018). High-throughput phenotypic screening is faster and can capture more genetic information and comprehensive information for the effect of injuries caused by heat stress (Crain et al., 2018; Schmidt et al., 2020). Crain et al. (2018) evaluated a portable phenotypic system named "Phenocart," which was used to record more than 1.1 million phenotypic observations in 1,170 wheat germplasm resources under drought and heat stress, and more than 2,000 GBS markers were identified and genotyped using genotyping sequencing (GBS) technique (Crain et al., 2018). An X-ray computed tomographic analysis was carried out on 203 diverse wheat accessions under heat stress. It takes only 7 min per ear to scan the main shape of the seed (smaller, shriveled seeds with an increased seed surface), and computed tomography evaluating grain set with an accuracy of 95–99% (Schmidt et al., 2020). The application of high-throughput plant phenomics, especially for abiotic stress, will greatly accelerate breeding efficiency. They suggest that advances in yield prediction models and the ability to generate data from genomic and phenotypic data will make these selection strategies easy to adopt by plant breeders for improved genetic gain rates.

Identification of QTL/Genes Related to Heat Tolerance

Over the last three decades, efforts have been made to elucidate the genetic basis of heat stress during grain filling (Ni et al., 2018). The QTLs associated with heat tolerance were identified on all 21 wheat chromosomes in wheat (**Table 4**; Pinto et al., 2016; Ogbonnaya et al., 2017; Bhusal et al., 2018), of which, some of the QTLs detected by different researchers or under different genetic backgrounds were located at the same or similar regions. QTLs for stay-green related traits were identified mainly on chromosome 2A and 7D, and several important QTLs mainly associated with yield and CT were detected on chromosome 3B. This indicates that certain chromosomal regions may have genes closely related to heat tolerance in wheat, and these promising molecular markers could be used in wheat molecular assisted breeding in the future. For example, 14 SSR markers linked to some important traits, including grain filling duration, HSI grain filling duration, HSI single kernel weight of main spike, and HSI kernel weight under heat stress have been used to screen varieties for heat tolerance (Sadat et al., 2013). Recently published sequencing information will be of great benefit for map-based cloning of major QTLs controlling heat tolerance during grain filling (IWGSC RefSeq 1.0; https://urgi.versailles.inra.fr/blast_iwgsc/blast.php; IWGSC, 2018). Most of these QTLs were identified during grain-filling stage, while fewer QTLs were identified for heat stress tolerance during flowering in wheat. Only a genome-wide association analysis of spike ethylene under heat stress at the anthesis stage was reported using an Illumina iSelect 90K SNP genotyping array in 130 diverse wheat elite lines (Valluru et al., 2017).

QTL Clusters in Same or Similar Regions

Most of the QTLs were found to be associated with heat tolerance in wheat grain filling, and there existed QTL clusters in same or similar regions on chromosome 1B, 2D, and 5AS (**Table 4**). Same QTL region on 1B was identified with heat tolerance for grain-filling duration (Yang et al., 2002; Mason et al., 2010; Acuna-Galindo et al., 2015; Sharma et al., 2016) and for kernel weight (Mason et al., 2010) closely linked to markers *gwm11* and *gwm268*. A strong QTL for yield found on 1B (Pinto et al., 2016) co-located with a QTL for green leaf duration flanking markers *wPt3477* to *Xbarc119* was detected in spring wheat grown under heat stress in greenhouse experiments (Naruoka et al., 2012). A stable QTL for flag leaf wax content was identified on chromosome 1B flanked with *wmc419* and *wmc156* (Mondal et al., 2015), which was co-located with a QTL for non-glaucousness spike in a similar position (Dubcovsky et al., 1997). Two HSI QTLs mapped to chromosome 2D were linked with *gwm261* and *gwm484* located closely with a GFD QTLs on chromosomes 2D (Tiwari et al., 2013). The yield-related marker-trait associations (MTAs) identified on chromosome 2D between 96 and 104 cM (Ogbonnaya et al., 2017) were previously identified as stable MTAs for grain yield using 9 K SNP markers within the same region (Edae et al., 2014). *Hgfd.iiwbr-5A* and *QLgfd.iiwbr-5A* associated with early and late grain filling efficiency detected by Sharma et al. (2016) were also located on the short arm of chromosome 5A, which is very close to a meta-QTL MQTL39 (close to *gwm639*) for grain filling reported by Acuna-Galindo et al. (2015).

Important QTLs Mainly Associated With Yield and Canopy Temperature

Numerous important QTLs controlling heat tolerance during grain-filling were identified on chromosome 3B, and were mainly associated with yield and CT (**Table 4**). An important QTL region flanked with markers *wmc527* and *wmc326* on chromosome 3B was identified to be associated with HSI of yield components explaining 19.0–21.2% genetic variance using a Halberd × Cutter RIL population (Mason et al., 2010). Two key QTLs were detected on chromosome 3B using a set of 255 doubled haploid lines, which had a large effect on CT and grain yield, accounting for

TABLE 3 | Heat-tolerant and heat-sensitive wheat genotypes and the selected indicators and performance to high-temperature stress.

Selected Indicators	Heat stress method	Heat stress time	Heat tolerant genotypes	Performance of tolerant genotypes	Sensitive genotypes	Performance of sensitive genotypes	References
Heat susceptibility index estimated for 1000 grain weight, grain yield per plant, grain weight of the main-spike and flag leaf senescence scale	Artificial temperature-rising facility made from hollow steel pipes covered with a white polythene plastic film	DAA7-21, 9.00–17.00	Gaoyou 9415, Hemai 13, Hindi62, Jimai 22, Kexin 9, Shannong 8355, Taishan 23, Yannong 5286, Zimai 7,	The HSI values were less than 1 for thousand kernel weight, grain yield per plant and grain weight per spike			Cao et al., 2015
Canopy temperature, grain yield and its components	Late and very late sown conditions.	Terminal heat stress	HI 8627, HI 8638, HI 8498, HI 896, HI 8691, MACS 3125	Lower canopy temperature, Higher grain yield/plant, biomass/plant, harvest index and test grain weight over years			Gautam et al., 2015
Heat susceptibility index, geometric mean yield and cell membrance thermostability	Under plastic film covered shelter	Began at the 15th day after flowering to harvest DAA15-mature	Nongda 212, Heng 6632, Nongda 3492, Jimai 19, Nongda 413, Nongda 2149, Hengguan 216	Lower heat susceptibility index, higher geometric mean yield and better cell membrance thermostability			Geng et al., 2016
HSI of thousand-kernel weight	Under plastic film covered shelter	From DAA10 to mature	Nongda 189, CA0518, and Jingdong 8	Performed high yield and high 1000 grain weight under both normal and heat-stress environments	Nongda 211, Shimai 15, Jimai 22, Nongda 3432, and Shannong 2149	Performed high yield and high TKW in normal environments, but low yield and low TKW in heat stress environments, and were characterized with poor resistance to heat stress.	Han et al., 2010
Chlorophyll content, grain quality and adversity index of thousand-kernel weight	The artificial intelligence greenhouse	DAA10-20, 9:00–16:00	Shannong 23, Zhoumai 18, Taishan 9818		Shiluan 02-1, Jinan 17	The chlorophyll content in flag leaf of wheat cultivars and thousand-kernel weight decreased, protein content was significantly increased while the starch content was significantly decreased.	Li et al., 2017
Membrane stability index, SPAD value, Fv/Fm ratio and Pn	Sown late	From flowering to grain maturity	DBW 14, RAJ 3765, HD 2643 and HALNA	Higher membrane stability index, chlorophyll content, photosynthesis rate, harvest index under heat stress conditions	HD 2987, SHANGHAI, HD 2402 and WH 730	Lower membrane stability index, chlorophyll content, photosynthesis rate, harvest index under heat stress conditions	Nagar et al., 2015
Stay-green character, water use efficiency, grain filling rate, grain filling duration, grain yield and harvest index	Placing pots in glass canopies with temperature of 4–5°C above than the ambient until maturity	The heat stress was imposed separately at booting, heading, anthesis and post anthesis stages until maturity.	Mairaj-2008	Stay green and take more duration for grain filling	BARS-2009, Shafaq-2006	Poor grain filling and less grain yield, rapid leaf senescence	Nawaz et al., 2013
The adversity resistance indices of functional period of flag leaf and 1,000-kernel weight	In the greenhouse	DAA10-20;09:00–16:00	Shannong 23, Liangxing 77, Shannong19, Luohan 7, Chang 4738	Both normalized greenness intensity of wheat canopy and 1,000-kernel weight were decreased, functional period of flag leaf was shorted, the grain protein content significantly increased and starch content significantly reduced	Jinan 17, Jimai 20, Shiluan 02-1, Zhoumai 24		Yi et al., 2015
Heat susceptibility index of 1,000 grain weight	Plastic film covered shelter	From flowering to grain maturity	Xinchun 37, Xinchun 2, Xinchun 38	HSI less than 1	Xinchun 13, Xinchun 18, Xinchun 33	HSI more than 1	Zhang et al., 2020

TABLE 4 | QTLs for traits associated with terminal heat tolerance in wheat.

Chromosome	Markers	Similar QTL region	Stable or major QTL	Phenotypic variation explanation (PVE)	Associated trait	References
1B	*gwm11, gwm268*	*		10.6–11.0%	Grain filling duration, kernel yield	Yang et al., 2002; Mason et al., 2010; Sharma et al., 2016
	wPt3477, Xbarc119	*		10.0%	Yield, green leaf duration	Naruoka et al., 2012; Pinto et al., 2016
	wmc419, wmc156	*		9.0–10.0%	Flag leaf wax content, spike non-glaucousness	Dubcovsky et al., 1997; Mondal et al., 2015
2A	*gwm356, XCGT.TGCG-349*		*	10.0–26.0%	Senescence-related traits	Vijayalakshmi et al., 2010
	nine QTLs (close to gwm372)		*	3.81–18.05%	Chlorophyll fluorescence and chlorophyll content	Bhusal et al., 2018
2D	*gwm261, gwm484*	*		More than 11.0%	Temperature depression of main spike, flag leaf length and width,	Tiwari et al., 2013
	wPt-0153, wPt-730427	*		5.5–5.61%	Yield-related traits	Edae et al., 2014; Ogbonnaya et al., 2017
3B	*wmc527, wmc326*		*	19.0–21.2%	HSI of yield components	Mason et al., 2010
	wPt-9388, wPt-8021	*	*	Up to 22.0%	CCanopy temperature, grain yield	Pinto et al., 2010; Bennett et al., 2012
	barc229, barc164	*	*	4.5–9.0%	Temperature depression of main spike, HSI_single kernel weight main spike	Mason et al., 2011; Mondal et al., 2015
	wPt-1940, barc0164	*	*	7.0–13.5%	Total green biomass, the velocity of greenness loss and the proportion of plant greenness lost mid grain filling, green leaf duration	Naruoka et al., 2012; Pinto et al., 2016
5A	*Xgwm293, gwm639, Vrn-A1*	*		12.0%	Grain filling duration; early and late grain filling efficiency	Yang et al., 2002; Acuna-Galindo et al., 2015; Sharma et al., 2016; Ogbonnaya et al., 2017
6D	*cfd42*	*	*	32.1%	Spike temperature depression	Mason et al., 2010, 2011
7B	*Xgwm1025–Xgwm745, Xgwm577*	*	*	10.4–20.3%, 25.0%	Canopy temperature depression	Barakat et al., 2011; Paliwal et al., 2012
7D	*acc/cat-10*	*		15.0%	Stay-green, grain filling, canopy temperature and days to heading, permanence of greenness	Kumar et al., 2010; Vijayalakshmi et al., 2010; Pinto et al., 2016

*The meaning of * is "Similar QTL region" and "Stable or major QTL".*

up to 22% of the variance for these traits; in particular, the locus on chromosome arm 3BL had its largest effect under the heat stress conditions, with the RAC875 allele increasing grain yield by 131 kg/ha (Bennett et al., 2012), while Pinto et al. (2010) also detected a QTL of relatively large effect in a similar region under similar heat stress conditions. One stable QTL linked with markers *barc229* and *barc164* influencing HSI single kernel weight main spike and temperature depression of main spike was mapped on chromosome 3B using the same Halberd × Karl92 RIL population across environments (Mason et al., 2011; Mondal et al., 2015). In agreement with the results of Pinto et al. (2016), in the Seri × Babax RIL population on 3B chromosomes seemed to contain genes driving total green biomass, the velocity of greenness loss, and the proportion of plant greenness lost in the middle of grain filling. Naruoka et al. (2012) also found that the 3B chromosomes controlled duration-related QTL of green leaf in spring wheat grown under heat and drought stress. In addition, major and stable QTLs contributing 10.4% ∼ 32.1% phenotypic variation for spike temperature depression and CT depression were detected on chromosome 6D in the Halberd × Karl92 population RILs (Mason et al., 2010, 2011) and on chromosomes 7B in the NW1014 × HUW468 RILs (Paliwal et al., 2012) (**Table 4**).

QTLs for Stay-Green Related Traits

Stay-green is reported to be induced by heat stress and the duration of the leaves staying green is dependent on the genetic background (Kumar et al., 2010). QTLs for stay-green related traits under heat stress were identified mainly on chromosome 2A and 7D in wheat (**Table 4**). QTLs for such traits were mapped

TABLE 5 | Putative genes for heat stress in wheat.

Gene	Source	Expression analysis	Function	References
TaZnF	Full CDS of *TaZnF* was cloned in pGBKT7 vector	*Arabidopsis*	Play important roles in various plant processes including regulation of growth and development, signaling networks, responses to abiotic stresses etc.	Agarwal and Khurana, 2018
TaWRKY1; *TaWRKY33*	Clone from wheat Xiaobaimai	Wheat	*TaWRKY1* was slightly up-regulated by high-temperature and abscisic acid (ABA), and down-regulated by low-temperature. *TaWRKY33* was involved in high responses to high-temperature, low-temperature, ABA and jasmonic acid methylester (MeJA).	He et al., 2016
miR430	miRNome analysis from wheat HD2985	Wheat	Negative regulation of the target gene expression in response to terminal heat stress.	Kumar et al., 2017
RuBisCo activase (Rca) gene	Whole transcriptome analysis	Wheat	A positive correlation was established between the Rca enzyme activity and radical scavenging potential in the leaves	Kumar et al., 2019
TaBI-1.1	RNA sequencing analysis from wheat Xiaobaimai	*Arabidopsis*	Co-localized with *TaFKBP62* on the endoplasmic reticulum (ER) membrane and enhanced heat stress tolerance.	Lu et al., 2018

on chromosome 2A within markers interval *gwm356* and *XCGT.TGCG-349* (Vijayalakshmi et al., 2010). Nine QTLs were clustered on chromosome 2A affecting chlorophyll fluorescence and chlorophyll content; *Qchc.iiwbr-2A*, linked with marker *gwm372* that explained 3.8–18.1% of phenotypic variation, was the consistent QTL on the same locus (Bhusal et al., 2018). The maximum phenotypic variance of 15.0% QTL linked with marker *acc/cat-10* was detected on chromosome 7D associated with stay-green, which was co-located with the QTL for grain filling, CT, and days to heading (Pinto et al., 2016), and this locus has been previously described as associated with permanence of greenness under high temperatures in wheat (Kumar et al., 2010; Vijayalakshmi et al., 2010).

Putative Genes Were Revealed in Response to Heat Stress in Wheat

Discovery of novel genes is made more efficient *via* the combination of transcriptomics, proteomics, metabolomics, and phenomics; some putative genes were revealed by omics techniques in response to high-temperature stress in wheat at the grain filling stage (**Table 5**). Differentially expressed proteins through proteomics approach or transcript profiling are mainly involved in carbohydrate metabolism (Majoul et al., 2003; Laino et al., 2010), starch synthesis (Majoul et al., 2003), ATP synthesis (Majoul et al., 2003; Wang et al., 2015), HSPs (Laino et al., 2010; Wang et al., 2015), photosynthesis (Wang et al., 2015; Kumar et al., 2019), and some defense-related proteins (Laino et al., 2010), translation initiation factors (Majoul et al., 2003), and antioxidant enzymes (Wang et al., 2015). Whole transcriptome analysis of thermotolerant wheat *HD2985* found a putative Rubisco to be significantly upregulated under terminal heat stress. A positive correlation was established between the RCA enzyme activity and radical scavenging potential in the leaves of wheat (Kumar et al., 2017, 2019). Similarly, a novel candidate gene *miR430* on 3B was found using *de novo* assembly and cloned from wheat cv. *HD2985*, which can be used to manipulate the expression of target genes under heat stress toward enhancing thermotolerance for the development of "climate-smart" wheat crop (Kumar et al., 2017). *TaBI-1.1*, a wheat *BI-1* conserved gene, and *TaFKBP62*, a *TaBI-1.1*-interacting protein that colocalized with *TaBI-1.1* on the endoplasmic reticulum membrane and enhanced heat stress tolerance, were identified by an RNA sequencing analysis of heat-treated wheat *Xiaobaimai* (Lu et al., 2018). In addition, *TaZnF* which belongs to C4HC3-type zinc finger transcription factor was found to be highest in the seed and it starts at the post anthesis period 3–5 DAA. Overexpression of *TaZnF* in *Arabidopsis* thaliana conferred improved tolerance to heat during their growth and development, had larger primary roots, more lateral branching, bigger, and more numerous leaves, resulting in more yield (Agarwal and Khurana, 2018). *TaWRKY1* and *TaWRKY33* transgenic wheat plants exhibited enhanced tolerance to heat stress (He et al., 2016).

Although these genes have been shown to be involved in heat stress signaling, more components remain to be identified and characterized in effectively elucidating the mechanism of thermotolerance. Gene editing techniques have been used to improve abiotic stress resistance of crops. By knocking out *OsARM1*, *OsNramp5*, and *OsHAK1*, breeders have developed rice strains with low levels of cadmium, radioactive cesium, and arsenic, respectively (Nieves-Cordones et al., 2017; Tang et al., 2017; Wang et al., 2017). In 2018, research on the OsPYL abscisic acid receptor gene family revealed that pyl1/4/6 triple knockout rice created by CRISPR/Cas9 editing had increased grain yield, greater high-temperature tolerance, and reduced pre-harvest sprouting compared with the wild type (Miao et al., 2018). This provides a possibility for the application of gene editing technology in heat tolerance enhancement and molecular level mechanism analysis of wheat, which requires attention in the future.

CONCLUSION AND FUTURE PERSPECTIVES

The high temperature during wheat reproductive stage has been receiving increased attention due to climate change. This review assessed the effects of heat stress on leaf photosynthetic capacity and grain yield formation in wheat, the associated physiological mechanisms of heat tolerance, and the breeding strategies. Heat stress during the reproductive stage causes great loss to wheat production through compromise in both photosynthetic capacity and sink size and activities. The heat during anthesis is fatal for grain setting through disturbing reproductive success, while the heat after anthesis reduces starch content by decreasing the activity of key enzymes in starch synthesis and grain filling duration. Antioxidant system, HSPs, and hormones were stimulated to protect the damage to cell and enzyme integrity from heat stress. The trait of staying-green acts together in protecting heat damage.

Identified genomic region and genes will play an important role for wheat improvement in terms of introgression of heat-tolerant genes/QTLs into an elite variety or pyramiding of all heat-tolerant genes into an agronomically superior variety/genotype, which will provide markers to assist selection for breeding strategy. It is noted that most of QTLs or genes were identified mainly associated with grain filling under heat stress. Hence, more research about the QTLs detected with traits of seed setting under high temperature should be done in the future. In addition, candidate genes involved in regulating heat tolerance will be available in breeding heat-tolerant varieties using the gene editing technology. The great potential of plant phenotyping in identification of more valuable traits using high-throughput image system facilitates to clarify the molecular network of heat tolerance. As such, this overview provides a thorough understanding of the impact of heat stress from leaf source to grain sink, protection mechanisms from heat damage, as well as associated molecular regulation and breeding contribution.

AUTHOR CONTRIBUTIONS

YZ and YS conceived this review. ML, JF, and YZ collected information and drafted this review. ML, JF, and HZ drafted tables. ML, UN, JL, and YS finalized the study. All authors read the manuscript and approved it for publication.

FUNDING

The study was supported by grants from the National Natural Science Foundation of China (No. 31901540), the Anhui's University Natural Science Research Project (No. KJ2019A0175), and the National Key Research and Development Plan Program of China (No. 2017YFD0300204-3).

REFERENCES

Abdelrahman, M., El-Sayed, M., Jogaiah, S., Burritt, D. J., and Lam-Son Phan, T. (2017). The "STAY-GREEN" trait and phytohormone signaling networks in plants under heat stress. *Plant Cell Rep.* 36, 1009–1025. doi: 10.1007/s00299-017-2119-y

Acuna-Galindo, M. A., Mason, R. E., Subramanian, N. K., and Hays, D. B. (2015). Meta-analysis of wheat QTL regions associated with adaptation to drought and heat stress. *Crop Sci.* 55, 477–492. doi: 10.2135/cropsci2013.11.0793

Agarwal, P., and Khurana, P. (2018). Characterization of a novel zinc finger transcription factor (*TaZnF*) from wheat conferring heat stress tolerance in *Arabidopsis*. *Cell Stress Chaperones*. 23, 253–267. doi: 10.1007/s12192-017-0838-1

Akter, N., and Islam, M. R. (2017). Heat stress effects and management in wheat: a review. *Agron. Sustain. Dev.* 37:37. doi: 10.1007/s13593-017-0443-9

Ali, A., Cao, J., Jiang, H., Chang, C., Zhang, H., Sheikh, S. W., et al. (2019). Unraveling molecular and genetic studies of wheat (*Triticum aestivum* L.) resistance against factors causing pre-harvest sprouting. *Agronomy* 9, 117. doi: 10.3390/agronomy9030117

Altenbach, S. B. (2012). New insights into the effects of high temperature, drought and post-anthesis fertilizer on wheat grain development. *J. Cereal Sci.* 56, 39–50. doi: 10.1016/j.jcs.2011.12.012

Ashraf, M., and Harris, P. J. C. (2013). Photosynthesis under stressful environments: An overview. *Photosynthetica*. 51, 163–190. doi: 10.1007/s11099-013-0021-6

Asthir, B., Kaur, S., and Mann, S. K. (2009). Effect of salicylic and abscisic acid administered through detached tillers on antioxidant system in developing wheat grains under heat stress. *Acta Physiol. Plant.* 31, 1091–1096. doi: 10.1007/s11738-009-0335-y

Baczek-Kwinta, R., Koziel, A., and Seidler-Lozykowska, K. (2011). Are the fluorescence parameters of German chamomile leaves the first indicators of the anthodia yield in drought conditions? *Photosynthetica*. 49, 87–97. doi: 10.1007/s11099-011-0013-3

Baker, N. R. (2008). Chlorophyll fluorescence: A probe of photosynthesis in vivo. *Annu. Rev. Plant Biol.* 59, 89–113. doi: 10.1146/annurev.arplant.59.032607.092759

Baker, N. R., and Rosenqvist, E. (2004). Applications of chlorophyll fluorescence can improve crop production strategies: an examination of future possibilities. *J. Exp. Bot.* 55, 1607–1621. doi: 10.1093/jxb/erh196

Balla, K., Rakszegi, M., Li, Z., Bekes, F., Bencze, S., and Veisz, O. (2011). Quality of winter wheat in relation to heat and drought shock after anthesis. *Czech J. Food Sciences*. 29, 117–128. doi: 10.17221/227/2010-cjfs

Bányai, J., Karsai, I., Balla, K., Kiss, T., Bedo, Z., and Lang, L. (2014). Heat stress response of wheat cultivars with different ecological adaptation. *Cereal Res. Commun.* 42, 413–425. doi: 10.1556/crc.42.2014.3.5

Barakat, M. N., Al-Doss, A. A., Elshafei, A. A., and Moustafa, K. A. (2011). Identification of new microsatellite marker linked to the grain filling rate as indicator for heat tolerance genes in F-2 wheat population. *Austr. J. Crop Sci.* 5, 104–110. doi: 10.1080/00380768.2010.551281

Bennett, D., Reynolds, M., Mullan, D., Izanloo, A., Kuchel, H., Langridge, P., et al. (2012). Detection of two major grain yield QTL in bread wheat (Triticum aestivum L.) under heat, drought and high yield potential environments. *Theor. Appl. Genet.* 125, 1473–1485. doi: 10.1007/s00122-012-1927-2

Bheemanahalli, R., Sunoj, V. S. J., Saripalli, G., Prasad, P. V. V., Balyan, H. S., Gupta, P. K., et al. (2019). Quantifying the impact of heat stress on pollen germination, seed set, and grain filling in spring wheat. *Crop Sci.* 59, 684–696. doi: 10.2135/cropsci2018.05.0292

Bhusal, N., Sharma, P., Sareen, S., and Sarial, A. K. (2018). Mapping QTLs for chlorophyll content and chlorophyll fluorescence in wheat under heat stress. *Biologia Plantarum*. 62, 721–731. doi: 10.1007/s10535-018-0811-6

Bi, H., Zhao, Y., Li, H., and Liu, W. (2020). Wheat heat shock factor *TaHsfA6f* increases aba levels and enhances tolerance to multiple abiotic stresses in transgenic plants. *Int. J. Mol. Sci.* 21, 9. doi: 10.3390/ijms21093121

Bian, X. B., Chen, D. D., Wang, Q. S., and Wang, S. H. (2012). Effects of different day and night temperature enhancements on wheat grain yield and quality

after anthesis under free air controlled condition. *Scientia Agricultura Sinica*. 45, 1489–1498. doi: 10.3864/j.issn.0578-1752.2012.08.004

Bita, C. E., and Gerats, T. (2013). Plant tolerance to high temperature in a changing environment: scientific fundamentals and production of heat stress-tolerant crops. *Front Plant Sci*. 4, 273. doi: 10.3389/fpls.2013.00273

Cao, X., Mondal, S., Cheng, D., Wang, C., Liu, A., Song, J., et al. (2015). Evaluation of agronomic and physiological traits associated with high temperature stress tolerance in the winter wheat cultivars. *Acta Physiol. Plant.* 37, 6. doi: 10.1007/s11738-015-1835-6

Centritto, M., Brilli, F., Fodale, R., and Loreto, F. (2011). Different sensitivity of isoprene emission, respiration and photosynthesis to high growth temperature coupled with drought stress in black poplar (Populus nigra) saplings. *Tree Physiol.* 31, 275–286. doi: 10.1093/treephys/tpq112

Chauhan, H., Khurana, N., Agarwal, P., Khurana, J. P., and Khurana, P. (2013). A seed preferential heat shock transcription factor from wheat provides abiotic stress tolerance and yield enhancement in transgenic *Arabidopsis* under heat stress environment. *PLoS ONE*. 8:11. doi: 10.1371/journal.pone.0079577

Chauhan, H., Khurana, N., Nijhavan, A., Khurana, J. P., and Khurana, P. (2012). The wheat chloroplastic small heat shock protein (sHSP26) is involved in seed maturation and germination and imparts tolerance to heat stress. *Plant Cell Environ.* 35, 1912–1931. doi: 10.1111/j.1365-3040.2012.02525.x

Cheikh, N., and Jones, R. J. (1995). Heat stress effects on sink activity of developing maize kernels grown in vitro. *Physiologia Plantaritm*. 95, 59–66. doi: 10.1111/j.1399-3054.1995.tb00808.x

Chen, D. M., Ma, Y. A., Liu, B. H., Su, Y. H., and Wang, X. X. (2017). Appraisal and screening of heat resistant wheat germplasm resources. *J. Hebei Agricult. Sci.* 21, 64–69. 10. 16318/j. cnki. hbnykx. 2017. 04. 018

Chen, T. T., Li, G. Y., Islam, M. R., Fu, W. M., Feng, B. H., Tao, L. X., et al. (2019). Abscisic acid synergizes with sucrose to enhance grain yield and quality of rice by improving the source-sink relationship. *BMC Plant Biol.* 19, 525. doi: 10.1186/s12870-019-2126-y

Clarke, S. M., Cristescu, S. M., Miersch, O., Harren, F. J. M., Wasternack, C., and Mur, L. A. J. (2009). Jasmonates act with salicylic acid to confer basal thermotolerance in *Arabidopsis* thaliana. *New Phytol.* 182, 175–187. doi: 10.1111/j.1469-8137.2008.02735.x

Cobb, J. N., Declerck, G., Greenberg, A., Clark, R., and Mccouch, S. (2013). Next-generation phenotyping: requirements and strategies for enhancing our understanding of genotype-phenotype relationships and its relevance to crop improvement. *Theor. Appl. Genet.* 126, 867–887. doi: 10.1007/s00122-013-2066-0

Cossani, C. M., and Reynolds, M. P. (2012). Physiological traits for improving heat tolerance in wheat. *Plant Physiol.* 160, 1710–1718. doi: 10.1104/pp.112.207753

Couee, I., Sulmon, C., Gouesbet, G., and El Amrani, A. (2006). Involvement of soluble sugars in reactive oxygen species balance and responses to oxidative stress in plants. *J. Exp. Bot.* 57, 449–459. doi: 10.1093/jxb/erj027

Crain, J., Mondal, S., Rutkoski, J., Singh, R. P., and Poland, J. (2018). Combining high-throughput phenotyping and genomic information to increase prediction and selection accuracy in wheat breeding. *The Plant Genome*. 11, 170043. doi: 10.3835/plantgenome2017.05.0043

Dias, A. S., Bagulho, A. S., and Lidon, F. C. (2008). Ultrastructure and biochemical traits of bread and durum wheat grains under heat stress. *Braz. J. Plant Physiol.* 20, 323–333. doi: 10.1590/s1677-04202008000400008

Draeger, T., and Moore, G. (2017). Short periods of high temperature during meiosis prevent normal meiotic progression and reduce grain number in hexaploid wheat (Triticum aestivum L.). *Theor. Appl. Genet*. 130, 1785–1800. doi: 10.1007/s00122-017-2925-1

Dubcovsky, J., Echaide, M., Giancola, S., Rousset, M., Luo, M. C., Joppa, L. R., et al. (1997). Seed storage protein loci in RFLP maps of tetraploid and hexaploid wheat. *Theor. Appl. Genet.* 95, 1169–1180

Dupont, F. M., and Altenbach, S. B. (2003). Molecular and biochemical impacts of environmental factors on wheat grain development and protein synthesis. *J. Cereal Sci.* 38, 133–146. doi: 10.1016/s0733-5210(03)00030-4

Dutta, S., Mohanty, S., and Tripathy, B. C. (2009). Role of temperature stress on chloroplast biogenesis and protein import in pea. *Plant Physiol.* 150, 1050–1061. doi: 10.1104/pp.109.137265

Edae, E. A., Byrne, P. F., Haley, S. D., Lopes, M. S., and Reynolds, M. P. (2014). Genome-wide association mapping of yield and yield components of spring wheat under contrasting moisture regimes. *Theor. Appl. Genet.* 127, 791–807. doi: 10.1007/s00122-013-2257-8

Esfandiari, E., Shekari, F., Shekari, F., and Esfandiari, M. (2007). The effect of salt stress on antioxidant enzymes activity and lipid peroxidation on the wheat seedlings. *Not. Bot. Hort. Agrobot. Cluj*. 35:1. doi: 10.15835/nbha351251

Farhangi-Abriz, S., and Ghassemi-Golezani, K. (2019). Jasmonates mechanisms and functions in abiotic stress tolerance of plants. *Biocataly. Agricult. Biotechnol*. 20, 101210. doi: 10.1016/j.bcab.2019.101210

Farooq, M., Bramley, H., Palta, J. A., and Siddique, K. H. M. (2011). Heat stress in wheat during reproductive and grain-filling phases. *Crit. Rev. Plant Sci.* 30, 491–507. doi: 10.1080/07352689.2011.615687

Feng, B., Liu, P., Li, G., Dong, S. T., Wang, F. H., Kong, L. A., et al. (2014). Effect of heat stress on the photosynthetic characteristics in flag leaves at the grain-filling stage of different heat-resistant winter wheat varieties. *J. Agron. Crop Sci.* 200, 143–155. doi: 10.1111/jac.12045

Feng, C. N., Guo, W. S., Shi, J. S., Peng, Y. X., and Zhu, X. K. (2000). Effect of high temperature after anthesis on endosperm cell development and grain weight in wheat. *Acta Agronomica Sinica*. 26, 399–405

Fokar, M., Blum, A., and Nguyen, H. T. (1998). Heat tolerance in spring wheat. II. Grain filling. *Euphytica*. 104, 9–15

Frank, G., Pressman, E., Ophir, R., Althan, L., Shaked, R., Freedman, M., et al. (2009). Transcriptional profiling of maturing tomato (Solanum lycopersicum L.) microspores reveals the involvement of heat shock proteins, ROS scavengers, hormones, and sugars in the heat stress response. *J. Exp. Bot.* 60, 3891–3908. doi: 10.1093/jxb/erp234

Gautam, A., Sai Prasad, S. V., Jajoo, A., and Ambati, D. (2015). Canopy temperature as a selection parameter for grain yield and its components in durum wheat under terminal heat stress in late sown conditions. *Agric. Res.* 4, 238–244. doi: 10.1007/s40003-015-0174-6

Geissler, N., Hussin, S., and Koyro, H. W. (2009). Interactive effects of NaCl salinity and elevated atmospheric CO_2 concentration on growth, photosynthesis, water relations and chemical composition of the potential cash crop halophyte Aster tripolium L. *Environ. Exp. Bot.* 65, 220–231. doi: 10.1016/j.envexpbot.2008.11.001

Geng, X. L., Zhang, Y. L., Zang, X. S., Zhao, Y., Zhang, J. B., and You, M. S., et al. (2016). Evaluation the thermotolerance of the wheat(Triticum aestivum L.) cultivars and advanced lines collected from the northern China and north area of Huanghuai winter wheat regions. *J. Triticeae Crops*. 36, 172–181. doi: 10.7606/j. issn.1009-1041.2016.02.07

Giorno, F., Wolters-Arts, M., Mariani, C., and Rieu, I. (2013). Ensuring reproduction at high temperatures: the heat stress response during anther and pollen development. *Plants (basel, switzerland)*. 2, 489–506. doi: 10.3390/plants2030489

Goraya, G. K., Kaur, B., Asthir, B., Bala, S., Kaur, G., and Farooq, M. (2017). Rapid injuries of high temperature in plants. *J. Plant Biol.* 60, 298–305. doi: 10.1007/s12374-016-0365-0

Han, L. M., Zhang, Y., Peng, H. R., Qiao, W. C., He, M. Q., Wang, H. G., et al. (2010). Analysis of heat resistance for cultivars from north china winter wheat region by yield and quality traits. *Acta Agronomica Sinica*. 36, 1538–1546. doi: 10.3724/SP.J.1006.2010.01538

Hasanuzzaman, M., Nahar, K., Alam, M. M., Roychowdhury, R., and Fujita, M. (2013). Physiological, biochemical, and molecular mechanisms of heat stress tolerance in plants. *Int. J. Mol. Sci.* 14, 9643–9684. doi: 10.3390/ijms14059643

Hassan, M. I., Mohamed, E. A., El-Rawy, M. A., and Amein, K. A. (2016). Evaluating interspecific wheat hybrids based on heat and drought stress tolerance. *J. Crop Sci. Biotechnol*. 19, 85–98. doi: 10.1007/s12892-015-0085-x

He, G. H., Xu, J. Y., Wang, Y. X., Liu, J. M., Li, P. S., Chen, M., et al. (2016). Drought responsive WRKY transcription factor genesTaWRKY1 and TaWRKY33 from wheat confer drought and or heat resistance in *Arabidopsis*. *BMC Plant Biol.* 16, 116. doi: 10.1186/s12870-016-0806-4

Hedhly, A., Hormaza, J. I., and Herrero, M. (2009). Global warming and sexual plant reproduction. *Trends Plant Sci.* 14, 30–36. doi: 10.1016/j.tplants.2008.11.001

Hoenig, M., Plihalova, L., Husickova, A., Nisler, J., and Dolezal, K. (2018). Role of cytokinins in senescence, antioxidant defence and photosynthesis. *Int. J. Mol. Sci.* 19:4045. doi: 10.3390/ijms19124045

Hu, X. J., Chen, D. D., McLntyre, C. L., Dreccer, M. F., Zhang, Z. B., Drenth, J., et al. (2018). Heat shock factor C2a serves as a proactive mechanism for

heat protection in developing grains in wheat via an ABA-mediated regulatory pathway. *Plant Cell Environ.* 41, 79–98. doi: 10.1111/pce.12957

Hu, X. L., Liu, R. X., Li, Y. H., Wang, W., Tai, F. J., Xue, R. L., et al. (2010). Heat shock protein 70 regulates the abscisic acid-induced antioxidant response of maize to combined drought and heat stress. *Plant Growth Regul.* 60, 225–235. doi: 10.1007/s10725-009-9436-2

Hütsch, B. W., Jahn, D., and Schubert, S. (2019). Grain yield of wheat (Triticum aestivum L.) under long-term heat stress is sink-limited with stronger inhibition of kernel setting than grain filling. *J. Agron. Crop Sci.* 205, 22–32. doi: 10.1111/jac.12298

Iqbal, M., Raja, N., Yasmeen, F., Hussain, M., Ejaz, M., and Shah, M. A. (2017). Impacts of heat stress on wheat a critical review. *Adv. Crop Sci. Technol.* 5, 251–259. doi: 10.4172/2329-8863.1000251

Iwai, M., Yokono, M., Inada, N., and Minagawa, J. (2010). Live-cell imaging of photosystem II antenna dissociation during state transitions. *P Natl Acad Sci Usa P. Natl. Acad. Sci. U. S. A. P.* 107, 2337–2342. doi: 10.1073/pnas.0908808107

Jacob, P., Hirt, H., and Bendahmane, A. (2017). The heat-shock protein/chaperone network and multiple stress resistance. *Plant Biotechnol. J.* 15, 405–414. doi: 10.1111/pbi.12659

Jin, S. H., Li, X. Q., Wang, G. G., and Zhu, X. T. (2015). Brassinosteroids alleviate high-temperature injury in Ficus concinna seedlings via maintaining higher antioxidant defence and glyoxalase systems. *Aob Plants*. 7, plv009. doi: 10.1093/aobpla/plv009

Jing, J. G., Guo, S. Y., Li, Y. F., and Li, W. H. (2020). The alleviating effect of exogenous polyamines on heat stress susceptibility of different heat resistant wheat (Triticum aestivum L.) varieties. *Scientific Rep*. 10, 7467. doi: 10.1038/s41598-020-64468-5

Jing, H. X., Wang, C. Y., Zuo, X. L., Hu, J. B., Wang, Y. H., and Guo, T. C. (2010). Effect of post-anthesis high temperature stress on grain yield and protein content of different wheat cultivars. *J. Triticeae Crops.* 30, 459–463. doi: 10.7606/j.issn.1009-1041.2010.03.013

Kaur, V., and Behl, R. K. (2010). Grain yield in wheat as affected by short periods of high temperature, drought and their interaction during pre- and post-anthesis stages. *Cereal Res. Commun.* 38, 514–520. doi: 10.1556/crc.38.2010.4.8

Kaya, H., Takeda, S., Kobayashi, M. J., Kimura, S., Iizuka, A., Imai, A., et al. (2019). Comparative analysis of the reactive oxygen species-producing enzymatic activity of *Arabidopsis* NADPH oxidases. *Plant J.* 98, 291–300. doi: 10.1111/tpj.14212

Keunen, E., Peshev, D., Vangronsveld, J., Van den Ende, W., and Cuypers, A. (2013). Plant sugars are crucial players in the oxidative challenge during abiotic stress: extending the traditional concept. *Plant Cell Environ.* 36, 1242–1255. doi: 10.1111/pce.12061

Kumar, M., Kumar, R. R., Goswami, S., Verma, P., Rai, R. D., Chinnusamy, V., et al. (2017). miR430: the novel heat-responsive microRNA identified from miRNome analysis in wheat (Triticum aestivum L). *Indian J. Plant Physiol.* 22, 566–576. doi: 10.1007/s40502-017-0341-9

Kumar, R. R., Goswami, S., Dubey, K., Singh, K., Singh, J. P., Kumar, A., et al. (2019). RuBisCo activasea catalytic chaperone involved in modulating the RuBisCo activity and heat stress-tolerance in wheat. *J. Plant Biochem. Biotechnol.* 28, 63–75. doi: 10.1007/s13562-018-0463-9

Kumar, R. R., Goswami, S., Gadpayle, K. A., Singh, K., Sharma, S. K., Singh, G. P., et al. (2014). Ascorbic acid at pre-anthesis modulate the thermotolerance level of wheat (Triticum aestivum) pollen under heat stress. *J. Plant Biochem. Biotechnol.* 23, 293–306. doi: 10.1007/s13562-013-0214-x

Kumar, R. R., Goswami, S., Gupta, R., Verma, P., Singh, K., Singh, J. P., et al. (2016). The stress of suicide: temporal and spatial expression of putative heat shock protein 70 protect the cells from heat injury in wheat (triticum aestivum). *J. Plant Growth Regul.* 35, 65–82. doi: 10.1007/s00344-015-9508-7

Kumar, R. R., Goswami, S., Sharma, S. K., Singh, K., Gadpayle, K. A., Singh, S. D., et al. (2013). Differential expression of heat shock protein and alteration in osmolyte accumulation under heat stress in wheat. *J. Plant Biochem. Biotechnol.* 22, 16–26. doi: 10.1007/s13562-012-0106-5

Kumar, R. R., Sharma, S. K., Goswami, S., Verma, P., Singh, K., Dixit, N., et al. (2015). Salicylic acid alleviates the heat stress-induced oxidative damage of starch biosynthesis pathway by modulating the expression of heat-stable genes and proteins in wheat (Triticum aestivum). *Acta Physiol. Plant.* 37, 143. doi: 10.1007/s11738-015-1899-3

Kumar, U., Joshi, A. K., Kumari, M., Paliwal, R., Kumar, S., and Roeder, M. S. (2010). Identification of QTLs for stay-green trait in wheat (Triticum aestivum L.) in the 'Chirya 3' x 'Sonalika' population. *Euphytica*. 174, 437–445. doi: 10.1007/s10681-010-0155-6

Labuschagne, M. T., Elago, O., and Koen, E. (2009). Influence of extreme temperatures during grain filling on protein fractions, and its relationship to some quality characteristics in bread, biscuit, and durum wheat. *Cereal Chem.* 86, 61–66. doi: 10.1094/cchem-86-1-0061

Laino, P., Shelton, D., Finnie, C., De Leonardis, A. M., Mastrangelo, A. M., Svensson, B., et al. (2010). Comparative proteome analysis of metabolic proteins from seeds of durum wheat (cv. Svevo) subjected to heat stress. *Proteomics*. 10, 2359–2368. doi: 10.1002/pmic.200900803

Li, C. Y., Zhang, R. Q., Fu, K. Y., Li, C., and Li, C. (2017). Effects of high temperature on starch morphology and the expression of genes related to starch biosynthesis and degradation. *J. Cereal Sci.* 73, 25–32. doi: 10.1016/j.jcs.2016.11.005

Li, G. Y., Zhang, C. X., Zhang, G. H., Fu, W. M., Feng, B. H., Chen, T. T., et al. (2020). Abscisic acid negatively modulates heat tolerance in rolled leaf rice by increasing leaf temperature and regulating energy homeostasis. *Rice*. 13, 18. doi: 10.1186/s12284-020-00379-3

Li, H., Liu, S. S., Yi, C. Y., Wang, F., Zhou, J., Xia, X. J., et al. (2014). Hydrogen peroxide mediates abscisic acid-induced HSP70 accumulation and heat tolerance in grafted cucumber plants. *Plant Cell Environ.* 37, 2768–2780. doi: 10.1111/pce.12360

Li, X., Wei, J.-P., Ahammed, G. J., Zhang, L., Li, Y., Yan, P., et al. (2018). Brassinosteroids attenuate moderate high temperature-caused decline in tea quality by enhancing theanine biosynthesis in camellia sinensis L. *Front Plant Sci.* 9, 1016. doi: 10.3389/fpls.2018.01016

Li, Z., and Howell, S. H. (2021). Heat stress responses and thermotolerance in maize. *Int. J. Mol. Sci.* 22, 948. doi: 10.3390/ijms22020948

Lippmann, R., Babben, S., Menger, A., Delker, C., and Quint, M. (2019). Development of wild and cultivated plants under global warming conditions. *Curr. Biol.* 29, R1326–R1338. doi: 10.1016/j.cub.2019.10.016

Liu, B., Asseng, S., Wang, A. N., Wang, S., h., Tang, L., et al. (2017). Modelling the effects of post-heading heat stress on biomass growth of winter wheat. *Agric. For. Meteorol.* 247, 476–490. doi: 10.1016/j.agrformet.2017.08.018

Liu, H. C., Liao, H. T., Charng, Y. Y., Liu, H. C., Liao, H. T., and Charng, Y. Y. (2011). The role of class A1 heat shock factors (HSFA1s) in response to heat and other stresses in *Arabidopsis*. *Plant Cell Environ.* 34, 738–751. doi: 10.1111/j.1365-3040.2011.02278.x

Liu, P., Guo, W. S., Pu, H. C., Feng, C. N., Zhu, X. K., and Peng, Y. X. (2007). Effects of transient high temperature after anthesis on grain protein content and physiological mechanism in wheat (Triticum aestivum L.). *Acta Agronomica Sinica*. 33, 1516–1522. doi: 10.3321/j.issn:0496-3490.2007.09.019

Liu, X. Z., and Huang, B. (2002). Cytokinin effects on creeping bentgrass response to heat stress: II. leaf senescence and antioxidant metabolism. *Crop Sci.* 42, 466–472. doi: 10.2135/cropsci2002.0466

Liu, Y., Li, J., Zhu, Y., Jones, A., Rose, R. J., and Song, Y. (2019). Heat stress in legume seed setting: effects, causes, and future prospects. *Front. Plant Sci.* 10, 938. doi: 10.3389/fpls.2019.00938

Liu, Y. H., Offler, C. E., and Ruan, Y. L. (2013). Regulation of fruit and seed response to heat and drought by sugars as nutrients and signals. *Front Plant Sci.* 4, 282. doi: 10.3389/fpls.2013.00282

Lu, P. P., Zheng, W. J., Wang, C. T., Shi, W. Y., Fu, J. D., Chen, M., et al. (2018). Wheat Bax Inhibitor-1 interacts with TaFKBP62 and mediates response to heat stress. *BMC Plant Biol.* 18:259. doi: 10.1186/s12870-018-1485-0

Majoul, T., Bancel, E., Triboi, E., Ben Hamida, J., and Branlard, G. (2003). Proteomic analysis of the effect of heat stress on hexaploid wheat grain: Characterization of heat-responsive proteins from total endosperm. *Proteomics*. 3, 175–183. doi: 10.1002/pmic.200390026

Malik, J. A., and Lone, R. (2021). Heat shock proteins with an emphasis on HSP 60. *Mol. Biol. Rep.* 48, 6959–6969. doi: 10.1007/s11033-021-06676-4

Mason, R. E., Mondal, S., Beecher, F. W., and Hays, D. B. (2011). Genetic loci linking improved heat tolerance in wheat (Triticum aestivum L.) to lower leaf and spike temperatures under controlled conditions. *Euphytica*. 180, 181–194. doi: 10.1007/s10681-011-0349-6

Mason, R. E., Mondal, S., Beecher, F. W., Pacheco, A., Jampala, B., Ibrahim, A. M. H., et al. (2010). QTL associated with heat susceptibility index in

wheat (Triticum aestivum L.) under short-term reproductive stage heat stress. *Euphytica*. 174, 423–436. doi: 10.1007/s10681-010-0151-x

Mathur, S., Jajoo, A., Mehta, P., and Bharti, S. (2011). Analysis of elevated temperature-induced inhibition of photosystem II using chlorophyll a fluorescence induction kinetics in wheat leaves (Triticum aestivum). *Plant Biol.* 13, 1–6. doi: 10.1111/j.1438-8677.2009.00319.x

Miao, C., Xiao, L., Huaa, K., Zou, C., Zhao, Y., Bressan, R. A., et al. (2018). Mutations in a subfamily of abscisic acid receptor genes promote rice growth and productivity. *Proc. Natl. Acad. Sci. U. S. A*. 115, 6058–6063. doi: 10.1073/pnas.1804774115

Mittler, R., and Blumwald, E. (2010). Genetic engineering for modern agriculture: challenges and perspectives. *Ann. Rev Plant Biol*. 61, 443–462. doi: 10.1146/annurev-arplant-042809-112116

Mohanty, S., Grimm, B., and Tripathy, B. C. (2006). Light and dark modulation of chlorophyll biosynthetic genes in response to temperature. *Planta*. 224, 692–699. doi: 10.1007/s00425-006-0248-6

Mondal, S., Mason, R. E., Huggins, T., and Hays, D. B. (2015). QTL on wheat (Triticum aestivum L.) chromosomes 1B, 3D and 5A are associated with constitutive production of leaf cuticular wax and may contribute to lower leaf temperatures under heat stress. *Euphytica*. 201, 123–130. doi: 10.1007/s10681-014-1193-2

Munne-Bosch, S., Penuelas, J., Asensio, D., and Llusia, J. (2004). Airborne ethylene may alter antioxidant protection and reduce tolerance of holm oak to heat and drought stress. *Plant Physiol.* 136, 2937–2947. doi: 10.1104/pp.104.050005

Nagar, S., Singh, V. P., Arora, A., Dhakar, R., and Ramakrishnan, S. (2015). Assessment of terminal heat tolerance ability of wheat genotypes based on physiological traits using multivariate analysis. *Acta Physiol. Plant*. 37, 2. doi: 10.1007/s11738-015-2017-2

Naruoka, Y., Sherman, J. D., Lanning, S. P., Blake, N. K., Martin, J. M., and Talbert, L. E. (2012). Genetic analysis of green leaf duration in spring wheat. *Crop Sci.* 52, 99–109. doi: 10.2135/cropsci2011.05.0269

Nawaz, A., Farooq, M., Cheema, S. A., and Wahid, A. (2013). Differential response of wheat cultivars to terminal heat stress. *Int. J. Agricult. Biol*. 15, 1354–1358. doi: 10.1590/brag.2013.045

Ni, Z. F., Li, H. J., Zhao, Y., Peng, H. R., Hu, Z. R., Xin, M. M., et al. (2018). Genetic improvement of heat tolerance in wheat: Recent progress in understanding the underlying molecular mechanisms. *Crop J*. 6, 32–41. doi: 10.1016/j.cj.2017.09.005

Nieves-Cordones, M., Mohamed, S., Tanoi, K., Kobayashi, N. I., Takagi, K., Vernet, A., et al. (2017). Production of low-Cs+ rice plants by inactivation of the K+ transporter OsHAK1 with the CRISPR-Cas system. *Plant J*. 92, 43–56. doi: 10.1111/tpj.13632

Nishizawa, A., Yabuta, Y., and Shigeoka, S. (2008). Galactinol and raffinose constitute a novel function to protect plants from oxidative damage. *Plant Physiol.* 147, 1251–1263. doi: 10.1104/pp.108.122465

O'Brien, J. A., and Benkova, E. (2013). Cytokinin cross-talking during biotic and abiotic stress responses. *Front Plant Sci*. 4, 451. doi: 10.3389/fpls.2013.00451

Ogbonnaya, F. C., Rasheed, A., Okechukwu, E. C., Jighly, A., Makdis, F., Wuletaw, T., et al. (2017). Genome-wide association study for agronomic and physiological traits in spring wheat evaluated in a range of heat prone environments. *Theor. Appl. Genet.* 130, 1819–1835. doi: 10.1007/s00122-017-2927-z

Paliwal, R., Roeder, M. S., Kumar, U., Srivastava, J. P., and Joshi, A. K. (2012). QTL mapping of terminal heat tolerance in hexaploid wheat (T. *aestivum L.). Theor. Appl. Genet.* 125, 561–575. doi: 10.1007/s00122-012-1853-3

Peshev, D., and Ende, W. V. (2013). "Sugars as antioxidants in plants," in *Crop Improvement Under Adverse Conditions*, eds Tuteja N., Gill S. (New York, NY: Springer), p. 13. Peshev, D., Vergauwen, R., Moglia, A., Hideg, E., and Van den Ende, W. (2013). Towards understanding vacuolar antioxidant mechanisms: a role for fructans? *J. Exp. Bot.* 64, 1025–1038. doi: 10.1093/jxb/ers377

Pinto, R. S., Lopes, M. S., Collins, N. C., and Reynolds, M. P. (2016). Modelling and genetic dissection of staygreen under heat stress. *Theor. Appl. Genet.* 129, 2055–2074. doi: 10.1007/s00122-016-2757-4

Pinto, R. S., Molero, G., and Reynolds, M. P. (2017). Identification of heat tolerant wheat lines showing genetic variation in leaf respiration and other physiological traits. *Euphytica*. 213, 76. doi: 10.1007/s10681-017-1858-8

Pinto, S. R., Reynolds, M. P., Mathews, K. L., McIntyre, C. L., Olivares-Villegas, J. J., and Chapman, S. C. (2010). Heat and drought adaptive QTL in a wheat population designed to minimize confounding agronomic effects. *Theor. Appl. Genet.* 121, 1001–1021. doi: 10.1007/s00122-010-1351-4

Portis, A. R. (2003). Rubisco activase-Rubisco's catalytic chaperone. *Photosynth. Res.* 75, 11–27. doi: 10.1023/a:1022458108678

Qu, M., Bunce, J. A., Sicher, R. C., Zhu, X. C., Gao, B., et al. (2017). An attempt to interpret a biochemical mechanism of C-4 photosynthetic thermotolerance under sudden heat shock on detached leaf in elevated CO_2 grown maize. *PLoS ONE*. 12, e0187437. doi: 10.1371/journal.pone.0187437

Rexroth, S., Mullineaux, C. W., Ellinger, D., Sendtko, E., Roegner, M., and Koenig, F. (2011). The plasma membrane of the cyanobacterium gloeobacter violaceus contains segregated bioenergetic domains. *Plant Cell*. 23, 2379–2390. doi: 10.1105/tpc.111.085779

Rezaul, I. M., Feng, B., Chen, T., Fu, W., Zhang, C., Tao, L., et al. (2019). Abscisic acid prevents pollen abortion under high-temperature stress by mediating sugar metabolism in rice spikelets. *Physiologia Plantarum*. 165, 644–663. doi: 10.1111/ppl.12759

Ristic, Z., Bukovnik, U., Momcilovic, I., Fu, J. M., and Prasad, P. V. V. (2008). Heat-induced accumulation of chloroplast protein synthesis elongation factor, EF-Tu, in winter wheat. *J. Plant Physiol.* 165, 192–202. doi: 10.1016/j.jplph.2007.03.003

Ristic, Z., Bukovnik, U., and Prasad, P. V. V. (2007). Correlation between heat stability of thylakoid membranes and loss of chlorophyll in winter wheat under heat stress. *Crop Sci.* 47, 2067–2073. doi: 10.2135/cropsci2006.10.0674

Ruan, Y. L. (2014). Sucrose metabolism: gateway to diverse carbon use and sugar signaling. *Annu. Rev. Plant Biol.* 65, 33–67. doi: 10.1146/annurev-arplant-050213-040251

Sadat, S., Saeid, K. A., Bihamta, M. R., Torabi, S., Salekdeh, S. G. H., and Ayeneh, G. A. L. (2013). Marker assisted selection for heat tolerance in bread wheat. *World Appl. Sci. J*. 21, 1181–1189. doi: 10.5829/idosi.wasj.2013.21.8.2866

Saini, H. S., and Aspinall, D. (1982). Abnormal sporogenesis in wheat (Triticum aestivum L.) induced by short periods of high temperature. *Ann. Bot*. 49, 835–846

Sattar, A., Sher, A., Ijaz, M., Ul-Allah, S., Rizwan, M. S., Hussain, M., et al. (2020). Terminal drought and heat stress alter physiological and biochemical attributes in flag leaf of bread wheat. *PLoS ONE*. 15, e0232974. doi: 10.1371/journal.pone.0232974

Schmidt, J., Claussen, J., Worlein, N., Eggert, A., Fleury, D., Garnett, T., et al. (2020). Drought and heat stress tolerance screening in wheat using computed tomography. *Plant Methods*. 16, 15. doi: 10.1186/s13007-020-00565-w

Schoffl, F., Prandl, R., and Reindl, A. (1998). Regulation of the heat-shock response. *Plant Physiol.* 117, 1135–1141. doi: 10.1104/pp.117.4.1135

Sehgal, A., Sita, K., Siddique, K. H. M., Kumar, R., Bhogireddy, S., Varshney, R. K., et al. (2018). Drought or/and heat-stress effects on seed filling in food crops: impacts on functional biochemistry, seed yields, and nutritional quality. *Front Plant Sci*. 9, 1705. doi: 10.3389/fpls.2018.01705

Semenov, M. A. (2009). Impacts of climate change on wheat in England and Wales. *J. Royal Soc. Interface*. 6, 343–350. doi: 10.1098/rsif.2008.0285

Sharkey, T. D. (2005). Effects of moderate heat stress on photosynthesis: importance of thylakoid reactions, rubisco deactivation, reactive oxygen species, and thermotolerance provided by isoprene. *Plant Cell Environ.* 28, 269–277. doi: 10.1111/j.1365-3040.2005.01324.x

Sharma, A., Shahzad, B., Kumar, V., Kohli, S. K., Sidhu, G. P. S., Bali, A. S., et al. (2019). Phytohormones regulate accumulation of osmolytes under abiotic stress. *Biomolecules*. 9, 285. doi: 10.3390/biom9070285

Sharma, D., Singh, R., Rane, J., Gupta, V. K., Mamrutha, H. M., and Tiwari, R. (2016). Mapping quantitative trait loci associated with grain filling duration and grain number under terminal heat stress in bread wheat (Triticum aestivum L.). *Plant Breed.* 135, 538–545. doi: 10.1111/pbr.12405

Shi, W., Muthurajan, R., Rahman, H., Selvam, J., Peng, S., Zou, Y., et al. (2013). Source-sink dynamics and proteomic reprogramming under elevated night temperature and their impact on rice yield and grain quality. *New Phytol.* 197, 825–837. doi: 10.1111/nph.12088

Suzuki, N., Bassil, E., Hamilton, J. S., Inupakutika, M. A., Zandalinas, S. I., Tripathy, D., et al. (2016). ABA is required for plant acclimation to a combination of salt and heat stress. *PLoS ONE*. 11, e0147625. doi: 10.1371/journal.pone.0147625

Suzuki, N., Miller, G., Morales, J., Shulaev, V., Angel Torres, M., and Mittler, R. (2011). Respiratory burst oxidases: the engines of ROS

signaling. *Curr. Opin. Plant Biol.* 14, 691–699. doi: 10.1016/j.pbi.2011.07.014

Tang, L., Mao, B., Li, Y., Lv, Q., Zhang, L., Chen, C., et al. (2017). Knockout of OsNramp5 using the CRISPR/Cas9 system produces low Cd-accumulating indica rice without compromising yield. *Scientific Rep*. 7, 14438. doi: 10.1038/s41598-017-14832-9

Thomas, H., and Ougham, H. (2014). The stay-green trait. *J. Exp. Bot*. 65, 3889–3900. doi: 10.1093/jxb/eru037

Thomas, X., Campos, L., Mounier, C., Cornillon, J., Flandrin, P., Le, Q. H., et al. (2005). Expression of heat-shock proteins is associated with major adverse prognostic factors in acute myeloid leukemia. *Leuk. Res.* 29, 1049–1058. doi: 10.1016/j.leukres.2005.02.010

Tian, B., Talukder, S. K., Fu, J., Fritz, A. K., and Trick, H. N. (2018). Expression of a rice soluble starch synthase gene in transgenic wheat improves the grain yield under heat stress conditions. *In Vitro Cell. Development. Biol. Plant*. 54, 216–227. doi: 10.1007/s11627-018-9893-2

Tiwari, C., Wallwork, H., Dhari, R., Arun, B., Mishra, V. K., and Joshi, A. K. (2012). Exploring the possibility of obtaining terminal heat tolerance in a doubled haploid population of spring wheat (Triticum aestivum L.) in the eastern Gangetic plains of India. *Field Crops Res.* 135, 1–9. doi: 10.1016/j.fcr.2012.06.006

Tiwari, C., Wallwork, H., Kumar, U., Dhari, R., Arun, B., Mishra, V. K., et al. (2013). Molecular mapping of high temperature tolerance in bread wheat adapted to the Eastern Gangetic Plain region of India. *Field Crops Res.* 154, 201–210. doi: 10.1016/j.fcr.2013.08.004

Ullah, A., Nadeem, F., Nawaz, A., Siddique, K. H. M., and Farooq, M. (2021). Heat stress effects on the reproductive physiology and yield of wheat. *J. Agron. Crop Sci.* 28,1–17. doi: 10.1111/jac.12572

Valluru, R., Reynolds, M. P., Davies, W. J., and Sukumaran, S. (2017). Phenotypic and genome-wide association analysis of spike ethylene in diverse wheat genotypes under heat stress. *New Phytol.* 214, 271–283. doi: 10.1111/nph.14367

Van den Ende, W., and Valluru, R. (2009). Sucrose, sucrosyl oligosaccharides, and oxidative stress: scavenging and salvaging? *J. Exp. Bot.* 60, 9–18. doi: 10.1093/jxb/ern297

Vijayalakshmi, K., Fritz, A. K., Paulsen, G. M., Bai, G., Pandravada, S., and Gill, B. S. (2010). Modeling and mapping QTL for senescence-related traits in winter wheat under high temperature. *Mol. Breed.* 26, 163–175. doi: 10.1007/s11032-009-9366-8

Wahid, A., Gelani, S., Ashraf, M., and Foolad, M. R. (2007). Heat tolerance in plants: an overview. *Environ. Exp. Bot.* 61, 199–223. doi: 10.1016/j.envexpbot.2007.05.011

Wang, F. Z., Chen, M. X., Yu, L. J., Xie, L. J., Yuan, L. B., Qi, H., et al. (2017). *OsARM1*, an R2R3 MYB transcription factor, is involved in regulation of the response to arsenic stress in rice. *Front Plant Sci*. 8, 868. doi: 10.3389/fpls.2017.01868

Wang, K., Zhang, X., and Ervin, E. (2012). Antioxidative responses in roots and shoots of creeping bentgrass under high temperature: effects of nitrogen and cytokinin. *J. Plant Physiol.* 169, 492–500. doi: 10.1016/j.jplph.2011.12.007

Wang, X., Dinler, B. S., Vignjevic, M., Jacobsen, S., and Wollenweber, B. (2015). Physiological and proteome studies of responses to heat stress during grain filling in contrasting wheat cultivars. *Plant Sci. (Amsterdam, Neth.)*. 230, 33–50. doi: 10.1016/j.plantsci.2014.10.009

Wu, X., Yao, X., Chen, J., Zhu, Z., Zhang, H., and Zha, D. (2014). Brassinosteroids protect photosynthesis and antioxidant system of eggplant seedlings from high-temperature stress. *Acta Physiol. Plant.* 36, 251–261. doi: 10.1007/s11738-013-1406-7

Yan, S. H., Wang, Z. L., Dai, Z. M., Li, W. Y., Fu, G. Z., He, M. R., et al. (2007). Activities of enzymes involved in starch synthesis and accumulation in grains of two wheat cultivars with a different amylose content. *Acta Agronomica Sinica*. 33, 84–89. doi: 10.3321/j.issn:0496-3490.2007.01.014

Yan, S. H., Yin, Y. P., Li, W. Y., Liang, T. B., Li, Y., Wu, Y. H., et al. (2008). Effect of high temperature during grain filling on starch accumulation, starch granule distribution, and activities of related enzymes in wheat grains. *Acta Agronomica Sinica*. 34, 1092–1096. doi: 10.3724/SP.J.1006.2008.01092

Yang, D. Q., Li, Y., Shi, Y. H., Cui, Z. Y., Luo, Y. L., Zheng, M. J., et al. (2016). Exogenous cytokinins increase grain yield of winter wheat cultivars by improving stay-green characteristics under heat stress. *PLoS ONE*. 11, e0155437. doi: 10.1371/journal.pone.0155437

Yang, D. Q., Wang, Z. L., Ni, Y. L., Yin, Y. P., Cai, T., Yang, W. B., et al. (2014). Effect of high temperature stress and spraying exogenous ABA post-anthesis on grain filling and grain yield in different types of stay-green wheat. *Scientia Agricultura Sinica*. 47, 2109–2125. doi: 10.3864/j.issn.0578-1752.2014.11.005

Yang, J., Fei, K., Chen, J., Wang, Z., Zhang, W., and Zhang, J. (2020). Jasmonates alleviate spikelet-opening impairment caused by high temperature stress during anthesis of photo-thermo-sensitive genic male sterile rice lines. *Food Energy Secur*. 9, e233. doi: 10.1002/fes3.233

Yang, J., Sears, R. G., Gill, B. S., and Paulsen, G. M. (2002). Quantitative and molecular characterization of heat tolerance in hexaploid wheat. *Euphytica*. 126, 275–282. doi: 10.1023/a:1016350509689

Yi, X. M., Sun, A. Q., Han, X. Y., Zhang, J. D., Wang, Z. L., Wang, C. W., et al. (2015). Identification of dry-hot wind resistance of major wheat cultivars (strains) in Huanghuai wheat region. *J. Triticeae Crop.* 35, 274–284. doi: 10.7606/ j. issn.1009-1041.2015.02.18

You, J., and Chan, Z. (2015). ROS regulation during abiotic stress responses in crop plants. *Front. Plant Sci*. 6, 1092. doi: 10.3389/fpls.2015.01092

Zavaleta-Mancera, H. A., Lopez-Delgado, H., Loza-Tavera, H., Mora-Herrera, M., Trevilla-Garcia, C., Vargas-Suarez, M., et al. (2007). Cytokinin promotes catalase and ascorbate peroxidase activities and preserves the chloroplast integrity during dark-senescence. *J. Plant Physiol.* 164, 1572–1582. doi: 10.1016/j.jplph.2007.02.003

Zhang, C. X., Feng, B. H., Chen, T. T., Fu, W. M., Li, H. B., Li, G. Y., et al. (2018). Heat stress-reduced kernel weight in rice at anthesis is associated with impaired source-sink relationship and sugars allocation. *Environ. Exp. Bot.* 155, 718–733. doi: 10.1016/j.envexpbot.2018.08.021

Zhang, H., and Zhou, C. (2013). Signal transduction in leaf senescence. *Plant Mol. Biol.* 82, 539–545. doi: 10.1007/s11103-012-9980-4

Zhang, J. B., Wang, X. B., Yan, Y. L., Xiao, J., Peng, H. R., and Cong, H. (2020). Evaluation the heat tolerance of the Xin Jiang spring wheat cultivars. *J. Triticeae Crops*. 40, 1055–1063. doi: 10.7606 /jissn.1009-−−104120200905

Zhang, L. T., Zhang, Z. S., Gao, H. Y., Xue, Z. C., Yang, C., Meng, X. L., et al. (2011). Mitochondrial alternative oxidase pathway protects plants against photoinhibition by alleviating inhibition of the repair of photodamaged PSII through preventing formation of reactive oxygen species in Rumex K-1 leaves. *Physiologia Plantarum*. 143, 396–407. doi: 10.1111/j.1399-3054.2011.01514.x

Zhou, J., Tardieu, F., Pridmore, T., Doonan, J., Reynolds, D., Hall, N., et al. (2018). Plant phenomics: history, present status and challenges. *J. Nanjing Agricult. Univ.* 41, 580–588. doi: 10.7685/jnau.201805100

Conflict of Interest: The authors declare that the research was conducted in the absence of any commercial or financial relationships that could be construed as a potential conflict of interest.

Publisher's Note: All claims expressed in this article are solely those of the authors and do not necessarily represent those of their affiliated organizations, or those of the publisher, the editors and the reviewers. Any product that may be evaluated in this article, or claim that may be made by its manufacturer, is not guaranteed or endorsed by the publisher.

frontiers | Frontiers in Plant Science

ORIGINAL RESEARCH
published: 25 May 2022
doi: 10.3389/fpls.2022.890830

Between Light and Shading: Morphological, Biochemical, and Metabolomics Insights Into the Influence of Blue Photoselective Shading on Vegetable Seedlings

*Luigi Formisano[1], Begoña Miras-Moreno[2], Michele Ciriello[1], Leilei Zhang[2], Stefania De Pascale[1], Luigi Lucini[2] and Youssef Rouphael[1]**

[1] Department of Agricultural Sciences, University of Naples Federico II, Portici, Italy, [2] Department for Sustainable Food Process, DiSTAS, Università Cattolica del Sacro Cuore, Piacenza, Italy

OPEN ACCESS

Edited by:
Ep Heuvelink, Wageningen University and Research, Netherlands

Reviewed by:
Sofia D. Carvalho, Universidad San Francisco de Quito, Ecuador
Lorenzo Guglielminetti, University of Pisa, Italy

***Correspondence:**
Youssef Rouphael
youssef.rouphael@unina.it

Specialty section:
This article was submitted to Crop and Product Physiology, a section of the journal Frontiers in Plant Science

Received: *06 March 2022*
Accepted: *26 April 2022*
Published: *25 May 2022*

Citation:
Formisano L, Miras-Moreno B, Ciriello M, Zhang L, De Pascale S, Lucini L and Rouphael Y (2022) Between Light and Shading: Morphological, Biochemical, and Metabolomics Insights Into the Influence of Blue Photoselective Shading on Vegetable Seedlings. Front. Plant Sci. 13:890830. doi: 10.3389/fpls.2022.890830

High nursery densities reduce the seedling quality due to the competition for light. High light intensity, shading, and blue light depletion activate morphophysiological and metabolomic responses in plants, resulting in size modification to gain an advantage over neighboring plants. Our research aimed to unravel the effects of light intensity and quality on nursery seedlings at the morphological and biochemical levels. To this aim, the effect of black shading and blue photoselective shading nets were investigated in terms of morphometric, ionomic, and untargeted metabolomics signatures in *Cucurbita pepo* L., *Citrullus lanatus* L., *Solanum lycopersicum* L., and *Solanum melongena* L. seedlings. Plant height, diameter, sturdiness index, leaf area, specific leaf area, shoot/root ratio, and mineral content (by ion chromatography-IC) were evaluated. In *C. pepo* L and *C. lanatus* L., the blue net reduced the shoot/root and chlorophyll a/b ratios and increased stem diameter and total chlorophyll content. The black net increased plant height, stem diameter, and sturdiness index in *Solanum lycopersicum* L. and *Solanum melongena* L. At the same time, unshading conditions reduced leaf area, specific leaf area, shoot/root ratio, and total chlorophyll content. The blue net improved the sturdiness index and quality of *C. pepo* L. and *C. lanatus* L. Such impact on morphological parameters induced by the different shading conditions was corroborated by a significant modulation at the metabolomics level. Untargeted metabolomic phytochemical signatures of the selected plants, and the subsequent multivariate analysis coupled to pathway analysis, allowed highlighting a broad and diverse biochemical modulation. Metabolomics revealed that both primary and secondary metabolism were largely affected by the different shading conditions, regardless of the species considered. A common pattern arose to point at the activation

of plant energy metabolism and lipid biosynthesis, together with a generalized down accumulation of several secondary metabolites, particularly phenylpropanoids. Our findings indicate an intriguing scientific interest in the effects of selective shading and its application to other species and different phenological stages.

Keywords: shading screen, plantlets, sturdiness index, red:blue ratio, metabolomics, plant metabolism, lipid biosynthesis, phenylpropanoids

INTRODUCTION

Nursery activities are the "backbone" of modern agricultural production systems, in addition to asserting additional assets for social and economic sustainability (Timpanaro et al., 2018; Rani et al., 2019; Rouphael et al., 2021). In the agricultural scene, the horticultural and nursery sectors have grown over the years due to their distinctive dynamism, the ongoing technological upgrading, and investment in new growing techniques to meet the increasing demand for high-quality seedlings (i.e., healthy, vigorous, and balanced development) and adaptability to different climates and soils. The adaptability of seedlings to changing environmental conditions is the cornerstone of nursery production. Drought, soil salinity, temperature, humidity, and sub-optimal nutrient levels are examples of environmental pressures that imperil seedling establishment, performance, and survival in their natural habitats (Franco et al., 2006). Pre-conditioning nursery techniques are crucial to producing robust plants with adequate morphology and high levels of organic reserves. These latter attributes are critical to ensure increased vegetative vigor during seedling establishment (Franco et al., 2006). Direct morphological parameters (such as plant height, stem diameter, root length, dry weight, and leaf area), derived parameters (such as the sturdiness index, the shoot/root ratio, and the leaf area ratio), and physiological parameters (such as mineral and chlorophyll content) are usually used for seedling quality assessment (Lin et al., 2019). For example, a lower sturdiness index (i.e., the ratio of stem height to stem diameter) reduces seedling lodging, while a low shoot/root ratio reduces mortality rates when grown in drought environments (Franco et al., 2006; Mañas et al., 2009). Mañas et al. (2009) reported that higher shoot dry weight (high content of photosynthetic reserves) increased the vigor and survival of seedlings after transplanting. At the same time, Grossnickle (2005) pointed out that high leaf area (excessive shoot growth) could lead to severe transplant shock as a consequence of water imbalances between shoot and root. Finally, a thicker stem and a larger root system increased resistance to transplant shock (Grossnickle and MacDonald, 2018b).

In plants, vegetative growth and development depend on cell division, cell elongation, directional growth, and branching (Ouzounis et al., 2015), where light is one of the environmental parameters that can drive many of these processes (Devlin et al., 2007). Plants are light-dependent and therefore have evolved sophisticated photoreceptors that control specific biochemical and physiological aspects to maximize photosynthetic performance by adapting to a specific light environment (Folta and Carvalho, 2015; Paradiso and Proietti, 2021). Usually, light-demanding species have higher photosynthetic activity, thicker roots, and long shoots. In contrast, shade-tolerating species increase leaf size under shading, show a higher chlorophyll content, and decrease their light compensation point to balance the reduced photosynthetic activity (Walter and Nagel, 2006; Ferrante and Mariani, 2018; Poorter et al., 2019).

However, modern nursery techniques based on high planting density can reduce seedling quality due to unwanted changes in key morphological parameters (Wang X. et al., 2020). In high-density seedlings, tight spaces cause a strenuous struggle for light, a scenario that triggers photo-morphogenetic adaptations to increase competitiveness among plants (Keuskamp et al., 2012; Paradiso and Proietti, 2021). To manage the challenging relationship between neighbors, plants can rely on two strategies: react (avoidance) or adapt (tolerance) (Morelli and Ruberti, 2002). Plants, through photoreceptors, detect shading as a reduced intensity in and/or changes in light quality (Morelli and Ruberti, 2002; Keuskamp et al., 2012). For example, depletion of blue radiation is an indicator of effective shading to which plants respond by elongating the stem and increasing the angle of incidence of the leaves (hyponastia) to take advantage of neighboring plants (Keuskamp et al., 2012). Stimulus-response induction is mediated by cryptochrome, a phototropin photoreceptor involved in the uptake of blue light and contributes largely to plant shape (Folta and Carvalho, 2015). Blue light depletion caused by self-shading can result in excessive stem and shoot growth, an undesirable aspect for nursery seedlings. Thus, forcing producers to use chemical size regulators that inhibit gibberellin production, resulting in shorter internodes and more controlled plant growth. Although morphological responses to blue light are genotype-dependent and can differ even among genotypes (Huché-Thélier et al., 2016), increasing blue radiation through alternative non-chemical methods could be a viable and environmentally sustainable aid to reduce nursery seedling size. However, the application of the blue spectrum in seedling cultivation has rarely been studied or documented in scientific manuscripts, and very little is known about the metabolic changes associated with planting exposition to the blue net. Considering the direct linkage between light and essential processes (not limited to photosynthesis) and its connection to the carbon and nitrogen fluxes (Li et al., 2020), studying the metabolic processes underlying selective shading is crucial in understanding the profound impact of shading in crops. In this sense, the hypothesis-free comprehensive profiling provided by untargeted

TABLE 1 | Effects of shading and light quality on morphometric indices of zucchini squash (*Cucurbita pepo* L.), watermelon (*Citrullus lanatus L.),* tomato (*Solanum lycopersicum L.),* and eggplant (*Solanum melongena L.)* seedlings.

Crop	Treatment	Plant height	Leaf area	Shoot dry weight	Root dry weight	Shoot/root ratio
		(cm plant^{-1})	(cm^2 plant^{-1})	(mg plant^{-1})		
	No shading	2.364 ± 0.018*b*	43.675 ± 0.330*a*	356.167 ± 9.076*a*	108.433 ± 3.795	3.674 ± 0.352
Zucchini squash	Black net	2.821 ± 0.014*a*	43.477 ± 0.135*a*	340.233 ± 2.747*a*	100.067 ± 1.486	3.811 ± 0.007
	Blue net	2.338 ± 0.019*b*	42.254 ± 0.147*b*	304.300 ± 7.199*b*	101.433 ± 0.837	3.458 ± 0.024
	Significance	***	**	**	*Ns*	*ns*
	No shading	2.820 ± 0.091*c*	20.561 ± 0.690*b*	321.867 ± 1.068*a*	86.200 ± 1.914*b*	4.201 ± 0.117*a*
Watermelon	Black net	3.752 ± 0.087*a*	21.904 ± 0.609*b*	296.100 ± 5.575*b*	77.100 ± 1.415*c*	3.980 ± 0.052*a*
	Blue net	3.262 ± 0.045*b*	24.893 ± 0.323*a*	327.033 ± 1.281*a*	100.567 ± 0.437*a*	3.404 ± 0.055*b*
	Significance	***	**	***	***	***
	No shading	5.309 ± 0.123*c*	7.421 ± 0.069*c*	119.133 ± 2.811*b*	44.067 ± 0.606*b*	2.694 ± 0.023*b*
Tomato	Black net	7.915 ± 0.077*a*	11.776 ± 0.053*a*	148.933 ± 6.438*a*	52.933 ± 1.386*a*	2.820 ± 0.059*ab*
	Blue net	6.516 ± 0.095*b*	10.568 ± 0.030*b*	133.267 ± 3.689*ab*	44.900 ± 0.361*b*	2.962 ± 0.055*a*
	Significance	***	***	*	***	*
	No shading	3.589 ± 0.011*c*	17.587 ± 0.613*c*	127.833 ± 2.210*b*	71.567 ± 0.940*a*	1.807 ± 0.073*c*
Eggplant	Black net	5.046 ± 0.086*a*	27.274 ± 0.504*b*	157.233 ± 3.830*a*	61.100 ± 1.206*b*	2.985 ± 0.119*a*
	Blue net	4.145 ± 0.031*b*	31.425 ± 0.335*a*	163.900 ± 2.743*a*	64.700 ± 0.351*b*	2.622 ± 0.033*b*
	Significance	***	***	***	***	***

*Different letters within columns indicate significant mean differences according to Tukey's HSD test (p = 0.05). ns, *, ** and *** denote non-significant or significant effects at p ≤ 0.05, 0.01, and 0.001, respectively. Data are mean values ± standard error, n = 3.*

metabolomics may provide a holistic overview of the different biochemical processes triggered by selective shading, thus providing valuable insights into the metabolic reprogramming induced in crops.

Based on these assumptions, the objective of our research was to evaluate the effects of intensity (No shading) and quality (Blue net) of light on morphometric and quality parameters, colorimetric indices, mineral concentration, and pigment concentration, in *Solanaceae* and *Cucurbitaceae* seedlings, compared to ordinary summer shading practices in the nursery (Black net). At the same time, metabolic reprogramming was investigated through untargeted metabolomics in light-demanding species such as zucchini squash (*Cucurbita pepo* L.), watermelon (*Citrullus lanatus* L.), tomato (*Solanum lycopersicum* L.), and eggplant (*Solanum melongena* L.) seedlings for nursery production in the Mediterranean environment. To our knowledge, this is the first study that has investigated these aspects and will be of prime interest to seedling producers.

MATERIALS AND METHODS

Experimental Design, Plant Material, and Technical Characteristics of the Nets

The experimental trial evaluated the intensity and quality of light on nursery seedlings. It was carried out in spring-summer 2021 at "Vivai Giuseppe Bene" nursery farm, located in Poggiomarino (Naples, Italy, 40°79′ N, 14°53′ E, 46 m.s.l.). The experiment protocol was based on comparing a blue photoselective shading net, a commercial black shading net (as of Control), and a transparent plastic film in ethyl vinyl acetate that covered high tunnels 10 m wide, 35 m long, and 3.5 and 5 m high at the eaves and ridge, respectively. The shading nets were in factorial combination with *Cucurbitaceae* shading-demanding species seedlings as zucchini squash (*Cucurbita pepo* L. cv. San Pasquale, Pagano Domenico and Figli, Scafati, Italy) and watermelon (*Citrullus lanatus* L. cv. Crimson Sweet, Pagano Domenico and Figli, Scafati, Italy) and *Solanaceae* shading-demanding species seedlings as tomato (*Solanum lycopersicum* L., cv. OR Grandborghese, Four-Blumen Vegetable seeds, Piacenza, Italy) and eggplant (*Solanum melongena* L., cv. Mirabelle F1—Seminis, Milan, Italy), sown in polystyrene plug trays (experimental unit) (*Cucurbitaceae*: 60 plants/tray; *Solanaceae*: 180 plants/tray). The experimental design was randomized into three replicates. Seeds were sown on June 29, 2021, covered with a thin layer of vermiculite and placed in a germination chamber for 36 h (until seed coats cracked and the shoots just started to emerge). On July 2, the trays were moved under the nets. The characteristics of the nets were as follows: (1) ChromatiNet[§] Blue (hereafter "Blue net"; shading factor: 40%; red:blue ratio = 1; Ginegar Plastic Products Ltd., Kibbutz Ginegar, Israel); (2) 2635NE Agri LDF black (hereafter "Black net"; shading factor: 40%; red:blue ratio = 1.4; Arrigoni S.p.A, Uggiate Trevano, Italy); and (3) Sunlux 200 EVO plastic film (hereinafter "No shading"; shading factor: 20%; red:blue ratio = 1.4; Comagri S.r.l., Grumello del Monte, Italy). The photosynthetically active radiation (PAR) was continuously recorded using WatchDog A150 dataloggers (Spectrum Technologies Inc., Aurora, IL, United States) (**Supplementary Figure 1**) while the red:blue ratio, the spectral irradiance (W m^{-2} nm^{-1}), and the degree of light extinction of the nets were evaluated using a portable spectral radiometer (MSC15, Gigahertz-Optik, Turkenfeld, Germany) (**Supplementary Figures 2**, **3**).

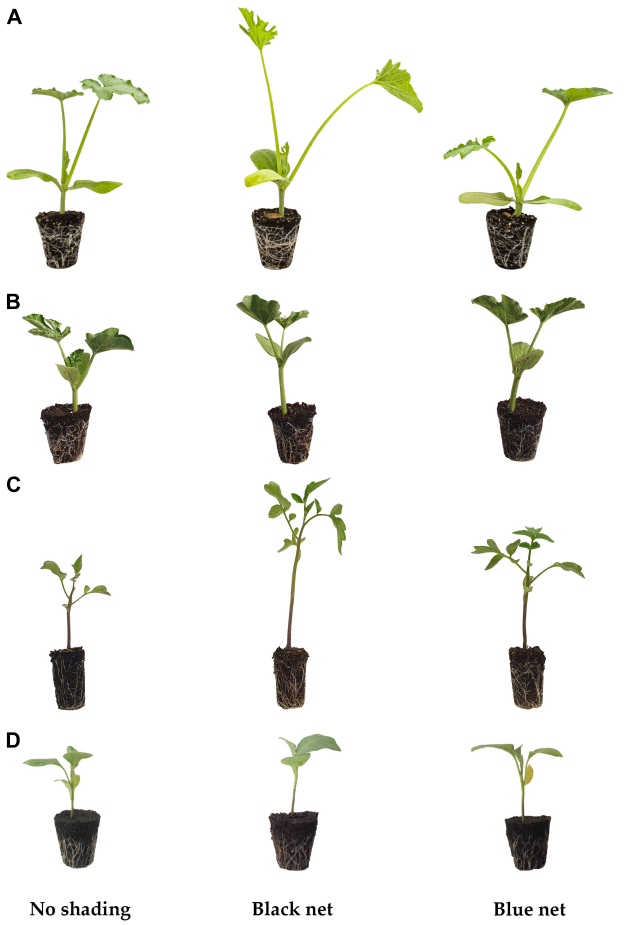

FIGURE 1 | Illustrative picture of the effects of light intensity and quality on the seedling height of zucchini squash (*Cucurbita pepo* L.) **(A)**, watermelon (*Citrullus lanatus* L.) **(B)**, tomato (*Solanum lycopersicum* L.) **(C)**, and eggplant (*Solanum melongena* L.) **(D)**.

Sampling and Determination of Morphometric and Quality Indices of Seedlings

Seedlings were sampled when they reached their marketable size (at two true leaves for zucchini squash and watermelon and three true leaves for tomato and eggplant). Specifically, zucchini squash, watermelon, tomato, and eggplant seedlings were sampled at 14, 19, 21, and 27 days after sowing, respectively. Twenty defect-free plants per experimental unit were harvested (avoiding border plants), weighed, and separated into leaves, stems, and roots. Plant height (cm plant^{-1}) was measured, and leaf area (cm^2 plant^{-1}) was assessed by digital image analysis using ImageJ v1.52a software (United States National Institutes of Health, Bethesda, MD, United States). A leaf tissue subsample was immediately stored at –20°C for pigment determination, while another subsample was immediately frozen at –80°C and subjected to a freeze-drying cycle (Alpha 1–4 Martin Christ Gefriertrocknungsanlagen GmbH, Osterode am Harz, Germany) for metabolomic analyzes. The diameter of the stem was measured using a digital caliper (± 0.02 mm accuracy; RS PRO, Sesto San Giovanni, Italy). The roots were gently cleaned in water, spread on a graph paper, and measured in length (cm plant^{-1}). All tissues collected were oven-dried at 70°C to constant weight (∼72 h) to determine the dry weight (mg plant^{-1}). The dried leaves and stems were ground with an MF10.1 cutting head mill (IKA®, Staufen im Breisgau, Germany) and sieved with an MF0.5 sieve (hole size 0.5 mm; IKA®, Staufen im Breisgau, Germany) for mineral determination. Then, derived quality indices such as the shoot/root ratio, sturdiness index (stem height/root collar diameter), and specific leaf area (LAR, cm^2 mg^{-1} plant^{-1}; leaf area/total dry weight) were calculated.

Soil Plant Analysis Development Index and Leaf Color Determination

At harvest, the soil plant analysis development (SPAD) index (greenness index) was measured on twenty young and fully expanded leaves of each experimental unit using a portable chlorophyll meter (SPAD-502, Minolta Camera Co., Ltd., Osaka, Japan) and CIELab colorimetric coordinates by a Minolta CR-300 colorimeter (Minolta Co., Ltd., Osaka, Japan) calibrated with a corresponding Minolta standard.

Mineral Determination

The determination of cations [potassium (K), calcium (Ca), and magnesium (Mg)] and anions [nitrate and phosphorus (P)] in zucchini squash, watermelon, tomato, and eggplant seedlings were assessed by ion chromatography according to the method described in detail by Formisano et al. (2021a). Briefly, 0.25 g of finely ground dry material was mixed with 50 ml of ultrapure water (Arium® Advance EDI pure water system, Sartorius, Goettingen, Germany), placed in a shaking water bath for 10 min (100 rpm; Julabo, Seelbach, Baden-Württemberg, Germany), and centrifuged for 10 min (6,000 rpm, R-10M centrifuges, Remi Elektrotechnik Ltd., Mumbai, India). A 0.25-µL aliquot of the supernatant was filtered and processed by anionic chromatography coupled to an electrical conductivity detector (ICS-3000, Thermo Scientific™ Dionex™, Sunnyvale, CA, United States). Columns, pre-columns, and self-regenerating suppressors were purchased from Thermo Scientific™ Dionex™ (Sunnyvale, CA, United States). Cations separation was performed isocratically using 25 mM methanesulfonic acid as an eluent (Sigma Aldrich, Milan, Italy). Anions separation was performed in a gradient mode (5–30 mM KOH with a 1.5 mL min^{-1} flow). The integration and quantification of minerals were performed using Chromeleon™ 6.8 Chromatography Data System (CDS) software (Thermo Scientific™ Dionex™, Sunnyvale, CA, United States), comparing the peak areas of the samples with those of the standards. Anions and cations concentrations were expressed as g kg^{-1} dry weight (dw), except for nitrate, which was expressed as mg kg^{-1} fresh weight (fw). Each treatment was analyzed in triplicate.

Pigments Determination

Pigments (total chlorophyll, a, b, and carotenoids) were determined as described by Formisano et al. (2021b). Briefly,

0.5 g of fresh leaves were extracted in ammonia acetone, crushed in a ceramic mortar, and centrifuged at 2,000 rpm for 10 min using an R-10 M centrifuge (Remi Elektrotechnik Limited, Mumbai, India). The contents of chlorophyll a, chlorophyll b, and carotenoids were determined by UV-Vis spectrophotometry (ONDA V-10 Plus, Giorgio Bormac srl, Carpi, Italy) with an absorbance of 647, 664, and 470 nm, respectively. Total chlorophylls were calculated as chlorophyll a + chlorophyll b. In addition, the chlorophyll a/chlorophyll b ratio was calculated. Total chlorophylls and carotenoids were expressed as mg g^{-1} fw.

Metabolomics Analysis

The untargeted metabolomics profiling of the four seedling species was carried out by extracting 0.5 g of dried leaves in 5 mL of extraction solvents, composed of 80% *v/v* methanol + 20% *v/v* ultrapure water and acidified with 0.1% formic acid (Merck KGaA, Darmstadt, Germany). The samples were subsequently homogenized using a Polytron® PT1200 E (Kinematica AG, Malters, Switzerland) homogenizer and centrifuged at 8,000 × *g* for 15 min. The supernatants were filtered with a 0.22 mm syringe filter and transferred in glass vials ready to be injected (volume of 6 μL) into the ultra-high-pressure liquid chromatography coupled to a quadrupole time of flight mass spectrometer (UHPLC-QTOF-MS; Agilent Technologies, Stevens Creek Blvd, Santa Clara, CA, United States) as previously reported (Benjamin et al., 2019). In detail, the chromatographic separation was achieved by using an Agilent InfinityLab Poroshell 120 pentafluorophenyl (PFP) column (2.1 × 100 mm, 1.9 μm) (Agilent Technologies, Stevens Creek Blvd, Santa Clara, CA, United States) and a binary mixture of water and acetonitrile acidified with 0.1% (*v/v*) formic acid as mobile phase (LC-MS grade, VWR, Milan, Italy). The data analysis after the samples acquisition was carried out using Agilent Profinder B 0.10.0 (Agilent Technologies, Stevens Creek Blvd, Santa Clara, CA, United States) in order to align and annotate the features according to the "find-by-formula" algorithm against the PlantCyc 12.6 database (Schläpfer et al., 2017), retaining only those compounds putatively annotated within 75% of replications in at least one condition (Lucini et al., 2019). Monoisotopic accurate mass was used together with the entire isotopic profile, achieving level 2 of confidence in annotation (Salek et al., 2015).

Statistical Analysis

Data from each species were subjected to a one-way ANOVA using IBM SPSS Statistics software (SPSS Inc., Chicago, IL, United States) version 26 for Windows 11 and presented as mean ± standard error, $n = 3$. Statistical significance was determined using Tukey's HSD test at the $p = 0.05$ level. All seedling responses to changing light intensity and quality on morphometric and quality indices, minerals, colorimetric parameters, and pigment accumulation were summarized *via* color heatmaps generated using the web-based tool ClustVis[1]. The Euclidean distance was used as a measure of similarity and hierarchical clustering with full link heatmaps, and the data were normalized [ln(x + 1)] and displayed using a false-color scale (red = increase in values; blue = decrease in values) (Modarelli et al., 2020).

The chemometric interpretation of the metabolic features was conducted with Mass Profiler Professional B 0.15.1 (Agilent Technologies, Stevens Creek Blvd, Santa Clara, CA, United States), as previously described in our study (Benjamin et al., 2019). Using this software, the raw metabolomic data set was transformed and normalized and then used for fold-change analysis. For this purpose, supervised orthogonal projections to latent structures discriminant analysis (OPLS-DA), using SIMCA 16 (Umetrics, Malmo, Sweden), was performed considering all the species together and only the nets as a factor. Subsequently, the OPLS-DA model was validated, and model fitness parameters (goodness of fit: R^2Y; goodness of prediction: Q^2Y) were inspired through the permutation test ($n = 100$) and Hotelling's T2 (95% and 99% confidence limit for the suspect and strong outliers, respectively). Then, the variable importance in projection (VIP ≥ 1.3) was adopted to identify discriminant metabolites among different treatments for the four species, and the resulted compounds were subjected to a fold-change (FC) to better understand the differences among treatments compared to the unshading plants. After that, VIP markers were uploaded into the Omic Viewer Pathway Tool of PlantCyc (Stanford, CA, United States) to identify the pathways and processes affected by treatments.

RESULTS AND DISCUSSION

Effects of Light Intensity and Quality on Morphometric and Seedling Quality Indices

Light plays a pivotal role in regulating physiological and critical processes in plants (Devlin et al., 2007; Folta and Carvalho, 2015; Ajdanian et al., 2019). Through complex mechanisms, plants capture light reaching their leaves and activate molecular pathways to acclimate to specific light environments (Paik and Huq, 2019). However, the productive performance also depends on light quality, which can trigger particular gene expressions that have a different impact on plant survival (Franco et al., 2006; Huché-Thélier et al., 2016; Lin et al., 2019; Paradiso and Proietti, 2021). The morphometric indices in **Table 1** show a significant effect of light intensity and quality on plant height. Except for zucchini squash seedlings, shading treatments (Black and Blue net) increased, on average, watermelon, tomato, and eggplant seedling size by 24.36%, 35.91%, and 28.04%, respectively, compared to the unshaded treatment (No shading).

The increase in plant height in our experiment is a typical phenotypic response to the so-called "shade avoidance syndrome" in light-demanding plants (**Figure 1**; Keuskamp et al., 2012). In the shade, light-demanding plants detect light depletion through specific photoreceptors such as phytochromes (Morelli and Ruberti, 2002), and they trigger morphological changes that promote stem elongation through a complex network of hormones and transcriptional regulators

[1]https://biit.cs.ut.ee/clustvis/; accessed January 3, 2022.

(Smith, 1995; Smith and Whitelam, 1997; Ballaré, 1999; Morelli and Ruberti, 2000). As reported by Casal (2013) and Ballaré and Pierik (2017), under shading, the active state of phytochrome B (Pfr) is converted to the inactive state (Pr). This conversion releases the negative feedback of phytochrome B on phytochrome interacting factors (PIFs), leading to auxin and gibberellin production that results in cell elongation, thus ensuring better light accessibility to plants. Similarly, plants' changes in the spectral light quality are detected as a warning signal of future competition. The literature has well documented that the depletion of blue light, or its limited availability, can prompt stem elongation due to an attenuation of the cryptochrome-PIFs interaction (Folta and Carvalho, 2015; Ma et al., 2016; Pedmale et al., 2016). In the present investigation, increasing the percentage of blue light in the light spectrum by photoselective blue net (Black net: R/B = 1.4, Blue net: R/B = 1; **Supplementary Figure 2**) decreased the height of plants, compared to the black net (**Table 1**). Similar to phytochromes, the effects of blue light on cryptochromes generate signals that suppress gibberellin and auxin syntheses, affecting gene expression involved in elongation repression (Folta et al., 2003). Our results are consistent with previous studies on light-demanding plants such as tomato seedlings (Glowacka, 2004; Nanya et al., 2012; Wollaeger and Runkle, 2014; Hernández et al., 2016; Snowden et al., 2016), cucumber (*Cucumis sativus* L.) (Snowden, 2015; Hernández and Kubota, 2016), broccoli (*Brassica oleracea* var. italica), kohlrabi (*Brassica oleracea* Gongylodes) (Li et al., 2019) and pepper (*Capsicum annuum* L.) (Snowden, 2015) seedlings grown under an LED light.

The leaf area showed divergent trends between *Cucurbitaceae* and *Solanaceae* (**Table 1**). The unshading condition reduced leaf area in tomato and eggplant seedlings compared to the shading treatments. Probably, under high light intensity, light-demanding plants decrease leaf expansion to catch less light and limit any damage to the photosystem. The reduction in leaf area also explains the lower shoot dry weight registered for the same species (**Table 1**). Shoot dry weight reflects the net gain from photosynthesis, and its accumulation is mainly driven by the source: the sink of photosynthesis. In fact, high shoot dry weight indicates a better growth potential (Mañas et al., 2009). However, Grossnickle (2005) suggested that a high leaf weight could lead to increased transplant stress under suboptimal conditions (e.g., drought and heat) because the root system might not provide sufficient water to the leaves to maintain adequate water balance during the establishment phase. The different responses observed for leaf area and shoot dry weight in *Cucurbitaceae* could be derived from their less permanence in the nursery (12–15 days for *Cucurbitaceae* vs. 20–30 days for *Solanaceae*) and the genotypic effect (**Table 1**). In zucchini squash, regardless of light intensity, the ratio R/B = 1.4 (No shading and black net) increased leaf area and shoot dry weight, which is consistent with the findings of Hernández and Kubota (2014), who reported an increase in shoot dry weight due to a higher allocation of dry weight to the leaves. In contrast, as in eggplant seedlings, the highest leaf area in watermelon was obtained under the blue net (R/B = 1). Our results are in agreement with the reviewed literature, where XiaoYing et al. (2011) reported that an R/B = 1 ratio promoted leaf expansion in tomato seedlings by improving light absorption, while Lian et al. (2002) and Kim et al. (2004) reported similar results on light-demanding species such as Lilium (*Lilium oriental* "Pesaro") and Chrysanthemum (*Dendranthema grandiflorum* Kitam "Cheonsu").

Except for zucchini squash seedlings, shading increased the leaf area ratio (LAR; **Table 2**). As Freschet et al. (2018) reported, the LAR increased under shading due to the increased leaf area rather than the dry weight of the leaf. This result is confirmed in tomato and eggplant seedlings, where leaf areas were, on average, 50.54 and 66.88% higher than that in the unshading condition.

Regarding the effects of light quality on the root system, it should be noted that blue light promoted root growth in watermelon seedlings, resulting in a lower shoot/root ratio (**Table 1**). The shoot/root ratio is a crucial index for seedlings as it correlates with their survival (Franco et al., 2006). Indeed, reducing the shoot/root ratio reduces the plant mortality rate at transplant establishments (Franco et al., 2006). An inadequately developed root system cannot provide enough water to large shoots, making plants unsuitable for active growth (Johkan et al., 2010). In zucchini squash seedlings, the intensity and quality of light did not affect root dry weight and, consequently, shoot/root ratio. While in shading treatments, root length increased, on average, by 6.85%, compared to the unshading condition (**Table 2**). A different situation was observed for *Solanaceae*. In tomato seedlings, the black net promoted root growth (> root dry weight), while the same trend was not found in eggplant seedlings, where the blue net lowered the shoot/root ratio in shading conditions (**Table 1**). However, the lowest shoot/root ratio (1.807) was recorded under unshading conditions due to the higher root dry weight (**Table 1**).

In addition to the root system and plant height, the diameter of the stem plays a crucial role in seedling survival and growth. A larger stem diameter reduces transplant stress by improving water transport and uptake (Grossnickle and MacDonald, 2018a,b). Compared to the black net, the blue net increased the stem diameter in zucchini squash and watermelon, while no effect was observed in tomato seedlings (**Table 2**). The lowest value was obtained in the No shading treatment in eggplant seedlings, which justified the lower shoot dry weight (**Tables 1**, **2**). As Grossnickle and MacDonald (2018b) indicated, the divergent results revealed that the relationship between big stem diameter and seedling survival is not universal. The effects of blue light on stem diameter increase were previously reported in mature light-demanding plants of canola (*Brassica napus* "Modena") (Tehrani et al., 2016) and cress (*Lepidium sativum* L.) (Ajdanian et al., 2019) grown under the LED light.

The different responses of plants to the quantity and quality of light on the height and diameter of the stem were mirrored in the sturdiness index (**Table 2**). In nursery production, a lower sturdiness index indicates a better-quality plant and is an indirect parameter for evaluating the seedlings' survival rate and growth performance (Grossnickle and MacDonald, 2018b). In our study, regardless of family and species, unshading conditions and the blue net increased plant compactness (lower sturdiness index) compared to the black net (**Table 2**). The increased plant compactness was directly related to the plant height reduction

TABLE 2 | Effects of shading and light quality on quality indices of zucchini squash (*C. pepo*), watermelon (*C. lanatus),* tomato (*S. lycopersicum),* and eggplant (*S. melongena)* seedlings.

Crop	Treatment	Stem diameter	Root length	Sturdiness index	Leaf area ratio
		(cm plant^{-1})			(cm^2 mg^{-1} plant^{-1})
Zucchini squash	No shading	0.442 ± 0.001ab	11.042 ± 0.081c	5.416 ± 0.022b	0.123 ± 0.002*b*
	Black net	0.436 ± 0.003b	12.077 ± 0.100a	6.682 ± 0.410a	0.128 ± 0.001b
	Blue net	0.456 ± 0.007a	11.519 ± 0.029b	5.249 ± 0.047b	0.139 ± 0.003a
	Significance	*	***	**	**
Watermelon	No shading	0.433 ± 0.003b	11.043 ± 0.536b	6.267 ± 0.134c	0.064 ± 0.002b
	Black net	0.404 ± 0.006c	12.995 ± 0.173a	9.974 ± 0.189a	0.074 ± 0.001a
	Blue net	0.477 ± 0.002a	11.633 ± 0.394ab	7.175 ± 0.159b	0.076 ± 0.001a
	Significance	***	*	***	**
Tomato	No shading	0.262 ± 0.003	11.331 ± 0.176a	20.304 ± 0.927c	0.062 ± 0.001b
	Black net	0.266 ± 0.004	10.876 ± 0.426a	30.508 ± 0.854a	0.079 ± 0.003a
	Blue net	0.261 ± 0.000	9.371 ± 0.173b	26.993 ± 0.043b	0.079 ± 0.002a
	Significance	*ns*	**	***	**
Eggplant	No shading	0.232 ± 0.006b	10.048 ± 0.075b	15.600 ± 0.170b	0.137 ± 0.003b
	Black net	0.250 ± 0.003a	10.929 ± 0.137a	20.312 ± 0.115a	0.174 ± 0.007a
	Blue net	0.261 ± 0.002a	11.314 ± 0.187a	15.914 ± 0.155b	0.192 ± 0.003a
	Significance	**	**	***	***

*Different letters within columns indicate significant mean differences according to Tukey's HSD test (p = 0.05). ns, *** and *** denote non-significant or significant effects at p ≤ 0.05, 0.01, and 0.001, respectively. Data are mean values ± standard error, n = 3.*

TABLE 3 | Effects of shading and light quality on SPAD index and CIELab colorimetric parameters of zucchini squash (*C. pepo*), watermelon (*C. lanatus),* tomato (*S. lycopersicum),* and eggplant (*S. melongena)* seedlings.

Crop	Treatment	SPAD index	L*	a*	b*
Zucchini squash	No shading	41.102 ± 0.564	45.861 ± 0.308a	−16.977 ± 0.272	24.034 ± 0.346a
	Black net	41.593 ± 0.483	42.325 ± 0.368b	−16.017 ± 0.126	21.625 ± 0.189b
	Blue net	42.212 ± 0.054	41.576 ± 0.380b	−16.248 ± 0.366	21.469 ± 0.255b
	Significance	ns	***	ns	***
Watermelon	No shading	47.733 ± 0.044b	47.459 ± 0.056a	−15.696 ± 0.056b	24.374 ± 0.107a
	Black net	47.421 ± 0.061b	46.935 ± 0.134b	−14.850 ± 0.104a	21.779 ± 0.146b
	Blue net	48.932 ± 0.128a	46.475 ± 0.092c	−14.797 ± 0.023a	21.245 ± 0.018c
	Significance	***	***	***	***
Tomato	No shading	43.369 ± 0.477a	47.749 ± 0.202b	−15.596 ± 0.085a	25.400 ± 0.211b
	Black net	37.055 ± 0.486b	49.749 ± 0.172a	−17.784 ± 0.035c	30.038 ± 0.080a
	Blue net	37.157 ± 0.127b	49.943 ± 0.061a	−17.405 ± 0.059b	29.895 ± 0.044a
	Significance	***	***	***	***
Eggplant	No shading	39.955 ± 0.068a	44.750 ± 0.236b	−13.294 ± 0.129a	21.855 ± 0.178b
	Black net	37.336 ± 0.075b	45.848 ± 0.078a	−15.623 ± 0.018c	25.464 ± 0.693a
	Blue net	36.352 ± 0.087c	43.879 ± 0.122c	−14.301 ± 0.122b	22.203 ± 0.064b
	Significance	***	***	***	**

*Different letters within columns indicate significant mean differences according to Tukey's HSD test (p = 0.05). ns, **, and*** denote non-significant or significant effects at p ≤ 0.01 and 0.001, respectively. Data are mean values ± standard error, n = 3.*

TABLE 4 | Effects of shading and light quality on minerals accumulation of zucchini squash (*C. pepo*), watermelon (*C. lanatus),* tomato (*S. lycopersicum),* and eggplant (*S. melongena)* seedlings.

Crop	Treatment	Nitrate	P	K	Ca	Mg
		(mg kg^{-1} fw)	(g kg^{-1} dw)			
	No shading	95.494 ± 0.612c	1.661 ± 0.010b	34.934 ± 0.076a	4.009 ± 0.063a	1.906 ± 0.022b
Zucchini squash	Black net	282.574 ± 5.331a	1.759 ± 0.020a	34.391 ± 0.122b	3.741 ± 0.030b	2.039 ± 0.039a
	Blue net	198.165 ± 1.745b	1.762 ± 0.017a	33.899 ± 0.117c	3.645 ± 0.022b	1.952 ± 0.007ab
	Significance	***	**	***	**	*
	No shading	17.315 ± 0.712b	0.555 ± 0.008b	26.681 ± 0.206	5.982 ± 0.168c	1.757 ± 0.018c
Watermelon	Black net	21.312 ± 0.418a	0.579 ± 0.003ab	26.598 ± 0.117	7.156 ± 0.047b	1.935 ± 0.031b
	Blue net	22.426 ± 0.165a	0.591 ± 0.005a	26.675 ± 0.150	9.268 ± 0.243a	2.168 ± 0.050a
	Significance	***	**	*ns*	***	***
	No shading	81.002 ± 2.047a	0.686 ± 0.005b	16.148 ± 0.363b	3.842 ± 0.133b	1.495 ± 0.032b
Tomato	Black net	74.137 ± 2.800ab	0.605 ± 0.004c	16.807 ± 0.217b	6.842 ± 0.042a	1.913 ± 0.012a
	Blue net	65.958 ± 1.625b	0.780 ± 0.023a	18.503 ± 0.121a	6.597 ± 0.040a	1.999 ± 0.030a
	Significance	**	***	**	***	***
	No shading	133.763 ± 8.286c	2.814 ± 0.054a	40.201 ± 0.539a	3.336 ± 0.066a	1.929 ± 0.058b
Eggplant	Black net	237.072 ± 9.772a	1.390 ± 0.035c	35.203 ± 0.634b	3.049 ± 0.094ab	2.097 ± 0.065b
	Blue net	169.909 ± 4.223b	2.289 ± 0.007b	35.884 ± 0.386b	2.708 ± 0.106b	2.628 ± 0.045a
	Significance	***	***	***	**	***

*Different letters within columns indicate significant mean differences according to Tukey's HSD test (p = 0.05). ns, *, ** and *** denote non-significant or significant effects at p ≤ 0.05, 0.01, and 0.001, respectively. Data are mean values ± standard error, n = 3.*

TABLE 5 | Effects of shading and light quality on the accumulation of pigments of zucchini squash (*C. pepo*), watermelon (*C. lanatus),* tomato (*S. lycopersicum),* and eggplant (*S. melongena)* seedlings.

Crop	Treatment	Total Chlorophyll	Carotenoids	Chlorophyll a/b
		(mg g^{-1} fw)		
	No shading	1.741 ± 0.022c	0.237 ± 0.006a	1.378 ± 0.030a
Zucchini squash	Black net	1.885 ± 0.002b	0.210 ± 0.004b	1.308 ± 0.017a
	Blue net	2.074 ± 0.002a	0.145 ± 0.002c	1.125 ± 0.025b
	Significance	***	***	***
	No shading	1.397 ± 0.009b	0.345 ± 0.001	1.838 ± 0.005
Watermelon	Black net	1.359 ± 0.006b	0.346 ± 0.002	1.884 ± 0.045
	Blue net	1.524 ± 0.015a	0.349 ± 0.002	1.774 ± 0.036
	Significance	***	ns	ns
	No shading	1.040 ± 0.026b	0.363 ± 0.002a	1.768 ± 0.032b
Tomato	Black net	1.161 ± 0.006a	0.366 ± 0.001a	1.967 ± 0.014a
	Blue net	1.138 ± 0.007a	0.348 ± 0.003b	1.982 ± 0.021a
	Significance	**	**	***
	No shading	1.395 ± 0.004c	0.335 ± 0.003a	1.691 ± 0.020a
Eggplant	Black net	1.450 ± 0.011b	0.317 ± 0.003b	1.642 ± 0.003a
	Blue net	1.529 ± 0.017a	0.296 ± 0.005c	1.539 ± 0.007b
	Significance	***	***	***

*Different letters within columns indicate significant mean differences according to Tukey's HSD test (p = 0.05). ns, ** and *** denote non-significant or significant effects at p ≤ 0.01, and 0.001, respectively. Data are mean values ± standard error, n = 3.*

and stem diameter increase obtained in the above treatments (**Tables 1**, **2**).

Effects of Light Intensity and Quality on Colorimetric Indices of Seedlings

The perception of the world around us is determined by the mutual interaction between physical stimuli and sensory responses. Color is one of the most important sensory attributes, influencing consumer choice and decision and predicting sensorial quality attributes in food (Pathare et al., 2013). However, perceived color differences in plants are due to the concentration of natural pigments such as carotenoids, chlorophylls, anthocyanins, and flavonoids that differ according to several factors such as genotype, phenological stage, postharvest treatments, and especially

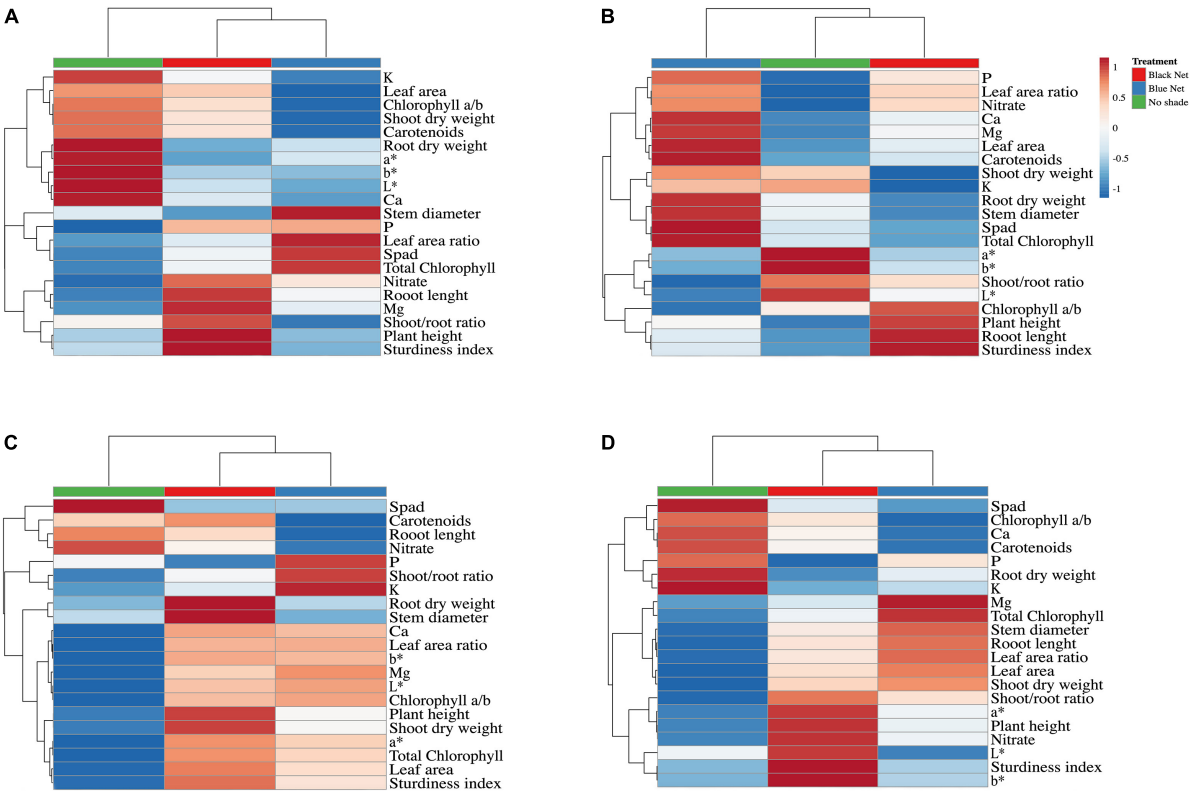

FIGURE 2 | Heatmap analysis summarizing the results of morphometric and quality indices, minerals, colorimetric parameters, and accumulation of pigments of zucchini squash (*C. pepo*) **(A)**, watermelon (*C. lanatus*) **(B)**, tomato (*S. lycopersicum*) **(C)**, and eggplant (*S. melongena*) **(D)** seedlings. Original values are ln(x + 1)-transformed. Columns with similar annotations are collapsed by taking the mean inside each group. The rows are centered; unit variance scaling is applied to the rows. Both rows and columns are clustered using Euclidean distance and complete linkage.

growth conditions (Pathare et al., 2013). Although there are no scientific contributions in the literature highlighting the key role of non-edible plant color in consumer preferences, color is also crucial in the nursery production of premium quality seedlings characterized by high compactness and vivid colors. Glossy, bright green leaf surfaces indicate high quality, associated with good water and nutritional status, and a good, well-formed, non-spiralized, non-senescent root system. Except for zucchini squash, the findings in **Table 3** showed a significant influence of the different treatments on the CIELab colorimetric parameters and the SPAD index. However, the species' response to the change in the intensity and quality of light was not univocal. In watermelon, the effects of the blue net on the morphometric and qualitative parameters were coupled with an increase in the SPAD index and a reduction in b*, compared to the other treatments (black net and No shading; **Tables 1**, **2**). However, the blue net led to the lowest L* (46.475) while the highest L* (47.459) was obtained in the No shading treatment. The same increasing trend was observed for L* and b* in zucchini squash in the No shading treatment (**Table 3**). In *Solanaceae*, the highest SPAD index was obtained in the No shading treatment. However, this finding was not associated with improved morphometric and qualitative indexes of plants grown under the same conditions (**Tables 1**, **2**). However, the most negative a* values were recorded under the black net. The lowest L* in tomato (47.749) was recorded in the No shading treatment, while in eggplant (43.879), it was recorded in the blue net treatment.

Effects of Light Intensity and Quality on Mineral and Pigment Accumulation in Seedlings

The change in intensity and quality of light affects the hormonal pathways of signal molecules involved in transmitting light signals to the roots, which regulates the uptake of nutrients in seedlings (Turnbull, 2011). Except for tomato seedlings, the unshading condition reduced nitrate (on average, −60.27, −20.82, −34.26%, in zucchini squash, watermelon, and eggplant, respectively) compared to shadings conditions (**Table 4**). Under unshading conditions, the demand for sugars and organic nitrogen is high (higher photosynthetic activity), and vacuolar nitrate is exchanged for soluble sugars and organic acids. Moreover, under shading conditions, nitrate may be a readily available vacuolar osmoticum (Poorter et al., 2019). This could explain the reduction of nitrate in our study under unshaded conditions. Compared to the No shading treatment, the blue net reduced nitrate by 18.57% in tomato seedlings. Similarly, Ohashi-Kaneko et al. (2007) and Li et al. (2019) reported

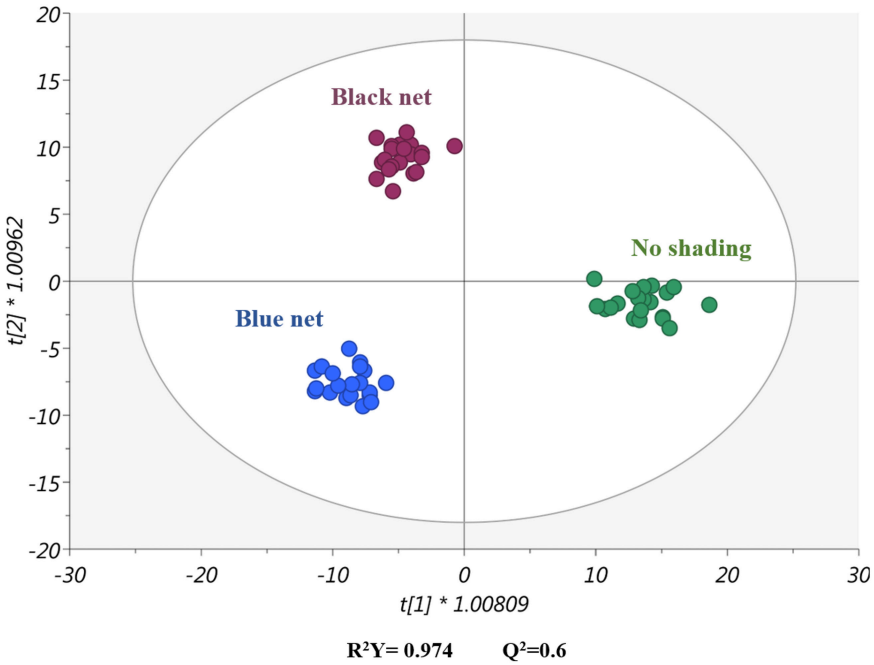

FIGURE 3 | A score plot of orthogonal projection to latent structures discriminant analysis (OPLS-DA) supervised modeling carried out on untargeted metabolomics profiles of zucchini squash (*C. pepo*), watermelon (*C. lanatus*), tomato (*S. lycopersicum*), and eggplant (*S. melongena*) leaves and considering the light quality and intensity as a factor.

nitrate reduction in plants exposed to blue light. A similar trend was observed in zucchini squash and eggplant seedlings (**Table 4**). Nitrate performs critical physiological and biochemical functions in adult plants (Hasanuzzaman et al., 2018). However, there is a lack of references and contributions explaining the importance of nitrate in vegetable seedlings in the literature. On the contrary, many authors have investigated the importance of nutritional status in forest seedlings, finding a link between nutritional status and survival in the field. Professional nursery growers use different cultural practices to harden container-grown seedlings, such as reducing day length and temperature but, most importantly, changing the fertilization regime to high-quality stock seedlings (Grossnickle, 2012). Proper fertilization in the nursery can affect the survival of seedlings after planting because they have limited ability to take the necessary nutrients from the soil during the establishment phase. A comparative study of forest seedlings (Van den Driessche, 1991) showed that adequate nursery fertilization increased field survival by about 60%. Similarly, Van den Driessche (1984) and Van den Driessche (1988) observed survival in seedlings of *Pseudotsuga menziesii* (Mirb.) Franco) was related to nitrogen concentration at planting.

Phosphorus is an essential macronutrient involved in photosynthesis, energy metabolism, respiration, and maintenance of cellular structures. It drives enzyme activation, stimulates root and stem development, and constitutes ATP and nucleic acids (DNA and RNA) (Malhotra et al., 2018). Xu et al. (2021) reported that phosphorus utilization efficiency increases with high light intensity within a threshold, beyond which adverse effects on nutrient uptake were observed. However, as observed in our study, the species do not have a univocal response (**Table 4**). In zucchini squash seedlings under unshading treatment, phosphorus decreased by 5.57%, compared to the black net. On the contrary, an opposite trend was observed in tomato and eggplant seedlings (+ 13.39 and + 102.45%, respectively), compared to the black net.

Potassium is the most abundant inorganic cation in plants that performs a wide range of metabolic functions such as osmoregulation and cell homeostasis and takes a role in enzymatic activation and protein synthesis (Amtmann and Rubio, 2012). The No shade treatment significantly increased potassium in eggplant seedlings (on average, + 13.14%) compared to shading treatments, while in tomato seedlings, the highest potassium values were obtained under the blue net (**Table 4**). Probably, blue radiation directly influenced potassium uptake. In fact, it was reported in the literature that blue light can regulate stomatal opening and, consequently, promote nutrient uptake through transpiration-induced mass flow (Kinoshita et al., 2001; Van Ieperen et al., 2012). Watermelon seedlings did not show significant differences in potassium between treatments, while in zucchini squash seedlings, the highest value (34.934 g kg^{-1} dw) was obtained in the No shading treatment (**Table 4**).

Like potassium, the highest calcium was obtained in the No shading condition in zucchini squash. In contrast, shade provided the highest calcium values in watermelon and tomato compared to the No shading treatment (**Table 4**). Under shading treatments, the highest magnesium content in watermelon, tomato, and eggplant seedlings was obtained (**Table 4**). Specifically, watermelon and eggplant showed an

increase in magnesium under the blue net, while there was no difference between shading nets in tomato seedlings. However, it should be noted that the increase in magnesium under shading treatments in tomato and eggplant seedlings was well correlated with the increase in total chlorophyll (**Table 5**). Mg is the central atom of the chlorophyll a and b porphyrin ring of green plants (Bohn et al., 2004).

Plants are endowed with sophisticated photoreceptors that transduce the light signal. Chlorophylls (a and b) absorb photons in the blue and red regions and drive metabolic processes by "collecting" energy (Carvalho et al., 2011). It is not surprising that changing the intensity and quality of light affected pigment biosynthesis. Regardless of light intensity, the light quality modification (Blue net) increased total chlorophyll in zucchini squash, watermelon and eggplant, compared to the No shading and black net treatments (**Table 5**). Plants adapt their chlorophyll pigment content to the light spectrum, and our results are in line with previous findings in lettuce (Son et al., 2012) and cucumber (Li et al., 2019). Similarly, Hogewoning et al. (2010) reported an increase in total chlorophyll in cucumber under R/B = 1 ratio, the same as the blue net used in our experiment. In watermelon, the increase in total chlorophyll under the blue net showed the same trend as the SPAD index (**Table 3**), as previously reported by Son et al. (2012) in lettuce. In tomato seedlings, the highest chlorophyll content was recorded in shading treatments (**Table 4**). Probably, tomato plants felt the reduction in light intensity (but not quality) and produced more photosynthetic pigments to absorb more light energy. Although chlorophyll content is reported in the literature as positively associated with photosynthetic capacity and indirectly with productivity (Son et al., 2012), our results do not correlate positively with shoot dry weight (**Table 1**). However, for nursery seedlings, this result could positively correlate with survival during plant establishment, in addition to providing a productive boost to adult plants.

Common adaptations to irradiation include an increase in the chlorophyll a/b ratio, a parameter that is proposed as a biological assay to evaluate the light environment (Fritschi and Ray, 2007). However, **Table 5** does not show a clear trend among species for this parameter. Under the blue net, in zucchini squash and eggplant seedlings, chlorophyll a/b ratio decreased as total chlorophyll increased, attributable to an increased chlorophyll b production under blue light (data not shown). In contrast, we observed an increase in chlorophyll a/b in tomato seedlings grown under shading compared to the No shading condition. Watermelon did not show significant differences in chlorophyll a/b or carotenoid for both intensity and quality of light.

Carotenoids are accessory pigments that capture light and transfer energy to chlorophylls and have photoprotective and antioxidant functions (Carvalho et al., 2011). In zucchini squash and eggplant seedlings, carotenoids increased as the light intensity increased (on average, + 33.52 and + 9.48%, respectively), compared to shading conditions. Our results reflect the role of carotenoids in protecting the leaves from excessive light. Carotenoids probably protected the photosynthetic machinery from high light intensity under No shading treatment (Dietz, 2015). Not least, in tomato seedlings, the blue net reduced carotenoids by 4.92 and 4.13%, compared to the black net and the No shading treatments, respectively.

Cluster Heatmap of the Effects of Light Intensity and Quality on Morphometric and Quality Indices, Minerals, Colorimetric Parameters, and Pigments Accumulation in Seedlings

Heat maps were made to provide a detailed view of the seedlings' morphometric, quality, mineral, color, and pigment parameters under different light treatments (light intensity and quality). In general, a different response was observed between families (*Solanaceae* and *Cucurbitaceae*) and between species.

Except for watermelon (**Figure 2B**), heatmaps analyses of aggregate data in zucchini squash (**Figure 2A**), tomato (**Figure 2C**), and eggplant (**Figure 2D**) identified two main clusters corresponding to the high light intensity treatment (No shading) and shading treatments (Black net and Blue net) (**Figure 2**). Two separate sub-clusters (Black net and Blue net) were defined under the second cluster indicating that shading was the main clustering factor, while light spectrum modification was the second.

In zucchini squash, blue net reduced leaf area, chlorophyll a/b ratio, shoot and root dry weight, shoot/root ratio, sturdiness index, increased stem diameter, specific leaf area, and total chlorophyll content (**Figure 2A**). Similarly, the blue net increased the stem diameter, total chlorophyll content, calcium and magnesium concentrations, and carotenoids in watermelon while reducing the shoot/root ratio and the chlorophyll a/b ratio (**Figure 2B**). In contrast to the findings of *Cucurbitaceae*, in tomato and eggplant seedlings, the blue net had less effect on size reduction (**Figure 2**). In tomato seedlings, an increase in stem diameter was observed under a black shading net, leading at the same time to the rise in height and thus to a higher sturdiness index (**Figure 2C**). In tomato seedlings, unshading conditions resulted in lower leaf area, lower chlorophyll a/b ratio, lower plant height, lower shoot/root ratio and root dry weight, lower sturdiness index, lower specific leaf area, lower total chlorophyll content (**Figure 2C**). In eggplant seedlings, the black net increased plant height and high sturdiness index. High light intensity reduced the shoot/root ratio and shoot dry weight, leaf area, specific leaf area, root length, total chlorophyll, and stem diameter while increasing the chlorophyll a/b ratio (**Figure 2D**).

Effects of Light Intensity and Quality on the Metabolic Profile of Seedlings

The metabolic profiles of *Cucurbitaceae* (zucchini and watermelon) and *Solanaceae* (tomato and eggplant) seedlings were obtained by using an untargeted metabolomics approach to better understand the effect of shading on the physiological process. More than 4,000 metabolites were detected through UHPLC-QTOF-MS analysis, and a comprehensive list of annotated compounds is reported in the **Supplementary Table 1**. To identify a general trend in plant response to light modulation, only the shading conditions were considered as a factor for supervised multivariate statistics, and all the species were

investigated together for the metabolomics analysis. The entire dataset was analyzed using the supervised OPLS-DA, resulting in a clear separation of samples in the score plot based on the net shading (**Figure 3**). In fact, the first latent vector t[1] clearly indicated that shading triggered a specific metabolic signature different from the unshading plants. Moreover, the second latent vector t[2] showed that shading plants presented a distinctive metabolic profile depending on the net (blue or black).

Therefore, as suggested by the morphometric and quality indices of seedlings, the metabolic profiles indicated a precise modulation of the leaf at the molecular level when changing light quality and intensity, which corroborates morphological changes. In this sense, Wang P. et al., 2020 reported the modulation of the biochemical fingerprint of tea plants under different light intensities, in particular under three supplemental intensities of blue light.

Once confirmed that shading strongly modulated the leaf metabolic profile regardless of the plant species, the discriminant metabolites that explain the separation of profiles in the score plot were selected by the variable importance in projection (VIP) analysis. In particular, the compound having a VIP score > 1.3 was retained for further investigation (**Supplementary Table 2**). Venn diagrams show that most compounds overlap for the black and blue net, indicating a shared effect of shading (**Figure 4A**) according to previous studies that pointed out light quality and intensity as essential factors in plant metabolism (Li et al., 2020; Wang P. et al., 2020). However, 45 and 24 compounds were down and up accumulated, respectively, in the sole presence of the black net. In comparison, 25 and 45 compounds were down and up accumulated, respectively, exclusively in the presence of the blue net. Regardless of the specific metabolites, both black and blue net presented a high ratio of down/up accumulated compounds since the black net decreased the biosynthesis of 153 compounds while increasing the biosynthesis of 86 while for the blue net 133 compounds decreased and 107 increased. Looking at the specific metabolites, the most discriminant markers were those related to terpenes and phenylpropanoids possessing the highest VIP score and indicating their strong implication in plant response to light intensity and quality, as previously reported (Wang P. et al., 2020). Nevertheless, several classes of metabolites including primary and secondary metabolism were found to be discriminant in plant response. The influence of blue light quality and intensity on plant metabolism has been previously confirmed through the metabolomic and transcriptomic approaches that revealed that low-intensity blue light, medium-intensity blue light, and high-intensity blue light triggered a reprogramming in essential physiological processes and secondary metabolism (Wang P. et al., 2020). Moreover, it has been reported that shading alters nitrogen and carbon metabolism, which explains the changes observed at the biochemical level and is supported by the nitrate concentration data under shading (Li et al., 2020; **Table 4**).

Considering the chemical diversity of VIP compounds, these 238 metabolites were further analyzed by classifying them into the plant biosynthetic pathways (**Figure 4B**). **Figure 4B** depicts the biochemical reprogramming triggered by light intensity and quality in plant leaves regardless of the species. Overall, shading seemed to positively modulate those pathways related to primary metabolism (i.e., amino acids, nucleotides, and carbohydrate biosynthesis) while compromising secondary metabolism. However, those molecules involved in several essential processes as phosphoenolpyruvate or cabamoyl-aspartate increased under shading while citrate and isocitrate decreased as a common response. Previously studies reported that energy metabolism was affected by shading. In particular, Li et al. (2020) observed a decrease in sugar content and suggested a lower need for energy under shading conditions that lead to changes in carbon flux from the synthesis of glucose to a feedback mechanism by shifting stored glucose to amino acid metabolism instead of normal carbon metabolism.

On the one hand, according to our results, Lakshmanan et al. (2015) observed an increase in the flux of metabolic pathways after blue light treatment in *Arabidopsis thaliana,* including the biosynthesis of lipids. Our findings revealed that fatty acids and lipid biosynthesis were positively regulated by the blue net rather than the black net. In agreement with our results, Wang P. et al., 2020 observed that blue light promoted lipid biosynthesis, mainly sterols and sphingolipids that are membrane structural components and might act as signal molecules. Notably, compounds classified into "cofactors, carriers, and vitamin biosynthesis" were modulated by black and blue shading. 6-methoxy-3-methyl-2-all-*trans*-decaprenyl-1,4-benzoquinol, 3-demethylubiquinol-9, 3-demethylubiquinol-9, and 3-non-aprenyl-4-hydroxybenzoate decreased under shading while 3,4-dihydroxy-5-all-*trans*-decaprenylbenzoate increased, pointing out the modulation of the ubiquinone pathway and respiratory electron transport in this response. In contrast, thiamine and thiamine diphosphate were positively regulated by the blue net and negatively modulated by the black net. Moreover, several compounds related to the biosynthesis of chlorophylls upstream (i.e., Mg-protoporphyrin, haematoporphyrin, uroporphyrin) were positively modulated under shading, according to the physiological measures including the uptake of Mg, while chlorophyll degradation products (protochlorophyll a) decreased (Bohn et al., 2004; Hernández and Kubota, 2016).

On the other hand, secondary metabolism biosynthesis was strongly repressed by both the blue and black nets. This repression is reflected in the marked down accumulation of nitrogen-containing compounds, which were the most affected class of secondary metabolites. This might be explained by the modulation in amino acid metabolism, phenylpropanoids, and terpenes being more marked for black shading (Li et al., 2020). Despite this, blue net provokes an accumulation of precursors of N-containing metabolites and the accumulation of some phenylpropanoids [dalnigrein 7-*O*-β-D-apiofuranosyl-(1–6)-β-D-glucopyranoside, amorphigenin, cyanidin 3-*O*-(6″-*O*-malonyl)-β-glucoside, 4-hydroxycoumarin] according to previous results. In fact, light intensity and shading regulate the expression of the genes and the activity of enzymes involved in the biosynthesis of flavonoids, anthocyanin, catechins, and flavanols (Li et al., 2020). In particular, blue light not only affects the synthesis of flavonoids, even if this modulation (positive or negative) depends on plant species, but also the light intensity (Wang P. et al., 2020). In addition,

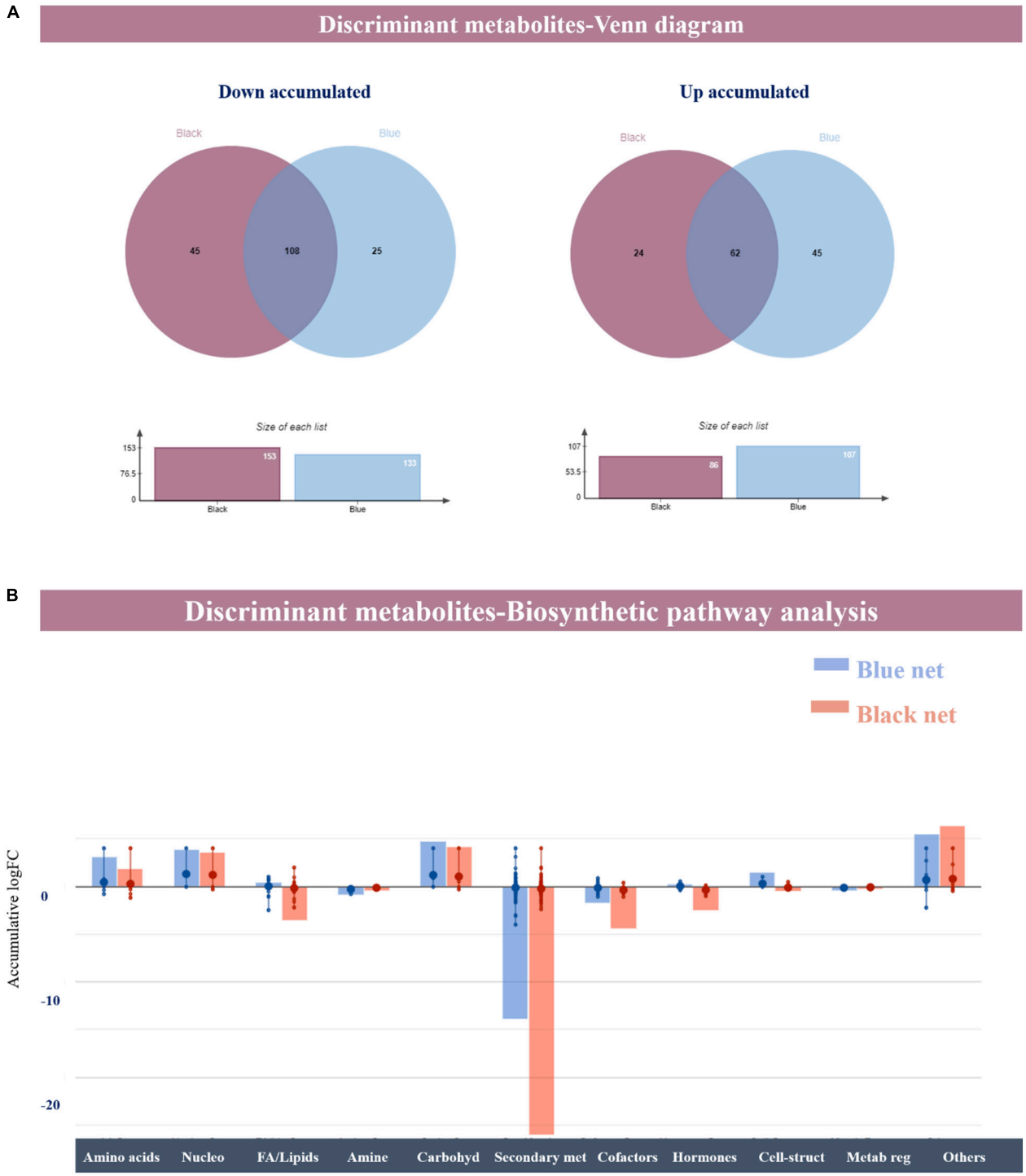

FIGURE 4 | (A) A Venn diagram summarizing the discriminant metabolites down and up accumulated under blue and black nets compared to the unshading plants, as resulted from the variable importance in projection (VIP) analysis (VIP score 1.3). **(B)** Metabolic processes are impaired by shading (blue and black net). Metabolites resulted as discriminant from the VIP analysis, and their fold-change values were elaborated using the Omic Viewer Dashboard of the PlantCyc Pathway Tool software (www.pmn.plantcyc.com). The large dots represent the average (mean) of all log Fold-change (FC) for metabolites, and the small dots represent the individual log FC for each metabolite. The x-axis represents each set of subcategories, while the y-axis corresponds to the cumulative log FC. Nucleo: nucleosides and nucleotides; FA/Lipids: fatty acids and lipids; Amines: amines and polyamines; Carbohyd: carbohydrates; Secondary met: secondary metabolism; Cofactors: cofactors, prosthetic groups, electron carriers, and vitamins; Cell-structures: plant cell structures; Metab reg: metabolic regulators.

flavonoid metabolism is also influenced by the TCA cycle and the biosynthesis of carbohydrates and amino acids, indicating a complex network between primary and secondary metabolism under shading rather than a direct effect on the specific expression of key genes (Li et al., 2020). In contrast, terpenoids seemed to be shading-specific modulated and seemed to be particularly altered by shading, as suggested by the VIP analysis. Precursors, such as mevalonate and squalene, and their final products as sterol and carotenoids and terpene hormones as brassinosteroids were specifically modulated, with their effect being stronger under blue shading in agreement with the general modulation of lipids under shading.

CONCLUSION

Light drives many vital processes in plants, which show different morphophysiological responses to varying degrees of light intensity and quality as an adaptation. For example, shading increases leaf area and pigment content, while high light intensity increases photosynthetic activity and shoot growth. However, changing light quality also induces adaptive changes in plants. Due to self-shading, blue light depletion in high-density plants reduces seedling quality (less compactness), driving producers to use chemical size regulators. In our study, we demonstrated that the response of plants to changing light intensity and quality is species-specific. Moreover, the untargeted metabolomics approach allowed us to identify a common pattern across species in response to shading. Considering that light controls essential biochemical and physiological processes, our results highlighted that both primary and secondary metabolism, together with the phytohormone profile, were largely affected by shading, resulting in a biochemical modulation much broader than photosynthesis and phytohormone profiles. These common patterns included plant energy metabolism and lipid biosynthesis and included a down accumulation of secondary pathways, particularly regarding phenylpropanoids.

The morphological changes induced by the different shading conditions corroborate the shift in metabolomic signatures we observed, indicating that a set of biological processes are modulated by shading. The comprehension of the mechanisms involved pivotally supports the implementation of photoselective shading in dedicated applications, toward the definition of more resilient crop production. Such information is of general relevance and is even more important in cropping systems under less favorable intense light conditions, where photoselective shading could represent a sustainable approach. The blue photoselective net used in our experiment modified the spectral quality of light at the canopy level, changing the blue and red portions of the light spectrum (and the relative red: blue ratio) and affecting seedling size as well as nutritional, biochemical, and physiological condition. However, a robust genotype-dependent response to light modification is evident, making further studies in other vegetable seedlings necessary to expand knowledge of the effects of blue photoselective nets.

DATA AVAILABILITY STATEMENT

The original contributions presented in the study are included in the article/**Supplementary Material**, further inquiries can be directed to the corresponding author/s.

AUTHOR CONTRIBUTIONS

LF, SDP, and YR: conceptualization and project administration. LF, BM-M, MC, LZ, SDP, LL, and YR: methodology, validation, formal analysis, investigation, writing—original draft preparation, and writing—review and editing. LF, BM-M, MC, and LZ: software and data curation. YR and SDP: resources. YR: visualization and supervision. SDP: funding acquisition. All authors contributed to the article and approved the submitted version.

ACKNOWLEDGMENTS

We would like to thank Marco Infante for technical assistance during the experiment and to Christophe El-Nakhel for critically reading the original version of the manuscript.

SUPPLEMENTARY MATERIAL

The Supplementary Material for this article can be found online at: https://www.frontiersin.org/articles/10.3389/fpls.2022.890830/full#supplementary-material

Supplementary Figure 1 | Effects of shading nets on photosynthetically active radiation (PAR). Data are mean values ± standard error, $n = 3$. All mean effects were subjected to a one-way ANOVA analysis. Statistical significance was determined with Tukey's HSD test at the $p = 0.05$ level.

Supplementary Figure 2 | Red:blue ratios of plastic film (No shade), black shading net (Black net), and blue photoselective shading net (Blue net).

Supplementary Figure 3 | Complete light spectrum under each net at the surface level of the plants.

Supplementary Table 1 | Metabolic profile of *Cucurbitaceae* (zucchini and watermelon) and *Solanaceae* (tomato and eggplant) seedling.

Supplementary Table 2 | List of compounds with a variable importance in projection (VIP) score > 1.3.

REFERENCES

Ajdanian, L., Babaei, M., and Aroiee, H. (2019). The growth and development of cress (*Lepidium sativum*) affected by blue and red light. *Heliyon* 5:e02109. doi: 10.1016/j.heliyon.2019.e02109

Amtmann, A., and Rubio, F. (2012). "Potassium in plants," in *eLS*, ed. A. M. Hetherington (Chichester: John Wiley & Sons, Ltd). doi: 10.1002/9780470015902.a0023737

Ballaré, C. L. (1999). Keeping up with the neighbours: phytochrome sensing and other signalling mechanisms.

Trends Plant Sci. 4, 97–102. doi: 10.1016/S1360-1385(99)01383-7

Ballaré, C. L., and Pierik, R. (2017). The shade-avoidance syndrome: multiple signals and ecological consequences. *Plant Cell Environ.* 40, 2530–2543. doi: 10.1111/pce.12914

Benjamin, J. J., Lucini, L., Jothiramshekar, S., and Parida, A. (2019). Metabolomic insights into the mechanisms underlying tolerance to salinity in different halophytes. *Plant Physiol. Biochem.* 135, 528–545. doi: 10.1016/j.plaphy.2018.11.006

Bohn, T., Walczyk, T., Leisibach, S., and Hurrell, R. F. (2004). Chlorophyll-bound magnesium in commonly and consumed vegetables and fruits: relevance to magnesium nutrition. *J. Food Sci.* 69, S347–S350. doi: 10.1111/j.1365-2621.2004.tb09947.x

Carvalho, R. F., Takaki, M., and Azevedo, R. A. (2011). Plant pigments: the many faces of light perception. *Acta Physiol. Plant.* 33, 241–248. doi: 10.1007/s11738-010-0533-7

Casal, J. J. (2013). Photoreceptor signaling networks in plant responses to shade. *Annu. Rev. Plant Biol.* 64, 403–427. doi: 10.1146/annurev-arplant-050312-120221

Devlin, P. F., Christie, J. M., and Terry, M. J. (2007). Many hands make light work. *J. Exp. Bot.* 58, 3071–3077.

Dietz, K. J. (2015). Efficient high light acclimation involves rapid processes at multiple mechanistic levels. *J. Exp. Bot.* 66, 2401–2414. doi: 10.1093/jxb/eru505

Ferrante, A., and Mariani, L. (2018). Agronomic management for enhancing plant tolerance to abiotic stresses: high and low values of temperature, light intensity, and relative humidity. *Horticulturae* 4:21. doi: 10.3390/horticulturae4030021

Folta, K. M., and Carvalho, S. D. (2015). Photoreceptors and control of horticultural plant traits. *HortScience* 50, 1274–1280. doi: 10.21273/hortsci.50.9.1274

Folta, K. M., Pontin, M. A., Karlin-Neumann, G., Bottini, R., and Spalding, E. P. (2003). Genomic and physiological studies of early cryptochrome 1 action demonstrate roles for auxin and gibberellin in the control of hypocotyl growth by blue light. *Plant J.* 36, 203–214. doi: 10.1046/j.1365-313X.2003.01870.x

Formisano, L., Ciriello, M., El-Nakhel, C., De Pascale, S., and Rouphael, Y. (2021a). Dataset on the effects of anti-insect nets of different porosity on mineral and organic acids profile of *Cucurbita pepo* L. Fruits and leaves. *Data* 6:50. doi: 10.3390/data6050050

Formisano, L., Ciriello, M., El-Nakhel, C., Poledica, M., Starace, G., Graziani, G., et al. (2021b). Pearl grey shading net boosts the accumulation of total carotenoids and phenolic compounds that accentuate the antioxidant activity of processing tomato. *Antioxidants* 10:1999. doi: 10.3390/antiox10121999

Franco, J. A., Martínez-Sánchez, J. J., Fernández, J. A., and Bañón, S. (2006). Selection and nursery production of ornamental plants for landscaping and xerogardening in semi-arid environments. *J. Hortic. Sci. Biotechnol.* 81, 3–17. doi: 10.1080/14620316.2006.11512022

Freschet, G. T., Violle, C., Bourget, M. Y., Scherer-Lorenzen, M., and Fort, F. (2018). Allocation, morphology, physiology, architecture: the multiple facets of plant above- and below-ground responses to resource stress. *New Phytol.* 219, 1338–1352. doi: 10.1111/nph.15225

Fritschi, F. B., and Ray, J. D. (2007). Soybean leaf nitrogen, chlorophyll content, and chlorophyll a/b ratio. *Photosynthetica* 45, 92–98. doi: 10.1007/s11099-007-0014-4

Glowacka, B. (2004). The effect of blue light on the height and habit of the tomato (Lycopersicon esculentum Mill.). *Folia Hortic.* 16, 3–10.

Grossnickle, S. C. (2005). Importance of root growth in overcoming planting stress. *New For.* 30, 273–294. doi: 10.1007/s11056-004-8303-2

Grossnickle, S. C. (2012). Why seedlings survive: influence of plant attributes. *New For.* 43, 711–738. doi: 10.1007/s11056-012-9336-6

Grossnickle, S. C., and MacDonald, J. E. (2018a). Seedling quality: History, application, and plant attributes. *Forests* 9:283. doi: 10.3390/F9050283

Grossnickle, S. C., and MacDonald, J. E. (2018b). Why seedlings grow: influence of plant attributes. *New For.* 49, 711–738. doi: 10.1007/s11056-017-9606-4

Hasanuzzaman, M., Fujita, M., Oku, H., Nahar, K., and Hawrylak-Nowak, B. (2018). *Plant Nutrients and Abiotic Stress Tolerance*. Singapore: Springer, 221–252.

Hernández, R., Eguchi, T., Deveci, M., and Kubota, C. (2016). Tomato seedling physiological responses under different percentages of blue and red photon flux ratios using LEDs and cool white fluorescent lamps. *Sci. Hortic.* 213, 270–280. doi: 10.1016/j.scienta.2016.11.005

Hernández, R., and Kubota, C. (2014). Growth and morphological response of cucumber seedlings to supplemental red and blue photon flux ratios under varied solar daily light integrals. *Sci. Hortic.* 173, 92–99. doi: 10.1016/j.scienta.2014.04.035

Hernández, R., and Kubota, C. (2016). Physiological responses of cucumber seedlings under different blue and red photon flux ratios using LEDs. *Environ. Exp. Bot.* 121, 66–74. doi: 10.1016/j.envexpbot.2015.04.001

Hogewoning, S. W., Trouwborst, G., Maljaars, H., Poorter, H., van Ieperen, W., and Harbinson, J. (2010). Blue light dose-responses of leaf photosynthesis, morphology, and chemical composition of *Cucumis sativus* grown under different combinations of red and blue light. *J. Exp. Bot.* 61, 3107–3117. doi: 10.1093/jxb/erq132

Huché-Thélier, L., Crespel, L., Gourrierec, J. L., Morel, P., Sakr, S., and Leduc, N. (2016). Light signaling and plant responses to blue and UV radiations-Perspectives for applications in horticulture. *Environ. Exp. Bot.* 121, 22–38. doi: 10.1016/j.envexpbot.2015.06.009

Johkan, M., Shoji, K., Goto, F., Hashida, S. N., and Yoshihara, T. (2010). Blue light-emitting diode light irradiation of seedlings improves seedling quality and growth after transplanting in red leaf lettuce. *HortScience* 45, 1809–1814. doi: 10.21273/hortsci.45.12.1809

Keuskamp, D. H., Keller, M. M., Ballaré, C. L., and Pierik, R. (2012). Blue light regulated shade avoidance. *Plant Signal. Behav.* 7, 514–517. doi: 10.4161/psb.19340

Kim, S. J., Hahn, E. J., Heo, J. W., and Paek, K. Y. (2004). Effects of LEDs on net photosynthetic rate, growth and leaf stomata of chrysanthemum plantlets in vitro. *Sci. Hortic.* 101, 143–151. doi: 10.1016/j.scienta.2003.10.003

Kinoshita, T., Doi, M., Suetsugu, N., Kagawa, T., Wada, M., and Shimazaki, K. I. (2001). Phot1 and Phot2 Mediate Blue Light Regulation of Stomatal Opening. *Nature* 414, 656–660. doi: 10.1038/414656a

Lakshmanan, M., Lim, S. H., Mohanty, B., Kim, J. K., Ha, S. H., and Lee, D. Y. (2015). Unraveling the light-specific metabolic and regulatory signatures of rice through combined in silico modeling and multiomics analysis. *Plant Physiol.* 169, 3002–3020. doi: 10.1104/pp.15.01379

Li, Y., Jeyaraj, A., Yu, H., Wang, Y., Ma, Q., Chen, X., et al. (2020). Metabolic regulation profiling of carbon and nitrogen in tea plants [*Camellia sinensis* (L.) O. Kuntze] in response to shading. *J. Agric. Food Chem.* 68, 961–974. doi: 10.1021/acs.jafc.9b05858

Li, Y., Zheng, Y., Liu, H., Zhang, Y., Hao, Y., Song, S., et al. (2019). Effect of supplemental blue light intensity on the growth and quality of Chinese kale. *Hortic. Environ. Biotechnol.* 60, 49–57. doi: 10.1007/s13580-018-0104-1

Lian, M.-L., Murthy, H. N., and Paek, K.-Y. (2002). Effects of light emitting diodes (LEDs) on the in vitro induction and growth of bulblets of Lilium oriental hybrid 'Pesaro.'. *Sci. Hortic.* 94, 365–370. doi: 10.1016/s0304-4238(01)00385-5

Lin, K. H., Wu, C. W., and Chang, Y. S. (2019). Applying Dickson quality index, chlorophyll fluorescence, and leaf area index for assessing plant quality of Pentas lanceolata. *Not. Bot. Horti Agrobot. Cluj-Napoca* 47, 169–176. doi: 10.15835/nbha47111312

Lucini, L., Colla, G., Miras Moreno, M. B., Bernardo, L., Cardarelli, M., Terzi, V., et al. (2019). Inoculation of *Rhizoglomus irregulare* or *Trichoderma* atroviride differentially modulates metabolite profiling of wheat root exudates. *Phytochemistry* 157, 158–167. doi: 10.1016/j.phytochem.2018.10.033

Ma, D., Li, X., Guo, Y., Chu, J., Fang, S., Yan, C., et al. (2016). Cryptochrome 1 interacts with PIF4 to regulate high temperature-mediated hypocotyl elongation in response to blue light. *Proc. Natl. Acad. Sci. U.S.A.* 113, 224–229. doi: 10.1073/pnas.1511437113

Malhotra, H., Sharma, V. S., and Pandey, R. (2018). "Phosphorus nutrition: Plant growth in response to deficiency and excess," in *Plant Nutrients and Abiotic Stress Tolerance*, eds M. Hasanuzzaman, M. Fujita, H. Oku, K. Nahar, and B. Hawrylak-Nowak (Singapore: Springer), 171–190. doi: 10.1007/978-981-10-9044-8_7

Mañas, P., Castro, E., and De Las Heras, J. (2009). Quality of maritime pine (*Pinus pinaster* Ait.) seedlings using waste materials as nursery growing media. *New For.* 37, 295–311. doi: 10.1007/s11056-008-9125-4

Modarelli, G. C., Arena, C., Pesce, G., Dell'Aversana, E., Fusco, G. M., Carillo, P., et al. (2020). The role of light quality of photoperiodic lighting on

photosynthesis, flowering and metabolic profiling in *Ranunculus asiaticus* L. *Physiol. Plant.* 170, 187–201. doi: 10.1111/ppl.13122

Morelli, G., and Ruberti, I. (2000). Shade avoidance responses. driving auxin along lateral routes. *Plant Physiol.* 122, 621–626. doi: 10.1104/pp.122.3.621

Morelli, G., and Ruberti, I. (2002). Light and shade in the photocontrol of *Arabidopsis* growth. *Trends Plant Sci.* 7, 399–404. doi: 10.1016/S1360-1385(02)02314-2

Nanya, K., Ishigami, Y., Hikosaka, S., and Goto, E. (2012). "Effects of blue and red light on stem elongation and flowering of tomato seedlings," in *Acta Horticulturae*, eds S. Hemming and E. Heuvelink (Wageningen: The Netherlands: ISHS Acta Horticulturae), 261–266. doi: 10.17660/ActaHortic.2012.956.29

Ohashi-Kaneko, K., Tarase, M., Noya, K. O. N., Fujiwara, K., and Kurata, K. (2007). Effect of light quality on growth and vegetable quality in leaf lettuce, spinach and komatsuna. *Environ. Control Biol.* 45, 189–198. doi: 10.2525/ecb.45.189

Ouzounis, T., Rosenqvist, E., and Ottosen, C. O. (2015). Spectral effects of artificial light on plant physiology and secondary metabolism: a review. *HortScience* 50, 1128–1135. doi: 10.21273/hortsci.50.8.1128

Paik, I., and Huq, E. (2019). Plant photoreceptors: Multi-functional sensory proteins and their signaling networks. *Semin. Cell Dev. Biol.* 92, 114–121. doi: 10.1016/j.semcdb.2019.03.007

Paradiso, R., and Proietti, S. (2021). Light-Quality manipulation to control plant growth and photomorphogenesis in greenhouse horticulture: the state of the art and the opportunities of modern LED Systems. *J. Plant Growth Regul.* 41, 742–780. doi: 10.1007/s00344-021-10337-y

Pathare, P. B., Opara, U. L., and Al-Said, F. A. J. (2013). Colour Measurement and analysis in fresh and processed foods: a review. *Food Bioproc. Tech.* 6, 36–60. doi: 10.1007/s11947-012-0867-9

Pedmale, U. V., Huang, S. S. C., Zander, M., Cole, B. J., Hetzel, J., Ljung, K., et al. (2016). Cryptochromes interact directly with pifs to control plant growth in limiting blue light. *Cell* 164, 233–245. doi: 10.1016/j.cell.2015.12.018

Poorter, H., Niinemets, Ü, Ntagkas, N., Siebenkäs, A., Mäenpää, M., Matsubara, S., et al. (2019). A meta-analysis of plant responses to light intensity for 70 traits ranging from molecules to whole plant performance. *New Phytol.* 223, 1073–1105. doi: 10.1111/nph.15754

Rani, A., Donovan, N., and Mantri, N. (2019). Review: The future of plant pathogen diagnostics in a nursery production system. *Biosens. Bioelectron.* 145:111631. doi: 10.1016/j.bios.2019.111631

Rouphael, Y., Colla, G., Hoagland, L., Giordano, M., El-Nakhel, C., and Cardarelli, M. (2021). Vegetal-protein hydrolysates based microgranule enhances growth, mineral content, and quality traits of vegetable transplants. *Sci. Hortic.* 290:110554. doi: 10.1016/j.scienta.2021.110554

Salek, R. M., Neumann, S., Schober, D., Hummel, J., Billiau, K., Kopka, J., et al. (2015). COordination of Standards in MetabOlomicS (COSMOS): facilitating integrated metabolomics data access. *Metabolomics* 11, 1587–1597. doi: 10.1007/s11306-015-0810-y

Schläpfer, P., Zhang, P., Wang, C., Kim, T., Banf, M., Chae, L., et al. (2017). Genome-wide prediction of metabolic enzymes, pathways, and gene clusters in plants. *Plant Physiol.* 173, 2041–2059. doi: 10.1104/pp.16.01942

Smith, H. (1995). Physiological and ecological function within the phytochrome family. *Annu. Rev. Plant Physiol. Plant Mol. Biol.* 46, 289–315. doi: 10.1146/annurev.pp.46.060195.001445

Smith, H., and Whitelam, G. C. (1997). The shade avoidance syndrome: Multiple responses mediated by multiple phytochromes. *Plant Cell Environ.* 20, 840–844. doi: 10.1046/j.1365-3040.1997.d01-104.x

Snowden, M. C. (2015). *Effects of Blue and Green Light on Plant Growth and Development at Low and High Photosynthetic Photon Flux* Master of Science Thesis. Logan, UT: Utah State Univ. Digit, 57.

Snowden, M. C., Cope, K. R., and Bugbee, B. (2016). Sensitivity of seven diverse species to blue and green light: interactions with photon flux. *PLoS One* 11:e0163121. doi: 10.1371/journal.pone.0163121

Son, K.-H., Park, J.-H., Kim, D., and Oh, M.-M. (2012). Leaf shape index, growth, and phytochemicals in two leaf lettuce cultivars grown under monochromatic light-emitting diodes. *Hortic. Sci. Technol.* 30, 664–672. doi: 10.7235/hort.2012.12063

Tehrani, P. F., Majd, A., Mahmoodzadeh, H., and Satari, T. N. (2016). Effect of red and blue light-emitting diodes on germination, morphological and anatomical features of *Brassica napus*. *Adv. Stud. Biol.* 8, 173–180. doi: 10.12988/asb.2016.6832

Timpanaro, G., Urso, A., and Foti, V. T. (2018). Technical and scale efficiency in nursery enterprises in an area of significant widespread horticulture in Italy. *HortScience* 53, 208–216. doi: 10.21273/HORTSCI12344-17

Turnbull, C. (2011). Long-distance regulation of flowering time. *J. Exp. Bot.* 62, 4399–4413. doi: 10.1093/jxb/err191

Van den Driessche, R. (1984). Relationship between spacing and nitrogen fertilization of seedlings in the nursery, seedling mineral nutrition, and outplanting performance. *Can. J. For. Res.* 14, 431–436. doi: 10.1139/x84-076

Van den Driessche, R. (1988). Nursery growth of conifer seedlings using fertilizers of different solubilities and application time, and their forest growth. *Can. J. For. Res.* 18, 172–180. doi: 10.1139/x88-027

Van den Driessche, R. (1991). "Effects of nutrients on stock performance in the forest," in *Mineral Nutrition of Conifer Seedlings*, ed. R. van den Driessche (Boca Raton, FL: CRC Press), 229–260.

Van Ieperen, W., Savvides, A., and Fanourakis, D. (2012). Red and blue light effects during growth on hydraulic and stomatal conductance in leaves of young cucumber plants. *Acta Hortic* 956, 223–230. doi: 10.17660/actahortic.2012.956.24

Walter, A., and Nagel, K. A. (2006). Root growth reacts rapidly and more pronounced than shoot growth towards increasing light intensity in tobacco seedlings. *Plant Signal. Behav.* 1, 225–226. doi: 10.4161/psb.1.5.3447

Wang, P., Chen, S., Gu, M., Chen, X., Chen, X., Yang, J., et al. (2020). Exploration of the effects of different blue led light intensities on flavonoid and lipid metabolism in tea plants via transcriptomics and metabolomics. *Int. J. Mol. Sci.* 21:4606. doi: 10.3390/ijms21134606

Wang, X., Gao, X., Liu, Y., Fan, S., and Ma, Q. (2020). Progress of research on the regulatory pathway of the plant shade-avoidance syndrome. *Front. Plant Sci.* 11:439. doi: 10.3389/fpls.2020.00439

Wollaeger, H. M., and Runkle, E. S. (2014). Growth of impatiens, petunia, salvia, and tomato seedlings under blue, green, and red light-emitting diodes. *HortScience* 49, 734–740. doi: 10.21273/hortsci.49.6.734

XiaoYing, L., ShiRong, G., ZhiGang, X., XueLei, J., and Tezuka, T. (2011). Regulation of chloroplast ultrastructure, cross-section anatomy of leaves, and morphology of stomata of cherry tomato by different light irradiations of light-emitting diodes. *HortScience* 46, 217–221. doi: 10.21273/hortsci.46.2.217

Xu, J., Guo, Z., Jiang, X., Ahammed, G. J., and Zhou, Y. (2021). Light regulation of horticultural crop nutrient uptake and utilization. *Hortic. Plant J.* 7, 367–379. doi: 10.1038/s41467-021-20964-4

Conflict of Interest: The authors declare that the research was conducted in the absence of any commercial or financial relationships that could be construed as a potential conflict of interest.

Publisher's Note: All claims expressed in this article are solely those of the authors and do not necessarily represent those of their affiliated organizations, or those of the publisher, the editors and the reviewers. Any product that may be evaluated in this article, or claim that may be made by its manufacturer, is not guaranteed or endorsed by the publisher.

frontiers | Frontiers in Plant Science

REVIEW
published: 25 May 2022
doi: 10.3389/fpls.2022.884572

γ-Aminobutyrate Improves the Postharvest Marketability of Horticultural Commodities: Advances and Prospects

*Morteza Soleimani Aghdam[1], Edward J. Flaherty[2] and Barry J. Shelp[2]**

[1] Department of Horticultural Science, Imam Khomeini International University, Qazvin, Iran, [2] Department of Plant Agriculture, University of Guelph, Guelph, ON, Canada

Postharvest deterioration can result in qualitative and quantitative changes in the marketability of horticultural commodities, as well as considerable economic loss to the industry. Low temperature and controlled atmosphere conditions (low O_2 and elevated CO_2) are extensively employed to prolong the postharvest life of these commodities. Nevertheless, they may suffer from chilling injury and other physiological disorders, as well as excessive water loss and bacterial/fungal decay. Research on the postharvest physiological, biochemical, and molecular responses of horticultural commodities indicates that low temperature/controlled atmosphere storage is associated with the promotion of γ-aminobutyrate (GABA) pathway activity, with or without the accumulation of GABA, delaying senescence, preserving quality and ameliorating chilling injury. Regardless of whether apple fruits are stored under low temperature/controlled atmosphere conditions or room temperature, elevated endogenous GABA or exogenous GABA maintains their quality by stimulating the activity of the GABA shunt (glutamate GABA succinic semialdehyde succinate) and the synthesis of malate, and delaying fruit ripening. This outcome is associated with changes in the genetic and biochemical regulation of key GABA pathway reactions. Flux estimates suggest that the GABA pool is derived primarily from glutamate, rather than polyamines, and that succinic semialdehyde is converted mainly to succinate, rather than γ-hydroxybutyrate. Exogenous GABA is a promising strategy for promoting the level of endogenous GABA and the activity of the GABA shunt in both intact and fresh-cut commodities, which increases carbon flux through respiratory pathways, restores or partially restores redox and energy levels, and improves postharvest marketability. The precise mechanisms whereby GABA interacts with other signaling molecules such as Ca^{2+}, H_2O_2, polyamines, salicylic acid, nitric oxide and melatonin, or with phytohormones such as ethylene, abscisic acid and auxin remain unknown. The occurrence of the aluminum-activated malate transporter and the glutamate/aspartate/GABA exchanger in the tonoplast, respectively, offers prospects for reducing transpirational water in cut flowers and immature green fruit, and for altering the development, flavor and biotic resistance of apple fruits.

Keywords: γ-aminobutyrate, biostimulants, horticultural commodities, marketability, postharvest stress

OPEN ACCESS

Edited by:
María Serrano, Miguel Hernández University of Elche, Spain

Reviewed by:
Milan Skalicky, Czech University of Life Sciences Prague, Czechia
Shaghef Ejaz, Bahauddin Zakariya University, Pakistan

***Correspondence:**
Barry J. Shelp
bshelp@uoguelph.ca

Specialty section:
This article was submitted to Crop and Product Physiology, a section of the journal Frontiers in Plant Science

Received: *26 February 2022*
Accepted: *11 April 2022*
Published: *25 May 2022*

Citation:
Aghdam MS, Flaherty EJ and Shelp BJ (2022) γ -Aminobutyrate Improves the Postharvest Marketability of Horticultural Commodities: Advances and Prospects. Front. Plant Sci. 13:884572. doi: 10.3389/fpls.2022.884572

INTRODUCTION

Fruits, vegetables and nuts are a crucial part of a healthy diet, which can help reduce risk factors for non-communicable diseases. Increasingly, consumers are concerned with the nutritional quality of these commodities (Kyriacou and Rouphael, 2018; Ziv and Fallik, 2021). Postharvest deterioration can result in qualitative and quantitative changes in their marketability, as well as incredible economic losses to the horticultural industry. Low temperature (LT) and controlled atmosphere (CA) conditions (low O_2 and elevated CO_2) are extensively employed to prolong the postharvest life of horticultural crops. However, horticultural crops may suffer from chilling injury and other physiological disorders, as well as excessive water loss and fungal decay (e.g., Lum et al., 2016b; Tarkowski et al., 2020; Ziv and Fallik, 2021).

The exogenous application of biostimulants, including naturally occurring plant metabolites and hormones such as polyamines (PA), salicylate, jasmonate, melatonin and γ-aminobutyrate (GABA), is being studied to improve plant tolerance/resistance to abiotic and biotic stresses under both open and closed environmental conditions (Bor and Turkan, 2019; Podlešákova et al., 2019; Akula and Mukherjee, 2020; Godoy et al., 2021; Shelp et al., 2021). The metabolism, transport, and signaling role(s) of GABA in plants were recently reviewed (Shelp et al., 2021; Xu et al., 2021b; Suhel et al., 2022). Stress-induced promotion of GABA pathways in vegetative plants, and the physiological, biochemical and molecular responses associated with enhancing stress tolerance *via* genetic manipulation of GABA metabolism and GABA receptors or the use of exogenous GABA were described (Shelp et al., 2021). Of particular interest is the demonstration that drought-induced GABA accumulation in the guard cell functions as an abscisic acid-independent mechanism for reducing stomatal reopening and transpirational water loss, thereby improving drought tolerance (Bown and Shelp, 2016; Mekonnen et al., 2016; Shelp et al., 2021; Xu et al., 2021b). GABA binds to aluminum-activated malate transporters (ALMT9/12 signaling pathway) and negatively regulates malate and/or Cl^- transport (Xu et al., 2021b).

This review focuses on postharvest horticultural commodities, with emphasis on botanical fruits, though some discussion of root, leaf and ornamental crops, as well as walnuts and mushrooms, is also included. First, we describe how LT and CA storage conditions improve marketability and promote GABA metabolism. Second, we discuss the genetic and biochemical control of GABA metabolism and signaling in apple fruits, and the use of exogenous GABA to preserve the postharvest quality of stored and fresh-cut horticultural commodities (i.e., delaying senescence, and enhancing resistance to chilling, browning, disease and physiological disorders) by promoting GABA shunt activity, energy generation, and antioxidant and secondary pathways. Third, we discuss prospects for enhancing postharvest drought tolerance, pathogen resistance, and flavor using exogenous GABA. Finally, we briefly comment on the safety and commercial production of GABA.

POSTHARVEST MARKETABILITY OF HORTICULTURAL COMMODITIES IS LINKED TO GABA METABOLISM, AND ANTIOXIDANT AND SECONDARY PATHWAYS

Low Temperature and Controlled Atmosphere Storage

During the postharvest storage of horticultural commodities, temperature and/or atmospheric conditions are adjusted so that ethylene production and respiratory rates are reduced, and ripening/senescence is delayed, resulting in the preservation of nutritional and sensory quality (**Table 1**). LT storage of mulberry leaves in air preserves color, while enhancing GABA accumulation (Li E. et al., 2018), as is often found in the vegetative organs of many plant species (Shelp et al., 2021). This result might be attributed to the elevated activity of glutamate (Glu) decarboxylase (GAD) and limited activity of the catabolic enzyme GABA transaminase (GABA-T) (**Figure 1**). In contrast, the LT storage of zucchini fruit promotes GABA catabolism, without causing its accumulation (Palma et al., 2014). The loss of GABA and the increase in GABA-T activity is more substantive in a chilling-tolerant cultivar than a chilling-sensitive cultivar, suggesting that GABA catabolism replenishes the tricarboxylic acid cycle (TCAC) to generate reducing equivalents and energy that could alleviate oxidative damage (Shelp et al., 2021). The authors have interpreted the increase in diamine oxidase (DAO) activity and putrescine (Put) accumulation as support for the involvement of Put catabolism in GABA production and the alleviation of chilling injury (**Figure 1**). Conditioning at 15°C prior to LT storage improves the tolerance in the chilling-sensitive zucchini cultivar by decreasing the GABA level and increasing the ATP level and activities of enzymatic antioxidants (peroxidase, catalase) (Carvajal et al., 2015). Improved chilling tolerance in peaches by hot water treatment prior to LT storage is associated with membrane stability (as indicated by less electrolyte leakage and lower malondialdehyde accumulation), and the maintenance of high levels of amino acid (including GABA and proline), polyamines (PAs) and radical scavenging capacity (phenols) (Wang L. et al., 2021).

Anoxia preserves the quality of drying green tea leaves and of soybean sprouts stored at room temperature (RT) and promotes GABA accumulation and the diversion of succinic semialdehyde (SSA) from succinate to γ-hydroxybutyrate (GHB) (Allan et al., 2003; **Table 1** and **Figure 1**). Several mechanisms could account for the accumulation of GABA: calmodulin (CaM) activation of CsGAD1; elevated expression of *CsGAD2*; oxidation of Put/proline; and, feedback inhibition of GABA transaminase (*Cs*GABA-T) activity (Mei et al., 2016; Liao et al., 2017; Shelp et al., 2021; **Table 1**). Complete inhibition of DAO activity by aminoguanidine (4–11 h of treatment) suggests that about 25% of the GABA is derived from the PA degradation pathways

TABLE 1 | Postharvest storage conditions improve the marketability of horticultural commodities and promote GABA metabolism.

Commodity	Storage conditions	Marketability	Biochemical and molecular responses	References
Mulberry leaves (*Morus alba* L.)	4°C, air for 5 days	Preserves color	• ↑ GABA, GAD activity; ↓ GABA-TP activity	Li E. et al., 2018
Zucchini fruit (*Cucurbita pepo* L.)	4°C, air for 14 days	Preserves FM	• ↓ GABA; ↑ Pro, free Put, and conj soluble Put • ↑ activities of GABA-T and DAO	Palma et al., 2014
Peach fruit (*Prunus persica* L.)	Hot water at 45°C for 10 min, then stored at 0°C for 35 days	Attenuates chilling injury	• ↑ GABA, arginine, Pro, Put, Spd, and Spm • ↑ Expression of *GAD1,4*, *GABA-T3, ARG*, *P5CS, OAT, ADC, ODC, PAL1,* and *4CL*, and corresponding activities • ↓ Expression of *ProDH, DAO* and *PAO1,4,5,* and corresponding activities • ↓ EL and MDA	Wang L. et al., 2021
Green tea leaves (*Commelia sinesis* [L.] O. Kuntze)	RT, 100 kPa N_2 during drying	Preserves quality	• ↑ GABA, alanine, and GHB	Allan et al., 2003
Soybean sprouts (*Glycine max* [L.] Merr.)	RT, 100 kPa N_2 for 100 h	Preserves quality	• ↑ GHB	Allan et al., 2003
Green tea leaves (*Commelia sinesis* [L.] O. Kuntze)	25°C, 100 kPa N_2 for 6 h	Induces GABA accumulation	• ↑ GABA; ↑ expression of *GAD2*, *GLYR1*, and *GDH1*; ↓ Glu • Expression of *GAD1,3, GABA-T1,2, SSADH1,2*, *GLYR2*, and *GDH2* unaffected • N_2 activates CaM-dependent GAD1 • N_2 and mechanical stress (i.e., picking) induce CaM-independent *GAD2*	Mei et al., 2016
	25°C, 100 kPa N_2 for 11 h	Induces GABA accumulation	• ↑ GABA, Put, Spm, and Spd; transient ↑ GAD activity; ↑ DAO activity; ↑ expression of *GAD1,2,3* • ↓ Glu	Liao et al., 2017
	25°C, 100 kPa N_2 or CO_2 for 6 h	Preserves quality	• ↑ GABA, Succ, Pro, and Put greater with CO_2 than N_2 • ↑ Glu, alanine, and pyruvate, and ↓ citrate, 2-OG and fumarate more with N_2 than CO_2	Chen et al., 2018
Mushroom [*Agaricus bisporus* (J.E. Lange) Imbach]	4°C, 100 kPa N_2 or CO_2 for 1 day	Preserves quality	• ↑ GABA; ↑ activities of GAD, GABA-TP, and PAO; ↓ Put, Spd, and Cad; may ↑ activities of ADC, ODC, PAO, and DAO • ↑ GABA and alanine, ↓ Arg, Orn, and DAO activity more with N_2 than CO_2 • ↑ Glu with CO_2; ↓ Glu with N_2	Chen et al., 2020
Broccoli florets (*Brassica oleracea* var. *italica* Plenck)	10°C, 20 kPa CO_2 + N_2 for 7 days	Delays senescence	• ↑ GABA and non-protein AAs • ↓ Glu, aspartate and protein AAs • ↓ GABA with re-aeration for 2 days	Hansen et al., 2001
Red tomato fruit (*Solanum lycopersicum* L.)	30°C, 11 kPa O_2 + 11 kPa CO_2 for 6 days	Delays ripening	↑ GABA, and GAD activity ↓ GABA-TOG activity; GABA-TP activity unaffected	Makino et al., 2008
	25°C, 2.4–3.5 kPa O_2 + 10 kPa CO_2 for 7 days	Delays ripening	• ↑ GABA; alanine and Glu unaffected • ↑ GAD activity, expression of *GAD1,2,3* • ↓ GABA-TOG activity.	Mae et al., 2012
	13°C, 10 kPa CO_2 in air for 12 days	Delays ripening	• ↑ GABA, and *GAD2,3* expression • ↓ Activities of GABA-TP, and SSADH; ↓ expression of *GABA-T1*, and *GYR1,2* • GAD activity and expression of *GAD1*, *GABA-T2,3*, and *SSADH* unaffected • ↓ GABA, ↑ *GABA-T2,3* expression upon re-aeration for 3 days	Deewatthanawong et al., 2010b
	20°C, 20 kPa CO_2 in air for 3 days	Delays ripening	• ↑ Expression of *GAD,* and *HSP* • ↓ Ethylene; ↓ expression of *ACS*, *ACO*, *PSY, PG*, and *INV* • ↓ *GAD* expression, ↑ expression of *ACS* and *ACO* upon re-aeration for 4 days	Rothan et al., 1997
Cherimoya fruit (*Annona cherimola* Mill.)	6°C, 20 kPa CO_2 in air for 3 days	Improves chilling tolerance and preserves quality	• ↑ GABA, and total PA • ↓ GABA, and total PA upon re-aeration for 3 days	Merodio et al., 1998
Strawberry fruit (*Fragaria* × *ananassa* Duch.)	2°C, 20 kPa CO_2 in air for 12 days	Delays ripening and preserves fruit color.	• ↑ GABA • GAD activity unaffected, but GABA-TP activity may ↓, depending upon cv	Deewatthanawong et al., 2010a

(Continued)

TABLE 1 | (Continued)

Commodity	Storage conditions	Marketability	Biochemical and molecular responses	References
	0°C, 20 kPa CO_2 in air for 12 days	Preserves quality and alleviates decay	• ↑ GABA, NAD^+; ↑ SDH and CCO activities • ↓ *GABA-TP* expression and activity, AEC, ATP, NADH, and NADH/NAD^+ • GAD activity, expression of *GAD1* and *GABA-T1* unaffected	Li D. et al., 2018
	4°C, 10 kPa CO_2 + 11 kPa O_2 for 10 days	Preserves quality	• ↓ GABA, Pro, OG • ↑ Fumarate, and Succ	Pott et al., 2020
Strawberry fruit (*Fragaria vesca* L.)	0°C, 20 kPa CO_2 in air for 3 days	Preserves FM and cell structure	• ↑ GABA (CO_2-independent), Glu, alanine, Pro, Succ, oxalate, and sugars • ↓ Malate; citrate unaffected	Blanch et al., 2012
Longan fruit (*Dimocarpus longan* Lour.)	4°C, 5 kPa O_2 + 5 kPa CO_2 for 18 days	Delays senescence	• ↓ GABA, and GAD activity • GABA-T activity fluctuates	Zhou et al., 2016
Peel from apple fruit (*Malus* × *domestica* Borkh. "Empire")	3°C, 2 kPa O_2 + 5 kPa CO_2 for 4 weeks	Delays senescence, but induces external injury	• ↑ GABA	Deewatthanawong and Watkins, 2010
Apple fruit ("Empire")	3°C, 2.5 kPa O_2 + 2.5 kPa CO_2	Delays senescence	• ↓ GABA upon aeration for 3 h	Trobacher et al., 2013a,b
	3°C, 2.5 kPa O_2 + 2.5 kPa CO_2 for 46 weeks	Delays senescence	• ↑ GABA; ↓ Glu after a transient peak • ↑ Total PAs, including free and soluble/insoluble conjug forms	Deyman et al., 2014a
	3°C, 2.5 kPa O_2 + 5 kPa CO_2 for 16 weeks	Delays senescence, but increases external injury	• ↑ GABA, alanine, Succ, GHB, Put, Spd, and Spm; ↓ Glu (short-term) • ↑ Expression of *GAD2*, *AO1*, *ALDH10A8* and *PAO2* (long-term, CO_2-dependent) • ↓ NADH (short-term) and NADH/NAD^+ (long-term); ↑ NADPH (long-term) and NADPH/$NADP^+$	Deyman et al., 2014b; Brikis et al., 2018
Apple fruit ("Honeycrisp")	3°C, 2.5 kPa O_2 + 5 kPa CO_2 for 24 weeks	Increases CA-related injury by 24 weeks	• ↑ GABA from 18 to 24 weeks	Chiu et al., 2015
	Conditioned at 10°C in air for 5 days, followed by 3°C in 2.5 kPa O_2 + 2.5 CO_2 for 35 weeks	Delays onset of CA-related injury	• ↓ GABA	Lum et al., 2016a
Pear fruit (*Pyrus communis* L.)	0°C, air for 167–180 days	Delays senescence	• ↑ GABA from 111–119 days to 167–180 days, depending on cv	Lum et al., 2017

Symbols: ↑, increases; ↓, decreases.

ACO, 1-aminocyclopropane-1-carboxylic acid oxidase; ACS, 1-aminocyclopropane-1-carboxylic acid synthase; ADC, arginine decarboxylase; AEC, adenylate energy charge; AA, amino acid; AO, Cu amine oxidase; ARG, arginase; 4CL, 4-coumarate/coenzyme A ligase; CA, controlled atmosphere; Cad, cadaverine; CaM, calmodulin; CCO, cytochrome c oxidase; conj, conjugated; cv, cultivar; DAO, diamine oxidase; EL, electrolyte leakage; GABA, γ-aminobutyrate; GABA-TP or GABA-TOG, pyruvate/glyoxylate or 2-oxoglutarate-dependent GABA transaminase; GAD, glutamate decarboxylase; GHB, γ-hydroxybutyrate; Glu, glutamate; GLYR, glyoxylate/succinic semialdehyde reductase; INV, acid invertase; MDA, malondialdehyde; NAD^+/NADH, oxidized/reduced dinucleotide; NADPH, reduced dinucleotide phosphate; OAT, ornithine δ-aminotransferase; ODC, ornithine decarboxylase; 2-OG, 2-oxoglutarate; P5CS, Δ^1-pyrroline-5-carboxylate synthetase; PA, polyamine; PAL, phenylalanine lyase; PAO, polyamine oxidase; PDC, pyruvate decarboxylase; Pro, proline; ProDH, proline dehydrogenase; PG, polygalacturonase; Pro, proline; PSY, phytoene synthase; Put, putrescine; RT, room temperature; SDH, succinate dehydrogenase; Spd, spermidine; Spm, spermine; SSADH, succinic semialdehyde dehydrogenase; Succ, succinate; TCAC, tricarboxylic acid cycle; TAA, total amino acids.

(Liao et al., 2017; **Figure 1**). However, this interpretation can be challenged. Based upon the increasing accumulation of Put with aminoguanidine over the same time period, we estimate that Put degradation would account for only 3% of the anoxia-induced rate of GABA accumulation. Notably, the spermidine (Spd) pool also decreases at an estimated rate of approximately 3% of the rate for GABA accumulation, suggesting that the terminal oxidation of Spd can substitute for the terminal oxidation of Put (Shelp et al., 2012b). This re-assessment of the published data is consistent with our recent interpretation of the ΔGABA/ΔPut stoichiometry published for wheat roots treated simultaneously with salinity and aminoguanidine (Shelp et al., 2021). While increasing DAO activity seems contrary to our interpretation of the metabolite data, it could reflect an "anticipation response" to the return to normoxia, as proposed for alanine transaminase and glutamate dehydrogenase (Limami et al., 2008).

The quality of green tea leaves at RT and of broccoli florets at LT is preserved under anaerobic conditions imposed by either

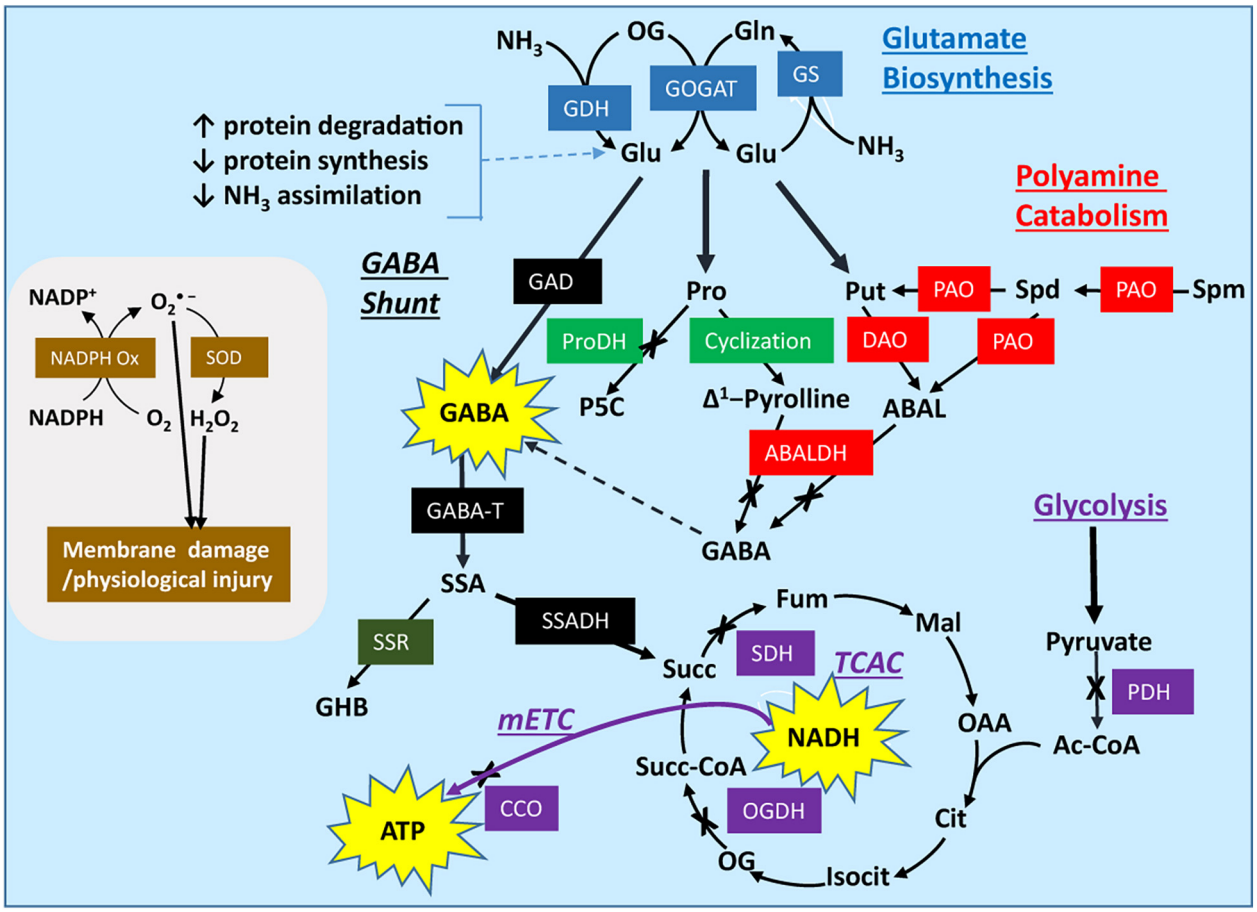

FIGURE 1 | Modeling the postharvest impact of low temperature and controlled atmosphere conditions on activities of the GABA shunt, polyamine catabolism, proline catabolism, respiratory processes, and oxidant systems in horticultural commodities. Low temperature, low O_2 and elevated CO_2 can limit the activities of pyruvate dehydrogenase, 2-oxoglutarate dehydrogenase, succinate dehydrogenase, and cytochrome c oxidase, leading to less NADH, FADH and ATP generation and more protein turnover. This is accompanied by a shift in redox balance. The elevated NADPH/$NADP^+$ ratio stimulates H_2O_2 production *via* NADPH oxidase and superoxide dismutase, and stimulates the expression/activities of non-enzymatic and enzymatic antioxidants (not shown). Under these conditions, the availability of Glu and the synthesis of polyamines, proline and GABA increase. Polyamines often accumulate, but evidence suggests that only about 3% of the stress-induced GABA is derived from putrescine or spermidine catabolism, which may be explained, at least in part, by O_2 and NAD^+ limitation of DAO, PAO, and ABALDH activities. Proline also accumulates, in part due to the decline in proline dehydrogenase activity, but there is no direct evidence for the conversion of proline into GABA *via* ABALDH (because 4-aminobutanal and Δ^1-pyrroline are in rapid non-enzymatic equilibrium, their oxidation is often considered to be catalyzed by ABALDH). The limiting activities are to some extent overcome by H^+ stimulation or Ca^{2+}/calmodulin activation of glutamate decarboxylase, which increases the biosynthesis of GABA and the carbon flux through succinic semialdehyde to succinate *via* GABA transaminase and succinic semialdehyde dehydrogenase, respectively. Only a minor portion of the NADPH is recycled *via* the diversion of succinic semialdehyde into γ-hydroxybutyrate. Consequently, stress-derived succinate stimulates the production of NADH and ATP *via* the non-cyclic tricarboxylic acid cycle and the mitochondrial electron transport chain. A representative oxidant system is shown on the left; it involves NADPH oxidase and superoxide dismutase, and contributes to membrane damage and physiological injury [Please refer to Shelp et al. (2021) for more detailed graphical representations]. Symbols: ↑, increase; ↓, decrease; colored rectangles, enzymes; X, biochemical reaction potentially inhibited by stress; thick arrows, multiple biochemical steps; moderately thick arrows, the GABA shunt. ABAL, 4-aminobutanal; ABALDH, 4-aminobutanal dehydrogenase; Ac-CoA, acetyl-CoA; Cit, citrate; CCO, cytochrome oxidase; DAO, diamine oxidase; Fum, fumarate; GABA; γ-aminobutyrate; GABA-T, pyruvate/glyoxylate-dependent GABA transaminase; GAD, glutamate decarboxylase; GDH, glutamate dehydrogenase; GHB, γ-hydroxybutyrate; Glu, glutamate; GOGAT, glutamate synthase; GS, glutamine synthetase; Isocit, isocitrate; MAL, malate; mETC, mitochondrial electron transport chain; NADPH Ox, NADPH oxidase; OG, 2-oxoglutarate; OGDH, 2-oxoglutarate dehydrogenase; PAO, polyamine oxidase; Pro, proline; PDH, pyruvate dehydrogenase; ProDH, proline dehydrogenase; Put, putrescine; SDH, succinate dehydrogenase; SOD, superoxide dismutase; Spd, spermidine; Spm, spermine; SSADH, succinic semialdehyde dehydrogenase; SSR, succinic semialdehyde reductase; Succ, succinate; Succ-CoA; succinyl-CoA; TCAC, tricarboxylic acid cycle; See **Table 4** legend for the remaining abbreviations.

anoxia or elevated CO_2 (Hansen et al., 2001; Chen et al., 2018; **Table 1**). However, the accumulation of GABA and succinate, and the depletion of Glu is more rapid with CO_2 than with N_2, whereas the accumulation of alanine is faster with N_2. There is greater Put and NADH accumulation, and less NADPH, citrate, 2-oxoglutarate (OG) and fumarate accumulation with CO_2 than air. Thus, the GABA shunt is more active with CO_2, but the inhibition of the TCAC and mitochondrial electron transport chain (mETC) occurs more quickly with N_2 (Chen et al., 2018). While the storage of mushrooms with 100% CO_2 at LT also

stimulates the production of Glu-derived GABA, storage with N_2 stimulates the production of both Glu-and PA-derived GABA (Chen et al., 2020), perhaps due in part to protein degradation. Notably, *Ab*GAD, unlike most plant GADs, does not possess a CaM-binding domain, and therefore its activity is likely to be stimulated by cytosolic acidification only.

Elevated CO_2 in air at LT improves chilling tolerance in cherimoya fruit (Merodio et al., 1998), and delays ripening/senescence in tomato and strawberry fruits (Deewatthanawong et al., 2010a,b; Blanch et al., 2012; Li D. et al., 2018; **Table 1**). These positive outcomes are typically accompanied by the accumulation of GABA and occasionally PAs, as well as limited flux of GABA-carbon through the GABA shunt into the TCAC and the mETC. Elevated CO_2, in combination with low O_2, delays the ripening/senescence of tomato fruit stored at RT (Makino et al., 2008; Mae et al., 2012), and longan (Zhou et al., 2016), strawberry (Pott et al., 2020) and "Empire" apple (Deewatthanawong and Watkins, 2010; Trobacher et al., 2013a; Deyman et al., 2014a,b; Brikis et al., 2018) fruits stored at LT. These findings have been attributed to the elevated generation of GABA from Glu, rather than PAs, and enhanced flux of GABA-carbon through the GABA shunt into a non-cyclic TCAC for generation of ATP (Shelp et al., 2012b; Brikis et al., 2018). Wang C. et al. (2014) previously suggested that Glu-derived GABA accumulation in melon roots can alleviate hypoxia damage by accelerating PA biosynthesis and conversion, as well as preventing PA degradation.

Some pome fruit are particularly sensitive to LT, CA storage (e.g., "Honeycrisp" apples and "Cold Snap" pears) (Chiu et al., 2015; Lum et al., 2016a, 2017; **Table 1**). In these cases, a dramatic increase in the GABA level coincides with CA-or senescence-related injury and is likely due to the disruption of cellular compartmentation and the release of acidic vacuolar contents to the cytosol (Bown and Shelp, 2006). Interestingly, conditioning of "Honeycrisp" apples at 10°C improves the resistance to CA-related injury, decreases the GABA level and increases the ratios of NAD(P)H/NAD(P) $^+$ (Lum et al., 2016a).

Overall, these studies indicate that LT, CA-mediated improvements in the postharvest marketability of horticultural products is generally associated with the promotion of GABA biosynthesis and GABA shunt activity, with or without the accumulation of GABA. The onset of CA-or senescence-related injury during prolonged storage may also be associated with the accumulation of GABA. Discrepancies in data from the various studies might be explained by: pretreatment and conditioning of plant materials prior to storage; the use of different cultivars and single time point determinations, rather than time courses; excessive handling or wounding of plant materials prior to metabolite extraction; and, the use of non-saturating levels of Glu and inhibitory levels of GABA and pyruvate, respectively, in *in vitro* assays of GAD and GABA-TP activities [for examples, compare Zhou et al. (2016), Li D. et al. (2018), and Chen et al. (2020) with Snedden et al. (1995), Van Cauwenberghe and Shelp (1999), Clark et al. (2009a), and Shelp et al. (2012a)]. Interpretation could vary somewhat because: (i) it is not possible to directly assess the Ca^{2+}/CaM stimulation of GAD activity *in situ*; (ii) the existence of a 2-OG-dependent plant GABA-T is questionable [for examples, compare Makino et al. (2008) and Deewatthanawong et al. (2010b) with Clark et al. (2009b), Koike et al. (2013), Trobacher et al. (2013a), Shimajiri et al. (2013), and Shelp et al. (2021)]; (iii) the expression of a gene does not establish that the encoded protein is operational; (iv) the understanding of precursor/product relations and flux is often incomplete (e.g., pool sizes alone do not indicate flux; Put accumulation does not establish greater contribution than Glu to GABA generation) (Shelp et al., 2012a); and, (v) there is often a failure to consider the importance of multiple isoforms of the GABA pathway enzymes (Shelp et al., 2012c, 2021).

Genetic and Biochemical Control of GABA Metabolism in Apple Fruits

Gene sequences for the key steps in GABA metabolism in apple fruit have been identified, allowing elucidation of the biochemical properties and subcellular location of multiple isoforms of the encoded proteins (**Table 2** and **Figure 1**). Three cytosolic GADs are present, but unlike *Md*GAD3, *Md*GAD1,2 are Ca^{2+}/CaM-dependent and more sensitive to pH (Trobacher et al., 2013b). There are also two mitochondrial pyruvate/glyoxylate-dependent GABA transaminases (*Md*GABA-Ts, designated as GABA-TP), two mitochondrial NAD^+-dependent SSADHs (*Md*SSADH1,2 or *Md*ALDH5F1,2), and two NADPH-dependent glyoxylate/succinic semialdehyde reductases (*Md*GLYR1,2 or *Md*SSR1,2) with different subcellular locations (Trobacher et al., 2013a; Brikis et al., 2017, 2018; Zarei et al., 2017). *Md*GLYR1 is cytosolic, whereas *Md*GLYR2 is both plastidial and mitochondrial. Two of the six apple fruit FAD-dependent polyamine oxidases (*Md*PAO2,4) are peroxisomal and likely catalyze the back-conversion of Spm and Spd to Spd and Put, respectively (Brikis et al., 2018). Three of the five *Md*CuAOs identified are peroxisomal (*Md*CuAO1,4-5), but only one of these, *Md*CuAO1, has been shown to exclusively utilize diamines (diaminopropane, Put and cadaverine) as substrates (Zarei et al., 2015a; Brikis et al., 2018). A candidate plastidial diamine oxidase activity has not yet been identified. Two NAD^+-dependent 4-aminobutanal dehydrogenases (ABALDH) exist in apple fruit (*Md*ALDH10A8,9 or *Md*AMADH1,2): one is peroxisomal and the other plastidial (Zarei et al., 2015b, 2016; Brikis et al., 2018).

The temporal patterns of specific metabolites have been compared to the expression of genes encoding the most biochemically relevant proteins in intact "Empire" apple fruit stored under LT and low O_2 with ambient or elevated CO_2 (0°C, 2.5 kPa O_2 and 0.03 or 5 kPa CO_2) (Brikis et al., 2018; **Table 2**). Five kPa CO_2 is known to elicit symptoms of external, but not internal, CO_2-induced injury in this cultivar within 16 weeks (Deyman et al., 2014b). Under LT, low-O_2 and ambient-CO_2 storage, there is a transient increase in amino acid availability, including Glu, early in the storage period (2–4 weeks), probably a reflection of protein hydrolysis (Brikis et al., 2018). This is accompanied by a rapid peak in the expression of *alanine transaminase* (*MdAla-T*), a marker of hypoxia (Cukrov et al., 2016), as well as in the pool of alanine (2–4 weeks), which decline slowly to a steady basal level (from 8 to 16 weeks) (Brikis et al., 2018). A rapid accumulation of GABA is also transient

TABLE 2 | Key proteins/genes of GABA metabolism and signaling in apple fruits subjected to low temperature, controlled atmosphere storage.

Protein/ gene name	Accession number	Subcellular location	Expression profile	References
MdGAD1[a]	KC812242	C[b]	U	Trobacher et al., 2013b; Brikis et al., 2018
MdGAD2	KC812243	C[b]	U	
MdGAD3	KC812244	C[b]	D	
MdGABA-T1	JX276380	M	U	Trobacher et al., 2013b; Brikis et al., 2018
MdGABA-T2	JX276381	M	U	
MdSSADH1	XM_008357890	M[b]	U	Brikis et al., 2018; Jung et al., 2019
MdSSADH2	XM_029110087[c]	M[b]	D	
MdGABP	XM_008341399	M[b]	–	Jung et al., 2019
MdSSR1	KT202799	C	TU	Brikis et al., 2017, 2018; Zarei et al., 2017
MdSSR2	KT202800	P/M	TU	
MdPAO2	KT184497	Px[b]	U	Brikis et al., 2018
MdPAO4	KT184499	Px[b]	U	
MdCuAO1	KM067895	Px	U	Zarei et al., 2015a; Brikis et al., 2018
MdCuAO4	KM067898	Px[b]	TU	
MdCuAO5	KM067899	Px[b]	TU	
MdALDH10A8	KP218041	P[b]	U	Zarei et al., 2015b; Zarei et al., 2016; Brikis et al., 2018
MdALDH10A9	KP218040	Px	U	
MdCAT9	XM_008368457	T[b]	–	Shelp and Zarei, 2017; Jung et al., 2019
MdALMT9	MDP0000252114	T[b]	–	Li et al., 2020

ES, extracellular/secretory pathway; U, upregulated; D, downregulated; T, tonoplast; TU, transiently upregulated; C, cytosol; M, mitochondrion; P, plastid; Px, peroxisome.
[a] *Proteins in bold lettering are likely to be the most abundant of the alternative forms (based on gene transcript abundance).*
[b] *Predicted.*

(2–4 weeks), but the pool size is approximately 60% of that for alanine, suggesting that the alanine is derived from both Ala-T and GABA-TP reactions. Notably, *MdGAD1* expression increases linearly up to 12 weeks and then remains steady, whereas *MdGAD2* expression increases up to only 4 weeks and then decreases, and *MdGAD3* expression decreases over the storage period. Succinate does not accumulate, but the burst of GABA is followed by a much smaller transient increase in GHB (**Figure 1**). Nevertheless, *MdSSADH1* expression increases up to 8 weeks and then slowly declines, whereas *MdSSADH2* expression decreases over the storage period. The expression of *MdSSR1* is transiently increased, peaking at 4–8 weeks, and may be correlated with GHB. While Put, Spd and spermine (Spm) represent potential precursors for GABA, their levels are only 1–5% of that for GABA. Furthermore, the Put level declines only slightly with the increase in GABA, while Spd accumulates slightly and Spm dramatically declines. The expression of *MdPAO2,4, MdCuAO1* and *MdALDH10A8,9* rapidly increases, peaking after 8, 2 and 4–8 weeks, respectively, whereas the expression of *MdCuAO4*-5 is transiently increased, peaking at 4 weeks.

With LT, low-O_2 and elevated-CO_2 storage, a pronounced transient peak of GABA is accompanied by a strong transient peak of succinate, and smaller transient peaks of GHB, Put, Spd and Spm (Brikis et al., 2018). With prolonged storage, only GABA and GHB exhibit subsequent increases. These changes are accompanied by minor, yet significant, increases in the expression of *MdGAD1*, *MdCuAO1* and *MdALDH10A8,9*. Thus, the GABA pattern might be interpreted as a CO_2-induced shift from Glu/CaM-mediated stimulation/activation of GAD activity to H^+-mediated stimulation of GAD activity (Trobacher et al., 2013b; Brikis et al., 2018). The patterns for succinate, GHB and Put might be explained by a combination of: elevated GABA production; differential effects of shifting redox balance on the activities of SSADH, TCAC, SSR, and ABALDH; and, limiting O_2 availability for DAO activity in bulky apple fruit (Shelp et al., 2012b; Brikis et al., 2018). Based on changing pool sizes, we can estimate the maximum rates of GABA and succinate synthesis to be ∼50 nmol g^{-1} fresh mass (FM) wk^{-1}, and the maximum rates of GHB synthesis and Put/Spd depletion to be ∼0.2 and ∼1.5 nmol g^{-1} FM wk^{-1}, respectively. Thus, the terminal oxidation of PAs and the direct decarboxylation of Glu can account for approximately 3 and 97%, respectively, of GABA synthesis. Moreover, only 3% of the SSA is diverted from succinate to GHB production. Overall, this study suggests that both genetic and biochemical mechanisms are involved in the metabolism of GABA in apple fruit stored under LT, CA conditions.

Han et al. (2018) have monitored the expression of the GABA shunt enzymes and the levels of important metabolites in "Cripps Pink" apple fruit stored at RT in air for 70 days. The *MdGAD*s exhibit different expression patterns, with *MdGAD1* expression increasing gradually with time, *MdGAD2* expression increasing until 30 days and then decreasing, and *MdGAD3* expression decreasing. The expression of *MdGABA-T1,2* and *MdSSADH1* increases gradually from 0 to 30 days, peaking at the same time as the ethylene climacteric peak (30 days). Thus, the expression of *MdGAD1*, *MdGAD2*, *MdGABA-T1,2*, and *MdSSADH1* in "Cripps Pink" apple fruit responds strongly under RT storage, essentially as in "Empire" apple fruit stored under LT, low O_2 and ambient or elevated CO_2 (Brikis et al., 2018). These findings, in conjunction with those of Brikis et al. (2018), lead us to conclude that the

TABLE 3 | The application of exogenous GABA improves the postharvest marketability of horticultural commodities by promoting GABA and antioxidant pathways.

Commodity	Storage conditions	Marketability	Biochemical and molecular responses	References
Peach fruit (*Prunus persica* L.)	1°C, 5 weeks	Chilling tolerance	• ↑ GABA, Pro, ATP, and ADP; ↑ activities of GAD, P5CS, OAT, SOD, CAT, APX, GPX, GST, GR, DHAR, and MDHAR • ↓ AEC, and ProDH activity	Shang et al., 2011; Yang et al., 2011
Banana fruit (*Musa* spp. Cavendish)	7°C, 20 days	Chilling tolerance	• ↑ Pro, and phenols; ↑ activities of P5CS, PAL, DPPH and FRAP scavenging capacity • ↓ PDH activity, MDA, and EL	Wang Y. et al., 2014
Zucchini fruit (*Cucurbita pepo* L.)	4°C, 14 days	Chilling tolerance	• ↑ Pro, malate, fumarate, ATP, and NADH; ↑ GABA-TP activity	Palma et al., 2019
Orange fruit [*Citrus* × *sinensis* (L.)]	3°C, 120 days	Chilling tolerance	• ↑ ASC, phenols, and anthocyanins; ↑ activities of SOD, CAT, and APX; ↑ PAL/PPO activity ratio, and DPPH scavenging capacity • ↓ H_2O_2, MDA, and EL	Habibi et al., 2019, 2020
Pomegranate fruit (*Punica granatum* L.)	4°C, 90 days	Chilling tolerance	• ↑ ASC, phenols, and anthocyanins; ↑ DPPH scavenging capacity • ↓ MDA, and EL	Nazoori et al., 2020
Persimmon fruit (*Diospyros kaki* Thunb.)	2°C, 45 days	Chilling tolerance, delays senescence	• ↑ TSS, ASC, phenols, and flavonoids; ↑ activities of SOD, CAT, APX, PAL, PPO, and DPPH scavenging capacity • ↓ H_2O_2, MDA, EL; ↓ activities of PG and PME	Niazi et al., 2021
Aonla fruit (*Emblica officinalis* Gaertn.)	5°C, 24 days	Chilling tolerance, delays senescence	↑ GABA, Pro, phenols, ASC, flavonoids, GSH Pro, ATP, and ADP; ↑ activities of GAD, GABA-T, P5CS, OAT, PAL, SOD, CAT, APX, and POD ↓ TSS, EL, MDA, H_2O_2, $O_2^{\bullet-}$; ↓ PPO activity	Ali et al., 2022
Cut anthurium flowers (*Anthurium andraeanum* L.)	4°C, 3 weeks	Chilling tolerance	• ↑ Pro, phenols, GB, and unSFA/SFA; ↑ activities of GABA-TP, SOD, CAT, APX, and GR; ↑ PAL/PPO activity ratio, and DPPH scavenging capacity • ↓ H_2O_2, MDA and EL; ↓ activities of GAD, PLD, and LOX	Aghdam et al., 2015, 2016a,b
Blueberry fruit (*Vaccinium corymbosum* L.	4°C, 2 weeks	Delays senescence	• Increases ASC, GSH, phenols, and flavonoids; ↑ activities of SOD, CAT, APX, GR, PAL, C4H, and 4CL • ↓ H_2O_2	Ge et al., 2018
Cornelian cherry fruit (*Cornus mas* L.)	4°C, 3 weeks	Delays senescence, preserves quality	• ↑ AA, phenols, flavonoids, and anthocyanins; ↑ activities of SOD, CAT, APX, and GR; ↑ PAL/PPO activity ratio, and DPPH scavenging capacity • ↓ Activities of LOX, PG, and PME; ↓ H_2O_2, MDA, and EL.	Aghdam et al., 2019; Rabiei et al., 2019
Mushrooom [*Agaricus bisporus* (J.E. Lange) Imbach]	4°C, 15 days	Retards cap browning, preserves nutritional and sensory quality	• ↑ *GAD* activity; ↑ *PAL* expression and corresponding activity; ↑ ASC, phenols, and DPPH scavenging activity • ↓ *GABA-T* expression, *PPO* expression and corresponding activity, MDA	Shekari et al., 2021
Pear fruit (*Pyrus ussuriensis* Maxim.)	0°C, 180 days, then 20°C, 12 days	Browning resistance	• ↑ Expression of *AOX*, *SOD*, and *CAT* and corresponding activities • ↓ ROS, and MDA	Li et al., 2019
Mango fruit (*Mangifera indica* L.)	15°C, 4 weeks	Preserves quality	• ↑ ASC, phenols, and flavonoids; ↑ CAT activity, and DPPH scavenging capacity • ↓ PPO activity	Rastegar et al., 2019
Apple fruit (*Malus* × *domestica* Borkh. "Cripps Pink")	RT, 10 weeks	Preserves titratable acidity and quality	• ↑ Expression of *GAD1*,*2*, *GABA-T1*,*2*, and *SSADH*, but *GAD3* unaffected • ↑ Succ, and malate; ↑ activities of cytNAD-MDH, and PEPC; ↓ activities of cytNADP-ME, and PEPCK • ↓ Respiration; ↓ ethylene, expression of *ACS*, *ACO,* and *ERF* before climacteric	Han et al., 2018
Apple fruit ("Honeycrisp")	Conditioned at 10°C for 1 week, followed by 3°C for 5 months	Decreases soft scald, bitter pit or senescent breakdown		Al Shoffe et al., 2021
Pear fruit (*Pyrus pyrifolia* Nakai)	4°C, 4 weeks or 25°C, 3 days	Resistance to blue mold rot (*Penicillium. expansum*)	• ↑ CAT activity; ↑ expression of *CHI, BGLU*, *PAL*, *POD*, and *PPO*, and corresponding activities	Yu et al., 2014; Fu et al., 2017
Orange fruit (*Citrus* × *sinensis* [L.] Osbeck)	RT, 80 days	Delays fruit rot	• ↑ Glu, Pro, and citrate; ↑ expression of *GABA-T*, and *GABP* at 80 days • ↓ Expression of *GAD2*, but not *GAD1*, at 20–80 days	Sheng et al., 2017

(Continued)

TABLE 3 | (Continued)

Commodity	Storage conditions	Marketability	Biochemical and molecular responses	References
Tomato fruit (*Solanum lycopersicum* L.)	25°C, 36 h	Resistance to *Alternaria* rot (*Alternaria alternata*)	• ↑ Expression of *GABA-TP1*, *SSADH*, *HXK*, and *PK*; ↑ activities of SDH, and MDH; ↑ ATP; ↑ expression of *SOD*, and *CAT*, and corresponding activities • Triggers SA signaling pathway and SAR; ↑ expression of *NPR1*, and *TAG1*; ↑ expression of *BGLU* and corresponding activity	Yang et al., 2017
Apple fruit ("Golden Delicious")	RT, 8 days	Blue mold resistance (*Penicillium. expansum*)	• ↑ GABA, and pyruvate; ↑ H_2O_2 (53 μmol g^{-1} FM), ASC, and GSH; ↑ activities of SOD, NADPH ox, CAT, GR, APX, DHAR, and MDHAR; ↑ activities of GAD, GDH, and GS; ↑ expression of *MT, MS, SAMS, SAMDC, ODC, ADC*, and *SPDS* • ↓ activities of GABA-T, and SSADH; ↓ expression of *PAO*, and *DAO*	Zhu et al., 2022
Walnut kernel (*Juglans regia* L.)	20°C, 18 weeks	Attenuates browning and oxidative rancidity	• ↑ unSFA/SFA ratio, phenols, oleic acid, linoleic acid, and linolenic acid; ↑ PAL/PPO activity ratio, and DPPH scavenging capacity • ↓ H_2O_2, MDA, palmitic acid, stearic acid, and LOX activity	Ebrahimzadeh et al., 2019

Symbols: ↑, increases; ↓, decreases.

ABALDH, 4-aminobutanal dehydrogenase; ACO, 1-aminocyclopropane-1-carboxylate oxidase; ACS, 1-aminocyclopropane-1-carboxylate synthase; ADC, arginine decarboxylase; ADP, adenosine diphosphate; AEC, Adenylate energy charge; AOX, alternative oxidase; APX, ascorbate peroxidase; ASC, ascorbate; ATP, adenosine triphosphate; BGLU, β-1,3-glucanase; C4H, cinnamate-4-hydroxylase; CAT, catalase; CHI, chitinase; 4CL, 4-coumarate/coenzyme A ligase; cyt, cytosolic; DAO, diamine oxidase; DHAR, dehydroascorbate reductase; DPPH, 2,2-diphenyl-1-picryl-hidrazil; EL, electrolyte leakage; ERF, ethylene-responsive factor; FRAP, ferric reducing antioxidant potential; GABA, γ-aminobutyric acid; GABA-TP or GABA-TOG, pyruvate-or 2-oxoglutarate-dependent GABA transaminase; GAD, glutamate decarboxylase; GABP, GABA permease; GB, glycine betaine; GDH, glutamate dehydrogenase; Glu, glutamate; GR, glutathione reductase; GS, glutamine synthetase; GSH, reduced glutathione; GPX, glutathione peroxidase; GST, glutathione S-transferase; H_2O_2, hydrogen peroxide; HXK, hexokinase; LOX, lipoxygenase; MDA, malondialdehyde; MDH, malate dehydrogenase; MDHAR, monodehydroascorbate reductase; ME, malic enzyme; MS, methionine synthase; MT, metallothionein; NADH, reduced dinucleotide; NADPH, reduced dinucleotide phosphate; NADPH Ox, NADPH oxidase; NPR, non-inducible pathogenesis-related; O_2, superoxide anion; OAT, ornithine δ-aminotransferase; ODC, ornithine decarboxylase; P5CS, Δ^1-pyrroline-5-carboxylate synthetase; PAL, phenylalanine ammonia lyase; PAO, polyamine oxidase; PDH, proline dehydrogenase; PEPC, phosphoenolpyruvate carboxylase; PEPCK, phosphoenolpyruvate carboxykinase; PG, polygalacturonase; PK, pyruvate kinase; PLD, phospholipase D; PME, pectin methylesterase; POD, peroxidase; PPO, polyphenol oxidase; PR, pathogenesis-related; Pro, proline; ProDH, proline dehydrogenase; Put, putrescine; RT, room temperature; SA, salicylate; SAM, S-adenosylmethionine; SAMS, S-adenosylmethionine synthetase; SAMDC, S-adenosylmethionine decarboxylase; SAR, systemic acquired resistance; SDH, succinate dehydrogenase; SFA, saturated fatty acids; SOD, superoxide dismutase; Spd, spermidine; SPDS, spermidine synthase; Spm, spermine; SSADH, succinic semialdehyde dehydrogenase; TAG, TAG transcription factor; TSS, total soluble sugars.

postharvest expression patterns for GABA shunt genes in apple fruits are more influenced by development, than by environment.

The temporal patterns for GABA (i.e., slow decrease of approximately 60% from 10 to 40 days, followed by a dramatic increase at 70 days, presumably due to fruit aging and cellular disintegration at the end of storage), succinate and malate (slow decrease of 40 and 20%, respectively, from 30 to 70 days) indicate that GABA does not accumulate under storage at RT, and that GABA is probably catabolized to succinate and malate (Han et al., 2018). The application of exogenous GABA increases the expression of *MdGAD1*, *MdGAD2, MdGABA-T1,2* and *MdSSADH1*, restrains the decrease in malate and succinate levels, decreases respiration and ethylene production rates, and delays the ethylene production peak (Han et al., 2018; **Table 3**). Notably, the application of exogenous Ca^{2+} decreases the Glu level (before 30 days), increases the levels of GABA, succinate and malate (10–60 days) and expression of *MdGAD1* (before 30 days), *MdGAD2* (20–40 days), *MdGABA-T1/2* (10–20 days) and *MdSSADH* (20–40 days), suppresses the respiration rate, and decreases the ethylene production peak (Han et al., 2021).

Together, these studies suggest that elevated endogenous GABA or exogenous GABA maintains the quality of apple fruit by stimulating the activity of the GABA shunt and the synthesis of malate, and delaying fruit ripening. Notably, the inhibition of ethylene-mediated ripening by 1-methylcyclopropene increases the GABA level in "Empire" and "Honeycrisp" apples and in "AC Harrow Crisp" pears stored under LT, CA conditions (Deyman et al., 2014a; Lum et al., 2016a; Flaherty et al., 2018). While the interaction between ethylene and GABA biosynthesis requires further study, exogenous GABA seems to elicit similar responses as LT, CA conditions.

Exogenous GABA Alleviates Chilling Injury, Bacterial/Fungal Decay, and Loss of Quality

The attenuation of LT injury in peach, banana, orange, pomegranate, persimmon and aonla fruits, as well as cut anthurium flowers, by exogenous GABA is evident from the preservation of membrane fluidity and stability (decrease in electrolyte leakage), which is accompanied by decreases in reactive oxygen species (ROS; e.g., hydrogen peroxide and superoxide radical), greater antioxidant and radical-scavenging capacities, the maintenance of intracellular ATP and NADH, and the accumulation of potential osmolytes (i.e., soluble sugars, PAs and proline) (Shang et al., 2011; Yang et al., 2011; Wang Y. et al., 2014; Aghdam et al., 2015, 2016a,b; Habibi et al., 2019, 2020; Nazoori et al., 2020; Niazi et al., 2021; Ali et al., 2022; **Table 3**).

Similar mechanisms are involved in: the delay of senescence and preservation of quality in LT-stored blueberries, cherries and mushrooms, RT-stored apples, and conditioned LT-stored apples (Ge et al., 2018; Han et al., 2018; Aghdam et al., 2019; Rabiei et al., 2019; Al Shoffe et al., 2021; Shekari et al., 2021); browning resistance and the preservation of quality in LT-stored pear and mango (Li et al., 2019; Rastegar et al., 2019); resistance against fungal infection in LT-or RT-stored

TABLE 4 | The postharvest marketability of fresh-cut horticultural commodities is improved by low temperature, controlled atmosphere conditions or exogenous GABA.

Commodity	Storage conditions	Treatment	Marketability	Biochemical and molecular responses	References
Carrot root (*Daucus carota* L.)	4°C for 9 h		Organoleptic quality unaffected	• ↑ GABA; ↑ expression of *GAD1, GAD2, GABA-T2* and *PAO*; ↑ activities of GAD, DAO, PAO, and ABALDH • ↓ Glu, Put, Spd, and Spm; ↓ *GABA-T1* expression; ↓ GABA-T activity	Hou et al., 2022
Pear fruit (*Pyrus pyrifolia* (f. Burm.) Nakai)	5°C, 10 kPa CO_2 + 11 kPa O_2, 6 days		Alleviates browning and preserves quality	• ↑ GABA and Pro; ↑ activities of GAD, GABA-T, P5CS, and OAT; ↑ linoleic acid (unSFA/SFA) • ↓ activities of PDH, PLD, and LOX; ↓ palmitic, oleic acid, and stearic acid; ↓ EL and MDA	Wang D. et al., 2021
Apple fruit (*Malus* × *domestica* Borkh. "Fuji")	4°C, 6 days	GABA	Resistance to various bacterial pathogens and browning	• ↑ expression of *CAT*, *PAL*, *CHI*, and *BGLU* and corresponding activities • ↑ expression of genes associated with caffeic acid, lignin, anthocyanin and coumarate biosynthesis; ↑ expression of *XTHs*, *PEI*s, *Ces*, *EXTs*, and *PRP*s • ↓ $O_2^{\bullet-}$ and H_2O_2 • ↓ phenols, flavonoids, and soluble pectin; ↓ expression of a *lacasse* gene; PPO expression unaffected	Gao et al., 2018a; Zhao et al., 2021
Potato tuber (*Solanum tuberosum* L.)	4°C, 6 days	GABA	Browning resistance	• ↑ SOD and CAT activities • ↓ PPO activity, $O_2^{\bullet-}$, H_2O_2, and MDA	Gao et al., 2018b

Symbols: ↑, increases; ↓, decreases.
XTH, xyloglucan endotransglucosylase/hydrolase; PEI, pectin esterase inhibitor; Ces, cellulose synthase; Ext, extensin; PRP, proline-rich protein; remaining abbreviations are given in ***Table 3****.*

pear, orange, strawberry and tomato fruits (Yu et al., 2014; Fu et al., 2017; Sheng et al., 2017; Yang et al., 2017); and resistance against various pathogens and browning in RT-stored walnut kernels (Ebrahimzadeh et al., 2019; **Table 3**). Notably, pathogen resistance is promoted by salicylate signaling and disease resistance proteins, and maintaining the integrity of the cell wall barrier (Yu et al., 2014; Fu et al., 2017; Yang et al., 2017; Gao et al., 2018a; Zhao et al., 2021; **Table 3**), and the loss of apple fruit acidity is retarded by accumulating malate and suppressing ethylene biosynthesis (Han et al., 2018; **Table 3**).

Hou et al. (2022) have shown that the fresh-cut process does not affect the organoleptic quality of carrots stored under LT for hours, though it appears to enhance GABA biosynthesis from both Glu and PAs (**Table 4**). This result is consistent with the previously reported impact of wounding/mechanical damage on GABA accumulation (Shelp et al., 2012a). Notably, the resistance to browning and bacterial pathogens in fresh-cut pear, apple and potato during prolonged LT storage is improved by both CA and exogenous GABA *via* the mechanisms described above (Gao et al., 2018a,b; Wang D. et al., 2021; Zhao et al., 2021).

In summary, the application of exogenous GABA to postharvest fruits, vegetables (including mushrooms), cut flowers, and walnuts delays senescence, attenuates chilling injury and fungal/bacterial-induced decay, and helps to preserve sensory and nutritional quality. GABA can promote activities of the GABA shunt, and the TCAC, antioxidant, secondary and phytohormone pathways, which in turn, reduce the stress-induced ROS level. However, the precise mechanisms whereby GABA interacts with other signaling molecules such as Ca^{2+}, H_2O_2, PAs, salicylic acid, nitric oxide and melatonin, or with phytohormones such as ethylene, abscisic acid and auxin remain unknown (Bor and Turkan, 2019; Podlešákova et al., 2019; Seifikalhor et al., 2019; Suhel et al., 2022).

PROSPECTS FOR IMPROVING THE POSTHARVEST MARKETABILITY OF HORTICULTURAL COMMODITIES WITH EXOGENOUS GABA

Stomatal Functioning and Tolerance/Resistance to Drought and Pathogens

In cut flowers, excessive transpiration can result in a loss of turgor, premature wilting of flowers and leaves, and accelerate flower senescence. Water loss *via* the stomata can also result in a loss of FM and quality in leafy vegetables and immature green fruits. Therefore, it may be beneficial to manipulate endogenous GABA by applying exogenous GABA to restrict stomatal opening and prevent water loss (Xu et al., 2021a). Stomatal closure may also aid in preventing bacterial and fungal pathogens from entering leaves or fruits (Gahir et al., 2021). Thus, regulation of stomatal function may be a promising strategy for improving postharvest quality and safety of horticultural products (van Meeteren and Aliniaeifard, 2016).

Vacuolar Functioning and Flavor

Malate is the predominant organic acid in ripe apple fruit, and most of this is found in the vacuole. The transport of malate across the apple tonoplast is probably mediated by the apple ALMT9 (*Md*Ma1) (Li et al., 2020; **Table 2**). Both the full-length

protein, *Md*Ma1, and its naturally occurring truncated protein, *md*ma1, localize to the tonoplast; when expressed in *Xenopus laevis* oocytes and *Nicotiana benthamiana* cells, *Md*Ma1 mediates a malate-dependent inward-rectifying current, whereas the ma1-mediated transmembrane current is much weaker, indicating that ma1 has significantly lower malate transport activity than Ma1. RNA interference suppression of *MdMa1* expression in "McIntosh" apple leaves, "Empire" apple fruit, and "Orin" apple calli significantly decreases the malate level. Notably, the most highly-related ortholog in *Arabidopsis*, ALMT9, transports mainly Cl^- into the vacuole, but is subject to negative regulation by cytosolic GABA (Bown and Shelp, 2016; Xu et al., 2021a,b). Thus, the application of GABA on apple fruit during LT storage could reduce malate accumulation and the acidity of apple fruits. Bai et al. (2015) have suggested that a major network of genes, including *MdALMT9*, is associated with the developmental regulation of apple fruit acidity in "Golden Delicious," but such a network has not been investigated during the ripening period (Ban and Xu, 2020). It could have implication for breeding apples or other fruits in order to preserve or enhance their flavor during postharvest storage.

Tomato SlCAT9 encodes a tonoplast Glu/Asp/GABA exchanger and its expression increases in tomato fruit during ripening (Snowden et al., 2015; **Table 2**). Such an exchanger might provide a mechanism for remobilizing GABA from the vacuole during cellular Glu uptake (Chung et al., 1992). On the other hand, ripening-specific overexpression of *SlCAT9* increases the accumulation of GABA, Glu and Asp by approximately 20-, one- and sixfold, respectively (Snowden et al., 2015). Notably, greater Glu and Asp accumulation in the vacuole contribute to umami taste development in tomato fruit during ripening (Takayama and Ezura, 2015). Elevated GABA accumulation in the vacuole of immature fruit might deter insect pests and pathogens, whereas lower GABA accumulation in tomato fruit during ripening might be beneficial for attracting insects and animals for successful seed dispersal (Takayama and Ezura, 2015; Shelp et al., 2021). The properties of apple CAT9 have not yet been characterized (**Table 2**), but they could have implications for altering the development, flavor and biotic resistance of apple fruits.

SAFETY AND COMMERCIAL PRODUCTION OF GABA

Natural GABA is ubiquitous in plants and animals, and exogenous GABA is readily catabolized (Tuin and Shelp, 1994; Hijaz and Killiny, 2019; Oketch-Rabah et al., 2021). Nevertheless, the application of exogenous GABA to horticultural commodities during postharvest storage is likely to result in GABA accumulation. GABA is marketed worldwide as a dietary ingredient, food supplement and medicinal agent/drug. Available evidence suggests that GABA ingestion is not associated with adverse health events, probably due to the inability of GABA to cross the human blood–brain barrier (Boonstra et al., 2015; Oketch-Rabah et al., 2021). Also, GABA meets the statutory requirement of reasonable certainty of no harm to the environment (The United States Environmental Protection Agency, 2004).

Large scale commercial production of GABA would be necessary to support its use in postharvest storage of horticultural commodities. While chemical synthesis of GABA is feasible, this process requires expensive and hazardous reagents and generates unwanted by-products (Grewal, 2020; Oketch-Rabah et al., 2021). GABA can be formed from Glu using purified GAD and the coenzyme pyridoxal-5'-phosphate, but the purification of GAD is expensive and the enzyme tends to be unstable. The preferred manufacturing method for commercial production of GABA is fermentation by lactic acid bacteria because of their GRAS (Generally Recognized As Safe) status, high stress tolerance, and ability to release GABA into the extracellular matrix (Grewal, 2020; Jin et al., 2021; Laroute et al., 2021; Yogeswara et al., 2021).

CONCLUDING REMARKS

Research on the postharvest physiological, biochemical, and molecular responses of horticultural commodities to LT and CA storage provides valuable information for conceiving new strategies to improve their marketability. These storage conditions are generally associated with the promotion of GABA pathway activity, with or without the accumulation of GABA, delaying senescence, preserving quality and ameliorating chilling injury. Induction and co-ordinated gene expression, together with the biochemical properties and subcellular location of the corresponding encoded proteins, suggest that *MdGAD1,2*, *MdGABA-T1,2, MdSSADH1, MdCuAO1*, and *MdALDH10A8,9* are important determinants of GABA pathway activity in stored apple fruits, regardless of the storage condition. Notwithstanding, the targeted metabolite profiles suggest that protein hydrolysis, Ca^{2+}/CaM activation or H^+ stimulation of GAD activity, and changing redox balance are especially significant under LT, CA conditions. Furthermore, flux estimates suggest that the GABA pool is primarily derived from Glu, rather than PAs, and that SSA is converted mainly to succinate, rather than GHB.

Exogenous GABA is a promising strategy for promoting the level of endogenous GABA and the activity of the GABA shunt, which results in increased carbon flux through respiratory pathways, leading to elevated levels of NADH, NADPH and ATP (Aghdam et al., 2018, 2020; Shelp et al., 2021). Adequate ATP and NADPH are essential for: (i) fortifying the activity of ROS avoidance and scavenging systems; (ii) promoting the accumulation of endogenous proline and PAs; (iii) promoting the activity of secondary pathways, which results in the generation of salicylate for promoting the expression and activity of PR proteins, as well as phenols, flavonoids, and anthocyanins for scavenging radicals; (iv) limiting the activity of phospholipase D and lipoxygenase, resulting in increased membrane stability and fluidity; and (v) enhancing NADPH oxidase activity for triggering H_2O_2 accumulation. As a result, chilling injury and fungal / bacterial decay are deterred during postharvest storage, delaying senescence, preserving nutritional quality, and improving the postharvest marketability of horticultural crops. The occurrence of the tonoplastic ALMT presents the

opportunity to restrict transpirational water loss by applying exogenous GABA to negatively regulate malate influx into the vacuole and light-induced stomatal opening in cut flowers and immature green fruit. Also, both the ALMT transporter and tonoplast CAT exchanger present the opportunity to manipulate fruit flavor. Available evidence suggests that exogenous GABA does not adversely affect human or environment health, though further optimization of microbial fermentation is probably necessary to ensure an adequate commercial supply of GABA for use as a biostimulant in the postharvest storage of horticultural commodities.

AUTHOR CONTRIBUTIONS

MA conceived and wrote the original manuscript, prepared original figures, and reviewed the revised manuscript. EF conducted the bioinformatics analysis, and reviewed the original and revised manuscripts. BS conceived and administered the project, and revised the original manuscript and figures. All authors have read and agreed to the published version of the manuscript.

FUNDING

This work was supported by the Imam Khomeini International University (MA) (12006) and the Natural Sciences and Engineering Research Council of Canada (BS) (400-367). The funding sources had no involvement in the study design; in the collection, analysis and interpretation of the data; in the writing of the report; and in the decision to submit the article for publication.

REFERENCES

Aghdam, M. S., Jannatizadeh, A., Luo, Z., and Paliyath, G. (2018). Ensuring sufficient intracellular ATP supplying and friendly extracellular ATP signaling attenuates stresses, delays senescence and maintains quality in horticultural crops during postharvest life. *Trends Food Sci. Technol.* 76, 67–81. doi: 10.1016/j.tifs.2018.04.003

Aghdam, M. S., Kakavand, F., Rabiei, V., Zaare-Nahandi, F., and Razavi, F. (2019). γ-Aminobutyric acid and nitric oxide treatments preserve sensory and nutritional quality of cornelian cherry fruits during postharvest cold storage by delaying softening and enhancing phenols accumulation. *Sci. Hortic.* 246, 812–817. doi: 10.1016/j.scienta.2018.11.064

Aghdam, M. S., Naderi, R., Jannatizadeh, A., Babalar, M., Sarcheshmeh, M. A., and Faradonbe, M. Z. (2016a). Impact of exogenous GABA treatments on endogenous GABA metabolism in anthurium cut flowers in response to postharvest chilling temperature. *Plant Physiol. Biochem.* 106, 11–15. doi: 10.1016/j.plaphy.2016.04.045

Aghdam, M. S., Naderi, R., Jannatizadeh, A., Sarcheshmeh, M. A. A., and Babalar, M. (2016b). Enhancement of postharvest chilling tolerance of anthurium cut flowers by γ-aminobutyric acid (GABA) treatments. *Sci. Hortic.* 198, 52–60. doi: 10.1016/j.scienta.2015.11.019

Aghdam, M. S., Naderi, R., Sarcheshmeh, M. A. A., and Babalar, M. (2015). Amelioration of postharvest chilling injury in anthurium cut flowers by γ-aminobutyric acid (GABA) treatments. *Postharv. Biol. Technol.* 110, 70–76. doi: 10.1016/j.postharvbio.2015.06.020

Aghdam, M. S., Palma, J. M., and Corpas, F. J. (2020). NADPH as a quality footprinting in horticultural crops marketability. *Tr. Food Sci. Technol.* 103, 152–161. doi: 10.1016/j.tifs.2020.07.002

Akula, R., and Mukherjee, S. (2020). New insights on neurotransmitters signaling mechanisms in plants. *Plant Signal. Behav.* 15:1737450. doi: 10.1080/15592324.2020.1737450

Al Shoffe, Y., Nock, J. F., Zhang, Y., and Watkins, C. B. (2021). Pre- and post-harvest γ-aminobutyric acid application in relation to fruit quality and physiological disorder development in 'Honeycrisp' apples. *Sci. Hortic.* 289:110431. doi: 10.1016/j.scienta.2021.110431

Ali, S., Anjum, M. A., Nawaz, A., Ejaz, S., Anwar, R., Khaliq, G., et al. (2022). Postharvest γ-aminobutyric acid application mitigates chilling injury of aonla (*Emblica officinalis* Gaertn.) fruit during low temperature storage. *Postharv. Biol. Technol.* 185:111803. doi: 10.1016/j.postharvbio.2021.111803

Allan, W. L., Peiris, C., Bown, A. W., and Shelp, B. J. (2003). Gammahydroxybutyrate accumulates in green tea and soybean sprouts in response to oxygen deficiency. *Can. J. Plant Sci.* 83, 951–953. doi: 10.4141/p03-085

Bai, Y., Dougherty, L., Cheng, L., and Xu, K. (2015). A co-expression gene network associated with developmental regulation of apple fruit acidity. *Mol. Genet. Genom.* 290, 1247–1263. doi: 10.1007/s00438-014-0986-2

Ban, S., and Xu, K. (2020). Identification of two QTLs associated with high fruit acidity in apple using pooled genome sequencing analysis. *Hortic. Res.* 7:171. doi: 10.1038/s41438-020-00393-y

Blanch, M., Sanchez-Ballesta, M. T., Escribano, M. I., and Merodio, C. (2012). Water distribution and ionic balance in response to high CO_2 treatments in strawberries (*Fragaria vesca* L. cv. Mara de Bois). *Postharv. Biol. Technol.* 73, 63–71. doi: 10.1016/j.postharvbio.2012.06.003

Boonstra, E., de Kleijn, R., Colzato, L. S., Alkemade, A., Forstmann, B. U., and Nieuwenhuis, S. (2015). Neurotransmitters as food supplements: the effects of GABA on brain and behavior. *Front. Psychol.* 6:1520. doi: 10.3389/fpsyg.2015.01520

Bor, M., and Turkan, I. (2019). Is there a room for GABA in ROS and RNS signalling? *Environ. Exp. Bot.* 161, 67–73. doi: 10.1016/j.envexpbot.2019.02.015

Bown, A. W., and Shelp, B. J. (2006). Gamma-aminobutyrate: defense against invertebrate pests. *Trends Plant Sci.* 11, 424–427. doi: 10.1016/j.tplants.2006.07.002

Bown, A. W., and Shelp, B. J. (2016). Plant GABA: not just a metabolite. *Trends Plant Sci.* 21, 811–813. doi: 10.1016/j.tplants.2016.08.001

Brikis, C. J., Zarei, A., Chiu, G. Z., Deyman, K. L., Liu, J., Trobacher, C. P., et al. (2018). Targeted quantitative profiling of metabolites and gene transcripts associated with 4-aminobutyrate (GABA) in apple fruit stored under multiple abiotic stresses. *Hortic. Res.* 5:61. doi: 10.1038/s41438-018-0069-3

Brikis, C. J., Zarei, A., Trobacher, C. P., DeEll, J. R., Akama, K., Mullen, R. T., et al. (2017). Ancient plant glyoxylate/succinic semialdehyde reductases: GLYR1s are cytosolic, whereas GLYR2s are localized to both mitochondria and plastids. *Front. Plant Sci.* 8:601. doi: 10.3389/fpls.2017.006

Carvajal, F., Palma, F., Jamilena, M., and Garrido, D. (2015). Preconditioning treatment induces chilling tolerance in zucchini fruit improving different physiological mechanisms against cold injury. *Ann. Appl. Biol.* 166, 340–354. doi: 10.1111/aab.12189

Chen, Q., Li, M.-S., Ding, W., Tao, M.-M., Li, M.-R., Qi, Q., et al. (2020). Effects of high N_2/CO_2 in package treatment on polyamine-derived 4-aminobutyrate (GABA) biosynthesis in cold-stored white mushrooms (*Agaricus bisporus*). *Postharv. Biol. Technol.* 162:111093. doi: 10.1016/j.postharvbio.2019.111093

Chen, Q., Zhang, Y., Tao, M., Li, M., Wu, Y., Qi, Q., et al. (2018). Comparative metabolic responses and adaptive strategies of tea leaves (*Camellia sinensis*) to N_2 and CO_2 anaerobic treatment by a nontargeted metabolomics approach. *J. Agric. Food Chem.* 66, 9565–9572. doi: 10.1021/acs.jafc.8b03067

Chiu, G. Z., Shelp, B. J., Bowley, S. R., DeEll, J. R., and Bozzo, G. G. (2015). Controlled atmosphere-related injury in 'Honeycrisp'apples is associated with γ-aminobutyrate accumulation. *Can. J. Plant Sci.* 95, 879–886. doi: 10.4141/CJPS-2015-061

Chung, I., Bown, A. W., and Shelp, B. J. (1992). The production and efflux of 4-aminobutyrate in isolated mesophyll cells. *Plant Physiol.* 99, 659–664. doi: 10.1104/pp.99.2.659

Clark, S. M., Di Leo, R., Dhanoa, P. K., Van Cauwenberghe, O. R., Mullen, R. T., and Shelp, B. J. (2009a). Biochemical characterization, mitochondrial localization, expression, and potential functions for an *Arabidopsis* γ-aminobutyrate transaminase that utilizes both pyruvate and glyoxylate. *J. Exp. Bot.* 60, 1743–1757. doi: 10.1093/jxb/erp044

Clark, S. M., Di Leo, R., Van Cauwenberghe, O. R., Mullen, R. T., and Shelp, B. J. (2009b). Subcellular localization and expression of multiple tomato γ-aminobutyrate transaminases that utilize both pyruvate and glyoxylate. *J. Exp. Bot.* 60, 3255–3267. doi: 10.1093/jxb/erp161

Cukrov, D., Zermiani, M., Brizzolara, S., Cestaro, A., Licausi, F., Luchinat, C., et al. (2016). Extreme hypoxic conditions induce selective molecular responses and metabolic reset in detached apple fruit. *Front. Plant Sci.* 7:146. doi: 10.3389/fpls.2016.00146

Deewatthanawong, R., and Watkins, C. B. (2010). Accumulation of γ-aminobutyric acid in apple, strawberry and tomato fruit in response to postharvest treatments. *Acta Hortic.* 877, 947–952. doi: 10.17660/actahortic.2010.877.127

Deewatthanawong, R., Nock, J. F., and Watkins, C. B. (2010a). γ-Aminobutyric acid (GABA) accumulation in four strawberry cultivars in response to elevated CO_2 storage. *Postharv. Biol. Technol.* 57, 92–96. doi: 10.1016/j.postharvbio.2010.03.003

Deewatthanawong, R., Rowell, P., and Watkins, C. B. (2010b). γ-Aminobutyric acid (GABA) metabolism in CO_2 treated tomatoes. *Postharv. Biol. Technol.* 57, 97–105. doi: 10.1016/j.postharvbio.2010.03.007

Deyman, K. L., Brikis, C. J., Bozzo, G. G., and Shelp, B. J. (2014a). Impact of 1-methylcyclopropene and controlled atmosphere storage on polyamine and 4-aminobutyrate levels in "Empire" apple fruit. *Front. Plant Sci.* 5:144. doi: 10.3389/fpls.2014.00144

Deyman, K. L., Chiu, G., Liu, J., Brikis, C. J., Trobacher, C. P., DeEll, J. R., et al. (2014b). Effects of elevated CO_2 and 1-methylcyclopropene on storage-related disorders of Ontario-grown 'Empire' apples. *Can. J. Plant Sci.* 94, 857–865. doi: 10.4141/CJPS-2014-040

Ebrahimzadeh, A., Pirzad, F., Tahanian, H., and Aghdam, M. S. (2019). Influence of gum arabic enriched with GABA coating on oxidative damage of walnut kernels. *Food Technol. Biotechnol.* 57, 554–560. doi: 10.17113/ftb.57.04.19.6380

Flaherty, E. J., Lum, G. B., DeEll, J. R., Subedi, S., Shelp, B. J., and Bozzo, G. G. (2018). Metabolic alterations in postharvest pear fruit as influenced by 1-methylcyclopropene and controlled atmosphere storage. *J. Agric. Food Chem.* 66, 12989–12999. doi: 10.1021/acs.jafc.8b04912

Fu, D., Sun, Y., Yu, C., Zheng, X., Yu, T., and Lu, H. (2017). Comparison of the effects of three types of aminobutyric acids on the control of *Penicillium expansum* infection in pear fruit. *J. Sci. Food Agric.* 97, 1497–1501. doi: 10.1002/jsfa.7891

Gahir, S., Bharath, P., and Raghavendra, A. S. (2021). Stomatal closure sets in motion long-term strategies of plant defense against microbial pathogens. *Front. Plant Sci.* 12:761952. doi: 10.3389/fpls.2021.761952

Gao, H., Wu, S., Zeng, Q., Li, P., and Guan, W. (2018a). Effects of exogenous γ-aminobutyric acid treatment on browning and food-borne pathogens in fresh-cut apples. *Postharv. Biol. Technol.* 146, 1–8. doi: 10.1016/j.postharvbio.2018.08.007

Gao, H., Zeng, Q., Ren, Z., Li, P., and Xu, X. (2018b). Effect of exogenous gamma-aminobutyric acid treatment on the enzymatic browning of fresh-cut potato during storage. *J. Food Sci. Technol.* 55, 5035–5044. doi: 10.1007/s13197-018-3442

Ge, Y., Duan, B., Li, C., Tang, Q., Li, X., Wei, M., et al. (2018). γ-Aminobutyric acid delays senescence of blueberry fruit by regulation of reactive oxygen species metabolism and phenylpropanoid pathway. *Sci. Hortic.* 240, 303–309. doi: 10.1016/j.scienta.2018.06.044

Godoy, F., Olivos-Hernández, K., Stange, C., and Handford, M. (2021). Abiotic stress in crop species: improving tolerance by applying plant metabolites. *Plants* 10, 186. doi: 10.3390/plants10020186

Grewal, J. (2020). Gamma-aminobutyric acid (GABA): a versatile bioactive compound. *Eur. J. Mol. Clin. Med.* 7, 3068–3075. doi: 10.1007/s00726-020-02885-6

Habibi, F., Ramezanian, A., Guillén, F., Serrano, M., and Valero, D. (2020). Blood oranges maintain bioactive compounds and nutritional quality by postharvest treatments with γ-aminobutyric acid, methyl jasmonate or methyl salicylate during cold storage. *Food Chem.* 306:125634. doi: 10.1016/j.foodchem.2019.125634

Habibi, F., Ramezanian, A., Rahemi, M., Eshghi, S., Guillén, F., Serrano, M., et al. (2019). Postharvest treatments with γ-aminobutyric acid, methyl jasmonate, or methyl salicylate enhance chilling tolerance of blood orange fruit at prolonged cold storage. *J. Sci. Food Agric.* 99, 6408–6417. doi: 10.1002/jsfa.9920

Han, S., Liu, H., He, Y., Nan, Y., Qu, W., and Rao, J. (2021). Effects of calcium treatment on malate metabolism and γ-aminobutyric acid (GABA) pathway in postharvest apple fruit. *Food Chem.* 334, 127479. doi: 10.1016/j.foodchem.2020.127479

Han, S., Nan, Y., Qu, W., He, Y., Ban, Q., Lv, Y., et al. (2018). Exogenous γ-aminobutyric acid treatment that contributes to regulation of malate metabolism and ethylene synthesis in apple fruit during storage. *J. Agric. Food Chem.* 66, 13473–13482. doi: 10.1021/acs.jafc.8b04674

Hansen, M. E., Sørensen, H., and Cantwell, M. (2001). Changes in acetaldehyde, ethanol and amino acid concentrations in broccoli florets during air and controlled atmosphere storage. *Postharv. Biol. Technol.* 22, 227–237. doi: 10.1016/s0925-5214(01)00093-x

Hijaz, F., and Killiny, N. (2019). Exogenous GABA is quickly metabolized to succinic acid and fed into the plant TCA cycle. *Plant Signal. Behav.* 14:e1573096. doi: 10.1080/15592324.2019.1573096

Hou, Y., Ren, H., Wang, K., Cao, S., Zheng, Y., Wei, Y., et al. (2022). Influence of fresh-cut process on γ-aminobutyric acid (GABA) metabolism and sensory properties in carrot. *J. Food Sci. Technol.* 59, 552–561. doi: 10.1007/s13197-021-05039-y

Jin, Y. H., Hong, J. H., Lee, J.-H., Yoon, H., Pawluk, A. M., Yun, S. J., et al. (2021). Lactic acid fermented green tea with *Levilactobacillus brevis* capable of producing γ-aminobutyric acid. *Fermentation* 7:110. doi: 10.3390/fermentation7030110

Jung, S., Lee, T., Cheng, C.-H., Buble, K., Zheng, P., Yu, J., et al. (2019). 15 years of GDR: new data and functionality in the genome database for rosaceae. *Nucleic Acids Res.* 47, D1137–D1145. doi: 10.1093/nar/gky1000

Koike, S., Matsukura, C., Takayama, M., Asamizu, E., and Ezura, H. (2013). Suppression of γ-aminobutyric acid (GABA) transaminases induces prominent GABA accumulation, dwarfism and infertility in the tomato (*Solanum lycopersicum* L.). *Plant Cell Physiol.* 54, 793–807. doi: 10.1093/pcp/pct035

Kyriacou, M. C., and Rouphael, Y. (2018). Towards a new definition of quality for fresh fruits and vegetables. *Sci. Hortic.* 234, 463–469. doi: 10.1016/j.scienta.2017.09.046

Laroute, V., Mazzoli, R., Loubière, P., Pessione, E., and Cocaign-Bousquet, M. (2021). Environmental conditions affecting GABA production in *Lactococcus lactis* NCDO 2118. *Microorganisms* 9:122. doi: 10.3390/microorganisms9010122

Li, C., Dougherty, L., Coluccio, A. E., Meng, D., El-Sharkawy, I., Borejsza-Wysocka, E., et al. (2020). Apple ALMT9 requires a conserved C-terminal domain. *Plant Physiol.* 182, 992–1006. doi: 10.1104/pp.19.01300

Li, D., Li, L., Xiao, G., Limwachiranon, J., Xu, Y., Lu, H., et al. (2018). Effects of elevated CO_2 on energy metabolism and gamma-aminobutyric acid shunt pathway in postharvest strawberry fruit. *Food Chem.* 265, 281–289. doi: 10.1016/j.foodchem.2018.05.106

Li, E., Luo, X., Liao, S., Shen, W., Li, Q., Liu, F., et al. (2018). Accumulation of γ-aminobutyric acid during cold storage in mulberry leaves. *Int. J. Food Sci. Technol.* 53, 2664–2672. doi: 10.1111/ijfs.13875

Li, J., Zhou, X., Wei, B., Cheng, S., Zhou, Q., and Ji, S. (2019). GABA application improves the mitochondrial antioxidant system and reduces peel browning in 'Nanguo' pears after removal from cold storage. *Food Chem.* 297, 124903. doi: 10.1016/j.foodchem.2019.05.177

Liao, J., Wu, X., Xing, Z., Li, Q., Duan, Y., Fang, W., et al. (2017). γ-Aminobutyric acid (GABA) accumulation in tea (*Camellia sinensis* L.) through the GABA shunt and polyamine degradation pathways under anoxia. *J. Agric. Food Chem.* 65, 3013–3018. doi: 10.1021/acs.jafc.7b00304

Limami, A. M., Glévarec, G., Ricoult, C., Cliquet, J.-B., and Planchet, E. (2008). Concerted modulation of alanine and glutamate metabolism in young *Medicago truncatula* seedlings under hypoxic stress. *J. Exp. Bot.* 59, 2325–2335. doi: 10.1093/jxb/ern102

Lum, G. B., Shelp, B. J., DeEll, J. R., and Bozzo, G. G. (2016b). Oxidative metabolism is associated with physiological disorders in fruits stored under multiple environmental stresses. *Plant Sci.* 245, 143–152. doi: 10.1016/j.plantsci.2016.02.005

Lum, G. B., Brikis, C. J., Deyman, K. L., Subedi, S., DeEll, J. R., Shelp, B. J., et al. (2016a). Pre-storage conditioning ameliorates the negative impact of 1-methylcyclopropene on physiological injury and modifies the response of antioxidants and γ-aminobutyrate in 'Honeycrisp' apples exposed to controlled-atmosphere conditions. *Postharv. Biol. Technol.* 116, 115–128. doi: 10.1016/j.postharvbio.2016.01.013

Lum, G. B., DeEll, J. R., Hoover, G. J., Subedi, S., Shelp, B. J., and Bozzo, G. G. (2017). 1-Methylcyclopropene and controlled atmosphere modulate oxidative stress metabolism and reduce senescence-related disorders in stored pear fruit. *Postharv. Biol. Technol.* 129, 52–63. doi: 10.1016/j.postharvbio.2017.03.008

Mae, N., Makino, Y., Oshita, S., Kawagoe, Y., Tanaka, A., Aoki, K., et al. (2012). Accumulation mechanism of γ-aminobutyric acid in tomatoes (*Solanum lycopersicum* L.) under low O_2 with and without CO_2. *J. Agric. Food Chem.* 60, 1013–1019. doi: 10.1021/jf2046812

Makino, Y., Soga, N., Oshita, S., Kawagoe, Y., and Tanaka, A. (2008). Stimulation of γ-aminobutyric acid production in vine-ripe tomato (*Lycopersicon esculentum* Mill.) fruits under modified atmospheres. *J. Agric. Food Chem.* 56, 7189–7193. doi: 10.1021/jf801516e

Mei, X., Chen, Y., Zhang, L., Fu, X., Wei, Q., Grierson, D., et al. (2016). Dual mechanisms regulating glutamate decarboxylases and accumulation of gamma-aminobutyric acid in tea (*Camellia sinensis*) leaves exposed to multiple stresses. *Sci. Rep.* 6:23685. doi: 10.1038/srep23685

Mekonnen, D. W., Flügge, U.-I., and Ludewig, F. (2016). Gamma-aminobutyric acid depletion affects stomata closure and drought tolerance of *Arabidopsis thaliana*. *Plant Sci.* 245, 25–34. doi: 10.1016/j.plantsci.2016.01.005

Merodio, C., Muñoz, M. T., Cura, B. D., Buitrago, D., Escribano, M., and Isabel, I. A. (1998). Effect of high CO_2 level on the titres of γ-aminobutyric acid, total polyamines and some pathogenesis-related proteins in cherimoya fruit stored at low temperature. *J. Exp. Bot.* 49, 1339–1347. doi: 10.1093/jexbot/49.325.1339

Nazoori, F., ZamaniBahramabadi, E., Mirdehghan, S. H., and Rafie, A. (2020). Extending the shelf life of pomegranate (*Punica granatum* L.) by GABA coating application. *J. Food Meas. Charact.* 14, 2760–2772. doi: 10.1007/s11694-020-00521-1

Niazi, Z., Razavi, F., Khademi, O., and Aghdam, M. S. (2021). Exogenous application of hydrogen sulfide and γ-aminobutyric acid alleviates chilling injury and preserves quality of persimmon fruit (*Diospyros kaki*, cv. Karaj) during cold storage. *Sci. Hortic.* 285:110198. doi: 10.1016/j.scienta.2021.110198

Oketch-Rabah, H. A., Madden, E. F., Roe, A. L., and Betz, J. M. (2021). United States pharmacopeia (USP) safety review of gamma-aminobutyric acid (GABA). *Nutrients* 13:2742. doi: 10.3390/nu13082742

Palma, F., Carvajal, F., Jamilena, M., and Garrido, D. (2014). Contribution of polyamines and other related metabolites to the maintenance of zucchini fruit quality during cold storage. *Plant Physiol. Biochem.* 82, 161–171. doi: 10.1016/j.plaphy.2014.06.001

Palma, F., Carvajal, F., Jiménez-Muñoz, R., Pulido, A., Jamilena, M., and Garrido, D. (2019). Exogenous γ-aminobutyric acid treatment improves the cold tolerance of zucchini fruit during postharvest storage. *Plant Physiol. Biochem.* 136, 188–195. doi: 10.1016/j.plaphy.2019.01.023

Podlešáková, K., Ugena, L., Spichal, L., Dolezal, K., and De Diego, N. (2019). Phytohormones and polyamines regulate plant stress responses by altering GABA pathway. *Nat. Biotechnol.* 48, 53–65. doi: 10.1016/j.nbt.2018.07.003

Pott, D. M., de Abreu e Limab, F., Soria, C., Willmitzer, L., Fernie, A. R., Nikoloski, Z., et al. (2020). Metabolic reconfiguration of strawberry physiology in response to postharvest practices. *Food Chem.* 321:126747. doi: 10.1016/j.foodchem.2020.126747

Rabiei, V., Kakavand, F., Zaare-Nahandi, F., Razavi, F., and Aghdam, M. (2019). Nitric oxide and γ-aminobutyric acid treatments delay senescence of cornelian cherry fruits during postharvest cold storage by enhancing antioxidant system activity. *Sci. Hortic.* 243, 268–273. doi: 10.1016/j.scienta.2018.08.034

Rastegar, S., Khankahdani, H. H., and Rahimzadeh, M. (2019). Effect of γ-aminobutyric acid on the antioxidant system and biochemical changes of mango fruit during storage. *J. Food Meas. Charact.* 14, 778–789. doi: 10.1007/s11694-019-00326-x

Rothan, C., Duret, S., Chevalier, C., and Raymond, P. (1997). Suppression of ripening-associated gene expression in tomato fruits subjected to a high CO_2 concentration. *Plant Physiol.* 114, 255–263. doi: 10.1104/pp.114.1.255

Seifikalhor, M., Aliniaeifad, S., Hassani, B., Nikman, V., and Lastochkina, O. (2019). Diverse role of γ-aminobutyric acid in dynamic plant responses. *Plant Cell Rep.* 38, 847–867. doi: 10.1007/s00299-019-02396-z

Shang, H., Cao, S., Yang, Z., Cai, Y., and Zheng, Y. (2011). Effect of exogenous gamma-aminobutyric acid treatment on proline accumulation and chilling injury in peach fruit after long-term cold storage. *J. Agric. Food Chem.* 59, 1264–1268. doi: 10.1021/jf104424z

Shekari, A., Hassani, R. N., and Aghdam, M. S. (2021). Exogenous application of GABA retards cap browning in *Agaricus bisporus* and its possible mechanism. *Postharv. Biol. Technol.* 174:111434. doi: 10.1016/j.postharvbio.2020.111434

Shelp, B. J., Aghdam, M. S., and Flaherty, E. J. (2021). γ-Aminobutyrate (GABA) regulated plant defense: mechanisms and opportunities. *Plants* 10:1939. doi: 10.3390/plants10091939

Shelp, B. J., Bozzo, G. G., Trobacher, C. P., Zarei, A., Deyman, K. L., and Brikis, C. J. (2012b). Hypothesis/review: contribution of putrescine to 4-aminobutyrate (GABA) production in response to abiotic stress. *Plant Sci.* 193–194, 130–135. doi: 10.1016/j.plantsci.2012.06.001

Shelp, B. J., Bozzo, G. G., Trobacher, C. P., Chiu, G., and Bajwa, V. S. (2012a). Strategies and tools for studying the metabolism and function of γ-aminobutyrate in plants. I. Pathway structure. *Botany* 90, 651–668. doi: 10.1139/B2012-030

Shelp, B. J., Bozzo, G. G., Zarei, A., Simpson, J. P., Trobacher, C. P., and Allan, W. L. (2012c). Strategies and tools for studying the metabolism and function of γ-aminobutyrate in plants. II. Integrated analysis. *Botany* 90, 781–793. doi: 10.1139/B2012-041

Shelp, B. J., and Zarei, A. (2017). Subcellular compartmentation of 4-aminobutyrate (GABA) metabolism in arabidopsis: An update. *Plant Signal. Behav.* 12:e1322244. doi: 10.1080/15592324.2017.1322244

Sheng, L., Shen, D., Luo, Y., Sun, X., Wang, J., Luo, T., et al. (2017). Exogenous γ-aminobutyric acid treatment affects citrate and amino acid accumulation to improve fruit quality and storage performance of postharvest citrus fruit. *Food Chem.* 216, 138–145. doi: 10.1016/j.foodchem.2016.08.024

Shimajiri, Y., Ozaki, K., Kainou, K., and Akama, K. (2013). Differential subcellular localization, enzymatic properties and expression patterns of γ-aminobutyric transaminases (GABA-T) in rice (*Oryza sativa*). *J. Plant Physiol.* 170, 196–201. doi: 10.1111/pbi.12050

Snedden, W. A., Arazi, T., Fromm, H., and Shelp, B. J. (1995). Calcium/calmodulin activation of soybean glutamate decarboxylase. *Plant Physiol.* 108, 543–549. doi: 10.1104/pp.108.2.543

Snowden, C. J., Thomas, B., Baxter, C. J., Smith, J. A. C., and Sweetlove, L. J. (2015). A tonoplast Glu/Asp/GABA exchanger that affects tomato fruit amino acid composition. *Plant J.* 81, 651–660. doi: 10.1111/tpj.12766

Suhel, M., Husain, T., Pandey, A., Singh, S., Dubey, N. K., Prasad, S. M., et al. (2022). An appraisal of ancient molecule GABA in abiotic stress tolerance in plants, and its crosstalk with other signaling molecules. *J. Plant Growth Regul.* doi: 10.1007/s00344-022-10610-8

Takayama, M., and Ezura, H. (2015). How and why does tomato accumulate a large amount of GABA in the fruit? *Front. Plant Sci.* 6:612. doi: 10.3389/fpls.2015.00612

Tarkowski, K. P., Signorelli, S., and Höfte, M. (2020). γ-Aminobutyric acid and related amino acids in plant immune responses: emerging mechanisms of action. *Plant Cell Environ.* 43, 1103–1116. doi: 10.1111/pce.13734

The United States Environmental Protection Agency (2004). *L-Glutamic Acid and Gamma Aminobutyric Acid: Order Denying Objections to Issuance of Tolerance. 40 CFR Part 180*, Vol. 69. Washington, DC: EPA.

Trobacher, C. P., Clark, S. M., Bozzo, G. G., Mullen, R. T., DeEll, J. R., and Shelp, B. J. (2013a). Catabolism of GABA in apple fruit: Subcellular localization and biochemical characterization of two γ-aminobutyrate transaminases. *Postharv. Biol. Technol.* 75, 106–113. doi: 10.1016/j.postharvbio.2012.08.005

Trobacher, C. P., Zarei, A., Liu, J., Clark, S. M., Bozzo, G. G., and Shelp, B. J. (2013b). Calmodulin-dependent and calmodulin-independent glutamate decarboxylases in apple fruit. *BMC Plant Biol.* 13:144. doi: 10.1186/1471-2229-13-144

Tuin, L. G., and Shelp, B. J. (1994). In situ [^{14}C]glutamate metabolism by developing soybean cotyledons I. Metabolic routes. *J. Plant Physiol.* 143, 1–7. doi: 10.1016/s0176-1617(11)82089-4

Van Cauwenberghe, O. R., and Shelp, B. J. (1999). Biochemical characterization of partially purified GABA:pyruvate transaminase from *Nicotiana tabacum*. *Phytochemistry* 52, 575–581. doi: 10.1016/s0031-9422(99)00301-5

van Meeteren, U., and Aliniaeifard, S. (2016). "Stomata and postharvest physiology," in *Postharvest Ripening Physiology of Crops*, ed. S. Pareek (Boca Raton, FL: CRC Press), 157–191.

Wang, C., Fan, L., Gao, H., Wu, X., Li, J., and Lv, G. (2014). Polyamine biosynthesis and degradation are modulated by exogenous gamma-aminobutyric acid in root-zone hypoxia stressed melon roots. *Plant Physiol. Biochem.* 82, 17–26. doi: 10.1016/j.plaphy.2014.04.018

Wang, D., Li, D., Xu, Y., Li, L., Belwal, T., Zhang, X., et al. (2021). Elevated CO_2 alleviates browning development by modulating metabolisms of membrane lipids, proline, and GABA in fresh-cut Asian pear fruit. *Sci. Hortic.* 281:109932. doi: 10.1016/j.scienta.2021.109932

Wang, L., Wang, Y., Hou, Y., Zhu, X., Zheng, Y., and Jin, P. (2021). Physiological and metabolomic analyses of hot water treatment on amino acids and phenolic metabolisms in peach cold tolerance. *Postharv. Biol. Technol.* 179:111593. doi: 10.1016/j.postharvbio.2021.111593

Wang, Y., Luo, Z., Huang, X., Yang, K., Gao, S., and Du, R. (2014). Effect of exogenous γ-aminobutyric acid (GABA) treatment on chilling injury and antioxidant capacity in banana peel. *Sci. Hortic.* 168, 132–137. doi: 10.1016/j.scienta.2014.01.022

Xu, B., Sai, N., and Gilliham, M. (2021b). The emerging role of GABA as a transport regulator and physiological signal. *Plant Physiol.* 187, 2005–2016. doi: 10.1093/plphys/kiab347

Xu, B., Long, Y., Feng, X., Zhu, X., Sai, N., Chirkova, L., et al. (2021a). GABA signalling modulates stomatal opening to enhance plant water use efficiency and drought resilence. *Nat. Commun.* 12:1952. doi: 10.1038/s41467-021-21694-3

Yang, A., Cao, S., Yang, Z., Cai, Y., and Zheng, Y. (2011). γ-Aminobutyric acid treatment reduces chilling injury and activates the defence response of peach fruit. *Food Chem.* 129, 1619–1622. doi: 10.1016/j.foodchem.2011.06.018

Yang, J., Sun, C., Zhang, Y., Fu, D., Zheng, X., and Yu, T. (2017). Induced resistance in tomato fruit by gamma-aminobutyric acid for the control of alternaria rot caused by *Alternaria alternata*. *Food Chem.* 221, 1014–1020. doi: 10.1016/j.foodchem.2016.11.061

Yogeswara, I. B. A., Kittibunchakul, S., Rahayu, E. S., Domig, K. J., Haltrich, D., and Nguyen, T. H. (2021). Microbial production and enzymatic biosynthesis of γ-aminobutyric acid (GABA) using *Lactobacillus plantarum* FNCC 260 isolated from Indonesian fermented foods. *Processes* 9:22. doi: 10.3390/pr9010022

Yu, C., Zeng, L., Sheng, K., Chen, F., Zhou, T., Zheng, X., et al. (2014). γ-Aminobutyric acid induces resistance against *Penicillium expansum* by priming of defence responses in pear fruit. *Food Chem.* 159, 29–37. doi: 10.1016/j.foodchem.2014.03.011

Zarei, A., Brikis, C. J., Bajwa, V. S., Chiu, G. Z., Simpson, J. P., DeEll, J. R., et al. (2017). Plant glyoxylate/succinic semialdehyde reductases: comparative biochemical properties, function during chilling stress, and subcellular localization. *Front. Plant Sci.* 8:1399. doi: 10.3389/fpls.2017.01399

Zarei, A., Trobacher, C. P., Cooke, A. R., Meyers, A. J., Hall, J. C., and Shelp, B. J. (2015a). Apple fruit copper amine oxidase isoforms: peroxisomal MdAO1 prefers diamines as substrates, whereas extracellular MdAO2 exclusively utilizes monoamines. *Plant Cell Physiol.* 56, 137–147. doi: 10.1093/pcp/pcu155

Zarei, A., Trobacher, C. P., and Shelp, B. J. (2015b). NAD^+-aminoaldehyde dehydrogenase candidates for 4-aminobutyrate (GABA) and β-alanine production during terminal oxidation of polyamines in apple fruit. *FEBS Lett.* 589, 2695–2700. doi: 10.1016/j.febslet.2015.08.005

Zarei, A., Trobacher, C. P., and Shelp, B. J. (2016). Arabidopsis aldehyde dehydrogenase 10 family members confer salt tolerance through putrescine-derived 4-aminobutyrate (GABA) production. *Sci. Rep.* 6:35115. doi: 10.1038/srep35115

Zhao, P., Li, W., Zhen, C., Wang, K., Qin, Z., and Gao, H. (2021). Transcriptomic analysis of the effects of γ-aminobutyric acid treatment on browning and induced disease resistance in fresh-cut apples. *Postharv. Biol. Technol.* 181:111686. doi: 10.1016/j.postharvbio.2021.111686

Zhou, M., Ndeurumio, K. H., Zhao, L., and Hu, Z. (2016). Impact of precooling and controlled-atmosphere storage on γ-aminobutyric acid (GABA) accumulation in longan (*Dimocarpus ongan* Lour.) fruit. *J. Agric. Food Chem.* 64, 6443–6450. doi: 10.1021/acs.jafc.6b01738

Zhu, J., Li, C., Sun, L., Cheng, Y., Hou, J., Fan, Y., et al. (2022). Application of γ-aminobutyric acid induces disease resistance in apples through regulation of polyamine metabolism, GABA shunt and reactive oxygen species metabolism. *Sci. Hortic.* 291:110588. doi: 10.1016/j.scienta.2021.110588

Ziv, C., and Fallik, E. (2021). Postharvest storage techniques and quality evaluation of fruits and vegetables for reducing food loss. *Agronomy* 11:133. doi: 10.3390/agronomy11061133

Conflict of Interest: The authors declare that the research was conducted in the absence of any commercial or financial relationships that could be construed as a potential conflict of interest.

Publisher's Note: All claims expressed in this article are solely those of the authors and do not necessarily represent those of their affiliated organizations, or those of the publisher, the editors and the reviewers. Any product that may be evaluated in this article, or claim that may be made by its manufacturer, is not guaranteed or endorsed by the publisher.

frontiers | Frontiers in Plant Science

ORIGINAL RESEARCH
published: 22 June 2022
doi: 10.3389/fpls.2022.889709

A Photosynthetic Light Acclimation Model Accounting for the Effects of Leaf Age, Chlorophyll Content, and Intra-Leaf Radiation Transfer

Jan Graefe[1]*, *Wenjuan Yu*[1,2] *and Oliver Körner*[1]

[1] Leibniz-Institute of Vegetable and Ornamental Crops (IGZ), Next-Generation Horticultural Systems, Grossbeeren, Germany, [2] Department of Functional Genome and Gene Safety, Chinese Academy of Agricultural Sciences, Beijing, China

OPEN ACCESS

Edited by:
Jung Eek Son,
Seoul National University,
South Korea

Reviewed by:
Nikolaos Katsoulas,
University of Thessaly, Greece
Quan Wang,
Shizuoka University, Japan
Dae Ho Jung,
Cheonan Yonam College,
South Korea

***Correspondence:**
Jan Graefe
graefe@igzev.de

Specialty section:
This article was submitted to Crop and Product Physiology, a section of the journal Frontiers in Plant Science

Received: 04 March 2022
Accepted: 30 May 2022
Published: 22 June 2022

Citation:
Graefe J, Yu W and Körner O (2022) A Photosynthetic Light Acclimation Model Accounting for the Effects of Leaf Age, Chlorophyll Content, and Intra-Leaf Radiation Transfer. Front. Plant Sci. 13:889709. doi: 10.3389/fpls.2022.889709

Mechanistic models of canopy photosynthesis usually upscale leaf photosynthesis to crop level. A detailed prediction of canopy microclimate with accurate leaf morphological and physiological model parameters is the pre-requisite for accurate predictions. It is well established that certain leaf model parameters (V_{cmax}, J_{max}) of the frequently adopted Farquhar and Caemmerer photosynthesis model change with leaf age and light interception history. Previous approaches to predict V_{cmax} and J_{max} focused primarily on light interception, either by cumulative intercepted photosynthetic photon flux density (PPFD) or by closely related proxy variables such as leaf nitrogen content per leaf area. However, for plants with monopodial growth, such as vertically grown tomatoes or cucumber crops, in greenhouse production, there is a strong relationship between leaf age and light interception, complicating the experimental and mathematical separation of both effects. We propose a modeling framework that separates age and light intensity-related acclimation effects in a crop stand: Improved approximation of intra-leaf light absorption profiles with cumulative chlorophyll content (*Chl*) is the basis, while parameters are estimated *via* Gaussian process regression from total *Chl*, carotenoid content (*Car*), and leaf mass per area (*LMA*). The model approximates light absorption profiles within a leaf and links them to leaf capacity profiles of photosynthetic electron transport. Published datasets for *Spinacia oleracea* and *Eucalyptus pauciflora* were used to parameterize the relationship between light and capacity profiles and to set the curvature parameter of electron transport rate described by a non-rectangular hyperbola on *Cucumis sativus*. Using the modified capacity and light absorption profile functions, the new model was then able to predict light acclimation in a 2-month period of a fully grown tomato crop. An age-dependent lower limit of the electron transport capacity per

unit *Chl* was essential in order to capture the decline of V_{cmax} and J_{max} over time and space of the investigated tomato crop. We detected that current leaf photosynthetic capacity in tomato is highly affected by intercepted light-sum of 3–5 previous days.

Keywords: light acclimation, J_{max}, chlorophyll, tomato, intra-leaf, age, *LMA*, V_{cmax}

INTRODUCTION

At the heart of most experimental and theoretical plant growth studies are measurements or predictions of primary CO_2 assimilation at different spatial and temporal scales. Mathematical or biological integration of instantaneous CO_2 assimilation rates over total leaf area and day/night cycle cumulates to daily biomass growth rates excluding certain losses. Therefore, there has been much work on modeling leaf photosynthesis (von Caemmerer et al., 2009), canopy microclimate (Russell et al., 1990; Körner et al., 2007; Myneni and Ross, 2012), and its proper integration (Bonan et al., 2021) over the last decades. In addition, mechanistic models of canopy photosynthesis require for upscaling from leaf photosynthesis rates an accurate description of microclimate and well-estimated leaf-model parameters at different canopy positions.

Certain parameters (e.g., V_{cmax} and J_{max}) of the frequently used Farquhar–Caemmerer–Berry (FCB) leaf photosynthesis model (von Caemmerer et al., 2009) are not constant over time and change with leaf age and past light interception. Photosynthetic acclimation to shade is a well-investigated process both at leaf (Lichtenthaler and Babani, 2004) and intra-leaf levels (Nishio et al., 1993). Focus was often set on light acclimation using either the cumulative intercepted photosynthetic photon flux density (PPFD) or closely related proxy variables, such as the leaf nitrogen content per leaf area, as predictors for V_{cmax} and J_{max} (Meir et al., 2002; Niinemets et al., 2004).

For plants with a monopodial growth habit, such as vertically grown tomatoes or cucumber crops, in greenhouse production (as common in commercial practice), there is a strong relationship between leaf age and light interception (Niinemets, 2016), complicating the experimental and mathematical separation of both effects. This may limit the generality of previously developed acclimation models, especially with the introduction of novel cultivation procedures, e.g., intra-canopy lighting (Joshi et al., 2019). To prevent the concurrent change of leaf age and intercepted light, plants could be grown horizontally (Trouwborst et al., 2011a). This, however, is unpractical and introduces artifacts, e.g., the vertical dominance among plant organs is disturbed.

In this article, we hypothesized that modeling light and age acclimation at the intra-leaf level is a feasible approach for estimating vertical parameter profiles over time, i.e., it enables the separation of age and light intensity-related effects in a crop stand. Besides reanalyzing several datasets from the literature, we performed a greenhouse experiment with a vertical growing tomato crop observing leaf parameters in different canopy depths over time. From that, we assessed the spatial-temporal evolution of V_{cmax} and J_{max}.

MATERIALS AND METHODS

Model Theory, Extension, and Parameter Estimation

Light Absorption Profiles Within a Leaf

The intra-leaf profile of incident and absorbed radiation can be well described by a two-stream-type approach of simultaneous downward and upward radiation transfer with cumulative chlorophyll (a + b) content c within the leaf mesophyll (Terashima et al., 2009). The absorbed light intensity I_a(c) from both streams can be approximated by a simple exponential profile of incident light I(c) times a two-stream absorption coefficient k_a (Badeck, 1995; Buckley and Farquhar, 2004).

$$I_a(c) = k_a I(c) = I_0\, p_1 k_a \exp\left(-kc^{p_2}\right) \tag{1}$$

With incident irradiance I_0 on the upper leaf side, effective extinction coefficient k, scaling parameter p_1, and exponent p_2. We introduced the exponent p_2 to allow for an improved fit of Equation 1 to the two-stream solution.

As neither in nature nor in experimental systems, light incidence is exclusively one-sided, Equation 1 was generalized for a two-sided incidence by Buckley and Farquhar (2004) as follows:

$$I_a\left(c,\ w_u, I_0, k\right) = I_0\, p_1 k_a \left(\mathrm{w_u} \exp\left(-kc^{p_2}\right) + (1 - w_u)\ \exp\left(-k(Chl - c)^{p_2}\right)\right) \tag{2}$$

with total chlorophyll content (Chl) per leaf area [c = (0, Chl)] and fractional light incidence w_u on the upper leaf side, where I_0 here denotes the total incident light on both leaf sides.

To obtain predictive equations for the introduced parameters (p_1, p_2, k_a, and k), we applied the *Prospect-D* leaf spectra model (Féret et al., 2017) and computed scattering and absorption coefficients (k_s and k_a) with a two-stream solution within the leaf mesophyll:

$$\begin{aligned} \frac{dI_d}{dc} &= -\left(k_s + k_a\right) I_d + k_s I_u \ \textit{with} \quad I_d(0) = (1 - r_e) + r_i\, I_u(0) \\ \frac{dI_u}{dc} &= \left(k_s + k_a\right) I_u - k_s I_d \qquad\qquad I_u\left(Chl\right) = r_i\, I_d\left(Chl\right) \end{aligned} \tag{3}$$

with downward and upward propagating diffuse radiation fluxes I_d and I_u, respectively. External r_e (air → epidermis) and internal leaf surface reflectance r_i (epidermis → air) are calculated from leaf spectral refraction index (n, Féret et al., 2017) and by solving

the Fresnel equations for diffuse incident light (Stern, 1964; Jacquemoud and Baret, 1990). The general solution of Equation 3 was obtained (refer to Jacquemoud and Ustin, 2019) with two free constants (C_1 and C_2) to be estimated from boundary conditions stated in Equation 3. With given total leaf reflectance and total transmittance (R, T),

$$\begin{aligned} R = &\ I_u\,(0, C_1,\ C_2)\,(1 - r_i) + r_e \\ T = &\ I_d(Chl,\ C_1,\ C_2)(1 - r_i) \end{aligned} \tag{4}$$

The radiation transfer parameters k_s and k_a are estimated from the solution of Equation 4, and the forward problem (Equation 3) to obtain $I_d(c)$ and $I_u(c)$ can be computed.

Parameter Estimation of Light Profile Function

In our approach, I_a(c) was subsequently parameterized (i.e., p_1, p_2, k_a, and k) by a five-step procedure using leaf *Chl*, leaf carotenoid content (*Car*), and leaf mass per area (*LMA*):

1. A set of 470 leaves from the Lopex and Angers leaf spectral dataset (Jacquemoud et al., 2003) were selected (i.e., selected leaves exceed the 5% percentile values of *Chl* and leaf mass water content over the whole dataset).
2. Solving Equations 3, 4 for those leaves resulted accordingly in $i = 1...470$ values for $k_{s,i}$ $k_{a,i}$ and corresponding profiles of incident radiation I(c) = $I_{d,i}$(c) + $I_{u,i}$(c).
3. The obtained spectral values of $I_{d,i}$(c, λ) + $I_{u,i}$(c, λ) between 400 and 700 nm were integrated according to a D55 CIE daylight spectral density distribution (Muschaweck, 2021) characterizing a typical daytime sky. The two-stream spectral absorption coefficients k_a(λ) were combined similarly to spectral light intensities. In addition, photosynthetic effective absorption (i.e., assuming 100% for chlorophylls and 70% for carotenoids; Laisk et al., 2014) was accounted for by using the absorption spectra for chlorophyll, carotenoid, leaf dry matter, and water from the Prospect D model.
4. Spectral integrated $I_{d,i}$(c) + $I_{u,i}$(c) were then used to fit p_1, p_2, and k in Equation 1.
5. All obtained parameter sets (p_1, k_a, k, n = 470) were analyzed *via* machine learning (Gaussian process regression, MATLAB R2020a, Regression Learner App) using the leaf parameters (features), namely, *Chl*, *Car*, and *LMA*.

Modeling Photosynthetic Electron Transport

To estimate the whole leaf electron transport rate J_{leaf}, electron transport rate per unit chlorophyll $J_c(c)$ is integrated over cumulative *Chl* (i.e., mesophyll thickness; Badeck, 1995; Buckley and Farquhar, 2004) using the Blackman response (linear slope and asymptote, Equation 5). This is a good approximation for the light response of electron transport rate at single cell or chloroplast level (Terashima and Saeki, 1985):

$$\begin{aligned} J_{leaf}(I_0,\ Chl) = &\int_0^{Chl} J_c\,(c)\ \mathrm{dc} \\ = &\ \min[\varphi\ I_a\left(c,\ w_{u,m}, I_0, k\right),\ J_{c,max}(c, w_{u,g},\ I_*, k^{'})\ ]dc \end{aligned} \tag{5}$$

with PSII quantum efficiency of electron transport φ, fractional upper light incidence during measurement $w_{u,m}$ and growth $w_{u,g}$, respectively, a modified extinction coefficient k', characteristic leaf irradiance I^* during light acclimation (Buckley and Farquhar, 2004), and maximum electron transport rate per unit chlorophyll $J_{c,\max}$. As a generalization of Equation 5, we apply a non-rectangular hyperbola with curvature parameter θ for $J_c(c)$ with the equation as follows:

$$J_c\,(c) = \ (\varphi I_a + J_{c,max} - \sqrt{(\varphi I_a + J_{c,max})^2 - 4\theta\varphi I_a J_{c,max}})/(2\theta) \tag{6}$$

Following Buckley and Farquhar (2004), $J_{c,max}$ is described as a function of absorbed radiation profile with a characteristic light intensity I^*. We adopted that approach and extended it in three ways, namely, (1) time-dependent minimum [$J_{c,max,mn}$(t)] and (2) maximum [$J_{c,max,mx}$(t)] values, respectively, and (3) a modified extinction coefficient $k' = p_3$k (Equation 7). With p_3 = 1, the capacity profile of electron transfer would match the light absorption profile perfectly.

$$\begin{aligned} &J_{c,max}\left(c, w_{u,g},\ I_*, k'\right) \\ &= min\left\{J_{c,max,mx}\,(t)\,,\ max\left[J_{c,max,mn}(t),\ \varphi I_a\left(c,\ w_{u,g}, I^*, k'\right)\ \right]\right\} \end{aligned} \tag{7}$$

The characteristic light intensity I^* is determined from the light intensity history (i.e., past days) of each specific leaf. Besides light-induced changes in *Chl*, *Car*, and *LMA*, which determine the intra-leaf profiles (k') and optical depth (*Chl*), I^* may be interpreted as a mathematical proxy for light-induced changes of key photosynthetic enzymes or complexes (e.g. cytochrome b_6f) to chlorophyll ratios (Evans and Seemann, 1989; Eichelmann et al., 2005; Schöttler and Tóth, 2014).

Equation 2 may be applied to leaf gas exchange measurements obtained from a cuvette system (e.g., LI-6400, LICOR Bioscience) with an actinic light source at one leaf side. For that, leaf transmittance needs to be taken into account. Denoting the reflectance of the lower chamber wall by r_{ch} and neglecting multiple reflections, one obtains $w_{u,m}$ = 1/(1 + $T{\cdot}r_{ch}$) and I_0' = I_0(1 + $T{\cdot}r_{ch}$). Total leaf transmittance T is also estimated from *Chl*, *Car*, and *LMA* using Gaussian process regression. For the LI-6400 standard lower chamber wall, we assumed r_{ch} = 0.5. The quantum efficiency φ of absorbed photons was estimated using an expression given by Yin et al. (2004)

$$\varphi = \ \frac{1 - f_{cyc}}{1 + (1 - f_{cyc})/\Phi_{2m}} \tag{8}$$

With assumed values for the fraction of cyclic electron flow f_{cyc} (0) and maximum e^- transport efficiency of PSII Φ_{2m} [0.88, refer to discussion in Kalaji et al. (2017)]. Equation 8 yields φ = 0.468. Other effects of leaf absorptance α_L and non-photosynthetic contributions f are fully accounted for by I_a (Equation 2). This is similar to the approach frequently used for bulk leaves (von Caemmerer et al., 2009)

$$\varphi' = \ \varphi\ \alpha_L\ (1 - f) \tag{9}$$

Mathematically, J_{max} is the integral of $J_{c,max}(c)$ over the cumulative *Chl*, but in the context of A/C_i curves, the retrieved J_{max} should be rather approximated as $J_{leaf}(I_0', Chl)$ at constant light intensity I_0. Assuming a unique proportionality between the capacities of electron transport and the Calvin cycle throughout the leaf, V_{cmax} is given by

$$V_{cmax} = p_4 \int_0^{Chl} J_{c,max}\left(c, w_{u,g}, I_*, k'\right) dc \quad (10)$$

with additional parameter p_4.

Empirical Data

Tomato Greenhouse Experiment

Experiment and Crop Management

Tomato seeds (*"Pannovy"*) were sown on 2 January 2018; 9 days after sowing, 48 seedlings were transplanted to stone-wool cubes and placed in a greenhouse controlled at 18°C at the Leibniz Institute of Vegetable and Ornamental Crops (IGZ), Großbeeren, Germany (52.35 N 13.31 E). On 22 February 2018, 48 tomato plants were selected by uniformity and placed on inert fleece mats with drip irrigation in four rows of each 12 plants in one central compartment (28.8 m^2) of the gas-exchange greenhouse (GEGH) at the IGZ (Kläring and Körner, 2020). The remaining seven compartments were equipped in the same way, i.e., border effects were minimized. For a starting period of 12 days, the temperature was controlled to 19°C and 15°C during day and night, respectively; air relative humidity (RH) was set to 80% and air CO_2 concentration was maintained at 400 μmol mol^{-1} during daytime. From 5 March 2018, the greenhouse temperature was set at 23°C, while all other setpoints remained unchanged. During all time, water and nutrients were adequately supplied by an automated non-recirculating system. The nutrient solutions were prepared after de Kreij et al. (2003) and were adjusted daily to constrain electric conductivity (EC) between 2.2 and 2.5 dS m^{-1} and to a mean pH of 5.6. The canopy was maintained at 4 m heights, and the mean leaf number was 18 leaves per plant (counting leaves > 10 cm in length).

Measurements and Computations

Each plant in the canopy was virtually subdivided into 8 vertical layers. For a leaf residing in layer *i*, the overlaying *Leaf Area Index* counted to the top ($LAI_{t,i}$) was estimated from $LAI_{t,i} = (\sum_1^i 2S_{L,j} + S_{L,i})/S_p$ with total ground area per plant S_P (4,167 cm^2) and one-sided leaf surface area $S_{L,j}$ (cm^2) in layer *j*. Note that one of the two leaves is included in target layer *i*. The area of a single leaf was derived from time-dependent length (L) and width (W) of leaves as $S_{L,i} = 0.2568 \cdot W(t_L) \cdot L(t_L) + 11.725$ where leaf age (t_L) dependence was adopted from Yu and Körner (2020).

Using hourly recorded air temperatures from a within canopy-installed psychrometer, we calculated the effective thermal time for tomato phenology using a response function with cardinal temperatures adopted from the CROPGRO-Tomato model (Boote et al., 2012). Outside the greenhouse, recorded and hourly averaged PPFD (I_0) was modified for greenhouse structure transmission losses and used to calculate the mean intercepted $PPFD_{i,d}$ for each measured leaf during the last *d* days.

$$\overline{PPFD_{i,d}} = \sum_{t-1}^{t-d} I_0(t)\exp(-kLAI_{t,i}(t'))/n \quad (11)$$

with crop diffuse extinction coefficient k (0.72, Heuvelink, 1996) and back extrapolated $LAI_{t,i}$ starting from the end of the previous day to *d* days backward with a total of *n* daylight hours. Note that the specific value of *d* is estimated during parameter estimation.

Leaf photosynthesis assessments on marked leaves started on 5th of April that was 42 days after transplanting. Three non-neighboring plants, located in the center of the greenhouse, were selected for measuring CO_2 response curves in different vertical canopy levels (1–8). Weekly measurements of photosynthesis CO_2-response curves (A-C_i curves, LI-COR 6400; LI-COR Inc., Lincoln, NE, United States) were performed on three plants for all leaves with a length of >10 cm starting with leaf number 9 and terminating with leaf number 39. This corresponded to a leaf-age range from 20 to 57 days at the end of the measurements. All A/C_i curves were obtained on one of the two-second leaflets of each leaf (counted from petiole-base). Leaf temperature was set at 25°C, and CO_2 concentration (C_a) was changed stepwise to 400, 350, 300, 300, 250, 200, 100, 400, 450, 500, 550, 600, 800, and 1,000 μmol mol^{-1} while keeping PPFD constant at 1,500 μmol $m^{-2}s^{-1}$ at an average leaf vapor pressure deficit of about 2.5 kPa. Several measurements were taken within a period of 10 s and averaged after fluxes had been either stabilized or the maximum measurement time of 120 s was encountered. For obtaining the main biochemical parameters of the FCB model (i.e., V_{cmax}, J_{max} at 25°C) from gas exchange measurements, the fitting approach proposed by Ethier and Livingston (2004) was applied, which implicitly accounts partly for the mesophyll conductance effect. Notably, 2–3 single FCB estimates of V_{cmax} and J_{max} per layer and date were averaged.

A handheld spectrophotometer device (Pigment Analyzer PA-1101, CP, Falkensee, Germany), which measures spectral remission between 320 and 1,120 nm at a spectral resolution (SR) of 3.3 nm (Kläring and Zude, 2009), was used on the same plants and leaves (upper side) as used for gas exchange measurements. We applied the Angers optical dataset (Jacquemoud et al., 2003, SR = 1 nm, dicot leaves) to calibrate the optical output of the Pigment Analyzer according to the following equation:

$$Chl\left(\frac{\mu g}{cm^2}\right) = 57.74\frac{R713 - R709}{R703 - R699} - 18.11 \quad (12)$$

with estimated total chlorophyll (a + b) content per leaf area and measured remissions (of reflectance) (R*) at wavelengths 713, 709, 703, and 699 nm. For calibration (R^2 = 0.955, n = 204), only non-senesced leaves were selected from the dataset while accounting for different SRs between the reference dataset and the device. For *noise* reduction, we only estimated the mean functions of *Chl* with the relative insertion level (bottom leaves = 0) for April and May (*robust linear regression with*

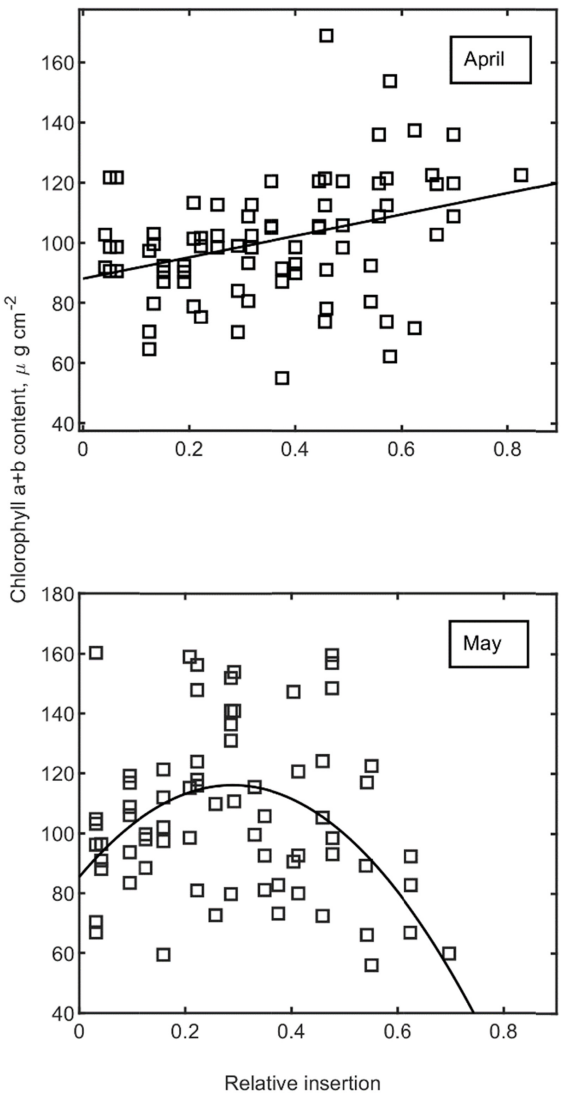

FIGURE 1 | Estimated vertical profiles of chlorophyll content as a function of relative insertion (top leaves = 1, bottom leaves = 0) for the months of April and May. Single estimates (symbols) with linear and quadratic regression functions for April and May, respectively.

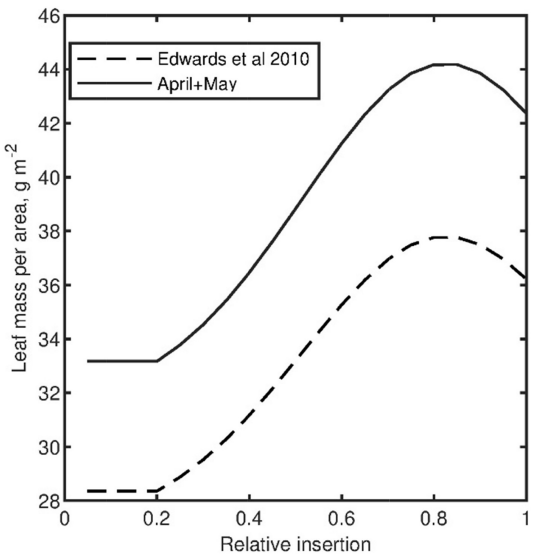

FIGURE 2 | Adopted vertical profile function of leaf mass per area (LMA) (without starch) during the tomato experiment based on LMA measurements of bottom leaves (relative insertion = 0) and an empirical equation form parameterized from Edwards et al. (2010).

bisquare weights, *robustfit procedure*, MATLAB 2020a, refer to **Figure 1**).

Estimated mean *Chl*(z) profile functions (**Figure 1**) were further modified by the received sum of $PPFD_i$ (mol m^{-2}) during expansion (21 days) of each leaf *i*, where the effect was assumed to decrease linearly to zero down to an insertion level (z_i) of $z_i = 0.5$, i.e., this initial enhancing effect was assumed to be fully diminished for the lower half of the canopy.

$$Chl_i^{'}(z_i) = Chl(z_i) + m(PPFD_i - \overline{PPFD})\ 2\ \max(0, -0.5 + z_i) \quad (13)$$

The coefficient ($m = 0.0447$) was estimated from a regression of corresponding data presented by Trouwborst et al. (2011a) and assumed to apply in an additive manner to the mean profiles in Equation 13. $\overline{PPFD}$ denotes the mean intercepted PPFD during April and May accordingly, while Chl(z_i) stands for the expected mean Chl content computed from relative leaf insertion level alone (mean curves in **Figure 1**).

The vertical profile of *LMA*, which is also required to estimate leaf optical parameters, was described as an empirical function of leaf position, total leaf number, and bottom value of *LMA* from a reanalysis of functions provided by Edwards et al. (2010) (**Figure 2**). Specifically, we considered starch as a source of variation in *LMA* that does not add useful information for leaf optical properties modeling. Therefore, a starch-free *LMA* profile was parameterized from a set of published expressions for two cultivars and several months (Edwards et al., 2010). Average *LMA* values obtained at the end of the experiment over the whole canopy were compared well with the calculated mean *LMA* over the adopted *LMA* profile function.

Photosynthetic Capacity in Spinach, Eucalyptus, and Cucumber

The profiles of photosynthetic capacity were analyzed with published data of three different crops, i.e., spinach (*Spinacia oleracea*), eucalyptus (*Eucalyptus pauciflora*), and cucumber (*Cucumis sativus*).

Photosynthetic capacity vs. cumulative chlorophyll content for *S. oleracea* and vertical *E. pauciflora* leaves were obtained from Nishio et al. (1993) and Evans and Vogelmann (2006), respectively. The effective extinction coefficient *k* was estimated through Gaussian process regression functions using leaf features *Chl*, *LMA*, and *Car* (refer to **Table 2**). The measured relative capacity profiles [C_n(c)] were then compared to a normalized

form of Equation 7, with estimated φ, $p_1 k_a$, and I^*.

$$C_n(c) = \varphi I_a\left(c,\ w_{u,g}, I_*, k'\right) / \varphi I_a\left(0,\ w_{u,g}, I_*, k'\right) \quad (14)$$

Measured properties of horizontal cucumber leaves and photosynthetic light response 7 days after a step change in growth irradiance at 4 different light transitions were tested (**Table 1**; Trouwborst et al., 2011b). The provided values of $J_{\max}$ and net photosynthesis rates A_n at 25°C were converted to leaf electron transfer rates J_{leaf}, assuming 50% reduction of dark respiration (R_d) in light,

$$J_{Leaf} = \frac{(A_n + 0.5R_d)(4.5C_i + 10.5\Gamma_*)}{(1 - \Gamma_*/C)\, C_i} \quad (15)$$

with CO_2 compensation point Γ_* set to 42.75 ppm (Bernacchi et al., 2001) and leaf internal CO_2 concentration C_i (ppm).

RESULTS

Empirical Description of Simplified Leaf Radiation Transfer Parameters

A major prerequisite for the following analysis is the validity of Equation 1 with profile parameters estimated from bulk leaf properties *Chl*, *Car*, and *LMA*. Setting the coefficient p_2 to 0.664 for all leaves improved the fit of Equation 1 to computed profiles of $I_d(c) + I_u(c)$ (Equations 3, 4). The root mean squared error (RMSE) decreased from 0.0263 with $p_2 = 1$ (i.e., the standard approach) to an RMSE of 0.01 ($p_2 = 0.664$). **Figure 3** shows that the remaining parameters (p_1, k, and k_a) can be fairly well predicted from leaf properties *Chl*, *Car*, and *LMA* using Gaussian process regression. Due to the two-stream nature of radiation transfer and manifested by the p_1 parameter, radiation intensities may exceed 1 (**Figure 3A**). It is more feasible to estimate the product $p_1 k_a$ (**Figure 3D**) than its terms separately.

Testing for the Coincidence of Photosynthetic Capacity and Light Absorption

To test Equation 7, we compared the profiles of the normalized light gradient $I_a\left(c,\ w_{u,g}, I_*, k\, p_3\right) / I_a\left(0,\ w_{u,g}, I_*, k\, p_3\right)$ with published profiles of maximum photosynthetic capacity in Spinach (Nishio et al., 1993; Terashima et al., 2009) and *E. pauciflora* (Evans and Vogelmann, 2006; **Figure 4**). While estimating k from given values of *Chl*, *Car*, and *LMA*, we could not justify a perfect match between light absorption and capacity profiles as fitted p_3 was always significantly lower than one [5% confidence region for all fitted p_3 = (0.156, 0.789)]. As those datasets are most suitable for the identification of p_3, we set it in the following to the mean of the obtained 3 estimates ($p_3 = 0.54$).

Testing Modified Electron Transfer by Light Acclimation in Cucumber

Published data for electron transport of cucumber leaves (Trouwborst et al., 2011b) could be predicted with fitting parameters to Equation 5 (**Table 2** and **Figure 5**). The estimated empirical model for I^* is as follows:

$$I^* = p_{i1}\left(p_{i2} I_1 + \left(1 - p_{i2}\right) I_2\right) \quad (16)$$

With p_{i2} being significantly greater than zero (**Table 2**), a large influence exists from the preceding light intensity prior to step change. Note that calculated I^* is here greater than the mean intensity during growth.

The minimum of $J_{c,max}$ ($J_{c,max,mn}$) was only active at constant low light treatment (LL-LL). The estimated value for θ (0.962) will also be used in subsequent steps.

V_{cmax} and J_{max} in Different Canopy Levels and Leaf Ages in a Tomato Crop

Parameter Estimation

Overall, the tested mechanistic model for photosynthetic light acclimation proved to be successful (**Figure 6**). The model could explain 68 or 72% of the observed variance for V_{cmax} and $J_{\max}$, respectively (**Table 3**). The estimated empirical model for I^* is as follows:

$$I^* = p_{i1}\overline{PPFD_{i,d}} \quad (17)$$

Best fitting results (in terms of the sum of squares) were obtained manually with d = 3, e.g., 3 previous days were used to compute $\overline{PPFD_{i,d}}$ for each leaf (equally weighted mean calculation). Alternative non-linear time weighting schemes improved the model fit marginally toward d values of 4–5 days.

The proportionality constant p_{i1} could be well identified for this dataset but at a lower value compared to cucumber (**Table 2**).

For the time dependence of minimum and maximum $J_{c,max}$ ($J_{c,max,mn}$, $J_{c,max,mx}$), which is here considered an aging process, the following relation was adopted.

$$J_{c,max,mn} = p_{J0} + p_{J1} PR_{sum}^{0.5} \qquad J_{c,max,mx} = n\, J_{c,max,mn} \quad (18)$$

with an hourly sum of the phenology response since leaf appearance PR_{sum} and empirical parameters p_{J0} and p_{J1}. The factor n was set to 2.6, the mean ratio obtained from experimental estimates (Evans and Seemann, 1989) on bulk leaves of several species.

For about 46% of the tested leaves, the photosynthetic capacity was constrained by PR_{sum}, i.e., $J_{c,max,mn}(t)$ was set as a lower limit in Equation 7.

Model Simulation

Assuming constant leaf properties and light intensities, different limitation onsets of electron flow by aging and light adaptation were investigated. At low light intensities (PPFD = 250 μmol m^{-2} s^{-1}, **Figure 7A**) the computed mean rate of electron transfer (symbols in **Figures 7A–C**) was almost entirely determined by the ontogenetic prescribed lower limit of electron transfer which decreases monotonically over time. Similarly, the calculated V_{cmax} (**Figure 7D**) was decreasing continuously over time. In contrast, at higher PPFD (750 μmol m^{-2} s^{-1}, **Figure 7C**), the electron flow could be determined by (constant) light acclimation and was later constrained by the upper limit of the ontogenetic prescribed range of electron flow (**Figure 4C**).

TABLE 1 | Leaf properties used for model testing of photosynthetic capacity profile and electron transport rates.

Species	PPFD μmol m^{-2} s^{-1}	*Chl* μg cm^{-2}	*LMA* g m^{-2}	*Chl2Car*	$w_{u,g}$
Spinacia o.[1]	800	56.3	48	4.46	0.9
	200	48.8	37	4.84	0.9
Eucalyptus p. [2]	Natural	44.8	240	4.25	0.5
Cucumis s. [3]	200→200	57	27.6	5.3	0.9
	50→200	54.9	24.3	5.4	0.9
	200→50	56.3	23.3	5.4	0.9
	50→50	40.0	15.4	5.5	0.9

[1]*Nishio et al. (1993)*; [2]*Evans and Vogelmann (2006)*; [3]*Trouwborst et al. (2011b)*. *Chl, chlorophyll a + b; LMA, Leaf mass area; Chl2Car, chlorophyll to carotenoid ratio; $w_{u,g}$, fractional light interception at upper leaf side.*

TABLE 2 | Parameter estimates for the fit of Equation 6 to electron transport rate of differently light acclimated cucumber leaves.

Parameter	p_{i1}	p_{i2}	θ	$J_{c,max,mn}$
Unit	–	–	–	mmol e^- (mol Chl) $^{-1}$ s^{-1}
Value (CI)	1.51 (1.4–1.6)	0.446 (0.36–0.53)	0.962 (0.93–0.99)	161 (150–174)

Seven days after step change in light intensity. $w_{u,g}$ = 0.9 (assumed), p_3 = 0.54, RMSE = 4.22, n = 20. CI: p = 5% confidence interval.

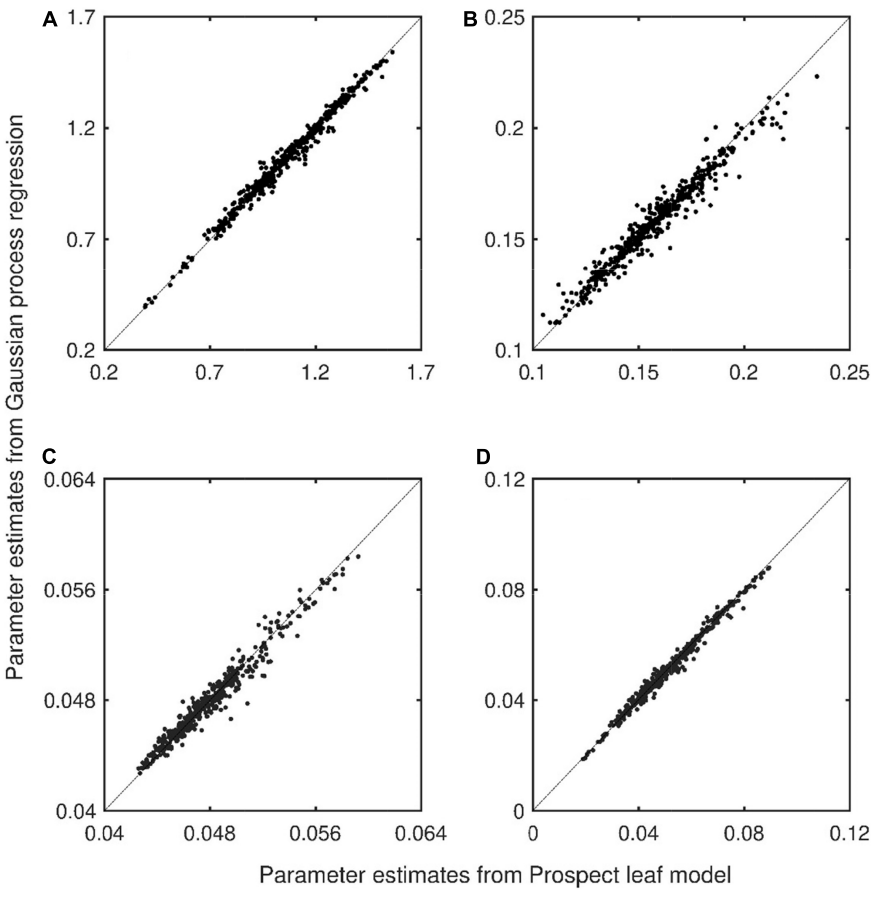

FIGURE 3 | Estimated parameters from the Prospect model (using Equations 1–4) vs. empirical regression estimates using Gaussian process regression y = f(*Chl, LMA, Car*) with 1:1 line. n = 470, Lopex and Angers leaf optical properties datasets, **(A)** scaling parameter p_1, **(B)** effective leaf extinction coefficient k, **(C)** absorption coefficient k_a, and **(D)** the product of p_1 and k_a. Optical depth is the chlorophyll content (*Chl*; μg/cm^2).

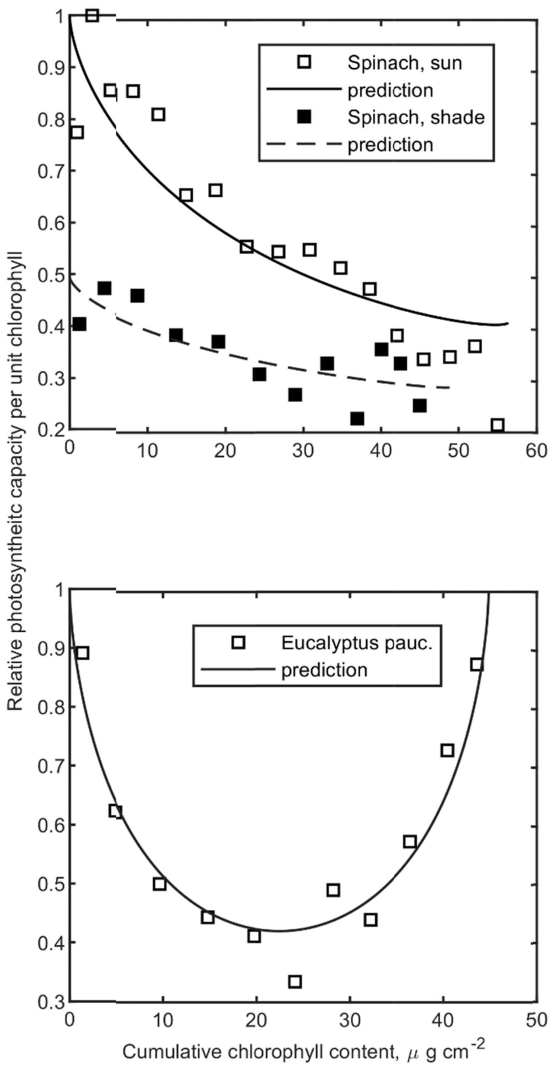

FIGURE 4 | Relative photosynthetic capacity vs. cumulative *Chl*. **(Upper graph)** Sun [k = 0.1457, fitted p_3 = 0.53 (0.458–0.628)] and shade [k = 0.1455, fitted p_3 = 0.36 (0.156–0.559)]-treated horizontal spinach leaves ($w_{u,g}$ = 0.9, Nishio et al., 1993). **(Lower graph)** Vertical isobilateral leaves of E. *pauciflora* (k = 0.2535, fitted p_3 = 0.73 (0.675–0.789), $w_{u,g}$ = 0.5, Evans and Vogelmann, 2006). Confidence limits are given in parenthesis, p = 0.05.

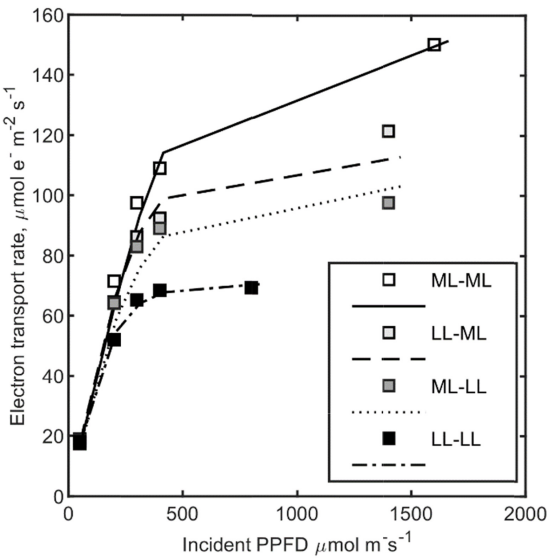

FIGURE 5 | Measured electron transport rates (symbols) and predictions by Equation 6 (lines) vs. incident photosynthetic photon flux density (PPFD) at 7 days after a step change in light intensity for cucumber leaves (Trouwborst et al., 2011b), ML-ML (I_1:200 → I_2:200 μmol m^2 s^{-1}), LL-ML (I_1:50 → I_2:200 μmol m^2 s^{-1}), LL-ML (I_1:200 → I_2:50 μmol m^{-2} s^{-1}), and LL-LL (I_1:50 → I_2:50 μmol m^{-2} s^{-1}). Plants were measured after 7 days growing at intensity I_2. Lines connect computations at assessed PPFD (i.e., symbols). n = 20, root mean squared error = 4.22 μmol e$^-$ m^{-2} s^{-1}.

This scenario results in an almost time-invariant behavior of V_{cmax} (**Figure 4D**).

DISCUSSION

Model-Framework Validity

We present a novel mathematical framework (Equations 2, 5–10) to describe the time dependency of the FCB photosynthetic model parameters (φ', θ, J_{max}, and V_{cmax}) caused by progressing leaf phenology and light acclimation. The derived relations build on previous work to model light acclimation (Badeck, 1995) or whole leaf electron transport rates (Buckley and Farquhar, 2004). The proposed model framework requires an accurate specification of the incoming radiation field [PPFD(t), $w_{u,m}$, and $w_{u,g}$], additional leaf traits (*Chl*, *Car*, and *LMA*), and further parameters ($J_{c,max,mx}$, $J_{c,max,mn}$, I^*) that are likely functions of perceived temperatures and intercepted light intensities during leaf growth (Equations 16–18).

We tested the capability of the framework to predict published intra-leaf photosynthetic capacity profiles (**Figure 4**), light response curves for differently light-adapted cucumber leaves (**Figure 5**), and measured J_{max} and V_{cmax} values at different times and canopy depths in a tomato crop. To limit the degree of freedom for each step, we estimated several parameters hierarchically from independent datasets, e.g., $p_1 k_a$ and k using generated leaf optics data, p_3 from capacity profiles, and θ from light response curves.

Clearly, to explore the full validity of our proposed theory, more experimental work with vertically and horizontally grown tomato and cucumber crops is required. An evident key role in this matter was identified in leaf *Chl* content. Being an integration variable (e.g., Equation 10) it also influences intra-leaf absorption parameters *via* Gaussian process regression. This fits well with recent observations in various species of V_{cmax} and J_{max}-*Chl* relations being better predictors than leaf nitrogen (Qian et al., 2021). However, neither its repeatable measurement nor its empirical prediction of *Chl* in time and space seems to be trivial. For tomato, *Chl* is dependent on the received light intensity during leaf expansion (Equation 13), Trouwborst et al. (2011a), while it declines with canopy depth (**Figure 1**).

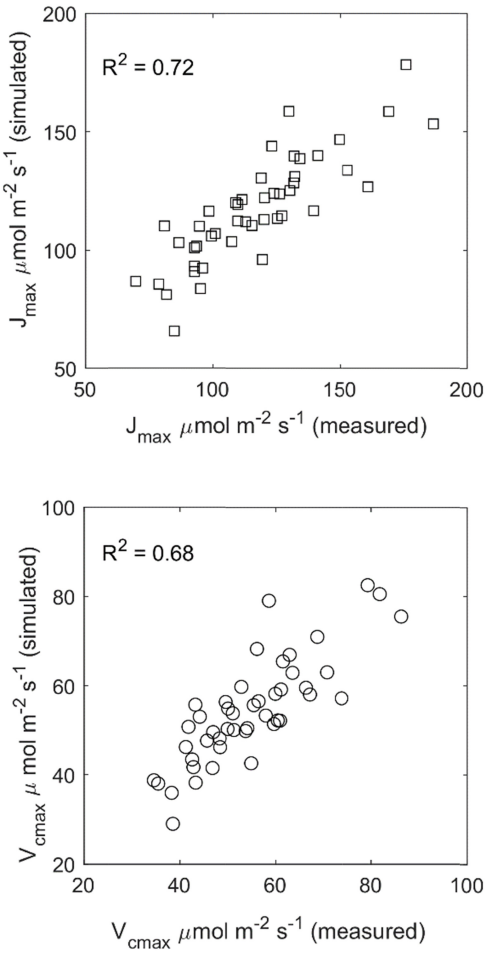

FIGURE 6 | Comparison of predicted vs. measured maximum rates of carboxylation (V_{cmax}) and electron transport (J_{max}) at different canopy depths over 2 months in a tomato canopy. n = 46. Refer to **Table 2** for more details.

Model Framework in a Current Scientific Context

Due to multiple and internal reflections (r_i) at the leaf epidermis-air interface (Equation 3), the total received irradiance at the topmost mesophyll layer may exceed the incident intensity (**Figure 3**). This phenomenon has been theoretically predicted and measured (Vogelmann and Björn, 1984). Therefore, the specific parameter p_1 was introduced (**Figure 3A**). A more effective way to predict the profile of absorbed radiation (Equation 2); however, is combining p_1 with k_a, i.e., $p_1 k_a$ (**Figure 4D**).

Analogously to the distribution of leaf photosynthetic capacity and leaf nitrogen content with canopy depth, a covariation of photosynthetic capacity profiles with intra-leaf absorbed radiation was observed (**Figure 4**). Consistently over all three observed capacity profiles, the agreement was imperfect: p_3 (on average 0.54) was significantly lower than 1. Earlier studies with whole leaves support our finding: A canopy scale meta-study estimated an analog reduction of the light extinction coefficient by 0.5 (Hikosaka et al., 2016).

The obtained estimate for θ = 0.962 for cucumber leaves (**Table 2**) corresponds well with an average figure of 0.965 reported by Terashima and Saeki (1985) for chloroplast and cell suspensions. Similarly, $J_{c,max,mn}$ estimated at 161 was similar to measurements in shaded cucumber leaves of 160 (PPFD = 120 μmol m^{-2} s^{-1}; Evans, 1989). For dicot plants common bean (*Phaseolus vulgaris*) and tobacco (*Nicotiana tabacum*), there is strong evidence that the ratio of the leaf cytochrome b_6f complex to chlorophyll content is the major target for both light acclimation and leaf aging (Schöttler and Tóth, 2014), which is linear related to electron flow (Evans and Seemann, 1989). Moreover, this ratio changes for tobacco by a factor of 2.45 from low to high light-adapted leaves (Schöttler and Tóth, 2014), which is close to the adopted value $J_{c,max,mx}/J_{c,max,mn}$ = 2.6 (Evans and Seemann, 1989) based on measured electron transport rates.

A strong correlation between V_{cmax} and J_{max} is well known. Wullschleger (1993) presented a V_{cmax} to J_{max} ratio of 0.431 for vegetable crops (17 species), obtained from A/C_i curves assuming implicitly a fixed curvature θ of leaf electron transfer. This ratio evolves automatically as parameter p_4 in Equation 10, with an estimated value of p_4 = 0.437 for tomato (**Table 3**), a remarkable agreement of Wullschleger's result and our estimate.

The bifacial nature of leaf morphology of dicot plants is often accompanied by different leaf reflectance and transmittances measured from the adaxial and abaxial leaf sides (De Lucia et al., 1991; Stuckens et al., 2009). This indicates different effective two-stream parameters depending on whether light is incident on the adaxial or abaxial leaf side. Therefore, additional research would be needed to investigate the necessity of introducing different parameters for the palisade and spongy mesophyll layers (Terashima et al., 2009). Especially for cases with significant light incidence from the lower leaf side, either during acclimation or measurement, this might be of importance.

Extensions to the Model Framework

The major foundation of this analysis is the assumption of the validity of the two-stream approximation of radiation

TABLE 3 | Parameter estimates for the fit of Equations 5, 10 to measure J_{max} and V_{cmax} in tomato.

Parameter	p_{i1}	p_4	p_{J0}	p_{J1}
Unit	–	–	mmol e^- (mol *Chl*) $^{-1}$ s^{-1}	mmol e^- (mol *Chl*) $^{-1}$ s^{-1} h^{-1}
Value CI	0.586 (0.54–0.63)	0.437 (0.41–0.47)	304 (273–336)	7.00 (5.8–8.1)

$w_{u,g}$ = 0.7, p_3 = 0.54, φ = 0.468, θ = 0.962, RMSE-J_{max} = 13.87, n = 46, RMSE-V_{cmax} = 7.02, n = 46. CI = 5% confidence intervals.

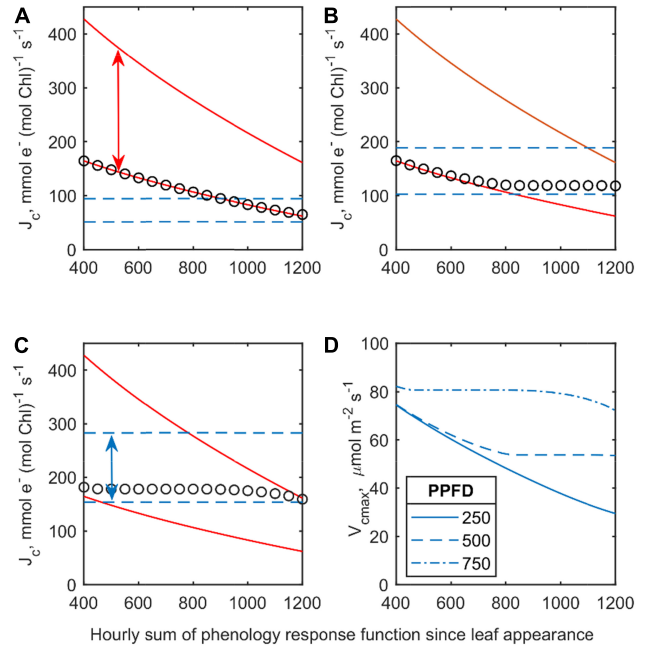

FIGURE 7 | (A–C) Simulated adaptation ranges of electron flow (lines) and final mean leaf rate (symbols) over time at different time constant PPFD: **(A)** 250 µmol m^{-2} s^{-1}, **(B)** 500 µmol m^{-2} s^{-1}, and **(C)** 750 µmol m^{-2} s^{-1}. Lower and upper red lines are $J_{x,max,mn}$ and $J_{x,max,mx}$, respectively. Lower and upper blue dashed lines are minima and maxima set by the profile of absorbed light, respectively. **(D)** Corresponding calculated rates of V_{cmax} over time.

transfer for leaves. This includes the need for identifying two parameters (k_s, k_a) from total leaf transmittance and reflectance while accounting for diffuse Fresnel reflectance/transmittances at the leaf boundaries (Equations 3, 4). This approach assumes perfectly diffused radiation streams, with equal probability of backward and forward scattering of photons, setting the anisotropy parameter for scattering g to zero. However, an accurate approximation to the radiation transfer equation for a scattering and absorbing slab was recently derived (Liemert et al., 2019). This solution could be a useful asset in improving parameter calibration of Equation 2 or similar functions, which eventually can lead to the derivation of better approximations; even different incidence angles and refraction index changes at the leaf surface can be accounted for Liemert et al. (2019). For that, an independent spectral parameterization of the anisotropy parameter g(λ) (or the scattering phase function) would be required. Measurements on various biological tissues indicate a rather smooth and slow change of g(λ) over the visible wavelength range (Jacques, 2013).

Ways for Practical Application

Both from a theoretical and experimental standpoint, the quantification of received radiation fluxes per leaf (patch) within plant canopies is not straightforward. In real (commercial cultivated) canopies, the leaf-specific and time-dependent estimation could be supported with imaging techniques. One solution would be the combination of a hemispherical gap fractions distribution from fisheye imaging (Eichelmann et al., 2005) with our model framework. Model predictions and accurate specification of the incoming radiation field could be a basis for a powerful monitoring tool in vertical crop stands. In addition, there is a growing number of functional structural plant model (FSPM) codes (Buck-Sorlin et al., 2011; Sarlikioti et al., 2011) and libraries (Bailey, 2019), which are in principle well suited to provide this information even on a leaf patch basis in virtual canopies.

CONCLUSION

In this study, we extended a previous leaf model for electron transport rate (Buckley and Farquhar, 2004) to account for the phenomenon of non-perfect acclimation of photosynthetic capacity to absorbed radiation within the mesophyll. Adopting the two-stream solution of radiation transfer with cumulative chlorophyll content, we derive the scattering and absorption coefficients from the total reflectance and transmittance of leaves. This allowed the derivation of an improved simplified model for absorbed radiation profile and corresponding lumped parameters, which can be estimated just from total chlorophyll, carotenoid, and dry mass content per leaf area using machine learning methods. A reanalysis of published datasets with this simplified model revealed a significant derivation of measured photosynthetic capacity profiles from calculated absorption profiles, while this deviation can be resolved empirically.

Furthermore, the applicability of the modified model was tested on light acclimation on published experimental data with cucumber (Trouwborst et al., 2011b) and with a self-performed tomato cultivation experiment. These tests revealed that ontogenetic constraints are likely to be superimposed on light intensity effects within the leaf mesophyll.

DATA AVAILABILITY STATEMENT

The raw data supporting the conclusions of this article will be made available by the authors, without undue reservation.

AUTHOR CONTRIBUTIONS

JG: model development, model conception and realization, manuscript writing, data management, simulations, and figures. WY: experimental measurements, first draft of manuscript, and model conception. OK: experimental design, experimental supervision, and manuscript writing. All authors contributed to the article and approved the submitted version.

ACKNOWLEDGMENTS

We thank Angela Schmidt and Robert Klose for their elaborate technical assistance.

REFERENCES

Badeck, F. W. (1995). Intra-leaf gradient of assimilation rate and optimal allocation of canopy nitrogen: a model on the implications of the use of homogeneous assimilation functions. *Aust. J. Plant Physiol.* 22, 425–439. doi: 10.1071/PP9950425

Bailey, B. N. (2019). Helios: A Scalable 3D Plant and Environmental Biophysical Modeling Framework. *Front. Plant Sci.* 10:1185. doi: 10.3389/FPLS.2019.01185/BIBTEX

Bernacchi, C. J., Singsaas, E. L., Pimentel, C., Portis, A. R. Jr., and Long, S. P. (2001). Improved temperature response functions for mod- els of Rubisco-limited photosynthesis. *Plant Cell Environ.* 24, 253–260. doi: 10.1046/j.1365-3040.2001.00668.x

Bonan, G. B., Patton, E. G., Finnigan, J. J., Baldocchi, D. D., and Harman, I. N. (2021). Moving beyond the incorrect but useful paradigm: reevaluating big-leaf and multilayer plant canopies to model biosphere-atmosphere fluxes – a review. *Agric. For. Meteorol.* 306:108435. doi: 10.1016/J.AGRFORMET.2021.108435

Boote, K. J., Rybak, M. R., Scholberg, J. M. S., and Jones, J. W. (2012). Improving the CROPGRO-tomato model for predicting growth and yield response to temperature. *HortScience* 47, 1038–1049. doi: 10.21273/hortsci.47.8.1038

Buckley, T. N., and Farquhar, G. D. (2004). A new analytical model for whole-leaf potential electron transport rate. *Plant Cell Environ.* 27, 1487–1502. doi: 10.1111/j.1365-3040.2004.01232.x

Buck-Sorlin, G., De Visser, P. H. B., Henke, M., Sarlikioti, V., Van Der Heijden, G. W. A. M., Marcelis, L. F. M., et al. (2011). Towards a functional structural plant model of cut-rose: simulation of light environment, light absorption, photosynthesis and interference with the plant structure. *Ann. Bot.* 108, 1121–1134. doi: 10.1093/aob/mcr190

de Kreij, C., Voogt, W., and Baas, R. (2003). *Nutrient Solutions and Water Quality for Soilless Cultures*. Available online at: https://library.wur.nl/WebQuery/wurpubs/fulltext/456342 (accessed June 9, 2022).

De Lucia, E. H., Shenoi, H. D., Naidu, S. L., and Day, T. A. (1991). Photosynthetic symmetry of sun and shade leaves of different orientations. *Oecologia* 87, 51–57. doi: 10.1007/BF00323779

Edwards, D., Jolliffe, P., and Ehret, D. (2010). Canopy profiles of starch and leaf mass per area in greenhouse tomato and the relationship with leaf area and fruit growth. *Sci. Hortic.* 125, 637–647. doi: 10.1016/j.scienta.2010.05.019

Eichelmann, H., Oja, V., Rasulov, B., Padu, E., Bichele, I., Pettai, H., et al. (2005). Adjustment of leaf photosynthesis to shade in a natural canopy: reallocation of nitrogen. *Plant Cell Environ.* 28, 389–401. doi: 10.1111/J.1365-3040.2004.01275.X

Ethier, G. J., and Livingston, N. J. (2004). On the need to incorporate sensitivity to CO2 transfer conductance into the Farquhar-von Caemmerer-Berry leaf photosynthesis model. *Plant Cell Environ.* 27, 137–153. doi: 10.1111/j.1365-3040.2004.01140.x

Evans, J. R. (1989). Partitioning of Nitrogen Between and Within Leaves Grown under Different Irradiances. *Fun. Plant Biol.* 16, 533-548.

Evans, J. R., and Seemann, J. R. (1989). "The allocation of protein nitrogen in the photosynthetic apparatus: costs, consequences, and control". in *Photosynthesis*, ed W. R. Briggs, (New York: A.R. Liss), 183–205.

Evans, J. R., and Vogelmann, T. C. (2006). Photosynthesis within isobilateral Eucalyptus pauciflora leaves. *New Phytol.* 171, 771–782. doi: 10.1111/j.1469-8137.2006.01789.x

Féret, J. B., Gitelson, A. A., Noble, S. D., Jacquemoud, S., and Féret, J.-B. (2017). PROSPECT-D: towards modeling leaf optical properties through a complete lifecycle PROSPECT-D: towards modeling leaf optical properties through a complete lifecycle 1. *Remote Sens. Environ* 193, 204–215. doi: 10.1016/j.rse.2017.03.004\"{\i}

Heuvelink, E. (1996). *Tomato Growth and Yield: Quantitative Analysis and Synthesis*. Available online at: https://search.proquest.com/openview/63d3499a7abf92da21725bb0410836dc/1?pq-origsite=gscholar&cbl=2026366&diss=y (accessed on Feb 22, 2022).

Hikosaka, K., Anten, N. P. R., Borjigidai, A., Kamiyama, C., Sakai, H., Hasegawa, T., et al. (2016). A meta-analysis of leaf nitrogen distribution within plant canopies. *Ann. Bot.* 118, 239–247. doi: 10.1093/aob/mcw099

Jacquemoud, S., and Baret, F. (1990). PROSPECT: A Model of Leaf Optical Properties Spectra. *Science* 91, 75–91. doi: 10.1364/AO.49.001687

Jacquemoud, S., Bidel, L., Francois, C., and Pavan, G. (2003). *ANGERS Leaf Optical Properties Database*. Available online at: http://opticleaf.ipgp.fr/index.php?page=database (Accessed June 9, 2022).

Jacquemoud, S., and Ustin, S. (2019). *Leaf Optical Properties*. Cambridge: Cambridge University Press, doi: 10.1017/9781108686457

Jacques, S. L. (2013). Optical properties of biological tissues: a review. *Phys. Med. Biol.* 58, R37–61. doi: 10.1088/0031-9155/58/14/5007

Joshi, N. C., Ratner, K., Eidelman, O., Bednarczyk, D., Zur, N., Many, Y., et al. (2019). Effects of daytime intra-canopy LED illumination on photosynthesis and productivity of bell pepper grown in protected cultivation. *Sci. Hortic.* 250, 81–88. doi: 10.1016/j.scienta.2019.02.039

Kalaji, H. M., Schansker, G., Brestic, M., Bussotti, F., Calatayud, A., Ferroni, L., et al. (2017). Frequently asked questions about chlorophyll fluorescence, the sequel. *Photosynth Res* 132, 13–66. doi: 10.1007/s11120-016-0318-y

Kläring, H. P., and Körner, O. (2020). Design of a real-time gas-exchange measurement system for crop stands in environmental scenarios. *Agronomy* 10:737. doi: 10.3390/agronomy10050737

Kläring, H. P., and Zude, M. (2009). Sensing of tomato plant response to hypoxia in the root environment. *Sci. Hortic.* 122, 17–25. doi: 10.1016/J.SCIENTA.2009.03.029

Körner, O., Aaslyng, J. M., Andreassen, A. U., and Holst, N. (2007). Microclimate prediction for dynamic greenhouse climate control. *HortScience* 42, 272–279. doi: 10.21273/HORTSCI.42.2.272

Laisk, A., Oja, V., Eichelmann, H., and Dall'Osto, L. (2014). Action spectra of photosystems II and i and quantum yield of photosynthesis in leaves in State 1. *Biochim. Biophys. Acta Bioenerg.* 1837, 315–325. doi: 10.1016/j.bbabio.2013.12.001

Lichtenthaler, H. K., and Babani, F. (2004). "Light adaptation and senescence of the photosynthetic apparatus. Changes in pigment composition, chlorophyll fluorescence parameters and photosynthetic activity," in *Chlorophyll a Fluorescence*, eds G. C. Papageorgiou and Govindjee (Dordrecht: Springer), 713–736. doi: 10.1007/978-1-4020-3218-9_28

Liemert, A., Martelli, F., Binzoni, T., and Kienle, A. (2019). P 3 solution for the total steady-state and time-resolved reflectance and transmittance from a turbid slab. *Appl. Opt.* 58, 4143–4148. doi: 10.1364/ao.58.004143

Meir, P., Kruijt, B., Broadmeadow, M., Barbosa, E., Kull, O., Carswell, F., et al. (2002). Acclimation of photosynthetic capacity to irradiance in tree canopies in relation to leaf nitrogen concentration and leaf mass per unit area. *Plant Cell Environ.* 25, 343–357. doi: 10.1046/j.0016-8025.2001.00811.x

Muschaweck, J. (2021). *JMO_Spectrum*. Available online at: https://www.mathworks.com/matlabcentral/images/matlab-file-exchange.svg)](https://uk.mathworks.com/matlabcentral/fileexchange/98044-jmo_spectrum) (Accessed June 9, 2022).

Myneni, R. B., and Ross, J. (2012). *Photon-Vegetation Interactions: Applications in Optical Remote Sensing and Plant Ecology*. Berlin: Springer Science & Business Media.

Niinemets, Ü (2016). Leaf age dependent changes in within-canopy variation in leaf functional traits: a meta-analysis. *J. Plant Res.* 129, 313–338. doi: 10.1007/s10265-016-0815-2

Niinemets, Ü, Kull, O., and Tenhunen, J. D. (2004). Within-canopy variation in the rate of development of photosynthetic capacity is proportional to integrated quantum flux density in temperate deciduous trees. *Plant Cell Environ.* 27, 293–313. doi: 10.1111/J.1365-3040.2003.01143.X

Nishio, J. N., Sun, J., and Vogelmann, T. C. (1993). Carbon fixation gradients across spinach leaves do not follow internal light gradients. *Plant Cell* 5, 953–961. doi: 10.2307/3869663

Qian, X., Liu, L., Croft, H., and Chen, J. (2021). Relationship Between Leaf Maximum Carboxylation Rate and Chlorophyll Content Preserved Across 13 Species. *J. Geophys. Res. Biogeosci.* 126:e2020JG006076. doi: 10.1029/2020JG006076

Russell, G., Marshall, B., and Jarvis, P. G. (1990). *Plant canopies: their growth, form and function*. Cambridge: Cambridge University Press.

Sarlikioti, V., De Visser, P. H. B., and Marcelis, L. F. M. (2011). Exploring the spatial distribution of light interception and photosynthesis of canopies by means of a functionalstructural plant model. *Ann. Bot.* 107, 875–883. doi: 10.1093/aob/mcr006

Schöttler, M. A., and Tóth, S. Z. (2014). Photosynthetic complex stoichiometry dynamics in higher plants: environmental acclimation and photosynthetic flux control. *Front. Plant Sci.* 5:188. doi: 10.3389/fpls.2014.00188

Stern, F. (1964). Transmission of isotropic radiation across an interface between two dielectrics. *Appl. Opt.* 3:111. doi: 10.1364/ao.3.000111

Stuckens, J., Verstraeten, W. W., Delalieux, S., Swennen, R., and Coppin, P. (2009). A dorsiventral leaf radiative transfer model: development, validation and improved model inversion techniques. *Remote Sens. Environ.* 113, 2560–2573. doi: 10.1016/J.RSE.2009.07.014

Terashima, I., Fujita, T., Inoue, T., Chow, W. S., and Oguchi, R. (2009). Green light drives leaf photosynthesis more efficiently than red light in strong white light: revisiting the enigmatic question of why leaves are green. *Plant Cell Physiol.* 50, 684–697. doi: 10.1093/pcp/pcp034

Terashima, I., and Saeki, T. (1985). A new model for leaf photosynthesis incorporating the gradients of light environment and of photosynthetic properties of chloroplasts within a leaf. *Ann. Bot.* 56, 489–499. doi: 10.1093/oxfordjournals.aob.a087034

Trouwborst, G., Hogewoning, S. W., Harbinson, J., and van Ieperen, W. (2011a). The influence of light intensity and leaf age on the photosynthetic capacity of leaves within a tomato canopy. *J. Hortic. Sci. Biotechnol.* 86, 403–407. doi: 10.1080/14620316.2011.11512781

Trouwborst, G., Hogewoning, S. W., Harbinson, J., and Van Ieperen, W. (2011b). Photosynthetic acclimation in relation to nitrogen allocation in cucumber leaves in response to changes in irradiance. *Physiol. Plant* 142, 157–169. doi: 10.1111/j.1399-3054.2011.01456.x

Vogelmann, T. C., and Björn, L. O. (1984). Measurement of light gradients and spectral regime in plant tissue with a fiber optic probe. *Physiol. Plant* 60, 361–368. doi: 10.1111/j.1399-3054.1984.tb06076.x

von Caemmerer, S., Farquhar, G., and Berry, J. (2009). "Biochemical Model of C3 Photosynthesis," in *Photosynthesis in Silico*, eds A. Laisk., L. Nedbal., and Govindjee, (Springer, Dordrecht), 209–230. doi: 10.1007/978-1-4020-9237-4_9.

Wullschleger, S. D. (1993). Biochemical limitations to carbon assimilation in C3 plants- A retrospective analysis of the A/Ci Curves from 109 species. *J. Exp. Bot.* 44, 907–920.

Yin, X., Yin, X., Van Oijen, M., and Schapendonk, A. H. C. M. (2004). Extension of a biochemical model for the generalized stoichiometry of electron transport limited C 3 photosynthesis. *Plant Cell Environ.* 27, 1211–1222.

Yu, W., and Körner, O. (2020). Effect of temperature and CO2 concentration on leaf expansion in a tomato crop canopy. *Acta Hortic.* 1296, 509–516. doi: 10.17660/ActaHortic.2020.1296.66

Conflict of Interest: The authors declare that the research was conducted in the absence of any commercial or financial relationships that could be construed as a potential conflict of interest.

Publisher's Note: All claims expressed in this article are solely those of the authors and do not necessarily represent those of their affiliated organizations, or those of the publisher, the editors and the reviewers. Any product that may be evaluated in this article, or claim that may be made by its manufacturer, is not guaranteed or endorsed by the publisher.

Advantages of publishing in Frontiers

OPEN ACCESS
Articles are free to read for greatest visibility and readership

FAST PUBLICATION
Around 90 days from submission to decision

HIGH QUALITY PEER-REVIEW
Rigorous, collaborative, and constructive peer-review

TRANSPARENT PEER-REVIEW
Editors and reviewers acknowledged by name on published articles

Frontiers
Avenue du Tribunal-Fédéral 34
1005 Lausanne | Switzerland

Visit us: www.frontiersin.org
Contact us: frontiersin.org/about/contact

REPRODUCIBILITY OF RESEARCH
Support open data and methods to enhance research reproducibility

DIGITAL PUBLISHING
Articles designed for optimal readership across devices

FOLLOW US
@frontiersin

IMPACT METRICS
Advanced article metrics track visibility across digital media

EXTENSIVE PROMOTION
Marketing and promotion of impactful research

LOOP RESEARCH NETWORK
Our network increases your article's readership